THE PHYSICAL REVIEW

VOLUME 85 [illegible] NUMBER

MARCH 15, [illegible]

Published for the
AMERICAN PHYSICAL [illegible]
by the
[illegible]

THE PHYSICAL REVIEW

A journal of experimental and theoretical physics established by E. L. Nichols in 1893

Published by the American Institute of Physics
for the
AMERICAN PHYSICAL SOCIETY

Officers

President

J. H. Van Vleck
Harvard University
Cambridge, Massachusetts

Vice-President

Enrico Fermi
Institute for Nuclear Studies
University of Chicago
Chicago 37, Illinois

Secretary

K. K. Darrow
Bell Telephone Laboratories
Office:
Columbia University
New York 27, New York

Treasurer

G. B. Pegram
Columbia University
New York 27, New York

Local Secretary
for the Pacific Coast

J. Kaplan
University of California at Los Angeles
Los Angeles, California

Managing Editor

S. A. Goudsmit
Brookhaven National Laboratory
Upton, Long Island
New York

BOARD OF EDITORS

Editor

S. A. Goudsmit

Assistant Editor

S. Pasternack

Associate Editors

Hardy Bacher	M. Goldhaber	W. P. Allis
R. F. Christy	R. Hofstadter	F. G. Brickwedde
C. L. Critchfield	A. W. Lawson	W. B. Fretter
H. Draper	A. Pais	Conyers Herring
T. H. Johnson	R. Serber	H. W. Lewis
Bruno Rossi	C. H. Townes	Abraham Wolf

Manuscripts for publication should be submitted to S. A. Goudsmit, Brookhaven National Laboratory, Upton, Long Island, New York. The authors' institutions are requested to pay a publication charge of $10 a page which, if honored, entitles them to 100 free reprints. Instructions will be sent with galley proofs.

Proof and all correspondence concerning papers in the process of publication should be addressed to the Publication Manager, American Institute of Physics, 57 East 55 Street, New York 22, New York.

Subscription Price

United States and Canada $25.00
Elsewhere $27.00

Back Numbers

Yearly back number rate unless *complete year is available*:
Prior to 1949: $20.00
Thereafter: $27.00

Single copies: $2.00 each, prior to July, 1929;
$1.50 each, July, 1929–December, 1941;
$2.00 each, January, 1942–December, 1946;
$1.00 each, January, 1947–December, 1948;
$1.25 each, thereafter.

General index, 1893–1920: $4.00.

Subscriptions, renewals, and orders for back numbers should be addressed to the American Institute of Physics, 57 East 55 Street, New York 22, New York.

Changes of address in the case of members of the American Physical Society should be addressed to the Treasurer; in the case of other subscribers to the American Institute of Physics.

[a] Per Section 4, Member of Physics Department, Cornell University, Ithaca, New York.

The Physical Review is published semimonthly at Prince and Lemon Streets, Lancaster, Pennsylvania.

Entered as second-class matter January 6, 1947, at the Post Office at Lancaster, Pennsylvania, under the Act of March 3, 1879.

Acceptance for mailing at special rate of postage provided for by paragraph (d-2), section 34.40, P. L. & R. of 1948, authorized January 27, 1947.

CONTENTS

JANUARY 1, 1952

Adiabatic Thermal Changes in Barium Titanate Ceramic at Low Temperatures . . . ROLAND W. SCHMITT 1

Internal Conversion Angular Correlations . . . M. E. ROSE, L. C. BIEDENHARN, AND G. B. ARFKEN 5

Note on the Adiabatic Thermomagnetic Effects . . . HERBERT B. CALLEN 16

Range Straggling of a Nonrelativistic Charged Particle . . . H. W. LEWIS 20

Rotational Magnetic Moments of $^1\Sigma$ Molecules . J. R. ESHBACH AND M. W. P. STRANDBERG 24

On the Critical State of Normal Fluids . . . LOUIS GOLDSTEIN 35

Nuclear Magnetic Moment and *j-j* Coupling Shell Model . . . MASATAKA MIZUSHIMA AND MINORU UMEZAWA 37

Motion of an Electron in a Perturbed Periodic Potential . . . E. N. ADAMS, II 41

Cross Section for the Radiative Capture of Protons by C^{13} at 129 kev . . . ERIC JOHN WOODBURY AND WILLIAM ALFRED FOWLER 51

Polarization of Scattered Quanta . . . J. I. HOOVER, W. R. FAUST, AND C. F. DOHNE 58

Theory of Molecular Hydrogen and Deuterium in Magnetic Fields . . NORMAN F. RAMSEY 60

Superposition of Configurations in the Ground State of He I . . LOUIS C. GREEN, MARJORIE M. MULDER, C. W. UFFORD, E. SLAYMAKER, ELEANOR KRAWITZ, AND R. T. MERTZ 65

Pressure Effects of Argon and Helium on the Resonance Lines of Silver . . . EUGENE D. CLAYTON AND SHANG-YI CH'EN 68

Magnetic Susceptibility of Uranium . . . C. J. KRIESSMAN, JR., AND T. R. MCGUIRE 71

High Energy Neutron Collisions with Helium . . . CLIFFORD SWARTZ 73

Study of the Multiple Scattering of Fast Charged Particles in a Gas. II. (Negative and Positive Beta-Particles) . GERHART GROETZINGER, WATTS HUMPHREY, JR., AND FRED L. RIBE 78

Production of Polarized Protons and the Inversion of Energy Levels of the P_1–P_1 Doublet in Li^5 . . . M. HEUSINKVELD AND GEORGE FREIER 80

Superconductivity of Vanadium . . . AARON WEXLER AND WILLIAM S. CORAK 85

Multiple Scattering of Fast Particles in Photographic Emulsions . . . L. VOYVODIC AND E. PICKUP 91

Internal Conversion in Pr^{141}, In^{114}, Ba^{137}, and Cd^{110} . . . W. C. KELLY 101

Magnetic Properties of a Hollow Superconducting Lead Sphere . . . JULIUS BABISKIN 104

Range of 18-Mev Protons in Aluminum . . . E. L. HUBBARD AND K. R. MACKENZIE 107

Beta-Spectra of P^{32} and P^{33} . . ERLING N. JENSEN, R. T. NICHOLS, J. CLEMENT, AND A. POHM 112

Distribution of Multiplicities of Neutrons Produced by Cosmic-Ray μ-Mesons Captured in Lead . . . MARSHALL F. CROUCH AND ROBERT D. SARD 120

Eigenvalue Problem in Quantum Electrodynamics . . . MAURICE NEUMAN 129

Letters to the Editor:

Radiations of RaD . . . R. C. BANNERMAN AND S. C. CURRAN 134

Information and Thermodynamics . . . JEROME ROTHSTEIN 135

Slow Neutron Fission of Am^{241}, Am^{242m}, and Am^{243} . . . K. STREET, JR., A. GHIORSO, AND S. G. THOMPSON 135

Light Emission from Silicon Carbide . . . R. W. SILLARS 136

Production of Halogen Negative Ions at the Surface of a Thoriated Tungsten Filament . . . J. W. TRISCHKA, D. T. F. MARPLE, AND A. WHITE 136

Radioactive Pm^{148} and Pm^{150} . . . JOHN K. LONG AND M. L. POOL 137

Connection between γ-γ and Internal Conversion Angular Correlations . . . J. W. GARDNER 137

Search for Long-Lived Nb^{94} . . . R. E. HEIN, C. M. FOWLER, AND R. H. MCFARLAND 138

Equation of Motion of the Landé Electron . . . PAUL MOLMUD 139

Identification of CO in the Solar Atmosphere . . . LEO GOLDBERG, ROBERT R. MCMATH, ORREN C. MOHLER, AND A. KEITH PIERCE 140

Far Infrared Transmission of Silicon and Germanium . . . R. C. LORD 140

Phase Transition of $ND_4D_2PO_4$ . . . B. T. MATTHIAS 141

Charge-Symmetrical Interaction between Nucleons and Leptons . . . V. VOTRUBA 141

Lifetime of an Excited State of $_{66}Dy^{162}$ and Upper Limits for Some Other Nuclei . F. K. MCGOWAN 142

Nuclear Reaction Energies . . . D. M. VAN PATTER, A. SPERDUTO, P. M. ENDT, W. W. BUECHNER, AND H. A. ENGE 142

Interactions between Nuclear Spins in Molecules . . . N. F. RAMSEY AND E. M. PURCELL 143

Possible Natural Radioactivity of Neodymium . . . GEORGE L. MULHOLLAND AND TRUMAN P. KOHMAN 144

Hyperfine Structure Anomaly of the Rb Isotopes . . . S. A. OCHS AND P. KUSCH 145

Condition for Radiation from a Solar Plasma . . . J. FEINSTEIN 145

Decay Series Nd^{146}–Pr^{146}–Ce^{142} . . . CHARLES I. BROWNE, JOHN O. RASMUSSEN, JOSEPH P. SURLS, AND DONALD F. MARTIN 146

Quadrupole Radiation in nD Capture . . . N. AUSTERN 147

Absence of Spontaneous Emission of Neutrons from Samarium . . . S. D. CHATTERJEE AND R. N. OLCOTT 147

Bipolar Expansion of Coulombic Potentials. Addenda . . . ROBERT J. BUEHLER AND JOSEPH O. HIRSCHFELDER 149

Disintegration of the Ground-State Sr^{85} and Metastable Energy Level of 514 kev in Rb^{85} . . . W. S. EMMERICH AND J. D. KURBATOV 149

Studies on the Linearity of a Scintillation Gamma-Ray Spectrometer . . . V. O. ERIKSEN AND G. JENSSEN 150

Heat Capacity and Lattice Defects of Silver Chloride . . . . . Koichi Kobayashi 150
Measurements of Some *K*-Shell Internal Conversion Coefficients . . . . . F. K. McGowan 151
Classification of the γ-Radiation of Hf^{177} . . . F. K. McGowan, E. D. Klema, and P. R. Bell 152
Isomeric Transition in Ge^{77} . . . . . Allan C. G. Mitchell and Alan B. Smith 153
Ions of Mass 19 from Water . . . . . Francis J. Norton 154
Experimentally Derived Configurational Coordinate Curves for Phosphors . . Clifford C. Klick 154
Protons and Deuterons from Li^6+T Reactions . . . . . T. P. Peffer, K. W. Allen, E. Almqvist, and J. T. Dewan 155
Decay of the π-Meson . . . . . M. Ruderman 157
Some Comments on the Mechanism of Fission . . . . . Glenn T. Seaborg 157
Melting Pressure of He^3 . . . . . B. Weinstock, B. M. Abraham, and D. W. Osborne 158
Nuclear Interactions of the Decay Products of a Neutral V-Particle . . . . . Herbert Bridge, Hans Courant, and Bruno Rossi 159

Proceedings of the American Physical Society:

Minutes of the 1951 Fall Meeting of the Ohio Section at Antioch College, Yellow Springs, Ohio . . 160

January 15, 1952

Production Cross Sections for π^+- and π^--Mesons by 340-Mev Protons on Carbon and Lead at 90° to the Beam . . . . . C. Richman, M. Weissbluth, and H. A. Wilcox 161
Suggested Interpretation of the Quantum Theory in Terms of "Hidden" Variables. I . . . . . David Bohm 166
Suggested Interpretation of the Quantum Theory in Terms of "Hidden" Variables. II . . . . . David Bohm 180
Neutrons from the Disintegration of the Separated Isotopes of Silicon by Deuterons . . . . C. E. Mandeville, C. P. Swann, S. D. Chatterjee, and D. M. Van Patter 193
Radiative Capture of Protons by C^{13} . . . . . John D. Seagrave 197
π-Meson Production by Protons on Nuclei . . . . . Ernest M. Henley 204
Thermal Rayleigh Disk Measurements in Liquid Helium II . . . . . John R. Pellam and William B. Hanson 216
Fermi Energy of Metallic Lithium . . . . . Richard A. Silverman 227
Radiative Corrections to Compton Scattering . . . . . L. M. Brown and R. P. Feynman 231
Mean-Value Calculations for Projected Multiple Scattering . . . . . W. T. Scott 245
Fast Protons from the Capture of π^- Mesons in Photographic Emulsions . . . . . Frank L. Adelman 249
Limits of Stability of the Heavy Elements and the Effects of Nuclear Shell Structure . . . . . P. S. Greifinger 253
Force between Particles in a Nonlinear Field Theory . . . . . Nathan Rosen and Herbert B. Rosenstock 257
Fine Structure of the Hydrogen Atom. III . . . . . Willis E. Lamb, Jr. 259
Dissociation of Hydrogen Molecules by Vibrational Excitation and Three-Body Recombination Coefficient. II . . . . . E. Bauer 277
Investigation of Alpha-Particle Groups from $Al^{27}(d, \alpha)Mg^{25}$ . . . . . E. C. Toops, M. B. Sampson, and F. E. Steigert 280
Angular Distribution in the High Energy Deuteron Photoeffect . . . . . N. Austern 283
Absorption of Gamma-Rays from Co^{60} . . . . . Sakae Shimizu, Tetsuya Hanai, and Sunao Okamoto 290
Energy Spectrum of Primary Cosmic Radiation . . . . . M. F. Kaplon, B. Peters, H. L. Reynolds, and D. M. Ritson 295
Variation of Intensity of Fast Cosmic-Ray Neutrons with Altitude . . . . . L. F. Curtiss and P. S. Gill 309
Absorption of Selenium in the Soft X-Ray Region . . . . . M. Parker Givens and Walter P. Siegmund 313
Ferroelectricity and Antiferroelectricity of a Crystal Containing Rotatable Polar Molecules . . . . . Yutaka Takagi 315
Interaction between the *d*-Shells in the Transition Metals. IV. The Intrinsic Antiferromagnetic Character of Iron . . . . . C. Zener 324
Theory of Antiferromagnetic Resonance . . . . . F. Keffer and C. Kittel 329
Collective Description of Electron Interactions: II. Collective *vs* Individual Particle Aspects of the Interactions . . . . . David Pines and David Bohm 338
Theory of Conductivity of Semiconductors . . . . . George Jaffé 354

Letters to the Editor:

Transition Effect for Neutron Production in Lead . . . . . S. B. Treiman and W. Fonger 364
Neutron Diffraction Investigation of the Atomic Magnetic Moment Orientation in the Antiferromagnetic Compound CrSb . . . . . A. I. Snow 365
Nutational Resonance . . . . . H. C. Torrey 365
Solar Component of the Primary Cosmic Radiation . . . J. A. Simpson, W. Fonger, and L. Wilcox 366
Investigation of the Double Beta-Decay of $_{50}Sn^{124}$ . . Marvin I. Kalkstein and W. F. Libby 368
L-Electron Capture and Alpha-Decay in Np^{235} . . . . . Ralph A. James, Albert Ghiorso, and Donald Orth 369
Charged π-Meson Production from Deuterium . . . . . S. Passman, M. M. Block, and W. W. Havens, Jr. 370

Three-Quantum Annihilation and Positronium . . . . . S. DeBenedetti and R. Siegel 371
Negative Ion Formation in Oxygen . . . . . Ronald Geballe and Melvin A. Harrison 372
Yield of Neutral Mesons from Proton Bombardment of Light Nuclei . . . . . R. W. Hales, R. H. Hildebrand, N. Knable, and B. J. Moyer 373
Neutral V-Particle Decay and the Negative Proton . . . . . L. I. Schiff 374
Saturation Magnetic Moment of Alloys on the Collective Electron Theory . . . . J. E. Goldman 375
Electronic Specific Heat in Chromium and Magnesium . . . . . S. A. Friedberg, I. Estermann, and J. E. Goldman 375
Relativistic Modification of Bose and Fermi Statistics . . A. E. Scheidegger and C. D. McKay 376
Half-Life of Positrons in Condensed Materials . . . . . S. DeBenedetti and H. J. Richings 377
New Method of Obtaining Focused Images with X-Rays . . . . . G. N. Ramachandran 378
Antiproton Annihilation . . . . . Israel Reff 379
Anisotropy in Paramagnetic Resonance Absorption of Picryl-n-Amino Carbazyl . . . . . Victor W. Cohen, C. Kikuchi, and John Turkevich 379
Sublimation and Condensation of Carbon Dioxide, Nitrogen, and Oxygen in an Expansion Chamber . . . . . B. M. Cwilong and M. H. Edwards 380
Photocontrolled Low Frequency Dielectric Dispersion . . . . . J. Ross Macdonald 381
$L(L+1)$ Correction in the Spectra of the Iron Group . . . . . Giulio Racah 381
$L(L+1)$ Correction to the Slater Formulas for the Energy Levels . . . . . R. E. Trees 382
Magnetic Threshold Field Curve of a Superconductor . . . . . R. P. Hudson 382
Gravitational Deflection of Photons with Nonvanishing Rest Mass . . . . Albert D. Wheelon 383
Effect of Neutron Irradiation on Metallic Diffusion . . . . . T. H. Blewitt and R. R. Coltman 384
Properties of Powdered $BaTiO_3$ . . . . . V. E. Derr and M. D. Earle 384
Molecular Spectrum of Iodine Excited in the Presence of an Inert Gas . . . . . K. Wieland and Jürg Waser 385
Radioactive Decay of Hg^{197} and Hg^{203} . . . . . J. M. Cork, D. W. Martin, J. M. LeBlanc, and C. E. Branyan 386

Proceedings of the American Physical Society:

Minutes of the Meeting of the Division of Electron Physics at the National Bureau of Standards, Washington, D. C., November 1–3, 1951 388

February 1, 1952

Numerical Variational Method . . . . . R. E. Meyerott, P. J. Luke, W. W. Clendenin, and S. Geltman 393
Wave Function of Ionized Lithium . . P. J. Luke, R. E. Meyerott, and W. W. Clendenin 401
Energetic Protons from Nuclei Exposed to 300-Mev Bremsstrahlung . . . James C. Keck 410
Proton-Proton Scattering at 240 Mev . . . . . C. L. Oxley and R. D. Schamberger 416
240-Mev Proton-Deuteron Scattering . . . . . Robert D. Schamberger 424
Energy Levels in C^{12} from $Be^9(\alpha, n)C^{12}$. W. H. Guier, H. W. Bertini, and J. H. Roberts 426
Further Work on Heavy Collateral Radioactive Chains . . . . . W. W. Meinke, A. Ghiorso, and G. T. Seaborg 429
Magnetic Moments of Even-Odd Nuclei . . . . . Jack P. Davidson 432
Disintegration of Lithium by Deuteron Bombardment . L. M. Baggett and S. J. Bame, Jr. 434
Absolute Excitation Function of the $Be^9(d, t)$ Reaction . . . . . Richard L. Wolfgang and W. F. Libby 437
Secondary Emission from Composite Surfaces . . . . . Harold Jacobs, Jack Martin, and Frank Brand 441
Nuclear Disintegration by Positron-K Electron Annihilation . R. D. Present and S. C. Chen 447
Magnetic Susceptibility of Chromium . . . . . T. R. McGuire and C. J. Kriessman 452
Air-Shower Cores . . . . . W. E. Hazen 455
Soft Radiation at Balloon Altitudes . . C. L. Critchfield, E. P. Ney, and Sophie Oleksa 461
Problems Connected with the Prohibition of Self-Interactions in Integro-Causal Quantum Field-Theory . . . . . Frederik J. Belinfante 468
Spin and Quadrupole Moment of O^{17} . S. Geschwind, G. R. Gunther-Mohr, and G. Silvey 474

Letters to the Editor:

Calculation of the g Factor of Metallic Sodium . . . . . Y. Yafet 478
Nuclear Magnetic Resonance of Titanium and Arsenic . . . . . C. D. Jeffries, H. Loeliger, and H. H. Staub 478
Nuclear Magnetic Moment of Tc^{99} . . . . . Harold Walchli, Ralph Livingston, and William J. Martin 479
Structural Changes in the Ferroelectric Transition of KH_2PO_4 . B. C. Frazer and R. Pepinsky 479
Production of Large Tensile Stresses by Dislocations . . . . . J. S. Koehler 480
Abundance of CO in the Sun and in the Earth's Atmosphere . . . . Leo Goldberg, Robert R. McMath, Orren C. Mohler, and A. Keith Pierce 481
α-Half-Life of Am 241 . . . . . B. G. Harvey 482
Measurement of the Electron-Neutron Interaction . . . . . M. Hamermesh, G. R. Ringo, and A. Wattenberg 483
Self-Energies of Nucleons and the Mass Spectra of Heavy Particles . . . . . H. Enatsu 483
Observations on the Photoelectric Work Functions and Low Speed Electron Diffraction from Thin Films of Silver on the (100) Face of a Silver Single Crystal . . . . . Edward N. Clarke and H. E. Farnsworth 484
Changes in Work Functions of Vacuum Distilled Gold Films . . . . . Chung Fu Ying and H. E. Farnsworth 485
Nuclear Cross Sections for Negative Pions of Energy 109 and 133 Mev . . . . . R. L. Martin, H. L. Anderson, and G. Yodh 486
Spin Paramagnetism of Cr^{+++} at Liquid Helium Temperatures and High Magnetic Fields . . . . Warren E. Henry 487

Beta-Spectra of Cerium 144 and Praseodymium 144 . . . Cheng Lin-sheng, G. John, and J. D. Kurbatov 487
Formation of Triplet Positronium in Gases . . . T. A. Pond 489
Fine Structure Splitting in the Ground State of Positronium . . . T. A. Pond and R. H. Dicke 489
Photoproduction of Neutral Mesons from Deuterium . . . W. Heckrotte, L. R. Henrich, and J. V. Lepore 490
Coherent Neutron Scattering Cross Section of C^{13} . . . W. C. Koehler and E. O. Wollan 491
Two-Model Interpretation of a Nuclear Spectrum . . . D. R. Inglis 492
Interpretation of Observed Pressure-Dependent Recombination Coefficients . . . Leonard B. Loeb and Wulf B. Kunkel 493
Spin and Quadrupole Moment of Se^{79} . . . W. A. Hardy, G. Silvey, and C. H. Townes 494
Splitting of Bands in Solids . . . E. Katz 495
Elastic Photoproduction of π^0 Mesons in Deuterium . . . N. C. Francis and R. E. Marshak 496
Inelastic Cross Sections for 240-Mev Protons . . . Alfred M. Perry, Jr. 497
Build-Up Factors for Transmission of Co^{60} Gamma-Rays through Concrete and Lead . W. R. Dixon 498
Preparation of Ra^{225} and Ac^{289} . . . F. Depocas and B. G. Harvey 499
Distribution of Components of Ternary Isotopic Mixture along Clusius-Dickel Column . . . F. K. Elder, Jr., and R. E. McDonald 500
Beta-Activity of Si^{31} and the Masses of the Al and Si Isotopes . . . Henry T. Motz 501
Atomic Heat of Lead in the Region of its Transition to Superconductivity . . . J. R. Clement and E. H. Quinnell 502
Beam System for Reduction of Doppler Broadening of a Microwave Absorption Line . . . H. R. Johnson and M. W. P. Strandberg 503

February 15, 1952

Mesonic Proper-Field . Hiroomi Umezawa, Yasushi Takahashi, and Susumu Kamefuchi 505
Nuclear Scattering of 1-Mev Electrons and Positrons . . . Harry J. Lipkin 517
Disintegration of the Deuteron by π^+ Mesons and the Spin of the π^+ Meson . . . Donald L. Clark, Arthur Roberts, and Richard Wilson 523
Pairing Effect in Nuclei and the Beta-Labile Elements . . . Truman P. Kohman 530
Nuclear Magnetic Moment of S^{33} from Microwave Spectroscopy . . . J. R. Eshbach, R. E. Hillger, and M. W. P. Strandberg 532
Meson Tail Effect and Treatment of Proton-Proton Scattering Data . . . M. C. Yovits, R. L. Smith, Jr., M. H. Hull, Jr., J. Bengston, and G. Breit 540
Neutron Scattering Lengths . . . D. C. Peaslee 555
Hyperfine Structure and Isotope Shift in the Spectrum of Tellurium . . . John S. Ross and Kiyoshi Murakawa 559
Proton Bremsstrahlung at 140 Mev . . . Richard Wilson 563
Genetic Relationships and Fission Yields of Members of the Mass-115 Decay Chain . . . Arthur C. Wahl and Norman A. Bonner 570
Neutron Yield from the Nuclear Photoeffect . . . J. S. Levinger and H. A. Bethe 577
Reaction $Be^9(p, \alpha\gamma)Li^6$ . . . R. B. Day and R. L. Walker 582
(p, n) Reaction on Separated Isotopes of Chromium . . . J. A. Lovington, J. J. G. McCue, and W. M. Preston 585
Intrinsic Magnetization in Alloys . . . W. J. Carr, Jr. 590
Neutron Transmission Cross Sections in the Kilovolt Region . . . Carl T. Hibdon, Alexander Langsdorf, Jr., and Robert E. Holland 595
Fission Neutron Spectrum of U^{235} . . . Norris Nereson 600
Spin-Spin Relaxation in a Simple System . . . Julian Eisenstein 603
Absorption Curve of the Cosmic Radiation in the Stratosphere . . . Marcel Schein and Victor H. Yngve 607
Semiconductivity and Diamagnetism of Polycrystalline Graphite and Condensed Ring Systems . . . S. Mrozowski 609
Multiple Scattering of Waves. II. The Effective Field in Dense Systems . . . Melvin Lax 621
Masses of Lead and Bismuth . . . P. I. Richards, E. E. Hays, and S. A. Goudsmit 630
Divergence of Perturbation Theory in Quantum Electrodynamics . . . F. J. Dyson 631
Geometrical Optics and the Theory of Multiple Small Angle Scattering . . . George H. Vineyard 633
Impulse Approximation . . . Geoffrey F. Chew and Gian Carlo Wick 636
Classification of Energy Levels in Al^{25} . . . Louis J. Koester, Jr. 643
Point Transformations in Quantum Mechanics . . . Bryce Seligman DeWitt 653
Further Calculations of X-Ray Diffusion in an Infinite Medium . . . L. V. Spencer and Fannie Stinson 662
Motion of a Ferromagnetic Domain Wall in Fe_3O_4 . . . John K. Galt 664
Ion Clustering . . . Stanley Bloom and Henry Margenau 670

Letters to the Editor:

Atmospheric Absorption of Solar Infrared Radiation . . . Romuald Anthony 674
Diurnal Variations in High Energy Cosmic-Ray Intensities . Paul H. Barrett and Y. Eisenberg 674
Scattering of 0.5-Mev Circularly Polarized Photons in Magnetized Iron . . . Forrest P. Clay and Frank L. Hereford 675
Phenomena Associated with Negative μ-Mesons Stopped in Photographic Emulsions . W. F. Fry 676
Striations in the Hydrogen Glow Discharge . . . W. A. Gambling 677
Properties of Thermally Produced Acceptors in Germanium . . . C. S. Fuller, H. C. Theuerer, and W. van Roosbroeck 678

Lateral Spread of Cosmic-Ray Showers in Air and Lead . . . . . H. S. Green and H. Messel 679
Drift Mobility of Electrons in Silicon . . . . . J. R. Haynes and W. C. Westphal 680
Photomeson Production in Carbon and Hydrogen . . . . . B. T. Feld, D. H. Frisch, I. L. Lebow, L. S. Osborne, and J. S. Clark 680
Photomeson Production from Deuterium . . . . . I. L. Lebow, B. T. Feld, D. H. Frisch, and L. S. Osborne 681
Hyperfine Structure in the Paramagnetic Resonance of the Ion $(SO_3)_2NO^{--}$ . . . . . G. E. Pake, J. Townsend, and S. I. Weissman 682
Hyperfine Structure in the Spectrum of Erbium . . . . Kiyoshi Murakawa and Shigeki Suwa 683
Is There a Neutral μ-Meson? . . . . . G. E. Uhlenbeck and C. S. Wang Chang 684
Auger Enhancement of the $M\alpha$ X-Ray Satellite Lines . . . . . F. R. Hirsh, Jr. 685
Comment on the "Impulse Approximation" . . . . . J. Ashkin and G. C. Wick 686
Nonlinearities Due to Vacuum Polarization in Meson-Nucleon Interactions . . . B. J. Malenka 686
Search for Double Beta-Decay in Palladium . . . . . Rolf G. Winter 687
Measurements on the *I*, *F*, and *A* Lines of Thorium by a New Method . . . . . H. Craig 688
Use of HD for Experiments on the Proton-Deuteron Magnetic Moment Ratio . Norman F. Ramsey 688
Determination of the Nuclear Magnetic Moment of Co^{60} Using the Method of Nuclear Alignment B. Bleaney, J. M. Daniels, M. A. Grace, H. Halban, N. Kurti, and F. N. H. Robinson 688
Comparison of Total Photoneutron Yield from 160- and 320-Mev Bremsstrahlung . . . . . Lawrence W. Jones and Kent M. Terwilliger 689
Effect of Intrinsic Moment of Electron on Spectroscopic Isotope Shift . . . . . G. Breit and W. W. Clendenin 689
Ferromagnetic Resonance in Single Crystals of Cobalt-Zinc Ferrite . . . . . Toshiiko Okamura and Yūzō Kojima 690
Low Energy γ-Transitions in Some Rare Earth Isotopes . . J. W. Mihelich and E. L. Church 690
Theory of Cooperative Phenomena . . . . . Gérard Fournet 692
Color Centers and Thermoluminescence in Alkali Halides . . . . . J. Sharma 692
Temperature Dependence of the Line-Half Width of Ferromagnetic Resonance in the Single Crystal of Zinc-Manganese Ferrite . Toshiiko Okamura, Yūzō Kojima, and Yosiharu Torizuka 693
Steady-State Transient Technique in Nuclear Resonance . . . . . R. Gabillard 694
High Energy Nucleon-Deuteron Scattering . . . . . P. B. Daitch and J. B. French 695
Some Polystyrene Solid Solutions as Scintillation Counters . Thomas Carlson and W. S. Koski 697
Absence of Secondary Maxima in the Transition Curve for Electronic Showers . . . . R. Maze 697
β-Decay of Radium *E* and the Pseudoscalar Interaction . . A. G. Pestchek and R. E. Marshak 698
Relaxation Effects in Ferromagnetic Resonance . . . . . N. Bloembergen and R. W. Damon 699

Proceedings of the American Physical Society:

Minutes of the Meetings at Chicago, October 24–27, 1951 700
Minutes of the 1951 Thanksgiving Meeting at Houston, Texas 738
Minutes of the Meeting at Berkeley, California, December 27–29, 1951 751

March 1, 1952

Radial Distribution Function of a Gas of Hard Spheres and the Superposition Approximation . . . . . B. R. A. Nijboer and L. Van Hove 777
Molecular Beam Electric Resonance Method Study of Thallium Monochloride . . . . . R. O. Carlson, C. A. Lee, and B. P. Fabricand 784
Molecular Beam Magnetic Resonance Spectra of $TlCl^{35}$ and $TlCl^{37}$ at Zero Field . . . . . H. J. Zeiger and D. I. Bolef 788
Molecular Beam Magnetic Resonance Spectra of $Rb^{87}F$ and $Rb^{87}Cl$ at Zero Field . . . . . D. I. Bolef and H. J. Zeiger 799
Total Cross Sections of 60-Mev Mesons in Hydrogen and Deuterium . . . . . P. J. Isaacs, A. M. Sachs, and J. Steinberger 803
Beta-Spectrum of RaD . . . . . G. M. Insch, J. G. Balfour, and S. C. Curran 805
Spontaneous Magnetization of a Two-Dimensional Ising Model . . . . . C. N. Yang 808
High Energy Induced Fluorescence in Organic Liquid Solutions (Energy Transport in Liquids). III . . . . . Milton Furst and Hartmut Kallman 816
Interactions of High Energy Nucleons with Nuclei. Part I . . . . . G. Bernardini, E. T. Booth, and S. J. Lindenbaum 826
Formation of a Boundary between Normal-Conducting and Superconducting Metal . . . . . M. P. Garfunkel and B. Serin 834
Electromagnetic Properties of Spin-One Particles . . . . . Daniel Leenov 841
Yield of Gamma-Rays and Neutrons from the Proton Bombardment of Fluorine . . . . . H. B. Willard, J. K. Bair, J. D. Kington, T. M. Hahn, C. W. Snyder, and F. P. Green 849
Hypothesis of Charge Independence for Nuclear Phenomena . . . . Kenneth M. Watson 852
Decay of Te^{125m} . . . . . J. C. Bowe and P. Axel 858
Mean Free Path of Neutral Penetrating Shower-Producing Radiation . . . . . H. W. Boehmer and H. S. Bridge 863
Relativistic Dynamics of a System of Particles Interacting at a Distance . . L. H. Thomas 868
Reaction $Cl^{37}(p, n)A^{37}$; Excited States in A^{38} . . . . . W. A. Schoenfeld, R. W. Duborg, W. M. Preston, and C. Goodman 873
Angular Momentum in Nonlocal Field Theory . . . . . D. R. Yennie 877
Multiple Compton Scattering of Low Energy Gamma-Radiation . . . . . R. C. O'Rourke 881
Angular Correlation of Electrons in Double Beta-Decay . . . . . H. Primakoff 888
Emission of Slow Positive and Negative Mesons from Nuclear Disruptions Produced by Cosmic Radiation . . . . . Herman Yagoda 891

Emulsion Cloud-Chamber Study of a High Energy Interaction in the Cosmic Radiation . . . M. KAPLON, B. PETERS, AND D. M. RITSON 900
Angular Correlation of Two Successive Nuclear Radiations . . . . . STUART P. LLOYD 904
On the Quantum Theory for a Finite-Sized Electron. I . . . . . GEORGE J. YEVICK 911

Letters to the Editor:

Origin of High Permeability in Permalloy . . . . . SŌSHIN CHIKAZUMI 918
Activation of LiI Crystal Phosphors . . . . . W. BERNSTEIN AND A. W. SCHARDT 919
Graphs for the Kernel of the Bethe-Salpeter Equation . . . . . C. A. HURST 920
Resistivity of Evaporated Tellurium Films . . . . . TAKEMARO SAKURAI AND SEIJI MUNESUE 921
Production Cross Section and Energy Spectrum of the Neutral Mesons in Cosmic Rays . . . . . G. SALVINI AND Y. KIM 921
Nuclear Gyromagnetic Ratio of V^{50} and Measurements on Rb^{85} and Cl^{35} . . . . . H. E. WALCHLI, W. E. LEYSHON, AND F. M. SCHEITLIN 922
Tin Activation of LiI . . . . . JAMES SCHENCK AND R. L. HEATH 923
High Energy Photodisintegration of the Deuteron . . . . T. S. BENEDICT AND W. M. WOODWARD 924
Line Width of Paramagnetic Resonance and Exchange Interaction in Salts Containing Mn^{++} and Fe^{+++} . . . . . H. KUMAGAI, K. ŌNO, AND I. HAYASHI 925
Adiabatic Study of the 128°C Transition in Barium Titanate . . . . . SHEPARD ROBERTS 925
Slow Neutron Liquid Scintillation Detector . . . . . C. O. MUEHLHAUSE AND G. E. THOMAS 926
Relative Probabilities of Diverse Photonuclear Reactions from Zn^{64} and Fe^{56} . RYOKICHI SAGANE 926
Magnetic Moment of Zn^{67} . . . . . S. S. DHARMATTI AND H. E. WEAVER, JR. 927
Reaction $Li^6(l, p)Li^6$ . . . . . C. D. MOAK, W. M. GOOD, AND W. E. KUNZ 928
Convergent *S*-Matrix Formalism with Correspondence to Ordinary Quantum Mechanics . . . . P. KRISTENSEN AND C. MØLLER 928
Scattering of 50-Mev Positive Pions by Helium . . . . . A. M. THORNDIKE, E. C. FOWLER, W. B. FOWLER, AND R. P. SHUTT 929
Limits of Isotopic Abundance for Hafnium and Platinum . . . . . H. E. DUCKWORTH, R. F. WOODCOCK, G. S. STANFORD, A. COUTU, AND R. L. STEARNS 929
Interactions of Remote Impurity Centers in Phosphors . . . H. W. LEVERENZ AND D. O. NORTH 930
Stopping Power of a Metal for Charged Particles . . . . . DAVID PINES 931
Capture Gamma-Rays from 277-Kev Protons on N^{15} . . . . . C. H. JOHNSON, G. P. ROBINSON, AND C. D. MOAK 931
Extremely High Energy Nuclear Interactions . . . . . M. F. KAPLON AND D. M. RITSON 932
Primary Flux of High Energy Protons and α-Particles . . . . . M. F. KAPLON, D. M. RITSON, AND EDYTHE P. WOODRUFF 933
Neutrons and Gamma-Rays from the Proton Bombardment of Beryllium . . . . . T. M. HAHN, C. W. SNYDER, H. B. WILLARD, J. K. BAIR, E. D. KLEMA, J. D. KINGTON, AND F. P. GREEN 934
Total Cross Sections of Negative Pions in Hydrogen . . . . . H. L. ANDERSON, E. FERMI, E. A. LONG, R. MARTIN, AND D. E. NAGLE 934
Ordinary and Exchange Scattering of Negative Pions by Hydrogen . . . . . E. FERMI, H. L. ANDERSON, A. LUNDBY, D. E. NAGLE, AND G. B. YODH 935
Total Cross Sections of Positive Pions in Hydrogen . . . . . H. L. ANDERSON, E. FERMI, E. A. LONG, AND D. E. NAGLE 936
Conductivity of Cold-Worked Metals . . . . . D. L. DEXTER 936
Long-Range Proton-Proton Tensor Force . . . . . NORMAN F. RAMSEY 937
Gyromagnetic Ratios of Li^7, Na^{23}, Al^{27}, and P^{31} . . . . . T. KANDA, Y. MASUDA, R. KUSAKA, Y. YAMAGATA, AND J. ITOH 938
Experiments with Audiofrequencies on Superconductors . . . . . B. SERIN AND C. A. REYNOLDS 938
Variational Calculation of Scattering Cross Sections . . . . . E. GERJUOY AND DAVID S. SAXON 939
Critical Domain Size in Ferroelectrics . . . . . W. KÄNZIG AND M. PETER 940
Search for Natural Radioactivity of Calcium 48 . . . JOHN W. JONES AND TRUMAN P. KOHMAN 941
Half-Life of the 1.3-Mev Excited State in K^{41} . . . . . L. G. ELLIOTT 942
Tetraneutron . . . . . K.-H. SUN, F. A. PECJAK, AND A. J. ALLEN 942
Radiative $\pi^- - \mu$ Decay . . . . . TETSUO EGUCHI 943
Internal Conversion in the L-Shell . . . . . H. GELLMAN, B. A. GRIFFITH, AND J. P. STANLEY 944
Fine Structure and Angular Correlation in Po^{210} . . . . . S. DE BENEDETTI AND G. H. MINTON 944
Zinc as an Acceptor in Germanium . . . . . W. C. DUNLAP, JR. 945
Proton Bombardment of Lithium . . . . . J. K. BAIR, H. B. WILLARD, C. W. SNYDER, T. M. HAHN, J. D. KINGTON, AND F. P. GREEN 946

MARCH 15, 1952

Invariance Conditions on the Scattering Amplitudes for Spin ½ Particles . . . . . L. WOLFENSTEIN AND J. ASHKIN 947
Radiative Correction for the Collision Loss of Fast Particles . . . . . J. M. JAUCH 950
Interaction of a Charged Pi-Meson with the Deuteron . . . . . W. B. CHESTON 952
Symmetry Effects on Nuclear Dipole Radiation with Application to a Bound Excited State of $_2He^4$ . . . . . LYNNE E. H. TRAINOR 962
Electrodynamic Displacement of Atomic Energy Levels. I. Hyperfine Structure . . . . . ROBERT KARPLUS AND ABRAHAM KLEIN 972
Isotope Effect in the Imprisonment of Resonance Radiation . . . . . T. HOLSTEIN, D. ALPERT, AND A. O. MCCOUBREY 985
Response of Anthracene Scintillation Crystals to High Energy μ-Mesons . . . . . THEODORE BOWEN AND FRANCIS X. ROSER 992
Differential Range Spectrum of Cosmic-Ray Mesons at Sea Level . . . CARL M. YORK, JR. 998
Energy of a Bloch Wall on the Band Picture. I. Spiral Approach . . . . CONYERS HERRING 1003
Neutron Capture γ-Rays from Phosphorus, Sulfur, Chlorine, Potassium, and Calcium . . . . . B. B. KINSEY, G. A. BARTHOLOMEW, AND W. H. WALKER 1012
Proton-Proton Scattering at 240 Mev by a Magnetic Deflection Method . O. A. TOWLER, JR. 1024

Some Experiments on Flow in the Unsaturated Helium II Film . . . . . EARL LONG AND LOTHAR MEYER 1030
Phase Transitions in Adsorbed Films . . . . . LOTHAR MEYER AND EARL LONG 1035

Letters to the Editor:

Exchange Integral in the 3*d* Shell . . . . . HARVEY KAPLAN 1038
Radioactivity of $Eu^{152,154}$ . . . . . ROBERT KATZ AND MILFORD R. LEE 1038
Masses of Pb^{208}, Th^{232}, U^{234}, U^{235}, and U^{238} . . . . . GEORGE S. STANFORD, HENRY E. DUCKWORTH, BENJAMIN G. HOGG, AND JAMES S. GEIGER 1039
M_5 and M_4 X-Ray Absorption Edges of Tantalum . DONALD D. DOUGHTY AND J. W. MCGRATH 1040
Electromagnetic Effects Due to Spin-Orbit Coupling . . . . . J. HANS D. JENSEN AND M. GOEPPERT-MAYER 1040
Polarization of the 6.13-Mev Gamma-Rays Emitted in the Reaction $F^{19}(p, \alpha)O^{16*}(\gamma)O^{16}$ . . . . . A. P. FRENCH AND J. O. NEWTON 1041
Dielectric Constant and Permeability of Various Ferrites in the Microwave Region . . . . . TOSHIHIKO OKAMURA, TADAO FUJIMURA, AND MUNEYUKI DATE 1041
Closing of the Proton Sub-Shell at Z 58 . . . . . G. P. DUBE AND S. JHA 1042
Ionization Loss of Energy of Relativistic Mu-Mesons in Argon . . . . . J. E. KUPPERIAN, JR., AND E. D. PALMATIER 1043
Transmission and Spectral Response of Lead Sulfide and Lead Telluride . . . . . M. A. CLARK AND R. J. CASHMAN 1043
Critical Velocity of Superflow in Liquid Helium II . . . . . H. M. FRIED AND P. R. ZILSEL 1044
Test for the Charge-Symmetry Hypothesis . . . . . RICHARD L. GARWIN 1045
Proposed Test of the Nuclear Shell Model . . . . . H. A. BETHE AND S. T. BUTLER 1045
Radiations of Rh^{99}, Rh^{101}, Rh^{105}, and Ru^{105} . . . . C. L. SCOVILLE S. C. FULTZ, AND M. L. POOL 1046
Energy Absorption During Twin Formation in Zinc Single Crystals . . . . . E. I. SALKOVITZ 1046
Zeeman Effect and Hyperfine Splitting of Positronium . . . . . MARTIN DEUTSCH AND SANBORN C. BROWN 1047
Multiple Gamma-Ray Scattering in Lead . . . . . J. O. ELLIOT, R. T. FARRAR, R. D. MYERS, AND C. F. RAVILIOUS 1048
Bernoulli's Theorem for Viscous Fluids . . . . . J. J. VAN DEEMTER 1049
Natural Scintillations from Uranyl Nitrate Crystals . . . . . S. G. COHEN AND Y. FEIGE 1049
Magic Numbers and the Isotope Shift in Atomic Spectra of Heavy Elements . . . . . P. BRIX AND H. KOPFERMANN 1050
Attempt to Produce Nuclear Orientation in Mercury Vapor . FRANCIS BITTER AND JEAN BROSSEL 1051
Scattering of 9.6-Mev Protons by Carbon, Aluminum, and Magnesium . . . . . C. J. BAKER, J. N. DODD, AND D. H. SIMMONS 1051
Elastic Scattering of Deuterons by Deuterons . . . . . RICHARD J. RUNGE 1052
Absorption Experiment to Detect the Cosmic-Ray Albedo at High Altitudes . . J. R. WINCKLER 1053
Application of Čerenkov Radiation to the Cosmic-Ray Albedo Problem . . . . J. R. WINCKLER 1054
Second γ-Transition ($d_{3/2} \rightarrow s_{1/2}$) in Xe^{135m} . . . . . S. THULIN AND I. BERGSTRÖM 1055
Probing the Space-Charge Layer in a p-n Junction . . . . . G. L. PEARSON, W. T. READ, AND W. SHOCKLEY 1055
Electron Interferometer . . . . . L. MARTON 1057
Stopping Power of Heavier Substances . . . . . J. LINDHARD AND M. SCHARFF 1058
Electromagnetic Interference Effects in Charged Meson-Proton Scattering . . . M. F. KAPLON 1059
Velocity of 170-Mev Gamma-Rays . . . . . DAVID LUCKEY AND JOHN W. WEIL 1060
Elastic and Plastic Properties of Very Small Metal Specimens . . . . . CONYERS HERRING AND J. K. GALT 1060
Pure Nuclear Electric Quadrupole Resonance of N^{14} in Three Molecular Solids . . . . . G. D. WATKINS AND R. V. POUND 1062
Photodissociation of the Deuteron by High Energy Gamma-Rays . . . . . SRISHI KIKUCHI 1062
Silver-Activated Alkali Halides . . . . . H. W. ETZEL, J. H. SCHULMAN, R. J. GINTHER, AND E. W. CLAFFY 1063

Errata 1064
Author Index to Volume 85 1066
Analytic Subject Index to Volume 85 1082
Volume Table of Contents iii

THE
PHYSICAL REVIEW

A journal of experimental and theoretical physics established by E. L. Nichols in 1893

SECOND SERIES, VOL. 85, NO. 6 MARCH 15, 1952

Invariance Conditions on the Scattering Amplitudes for Spin ½ Particles

L. WOLFENSTEIN AND J. ASHKIN
Carnegie Institute of Technology, Pittsburgh, Pennsylvania
(Received December 5, 1951)

The most general form of the scattering matrix in spin space for two spin ½ particles is derived subject to invariance under rotation, reflection, and time-reversal. The result may be used to prove a relationship important for polarization experiments and previously stated without proof.

A COMPLETE description of the scattering of two particles of spin ½ is given by a matrix specifying the amplitude of any outgoing spin and momentum state as a function of the incident spin and momentum. This matrix will be written

$$M(\sigma_1, \sigma_2, \mathbf{k}_i, \mathbf{k}_f)$$

and is to be considered as an operator in the four-dimensional spin space operating on the initial spin state. Here $\mathbf{k}_i$ and $\mathbf{k}_f$ are the initial and final momenta of one of the particles (in the c.m. system) and σ_1 and σ_2 are the Pauli spin operators for the two particles. The treatment is nonrelativistic.

I. RELATION OF M TO EXPERIMENT

A polarization state for a system of two spin ½ particles is, in general, described as a mixture of many separate pure spin states in which the system may be found at any particular time. If the polarization state of the particles before the collision is specified, the most general scattering problem is that of finding the outgoing polarization state and intensity as a function of the angle of scattering.

A polarization state of the system can be completely specified by the average values of a suitable array of 16 observables[1] pertaining to the spins of the two particles. This is most easily shown with the help of the von Neumann density matrix ρ for a mixture of states:

$$\rho=\sum_n P_n\chi_n\chi_n^\dagger,$$

where χ_n is a column vector with four components representing one of the spin states present in the mixture, $\chi_n^\dagger$ is the adjoint row vector, and P_n is the relative probability of finding the system in state χ_n. Knowledge of the matrix ρ suffices to obtain the average value $\langle S\rangle$ of any spin operator S, for the mixture, through the relation

$$\langle S\rangle \operatorname{Tr}(\rho)=\operatorname{Tr}(\rho S). \tag{1}$$

Since the matrix ρ is Hermitian and 4×4, it is fixed by giving 16 real numbers which may be chosen as the average values of a complete set of 16 Hermitian operators S^α in the spin space. A set of operators will be called complete if it obeys the orthogonality relations

$$\operatorname{Tr}S^\alpha S^\nu=4\delta_{\mu\nu}. \tag{2}$$

For example, the operators 1, σ_{1x}, σ_{1y}, σ_{1z}, σ_{2x}, σ_{2y}, σ_{2z}, and the nine products of one of the Pauli spin operators for particle 1 with one of those for particle 2 form such a set of operators. Any matrix must be expressible linearly in the S^α. Thus

$$\rho=\tfrac{1}{4}\sum_\alpha S^\alpha \operatorname{Tr}(\rho S^\alpha)=\tfrac{1}{4}\operatorname{Tr}(\rho)\sum_\alpha\langle S^\alpha\rangle S^\alpha \tag{3}$$

showing how ρ is characterized by the $\langle S^\alpha\rangle$.

The desired relation between ingoing and outgoing polarization states is obtained by giving averages $\langle S^\alpha\rangle_f$ in the final state in terms of the $\langle S^\alpha\rangle_i$ for the initial state. By the definition of the matrix M,[2] the density matrix for the final polarization state at any angle is

$$\rho_f=\sum_n P_{ni}M\chi_{ni}\chi_{ni}^\dagger M^\dagger=M\rho_i M^\dagger. \tag{4}$$

Using Eqs. (1) through (4) we get, therefore,

$$\langle S^\alpha\rangle_f I=\tfrac{1}{4}\sum_\nu\langle S^\nu\rangle_i \operatorname{Tr}(MS^\nu M^\dagger S^\alpha), \tag{5}$$

[1] It is convenient throughout to include the unity operator as one of the operators whose average values specify the polarization state; that is, the normalization of the state will be considered as part of the specification of the polarization state.

[2] Matrix notation is used only for the spin dependence of M and not for the momentum dependence. Thus $\mathbf{k}_i$ and $\mathbf{k}_f$ are fixed parameters in Eq. (4) and those that follow.

where

$$I=\mathrm{Tr}(\rho_f)/\mathrm{Tr}(\rho_i) \tag{5a}$$

is the differential scattering cross section at the angle in question.

Two special cases of interest are (a) the polarization of particles 1 produced by the scattering of an unpolarized beam on an unpolarized target, and (b) the differential scattering cross section of initially polarized particles 1 against initially unpolarized particles 2. In the first case all $\langle S^{\nu}\rangle_i$ equal zero in Eq. (5) except for the unity operator, yielding

$$\langle\boldsymbol{\sigma}_1\rangle_f I_0=\tfrac{1}{4}\,\mathrm{Tr}M^{\dagger}\boldsymbol{\sigma}_1 M. \tag{6}$$

In the second case one obtains

$$I=\tfrac{1}{4}\,\mathrm{Tr}M^{\dagger}M+\tfrac{1}{4}\langle\boldsymbol{\sigma}_1\rangle_i\cdot\mathrm{Tr}M^{\dagger}M\boldsymbol{\sigma}_1, \tag{7}$$

or, for the case of a beam completely polarized in the direction $\mathbf{N}(\langle\boldsymbol{\sigma}_1\rangle_i=\mathbf{N})$,

$$I=I_0+I_p=\tfrac{1}{4}\,\mathrm{Tr}M^{\dagger}M+\tfrac{1}{4}\,\mathrm{Tr}M^{\dagger}M\boldsymbol{\sigma}_1\cdot\mathbf{N}, \tag{7a}$$

where I_0 is the scattering cross section for an unpolarized beam and I_p is the contribution to the cross section due to initial polarization. In previous papers[3] it is stated as obvious that the quantities in Eqs. (6) and (7a) are related by

$$I_p/I_0=\mathbf{N}\cdot\langle\boldsymbol{\sigma}_1\rangle_f \tag{8}$$

implying that

$$\mathrm{Tr}M^{\dagger}\boldsymbol{\sigma}_1 M=\mathrm{Tr}M^{\dagger}M\boldsymbol{\sigma}_1. \tag{8a}$$

Since the $\boldsymbol{\sigma}$ matrices do not commute with M, this is not a mathematical identity; it will be shown herein, however, that this relation follows from the condition on M of invariance under time reversal.

II. MOST GENERAL FORM OF M

The most general form of the matrix M may be found following a procedure similar to that used by Eisenbud and Wigner[4] to find the most general form of the interaction Hamiltonian for two particles of spin $\frac{1}{2}$. Conditions placed on the matrix M are invariance under space rotations and reflections and time reversal. The matrix M must be a scalar obtained by combining the sixteen linearly independent matrices in spin space:

$$\begin{aligned}
&1 && \text{(scalar)}\\
&(\boldsymbol{\sigma}_1\cdot\boldsymbol{\sigma}_2-1) && \text{(scalar)}\\
&(\boldsymbol{\sigma}_1+\boldsymbol{\sigma}_2) && \text{(axial vector)}\\
&(\boldsymbol{\sigma}_1-\boldsymbol{\sigma}_2) && \text{(axial vector)}\\
&(\boldsymbol{\sigma}_1\times\boldsymbol{\sigma}_2) && \text{(axial vector)}\\
&t_{\alpha\beta}=(\sigma_{1\alpha}\sigma_{2\beta}+\sigma_{1\beta}\sigma_{2\alpha}) && \text{(symmetric tensor)}
\end{aligned}$$

with functions of the momenta:

$$\left.\begin{aligned}
&1 && \text{(scalar)}\\
&\mathbf{k}_f-\mathbf{k}_i=\mathbf{K} && \text{(polar vector)}\\
&\mathbf{k}_f\times\mathbf{k}_i=\mathbf{n} && \text{(axial vector)}\\
&\mathbf{n}\times\mathbf{K}=\mathbf{P} && \text{(polar vector)}\\
&K_\alpha K_\beta,\ n_\alpha n_\beta, && \\
&P_\alpha P_\beta,\ K_\alpha P_\beta+K_\beta P_\alpha && \text{(symmetric tensors).}
\end{aligned}\right\}$$

Any of these functions of momenta may be multiplied by an arbitrary function of the scalars $\mathbf{k}_i\cdot\mathbf{k}_f$ and $k_i^2(=k_f^2)$. Each of the symmetric tensors above have only five independent components, since the sum of the diagonal elements of the tensor is one of the scalars. Among the functions of momenta, only those symmetric tensors are listed which do not change sign under space inversion.

The resulting forms invariant under space rotation and reflection are:

$$1,\ (\boldsymbol{\sigma}_1\cdot\boldsymbol{\sigma}_2-1),\ (\boldsymbol{\sigma}_1+\boldsymbol{\sigma}_2)\cdot\mathbf{n}, \tag{I}$$

$$(\boldsymbol{\sigma}_1-\boldsymbol{\sigma}_2)\cdot\mathbf{n}, \tag{II}$$

$$(\boldsymbol{\sigma}_1\times\boldsymbol{\sigma}_2)\cdot\mathbf{n}, \tag{III}$$

$$\left.\begin{aligned}
&\textstyle\sum_{\alpha\beta} l_{\alpha\beta}K_\alpha K_\beta,\ \sum_{\alpha\beta} l_{\alpha\beta}n_\alpha n_\beta,\\
&\textstyle\sum_{\alpha\beta} l_{\alpha\beta}P_\alpha P_\beta,\\
&\textstyle\sum_{\alpha\beta} l_{\alpha\beta}(K_\alpha P_\beta+K_\beta P_\alpha).
\end{aligned}\right\} \tag{IV}$$

The set (IV) is equivalent to

$$\boldsymbol{\sigma}_1\cdot\mathbf{K}\boldsymbol{\sigma}_2\cdot\mathbf{K},\ \boldsymbol{\sigma}_1\cdot\mathbf{n}\boldsymbol{\sigma}_2\cdot\mathbf{n},\ \boldsymbol{\sigma}_1\cdot\mathbf{P}\boldsymbol{\sigma}_2\cdot\mathbf{P}, \tag{IVa}$$

$$(\boldsymbol{\sigma}_1\cdot\mathbf{K}\boldsymbol{\sigma}_2\cdot\mathbf{P}+\boldsymbol{\sigma}_1\cdot\mathbf{P}\boldsymbol{\sigma}_2\cdot\mathbf{K}). \tag{IVb}$$

Only two of the forms (IVa) are really independent, since the three may be combined to give $\boldsymbol{\sigma}_1\cdot\boldsymbol{\sigma}_2$.

If time-reversed quantities are indicated by a prime superscript, the effects of time reversal[5] may be summarized by

$$\boldsymbol{\sigma}'=-\boldsymbol{\sigma},\quad \mathbf{k}_i'=-\mathbf{k}_f,\quad \mathbf{k}_f'=-\mathbf{k}_i,$$

and therefore,

$$\mathbf{K}'=\mathbf{K},\quad \mathbf{n}'=-\mathbf{n},\quad \mathbf{P}'=-\mathbf{P}.$$

It is seen that (III) and (IVb) change sign under time-reversal and these are therefore ruled out. Thus the most general form of M is

$$\begin{aligned}M=A+B(\boldsymbol{\sigma}_1\cdot\boldsymbol{\sigma}_2-1)+C(\boldsymbol{\sigma}_1+\boldsymbol{\sigma}_2)\cdot\mathbf{n}+D(\boldsymbol{\sigma}_1-\boldsymbol{\sigma}_2)\cdot\mathbf{n}\\ +E(\boldsymbol{\sigma}_1\cdot\mathbf{K})(\boldsymbol{\sigma}_2\cdot\mathbf{K})+F(\boldsymbol{\sigma}_1\cdot\mathbf{P})(\boldsymbol{\sigma}_2\cdot\mathbf{P}),\end{aligned} \tag{9}$$

where the coefficients are functions of the scalars k_i^2 and $\mathbf{k}_i\cdot\mathbf{k}_f$, that is, of the energy and $\cos\theta$, where θ is the c.m. scattering angle.

Substituting from Eq. (9) into Eqs. (6) and (7a) one finds

$$\mathbf{N}\cdot\langle\boldsymbol{\sigma}_1\rangle_f I_0=I_p=\mathbf{N}\cdot\mathbf{n}\,2\,\mathrm{Re}\{CA^*+D(A^*-2B^*)\}, \tag{10}$$

thus proving Eq. (8). If the forms (III) or (IVb) were

[3] L. Wolfenstein, Phys. Rev. **75**, 1664 (1949), Phys. Rev. **76**, 541 (1949). One of us (L.W.) takes this opportunity to apologize for having stated as obvious a relation which is far from being so.

[4] L. Eisenbud and E. Wigner, Proc. Nat. Acad. Sci. **27**, 281 (1941).

[5] E. P. Wigner, Göttinger Nachr. p. 546 (1932).

included in Eq. (9), this would no longer be true; thus the condition of invariance under time-reversal is necessary in order to prove Eq. (8). The important consequences of invariance under space reflections (and rotations) have been previously noted;[5] these include: (a) the polarization $\langle\boldsymbol{\sigma}_1\rangle_f$ resulting from an initially unpolarized beam is normal to the plane containing the initial and final momenta; and (b) the contribution I_p to the scattering due to the initial polarization of one particle is proportional to the component of $\langle\boldsymbol{\sigma}_1\rangle_i$ perpendicular to the initial direction of motion and contains as a factor $\sin\theta\cos\varphi$, where φ is the azimuthal angle measured from the normal to the plane defined by the initial momentum and polarization.

Of special interest is the 3×3 submatrix of M which involves scattering in triplet states only. The usual representation[6] of this matrix is $S_{m_s'm_s}$, where m_s' and m_s are the final and initial z-components of the total spin, respectively. Each of the conditions imposed here on M may be translated into this representation if it concerns matrix elements which are nonzero only between triplet states. For example, since the matrix (IVb) may be regarded as one of a complete set of matrices in terms of which M may be expanded, the condition that (IVb) cannot enter into the expansion is expressible by the vanishing of the trace of the product of M and (IVb). Computation of this trace yields

$$S_{11}-S_{00}-e^{2i\varphi}S_{1-1}=\sqrt{2}\,\cot\theta(e^{-i\varphi}S_{01}+e^{i\varphi}S_{10}). \quad (11)$$

This equation, which is seen to follow from the time-reversal condition, is not apparent in explicit formulations and thus may be used as a check on the accuracy of numerical calculations. Similarly the condition of invariance of M under space reflections may be translated into this representation:

$$\begin{aligned} &S_{11}=S_{-1-1}, \quad e^{-i\varphi}S_{-10}=-e^{i\varphi}S_{10}, \\ &e^{-i\varphi}S_{01}=-e^{i\varphi}S_{0-1}, \quad e^{2i\varphi}S_{1-1}=e^{-2i\varphi}S_{-11}. \end{aligned} \quad (12)$$

III. GENERAL PROOF OF EQUATION (8)

Equation (8) may be shown to be valid in the more general case of the scattering of a spin $\frac{1}{2}$ particle from a scatterer of spin I. As a complete set of operators in the combined spin spaces of the two particles one may use all the products of the form $(\sigma^\alpha\times s^\beta)$, where σ^α are the four spin operators of the spin $\frac{1}{2}$ particle and s^β are a complete set of $(2I+1)^2$ operators in the spin space of spin I particle. It is important to note that all the operators $(\sigma^\alpha\times s^\beta)$ have zero trace except the unity operator (1×1). The most general form of M may be written

$$M=a+b\boldsymbol{\sigma}_1\cdot\mathbf{n}+c\boldsymbol{\sigma}_1\cdot\mathbf{K}+d\boldsymbol{\sigma}_1\cdot\mathbf{P},$$

where a, b, c, and d are linear combinations of operators of the form s^β. To prove Eq. (8), one evaluates

$$\begin{aligned} 4I_0(I_p/I_0-\mathbf{N}\cdot\langle\boldsymbol{\sigma}_1\rangle_f)&=\mathrm{Tr}(M^\dagger M-MM^\dagger)\boldsymbol{\sigma}_1\cdot\mathbf{N} \\ &=2i\ \mathrm{Tr}\{\boldsymbol{\sigma}_1\cdot(\mathbf{n}\times\mathbf{P})(b^\dagger d-bd^\dagger)+\boldsymbol{\sigma}_1\cdot(\mathbf{n}\times\mathbf{K})(b^\dagger c-c^\dagger b) \\ &\quad+\boldsymbol{\sigma}_1\cdot(\mathbf{P}\times\mathbf{K})(d^\dagger c-c^\dagger d)\}\boldsymbol{\sigma}_1\cdot\mathbf{N}. \end{aligned} \quad (13)$$

Here contributions to the commutator of $M^\dagger$ and M from the noncommutation of a, b, c, and d have been omitted, since these terms must contain an s^β factor other than unity and so will have zero trace. Furthermore, for our considerations the factors $b^\dagger d-bd^\dagger$, $b^\dagger c-c^\dagger b$, and $d^\dagger c-c^\dagger d$ are not operators in the spin space of the spin I particle, but depend only on the vectors $\mathbf{k}_i$ and $\mathbf{k}_f$, because any term containing an operator s^β other than unity will yield zero trace. Following the arguments used previously one finds the transformation properties indicated in Table I. Since it is impossible to construct from $\mathbf{k}_i$ and $\mathbf{k}_f$ quantities having the transformation properties required for $bd^\dagger$, $bc^\dagger$, $dc^\dagger$, etc., it follows that each of the terms in Eq. (13) is zero.

TABLE I. Transformation properties of factors in Eq. (13). *S*—scalar. *PS*—pseudoscalar.

	Reflection-rotation	Time reflection
b	S	$+$
c	PS	$-$
d	PS	$+$
$b^\dagger d$, $bd^\dagger$	PS	$+$
$c^\dagger b$, $bc^\dagger$	PS	$-$
$d^\dagger c$, $dc^\dagger$	S	$-$

[5] J. Ashkin and T. Y. Wu, Phys. Rev. **73**, 973 (1948).

Radiative Correction for the Collision Loss of Fast Particles

J. M. JAUCH
State University of Iowa, Iowa City, Iowa
(Received December 10, 1951)

The correction for the collision loss of fast heavy particles because of the interaction with the radiation field is calculated approximately. The radiative corrections always result in a decrease of the collision loss. Only the collisions with energy loss $\epsilon > \gamma mc^2$ contribute significantly to this result. For $\gamma = 1000$ and $Z = 18$ (argon) the correction amounts to about 6 percent.

THE energy loss of fast particles by collisions with the atomic electrons has a minimum if the kinetic energy is approximately equal to the rest energy of the colliding particle. Beyond this value the theory predicts an expression for the specific energy loss which is essentially of the form[1]

$$-dW/dx = A \ln\gamma^2 + B, \tag{1}$$

with

$$A \simeq 4\pi ne^4/mc^2, \quad B \simeq (4\pi ne^4/mc^2) \ln(2mc^2/I), \quad \gamma = [1-(v^2/c^2)]^{-\frac{1}{2}}. \tag{2}$$

The formula (1) is derived on the basis of the assumption that the collision occurs with one single atom. If the mutual interaction of the atoms is included then the energy loss for very energetic particles decreases slightly because of the shielding effect of the closer atoms.

This effect has been calculated by a number of different workers, with slightly different results.[2] They agree, however, in predicting less ionization loss than the Bethe-Bloch formula and the gradual approach of a constant value. Recent experiments with ultrarelativistic particles in various materials tended to confirm this general behavior.[3]

A significant departure from the theoretical energy loss formula was recently reported, however, by Goodman, Nicholson, and Rathgeber.[4] They report the energy loss of cosmic-ray mesons to lie considerably below the theoretical value for values of γ up to about 10^3.

Since the collision loss depends only on the electromagnetic interaction of charged particles, the establishment of such a discrepancy would be of considerable theoretical interest. The only electromagnetic effect which could possibly be called upon to give an appreciable correction at ultrarelativistic energies would be the radiative corrections.

The radiative corrections to the collision of charged particles calculated with the methods of quantum electrodynamics are finite, if proper care is taken to remove infinities by the process of "renormalization." The rigorous calculation of the radiative corrections to the collision loss in this manner is rather involved and has not yet been done. It is, however, possible to obtain an estimate of the order of magnitude of this effect by reducing it to the problem of the radiative corrections to the scattering in a fixed Coulomb potential. This problem has been treated in detail by Schwinger.[5] The result is given in Eqs. (2.101) and (2.102) of Schwinger's paper.

In order to apply this result to the problem of collision loss we consider the problem in the center-of-mass system. If the atomic electron is for the moment considered as a free particle we could calculate the energy loss of the colliding particle by multiplying the probability for Coulomb scattering of the electron into a certain angle with the energy gain of the electron in the laboratory system associated with this scattering angle. We then sum this energy over all possible scattering angles to obtain the total energy loss per collision. A simple application of the Lorentz transformation to this problem shows that an electron which in the rest system is scattered into an angle θ by an infinitely heavy particle has in the laboratory system an energy

$$\epsilon(\theta) = mc^2\gamma^2\beta^2(1-\cos\theta), \tag{3}$$

with $\gamma^2 = 1/(1-\beta^2)$. The collision loss per unit path length is then obtained from the expression

$$-\frac{dw}{dx} = 2\pi nmc^2\gamma^2\beta^2 \int_{\theta_0}^{\pi} \sigma(\theta)(1-\cos\theta)\sin\theta d\theta, \tag{4}$$

where n is the number of electrons per unit volume. The integration over the angle θ cannot be extended to 0 for the lower limit, since for very small angle scattering the electrons cannot be considered as free.

If we calculate (4) with the differential cross section $\sigma(\theta)$ for Coulomb scattering

$$\sigma_0(\theta) = \left(\frac{e^2}{2\gamma m\beta^2c^2}\right)^2 \frac{1}{\sin^4\frac{1}{2}\theta} \tag{5}$$

[1] See for instance W. Heitler, *The Quantum Theory of Radiation* (Oxford University Press, London, 1947), p. 218, Eq. (1).
[2] E. Fermi, Phys. Rev. **57**, 485 (1940); O. Halpern and H. Hall, Phys. Rev. **73**, 477 (1948); G. C. Wick, Nuovo cimento **1**, 302 (1943); A. Bohr, Kgl. Danske Videnskab. Selskab, Nat.-fys. Medd. **24**, No. 19 (1948).
[3] See for instance D. R. Corson and M. R. Keck, Phys. Rev. **79**, 209 (1950); W. L. Whittemore and J. C. Street, Phys. Rev. **76**, 1786 (1949); E. Hayward, Phys. Rev. **72**, 937 (1948); F. L. Hereford, Phys. Rev. **74**, 574 (1948); E. Pickup and L. Voyvodic, Phys. Rev. **80**, 89 (1950).
[4] Goodman, Nicholson, and Rathgeber, Proc. Phys. Soc. (London) **A64**, 96 (1951).
[5] J. Schwinger, Phys. Rev. **76**, 790 (1949).

we obtain

$$-dw/dx=\tfrac{1}{2}\pi(ne^4/m\beta^2c^2)J, \tag{6}$$

where

$$J=\int_{\theta_0}^{\pi}\frac{1-\cos\theta}{\sin^4\tfrac{1}{2}\theta}\sin\theta d\theta=8\ln\left(\frac{1}{\sin\tfrac{1}{2}\theta_0}\right). \tag{7}$$

Formula (6) thus gives

$$-dw/dx=4\pi(ne^4/m\beta^2c^2)\ln(2/\theta_0). \tag{8}$$

The minimum scattering angle may be obtained by comparison with the rigorous formula or by arguments for the limit of energy transfer for bound electrons.[6]

$$\theta_0\sim I/mc^2\beta^2\gamma^2, \tag{9}$$

from which we obtain

$$-dw/dx=4\pi(ne^4/m\beta^2c^2)\ln(2mc^2\beta^2\gamma^2/I). \tag{10}$$

In order to obtain an order of magnitude estimate of the radiative correction we replace $\sigma_0(\theta)$ by

$$\sigma(\theta)=\sigma_0(\theta)[1-\delta(\theta)], \tag{11}$$

where $\delta(\theta)$ is the radiative correction for the scattering in a Coulomb field calculated by Schwinger.

$$\delta(\theta)=(4\alpha/\pi)[A(\ln(2\gamma\sin\tfrac{1}{2}\theta)-\tfrac{1}{2})+B+C\sin^2\tfrac{1}{2}\theta f(\theta)], \tag{12}$$

with

$$A=\ln(E/\Delta E)-13/12,\quad B=17/72,\quad C=\tfrac{1}{4}.$$

Here ΔE is the uncertainty of the energy change of the scattered electron, subject only to the condition

$$0<\Delta E\ll E-mc^2. \tag{13}$$

$f(\theta)$ is a slowly varying function of the angle θ, which we do not need to know since the contribution from this term turns out to be entirely negligible. Formula (12) is only valid for energies and scattering angles such that

$$\gamma\sin\tfrac{1}{2}\theta\gg1. \tag{14}$$

For the extreme relativistic case to be considered here, the limiting angle θ_1 defined by

$$\gamma\sin\tfrac{1}{2}\theta_1=1,\quad \theta_1\simeq2/\gamma, \tag{15}$$

turns out to be very much larger than θ_0, although it is still small compared to one. Thus we have

$$\theta_0\ll\theta_1\ll1. \tag{16}$$

For angles $\theta<\theta_1$ we must use another limiting formula for δ. In this case δ is proportional to $\theta^2\ll1$ and thus the contribution to the effect from this region turns out to be negligible.

Thus we may use formula (12) throughout and limit the scattering angle for the correction term to $\theta=\theta_1$. Comparing with (3) we see that radiative corrections to collision loss are only important for collisions such that the energy transferred to the electron is of order $mc^2\gamma$ or more.

If we write for the energy loss per unit length,

$$-dw/dx=F(1-\Delta), \tag{17}$$

with F given by (10), we find with the help of (11), (12), and (13) for the relative decrease of the radiation loss

$$\Delta=\frac{\alpha}{2\pi}\int_{\theta_1}^{\pi}[A\{\ln(2\gamma\sin\tfrac{1}{2}\theta)-\tfrac{1}{2}\}+B]\times\frac{1-\cos\theta}{\sin^4\tfrac{1}{2}\theta}\sin\theta d\theta\Big/\ln\left(\frac{2mc^2\beta^2\gamma^2}{I}\right). \tag{18}$$

The integration involves only the two integrals

$$\int_{\theta_1}^{\pi}\frac{1-\cos\theta}{\sin^4\tfrac{1}{2}\theta}\sin\theta d\theta=8\ln\left(\frac{1}{\sin\tfrac{1}{2}\theta_1}\right)=8\ln\gamma, \tag{19}$$

$$\int_{\theta_1}^{\pi}\frac{\ln(2\gamma\sin\tfrac{1}{2}\theta)}{\sin^4\tfrac{1}{2}\theta}(1-\cos\theta)\sin\theta d\theta=8\ln\gamma(\ln\gamma+\ln2-\tfrac{1}{4}). \tag{20}$$

Substituting these expressions in (18), we find for Δ

$$\Delta=\frac{(4\alpha/\pi)\ln\gamma[\{\ln(E/\Delta E)-13/12\}\times(\ln\gamma-1+\ln2)+17/72]}{\ln(2mc^2\beta^2\gamma^2/I)}. \tag{21}$$

This represents the relative decrease of collision loss resulting from radiative corrections.

In this formula there occurs still the as yet undetermined quantity $E/\Delta E$. Here ΔE represents the energy loss of the electron resulting from the emission of low energy photons. In the theory which includes radiative corrections the cross section for elastic scattering ($\Delta E\to0$) would actually vanish. In an actual experiment this is not what is observed, however. There is always in the nature of the experiment a limitation ΔE on the accuracy of the energy determination and this is the value to be inserted in Eq. (12).

In our case the limitation on the energy determination arises from the fact that because of the finite extension of the electron in an atom, the kinetic energy E of the electron before collision is uncertain by an amount

$$\Delta E/E\simeq\Delta p/p=(\gamma h/a)(1/\gamma mc)=Z^{\frac{1}{3}}/137, \tag{22}$$

where we have used $a\simeq a_0Z^{-\frac{1}{3}}$, $a_0=h^2/mc^2$, for the extension of the electron at rest.

If we insert this expression for $\Delta E/E$ in (17), we obtain the final result

$$\Delta(Z,\gamma)=\frac{(4\alpha/\pi)\ln\gamma[\{\ln(137/Z^{\frac{1}{3}})-13/12\}\times(\ln2\gamma-1)+17/72]}{\ln(2mc^2\beta^2\gamma^2/I)}, \tag{23}$$

[6] See for instance E. J. Williams, Revs. Modern Phys. **17**, 217 (1945), especially p. 223 ff.

TABLE I. Relative decrease Δ of radiation loss in percent due to radiative correction for energies γMc^2 of heavy particle, $Z=18$ (argon).

γ	10	20	50	100	200	500	1000
$\Delta\times100$	1.06	1.68	2.57	3.24	4.1	5.15	6

for the relative decrease of the collision loss per unit path length. The evaluation of this for the case of argon ($Z=18$) gives the result summarized in Table I.

The correction Δ would be a correction over and above the correction due to the density effect. It is difficult to compare this result with existing experiments. At the present time we can only conclude that if precise experiments at ultrarelativistic energies become available, the radiative correction would have to be included in the theoretical discussion. The method used here cannot claim any accuracy better than about a factor of two, and for a detailed comparison with experiment it would be necessary to refine the calculation.

Note added in proof: While this paper was in print there appeared a paper by H. D. Rathgeber [Z. Naturforsch. **6a**, 598 (1951)] on the energy loss of fast mesons in water. It is found that the energy loss of measons stays nearly constant in the range from 2 to 20×10^9 ev while according to the Bethe-Bloch theory it should increase 29 percent in this range. 16 percent of these can be accounted for as being due to the density effect, thus leaving 13 percent unexplained. The radiative correction here calculated would result in a further decrease of about 3–4 percent. Although the method of calculation used here does not claim accuracy better than about a factor of two, it seems difficult to explain the whole of the discrepancy found by Rathgeber as due to radiative corrections alone.

PHYSICAL REVIEW VOLUME 85, NUMBER 6 MARCH 15, 1952

The Interaction of a Charged Pi-Meson with the Deuteron*

W. B. CHESTON†
University of Rochester, Rochester, New York
(Received August 23, 1951)

The radiative absorption, charge-exchange scattering, elastic and inelastic scattering of a π^+ meson by the deuteron are calculated in conventional weak-coupling theory for the pseudoscalar field with both direct and gradient coupling. The nucleon-nucleon interaction is treated phenomenologically and the "impulse" approximation employed. The behavior of the ratio $\sigma_{\text{nonradiative}}/\sigma_{\text{radiative}}$ for the *PS* theory is different from that for the *PV* theory. The charge-exchange scattering of a *PS* meson exhibits a minimum for forward scattering for both types of coupling but otherwise mirrors the behavior of the charge-exchange cross section for a neutron target. The elastic and inelastic scattering cross sections are comparable for an incident 25-Mev meson, and small energy transfers to the deuteron are favored, in contrast to the case in which the target nucleus is more complex.

INTRODUCTION

IN this paper, we shall investigate the interaction of a charged π-meson of positive energy with the deuteron. The nonradiative absorption of a π^+ meson by the deuteron ($\pi^++d\rightarrow p+p$) and its inverse ($p+p\rightarrow\pi^++d$) have been the subjects of a previous paper[1] by the author. The reactions to be considered here are:

$$\pi^++d\rightarrow\begin{cases}p+p+\gamma & \text{radiative absorption}\\ p+p+\pi^0 & \text{charge-exchange scattering}\\ d+\pi^+ & \text{elastic scattering}\\ n+p+\pi^+ & \text{inelastic scattering.}\end{cases}$$

Recent experimental results on the reactions[2,3] $\pi^++d\rightleftarrows p+p$ prove that the π^+ meson has zero spin. In addition, comparison of the theoretical results[4] with the experimental data[5] on the reactions π^- (*K*-shell) $+d\rightarrow n+n$ and $n+n+\gamma$ show that if the π^- meson has zero spin, it has odd parity (*PS*). If one assumes that the π^+ and π^- mesons differ only in the sign of their Coulombic charge, then one may assign zero spin and odd parity to the charged π-meson field. The calculation of the above reactions will be carried out assuming both direct (*PS*) and gradient (*PV*) coupling of the *PS* π-meson to a nucleon. Although the two nucleon interaction will be treated phenomenologically, it will be consistent to consider direct coupling for the *PS* field since we shall take account of the possibility of the meson interacting with negative energy state nucleons. The nucleons will be assumed to be Dirac particles, and transitions through intermediate negative energy states will be included. The calculation is performed assuming a positive charge for the π-meson; however, since the Coulomb force between the meson and the nucleus is ignored, the derived expressions are independent of the sign of the charge of the meson. The π^+ meson is con-

* This work was assisted by the AEC.
† Now at Washington University, St. Louis, Missouri.
[1] W. Cheston, Phys. Rev. **83**, 1118 (1951).
[2] Clark, Roberts, and Wilson, Phys. Rev. **83**, 649 (1951).
[3] Cartwright, Richman, Whitehead, and Wilcox, Phys. Rev. **81**, 652 (1951); Crawford, Crowe, and Stevenson, Phys. Rev. **82**, 97 (1951).
[4] S. Tamor, Phys. Rev. **82**, 38 (1951).
[5] W. Panofsky (private communication).

sidered since the final state nucleons (two protons) in the radiative and nonradiative and charge-exchange scattering are easier to detect experimentally than those (two neutrons) which would result if the π^- meson had been considered.

GENERAL PROCEDURE

The reactions listed above will be treated as second-order processes on the assumption that the meson-nucleon coupling is weak (e.g., $g^2/\hbar c<1$). The weak coupling theory has been sufficiently successful in explaining the qualitative features of the data on the meson-nucleon reactions[6] to justify a study of the chief meson-deuteron reactions. We shall attempt to clarify in what respects the meson-deuteron and meson-nucleon reactions differ from each other and to extract those predictions which are not too sensitive to the details of the meson theory. Wherever possible, the results of the meson-deuteron calculations will be compared directly to the results of the meson-nucleon calculations.

Following Tamor[4] and Chew,[7] it will be assumed that the nucleon in the deuteron which interacts with the initial state quantum also interacts with the final state quantum. The possibility of, say, nucleon 1 interacting with the initial quantum and nucleon 2 with the final quantum will be assumed to be small and will be ignored. This is equivalent to the assumption that the characteristic time for the interaction of a nucleon with the initial and final state quanta is short compared to the period of the deuteron. The rather loose binding of the nucleons in the deuteron makes this a good approximation.

In general, the matrix element which must be evaluated in these problems may be written in this approximation:

$$M=\sum_{i=1}^{2}\int\Psi_f^*(\mathbf{R}_i,\boldsymbol{\sigma}_i,\boldsymbol{\tau}_i)\left\{\frac{\exp(-i\mathbf{k}'\cdot\mathbf{R}_i)}{(2E')^{\frac{1}{2}}}I\frac{\exp(i\mathbf{k}\cdot\mathbf{R}_i)}{(2E)^{\frac{1}{2}}}\right\}\times\Psi_0(\mathbf{R}_i,\boldsymbol{\tau}_i,\boldsymbol{\sigma}_i)d\mathbf{R}_1d\mathbf{R}_2,$$

where $\mathbf{R}_i$ = space coordinate of the ith nucleon; $\boldsymbol{\sigma}_i$ = spin coordinate of the ith nucleon; $\boldsymbol{\tau}_i$ = isotopic spin coordinate of the ith nucleon; $(\mathbf{k}, E)$ = momentum-energy 4-vector of the initial quantum; $(\mathbf{k}', E')$ = momentum-energy 4-vector of the final quantum; and I = operator which transforms the initial two-nucleon state (deuteron) into the final state and represents the relativistic summation over plane-wave intermediate states. I will be evaluated for the different processes using the methods of Feynman.[8] For Ψ_0, the deuteron wave function, we shall choose the representation employed in our previous paper on the nonradiative absorption of a π^+ meson by the deuteron:

$$\Psi_0=\frac{N}{(4\pi)^{\frac{1}{2}}}\frac{e^{-\gamma R}-e^{-\beta R}}{R}|T_m\rangle\frac{|\tau_n{}^1\tau_p{}^2-\tau_n{}^2\tau_p{}^1\rangle}{\sqrt{2}}.$$

In the case of the radiative absorption reaction, plane waves will be assumed for the final two-nucleon wave function. This will be a good approximation since we shall only interest ourselves in the total cross section for the process. The validity of the plane wave approximation follows from the fact that the distribution at any angle in the gamma-ray energy k' will be highly peaked at k_{max}'; little error is made if the square of the matrix element is given its value at k_{max}' and taken outside the integral over the density of states. The integral can then be extended over all energies instead of over just those allowed by the process. Since we thus sum over a complete set of functions for the two nucleons, this complete set can be the set of plane waves or the set of distorted waves insofar as the total cross section is concerned.

For the remaining reactions, the distortion of the final two-nucleon wave function will only be assumed to act in the S-state. The form of the even part of the final wave function is written:

$$\psi_{even}=\frac{e^{i\mathbf{k}\cdot\mathbf{R}}+e^{-i\mathbf{k}\cdot\mathbf{R}}}{\sqrt{2}}-\sqrt{2}\frac{\sin kR}{kR}+\sqrt{2}f(R)\frac{\sin(kR+\delta)}{kR},$$

where δ = S-phase shift, and $f(R)$ = zero energy wave function for the $n-p$ or $p-p$ systems. Since the major part of the cross section will come from that region in which the final state nucleons have below 10-Mev kinetic energy, we may use the expression for the phase-shifts which is independent of the shape of the nucleon-nucleon potential:[9]

$$k\cot\delta=-\alpha+\tfrac{1}{2}k^2r_0,$$

where α = scattering length, and r_0 = effective range of the nucleon-nucleon interaction.

The matrix element for the interaction of a π^+ meson with the deuteron may be calculated in the initial stages in the same manner as the interaction of a π^+ meson with a free nucleon. It is only in the final stages of the calculation, in which one is forced to restrict the number of final states for the nucleon, that the effect of the nucleon's presence in the deuteron will become apparent.

RADIATIVE ABSORPTION

It is assumed that only that nucleon in the deuteron which is originally a neutron can interact with the meson and photon fields:

$$\pi^+ + \begin{pmatrix} n \\ + \\ p \end{pmatrix} \begin{matrix} \rightarrow p+\gamma \\ \\ \rightarrow p. \end{matrix}$$

[6] R. E. Marshak, Revs. Modern Phys. **23**, 137 (1951).
[7] G. Chew, Phys. Rev. **80**, 196 (1950).
[8] R. Feynman, Phys. Rev. **76**, 749 (1949); Phys. Rev. **76**, 769 (1949).
[9] H. Bethe, Phys. Rev. **76**, 38 (1949); J. Blatt and J. Jackson, Phys. Rev. **76**, 18 (1949).

The matrix element for the radiative absorption of a π^+ meson by a neutron will only be calculated in the $PS(PV)$ theory. The equivalence theorem between the $PS(PV)$ and $PS(PS)$ theories[10] for this reaction is approximately valid, although conservation of energy for the reaction $\pi^+ + n \rightarrow p + \gamma$ does not hold when the absorbing neutron is in the deuteron. We shall ignore the contribution of the anomalous magnetic moments of the nucleons. Although the anomalous magnetic moments have been shown to give large contributions to PS π^0 production in photon-nucleon collisions, their contributions to charged meson production (the inverse of the process $\pi^+ + n \rightarrow p + \gamma$) are negligibly small.[11]

The three terms which enter into the matrix element may be written as follows[12] (setting $\hbar = c$ (velocity of light) $= M$ (nucleon mass) $= 1$):

$$4\pi \frac{ge}{\mu} \mathfrak{N} \frac{1}{\mathfrak{P}_0 + \mathfrak{k} - 1} \gamma_5 \mathfrak{k}, \tag{1}$$

$$4\pi \frac{ge}{\mu} \gamma_5 \mathfrak{k}'' \frac{1}{k'' \cdot k'' - \mu^2} (A \cdot k + A \cdot k''), \tag{2}$$

$$-4\pi \frac{ge}{\mu} \gamma_5 \mathfrak{A}, \tag{3}$$

where k = initial meson momentum-energy 4-vector; k'' = intermediate meson momentum-energy 4-vector; P_0 = initial nucleon momentum-energy 4-vector; and A = 4-vector polarization of the photon field. The first term represents the absorption of the π^+ meson by the neutron with the subsequent interaction of the proton current with the photon field:

$$\pi^+ + n \rightarrow p' \rightarrow p + \gamma.$$

The second term represents the interaction of the π^+ meson current with the photon field and the subsequent absorption of the π^+ meson by the neutron:

$$\pi^+ + n \rightarrow \gamma + \pi^{+\prime} + n \rightarrow \gamma + p.$$

The third term represents the "catastrophic" absorption of a π^+ meson by the neutron with the emission of a gamma-ray:

$$\pi^+ + n \rightarrow \gamma + p.$$

Throughout the calculation, it will be assumed that the terms depending on the momentum of the initial state neutron are negligible. This may be called the "target at rest" approximation. The matrix element is a slowly varying function of the target momentum; in addition, the kinematic factors which appear when we pass over to the case of the deuteron will strongly favor zero momentum for the target nucleons since the Fourier transform of the deuteron wave function is highly peaked at zero momentum.

The matrix element for the radiative absorption of a π^+ meson by a neutron is then, in nonrelativistic approximation:

$$M_n = 4\pi \frac{ge}{\mu} \frac{1}{(\mu^2+2E)} \Big\{ -2E\sigma + \left(1 - \frac{\mu^2+2E}{Ek' - \mathbf{k}\cdot\mathbf{k}'}\right)(\sigma\cdot\kappa)\mathbf{k} - (\sigma\cdot\kappa)(\sigma\times\mathbf{k}) \Big\} \cdot \mathbf{A},$$
$$\mathbf{k}' - \mathbf{k} = \kappa.$$

In the above, use has been made of the following device for obtaining the nonrelativistic approximation to the matrix element of an operator θ:

$$\langle f|\theta|i\rangle \sim \left\langle f \left| \frac{\mathfrak{P}'+1}{2} \theta \frac{\mathfrak{P}_i+1}{2} \right| i \right\rangle.$$

We must now take care of the fact that the absorbing neutron is in the deuteron. The matrix element for the radiative absorption of a π^+ meson by the deuteron is:

$$M = \sum_{i=1}^{2} \int \Psi_f^*(\mathbf{R}_i, \sigma_i, \tau_i) \{M_n{}^i \tau_+{}^i\} \times \frac{\exp(i\kappa\cdot\mathbf{R}_i)}{(4Ek')^{\frac{1}{2}}} \Psi_0(\mathbf{R}_i, \sigma_i, \tau_i) d\mathbf{R}_1 d\mathbf{R}_2,$$

where

$$\tau_+ |\text{neutron}\rangle = |\text{proton}\rangle,$$
$$\tau_+ |\text{proton}\rangle = 0.$$

Performing the indicated isotopic spin operation and passing over to the center-of-mass system, we find:

$$M = (8Ek')^{-\frac{1}{2}} \int \Psi_f^*(\mathbf{R}; \sigma_1, \sigma_2) \{M_n{}^{(1)} \exp(\tfrac{1}{2} i\kappa\cdot\mathbf{R}) - M_n{}^{(2)} \exp(-\tfrac{1}{2} i\kappa\cdot\mathbf{R})\} \psi_0(R) |T_m\rangle d\mathbf{R}.$$

For transitions to even parity plane wave final states:

$$M^{\text{even}} = \left\langle s \left| \frac{M_n{}^{(1)} - M_n{}^{(2)}}{(16Ek')^{\frac{1}{2}}} \right| T_m \right\rangle \{a_+ + a_-\},$$

where

$$a_\pm = \int \psi_0(R) \exp[i(\mathbf{K} \pm \tfrac{1}{2}\kappa)\cdot\mathbf{R}] d\mathbf{R},$$

and $\mathbf{K}$ = final nucleon momentum in the nucleon center-of-mass system. Using the expression for M_n found previously, we may write

$$M^{\text{even}} = -\frac{\pi ge}{\mu(\mu^2+2E)(Ek')^{\frac{1}{2}}} \langle s | \{\alpha\Delta\sigma + \beta(\Delta\sigma\cdot\kappa)\mathbf{k} + (\Delta\sigma\times\kappa)\times\mathbf{k}\} \cdot \mathbf{A} | T_m \rangle,$$

[10] F. Dyson, Phys. Rev. **73**, 929 (1948).
[11] M. Kaplon, Phys. Rev. **83**, 712 (1951).
[12] We use the following notation: boldface roman $\mathbf{k}$ for a 3-vector, boldface italic k for a 4-vector, and lightface German $\mathfrak{k}$ for $\Sigma\gamma_\mu k_\mu$.

where

$$\alpha=2E,\quad \beta=\frac{\mu^2+2E}{Ek'-\mathbf{k}\cdot\mathbf{k}'}-1,\quad \Delta\sigma=\sigma_1-\sigma_2.$$

The differential cross section in the laboratory system ignoring the odd-parity states contribution is then

$$\frac{d\sigma}{d\cos\alpha}=\frac{2N^2g^2e^2}{3\mu^3k(\mu^2+2E)^2}\int_0^{k_{\max}'(\alpha)}B^{\text{even}}K\Theta^2k'dk',$$

where

$$16\pi N^2B^{\text{even}}\equiv\int_{-1}^{+1}\{a_+ + a_-\}^2d(\cos\theta);\quad \theta=\sphericalangle(\boldsymbol{\kappa},\mathbf{K})$$

$$B^{\text{even}}=\frac{1}{\Gamma_1^+\Gamma_1^-}+\frac{1}{\Gamma_2^+\Gamma_2^-}+\frac{1}{2\Gamma_1K\kappa}\ln\frac{\Gamma_1^+}{\Gamma_1^-}+\frac{1}{2\Gamma_2K\kappa}\ln\frac{\Gamma_2^+}{\Gamma_2^-}$$
$$-\frac{2}{K\kappa(\Gamma_2^2-\Gamma_1^2)}\left[\Gamma_2\ln\frac{\Gamma_1^+}{\Gamma_1^-}-\Gamma_1\ln\frac{\Gamma_2^+}{\Gamma_2^-}\right],$$

$$\begin{pmatrix}\Gamma_1\\ \Gamma_2\end{pmatrix}=\begin{pmatrix}\gamma^2\\ \beta^2\end{pmatrix}+K^2+\tfrac{1}{4}\kappa^2;\quad \Gamma_i^{\pm}=\Gamma_i\pm K\kappa,$$

$$\Theta^2=8E^2+4E\{k^2(1+\cos^2\alpha)-2\mathbf{k}\cdot\mathbf{k}'\}$$
$$+L^2k^2\sin^2\alpha(\mathbf{k}-\mathbf{k}')^2-4E(1+L)k^2\sin^2\alpha,$$

$$L=(\mu^2+2E)/(Ek'-\mathbf{k}\cdot\mathbf{k}'),\quad \alpha=\sphericalangle(\mathbf{k},\mathbf{k}').$$

The integration over k' must be performed numerically.

The contribution to the cross section due to transitions to final nucleon states of odd parity will be small compared to the contribution from the even parity states. The major portion of each contribution will come from that region in which the final nucleons have essentially zero energy in the nucleon center-of-mass system. For absorption of a 25-Mev π^+ meson, the ratio $I^{\text{odd}}/I^{\text{even}}$ is about 0.1 where

$$I^{\text{even(odd)}}=\int B^{\text{even(odd)}}Kk'dk',$$

$$16\pi N^2B^{\text{odd}}\equiv\int_{-1}^{+1}\{a_+-a_-\}^2d(\cos\theta).$$

The spin sums, however, favor the odd-parity transitions. The total cross section for an incident 25-Mev π^+ meson is 3.6 $g^2/\hbar c\times10^{-27}$ cm^2. This is less than the cross section for the radiative absorption of a 25-Mev π^+ meson by a free neutron, which is calculated to be 5.9 $g^2/\hbar c\times10^{-27}$ cm^2 using the value of the cross section for the inverse process[11] and detailed balancing. The reduction of the cross section when the neutron is in the deuteron is due primarily to the operation of the Pauli principle.

If we define

$$R=\sigma_{\pi^++d\to p+p}/\sigma_{\pi^++d\to p+p+\gamma},$$

then, using the total cross section for the nonradiative absorption calculated in a previous paper,[1] we find

$$R_{25}=2.5.$$

Tamor[4] has shown that the ratio of the transition probabilities, R_K, in the $PS(PV)$ theory for the two competing reactions

$$\pi^-(K\text{-shell})+d\to\begin{cases}n+n\\ n+n+\gamma,\end{cases}$$

is 2.1. Assuming that the π^- and π^+ mesons have the same spin and parity, we note that for the PS theory, R is essentially constant from 0 to 25-Mev meson energy. For a PV meson, on the other hand, several authors[4,12] have demonstrated that nonradiative absorption of a π^- meson from the K-shell of the mesic-deuterium atom should occur twice as frequently as radiative absorption. This prediction was based on the conservation of angular momentum and parity and the assumption that the different sub-states formed by the deuteron and spin one meson (i.e., $J=0,1,2$) are occupied according to their statistical weights. For the absorption of a charged spin one meson from the continuum, this result no longer holds and one must compare transition probabilities directly. This should offer a method of distinguishing between the PS and PV theories since Tamor[4] has shown that the ratio of transition probabilities for the PV theory at zero energy is about 130 compared to 2.1 for the PS theory.

CHARGE-EXCHANGE SCATTERING

As was the case in the radiative absorption of a π^+ meson by the deuteron, only that nucleon which is originally the neutron in the deuteron can interact with the π^+ and π^0 meson fields. We must therefore calculate the matrix element for the charge-exchange scattering of a π^+ meson by the neutron. Since the equivalence theorem does not hold for this reaction, we shall calculate the cross section for both the $PS(PV)$ and $PS(PS)$ theories.

The matrix element for the charge-exchange scattering of a π^+ meson by the neutron in the $PS(PV)$ theory may be written as the sum of two terms: (1) represents the absorption of the π^+ meson with subsequent emission of the π^0 meson; (2) represents the emission of the π^0 meson with the subsequent absorption of the π^+ meson:

$$-4\pi\frac{gg_p}{\mu\mu_0}\gamma_5\mathfrak{k}'\frac{1}{\mathfrak{P}_0+\mathfrak{k}'-1}\gamma_5\mathfrak{k},\qquad(1)$$

$$-4\pi\frac{gg_n}{\mu\mu_0}\gamma_5\mathfrak{k}\frac{1}{\mathfrak{P}_0-\mathfrak{k}'-1}\gamma_5\mathfrak{k}',\qquad(2)$$

[12] Brueckner, Serber, and Watson, Phys. Rev. 81, 575 (1950).

TABLE I. Coefficients of $(g_p^2/\hbar c)$, $(g_n^2/\hbar c)$, and $(g_p g_n/\hbar c)$ in the expression for the charge-exchange differential cross section in units of $g^2/\hbar c \times 10^{-28}$ cm². The kinetic energy of the incident meson is 25 Mev. The *PS* theory with gradient coupling is assumed.

Angle of scattering	g_p^2	g_n^2	$g_n g_p$
0°	0.29	0.11	−0.35
30°	11.9	7.2	−7.1
60°	17.2	7.8	5.4
90°	7.9	8.9	16.7
120°	4.8	20.8	−9.2
180°	8.2	40.8	−36.2

where g_n = coupling constant of π^0 meson to the neutron, and g_p = coupling constant of π^0 meson to the proton. Those parts of the nonrelativistic approximation to the matrix elements which do not contain terms involving the Pauli spin operators are

(1)

$$4\pi\frac{gg_p}{\mu\mu_0}\frac{E'}{2E+\mu^2}\left[\mu^2+\frac{2}{E'}\mathbf{k}\cdot\mathbf{k}'\right],$$

(2)

$$4\pi\frac{gg_n}{\mu\mu_0}\frac{E}{2E'-\mu_0^2}\left[\mu_0^2-\frac{2}{E}\mathbf{k}\cdot\mathbf{k}'\right].$$

The leading spin dependent terms are

(1) (2)

$$2\pi i\frac{gg_p}{\mu\mu_0}\boldsymbol{\sigma}\cdot\mathbf{k}'\times\mathbf{k}\frac{4+\mu^2+2E}{\mu^2+2E},\quad 2\pi i\frac{gg_n}{\mu\mu_0}\boldsymbol{\sigma}\cdot\mathbf{k}'\times\mathbf{k}\frac{4+\mu_0^2-2E'}{2E'-\mu_0^2}.$$

The nonrelativistic approximations written above were obtained by the same method used for the radiative absorption reaction and are evaluated in the "target at rest" approximation.

If we let M_n represent the matrix element for the charge-exchange scattering of a π^+ meson by the neutron in the *PS*(*PV*) theory, then the corresponding matrix element for the charge-exchange scattering of a π^+ meson by the deuteron for transitions to triplet plane wave final states may be written:

$$M^t=\left\langle T_m'\left|\frac{M_n^{(1)}+M_n^{(2)}}{(16EE')^{\frac{1}{2}}}\right|T_m\right\rangle\{a_--a_+\}.$$

For transitions to final singlet plane wave states:

$$M^s=\left\langle s\left|\frac{M_n^{(1)}-M_n^{(2)}}{(16EE')^{\frac{1}{2}}}\right|T_m\right\rangle\{a_-+a_+\}.$$

Using the explicit expression for M_n found above, these matrix elements become

$$M^t=\frac{4\pi g}{\mu\mu_0}\left\langle T_m'\left|\left\{\frac{g_p}{2E+\mu^2}\left[E'\left(\mu^2+\frac{2}{E'}\mathbf{k}\cdot\mathbf{k}'\right)+\frac{i}{4}(\boldsymbol{\sigma}^1+\boldsymbol{\sigma}^2)\cdot\mathbf{k}'\times\mathbf{k}(4+\mu^2+2E)\right]+\frac{g_n}{2E'-\mu_0^2}\left[E\left(\mu_0^2-\frac{2}{E}\mathbf{k}\cdot\mathbf{k}'\right)+\frac{i}{4}(\boldsymbol{\sigma}^1+\boldsymbol{\sigma}^2)\cdot\mathbf{k}'\times\mathbf{k}(4+\mu_0^2-2E')\right]\right\}\right|T_m\right\rangle\{a_--a_+\}$$

$$M^s=\frac{\pi ig}{\mu\mu_0}\langle s|\Delta\boldsymbol{\sigma}\cdot\mathbf{k}'\times\mathbf{k}|T_m\rangle\times\left\{g_p\frac{4+\mu^2+2E}{2E+\mu^2}+g_n\frac{4+\mu_0^2-2E'}{2E'-\mu_0^2}\right\}\{a_++a_-\}.$$

The differential cross section follows immediately and is

$$\frac{d\sigma}{d\cos\alpha}=\frac{2N^2}{k}\int_0^{k'_{\max}(\alpha)}\frac{K}{E'}\{B^{\text{odd}}\langle M^{t2}\rangle+B^{\text{even}}\langle M^{s2}\rangle\}\frac{k'^2dk'}{(4\pi)^2}$$

$$16\pi N^2B^{\text{odd}}\equiv\int_{-1}^{+1}\{a_+-a_-\}^2d\cos\theta$$

$$B^{\text{odd}}=\frac{1}{\Gamma_1^+\Gamma_1^-}+\frac{1}{\Gamma_2^+\Gamma_2^-}-\frac{1}{2\Gamma_1K\kappa}\ln\frac{\Gamma_1^+}{\Gamma_1^-}-\frac{1}{2\Gamma_2K\kappa}\ln\frac{\Gamma_2^+}{\Gamma_2^-}-\frac{2}{K\kappa(\Gamma_2^2-\Gamma_1^2)}\left[\Gamma_1\ln\frac{\Gamma_1^+}{\Gamma_1^-}-\Gamma_2\ln\frac{\Gamma_2^+}{\Gamma_2^-}\right],$$

where $\langle\ \rangle\equiv$average over final nucleon spin states. In obtaining the differential cross section, the integration over the directions of the final state nucleons in the nucleon center-of-mass has been performed using $\boldsymbol{\kappa}$ as the polar axis. The coefficients of g_ng_p, g_n^2, and g_p^2 in the expression for the differential cross section for an incident 25-Mev meson are listed in Table I at five different angles of scattering in the laboratory system.

If the matrix element is a slowly varying function of k' over the region of integration, then we can compare the charge-exchange scattering of a π^+ meson by the deuteron to the charge-exchange scattering by a neutron. If the above condition holds, then we may write the differential cross section for the deuteron reaction as

$$\frac{d\sigma}{d\cos\alpha}=\frac{2N^2}{k}\{\langle M^{t2}\rangle I_t(\alpha)+\langle M^{s2}\rangle I_s(\alpha)\}.$$

The differential cross section for the reaction π^+

$+n\rightarrow p+\pi^0$ is

$$\frac{d\sigma}{d\cos\alpha}=\frac{2\pi}{k}<M_n^2>\frac{q^2}{q(1+E'')-E''k\cos\alpha},$$

where $(\mathbf{q}, E'')$ = energy-momentum 4-vector of scattered meson in the laboratory system. At 90°, the coefficients of g_n^2, g_p^2, and g_ng_p in the expression for the cross section for the deuteron reaction vary slowly for those values of k' which give the major contribution to the cross section. Therefore the square of the matrix element may be removed from the integral over the density of states at this angle. In addition, at 90°:

$$<M_t^2>\sim\tfrac{2}{3}<M_n^2>,$$
$$<M_s^2>\sim\tfrac{1}{3}<M_n^2>.$$

Therefore, for an incident 25-Mev meson,

$$R_{d/n}=|(d\sigma/d\cos\alpha)_{\text{deuteron}}/(d\sigma/d\cos\alpha)_{\text{neutron}}|_{90^\circ}\sim 0.35.$$

This is a reasonable value since we expect the ratio to be less than 0.5. The factor $\frac{1}{2}$ arises because the two final state nucleons are identical in the deuteron reaction. Additional factors tending to decrease the ratio result from the properties of the overlap integrals:

$$\int\psi_0\exp(\tfrac{1}{2}i\kappa\cdot\mathbf{R})[(e^{i\mathbf{K}\cdot\mathbf{R}}\pm e^{-i\mathbf{K}\cdot\mathbf{R}})/\sqrt{2}]d\mathbf{R}<1.$$

The approximation concerning the constancy of the matrix element over the allowed range of k' is not a good one as soon as $\cos\alpha$ approaches unity. However, the order of magnitude of $R_{d/n}$ at 0° can be obtained by a comparison of $I_t(0°)$ to $I_t(90°)$. We find for an incident 25-Mev meson:

$$I_t(0°)/I_t(90°)\sim 1.3\times 10^{-3}.$$

We therefore expect a minimum in the cross section for forward scattering.

The value of $R_{d/n}$ at 90° estimated above is not a good one if we assume a symmetrical meson theory (e.g., $g_n=-g_p$). This is because the matrix element at 90° will now vary rapidly with k' due to the near cancellation at this angle for the symmetrical theory. Table II shows the variation in $d\sigma/d\cos\alpha$ with angle for an incident 25-Mev meson in the case of the deuteron reaction for $g_n=-g_p$. All values are normalized to $d\sigma/d\cos 180°=1$ since the cross section exhibits no anomalies at this angle. In addition, Table II also shows the variation of $d\sigma/d\cos\alpha$ with angle for an incident 25-Mev meson in the case of the neutron for $g_n=-g_p$. These values were obtained using the analytic expressions given by Ashkin, Simon, and Marshak[14] modified[15] to take into account the mass difference between the charged and neutral mesons. These values are also normalized to $d\sigma/d\cos 180°=1$.

[14] Ashkin, Simon, and Marshak, Prog. Theor. Phys. **5**, 634 (1950).

[15] T. Auerbach (private communication).

The values at 90° are quite different for the two reactions. The cancellation in the matrix element for $g_n=-g_p$ seems to be more complete in the case of the deuteron. This is due to the neglect in the matrix element of terms which are, at first thought, negligible compared to those considered. At 90°, however, the almost complete cancellation of the large terms causes the small terms to assume an important role. These small relativistic terms cannot be consistently included in the deuteron calculation since only terms up to and including $(v/c)_{\text{nucleon}}$ may be used in the matrix element; the decomposition of the matrix element for the deuteron calculation into matrix elements between plane waves is only valid if terms in $(v/c)_{\text{nucleon}}^2$ and higher can be neglected. It is therefore assumed that a more correct theory for the deuteron would give approximately 10^{-2} for the ratio $(d\sigma/d\cos 90°)/(d\sigma/d\cos 180°)$ instead of approximately 10^{-3}.

In the case of the $PS(PS)$ theory, the prediction concerning the small value of the cross section for forward scattering remains unchanged. The precipitous drop in the cross section at 90° when use is made of the symmetrical theory does not occur in the $PS(PS)$ theory since the scattering from an individual nucleon does not exhibit any cancellation at 90°. The matrix element for the charge-exchange scattering of a π^+ meson by a neutron may be written in the $PS(PS)$ theory as

$$-\frac{4\pi g}{\mu\mu_0}\left\{g_p\gamma_5\frac{1}{\mathfrak{P}_0+\mathfrak{k}-1}\gamma_5+g_n\gamma_5\frac{1}{\mathfrak{P}_0-\mathfrak{k}'-1}\gamma_5\right\}.$$

The nonrelativistic approximation to this operator is immediate:

$$M_n=\frac{4\pi g}{\mu\mu_0}\left\{g_p\frac{E}{\mu^2+2E}+g_n\frac{E'}{2E'-\mu_0^2}\right\}.$$

The terms which have been neglected in the above are of order $(v/c)_{\text{meson}}\times(v/c)_{\text{nucleon}}$ smaller than those considered. The total cross section for an incident 25-Mev π^+ meson is

$$\sigma=\{0.50g_p^2/\hbar c+1.81g_n^2/\hbar c+2.06g_pg_n/\hbar c\}(g^2/\hbar c)\times 10^{-28}\ \text{cm}^2.$$

The angular distribution is determined by the expres-

TABLE II. Differential cross section for the charge-exchange scattering of a 25-Mev π^+ meson from the deuteron and from the neutron in the $PS(PV)$ theory with $g_n=-g_p$. All values normalized to $d\sigma/d\cos 180°=1$.

Angle of scattering	Deuteron	Neutron
0°	8.8×10^{-3}	1.2
30°	0.31	0.76
60°	0.23	0.45
90°	1.6×10^{-2}	1.0×10^{-2}
120°	0.41	0.59
180°	1	1

sion I_t defined previously. For $g_n=-g_p$ the $PS(PS)$ cross section becomes small. This effect is also present in the $PS(PS)$ theory for the charge-exchange scattering from a single nucleon.

ELASTIC SCATTERING

The elastic and inelastic scattering of a π^+ meson differ in one major respect from the reactions previously considered. Both the neutron and the proton in the deuteron can scatter the meson. This will cause an added interference effect not found in the reactions considered previously. Once again the approximation will be made that, as far as the nucleon which is interacting with the meson fields is concerned, the other nucleon merely "goes along for the ride."

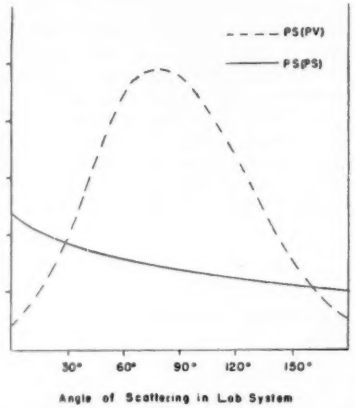

FIG. 1. Angular distribution in the laboratory system of π^+ mesons elastically scattered from the deuteron. The kinetic energy of the incident meson is 25 Mev.

The matrix element for the elastic scattering of a π^+ meson by the deuteron can be written:

$$M=\sum_{i=1}^{2}\int\Psi_f^*\left\{\frac{M_n{}^i\tau_n{}^i+M_p{}^i\tau_p{}^i}{(4EE')^{\frac{1}{4}}}\right\}\exp(i\boldsymbol{\kappa}\cdot\mathbf{R}_i)d\mathbf{R}_1d\mathbf{R}_2,$$

where M_n = matrix element for the reaction:

$$\pi^++n\rightarrow p'\rightarrow\pi^{+\prime}+n'$$

M_p = matrix element for the reaction:

$$\pi^++p\rightarrow\pi^{+}+n''+\pi^{+\prime}\rightarrow\pi^{+\prime}+p'$$

$\tau_n|\text{neutron}>=|\text{neutron}>$,

$\tau_n|\text{proton}>=0$,

etc.

Since the deuteron is charge antisymmetric, performing the indicated isotopic spin operation, we find

$$M=\frac{1}{(16EE')^{\frac{1}{4}}}\int\Psi_f^*(\sigma_1,\sigma_2;\mathbf{R}_1,\mathbf{R}_2)\times\{(M_n{}^{(1)}+M_p{}^{(1)})\exp(i\boldsymbol{\kappa}\cdot\mathbf{R}_1)+(M_n{}^{(2)}+M_p{}^{(2)})\exp(i\boldsymbol{\kappa}\cdot\mathbf{R}_2)\}\times\Psi_0(\sigma_1,\sigma_2;\mathbf{R}_1,\mathbf{R}_2)d\mathbf{R}_1d\mathbf{R}_2.$$

Integration over the center-of-mass coordinates yields

$$M=1/2(2\pi)^3(4EE')^{\frac{1}{4}}\int a_{\mathbf{K}}{}^*a_{\mathbf{K}}\langle T_m'|M^{(1)}+M^{(2)}|T_m\rangle dK$$

$$M^{(i)}=M_n{}^{(i)}+M_p{}^{(i)};\quad \mathbf{K}^+=\mathbf{K}+\tfrac{1}{2}\boldsymbol{\kappa}.$$

As was the case in the reactions previously considered, we shall make the "target at rest" approximation:

$$M=\frac{<T_m'|M^{(1)}+M^{(2)}|T_m>}{2(2\pi)^3(4EE')^{\frac{1}{4}}}\int a_{\mathbf{K}}{}^*a_{\mathbf{K}}d\mathbf{K}.$$

The indicated integration is immediate yielding

$$M=\frac{\langle T_m'|M^{(1)}+M^{(2)}|T_m\rangle}{(16EE')^{\frac{1}{4}}}\int\psi_0{}^2(R)\exp\left(\frac{i}{2}\boldsymbol{\kappa}\cdot\mathbf{R}\right)d\mathbf{R}$$

$$=\frac{\langle T_m'|M^{(1)}+M^{(2)}|T_m\rangle}{(16EE')^{\frac{1}{4}}}a'^2.$$

The matrix element for the scattering of π^+ meson by a neutron and by a proton may be calculated using the Feynman techniques. In the case of the elastic scattering of the π^+ meson by the deuteron we must form M_n+M_p. The nonrelativistic approximations to M_n and M_p may be found by setting $g=g_p=g_n$ and $\mu=\mu_0$ in the charge-exchange scattering matrix elements. If we let A be that part of the interaction operator which does not contain $\boldsymbol{\sigma}$ and B be that part which does depend on $\boldsymbol{\sigma}$, then the differential cross section in the laboratory for the elastic scattering of a π^+ meson by the deuteron is

$$\frac{d\sigma}{d\cos\alpha}=\frac{4\pi k'^2}{k}\frac{a'^2}{E'(k'-k\cos\alpha)+2k'}\{A^2+\tfrac{2}{3}B^2\}.$$

a'^2 is a maximum for forward scattering ($\kappa=0$) and decreases as the angle of scattering increases. We know that in the $PS(PV)$ theory, M_n+M_p increases as the angle of scattering increases from 0° to 90°. The rate of increase of M_n+M_p with increasing scattering angle in this region overpowers the decrease in a'^2 for the momentum transfers which enter into this problem. For the $PS(PS)$ theory, M_n+M_p is essentially constant from 0° to 180°. Therefore, the PS theory with direct coupling predicts a maximum for forward scattering

whereas the PS theory with gradient coupling predicts a maximum at approximately 90°.

The differential cross section for elastic scattering of a 25-Mev π^+ meson by the deuteron in the PS theories is shown in Fig. 1. The total cross sections at 25 Mev are

$$\sigma_{PS(PS)}=3.6\times10^{-27}\ (g^2/\hbar c)^2\ \text{cm}^2,$$

$$\sigma_{PS(PV)}=2.4\times10^{-26}\ (g^2/\hbar c)^2\ \text{cm}^2.$$

The total cross sections for the scattering of a 25-Mev meson by a nucleon have been calculated by Auerbach[15] and are

$$\left.\begin{aligned}\sigma_{PS(PS)}&=0.86\times10^{-27}\ (g^2/\hbar c)^2\ \text{cm}^2\\ \sigma_{PS(PV)}&=1.67\times10^{-26}\ (g^2/\hbar c)^2\ \text{cm}^2\end{aligned}\right\}\pi^++n\rightarrow n+\pi^+,$$

$$\left.\begin{aligned}\sigma_{PS(PS)}&=1.21\times10^{-27}\ (g^2/\hbar c)^2\ \text{cm}^2\\ \sigma_{PS(PV)}&=1.53+10^{-26}\ (g^2/\hbar c)^2\ \text{cm}^2\end{aligned}\right\}\pi^++p\rightarrow p+\pi^+.$$

If $M_n=M_p$ and did not contain terms which depended on the nucleon spin, we would expect a cross section for elastic scattering by the deuteron to be approximately four times the cross section for the scattering from an individual nucleon. Since a'^2 is less than unity except in the forward direction, and in addition, since M_n is only approximately equal to M_p even in the $PS(PS)$ theory, we would expect some reduction in the factor four. In the $PS(PV)$ theory, destructive interference in certain regions as well as terms depending on the nucleon spin cause a further decrease in the factor four. The actual numbers quoted above bear out this general argument. The energy dependence of the deuteron cross section mirrors the scattering from a single nucleon as calculations at 50 and 100 Mev have shown.

The cross sections for the elastic scattering of a π^+ meson at 50 and 100 Mev in the $PS(PV)$ theory are

$$\sigma(50\ \text{Mev})=6.2\times10^{-26}\ (g^2/\hbar c)^2\ \text{cm}^2,$$

$$\sigma(100\ \text{Mev})=11.2\times10^{-26}\ (g^2/\hbar c)^2\ \text{cm}^2.$$

Several other authors[16,17] have investigated the elastic scattering of a π^+ meson by the deuteron in the PS theories. Blair[16] has found results in general agreement with the results quoted above. However, Ferretti and Gallone[17] find that the ratio of the square of the matrix element for the scattering by the deuteron to the square of the matrix element for the scattering from a proton is about 1/10 at 25 Mev. This result is in disagreement with the results of Blair and those quoted here and is difficult to understand since destructive interference effects only play a role for forward scattering in the $PS(PV)$ theory and do not exist at all in the case of the $PS(PS)$ theory.

[16] J. Blair, Phys. Rev. **83**, 1246 (1951).
[17] B. Ferretti and S. Gallone, Phys. Rev. **77**, 153 (1950).

INELASTIC SCATTERING

The inelastic scattering of a π^+ meson by the deuteron is carried out in a manner similar to that employed for elastic and charge-exchange scattering. In contrast to the previous reactions, no states are excluded from the final state nucleons by the Pauli principle or by the requirement that the final state be bound. For reasons which will become evident, it is convenient to group the final states into the following categories:

SE singlet spin—even parity,
SO singlet spin—odd parity,
TE triplet spin—even parity,
TO triplet spin—odd parity.

SE

The matrix element for this transition is

$$M^{SE}=\sum_{i=1}^{2}\int\frac{<\tau_n{}^1\tau_p{}^2+\tau_p{}^1\tau_n{}^2|}{\sqrt{2}}\times\left\{\frac{M_n{}^i\tau_n{}^i+M_p{}^i\tau_p{}^i}{(4EE')^{\frac{1}{2}}}\right\}\frac{|\tau_n{}^1\tau_p{}^2-\tau_n{}^2\tau_p{}^1>}{\sqrt{2}}\times\exp(i\mathbf{x}\cdot\mathbf{R}_i)\Psi_{SE}{}^*(\mathbf{R}_1,\mathbf{R}_2;\sigma_1,\sigma_2)\times\Psi_0(\mathbf{R}_1,\mathbf{R}_2;\sigma_1,\sigma_2)d\mathbf{R}_1d\mathbf{R}_2.$$

Carrying out the indicated isotopic spin operation and considering plane wave final states, M_{SE} becomes

$$M_{SE}=\frac{1}{2\sqrt{2}}\left\langle S\left|\frac{\theta_1'-\theta_2'}{(4EE')^{\frac{1}{2}}}\right|T_m\right\rangle\{a_++a_-\},$$

where $\theta_i'=M_n{}^i-M_p{}^i$.

The matrix element for a SE transition will be small for two reasons: (1) destructive interference between M_n and M_p; (2) only the spin dependent terms will contribute. This may be seen in still another way which is perhaps more general. The intermediate state nucleons can only occupy SE or TO states since they are identical. If we consider only the S-part of the initial meson wave function, then the transition must proceed through the TO intermediate state by conservation of parity (the PS meson has an intrinsic odd parity). However, conservation of angular momentum and parity between initial and final states requires the nucleons and the meson to be in states of $l=2$ in the final state. This will make transitions through TO intermediate states vanishingly small. The transition to SE final states can be carried out through the SE intermediate states, but for this transition the odd angular momentum states of both the initial and final state mesons must contribute if parity and angular momentum are to be conserved. This reduces M_{SE} in comparison to those matrix elements in which the S-part of one of the mesons can contribute.

If we define B' as the spin dependent part of $\theta_1'-\theta_2'$, then the differential cross section for transitions to SE final states is

$$\frac{d\sigma}{d\cos\alpha}=\frac{2N^2}{3k}\int_0^{k'^{\max(\alpha)}}|B'|^2\frac{K}{E'}B^{\text{even}}\frac{k'^2dk'}{(4\pi)^2}.$$

TE

In this case, the matrix element is formally the same as in the elastic scattering reaction:

$$M^{TE}=\sum_{i=1}^{2}\int\frac{<\tau_n^1\tau_p^2-\tau_p^1\tau_n^2|}{\sqrt{2}}\times\left\{\frac{M_n^i\tau_n^i+M_p^i\tau_p^i}{(4EE')^{\frac{1}{2}}}\right\}\frac{|\tau_n^1\tau_p^2-\tau_n^2\tau_p^1>}{\sqrt{2}}\times\exp(i\mathbf{k}\cdot\mathbf{R}_i)\Psi_{SE}^*(\mathbf{R}_1,\mathbf{R}_2;\boldsymbol{\sigma}_1,\boldsymbol{\sigma}_2)\times\Psi_0(\mathbf{R}_1,\mathbf{R}_2;\boldsymbol{\sigma}_1,\boldsymbol{\sigma}_2)d\mathbf{R}_1d\mathbf{R}_2.$$

Carrying out the indicated isotopic spin operation and considering plane wave final states,

$$M^{TE}=\frac{1}{2\sqrt{2}}\left\langle T_m'\left|\frac{\{\theta_1+\theta_2\}}{(4EE')^{\frac{1}{2}}}\right|T_m\right\rangle\{a_++a_-\},$$

$$\theta_i=M_n^i+M_p^i.$$

In contrast to the case of M^{SE}, here transitions through TO intermediate states are not small and can proceed through the S-part of either the final or initial meson. If A and B are given the same definition as in the section on elastic scattering, then the differential cross section for transitions to TE final states is

$$\frac{d\sigma}{d\cos\alpha}=\frac{2N^2}{k}\int_0^{k'^{\max(\alpha)}}\frac{K}{E'}\{A^2+\tfrac{2}{3}B^2\}B^{\text{even}}\frac{k'^2dk'}{(4\pi)^2}.$$

SO

M^{SO} is identical to M^{TE} with Ψ_{TE}^* replaced by Ψ_{SO}^*. M^{SO} can therefore be written:

$$M^{SO}=\frac{1}{2\sqrt{2}}\left\langle S\left|\frac{\theta_1-\theta_2}{(4EE')^{\frac{1}{2}}}\right|T_m\right\rangle\{a_+-a_-\}.$$

The differential cross section for transitions to SO final states is then

$$\frac{d\sigma}{d\cos\alpha}=\frac{2N^2}{3k}\int_0^{k'^{\max(\alpha)}}\frac{K}{E'}B^{\text{odd}}B^2\frac{k'^2dk'}{(4\pi)^2}.$$

Transitions through SE intermediate states are possible by means of the P-part of one of the meson wave functions and the S-part of the other meson wave function. The P-part of one of the meson wave functions is needed for the transition from the initial to the intermediate SE state. However, the S-part of the wave function of the remaining meson is all that is needed for the transition from the SE intermediate state to the SO final state. Even though $B^{\text{even}}\sim 16B^{\text{odd}}$ for a 25-Mev meson, M^{SO} will be larger than M^{SE}.

TO

M^{TO} is identical to M^{SE} with Ψ_{SE}^* replaced by Ψ_{TO}^*. M^{TO} can therefore be written:

$$M^{TO}=\frac{1}{2\sqrt{2}}\left\langle T_m'\left|\frac{\theta_1'+\theta_2'}{(4EE')^{\frac{1}{2}}}\right|T_m\right\rangle\{a_+-a_-\}.$$

If A' is defined as that part of θ_i' which does not depend on $\boldsymbol{\sigma}$ and B' is defined as that part of θ_i' which does depend on $\boldsymbol{\sigma}$, then the differential cross section for transitions to TO final states is

$$\frac{d\sigma}{d\cos\alpha}=\frac{2N^2}{k}\int_0^{k'^{\max(\alpha)}}\frac{K}{E'}B^{\text{odd}}\{A'^2+\tfrac{2}{3}B'^2\}\frac{k'^2dk'}{(4\pi)^2}.$$

Destructive interference between the neutron and proton in addition to the small amplitude of the final nucleon states makes this transition small compared to the TE and SO transitions.

The angular distribution in the laboratory for the PS theories is shown in Fig. 2 for an incident 25-Mev meson. The total cross sections at this energy are

$$\sigma_{PS(PS)}=2.4\times10^{-27}\ (g^2/\hbar c)^2\ \text{cm}^2,$$

$$\sigma_{PS(PV)}=1.6\times10^{-26}\ (g^2/\hbar c)^2\ \text{cm}^2.$$

The effect of the distortion of the final state $n-p$ wave function is small. At 90°, the value of the cross

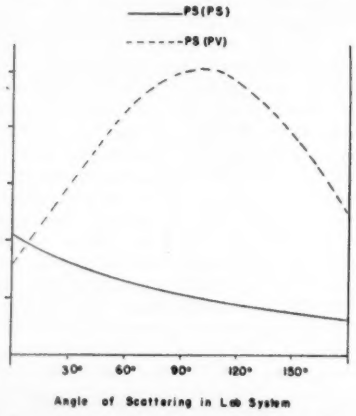

FIG. 2. Angular distribution in the laboratory system of π^+ mesons inelastically scattered from the deuteron. The kinetic energy of the incident meson is 25 Mev.

section is increased by approximately 2 percent over its value for plane wave final states. However, as is the case for those reactions in which a photon is the final state quantum, the distribution in energy of the final state meson at a given angle is greatly modified. Figure 3 shows the energy distribution for the final state meson for 90° scattering with and without taking into account the $n-p$ interaction. The small value of the meson energy half-width (2 Mev), in addition to the fact that the major transition is to *TE* final states, causes the inelastic scattering differential cross section to exhibit the same properties as the differential cross section for elastic scattering, in which the final state meson energy distribution is a delta-function at a given angle and in which the transition is solely to *TE* states.

The ratio of the cross section for elastic scattering to that for inelastic scattering is 1.5 for both couplings at 25 Mev. Both the energy distribution of the final state nucleons and the ratio of the elastic and inelastic cross sections are similar to those associated with the reactions $p+p\rightarrow\pi^+ +d$, $p+p\rightarrow\pi^+ +n+p$ which have been measured experimentally at a comparable meson energy.

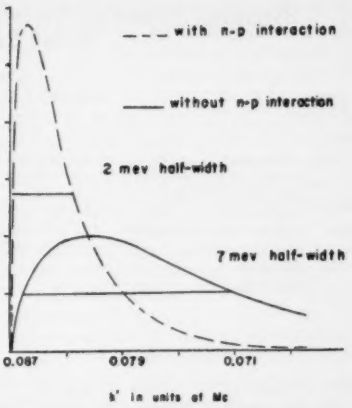

FIG. 3. Energy distribution of π^+ mesons inelastically scattered from the deuteron through 90°. The kinetic energy of the incident meson is 25 Mev. The effect of considering the interaction of the neutron and proton in the final state is shown.

DISCUSSION

Examination of the nonradiative absorption of a π^+ meson by the deuteron and the inverse reaction has made possible the determination of the spin of the π^+ meson. However, with our present knowledge of the deuteron wave function at small distances or, what is equivalent, the behavior of the nucleon-nucleon potential at small nucleon separations, the *PS* theory does not seem to be able to explain the large angular anisotropy[3] in the differential cross section for the nonradiative absorption reaction. In fact, assuming that the charged π-meson is *PS*, the differential cross section for the nonradiative absorption reaction suggests a method of investigating the extremely short-range properties of the $n-p$ and $p-p$ potentials. The radiative absorption reaction affords a method of choosing between the *PS* and *PV* theories for the charged π-meson since the behavior of the ratio $\sigma_{\text{nonradiative}}/\sigma_{\text{radiative}}$ is completely different for the two theories. This result is independent of the weak coupling theory and is based only on the form of the interaction operators for the two theories. The charge-exchange scattering reaction affords a method of investigating the charge-exchange scattering of a π^+ meson from a neutron, since the presence of the proton in the deuteron only restricts the number of states available to the final nucleons. The interference between the scattering of a π^+ meson from a neutron and from a proton is exhibited in the elastic and inelastic scattering of a π^+ meson by the deuteron. The theoretical cross sections for elastic and inelastic scattering from the deuteron at 25 Mev are comparable, and high energy for the final state meson is favored in the inelastic scattering reaction. This is in contrast to the experimental results[18] on the inelastic scattering of a π^+ meson from a more complex nucleus in which large energy transfers from the incident meson to the nucleus seem to be involved. In the case of the deuteron, the theoretical results predict low relative momenta for the final nucleons because of the strong interaction of the final state nucleons and the high Fourier amplitude for the low momentum components of the deuteron.

ACKNOWLEDGMENTS

The author wishes to thank Prof. R. E. Marshak for suggesting this problem and for his continued interest and guidance throughout the course of this work. He is also indebted to Dr. M. Kaplon and Mr. N. Francis for particular discussions.

[18] G. Bernardini, Phys. Rev. 82, 313 (1951).

Symmetry Effects on Nuclear Dipole Radiation with Application to a Bound Excited State of $_2He^4$*

LYNNE E. H. TRAINOR†
University of Minnesota, Minneapolis, Minnesota
(Received October 31, 1951)

The effect of nuclear symmetry properties on electric dipole transitions is investigated using the independent particle model and Wigner's theory of the symmetric Hamiltonian. Methods are given for the construction of completely symmetrized wave functions for the nuclear states on this model. Symmetry selection rules are found to operate, in addition to the usual selection rules, to reduce the amount of nuclear dipole radiation. A detailed study of the He^4 nucleus leads to the conclusion that if a resonant state at 21.6 Mev does exist with a strong dipole transition to the ground state, then a bound, excited state of the alpha-particle also exists. Spin-orbit and tensor forces are introduced to give a possible explanation of the angular distribution of gamma-rays when protons are captured by tritium.

I. INTRODUCTION

THE mechanism by which a nuclear structure absorbs or emits electromagnetic radiation is not well understood. Levinger and Bethe[1] proposed that results on nuclear absorption of betatron bremsstrahlung could be explained on the basis of single particle dipole transitions within alpha-particle subunits. But an entirely different model in which dipole absorption results from the antivibration of all neutrons as against all protons also gives general agreement.[2,3] For the present it appears that such experiments are insensitive tests of a nuclear model. The rather unexpected good agreement obtained with the individual particle model in the nuclear case[4] might be considered as good evidence that nuclear radiation is, to a good first approximation, produced by single particle transitions. Since nuclear forces are large, and since electric dipole moments require a separation of the nuclear center of charge from the nuclear center of mass, it is not surprising that the individual particle model considerably overestimates the transition probabilities for electric dipole radiation.

The present investigation assumes that radiative transitions are single particle transitions and that the energy states of light nuclei are classifiable according to Wigner's theory of the symmetric Hamiltonian.[5,6] This assumes a predominance of position dependent (Wigner and Majorana) forces. As a consequence of the symmetry properties of the nuclear states, the amount of electric dipole radiation is reduced according to certain symmetry selection rules. Introduction of spin and charge dependent forces results in a mixing of states of different symmetries, and the mode of description becomes less useful in the limit of large mixing. Where explicit use of wave functions is required, one needs a nuclear model. Since one is concerned here with radiative transitions and not with quantities such as binding energies which depend directly on particle correlations in the nucleus, the independent particle model[7] is used in conjunction with Wigner's theory. In many respects this is a matter of convenience since the essential results seem to depend only upon Wigner's theory and the assumption of single particle transitions, and not upon the explicit use of the independent particle model.

In Sec. II a discussion is given of the symmetry model used, and methods are developed for construction of the wave functions of nuclear states for this model. In Sec. III the nature of the electric dipole moment is considered and an important symmetry selection rule for dipole radiation is developed. The results of Secs. II and III are applied to the $_2He^4$ nucleus in Sec. IV.

II. NUCLEAR WAVE FUNCTIONS ON THE SYMMETRY MODEL

According to Wigner's theory the energy of a nuclear state is strongly dependent upon its symmetry character. In a first approximation one neglects Coulomb and spin-dependent forces as compared to forces depending on spatial coordinates alone. On the average antisymmetrically coupled particles are separated more than symmetrically coupled particles, and since nuclear forces are mostly attractive and of short range, one expects the energy to increase with the number of antisymmetric space couplings and to decrease with the number of symmetric space couplings. Each nucleon is assumed to explore the entire nucleus and each nucleon pair to contribute an average negative energy by mutual interaction. In addition to these ordinary forces, Majorana forces are assumed. A Majorana potential contains an operator which interchanges the space coordinates of two interacting particles. If the particles are symmetrically coupled in their space coordinates the

* Based on a thesis presented for the degree of Doctor of Philosophy at the University of Minnesota, September, 1951.
† Now under post-doctorate fellowship with the National Research Council of Canada, Ottawa, Canada.
[1] J. S. Levinger and H. A. Bethe, Phys. Rev. **78**, 115 (1950).
[2] M. Goldhaber and E. Teller, Phys. Rev. **74**, 1046 (1948).
[3] H. Steinwedel and J. Jensen, Phys. Rev. **79**, 1019 (1950).
[4] V. F. Weisskopf, Phys. Rev. **83**, 1073 (1951).
[5] E. Wigner, Phys. Rev. **51**, 106 (1937).
[6] E. Wigner, Phys. Rev. **51**, 947 (1937).
[7] G. Gamow and C. L. Critchfield, *Theory of Atomic Nucleus and Nuclear Energy-Sources* (Clarendon Press, Oxford, England, 1949).

total wave function retains its sign and the Majorana forces are attractive, but if the particles are antisymmetrically coupled in their space coordinates, the wave function changes sign and the Majorana forces are repulsive. For particle pairs that are neither symmetrically nor antisymmetrically coupled, the Majorana operator gives zero. Thus, if both ordinary and Majorana forces are corrected to take account of the greater average particle separation for antisymmetrically coupled pairs as compared to the symmetrically coupled pairs, the symmetry energy can be expressed as a negative constant times the difference in the number of symmetric and antisymmetric couplings.

In this approximation, nuclear wave functions will be classifiable according to their symmetry characters with respect to interchanges of spatial coordinates, in addition to classification according to total angular momentum, spin state, etc. Ground states of nuclei will be characterized by having the greatest possible number of symmetric couplings consistent with the Pauli exclusion principle and simultaneous minimization of the kinetic energies. Excited states correspond either to the use of higher kinetic energy states or to the use of states of less space symmetry, or to both. Because of the explicit dependence of energy upon the symmetry of nuclear states, states of definite energy will be described by wave functions of definite symmetry character in the space variables, or what is the same thing, by wave functions which belong to the irreducible representations of the symmetric group of order‡ A (the atomic mass number) with respect to interchanges of particle space coordinates. Since the total wave function is antisymmetric in the simultaneous interchange of all coordinates for any particle pair, it follows that the combined (ordinary and isotopic) spin function must belong to the associated irreducible representations of the symmetric group with respect to simultaneous interchanges of ordinary and isotopic spin coordinates. Thus the symmetry can be characterized in terms of the space symmetry alone, the spin symmetry being thereby fixed.

One is interested in the first few excited states of light nuclei. Ignoring the effect of symmetry on kinetic energy, the kinetic energies of these states on the present model will depend upon the nucleon distribution over independent particle states and will equal the sum of the independent energies.[8] The relative potential energies of nuclear states will depend upon their spatial symmetries. One does not know the energy separation of individual particle states, nor does one know the magnitude of the symmetry energy. Thus, the energy order of the possible excited states is not completely determined and appeal must be made to empirical evaluation from experimental results.

For any particular nucleus it is necessary to know first what symmetries can occur with a given distribution over space orbits, and second, what states can be formed with a given symmetry and distribution over space orbits. Nuclear wave functions must correspond to states of definite total angular momentum J and z component J_z. In the approximation of no spin-orbit coupling, these wave functions must also correspond to states of definite orbital momentum L and spin momentum S. A state is then completely specified by giving its J, J_z, S, L, T, and T_z values in addition to its symmetry classification; here T is the total isotopic spin quantum number.

A nuclear multiplet has both a definite ordinary spin multiplicity $2S+1$ and a definite isotopic spin multiplicity $2T+1$. The notation of Hund[9] is used here. Thus ^{32}B indicates a state with $T=2$ and $S=1$, where the letter B denotes a general orbital angular momentum term. For convenience, the four possible single particle spin-state wave functions are denoted by the boldface numbers **1**, **2**, **3**, and **4**:

1 corresponds to neutron, spin up,
2 corresponds to neutron, spin down,
3 corresponds to proton, spin up,
4 corresponds to proton, spin down.

The order in a series designating a product wave function gives the particle number. Thus **124** indicates the spin wave function in which particle one is in spin state **1**, particle two is in spin state **2**, and particle three is in spin state **4**, for a three-particle system. Though the methods of finding wave functions given here are general, particular attention is given to the four-particle nucleus since the results are to be applied to the alpha-particle.

A particular multiplet corresponds to a particular ordinary spin symmetry and a particular isotopic spin symmetry for a given nucleus. These may be combined in one or more ways to form one or more combined-spin symmetries, and correspondingly one or more space-wave symmetries. It is first necessary to know what space symmetries are possible for a given multiplet. One can then form general wave functions for multiplet terms of each possible space symmetry.

The possible combined-spin symmetries that can occur for a given multiplet may be found by determining which irreducible representations of the symmetric group are contained in the spin functions of the multiplet. For each multiplet it is necessary to consider only the highest term in the multiplet since the symmetry of spin wave functions is preserved under the operators which turn down ordinary and isotopic spins. For any particular multiplet only certain types of spin functions can occur in the highest term, *viz.*, those types with $S_z=S$ and $T_z=T$. Thus, for the four-particle

‡ Order, as used here, refers to the number of objects undergoing permutation, rather than to the number of permutations.

[8] In the center-of-mass system, only $A-1$ of the nucleons can be considered to contribute independently to the kinetic energy. The nonseparable part of the kinetic energy has been treated as a perturbation by D. R. Inglis, Phys. Rev. **51**, 534 (1937).

[9] F. Hund, Z. Physik **105**, 202 (1937).

TABLE I. Irreducible representations for four-particle spin functions.

Multiplets with $T \geqslant S$	Types of spin function occuring	Corresponding manifold of spin functions	Irreducible representations contained in manifold of spin functions
^{55}B	1111	(4)	[4]
^{53}B	1112	(3+1)	[4]+[3+1]
^{51}B	1122	(2+2)	[4]+[3+1]+[2+2]
^{53}B	1114	(3+1)	[4]+[3+1]
	1123	(2+1+1)	[4]+2[3+1]+[2+2] +[2+1+1]
^{51}B	1124	(2+1+1)	[4]+2[3+1]+[2+2] +[2+1+1]
	1223	(2+1+1)	[4]+2[3+1]+[2+2] +[2+1+1]
^{11}B	2233	(2+2)	[4]+[3+1]+[2+2]
	1144	(2+2)	[4]+[3+1]+[2+2]
	1234	(1+1+1+1)	[4]+3[3+1]+2[2+2] +3[2+1+1]+[1+1+1+1]

multiplet ^{51}B two types of spin function are possible, **1124** and **1223** since each has $S_z=0$ and $T_z=1$. The manifold (2+1+1) of 12 functions of the type **1124** contains several irreducible representations of the symmetric group of order 4, which can be found by means of formulas (22) and (23) of Wigner,[6]

$$(2+1+1)=[4]+2[3+1]+[2+2]+[2+1+1].$$

The same is true of the manifold (2+1+1) of 12 functions of the type **1223**. However, only those irreducible representations belong to the multiplet ^{51}B which do not belong to the $S_z=0$, $T_z=1$ terms of the higher 4-nucleon multiplets ^{53}B, ^{55}B, ^{53}B, ^{51}B, and ^{55}B. Tables I and II summarize the information and procedure for four-particle systems. The same procedure is applicable to systems with any number of particles. The x notation used in Table II has the advantage that as well as expressing the symmetries corresponding to the various irreducible representations of the symmetric group, it is convenient for forming the actual wave functions. The statement that a space wave function has the symmetry character $(\{xx\}_s xx)$ is equivalent to the statement that this wave function belongs to the irreducible representation [2+1+1] in which two of the four particles are symmetrically coupled. In this notation all symmetric couplings are explicitly indicated, whereas the appropriate antisymmetric couplings are implied, just as in the square bracket notation for irreducible representations. Only those multiplets with $T \geqq S$ have been listed in Tables I and II. Results for multiplets $^{\lambda\nu}B$ are identical with those for multiplets $^{\nu\lambda}B$ except for the transformations **2→3**, **3→2** in their spin functions.

In order to construct multiplet wave functions possessing definite symmetry for general terms it is convenient to consider each particle of the A nucleon system in a different space orbit since the manifold of functions consisting of products or sums of products of these orbital functions contain all irreducible representations of the symmetric group of order A. Since particles in the same orbit are symmetrically coupled in their space waves, two or more orbits in a set of symmetrically coupled orbits may later be considered to be identical without changing the symmetry properties of the wave function. For a particular multiplet it is necessary to construct only the wave function corresponding to the highest term in the multiplet since wave functions corresponding to lower terms can be obtained by using the infinitesimal rotation operators in ordinary spin space and isotopic spin space for "turning down" spins.

One can systematically form all wave functions for four-nucleon multiplets beginning with the highest possible multiplet by putting the requirements of proper symmetry of spin and space wave functions and total antisymmetry according to the Pauli principle on the most general linear combination of products of single particle spin and space wave functions, with the additional requirement that the resulting wave functions vanish when either the ordinary or isotopic spins are turned up. This is a rather cumbersome process. It is much simpler to note that if the symmetric couplings in spin and space functions are assured, then the required antisymmetric couplings are contained in the requirement of total antisymmetry according to the Pauli principle. The procedure can be best illustrated by an example. Suppose it is required to find the wave function for the ^{53}B multiplet with the space symmetry $(\{xx\}_s xx)$. Two types of spin function are possible, **4111** and **2113**, and the spin function must possess the associate symmetry $(x\{xxx\}_s)$. Using the letters a, b, c, and d to denote the four space orbit functions, and using the order in a product to denote the particle number, the required wave function can be expressed as a product of spin and space functions

$$(\{ab\}_s cd)(\mathfrak{C}_1(4\{111\}_s)+\mathfrak{C}_2(3\{112\}_s)+\mathfrak{C}_3(2\{113\}_s)),$$

where the symmetric couplings are to be expanded, e.g.,

$$(\{ab\}_s cd)=abcd+bacd,\ (3\{112\}_s)=3112+3121+3211.$$

The coefficients $\mathfrak{C}_1$, $\mathfrak{C}_2$, and $\mathfrak{C}_3$ are determined by requiring the wave function to vanish under the opera-

TABLE II. Allowed space symmetries for four-particle multiplets with $T \geqq S$.

Multiplet	Subtract irreducible representations belonging to	Irreducible representations remaining	Combined-spin symmetry	Associated space symmetry
^{55}B		[4]	$(\{xxxx\}_s)$	$(xxxx)$
^{53}B	^{55}B	[3+1]	$(\{xxx\}_s x)$	$(\{xx\}_s xx)$
^{51}B	^{55}B, ^{53}B	[2+2]	$(\{xx\}_s\{xx\}_s)$	$(\{xx\}_s\{xx\}_s)$
^{53}B	^{55}B, ^{53}B, ^{51}B	[4]	$(\{xxxx\}_s)$	$(xxxx)$
		[3+1]	$(\{xxx\}_s x)$	$(\{xx\}_s xx)$
		[2+2]	$(\{xx\}_s\{xx\}_s)$	$(\{xx\}_s\{xx\}_s)$
		[2+1+1]	$(\{xx\}_s xx)$	$(\{xxx\}_s x)$
^{51}B	^{55}B, ^{53}B, ^{51}B,	[3+1]	$(\{xxx\}_s x)$	$(\{xx\}_s xx)$
	^{53}B, ^{51}B	[2+1+1]	$(\{xx\}_s xx)$	$(\{xxx\}_s x)$
^{11}B	^{55}B, ^{53}B, ^{51}B, ^{51}B,	[4]	$(\{xxxx\}_s)$	$(xxxx)$
	^{11}B, ^{53}B, ^{51}B, ^{11}B	[2+2]	$(\{xx\}_s\{xx\}_s)$	$(\{xx\}_s\{xx\}_s)$
		[1+1+1+1]	$(xxxx)$	$(\{xxxx\}_s)$

tions of turning up ordinary and isotopic spins. This process yields $\mathcal{C}_1=2$, $\mathcal{C}_2=\mathcal{C}_3=-1$. Thus,

$$\begin{aligned}(\{ab\}_s cd)&[2(\mathbf{4111})-(3\{\mathbf{112}\}_s)-(2\{\mathbf{113}\}_s)]\\ &=(abcd+bacd)(2(\mathbf{4111})-\mathbf{3112}-\mathbf{3121}\\ &\qquad -\mathbf{3211}-\mathbf{2113}-\mathbf{2131}-\mathbf{2311})\\ &=2(a_4b_1c_1d_1+b_4a_1c_1d_1)-a_3b_1c_2d_1-b_3a_1c_2d_1\\ &\quad -a_3b_1c_1d_2-b_3a_1c_1d_2-a_2b_1c_1d_3-b_2a_1c_1d_3\\ &\qquad -a_2b_1c_3d_1-b_2a_1c_3d_1,\end{aligned}$$

where subscripts on space wave functions signify the product of the space function with the spin function indicated by the subscript. Thus, a_4 indicates the product of the space function $a(\mathbf{r})$ with the spin function representing a proton, spin down. The exclusion principle is automatically satisfied if one regards each of the above terms as representing the sum of the 24 product functions resulting from formal expansion of the appropriate determinant. For example,

$$a_4b_1c_1d_1\equiv\begin{vmatrix}a_4 & a_4 & a_4 & a_4\\ b_1 & b_1 & b_1 & b_1\\ c_1 & c_1 & c_1 & c_1\\ d_1 & d_1 & d_1 & d_1\end{vmatrix}=a_4b_1c_1d_1-a_4b_1d_1c_1+\text{etc.},$$

where the columns of the determinant are labeled according to particle number. From an assumed *ortho*-normalization of the space orbital functions, the complete normalization factor is $1/(16\times24)^{\frac{1}{2}}$.

The wave functions for maximum S_z and T_z for all four-particle multiplets with $T\geqq S$ are given in Table III in unexpanded form. The wave function for a multiplet ${}^{\lambda\tau}B$ may be obtained from the wave function of multiplet ${}^{r\lambda}B$ by the transformation of spin functions

$$\mathbf{2}\rightarrow\mathbf{3},\quad \mathbf{1}\rightarrow\mathbf{1},\quad \mathbf{3}\rightarrow\mathbf{2},\quad \mathbf{4}\rightarrow\mathbf{4}.$$

For a particular distribution of nucleons over individual particle orbital momentum states it is necessary to know what total angular momentum states can occur and with what symmetry. Hund[9] lists the results in several cases. A trivial example is given here since it will be used later. A more illustrative example is given in Appendix I. Consider the distribution of one p-wave and three s-wave nucleons, where a, b, and c are the p-wave orbital functions with $l_z=1$, 0 and -1, respectively, and s is the s-wave orbital function. The possible function manifolds are $(sssa)$, $(sssb)$, $(sssc)$, and each of these contains the $[4]$ and $[3+1]$ irreducible representations each once:

$$(3+1)=[4]+[3+1].$$

Both irreducible representations in the manifold $(sssa)$ must correspond to P-states of total orbital angular momentum with $L_z=1$. Likewise, the manifolds $(sssb)$ and $(sssc)$ contain the irreducible representations belonging to the $L_z=0$ and $L_z=-1$ components of these two P-states. This information in combination with the results of Table II yields Table IV.

The possible J values for a given distribution of nucleons over space orbits and a given symmetry follow from tables of the type of Table IV in conjunction with the vector coupling model for combining spins and orbital momenta. The wave functions for states of definite J value must be constructed by appropriate linear combinations of the wave functions (e.g., Table III) corresponding to a given multiplet and symmetry. Orbital functions a, b, c, etc., are identified to give the correct maximum J_z value, and the coefficients in the appropriate linear combination are determined by requiring the wave function to vanish under the operation of increasing the J_z value by one unit through the process of infinitesimal rotation. A state with a lower J_z value is obtained from the state of maximum J_z by infinitesimal rotation.

The unnormalized wave functions (in abbreviated form) corresponding to those states of ${}_2\mathrm{He}^4$ which arise from a four s-wave distribution and from a three s-wave, one p-wave distribution are given in Table V. The notation a, b, c for p-waves with $l_z=1$, 0, -1 is again used. Components with negative J_z values are obtained from those with positive J_z through the transformations

$$a\rightarrow c,\ c\rightarrow a,\ \mathbf{1}\rightarrow\mathbf{2},\ \mathbf{2}\rightarrow\mathbf{1},\ \mathbf{3}\rightarrow\mathbf{4},\ \mathbf{4}\rightarrow\mathbf{3}.$$

TABLE III. Wave functions for four-nucleon multiplets with $T\geqq S$.

Multiplet	Wave function
${}^{55}B(xxxx)$	$(abcd)(\mathbf{1111})$
${}^{52}B(\{xx\}_s xx)$	$(\{ab\}_s cd)(\mathbf{2111})$
${}^{51}B(\{xx\}_s\{xx\}_s)$	$(\{ab\}_s\{cd\}_s)(\mathbf{1212})$
${}^{50}B(xxxx)$	$(abcd)[(\{\mathbf{1123}\}_s)-3(\{\mathbf{1114}\}_s)]$
${}^{52}B(\{xx\}_s xx)$	$(\{ab\}_s cd)[2(\mathbf{4111})-(3\{\mathbf{112}\}_s)-(2\{\mathbf{113}\}_s)]$
${}^{50}B(\{xx\}_s\{xx\}_s)$	$(\{ab\}_s\{cd\}_s)(\mathbf{1312}+\mathbf{1213})$
${}^{50}B(\{xxx\}_s x)$	$(\{abc\}_s d)(\mathbf{1231})$
${}^{51}B(\{xx\}_s xx)$	$(\{ab\}_s cd)[(4\{\mathbf{112}\}_s)+3(2\{\mathbf{114}\}_s)+3(\mathbf{1}\{\mathbf{223}\}_s)+(3\{\mathbf{112}\}_s)]$
${}^{51}B(\{xxx\}_s x)$	$(\{abc\}_s d)(\mathbf{1232}+\mathbf{1421})$
${}^{51}B(xxxx)$	$(abcd)[(\{\mathbf{1234}\}_s)-2(\{\mathbf{2233}\}_s)-2(\{\mathbf{1144}\}_s)]$
${}^{51}B(\{xx\}_s\{xx\}_s)$	$(\{ab\}_s\{cd\}_s)(\mathbf{1441}+\mathbf{2332}+\mathbf{1234}+\mathbf{1324}+\mathbf{4231}+\mathbf{4321})$
${}^{51}B(\{xxxx\}_s)$	$(\{abcd\}_s)(\mathbf{1234})$

TABLE IV. Multiplets for a three s-wave, one p-wave distribution.

Space symmetry	Possible multiplets and orbital momentum states
$(\{xxxx\}_s)$	${}^{11}P$
$(\{xxx\}_s x)$	${}^{11}P_z$, ${}^{13}P_z$, ${}^{33}P$

III. SYMMETRY EFFECTS ON ELECTRIC DIPOLE RADIATION

The electric dipole moment for transition between an initial state $\Psi_0(\xi_1, \eta_1, \cdots, \zeta_A)$ and a final state $\Psi_f(\xi_1, \eta_1, \cdots, \zeta_A)$ of a nuclear system of atomic mass number A is given by

$$\frac{eh}{2m\omega}\int\Psi_f^*(\xi_1,\cdots,\zeta_A)\sum_{j=1}^{A}(1-\tau_{jz})\times_q\nabla_j\Psi_0(\xi_1,\cdots,\zeta_A)d\xi_1\cdots d\zeta_A, \quad (1)$$

TABLE V. Wave functions for lowest states of $_2He^4$.

State		Wave function
$^{11}S_0(\|xxxx\|_a)$	$J_z=0$	$(ssss)(1234)$
$^{11}P_1(\|xxxx\|_a)$	$J_z=1$	$(sssa)(1234-1243+4132-4231)$
	$J_z=0$	$(sssb)(1234-1243+4132-4231)$
$^{31}P_1(\|xxx\|_s x)$	$J_z=1$	$(sssa)(1432+1234+3421+1423)$
	$J_z=0$	$(sssb)(1432+1234+3421+1423)$
$^{13}P_2(\|xxx\|_s x)$	$J_z=2$	$(sssa)(1323+1431)$
	$J_z=1$	$\sqrt{2}(sssb)(1323+1431)+(sssa)(1423+1324+2431+1432)$
	$J_z=0$	$(sssc)(1323+1431)+(sssa)(1424+2432)+\sqrt{2}(sssb)(1423+1324+2431+1432)$
$^{13}P_1(\|xxx\|_a x)$	$J_z=1$	$\sqrt{2}(sssb)(1323+1431)-(sssa)(1423+1324+2431+1432)$
	$J_z=0$	$(sssc)(1323+1431)-(sssa)(1424+2432)$
$^{13}P_0(\|xxx\|_a x)$	$J_z=0$	$\sqrt{2}(sssc)(1323+1431)+\sqrt{2}(sssa)(1424+2432)-(sssb)(1423+1324+1432+2431)$
$^{33}P_2(\|xxx\|_s x)$	$J_z=2$	$(sssa)(1431+1233)$
	$J_z=1$	$\sqrt{2}(sssb)(1431+1233)+(sssa)(3241+1243+1432+1234)$
	$J_z=0$	$(sssc)(1431+1233)+(sssa)(3242+1244)+\sqrt{2}(sssb)(3241+1243+1432+1234)$
$^{33}P_1(\|xxx\|_a x)$	$J_z=1$	$(sssa)(3241+1243+1432+1234)-\sqrt{2}(sssb)(1431+1233)$
	$J_z=0$	$(sssa)(3242+1244)-(sssc)(1431+1233)$
$^{33}P_0(\|xxx\|_a x)$	$J_z=0$	$\sqrt{2}(sssa)(3242+1244)+\sqrt{2}(sssc)(1431+1233)-(sssb)(3241+1243+1432+1234)$

where $\mathbf{q}_j(\xi_j, \eta_j, \zeta_j)$ is the vector position of the jth particle in a fixed coordinate system, m is the nucleon mass (assumed to be equal for protons and neutrons), τ_{jz} is the z component of the isotopic spin vector for the jth particle, and ω is the frequency of the light quantum. The gradient operator ${}_q\nabla_j$ is taken with respect the coordinates (ξ_j, η_j, ζ_j) of the jth particle. One is concerned only with that part of the dipole moment which has to do with internal (center of mass) coordinates $\mathbf{r}_j(x_j, y_j, z_j)$. If x, y, z are the coordinates of the center of mass in the fixed system, one has the vector relations

$$\mathbf{q}_j=\mathbf{r}_j+\mathbf{r}, \quad j=1, 2, \cdots A, \tag{2}$$

and

$$\sum_{j=1}^{A}\mathbf{r}_j=0 \tag{3}$$

from which it follows that[10]

$$\sum_{j=1}^{A}(1-\tau_{jz})\,{}_q\nabla_j=\sum_{j=1}^{A}\left\{\frac{N}{A}(1-\tau_{jz})-\frac{Z}{A}(1+\tau_{jz})\right\}{}_r\nabla_j+\frac{4Z}{A}\nabla, \tag{4}$$

where ${}_r\nabla_j$ is taken with respect to the center-of-mass coordinates (x_j, y_j, z_j) of the jth particle and ∇ is taken with respect to the coordinates (x, y, z) of the center of mass. The last term on the right depends only on the coordinates of the center of mass and does not contribute to the internal electric moment. Since $A-1$ of the nucleons may be considered independent in the center-of-mass coordinates, one can transform the volume element $d\xi_1 d\eta_1 \cdots d\zeta_A$ into $A^3 dx_1 dy_1 \cdots dz_{A-1} dx dy dz$ where A^3 is the Jacobian of the transformation. Since the momentum of the photon is small the center-of-mass motion does not essentially change during the transition and one can write

$$\Psi_0(\xi_1, \eta_1, \cdots, \zeta_A)=\psi_0(x_1, y_1 \cdots, z_A)\phi(x, y, z),$$
$$\Psi_f(\xi_1, \eta_1, \cdots, \zeta_A)=\psi_f(x_1, y_1, \cdots, z_A)\phi(x, y, z).$$

Integrating (1) with a suitably normalized center-of-mass function ϕ over the volume element $dxdydz$ yields the internal dipole moment

$$\frac{eh}{2m\omega}\int\psi_f^*(x_1, y_1, \cdots, z_A)\sum_{j=1}^{A}\left\{\frac{N}{A}(1-\tau_{jz})-\frac{Z}{A}(1+\tau_{jz})\right\}$$
$$\times{}_r\nabla_j\psi_0(x_1, y_1, \cdots, z_A)dx_1dy_1\cdots dz_{A-1}$$

subject to the conditions (3),

$$=\frac{eh}{2m\omega}\int\psi_f^*(x_1, y_1, \cdots, z_A)\sum_{j=1}^{A}\left\{\frac{N}{A}(1-\tau_{jz})\right.$$
$$\left.-\frac{Z}{A}(1+\tau_{jz})\right\}{}_r\nabla_j\psi_0(x_1, y_1, \cdots, z_A)$$
$$\times\delta(\sum_{j=1}^{A}\mathbf{r}_j)dx_1dx_2\cdots dz_A, \tag{5}$$

where the conditions (3) are formally relaxed, but are expressed in the Dirac delta-function. By comparison of (1) and (5) it can be seen that in the center-of-mass system one can regard protons as possessing a charge eN/A and neutrons as possessing a charge $-eZ/A$.

Since the delta-function and the dipole operator are symmetric between all particle pairs, this exact expression can be used to investigate the effects of the symmetry of wave functions on the dipole moment. For the independent particle model the wave functions are products or sums of products of individual particle states and each particle contributes independently to the dipole moment. Independent contributions amount to relaxing the conditions imposed by the presence of the delta-function in (5). Since on this model each particle satisfies a separate Schrödinger equation, partial integration may then be carried out to yield the usual form of the dipole operator,

$$\frac{e}{2}\int\psi_f^*(x_1, y_1, \cdots, z_A)\sum_{j=1}^{A}\left\{\frac{N}{A}(1-\tau_{jz})-\frac{Z}{A}(1+\tau_{jz})\right\}$$
$$\times\mathbf{r}_j\psi_0(x_1, y_1, \cdots, z_A)dx_1\cdots dz_A. \tag{6}$$

In addition to the usual selection rules for electric dipole radiation which have to do with the space and ordinary spin functions in the initial and final states,

[10] H. A. Bethe, Revs. Modern Phys. 9, 69 (1937).

there are certain selection rules having to do with the isotopic spin functions in the present symmetry model. Of particular interest here is the important selection rule for nuclei with equal proton number Z and neutron number N which states that the electric dipole moment vanishes between a state of isotopic spin multiplicity λ and all other states with multiplicity $\lambda\pm 4n$ where n is a positive integer or zero. This can be seen in the following way.

For an antisymmetric coupling in the isotopic spin function, the operator $\tau_{1x}\cdot\tau_{2x}$ (where 1, 2 denote particle numbers) which transforms a neutron into a proton and vice versa, changes the sign of the wave function for an antisymmetric neutron-proton pair,

$$\tau_{1x}\tau_{2x}[\xi(1)\eta(2)-\eta(1)\xi(2)]=-[\xi(1)\eta(2)-\eta(1)\xi(2)],$$

but it does not change the sign for a symmetric neutron-proton pair,

$$\tau_{1x}\tau_{2x}[\xi(1)\eta(2)+\eta(1)\xi(2)]=[\xi(1)\eta(2)+\eta(1)\xi(2)].$$

Under transformation of all protons into neutrons and neutrons into protons, the total wave function is preserved if the number of antisymmetric couplings is even, but changes sign if this number is odd.

Since there are only two isotopic spin states, the distribution of particles over isotopic spin states is limited to two summands $(N+Z)$, and the corresponding manifold of isotopic spin functions does not contain all irreducible representations of the symmetric group of order $A=N+Z$. Those irreducible representations which are contained are only contained once, and quite generally,[11,12]

$$(N+Z)=[A]+[(A-1)+1]+[(A-2)+2]+\cdots+[N+Z]$$

for $N\geqq Z$. For $N\leqq Z$ the last irreducible representation is $[Z+N]$. For a symmetry partition $[(A-n)+n]$ the number of symmetric couplings in the corresponding wave function is $\frac{1}{2}(A-n)(A-n-1)+\frac{1}{2}n(n-1)$ and the number of antisymmetric couplings is just the number of symmetric couplings in the adjoint partition $[2+2+\cdots+2+1+\cdots+1]$, where there are n two's and $A-2n$ one's. It follows that the number of antisymmetric couplings in the wave functions corresponding to partition $[(A-n)+n]$ is just n.

It follows from the foregoing discussion that the operation of changing neutrons into protons and vice versa reverses the sign of the wave functions belonging to isotopic spin multiplicities $A-1$, $A-5$, $A-9$, etc., but leaves invariant the wave functions belonging to multiplicities $A+1$, $A-3$, $A-7$, etc. Consider the electric moment in either the exact form (5) or in the approximate form (6), say the latter. For $N=Z$,

$$\frac{e}{2}\int\psi_f^*(x_1,\cdots,z_A)\sum_{j=1}^{A}\left\{\frac{N}{A}(1-\tau_{jz})-\frac{Z}{A}(1+\tau_{jz})\right\}\times\tau_j\psi_0(x_1,\cdots,z_A)dx_1\cdots dz_A$$

$$=\frac{-e}{2}\int\psi_f^*(x_1,\cdots,z_A)\sum_{j=1}^{A}\tau_{jz}\tau_j\psi_0(x_1,\cdots,z_A)\times dx_1\cdots dz_A=\kappa\text{ (a number)}$$

$$=\frac{-e}{2}\int\psi_f^*(x_1,\cdots,z_A)\tau_{1z}^2\cdot\tau_{2z}^2\cdots\tau_{Az}^2\times\sum_{j=1}^{A}\tau_{jz}\tau_j\psi_0(x_1,\cdots,z_A)dx_1\cdots dz_A$$

$$=\frac{e}{2}\int\{\tau_{1z}\cdot\tau_{2z}\cdots\tau_{Az}\psi_f(x_1,\cdots,z_A)\}^*\times\sum_{j=1}^{A}\tau_{jz}\tau_j\{\tau_{1z}\cdot\tau_{2z}\cdots\tau_{Az}\psi_0(x_1,\cdots z_A)\}dx_1\cdots dz_A,$$

$$=\mp\kappa,$$

where the minus sign applies if $\psi_0(x)$ and $\psi_f(x)$ both change sign or both do not change sign under the operation of transforming protons into neutrons and vice versa, and the plus sign applies if one changes sign and the other does not. Use has been made of the commutivity of τ_{kz} and τ_{jz} for $j\neq k$, the anticommutivity for $j=k$, and of the property $\tau_{jz}^2=1$. If the minus sign applies, κ must be zero and the theorem as stated above is proven.

IV. APPLICATION OF THE SYMMETRY MODEL TO $_2He^4$

(a) A Bound Excited State of $_2He^4$

The experimental work on the $T(p,\gamma)He^4$ reaction by the Los Alamos group,[13] supported by their $T(p,n)He^3$ results,[14] indicates a possible excited state of the He^4 nucleus which can reach the ground state by the emission of a 21.6-Mev dipole gamma-ray. Flowers and Mandl[15] explain the Los Alamos results as nonresonant radiation from the capture of p-wave protons on tritium. However, these authors do not use completely symmetrized wave functions. Benveniste and Cork[16] placed an upper limit of 3×10^{-27} cm^2 for the reaction $He^4(p,p')He^{4*}$ at 45°, using the scattering of 31-Mev protons on helium. This upper limit is just below the resonant cross section reported by the Los

[11] F. D. Murnaghan, *The Theory of Group Representations* (Johns Hopkins Press, Baltimore, 1938).
[12] E. Wigner, *Gruppentheorie und ihre Anwendung auf die Quantenmechanik der Atomspektren* (Edward Brothers, Inc., Ann Arbor, 1944).
[13] Argo, Gittings, Hemmendinger, Jarvis, and Taschek, Phys. Rev. **78**, 691 (1950).
[14] Jarvis, Hemmendinger, Argo, and Taschek, Phys. Rev. **79**, 929 (1950).
[15] B. H. Flowers and F. Mandl, Proc. Roy. Soc. (London) **206**, 131 (1951).
[16] J. Benveniste and B. Cork, Phys. Rev. **83**, 894 (1951).

Alamos group. Falk and Phillips[17] extended the Los Alamos work up to 3.4-Mev proton energy. They find that the $p-\gamma$ cross section continues to rise beyond the 2.6-Mev resonance predicted by the Los Alamos group, and in general agreement with the theoretical work of Flowers and Mandl. They do not rule out a broad resonance superimposed on the rising nonresonant cross section. The rise rate of the cross section with proton energy is much less rapid than that obtained by the Los Alamos group—perhaps a point in favor of the latter since there are more experimental errors tending to depress the rise rate than to increase it.[18] Gaerttner and Yeater,[19] using γ-radiation from the 100-Mev betatron, find a maximum proton production from the photodisintegration of helium in the region of 27-Mev proton energy, but the results are not sufficiently good to indicate or rule out the presence of a resonance at a gamma-ray energy of 21.6 Mev. A phase shift analysis[18] of the results of Claassen *et al.*[20] for the inelastic scattering of protons on tritium are not in contradiction with a resonant ^1P-state of $_2\mathrm{He}^4$, although the data makes a unique interpretation difficult.

An excited state of the alpha-particle still seems to be an open question. As will be shown, no radiative transitions can occur from the first excited state to the ground state on the model used here. If a resonant state does exist which has a strong electric dipole transition moment to the ground state, it corresponds to the second excited state of this model in which case the first excited state is bound. An alternative is to regard the two excited states of the model as strongly coupled by spin-orbit or other forces.

Since the p-wave protons captured by tritium have no orbital angular momentum about the incident direction (z axis), only the following states of the compound nucleus are formed:

$$\begin{aligned} &^1P_1, \quad J_z=0 \\ &^3P_0, \quad J_z=0 \\ &^3P_1, \quad J_z=\pm 1, 0 \\ &^3P_2, \quad J_z=\pm 1, 0. \end{aligned}$$

Since the experimental angular distribution of gamma-rays is $\sin^2\theta$, and the cross section for the $p-\gamma$ reaction is large, the transition must be $^1P_1 \rightarrow {}^1S_0$. Using the Breit-Wigner single resonance formula, and the Los Alamos values of $\sigma_{res}=10^{-27}$ cm^2 at a proton energy $E=2.6$ Mev and half-width $\Gamma=1$ Mev, one obtains for the gamma-width,

$$\Gamma_\gamma \sim 1000(1+G)/G \text{ electron volts},$$

where G is the Gamow penetrability factor for the protons at this energy. Interpreted in terms of the formula for spontaneous emission probability

$$\Gamma_\gamma/\hbar = 4\omega^3(ez)^2/3\hbar c^3,$$

where ω is the frequency of the radiation, and z an effective length in the dipole moment (ez), one obtains a value of z equal to the radius of the alpha-particle within a factor of 2 or 3. This dipole moment is of the the same order of magnitude as that for a dipole moment between the $1s$ and $2p$ orbits of the individual particle model.

On the present model the ground state of the alpha-particle is $^1S_0(\{xxxx\}_s)$, and excited states correspond to promoting particles to higher individual orbits. The resulting states for four s-wave nucleons and for one p-wave and three s-wave nucleons are given in Table V, together with the corresponding wave functions. The energy difference between the $^1S_0(\{xxxx\}_s)$ state and the $^1P_1(\{xxxx\}_s)$ state is just equal to the energy difference of $1s$ and $2p$ orbits on the individual particle model, while the $^1P_1(\{xxxx\}_s)$ state is separated from the remaining (degenerate) P states of Table V by $4U$, where U is the symmetry energy associated with one less symmetric coupling or one more antisymmetric coupling.

Application of the theorem of Sec. III on combining isotopic spin multiplicities gives the result that the transition dipole moment vanishes for the transition $^1P_1(\{xxxx\}_s) \rightarrow {}^1S_0(\{xxxx\}_s)$. Hence, it is necessary to interpret the observed resonant state as the higher $^1P_1(\{xxx\}_s x)$. This result is more general than might first appear. The theorem of Sec. III still applies if one replaces the space part of the $^1S_0(\{xxxx\}_s)$ wave function by any function $f(\mathbf{r}_1, \mathbf{r}_2, \mathbf{r}_3, \mathbf{r}_4)$ which is completely symmetric in the space coordinates, and if one further replaces the space part of the $^1P_1(\{xxxx\}_s)$ wave function by $q(\mathbf{r}_i, \mathbf{r}_j, \mathbf{r}_k)a(\mathbf{r}_l)$, where q is any function completely symmetric in the space coordinates of the particles taken three at a time, and $a(\mathbf{r}_l)$ is the p-wave individual particle state. This removes the strong objection to the wave functions of Table V, that for several particles in the same s-wave, the positions will be highly correlated and the individual particle model a poor approximation. Although one can say little about the magnitude of the symmetry energy $4U$, it must be at least several Mev[21] and since the neutron threshold is roughly 20 Mev, one is forced to interpret the $^1P_1(\{xxxx\}_s)$ state as a bound, excited state of the alpha-particle.[22]

(b) Angular Distributions in the $\mathrm{T}(p,\gamma)\mathrm{He}^4$ Reaction

The experimental angular distribution of proton capture gamma-rays[12] is nearly pure $\sin^2\theta$, but a small amount of what is probably $1+\cos^2\theta$ is present. Since

[17] C. E. Falk and G. C. Phillips, Phys. Rev. **83**, 468 (1951).
[18] G. Breit, private communication.
[19] E. R. Gaerttner and M. L. Yeater, Phys. Rev. **83**, 146 (1951).
[20] Claassen, Brown, Freier, and Stratton, Phys. Rev. **82**, 589 (1951).
[21] W. H. Barkas, Phys. Rev. **55**, 691 (1939).
[22] H. A. Bethe and R. F. Bacher, Revs. Modern Phys. **8**, 83 (1937).

only the $J_z=0$ component of the $^1P_1$ state is formed in the capture process, one requires spin-orbit forces (or some other type of coupling) to mix the $^1P_1$ and $^3P_1$ states in order to account for the $1+\cos^2\theta$ admixture. The decided change in the angular distribution with incident proton energy suggests further that two Breit-Wigner resonances are competing in the capture process. To account for these results, both spin-orbit and tensor forces are introduced here. The spin-orbit operator for the independent particle approximation is taken to be

$$\Omega\sum_{j=1}^{A}\boldsymbol{\sigma}_j\cdot\mathbf{L}_j, \tag{7}$$

where $\boldsymbol{\sigma}_j$ and $\mathbf{L}_j$ are the Pauli vector and angular momentum operator for the jth particle, and Ω is a parameter to be evaluated. The tensor operator is taken to be

$$\textstyle\sum_{j,k}U_{jk}=\sum_{j,k}J(r_{jk})S_{jk}, \tag{8}$$

where the summation goes over all particle pairs, $\mathbf{r}_{jk}$ is the vector joining the jth and the kth particles, and

$$S_{jk}=[3(\boldsymbol{\sigma}_j\cdot\mathbf{r}_{jk})(\boldsymbol{\sigma}_k\cdot\mathbf{r}_{jk})-(\boldsymbol{\sigma}_j\cdot\boldsymbol{\sigma}_k)r_{jk}^2]/r_{jk}^2. \tag{9}$$

The assumptions are made that significant tensor coupling occurs only between the s-waves and the p-wave, and that each s-wave dipole source is located at the center of mass.

Using expressions (7), (8), and (9) and the wave functions in Table V, one finds that the spin-orbit operator can be diagonalized within the set of functions in Table V while the tensor operator couples in higher states. This coupling is assumed small because of the wide energy separation, and is disregarded. The resulting mixed states and their energy values are

$$\psi_1=(^3P_1+\mathfrak{A}\,^1P_1)/(\mathfrak{A}^2+1)^{\frac{1}{2}},\quad E_1=E''+\kappa+K \tag{10a}$$

$$\psi_2=(\mathfrak{A}\,^3P_1-{}^1P_1)/(\mathfrak{A}^2+1)^{\frac{1}{2}},\quad E_2=E''+\kappa-K \tag{10b}$$

$$\psi_3=(\mathfrak{B}\,^1P_1+{}^3P_1)/(\mathfrak{B}^2+1)^{\frac{1}{2}},\quad E_3=E'+\delta+(\delta^2+\epsilon^2)^{\frac{1}{2}} \tag{10c}$$

$$\psi_4=(^1P_1-\mathfrak{B}\,^3P_1)/(\mathfrak{B}^2+1)^{\frac{1}{2}},\quad E_4=E'+\delta-(\delta^2+\epsilon^2)^{\frac{1}{2}} \tag{10d}$$

while the nonmixed states are

$$^1S_0, \text{ with energy } E_0, \tag{11a}$$

$$^3P_2 \text{ and } {}^3P_2, \text{ with energy } E''-(4\epsilon/5\sqrt{2})-(2\kappa/5), \tag{11b}$$

$$^3P_0 \text{ and } {}^3P_0, \text{ with energy } E''+(4\epsilon/\sqrt{2})-4\kappa, \tag{11c}$$

where E' is the energy of the $^1P(\{xxxx\}_s)$ state and E'' the energy of the remaining degenerate $P(\{xxx\}_s x)$ states of Table V. Also,

$$\epsilon=\sqrt{2}\Omega,\quad 2\kappa=-\Omega+2U_t,\quad K=(\kappa^2+\epsilon^2)^{\frac{1}{2}},\quad \delta=\kappa+\tfrac{1}{2}(E''-E'), \tag{12}$$

where Ω is the spin-orbit parameter, and U_t is the tensor parameter which represents the value of $J(r)$ in expression (8) integrated over the radial variable in a p-wave. The mixture constants $\mathfrak{A}$, $\mathfrak{B}$ are related to these paramaters through

$$\mathfrak{A}=\epsilon/(K-\kappa),\quad \mathfrak{B}=[(\delta^2+\epsilon^2)^{\frac{1}{2}}-\delta]/\epsilon. \tag{13}$$

All of the states listed above remain degenerate with respect to their J_z values. All parameters, except for the unknown positive energy differences $E'-E_0$ and $E''-E'$, are expressible in terms of the basic parameters Ω and U_t.

The only states contributing to electric dipole transitions to ground are the mixed states ψ_1 and ψ_2 by virtue of the presence of the $^3P_1$ terms. The amount that each state contributes will depend upon the value of $\mathfrak{A}$ and the coupling to the incident proton wave. The amount of $1+\cos^2\theta$ depends upon the $^3P_1$ terms supplying $J_z=\pm1$ values to the $^3P_1$ term. If $\mathfrak{A}$ is either large or small compared to unity, the radiation from ψ_1 or ψ_2 will dominate.

The differential (p,γ) cross section is given by Bethe[10]

$$\begin{aligned}\sigma_\gamma{}^p(\theta)&=\sum_{m=-1}^{1}\sigma_{\gamma,(m)}{}^p(\theta)\\&=\sum_{m=-1}^{1}4\pi^3\lambda^2\sum_{r=1}^{2}\left|\frac{H_{r,(m)}{}^pH_\gamma{}^{r,(m)}}{E-E_r+i\gamma_r}\right|^2,\end{aligned} \tag{14}$$

where λ is the reciprocal wave number of the incident protons, E their energy, E_r is rth resonant energy and γ_r the half-width of the rth resonance. $H_{r,(m)}{}^p$ is the matrix element connecting the initial state χ [p-wave part of the incident plane wave protons plus tritium in the ground $^2S_{\frac{1}{2}}(\{xxx\}_s)$ state] with the $J_z=m$ component of the rth resonant state $\psi_r{}^{(m)}$ of the compound nucleus. $H_\gamma{}^{r,(m)}$ is the electromagnetic interaction matrix describing the electric dipole transition from the resonant state $\psi_r{}^{(m)}$ to the ground state φ_0 of helium [i.e., to the $^1S_0(\{xxxx\}_s)$ state] with the emission of a light quantum with z component of angular momentum equal to $-m$.

$H_{r,(m)}{}^p$ consists of two factors—one is the projection $(\chi,\psi_r{}^{(m)})$ which tells how much of $\psi_r{}^{(m)}$ is represented in the initial state χ, and the second is the interaction matrix $W_r{}^p$ which determines the transition probability for formation of a compound state, and therefore the level width for proton capture by tritium,

$$\begin{aligned}2\pi|H_{r,(m)}{}^p|^2&=(\chi^{(m)},\psi_r{}^{(m)})^2G(E)\Gamma_r{}^p\\&=2\pi(\chi^{(m)},\psi_r{}^{(m)})^2|W_r{}^p|^2,\end{aligned}$$

where $G(E)$ is the Gamow penetrability factor and $\Gamma_r{}^p$ the intrinsic proton width for the rth resonance level. In $H_{r,(m)}{}^p$ the incident proton wave must be normalized per unit energy range.

The $^2S_{\frac{1}{2}}(\{xxx\}_s)$ ground state of tritium has two J_z states with wave functions

$$s_1s_2s_3 \text{ for } J_z=\tfrac{1}{2},\quad s_1s_2s_4 \text{ for } J_z=-\tfrac{1}{2} \tag{15}$$

which combine with the p-wave protons to form triplet and singlet states

$$\begin{aligned}
&{}^1\chi^{(0)}=(24)^{-\frac{1}{2}}\{s_1s_2s_3b_4-s_1s_2s_4b_3\},\\
&{}^3\chi^{(1)}=(12)^{-\frac{1}{2}}\{s_1s_2s_3b_3\},\\
&{}^3\chi^{(0)}=(24)^{-\frac{1}{2}}\{s_1s_2s_3b_4+s_1s_2s_4b_3\},\\
&{}^3\chi^{(-1)}=(12)^{-\frac{1}{2}}\{s_1s_2s_4b_4\},
\end{aligned}\tag{16}$$

where a factor $1/\sqrt{3}$ has been included to transform the p-wave part of the incident plane wave to a normalized individual particle state b.[23] The further factors of $1/\sqrt{4}$ or $1/\sqrt{8}$ ensure normalization of the total incident wave. Each term in (16) is again a 4×4 determinant of functions with normalization $1/\sqrt{24}$. Using relations (15) and (16) and the wave functions of Table V, the appropriate transformation coefficients can be calculated.

The wave functions in $H_\gamma^{r,(m)}$ for the final state (helium ground state plus gamma-ray) must also be normalized per unit energy interval. Thus

$$|H_\gamma^{r,(m)}|^2=|W_\gamma^{r,(m)}|^2\rho(\hbar\omega),$$

where $\rho(\hbar\omega)$ is the number of final states per unit energy per unit solid angle,

$$\rho(\hbar\omega)=(\hbar\omega)^2/(2\pi\hbar c)^3,$$

ω is the angular frequency of the emitted radiation, and $W_\gamma^{r,(m)}$ is the dipole interaction matrix

$$i(4\pi^2\hbar\omega)^{\frac{1}{2}}\int\psi_r^{(m)*}\hat{e}\cdot\sum_{j=1}^{A}e_jx_j\varphi_0.$$

Here $\hat{e}$ is the unit vector in the polarization direction and e_j the effective charge on the jth nucleon. Setting

$$D=\int{}^{31}P_1^{(0)*}\sum_{j=1}^{A}e_jx_j\varphi_0dx_1\cdots dx_A,$$

one obtains after some calculation,

$$\begin{aligned}
\sigma_\gamma^p(\theta)=\mathcal{K}\mathfrak{A}^2&\left\{\frac{\Gamma_1^p}{(E-E_1)^2+\gamma_1^2}+\frac{\Gamma_2^p}{(E-E_2)^2+\gamma_2^2}\right.\\
&\left.-\frac{2(\Gamma_1^p\Gamma_2^p)^{\frac{1}{2}}((E-E_1)(E-E_2)+\gamma_1\gamma_2)}{((E-E_1)^2+\gamma_1^2)((E-E_2)^2+\gamma_2^2)}\right\}\left(\frac{1+\cos^2\theta}{2}\right)\\
+\mathcal{K}&\left\{\frac{\Gamma_1^p}{(E-E_1)^2+\gamma_1^2}+\frac{\mathfrak{A}^4\Gamma_2^p}{(E-E_2)^2+\gamma_2^2}\right.\\
&\left.+\frac{2(\Gamma_1^p\Gamma_2^p)^{\frac{1}{2}}\mathfrak{A}^2((E-E_1)(E-E_2)+\gamma_1\gamma_2)}{((E-E_1)^2+\gamma_1^2)((E-E_2)^2+\gamma_2^2)}\right\}\sin^2\theta,
\end{aligned}\tag{17}$$

where

$$\begin{aligned}
\mathcal{K}&=4\pi^2\lambda^2G(E)\rho(\hbar\omega)\hbar\omega D^2/48(\mathfrak{A}^2+1)^2\\
&=\lambda^2G(E)\Gamma_\gamma/128(\mathfrak{A}^2+1)^2,
\end{aligned}$$

and Γ_γ is the radiation width $4\omega^3D^2/3c^3$.

For $\mathfrak{A}\to0$ (no spin-orbit coupling) the distribution is pure $\sin^2\theta$. If the levels E_1 and E_2 are not too far apart, so that one can neglect the difference between singlet and triplet levels in so far as partial proton widths and total widths are concerned, $\sigma_\gamma^p(\theta)$ simplifies to

$$\begin{aligned}
\sigma_\gamma^p(\theta)=\frac{\lambda^2\Gamma_\gamma\Gamma_p}{128(\mathfrak{A}^2+1)^2}&\left[\left\{\frac{1}{x^2+\Gamma^2}+\frac{\mathfrak{A}^4}{y^2+\Gamma^2}\right.\right.\\
&\left.+\frac{2\mathfrak{A}^2(xy+\Gamma^2)}{(x^2+\Gamma^2)(y^2+\Gamma^2)}\right\}\sin^2\theta+\mathfrak{A}^2\left\{\frac{1}{x^2+\Gamma^2}\right.\\
&\left.\left.+\frac{1}{y^2+\Gamma^2}-\frac{2(xy+\Gamma^2)}{(x^2+\Gamma^2)(y^2+\Gamma^2)}\right\}\left(\frac{1+\cos^2\theta}{2}\right)\right],
\end{aligned}\tag{18}$$

where $x=E-E_1$, $y=E-E_2$, Γ is a mean value of γ_1 and γ_2, and Γ_p is $G(E)$ times a mean value of the intrinsic widths Γ_1^p and Γ_2^p.

Letting R be the intensity ratio of $\sin^2\theta$ to $1+\cos^2\theta$ radiation at any energy, one obtains from (18)

$$\tfrac{1}{2}x_0^2\mathfrak{A}^2R=(\mathfrak{A}^2+1)\{(\mathfrak{A}^2+1)x^2+2xx_0+\Gamma^2\}+x_0^2.\tag{19}$$

Here x_0 is the level separation E_1-E_2. Assuming $\mathfrak{A}^2\ll1$, then ψ_1 is the observed resonant state, and one obtains experimentally[18]

$$\begin{aligned}
&R=24 \quad \text{when } x=-0.34 \text{ Mev},\\
&R=18.6 \text{ when } x=-0.98 \text{ Mev},\\
&\Gamma=1 \text{ Mev}.
\end{aligned}\tag{20}$$

TABLE VI. Energy levels of $_2He^4$.

State	Level energy in Mev, Solution one	Solution two, $\Delta=6$ Mev	$\Delta=9$ Mev	$\Delta=12$ Mev
${}^{11}S_0$	0	0	0	0
$\dfrac{{}^{11}P_1-\mathfrak{B}{}^{13}P_1}{(\mathfrak{B}^2+1)^{\frac{1}{2}}}$	$21.5-\Delta$	14.3	11.8	8.9
$\dfrac{\mathfrak{B}{}^{11}P_1+{}^{13}P_1}{(\mathfrak{B}^2+1)^{\frac{1}{2}}}$	20.8	17.4	16.9	16.7
$\dfrac{\mathfrak{A}{}^{21}P_1-{}^{23}P_1}{(\mathfrak{A}^2+1)^{\frac{1}{2}}}$	20.7	16.1	16.1	16.1
$\dfrac{{}^{21}P_1+\mathfrak{A}{}^{23}P_1}{(\mathfrak{A}^2+1)^{\frac{1}{2}}}$	21.6	21.6	21.6	21.6
${}^{13}P_2$ and ${}^{23}P_2$	21.5	21.4	21.4	21.4
${}^{13}P_0$ and ${}^{23}P_0$	23.6	34.6	34.6	34.6

[23] See reference 7, page 252.

If $\mathfrak{A}^2 \ll 1$, Eq. (19) reduces to

$$\tfrac{1}{2}(x_0^2 \mathfrak{A}^2 R) = (x+x_0)^2 + \Gamma^2. \tag{21}$$

This approximation is justified if the value of $\mathfrak{A}^2$ so obtained does satisfy the condition $\mathfrak{A}^2 \ll 1$. Putting values (20) into Eq. (21), one obtains two possible solutions for the parameters x_0 and $\mathfrak{A}$, and correspondingly for the parameters ϵ, Ω, κ, and U_t:

Solution one	$x_0 = 0.89$ Mev	$\mathfrak{A}^2 = 0.14$
	$\epsilon = 0.29$ Mev	$\kappa = -0.34$ Mev
	$\Omega = -0.20$ Mev	$U_t = -0.44$ Mev.
Solution two	$x_0 = 5.5$ Mev	$\mathfrak{A}^2 = 0.075$
	$\epsilon = 1.4$ Mev	$\kappa = -2.36$ Mev
	$\Omega = -0.99$ Mev	$U_t = -2.85$ Mev.

In both cases, $\mathfrak{A}^2 \ll 1$ and the above approximation is justified. Since ψ_1 is predominant, it must be identified with the experimental resonance and its energy set equal to 21.6 Mev. Aside from the value $\Delta = E'' - E'$, the various energy levels are now fixed. The results are given in Table VI (for assumed values of Δ).

Since the neutron threshold is 20 Mev and since one would certainly not expect the symmetry energy Δ to be less than 6 Mev, solution one predicts a single bound, excited state of the alpha-particle and solution two predicts three such. Although one does not know enough about nuclear forces to distinguish between the two solutions on the basis of the predicted values of the spin-orbit and tensor parameters, the splitting of levels is probably more reasonable for solution one. More extensive angular distribution studies would distinguish between the solutions, or rule both out.

V. CONCLUDING REMARKS

A bound excited state of the alpha-particle remains an open question. If an excited state does exist at 21.6 Mev with a strong dipole transition moment to the ground state, then a bound excited state seems certain on the basis of symmetry arguments. The incident wave used by Flowers and Mandl[18] corresponds to an equal mixture of the $^{11}P_1$ and $^{31}P_1$ states of the compound nucleus, and since the $^{11}P_1$ state has a considerably lower energy it ought to couple in more strongly than the $^{31}P_1$ state, and therefore reduce the nonresonant cross section. Experimental work is not sufficiently extensive and precise to rule out alternative explanations.

The more general question of symmetry effects on dipole radiation transition probabilities should be mentioned.[34] A few direct calculations of dipole moments indicate that additional selection rules having to do with the symmetry properties of wave functions exist in addition to the selection rule proved in Sec. III and the usual selection rules for dipole radiation. As one proceeds to more complex nuclei, the symmetry is likely to be much more complex due to increased number of particles and to increased effect of Coulomb and other forces. Actual wave functions can then be expressed as linear superpositions of functions with definite symmetry properties. The symmetry selection rules still hold between these symmetry functions, in general reducing the amount of dipole radiation between actual nuclear states.

In conclusion the author would like to express his sincerest thanks to Professor C. L. Critchfield for his encouragement and guidance during the course of this work.

TABLE VII. Multiplets for a three p-wave distribution.

Space symmetry	Possible multiplets
$(\{xxx\}_a)$	^2F, ^2P
$(\{xx\}_s x)$	^2D, ^4D, ^2D, ^2P, ^2P, ^4P
(xxx)	^2S, ^4S

APPENDIX I. EXAMPLE OF POSSIBLE MULTIPLETS FOR GIVEN SPACE SYMMETRY AND NUCLEON DISTRIBUTION OVER SPACE ORBITS

Consider a 3 p-wave nucleon distribution with a, b, c denoting the p-wave functions with $l_z = 1, 0, -1$. The maximum possible L_z is 3 requiring a product aaa. For $L_z = 2$ the possible product is aab, for $L_z = 1$ the two products aac and abb are possible, and for $L_z = 0$ the two types bbb and abc are possible. The function manifolds corresponding to each type contain one or more irreducible representations of the symmetric group of order three:

$(aaa) = [3]$ similarly for (bbb),
$(aab) = [3]+[2+1]$ similarly for (aac) and (abb),
$(abc) = [3]+2[2+1]+[1+1+1]$.

Hence, the irreducible representations contained in the function manifolds for each L_z value are

$L_z = 3$ $[3]$,
$L_z = 2$ $[3]+[2+1]$,
$L_z = 1$ $2[3]+2[2+1]$,
$L_z = 0$ $2[3]+2[2+1]+[1+1+1]$.

The $L_z = 3$ representation $[3]$ must belong to an F state. For $L_z = 2$ the $[3]$ representation must belong to the $L_z = 2$ component of this F state. The remaining irreducible representation $[2+1]$ must belong to a D state. Proceeding in this fashion, P states occur which belong to the irreducible representations $[3]$ and $[2+1]$ while an S state occurs which belongs to the irreducible representation $[1+1+1]$. Combining this information with a table for three particles like Table II for four particles, one obtains the desired information as given in Table VII.

One notes that the function manifold (aaa) consists

[34] For the effect of symmetry on the photodisintegration of $_2He^4$ and H^3, see M. Verde, Helv. Phys. Acta 23, 453 (1950).

of only one function *aaa* which belongs to the irreducible representation [3]. The manifold (*aab*) consists of three functions, *aab*, *aba*, and *baa*, which can be combined into three linearly independent functions (*aab* $+baa+aba$), belonging to one-dimensional representation [3], (*aab* $-baa$) and (*aab* $+baa-2aba$) both belonging to the irreducible representation [2+1]. From the six functions in the manifold (*abc*), six linearly independent functions can be formed, two of which belong to each of the two two-dimensional representations [2+1], and one each to the one-dimensional representations [3] and [1+1+1].

PHYSICAL REVIEW VOLUME 85, NUMBER 6 MARCH 15, 1952

Electrodynamic Displacement of Atomic Energy Levels. I. Hyperfine Structure

ROBERT KARPLUS AND ABRAHAM KLEIN
Harvard University, Cambridge, Massachusetts

(Received November 23, 1951)

The vacuum fluctuations of the photon and pair fields modify the interaction of an electron with an electromagnetic field. The effects on the energy levels are conveniently described in terms of the mass operator and the vacuum polarization potential. A gauge-covariant expansion of the mass operator for the motion of an electron in a weak external electromagnetic field is derived; the expression contains terms quadratic in the field but includes only the lowest order electrodynamic correction. The modification in the Fermi formula is then computed by specializing the external field to consist of the Coulomb and magnetic dipole fields of the nucleus and by taking the matrix element of the operators in an S-state of a hydrogen-like atom. All changes can be described as a correction $\Delta g=-2Z\alpha^2(5/2-\ln 2)$ in the gyromagnetic ratio of the electron. The value of the fine structure constant deduced from measurements of the hyperfine structure becomes $\alpha^{-1}=137.0364$.

I. INTRODUCTION

THE success of the covariant reformulations of quantum electrodynamics is predicated in the first instance on their unambiguous prediction of the observable effects associated with the coupling of an electron to the vacuum fluctuations of the photon field. The experimental investigation of these phenomena depends primarily on experiments performed on hydrogen-like atoms. By this means, it has been possible to test the predictions of the theory concerning the effective static magnetic moment of the electron[1,2] and the electrodynamic shift of energy levels (Lamb shift).[3,4] In addition, the use of the magnetic moment result in the corrected Fermi formula,[5] in conjunction with a precise determination of the hyperfine structure splitting of the ground state of hydrogen,[6] has been the most accurate way of determining α, the fine structure constant.[5]

With the exception of the calculation of the static magnetic moment, which has been carried out to the inclusion of fourth-order (α^2) electrodynamic corrections,[2] the present theoretical predictions must be termed incomplete in several well-defined respects. These are the following: the dependence on the nuclear field has been obtained only through linear terms and for a slowly varying field; the α^2 electrodynamic correction has not been fully ascertained; and the nucleus has been treated as a structureless particle possessing a charge and a magnetic dipole moment.

It is the purpose of the present paper and of one that is to follow to describe methods of treating the prescribed nuclear field (or any external electromagnetic field) to higher approximation. The results will find twofold application. First we shall obtain corrections to the Fermi formula which arise from interference between the Coulomb and dipole fields of the nucleus. Second, we shall compute the contribution to the Lamb shift formula of terms which are quadratic in the Coulomb field.

The investigation proceeds from a Dirac equation modified to include the electron self-energy and the polarization potential induced in the vacuum.[7] The former is described by the mass operator, an integral operator whose general structure has been analyzed elsewhere.[7,8] We restrict our discussion to the electrodynamic correction of order α. The explicit field dependence of the mass operator is contained only in the Green's function for the electron in the prescribed field. Several procedures have been developed for the representation of this dependence to the desired order of approximation.[8,9] In this paper, we describe one of

[1] Koenig, Prodell, and Kusch, Phys. Rev. **83**, 687 (1951).
[2] R. Karplus and N. Kroll, Phys. Rev. **77**, 536 (1950).
[3] W. E. Lamb and R. C. Retherford, Phys. Rev. **81**, 222 (1951).
[4] Bethe, Brown, and Stehn, Phys. Rev. **77**, 370 (1950). Further references are given here.
[5] J. W. M. Dumond and E. R. Cohen, "A Least-Squares Adjustment of the Atomic Constants as of December 1950" (A report to the Natl. Research Council). See also Phys. Rev. **82**, 555 (1951).
[6] A. G. Prodell and P. Kusch, Phys. Rev. **79**, 1009 (1950).
[7] J. Schwinger, Proc. Natl. Acad. **7**, 432, 455 (1951).
[8] J. Schwinger, Phys. Rev. **82**, 664 (1951). We follow the notation of this paper, hereafter referred to as I.
[9] Some of these are discussed by R. P. Feynman, Phys. Rev. **84**, 108 (1951).

these methods which is suited to the treatment of a weak field, in which case a power series expansion is permissible. The construction of the Green's function is related to the construction of a transformation function and its associated momentum operators.[8] By direct expansion and extensive rearrangement, these are exhibited as gauge-covariant quantities correct to second order in the external field. In the resulting mass operator, a separation is effected between the infinite field independent part which is the mass renormalization and the finite field dependent part, which forms the starting point for further discussion and application.

The assumption of a weak field is adequate for the treatment of the coupling of the electron to the dipole field of the proton.[10] The largest contribution, which is the well-known $(\alpha/2\pi)$ correction to the static magnetic moment, is obtained by neglecting the high Fourier components of the magnetic field in the linear field term. For an S-state, the associated magnetic energy depends only on the density of the electron wave function at the origin, as in the Fermi formula. The essentially new results involve the corrections of relative order $Z\alpha$ compared to the above. From the structure of the mass operator, it will be seen that these arise from the behavior of the electron within a neighborhood of its Compton wavelength from the nucleus and are thus present only for an S-state. In a P-state, for example, there will be another factor of $Z\alpha$ arising from the reduced probability density near the origin.

The present considerations do not suffice for the treatment of the Lamb shift. There one encounters the well-known infrared difficulties arising from the fact that the bulk of the effect is not confined to the neighborhood of the nucleus. The emission of soft virtual quanta is thus given full play, with the resultant breakdown of an expansion in powers of the field. The presentation of a modified approach, which subverts this difficulty, the evaluation of results, as well as other methodological advances in the treatment of the mass operator are reserved for a subsequent paper.

II. PRELIMINARY CONSIDERATIONS

A. The Mass Operator; Green's Functions

The description of the motion of an electron in a prescribed electromagnetic field, including vacuum polarization and self-energy effects, will be based on a modified Dirac equation of the form[7,8]

$$\gamma_\mu(-i\partial_\mu - e\bar{A}_\mu(x))\psi(x) + \int M(x,x')\psi(x')d^4x' = 0. \quad (2.1)$$

Here $\bar{A}_\mu(x)$ is the four-potential of the external field augmented by the potential induced in the vacuum. $M(x,x')$ is the mass operator which formally contains self-energy effects to all orders. To the lowest order in e (second-order electrodynamic correction), it is given by

$$M(x,x') = m_0\delta(x-x') + ie^2\gamma_\mu G_+(x,x')\gamma_\mu D_+(x-x'), \quad (2.2)$$

where $G_+(x,x')$ is a Green's function for the Dirac equation in the external field, which is specified more precisely below, and $D_+(x-x')$ is a photon Green's function represented by (note that $ab = a_\mu b_\mu = \mathbf{a}\cdot\mathbf{b} - a_0 b_0$)

$$\begin{aligned} D_+(x-x') &= \int (2\pi)^{-4} d^4k e^{ik(x-x')}(k^2)^{-1} \\ &= \int (2\pi)^{-4} d^4k e^{ik(x-x')} i\int_0^\infty dt \exp[-itk^2] \\ &= (4\pi)^{-2}\int_0^\infty t^{-2}dt \exp[i(x-x')^2/4t]. \end{aligned} \quad (2.3)$$

In Eq. (2.3) it is implicitly understood that for k^2, one should read $k^2 - i\epsilon$, with ϵ small and positive so that the Green's function $D_+(x-x')$ contains only outgoing waves in the remote past and future.

The procedure for extracting the physical consequences of Eq. (2.1) rests, in the approximation considered, on a perturbation calculus which takes the wave equation in the given field as starting point and treats the polarization potential and the second term of Eq. (2.2) as the perturbing elements. Of these, the former has already been computed to the accuracy to which we shall require it and will be stated and used when needed. On the other hand, previous treatments of self-energy effects have, with the exception of Bethe's nonrelativistic calculation, been confined to a consideration of Eq. (2.2) in first Born approximation. Our first aim will be to explore means of representing the mass operator in explicit form to a higher order of approximation in the external field. We consider here one such means based on the direct expansion of $G_+(x,x')$, applicable when the field can be considered weak. The method in question was devised so as to exhibit the Green's function and any operator of which it is part in gauge-covariant form before any specialization of electromagnetic potential is made. It has already been applied in several forms in I to the problem of vacuum polarization by a slowly varying field of arbitrary strength. We briefly recall those aspects which are relevant to the present case.

The particle Green's function satisfies the operator equation

$$(\gamma\Pi + m)G_+ = 1. \quad (2.4)$$

The solution of Eq. (2.4) can be written in the symmetrical form

$$\begin{aligned} G_+ &= \tfrac{1}{2}\{m - \gamma\Pi, [m^2 - (\gamma\Pi)^2]^{-1}\} \\ &= i\int_0^\infty ds \exp[im^2 s]\tfrac{1}{2}\{m - \gamma\Pi, \exp[i(\gamma\Pi)^2 s]\}. \end{aligned} \quad (2.5)$$

[10] As will be seen below, this interaction is effective in an S-state only when the electron is within a Compton wavelength $(1/m)$ of the nucleus. At this distance, the kinetic energy of the electron, $p^2/2m \sim m$, whereas the potential energy (in the Coulomb field), α/r, $\sim \alpha m$. The magnetic coupling is smaller still by a factor of the order of the ratio of the electron to the proton mass. Thus, both interactions can be treated as small perturbations in this problem. It is also clear why we shall never consider terms which are quadratic in the magnetic coupling.

The introduction of the integral representation (2.5) implies that m^2 has a small negative imaginary part and that the Green's function G_+ is therefore the one which propagates with increasing phase in any time-like direction from the source. We might emphasize here once and for all that we shall be interested in the real part of any matrix element of the mass operator since we are concerned with energy level shifts. It will thus be unnecessary during our future work to take cognizance of the presence of the small imaginary addition to the mass that makes Eq. (2.5) well defined and of the corresponding addition to k^2 in Eq. (2.3). When we eventually perform an integration over the parameter s, it will be correct merely to treat oscillatory exponentials as if they were decaying exponentials. More formally we could make the substitution of variables $s'=is$ and integrate with respect to s' along its positive real axis.

The electron Green's function is the matrix element of the operator Eq. (2.5) with respect to space-time coordinates,

$$G_+(x', x'')=(x'|G_+|x''). \tag{2.6}$$

We employ the notation

$$(x'|\exp[i(\gamma\Pi)^2 s]|x'') \equiv (x'|U(s)|x'')\equiv(x'(s)|x''(0)) \tag{2.7}$$

which will be termed the "transformation function";

$$(x'|\Pi_\mu U(s)|x'')\equiv(x'(s)|\Pi_\mu(s)|x''(0)) =(-i\partial_\mu'-eA_\mu')(x'(s)|x''(0)) \tag{2.8}$$

and

$$(x'|U(s)\Pi_\mu|x'')\equiv(x'(s)|\Pi_\mu(0)|x''(0)) =(i\partial_\mu''-eA_\mu'')(x'(s)|x''(0)) \tag{2.9}$$

are the corresponding matrix elements of the momentum operators. The Green's function can thus be written[11]

$$G_+(x', x'')=i\int_0^\infty ds\exp[-im^2 s][m(x'(s)|x''(0)) -\tfrac{1}{2}\gamma(x'(s)|\Pi(s)|x''(0)) -\tfrac{1}{2}(x'(s)|\Pi(0)|x''(0))\gamma]. \tag{2.10}$$

The procedure is now to expand $(x'(s)|x''(0))$ about its value for a free particle up to terms quadratic in the external field, the result to be exhibited in gauge-covariant form. The matrix elements of the momentum operators are then obtained by means of Eqs. (2.7) and (2.8) and the results amalgamated to form the mass operator, Eq. (2.2). The details of this calculation are contained in Sec. III.

[11] The combination of momentum operator matrix elements that appears in Eq. (2.10) will henceforth be written for convenience as

$$-\tfrac{1}{2}(x'(s)|\gamma\Pi(s)+\Pi(0)\gamma|x''(0))$$

with the understanding that the more precise rendering is that of (2.10).

B. The Hyperfine Structure

In order to lay the basis for the application of the results of Sec. III to the calculation of corrections to the Fermi hyperfine structure formula, we shall briefly discuss pertinent background material.

The full vector potential of Eq. (2.1) has the form

$$\bar{A}_\mu(x)=A_\mu^E(x)+A_\mu^M(x)+A_\mu^{EP}(x)+A_\mu^{MP}(x), \tag{2.11}$$

where the superscripts E and M indicate electric and magnetic, respectively, and the additional superscript P indicates the corresponding vacuum polarization potential. $A^E(x)$ is the Coulomb potential of the nucleus,

$$\mathbf{A}^E=0, \quad A_0{}^E=-Ze/4\pi r \tag{2.12}$$

(e is the electronic charge), and belongs to the unperturbed problem. $A^M(x)$ is the vector potential of the proton considered as a point dipole. It is given by

$$\mathbf{A}^M=\boldsymbol{\mu}\times\mathbf{r}/4\pi r^3=\nabla\times(\boldsymbol{\mu}/4\pi r), \quad A_0{}^M=0, \tag{2.13}$$

where $\boldsymbol{\mu}$ is the proton dipole moment operator. The Fermi formula is the diagonal matrix element of the interaction of A^M with the electron current in the ground state of hydrogen. Since only the polarization current of the electron is relevant here, the interaction energy ΔE_0 has the form

$$\Delta E_0=-(e/2m)\int d\tau\bar{\psi}_c(\mathbf{r})\boldsymbol{\sigma}\psi_c(\mathbf{r})\cdot\mathbf{H}(\mathbf{r}). \tag{2.14}$$

For an S-state the spherical symmetry reduces the magnetic field to a δ-function,

$$\mathbf{H}=\nabla\times\mathbf{A}=\nabla\times(\nabla\times(\boldsymbol{\mu}/4\pi r))=\nabla\nabla\cdot(\boldsymbol{\mu}/4\pi r) -\nabla^2(\boldsymbol{\mu}/4\pi r)\to-\tfrac{2}{3}\nabla^2(\boldsymbol{\mu}/4\pi r)=\tfrac{2}{3}\boldsymbol{\mu}\delta(\mathbf{r}). \tag{2.15}$$

An adequate representation of the large and small components of the Coulomb wave function $\psi_c(\mathbf{r})$ by means of the corresponding Schrödinger wave function $\varphi_0(\mathbf{r})$ then gives the Fermi formula with the Breit correction[12,13]

$$\Delta E_0=-\tfrac{2}{3}\mu_0(\boldsymbol{\sigma}\cdot\boldsymbol{\mu})|\varphi_0(0)|^2(1+\tfrac{3}{2}(Z\alpha)^2). \tag{2.16}$$

The corrections we shall obtain will be exhibited as multiples of the leading term in Eq. (2.16).

The largest addition of electrodynamic origin is, of course, the relative change $(\alpha/2\pi)$ in the spin density of the electron, which will emerge again from our calculation. Further corrections are at least of relative order $Z\alpha^2$ compared to the reference term and may all be said to arise from the spatially distributed nature of quantum electrodynamic corrections. This statement is perhaps most clearly illustrated by preliminary consideration of the effects due to the interaction of the electron current with the vacuum polarization potentials. In this connection it proves convenient to intro-

[12] E. Fermi, Z. Physik **60**, 320 (1930).
[13] G. Breit, Phys. Rev. **35**, 1447 (1949).

duce the four-dimensional Fourier integral representation

$$A_\mu(x)=\int(2\pi)^{-2}d^4kA_\mu(k)e^{ik\cdot x}, \tag{2.17}$$

with analogous definitions for the current $J_\mu(x)$ and the field tensor $F_{\mu\nu}(x)$. The transforms that will be of particular interest in the following work are

$$\begin{aligned}
2\pi A_0{}^E(k)&=-\delta(k_0)Ze/k^2,\\
2\pi\mathbf{A}^M(k)&=\delta(k_0)i\mathbf{k}\times\boldsymbol{\mu}/k^2,\\
2\pi\mathbf{E}(k)&=\delta(k_0)Zei\mathbf{k}/k^2,\\
2\pi\mathbf{H}(k)&=\mathcal{E}(k_0)i\mathbf{k}\times(i\mathbf{k}\times\boldsymbol{\mu})/k^2\to\tfrac{2}{3}\boldsymbol{\mu}\delta(k_0),\\
2\pi J_0{}^E(k)&=-\delta(k_0)Ze,\\
2\pi\mathbf{J}^M(k)&=\delta(k_0)i\mathbf{k}\times\boldsymbol{\mu}.
\end{aligned} \tag{2.18}$$

The last expression for $\mathbf{H}(k)$ is the Fourier transform of the result Eq. (2.12). In terms of the definition Eq. (2.17)[14]

$$A_\mu{}^P(k)=\frac{\alpha}{4\pi}J_\mu(k)\int_0^1\frac{dvv^2(1-\frac{1}{3}v^2)}{m^2+\frac{1}{4}k^2(1-v^2)}. \tag{2.19}$$

From Eq. (2.18) it follows that

$$\begin{aligned}
\mathbf{H}^P(k)&=i\mathbf{k}\times\mathbf{A}^{MP}(k)\\
&=\frac{\alpha}{4\pi}\frac{\delta(k_0)}{2\pi}k^2\mathbf{H}(\mathbf{k})\int_0^1\frac{dvv^2(1-\frac{1}{3}v^2)}{m^2+\frac{1}{4}k^2(1-v^2)}.
\end{aligned} \tag{2.20}$$

The corresponding interaction energy is

$$-\mu_0\int d\mathbf{r}\bar{\psi}_c(\mathbf{r})\boldsymbol{\sigma}\psi_c(\mathbf{r})\cdot\tfrac{2}{3}\boldsymbol{\mu}\int\frac{d\mathbf{k}}{(2\pi)^3}e^{i\mathbf{k}\cdot\mathbf{r}}\frac{\alpha}{4\pi}k^2\times\int_0^1\frac{dvv^2(1-\frac{1}{3}v^2)}{m^2+\frac{1}{4}k^2(1-v^2)}. \tag{2.21}$$

The magnetic field is no longer confined to the origin, but, as is evident from its form, is spread out over a distance of the electron Compton wavelength, $1/m$. In fact, if one approximates $\psi_c(\mathbf{r})$ by $\varphi_0(0)$, expression (2.21) is easily seen to vanish. To obtain a nonvanishing result one requires the more accurate representation

$$\begin{aligned}
\psi_c(\mathbf{r})&\to\varphi_0(\mathbf{r})\cong\varphi_0(0)(1-Z\alpha rm),\\
\varphi^*(\mathbf{r})\varphi(\mathbf{r})&\cong|\varphi_0(0)|^2(1-2Z\alpha rm)
\end{aligned} \tag{2.22}$$

of the wave function in the neighborhood of the origin.

[14] J. Schwinger, Phys. Rev. **76**, 790 (1949).

The matrix element of Eq. (2.21) now becomes

$$\tfrac{2}{3}\mu_0\langle\boldsymbol{\sigma}\cdot\boldsymbol{\mu}\rangle|\varphi_0(0)|^2\frac{Z\alpha^3}{2\pi}\int\frac{d\mathbf{r}d\mathbf{k}}{(2\pi)^3}rk^2m\times\int_0^1\frac{dvv^2(1-\frac{1}{3}v^2)}{m^2+\frac{1}{4}k^2(1-v^2)}. \tag{2.23}$$

Further consideration of expression (2.23) is reserved for Sec. VI, where an analogous contribution from the Coulomb polarization potential taken in conjunction with a wave function modified by the magnetic field will also be considered. We merely note there that Eq. (2.23) is of prototype form, since it contains one factor of α of electrodynamic origin, one factor of $Z\alpha$ of Coulombic origin, and is linear in the magnetic coupling.

The $Z\alpha^2$ corrections that are contributed by the matrix elements of the mass operator will be considered in Secs. IV and V.

III. MASS OPERATOR

An expression for the mass operator in a weak, arbitrarily varying external electromagnetic field will now be derived up to quadratic terms in this field. Since the formulas are quite involved, it is useful to obtain as a preliminary result, the matrix element of the transformation function $U(s)$ to the necessary order of accuracy. The calculation of the momenta Π_μ from the transformation function then furnishes all the necessary ingredients for the Green's function which contains the entire dependence of the mass operator on the prescribed field.

In order to exhibit the gauge covariance of the transformation function, it will be expressed in the form

$$\begin{aligned}
(x'(s)|x''(0))&=(x'|U(s)|x'')\\
&=-i(4\pi s)^{-2}\Phi(x',x'')\\
&\quad\times\exp[i(x'-x'')^2/4s]U'(s;x',x''),
\end{aligned} \tag{3.1}$$

where the function $U'(s;x',x'')$ must depend on the field in a gauge invariant way and must reduce to unity as the field vanishes. An expansion of the form discussed in Sec. VI of reference 8 yields the transformation operator

$$\begin{aligned}
U(s)=\exp[-isp^2]+ise\int_{-1}^1\tfrac{1}{2}dv\exp[-isp^2\tfrac{1}{2}(1-v)]\\
\times(pA+Ap+\tfrac{1}{2}\sigma F-eA^2)\exp[-isp^2\tfrac{1}{2}(1+v)]\\
+(ise)^2\int_{-1}^1\tfrac{1}{2}dv_1\int_{-1}^{v_1}\tfrac{1}{2}dv_2\\
\times\exp[-isp^2\tfrac{1}{2}(1-v_1)](pA+Ap+\tfrac{1}{2}\sigma F)\\
\times\exp[-isp^2\tfrac{1}{2}(v_1-v_2)](pA+Ap+\tfrac{1}{2}\sigma F)\\
\times\exp[-isp^2\tfrac{1}{2}(1+v_2)],
\end{aligned} \tag{3.2}$$

which has the matrix element

$$
\begin{aligned}
&(x'|\,U(s)\,|x'')\\
&=\int(2\pi)^{-4}d^4p e^{ip(x'-x'')}\Big\{\exp[-isp^2]\\
&\quad+ise\int_{-1}^{1}\tfrac{1}{2}dv\int(2\pi)^{-2}d^4k e^{\frac{1}{2}ik(x'+x'')}\\
&\quad\times\exp[-is(p+\tfrac{1}{2}k)^2\tfrac{1}{2}(1-v)]\Big[2pA+\tfrac{1}{2}\sigma F\\
&\quad-e\int(2\pi)^{-2}d^4k'A(k')A(k-k')\Big]\\
&\quad\times\exp[-is(p-\tfrac{1}{2}k)^2\tfrac{1}{2}(1+v)]+(ise)^2\int_{-1}^{1}\tfrac{1}{2}dv_1\\
&\quad\times\int_{-1}^{v_1}\tfrac{1}{2}dv_2(2\pi)^{-4}d^4k_1d^4k_2e^{\frac{1}{2}i(k_1+k_2)(x'+x'')}\\
&\quad\times\exp[-is(p+\tfrac{1}{2}(k_1+k_2)^2\tfrac{1}{2}(1-v_1)]\\
&\quad\times[(2p+k_2)A^1+\tfrac{1}{2}\sigma F^1]\exp[-is(p-\tfrac{1}{2}k_1+\tfrac{1}{2}k_2)^2\\
&\quad\times\tfrac{1}{2}(v_1-v_2)][(2p-k^1)A^2+\tfrac{1}{2}\sigma F]\\
&\qquad\times\exp[-is(p-\tfrac{1}{2}k_1-\tfrac{1}{2}k_2)^2\tfrac{1}{2}(1+v_2)]\Big\},
\end{aligned}
$$

$$
\Big(A_\mu(k_i)=A_\mu{}^i=\int(2\pi)^{-2}d^4x e^{-ik_ix}A_\mu(x)\Big). \quad (3.3)
$$

The translations

$$
p_\mu\to(p+\tfrac{1}{2}kv)_\mu \quad\text{and}\quad p_\mu\to(p+\tfrac{1}{2}(k_1v_1+k_2v_2))_\mu \quad (3.4)
$$

of the momentum coordinates in the linear and in the quadratic expansion terms serve to eliminate all scalar products (pk) from the exponents and yield the common factor $\exp[-isp^2]$. It is then possible to carry out the integration over the variable p_μ by noting that

$$
\begin{aligned}
&\int(2\pi)^{-4}d^4p e^{ip(x'-x'')}p_\mu\exp[-isp^2]\\
&=\int(2\pi)^{-4}d^4p e^{ip(x'-x'')}\tfrac{1}{2}is^{-1}(\partial/\partial p_\mu)\exp[-isp^2]\\
&=\int(2\pi)^{-4}d^4p e^{ip(x'-x'')}(2s)^{-1}(x'-x'')_\mu\exp[-isp^2]\\
&=-i(4\pi s)^{-2}(2s)^{-1}(x'-x'')_\mu\exp[i(x'-x'')^2/4s] \quad (3.5)
\end{aligned}
$$

on an integration by parts. With the notation $(x'-x'')_\mu=\Delta x_\mu$, it then follows that

$$
\begin{aligned}
&\int(2\pi)^{-4}d^4p e^{ip\Delta x}\exp[-isp^2]\{1;\,p_\mu;\,p_\mu p_\nu;\,p_\mu p_\nu p_\lambda\}\\
&=-i(4\pi s)^{-2}\exp[i(\Delta x)^2/4s]\{1;\,(2s)^{-1}\Delta x_\mu;\\
&\qquad(2s)^{-2}\Delta x_\mu\Delta x_\nu-i(2s)^{-1}\delta_{\mu\nu};\,(2s)^{-3}\Delta x_\mu\Delta x_\nu\Delta x_\lambda\\
&\qquad-i(2s)^{-2}(\delta_{\mu\nu}\Delta x_\lambda+\delta_{\mu\lambda}\Delta x_\nu+\delta_{\nu\lambda}\Delta x_\mu)\}. \quad (3.6)
\end{aligned}
$$

The function $U'(s;x',x'')$ defined in Eq. (3.1) can now be written

$$
\begin{aligned}
&U'(s;x',x'')=[\Phi(x',x'')]^{-1}\Big\{1+ise\int_{-1}^{1}\tfrac{1}{2}dv\\
&\quad\times\int(2\pi)^{-2}d^4k e^{ik\xi}\exp[-is\tfrac{1}{4}k^2(1-v^2)]\\
&\quad\times\Big[((\Delta x/s)+kv)A+\tfrac{1}{2}\sigma F-e\int(2\pi)^{-2}d^4k'A(k')\\
&\quad\times A(k-k')\Big]+(ise)^2\int_{-1}^{1}\tfrac{1}{2}dv_1\int_{-1}^{v_1}\tfrac{1}{2}dv_2e^{ik\xi_{12}}\\
&\quad\times e^{ik\xi_{12}}(2\pi)^{-4}d^4k_1d^4k_2\exp[-is\tfrac{1}{8}K^2]\\
&\quad\times\{[((\Delta x/s)+k_2(1+v_2)+k_1v_1)A^1\\
&\quad+\tfrac{1}{2}\sigma F^1][((\Delta x/s)+k_2v_2-k_1(1-v_1))A^2\\
&\qquad+\tfrac{1}{2}\sigma F^2]-2iA^1A^2/s\}\Big\}, \quad (3.7)
\end{aligned}
$$

where

$$
\xi_{ik}=\tfrac{1}{2}[x_\mu'(1+v_i)+x_\mu''(1-v_i)] \quad (3.7')
$$

and

$$
K^2=k_1^2(1-v_1^2)+2k_1k_2(1-v_1)(1+v_2)+k_2^2(1-v_2^2).
$$

By a fairly extensive rearrangement it can now be shown that up to second-order terms in the external field the function $U'(s;x',x'')$ really depends only on gauge invariant quantities. This fact will be verified explicitly for the first-order terms

$$
\begin{aligned}
&ise\int_{-1}^{1}\tfrac{1}{2}dv(2\pi)^{-2}d^4k e^{ik\xi}\{[(\Delta x/s)+kv]A\\
&\qquad\times\exp[-is\tfrac{1}{4}k^2(1-v^2)]-(\Delta x/s)A\}. \quad (3.8)
\end{aligned}
$$

The last contribution in the bracket has come from an expansion of the gauge dependent exponential $[\Phi(x',x'')]^{-1}$. An integration by parts with respect to v of the middle term

$$
\begin{aligned}
&\int_{-1}^{1}\tfrac{1}{2}dv e^{ik\xi}v\exp[-is\tfrac{1}{4}k^2(1-v^2)]\\
&=(isk^2)^{-1}e^{ik\xi}(\exp[-is\tfrac{1}{4}k^2(1-v^2)]-1)\Big|_{-1}^{1}\\
&-(k\Delta x/sk^2)\int_{-1}^{1}\tfrac{1}{2}dv e^{ik\xi}(\exp[-is\tfrac{1}{4}k^2(1-v^2)]-1) \quad (3.9)
\end{aligned}
$$

shows the identity of Eq. (3.8) with

$$ise\int_{-1}^{1}\tfrac{1}{2}dv(2\pi)^{-2}d^4k e^{ikx}(\Delta xJ/sk^2)\times(\exp[-is\tfrac{1}{4}k^2(1-v^2)]-1), \quad (3.10)$$

since

$$k^2A_\mu-k_\mu(kA)=-ik_\nu F_{\nu\mu}=J_\mu. \quad (3.11)$$

By a similar treatment the second-order terms from the expansion of $[\Phi(x',x'')]^{-1}$, from the linear expansion term, and from the quadratic expansion term can be combined into an expression that depends only on field strengths and current densities and their derivatives. With the abbreviations

$$e_i(s)=\exp[-is\tfrac{1}{4}k_i^2(1-v_i^2)], \quad E(s)=\exp[-is\tfrac{1}{4}K^2] \quad (3.12)$$

for the ubiquitous exponential factors, as well as

$$\int d^4\bar{k}_j=\int_{-1}^{1}\tfrac{1}{2}dv_j\int(2\pi)^{-2}d^4k_j e^{ik_jx_j} \quad \text{and} \quad (3.13)$$

$$\int d^3\bar{K}=\int_{-1}^{1}\tfrac{1}{2}dv_1\int_{-1}^{v_1}\tfrac{1}{2}dv_2\int(2\pi)^{-4}d^4k_1d^4k_2e^{ik_1x_1}e^{ik_2x_2}$$

for the Fourier integral operators, the function $U'(s;x'x'')$ becomes

$$\begin{aligned}U'(s;x',x'')&=1+ise\int d^4\bar{k}\{(\Delta xJ/sk^2)(e(s)-1)+\tfrac{1}{2}\sigma Fe(s)\}\\&+(ise)^2\int d^3\bar{K}\{(\Delta xJ^1/sk_1^2)(\Delta xJ^2/sk_2^2)\\&\times[E(s)-e_1(s)-e_2(s)+1]\\&+i[(J^2F^1\Delta x/sk_2^2)(1-v_1)\\&-(J^1F^2\Delta x/sk_1^2)(1+v_2)]E(s)\\&+\tfrac{1}{2}(J^1J^2/sk_1^2k_2^2)[k_2\Delta x(1+v_2)-k_1\Delta x(1-v_1)\\&+sk_1^2v_1(1-v_1)-sk_2^2v_2(1+v_2)]E(s)\\&+\tfrac{1}{2}\sigma F^1(\Delta xJ^2/sk_2^2)[E(s)-e_1(s)]\\&+\tfrac{1}{2}\sigma F^2(\Delta xJ^1/sk_1^2)[E(s)-e_2(s)]\\&+[\tfrac{1}{2}\sigma F^1(k_1J^2/k_2^2)(1+v_2)-\tfrac{1}{2}\sigma F^2(k_2J^1/k_1^2)\\&\times(1-v_1)]E(s)-(1-v_1)(1+v_2)\tfrac{1}{2}F^1F^2E(s)\\&+\tfrac{1}{2}\sigma F^1\tfrac{1}{2}\sigma F^2E(s)\}. \quad (3.14)\end{aligned}$$

We may now proceed to an evaluation of the matrix elements of the momentum operators:

$$\begin{aligned}&(x'(s)|\,\Pi_\mu(s)\,|x''(0))=(-i\partial_\mu'-eA_\mu(x'))(x'(s)\,|x''(0))\\&=-i(4\pi s)^{-2}\exp[i(\Delta x)^2/4s]\Phi(x',x'')\\&\times\left\{\left[(\Delta x_\mu/2s)+e\int d^4\bar{k}\tfrac{1}{2}(1+v)(F\Delta x)_\mu\right]\right.\\&\left.\times U'(s;x',x'')-i\partial_\mu'U'(s;x',x'')\right\} \quad (3.15)\end{aligned}$$

and

$$\begin{aligned}&(x'(s)|\,\Pi_\mu(0)\,|x''(0))\\&=(i\partial_\mu''-eA_\mu(x''))(x'(s)\,|x''(0))\\&=-i(4\pi s)^{-2}\exp[i(\Delta x)^2/4s]\Phi(x',x'')\\&\times\left\{\left[(\Delta x_\mu/2s)-e\int d^4\bar{k}\tfrac{1}{2}(1-v)(F\Delta x)_\mu\right]\right.\\&\left.\times U'(s;x',x'')+i\partial_\mu''U'(s;x',x'')\right\}. \quad (3.16)\end{aligned}$$

Since the momenta enter the mass operator in the combination $\frac{1}{2}(\gamma\Pi(s)+\Pi(0)\gamma)$, only this quantity will be given in detail. The fact that the operator is a Dirac matrix suggests that the contributions to the momenta and to the transformation function be classified according to their spinor character. Thus we have the scalar part (a multiple of the unit matrix), the "spin" part (a multiple of $\sigma_{\mu\nu}$), and the pseudoscalar part (a multiple of γ_5) which is introduced by the decomposition

$$\tfrac{1}{2}\sigma F^1\tfrac{1}{2}\sigma F^2=\tfrac{1}{2}F^1F^2-i\,\mathrm{tr}[F^1\sigma F^2]+\gamma_5\tfrac{1}{2}F^1F^{2*} \quad (3.17)$$

and involves the dual of $F_{\mu\nu}$,

$$F_{\mu\nu}{}^*=\tfrac{1}{2}i\epsilon_{\mu\nu\lambda\sigma}F_{\lambda\sigma} \quad \text{(cf. Eqs. (I, 3.25–3.27))}. \quad (3.18)$$

In terms of integral operators that will be defined below, we can now write the Green's function for the Dirac field:

$$\begin{aligned}&G_+(x',x'')\\&=i\int_0^\infty ds\exp[-im^2s]\\&\times(x'(s)|\,m-\tfrac{1}{2}(\gamma\Pi(s)+\Pi(0)\gamma)\,|x''(0))\\&=(4\pi)^{-2}\int_0^\infty s^{-2}ds\exp[-im^2s+i(\Delta x)^2/4s]\Phi(x',x'')\\&\times\{[m-(\gamma\Delta x/2s)][1+A(s)+C(s)]\\&-\gamma_\mu[A_{+\mu}(s)+C_{+\mu}(s)]-\tfrac{1}{2}\{\gamma B_+(s)\\&+[(\gamma\Delta x/2s)-m]B(s),\tfrac{1}{2}\sigma F\}-\tfrac{1}{2}[\gamma B_-(s),\tfrac{1}{2}\sigma F]\\&-\tfrac{1}{2}\{\gamma D_+{}^2(s)+[(\gamma\Delta x/2s)-m]D^2(s),\tfrac{1}{2}\sigma F^1\}\\&-\tfrac{1}{2}[\gamma D_-{}^2(s),\tfrac{1}{2}\sigma F^1]-\tfrac{1}{2}\{\gamma D_+{}^1(s)\\&+[(\gamma\Delta x/2s)-m]D^1(s),\tfrac{1}{2}\sigma F^2\}\\&-\tfrac{1}{2}[\gamma D_-{}^1(s),\tfrac{1}{2}\sigma F^2]+\tfrac{1}{2}i\{\gamma G_+(s)\\&+[(\gamma\Delta x/2s)-m]G(s),\mathrm{tr}[F^1\sigma F^2]\}\\&+\tfrac{1}{2}i[\gamma G_-(s),\mathrm{tr}[F^1\sigma F^2]]\\&+[\gamma G_-(s)+mG(s)]\tfrac{1}{2}\gamma_5F^1F^{2*}\}. \quad (3.19)\end{aligned}$$

The symbols have the following significance:

$$A(s)=ise\int d^4k(\Delta xJ/sk^2)[e(s)-1]; \tag{3.20a}$$

$$A_{+\mu}(s)=ise\int d^4k\tfrac{1}{2}v[-i(F\Delta x/s)_\mu-vJ_\mu]e(s); \tag{3.20b}$$

$$B(s)=ise\int d^4k e(s)$$

$$\left(\text{whence } B(s)\tfrac{1}{2}\sigma F=ise\int d^4k\tfrac{1}{2}\sigma Fe(s)\right); \tag{3.20c}$$

$$B_{+\mu}(s)=ise\int d^4k\tfrac{1}{2}vk_\mu e(s); \tag{3.20d}$$

$$B_{-\mu}(s)=ise\int d^4k\tfrac{1}{2}k_\mu e(s); \tag{3.20e}$$

$$\begin{aligned}C(s)=(ise)^2\int d^3\bar{K}\{&(\Delta xJ^1/sk_1^2)(\Delta xJ^2/sk_2^2)\\&\times[E(s)-e_1(s)-e_2(s)+1]+\tfrac{1}{2}(J^1J^2/sk_1^2k_2^2)\\&\times[k_2\Delta x(1+v_2)-k_1\Delta x(1-v_1)\\&+sk_1^2v_1(1-v_1)-sk_2^2v_2(1+v_2)]E(s)\\&+i[(J^2F^1\Delta x/sk_2^2)(1-v_1)\\&-(J^1F^2\Delta x/sk_1^2)(1+v_2)]E(s)\\&+(v_1-v_2+v_1v_2)\tfrac{1}{2}F^1F^2E(s)\},\end{aligned} \tag{3.20f}$$

$$\begin{aligned}C_{+\mu}(s)=(ise)^2\int d^3\bar{K}\{&-\tfrac{1}{2}(v_1/s)J_\mu{}^1(\Delta xJ^2/sk_2^2)\\&\times[E(s)(v_1+(k_1k_2/k_1^2)(1+v_2))-v_1e_1(s)]\\&-\tfrac{1}{2}(v_2/s)J_\mu{}^2(\Delta xJ^1/sk_1^2)\\&\times[E(s)(v_2-(k_1k_2/k_2^2)(1-v_1))-v_2e_2(s)]\\&+(sk_1^2k_2^2)^{-1}[\tfrac{1}{2}J^1J^2(k_2(1+v_2)-k_1(1-v_1))_\mu\\&+ik_1^2(J^2F^1)_\mu(1-v_1)-ik_2^2(J^1F^2)_\mu(1+v_2)]\\&\times[\Delta x_\nu\tfrac{1}{2}(k_1v_1+k_2v_2)_\mu-i\delta_{\mu\nu}]E(s)\\&-\tfrac{1}{2}iv_1(F^1\Delta x)_\mu(\Delta xJ^2/sk_2^2)[E(s)-e_1(s)]\\&+\tfrac{1}{2}iv_2(F^2\Delta x)_\mu(\Delta xJ^1/sk_1^2)[E(s)-e_2(s)]\\&+[\tfrac{1}{2}(J^1J^2/k_1^2k_2^2)(k_1^2v_1(1-v_1)\\&-k_2^2v_2(1+v_2))+(v_1-v_2+v_1v_2)\tfrac{1}{2}F^1F^2]\\&\times\tfrac{1}{2}(k_1v_1+k_2v_2)_\mu E(s)\},\end{aligned} \tag{3.20g}$$

$$\begin{aligned}D^1(s)=(ise)^2\int d^3\bar{K}\{&(\Delta xJ^1/sk_1^2)(E(s)-e_2(s))\\&+(1+v_2)(k_2J^1/k_1^2)E(s)\};\end{aligned} \tag{3.20h}$$

$$\begin{aligned}D^2(s)=(ise)^2\int d^3\bar{K}\{&(\Delta xJ^2/sk_2^2)(E(s)-e_1(s))\\&-(1-v_1)(k_1J^2/k_2^2)E(s)\};\end{aligned} \tag{3.20i}$$

$$\begin{aligned}D_{+\mu}{}^1(s)=(ise)^2\int d^3\bar{K}\{&\tfrac{1}{2}v_2k_{2\mu}(\Delta xJ^1/sk_1^2)(E(s)-e_2(s))\\&-\tfrac{1}{2}iv_1(F^1\Delta x/s)_\mu E(s)\\&-\tfrac{1}{2}v_1J_\mu{}^1[v_1+(k_1k_2/k_1^2)(1+v_2)]E(s)\\&+\tfrac{1}{2}(k_1v_1+k_2v_2)_\mu(k_2J^1/k_1^2)E(s)\};\end{aligned} \tag{3.20j}$$

$$\begin{aligned}D_{+\mu}{}^2(s)=(ise)^2\int d^3\bar{K}\{&\tfrac{1}{2}v_1k_{1\mu}(\Delta xJ^2/sk_2^2)(E(s)-e_1(s))\\&-\tfrac{1}{2}iv_2(F^2\Delta x/s)_\mu E(s)\\&-\tfrac{1}{2}v_2J_\mu{}^2[v_2-(k_1k_2/k_2^2)(1-v_1)]E(s)\\&-\tfrac{1}{2}(k_1v_1+k_2v_2)_\mu(k_1J^2/k_2^2)E(s)\};\end{aligned} \tag{3.20k}$$

$$\begin{aligned}D_{-\mu}{}^1(s)=(ise)^2\int d^3\bar{K}\{&\tfrac{1}{2}k_{2\mu}(\Delta xJ^1/sk_1^2)(E(s)-e_2(s))\\&-\tfrac{1}{2}i(F^1\Delta x/s)_\mu E(s)\\&-\tfrac{1}{2}J_\mu{}^1[v_1+(k_1k_2/k_1^2)(1+v_2)]E(s)\\&+\tfrac{1}{2}(k_1+k_2)_\mu(k_2J^1/k_1^2)E(s)\};\end{aligned} \tag{3.20l}$$

$$\begin{aligned}D_{-\mu}{}^2(s)=(ise)^2\int d^3\bar{K}\{&\tfrac{1}{2}k_{1\mu}(\Delta xJ^2/sk_2^2)(E(s)-e_1(s))\\&-\tfrac{1}{2}i(F^2\Delta x/s)_\mu E(s)\\&-\tfrac{1}{2}J_\mu{}^2[v_2-(k_1k_2/k_2^2)(1-v_1)]E(s)\\&-\tfrac{1}{2}(k_1+k_2)_\mu(k_1J^2/k_2^2)E(s)\};\end{aligned} \tag{3.20m}$$

$$G(s)=(ise)^2\int d^3\bar{K}E(s); \tag{3.20n}$$

$$G_{+\mu}(s)=(ise)^2\int d^3\bar{K}\tfrac{1}{2}(k_1v_1+k_2v_2)_\mu E(s); \tag{3.20o}$$

$$G_{-\mu}(s)=(ise)^2\int d^3\bar{K}\tfrac{1}{2}(k_1+k_2)_\mu E(s). \tag{3.20p}$$

We may note that the A and C are scalar parts, that the B, D, and G are spin parts, and that the G are pseudoscalar parts.

There still remains the task of constructing the entire mass operator and of separating that part of it which merely represents an addition to the rest mass of the electron. In terms of the proper-time representation of the Green's function of the photon field, the mass

operator is written

$$M(x', x'') = m_0\delta(x'-x'') + ie^2(2\pi)^{-4} \times \Phi(x', x'') \int_0^\infty s^{-2}ds \int_0^s w^{-2}dw \times \exp[-im^2 s + i(\Delta x)^2/4w]\gamma_\lambda (\ )\gamma_\lambda, \quad (3.21)$$

where ( ) stands for the same bracket of Eq. (3.19) and the variable $w = (s^{-1}+t^{-1})^{-1}$ has replaced t of Eq. (2.3).

We may now observe that the leading terms in the correction to the rest mass,

$$-i(4\pi w)^{-2} \exp[i(\Delta x)^2/4w][-4m - 2(\gamma\Delta x/2s)] \quad (3.22)$$

are also the leading terms in the expansion of the operator

$$(x'(w)|-4m-(w/s)(\gamma\Pi(w)+\Pi(0)\gamma)|x''(0)) = \delta m(w; x', x'') \quad (3.23)$$

of which the wave function satisfying

$$(\gamma\Pi + m)\psi = 0 \quad (3.24)$$

is an eigenfunction,

$$\int \delta m(w; x', x'')\psi(x'')d^4x'' = -2m(2-w/s) \times \exp[im^2 w]\psi(x'). \quad (3.25)$$

If we adopt a procedure that treats the electrodynamic correction as a perturbation to be evaluated to first order, wave functions satisfying Eq. (3.24) may be used and the content of Eq. (3.21) can be rewritten

$$\int M(x', x'')\psi(x'')d^4x'' = \int (m\delta(x'-x'') + \bar{M}(x', x''))\psi(x'')d^4x'' \quad (3.26)$$

in terms of the observed mass of a free electron[7]

$$m = m_0 + (\alpha m/2\pi)\int_0^\infty s^{-2}ds \int_0^s dw(2-w/s) \times \exp[-im^2(s-w)] \quad (3.27)$$

and of the finite operator that describes the effect of the vacuum fluctuations of the field on the behavior of an electron in an external field,

$$\bar{M}(x', x'') = -(\alpha/4\pi)\int_0^\infty ds \exp[-im^2 s]\int_0^s dw \times \{s^{-2}(x'(w)|4m + (w/s)(\gamma\Pi(w)+\Pi(0)(\gamma))|x''(0)) + w^{-2}\gamma_\lambda(x'(s)|m - \tfrac{1}{2}(\gamma\Pi(s)+\Pi(0)\gamma)|x''(0))\gamma_\lambda \times \exp[\tfrac{1}{4}i(\Delta x)^2(w^{-1}-s^{-1})]\}. \quad (3.27')$$

By consulting Eq. (3.19) for the spinor character of the matrix element, one can combine the two parts of Eq. (3.27'). The following identities are useful in this connection:

$$\gamma_\lambda{}^2 = -4; \quad \gamma_\lambda\gamma_\delta\gamma_\lambda = 4\gamma_\delta \quad (3.28a)$$

$$\gamma_\lambda\gamma_\mu\gamma_\lambda = 2\gamma_\mu; \quad \gamma_\lambda\gamma_\mu\gamma_\delta\gamma_\lambda = -2\gamma_\mu\gamma_\delta \quad (3.28b)$$

$$\gamma_\lambda\sigma_{\mu\nu}\gamma_\lambda = 0; \quad (3.28c)$$

$$\gamma_\lambda[\gamma_\mu, \sigma_{\nu\rho}]\gamma_\lambda = -2[\gamma_\mu, \sigma_{\nu\rho}]; \quad \gamma_\lambda\{\gamma_\mu, \sigma_{\nu\rho}\}\gamma_\lambda = 2\{\gamma_\mu, \sigma_{\nu\rho}\}. \quad (3.28d)$$

The expansion of the mass operator Eq. (3.27') analogous to the expression (3.19) for the Green's function may now be written by inspection with the help of the operators $A(w)$, $B(w)$, etc.:

$$\begin{aligned}\bar{M}(x', x'') = -i\alpha(4\pi)^{-2}\int_0^\infty s^{-2}ds \int_0^s w^{-2}dw \\ \times\exp[-im^2 s + i\Delta x^2/4w]\Phi(x', x'') \\ \times([4m+\gamma\Delta x/s][A(s)-A(w)+C(s)-C(w)] \\ +2\gamma_\mu[A_{+\mu}(s)-A_{+\mu}(w)+C_{+\mu}(s)-C_{+\mu}(w)] \\ +4m[B(w)\tfrac{1}{2}\sigma F + D^1(w)\tfrac{1}{2}\sigma F^2 + D^2(w)\tfrac{1}{2}\sigma F^1 \\ -iG(w)\ \mathrm{tr}[F^1\sigma F^2] + (G(s)+G(w))\gamma_5\tfrac{1}{2}F^1F^{2*}] \\ -\{\gamma B_+(s)+(w/s)\gamma B_+(w)+(\gamma\Delta x/2s)(B(s) \\ +B(w)), \tfrac{1}{2}\sigma F\} + [\gamma B_-(s)-(w/s)\gamma B_-(w), \tfrac{1}{2}\sigma F] \\ -\{\gamma D_+{}^1(s)+(w/s)\gamma D_+{}^1(w)+(\gamma\Delta x/2s) \\ \times(D^1(s)+D^1(w)), \tfrac{1}{2}\sigma F^2\} - \{\gamma D_+{}^2(s) \\ +(w/s)\gamma D_+{}^2(w)+(\gamma\Delta x/2s)(D^2(s)+D^2(w)), \tfrac{1}{2}\sigma F^1\} \\ +i\{\gamma G_+(s)+(w/s)\gamma G_+(w)+(\gamma\Delta x/2s) \\ \times(G(s)+G(w)), \mathrm{tr}[F^1\sigma F^2]\} \\ +[\gamma D_-{}^1(s)-(w/s)\gamma D_-{}^1(w), \tfrac{1}{2}\sigma F^2] \\ +[\gamma D_-{}^2(s)-(w/s)\gamma D_-{}^2(w), \tfrac{1}{2}\sigma F^1] \\ -i[\gamma G_-(s)-(w/s)\gamma G_-(w), \mathrm{tr}[F^1\sigma F^2]] \\ +2[\gamma G_-(s)-(w/s)\gamma G_-(w)]\gamma_5\tfrac{1}{2}F^1F^{2*}]). \quad (3.29)\end{aligned}$$

It may be noticed that this operator has appreciable values only for $(\Delta x)^2 \lesssim m^{-2}$, for otherwise the exponential factors oscillate rapidly and average to zero on integration over the proper time parameters.

IV. FIRST-ORDER PART

Since we desire to obtain a result accurate to terms quadratic in the field, it is clear that the matrix elements of those terms in Eq. (3.29) which involve the field only linearly—all operators A and B—must be calculated more carefully than the quadratic terms. In particular, the field dependent terms that are contained in the rela-

tionships between $\gamma\Pi$ and $\gamma\Delta x/2s$, Eqs. (3.15) and (3.16), must be retained in the former while they may be ignored in the latter. Similarly, in the latter terms the factor $\Phi(x', x'')$ may be approximated by unity, while in the former it must be expanded to include linear terms. These rearrangements that must be carried out will now be considered without restricting the generality of the vector potential A_μ. We shall suppose, however, that a matrix element of the mass operator is taken between wave functions that satisfy Eq. (3.24); hence operators $\gamma(-i\partial'-eA(x'))$ and $\gamma(i\partial''-eA(x''))$ acting from the left or right, respectively, may be transferred to the wave function by an integration by parts and then replaced by $(-m)$.

The procedure is illustrated by its application to the first term in Eq. (3.29):[15]

$$
\begin{aligned}
&4m\exp[i(\Delta x)^2/4w]\Phi(x', x'')ise\\
&\times\int d^4k(-\tfrac{1}{2}\{\gamma\Delta x,\gamma J\}/sk^2)(e(s)-e(w))\\
&=4mise\int(-w/s)\Big[\gamma\Big(-i\partial'-eA(x')-\tfrac{1}{2}k(1+v)\\
&\quad-e\int d^4k_1\tfrac{1}{2}(1+v_1)(F^1\Delta x)\Big)\gamma J\\
&\quad+\gamma J\gamma\Big(i\partial''-eA(x'')+\tfrac{1}{2}k(1-v)\\
&\quad+e\int d^4k_1\tfrac{1}{2}(1-v_1)(F^1\Delta x)\Big)\Big]\Phi(x', x'')\\
&\quad\times\exp[i(\Delta x)^2/4w]d^4k(e(s)-e(w))/k^2\\
&=4m\exp[i(\Delta x)^2/4w]\Phi(x', x'')\\
&\quad\times\Big|ie\int d^4k[2m\gamma J-k^2\tfrac{1}{2}\sigma F][e(s)-e(w)]\Big/k^2\\
&\quad+(ie)^2w\int d^4k_1d^4k_2\Big[i\gamma J^2(\gamma F^1\Delta x)\tfrac{1}{2}(1-v_1)\\
&\quad-i(\gamma F^1\Delta x)\gamma J^2\tfrac{1}{2}(1+v_2)\Big](e_2(s)-e_2(w))\Big/k_2^2\Big|. \qquad (4.1)
\end{aligned}
$$

In carrying out this reduction as well as in the treatment of the other first-order terms the following identities help to simplify the results:

$$\{\gamma J,\gamma k\}=0; \qquad (4.2a)$$

$$\tfrac{1}{2}[\gamma J,\gamma k]=k^2\tfrac{1}{2}\sigma F; \qquad (4.2b)$$

$$\tfrac{1}{2}\{\gamma_\mu,\tfrac{1}{2}\sigma F\}=i\gamma_5(\gamma F^*)_\mu;\quad \tfrac{1}{2}\{\gamma k,\tfrac{1}{2}\sigma F\}=0; \qquad (4.2c)$$

$$\tfrac{1}{2}[\gamma_\mu,\tfrac{1}{2}\sigma F]=i(\gamma F)_\mu;\quad \tfrac{1}{2}[\gamma k,\tfrac{1}{2}\sigma F]=\gamma J. \qquad (4.2d)$$

[15] Note that d^4k conceals a dependence on the coordinates x' and x''.

If the gauge dependent factor is now expanded up to first-order terms, one obtains the contributions to the mass operator that are linear in the external field,

$$
\begin{aligned}
&\bar{M}_1(x', x'')\\
&=(\alpha/2\pi)\int_0^\infty s^{-2}ds\int_0^s dw\exp[im^2(s-w)]\\
&\quad\times\int(2\pi)^{-4}d^4p e^{ip\Delta x}\exp[-iw(p^2+m^2)]ie\\
&\quad\times\int d^4k\{[2m^2w(2-w/s)+iw/s]\\
&\quad\times[e(s)-e(w)]\gamma J/k^2+\tfrac{1}{2}[s+w-v^2(s-w)]\\
&\qquad\times e(s)\gamma J-mw(1-w/s)e(s)\tfrac{1}{2}\sigma F\}. \qquad (4.3)
\end{aligned}
$$

We have returned here to a Fourier representation of

$$-i(4\pi w)^{-2}\exp[i(\Delta x)^2/4w]$$

$$=\int(2\pi)^{-4}d^4p e^{ip\Delta x}\exp[-iwp^2]. \qquad (4.4)$$

The remaining parts of the terms we have considered are explicitly second order in the field,

$$
\begin{aligned}
&\bar{M}_2{}^I(x', x'')\\
&=(\alpha/2\pi)\int_0^\infty s^{-2}ds\int_0^s dw\exp[-im^2(s-w)]\\
&\quad\times\int(2\pi)^{-4}d^4p e^{ip\Delta x}\exp[-iw(p^2+m^2)](ie)^2\\
&\quad\times\int d^4k_1d^4k_2\{\tfrac{1}{2}iw(v_1-v_2)(\gamma F^1\Delta x)(\Delta x J^2)\\
&\quad\times[e_2(s)-e_2(w)]/k_2^2+imw(2-w/s)\\
&\quad\times(v_2J^2F^1\Delta x+\tfrac{1}{2}[\gamma J^2,\gamma F^1\Delta x])\\
&\quad\times[e_2(s)-e_2(w)]/k_2^2-\tfrac{1}{4}iw(v_2\{\gamma F^1\Delta x,\tfrac{1}{2}\sigma F^2\}\\
&\quad+v_1v_2[\gamma F^1\Delta x,\tfrac{1}{2}\sigma F^2])[e_2(s)-(w/s)e_2(w)]\\
&\quad-\tfrac{1}{4}iw(v_1\{\gamma F^1\Delta x,\tfrac{1}{2}\sigma F^2\}+[\gamma F^1\Delta x,\tfrac{1}{2}\sigma F^2])\\
&\quad\times[e_2(s)+(w/s)e_2(w)]+(\gamma J^2)(A^1\Delta x)\\
&\quad\times[2m^2w(2-w/s)+iw/s][e_2(s)-e_2(w)]/k_2^2\\
&\quad+\tfrac{1}{2}(\gamma J^2)(A^1\Delta x)[s+w-v_2^2(s-w)]e_2(s)\\
&\qquad-m(\tfrac{1}{2}\sigma F^2)(A^1\Delta x)w(1-w/s)e_2(s)\}. \qquad (4.5)
\end{aligned}
$$

They will be considered later together with the second-order terms C, D, and G in Eq. (3.29).

In the evaluation of the matrix element of Eq. (4.3) in an S-state of a hydrogenic atom,

$$\bar{M}_1=\int d\mathbf{r}'d\mathbf{r}''dl''\bar{\psi}_0(x')\bar{M}_1(x', x'')\psi_0(x''), \qquad (4.6)$$

it must be remembered that only corrections of orders α and $Z\alpha^2$ with respect to the matrix element of the hyperfine energy density $\frac{1}{2}\sigma F$ are required. Since a coefficient α appears explicitly, all other factors need be treated only to order $Z\alpha$. Thus the energy of the electron in this state can be approximated by the rest energy, so that the integration over t'' can be carried out when it is noticed that for a static potential

$$A_\mu(k)=A_\mu(\mathbf{k})\delta(k_0) \text{ and } \psi_0(x)=\psi_0(\mathbf{r})e^{-im^2t}. \quad (4.7)$$

Then one obtains

$$\bar{M}_1=\int d\mathbf{r}'d\mathbf{r}''\bar{\psi}_0(\mathbf{r}')(\alpha/2\pi)\int_0^\infty s^{-2}ds\int_0^\infty dw$$

$$\times\exp[-im^2(s-w)]\int(2\pi)^{-3}d\mathbf{p}e^{i\mathbf{p}\cdot\Delta\mathbf{r}}$$

$$\times\exp[-iwp^2]ie\int_{-1}^{1}\tfrac{1}{2}dv\int(2\pi)^{-3}d\mathbf{k}$$

$$\times e^{\frac{1}{2}i\mathbf{k}\cdot[\mathbf{r}'(1+v)+\mathbf{r}''(1-v)]}\{\quad\}\psi_0(\mathbf{r}'') \quad (4.8)$$

where $\{\quad\}$ stands for the bracket of Eq. (4.3).

The presence of the exponentials $e(s)$ and $e(w)$ in every term together with factor $e^{\frac{1}{2}i\mathbf{k}\cdot(\mathbf{r}'+\mathbf{r}'')}$ implies that most of the contribution to $\bar{M}_1$ comes from the region of space within one electronic Compton wavelength $1/m$ of the origin. The crudest approximation to $\bar{M}_1$ is therefore obtained when the small components of ψ_0 are neglected and the function itself is replaced by the value $\varphi_0(0)$ of the Pauli wave function at the origin. Only the last term in Eq. (4.3) fails to vanish, whence, with $u=1-w/s$,

$$\bar{M}_1=-(\alpha/2\pi)\int_0^\infty im^2ds\int_0^1 du\exp[-im^2su]$$

$$\times 2u(1-u)\tfrac{2}{3}\mu_0\langle\boldsymbol{\sigma}\cdot\boldsymbol{\mu}\rangle|\varphi_0(0)|^2$$

$$=-\tfrac{2}{3}\mu_0\langle\boldsymbol{\sigma}\cdot\boldsymbol{\mu}\rangle|\varphi_0(0)|^2(\alpha/2\pi). \quad (4.9)$$

This formula leads to an addition to the hyperfine structure separation due to the anomalous magnetic moment $\mu_0\alpha/2\pi$.

To obtain the corrections to this result one must use more accurate solutions of Eq. (3.24). The first-order effects of the magnetic field are included in the expression

$$\psi(x)=\psi_c(x)+e\int G_c(x,x')\boldsymbol{\gamma}\cdot\mathbf{A}^M(\mathbf{r}')\psi_c(x')d^4x', \quad (4.10)$$

which depends on the exact Coulomb wave function $\psi_c(x)$ and on the Coulomb Green's function G_c. The last term may be approximated quite crudely because the vector potential appearing in it, taken with the mass operator that is linear in the field, gives explicitly quadratic field-dependent terms. The Green's function is therefore replaced by that of the free particle,

$$G(x,x')=\int(2\pi)^{-4}d^4k e^{ik(x-x')}(m-\gamma k)/(m^2+k^2), \quad (4.11)$$

and the energy of the state is approximated by the rest energy

$$\psi(x)=\psi(\mathbf{r})e^{-im^2t}, \quad \psi_c(x)=\psi_c(\mathbf{r})e^{-im^2t}. \quad (4.12)$$

After the integration over t', the spatial dependence of the wave function is[16]

$$\psi(\mathbf{r})=\psi_c(\mathbf{r})+\int(2\pi)^{-3}(k^2)^{-1}d\mathbf{k}d\mathbf{r}'e^{i\mathbf{k}\cdot(\mathbf{r}-\mathbf{r}')}$$

$$\times[m(1+\gamma_0)-\boldsymbol{\gamma}\cdot\mathbf{k}]\boldsymbol{\gamma}\cdot\mathbf{A}^M(\mathbf{r}')\psi_c(\mathbf{r}'). \quad (4.13)$$

In terms of the Pauli wave function, the large components of this wave function for an S-state are

$$\varphi_0(\mathbf{r})+e\int(2\pi)^{-3}(k^2)^{-1}d\mathbf{k}d\mathbf{r}'e^{i\mathbf{k}\cdot(\mathbf{r}-\mathbf{r}')}\boldsymbol{\sigma}\cdot\mathbf{k}\boldsymbol{\sigma}\cdot\mathbf{A}^M(\mathbf{r}')\varphi_0(\mathbf{r}')$$

$$\cong\varphi_0(\mathbf{r})+e\int(2\pi)^{-3}(k^2)^{-1}d\mathbf{k}e^{i\mathbf{k}\cdot\mathbf{r}}i\boldsymbol{\sigma}\cdot(\mathbf{k}\times\mathbf{A}^M(k))\varphi_0(0)$$

$$\to\varphi_0(\mathbf{r})+\tfrac{2}{3}e\boldsymbol{\sigma}\cdot\boldsymbol{\mu}\varphi_0(0)/4\pi r, \quad (4.14)$$

where the second step results from the recognition that the constant $\varphi_0(0)$ is a sufficient approximation to the slowly varying wave function, and the third step anticipates the spherically symmetrical averaging in the matrix element. Finally, the small components of the wave function Eq. (4.13) are

$$-i(\boldsymbol{\sigma}\cdot\boldsymbol{\nabla}/2m)\varphi_0(\mathbf{r}) \quad (4.15)$$

to the required accuracy. With these wave functions, the evaluation of the Dirac matrices in Eq. (4.8) leads to the four kinds of terms,

$$\bar{\psi}_0(\mathbf{r}')e\boldsymbol{\gamma}J^M\psi_0(\mathbf{r}'')$$

$$\to\varphi_0^*(\mathbf{r}')[e\boldsymbol{\sigma}\cdot J^M(\mathbf{k})\boldsymbol{\sigma}\cdot(\mathbf{p}-\tfrac{1}{2}\mathbf{k}(1-v))$$

$$+\boldsymbol{\sigma}\cdot(\mathbf{p}+\tfrac{1}{2}\mathbf{k}(1+v))e\boldsymbol{\sigma}\cdot\mathbf{J}^M(\mathbf{k})]\varphi_0(\mathbf{r}'')/2m$$

$$\to\tfrac{2}{3}\mu_0\langle\boldsymbol{\sigma}\cdot\boldsymbol{\mu}\rangle k^2\varphi_0^*(\mathbf{r}')\varphi_0(\mathbf{r}'')/2\pi, \quad (4.16)$$

$$\bar{\psi}_0(\mathbf{r}')e\boldsymbol{\gamma}J^E\psi_0(\mathbf{r}'')$$

$$\to\tfrac{2}{3}\langle\boldsymbol{\sigma}\cdot\boldsymbol{\mu}\rangle 2Z\alpha\tfrac{1}{2}[\varphi_0^*(\mathbf{r}')\varphi_0(0)/r''$$

$$+\varphi_0^*(0)\varphi_0(\mathbf{r}'')/r']/2\pi, \quad (4.17)$$

$$\bar{\psi}_0(\mathbf{r}')e\tfrac{1}{2}\sigma F^M\psi_0(\mathbf{r}'')\to\tfrac{2}{3}e\langle\boldsymbol{\sigma}\cdot\boldsymbol{\mu}\rangle\varphi_0^*(\mathbf{r}')\varphi_0(\mathbf{r}'')/2\pi, \quad (4.18)$$

$$\bar{\psi}_0(\mathbf{r}')e\tfrac{1}{2}\sigma F^E\psi_0(\mathbf{r}'')\to 0. \quad (4.19)$$

The symmetry of $\bar{M}_1(x',x'')$ in $\mathbf{r}'$ and $\mathbf{r}''$ and the fact that it is large only near the origin imply that the ex-

[16] We are indebted to Norman M. Kroll for calling to our attention the necessity for this magnetic correction.

pansion of the Coulomb wave function

$$\varphi_0(\mathbf{r})=\varphi_0(0)(1-Z\alpha rm),$$
$$\varphi_0^*(\mathbf{r}')\varphi_0(\mathbf{r}'')=|\varphi_0(0)|^2(1-2Z\alpha r'm), \tag{4.20}$$

is sufficiently accurate to be used in Eq. (4.8). With all these approximations the matrix element simplifies to

$$\bar{M}_1=\tfrac{2}{3}\mu_0\langle\boldsymbol{\sigma}\cdot\boldsymbol{\mu}\rangle|\varphi_0(0)|^2(\alpha/2\pi)\int_0^\infty im^2ds\int_0^1 du$$
$$\times\exp[-ism^2u]\int_{-1}^1\tfrac{1}{2}dv\int(2\pi)^{-6}d\mathbf{p}d\mathbf{k}d\mathbf{r}'d\mathbf{r}''$$
$$\times e^{i\mathbf{p}\cdot(\mathbf{r}'-\mathbf{r}'')}e^{\frac{1}{2}i\mathbf{k}\cdot[\mathbf{r}'(1+v)+\mathbf{r}''(1-v)]}$$
$$\times\{[1-2Z\alpha r'm+4Z\alpha m/r'k^2][(2(1-u^2)$$
$$-(1-u)/im^2s)(e(s)-e(s(1-u)))$$
$$+\tfrac{1}{2}(2-u-uv^2)(k^2/m^2)e(s)]$$
$$-(1-2Z\alpha r'm)2u(1-u)e(s)\}. \tag{4.21}$$

The integrations of $\mathbf{r}''$ and $\mathbf{p}$ are trivial because

$$\int(2\pi)^{-3}d\mathbf{r}''\exp[i\mathbf{r}''\cdot(\tfrac{1}{2}\mathbf{k}(1-v)-\mathbf{p})]$$
$$=\delta(\mathbf{p}-\tfrac{1}{2}\mathbf{k}(1-v)). \tag{4.22}$$

The integrations over $\mathbf{r}'$ and k are of the form

$$\int(2\pi)^{-3}d\mathbf{r}'d\mathbf{k}e^{i\mathbf{k}\cdot\mathbf{r}'}\exp[-\tfrac{1}{4}isk^2\lambda_n]$$
$$\times\{1;\,k^2;\,r';\,r'k^2;\,(r'k^2)^{-1};\,(r')^{-1}\}$$
$$=\{1;\,0;\,2(i\lambda_n s/\pi)^{\frac{1}{2}};\,-4(i\lambda_n s\pi)^{-1};$$
$$-(i\lambda_n s/\pi)^{\frac{1}{2}};\,2(i\lambda_n s\pi)^{-\frac{1}{2}}\},\quad(n=1,2) \tag{4.23}$$

where

$\lambda_1=(1-v)(2-u(1-v))$ from terms involving $e(s)$,
$\lambda_2=2(1-v)(1-u)$ from terms involving $e(s(1-u))$. (4.24)

The proper time integrations are Γ functions. These operations leave the following integral over the two parameters u and v:

$$\bar{M}_1=\tfrac{2}{3}\mu_0\langle\boldsymbol{\sigma}\cdot\boldsymbol{\mu}\rangle|\varphi_0(0)|^2(\alpha/2\pi)\int_0^1 du\int_{-1}^1\tfrac{1}{2}dv$$
$$\times\{-2(1-u)(1-2Z\alpha u^{-\frac{1}{2}}\lambda_1^{\frac{1}{2}})$$
$$+[-2Z\alpha+4Z\alpha(-\tfrac{1}{2})][2(u^{-1}(1-u^2)$$
$$-u^{-\frac{1}{2}}(1-u))(\lambda_1^{\frac{1}{2}}-\lambda_2^{\frac{1}{2}})$$
$$-2(2-u-uv^2)u^{-\frac{1}{2}}\lambda_1^{-\frac{1}{2}}]\}. \tag{4.25}$$

With the help of a table of integrals Eq. (4.25) is evaluated to

$$\bar{M}_1=-\tfrac{2}{3}\mu_0\langle\boldsymbol{\sigma}\cdot\boldsymbol{\mu}\rangle|\varphi_0(0)|^2\{(\alpha/2\pi)$$
$$-\tfrac{1}{4}Z\alpha^2(60\ln 2-23)\}. \tag{4.26}$$

V. SECOND-ORDER TERMS

The host of second-order terms in Eqs. (3.29) and (4.5) must now be treated in a manner similar to the treatment of the first-order terms, except that an order of accuracy can be sacrificed in the expressions for the wave functions which are now approximated by their value at the position of the nucleus,

$$\psi_0(x)\cong\varphi_0(0)e^{-imt}. \tag{5.1}$$

To carry out the coordinate integrations it is convenient to return to momentum space with the aid of Eqs. (4.4) and the inverse of Eq. (3.6),

$$\Delta x_\mu\to 2wp_\mu,$$
$$\Delta x_\mu\Delta x_\nu\to 4w^2p_\mu p_\nu+2iw\delta_{\mu\nu}, \tag{5.2}$$
$$\Delta x_\mu\Delta x_\nu\Delta x_\lambda\to 8w^3p_\mu p_\nu p_\lambda+4iw^2(\delta_{\mu\nu}p_\lambda+\delta_{\mu\lambda}p_\nu+\delta_{\nu\lambda}p_\mu).$$

The coordinate integrations now lead to Dirac δ-functions relating the momentum variables k_1, k_2, and p as follows:

$$\bar{M}_2=(\alpha/4\pi)\int_0^\infty s^{-2}ds\int_0^s dw\exp[-im^2(s-w)]$$
$$\times\int(2\pi)^{-1}d\mathbf{k}_1d\mathbf{k}_2d^4p\exp[-iw(p^2+m^2)]$$
$$\times(ie)^2\int_{-1}^1\tfrac{1}{2}dv_1\int_{-1}^{v_1}\tfrac{1}{2}dv_2\delta(\mathbf{k}_1+\mathbf{k}_2)$$
$$\times\delta(\mathbf{p}+\tfrac{1}{2}\mathbf{k}_1(v_1-v_2))\delta(p_0-m)$$
$$\times\varphi_0^*(0)\{\quad\}\varphi_0(0), \tag{5.3}$$

where { } stands for the details of Eqs. (3.29) and (4.5); the terms of the latter have been symmetrized in the arguments v_1 and v_2. This bracket will now be evaluated in the light of the fact that it is of interest only when the arguments of the δ-functions vanish, when

$$\mathbf{k}_1=-\mathbf{k}_2,\quad\mathbf{p}=\tfrac{1}{2}\mathbf{k}_1\Delta v=-\tfrac{1}{2}\mathbf{k}_2\Delta v,\quad\Delta v=v_1-v_2. \tag{5.4}$$

These relations, coupled with the facts that the two field vectors are the product of an electric with a magnetic field and that in the final integration over k_1 only spherically symmetrical quantities can survive, greatly simplify Eq. (5.3). It is easy to verify that in addition to the anticommutators in Eqs. (3.29) and (4.5) only two terms,

$$\varphi_0^*(0)\tfrac{1}{2}\sigma F^1A^1\Delta x\varphi_0(0)$$
$$\to\tfrac{2}{3}\langle\boldsymbol{\sigma}\cdot\boldsymbol{\mu}\rangle|\varphi_0(0)|^2(2Z\alpha)(2mw/2\pi k_1^3) \tag{5.5a}$$

and

$$\varphi_0^*(0)[\gamma J^2, \gamma F^1\Delta x]\varphi_0(0) \rightarrow \tfrac{2}{3}\langle\boldsymbol{\sigma}\cdot\mathbf{u}\rangle|\varphi_0(0)|^2(2Z\alpha)(4imw/2\pi) \quad (5.5b)$$

in Eq. (4.5), fail to vanish.[17] The anticommutators are evaluated as follows (for the sake of brevity, the symbols of Eq. (3.20) are used to represent the integrands given there, and it is supposed that the substitution (5.2) is made):

$$\varphi_0^*(0)[\{(\gamma\Delta x/2s)(D^1(s)+D^1(w)),\tfrac{1}{2}\sigma F^2\} + \{(\gamma\Delta x/2s)(D^2(s)+D^2(w)),\tfrac{1}{2}\sigma F^1\}]\varphi(0) \rightarrow \tfrac{2}{3}\langle\boldsymbol{\sigma}\cdot\mathbf{u}\rangle|\varphi_0(0)|^2(2Z\alpha)4(m^2w^2-iw) \times[2E(s)-e_1(s)-e_2(s)+(w/s)(2E(w) -e_1(w)-e_2(w))]/2\pi k_1^2; \quad (5.5c)$$

$$\varphi_0^*(0)[\{\gamma(D_+^1(s)+(w/s)D_+^1(w)),\tfrac{1}{2}\sigma F^2\} + \{\gamma(D_+^2(s)+(w/s)D_+^2(w)),\tfrac{1}{2}\sigma F^1\}]\varphi_0(0) \rightarrow \tfrac{2}{3}\langle\boldsymbol{\sigma}\cdot\mathbf{u}\rangle|\varphi_0(0)|^2(2Z\alpha)(-2s) \times[(\Delta v)^2w(E(s)+(w/s)^2E(w)) + \Delta v(1-\Delta v)s(E(s)+(w/s)^3E(w))]/2\pi; \quad (5.5d)$$

$$-i\varphi_0^*(0)\{(\gamma\Delta x/2s)(G(s)+G(w)),\operatorname{tr}(F^1\sigma F^2)\}\varphi_0(0) \rightarrow \tfrac{2}{3}\langle\boldsymbol{\sigma}\cdot\mathbf{u}\rangle|\varphi_0(0)|^2(2Z\alpha)2sw\Delta v \times(E(s)+(w/s)^2E(w))/2\pi; \quad (5.5e)$$

$$-i\varphi_0^*(0)\{\gamma(G_+(s)+(w/s)G_+(w)),\operatorname{tr}(F^1\sigma F^2)\}\varphi_0(0) \rightarrow \tfrac{2}{3}\langle\boldsymbol{\sigma}\cdot\mathbf{u}\rangle|\varphi_0(0)|^2(2Z\alpha)(-2s^2\Delta v) \times(E(s)+(w/s)^2E(w))/2\pi; \quad (5.5f)$$

$$\varphi_0^*(0)\{\gamma F^1\Delta x,\tfrac{1}{2}\sigma F^2\}\varphi_0(0) \rightarrow \tfrac{2}{3}\langle\boldsymbol{\sigma}\cdot\mathbf{u}\rangle|\varphi_0(0)|^2(2Z\alpha)(4iw\Delta v/2\pi). \quad (5.5g)$$

One exponential factor simplifies,

$$E(s)=\exp[-\tfrac{1}{4}isk_1^2\Delta v(2-\Delta v)], \quad (5.6)$$

while the others can be combined (see Eq. (5.5c)),

$$\int_{-1}^{1}\tfrac{1}{2}dv_1\int_{-1}^{v_1}\tfrac{1}{2}dv_2(e_1(s)+e_2(s)) \rightarrow \int_{-1}^{1}\tfrac{1}{2}dv_1\int_{-1}^{1}\tfrac{1}{2}dv_2e_2(s) \quad (5.7)$$

so that they will be taken together with the contributions (5.5a, b, g) from Eq. (4.5).

Then, after the parameter $u=1-w/s$ is introduced, the remaining momentum integration is carried out. The relevant formulas are

$$\int d\mathbf{k}\exp[-\tfrac{1}{4}isk^2\lambda_i]\{1;(k^2)^{-1}\} = \{8\pi^{\frac{1}{2}}(is\lambda_i)^{-\frac{3}{2}};4\pi^{\frac{1}{2}}(is\lambda_i)^{-\frac{1}{2}}\}, \quad (5.8)$$

where the λ_i have the following significance:

$$\begin{aligned}&\lambda_1=\Delta v(2-\Delta v)\text{ from }E(s),\\ &\lambda_2=2\Delta v(1-u)\text{ from }E(w),\\ &\lambda_3=1-v_2^2+(\Delta v)^2(1-u)\text{ from }e_2(s),\\ &\lambda_4=(1-v_2^2+(\Delta v)^2)(1-u)\text{ from }e_2(w).\end{aligned} \quad (5.9)$$

The proper time integration, as before, involves half-integral Γ-functions. It leaves the two contribution to the hyperfine energy

$$\begin{aligned}\bar{M}_2^A&=\tfrac{2}{3}\mu_0\langle\boldsymbol{\sigma}\cdot\mathbf{u}\rangle|\varphi_0(0)|^2(2Z\alpha^2/2\pi)\\ &\times\int_{-1}^{1}\tfrac{1}{2}dv_1\int_{-1}^{v_1}\tfrac{1}{2}dv_2\int_0^1 du\{4(1-u)^2u^{-\frac{1}{2}}\\ &\times(\lambda_1^{-\frac{1}{2}}-\lambda_2^{-\frac{1}{2}})+4(1-u)u^{-\frac{1}{2}}\\ &\times(2\lambda_1^{-\frac{1}{2}}-(1-u)\lambda_2^{-\frac{1}{2}})-4(u^{\frac{1}{2}}\Delta v(1-\Delta v)\\ &+u^{-\frac{1}{2}}\Delta v)\lambda_1^{-\frac{1}{2}}-4u^{-\frac{1}{2}}(1-u)^2\Delta v\lambda_2^{-\frac{1}{2}}\}\\ &=\tfrac{2}{3}\mu_0\langle\boldsymbol{\sigma}\cdot\mathbf{u}\rangle|\varphi_0(0)|^2 4Z\alpha^2(1-\ln 2)\end{aligned} \quad (5.10)$$

and

$$\begin{aligned}\bar{M}_2^B&=\tfrac{2}{3}\mu_0\langle\boldsymbol{\sigma}\cdot\mathbf{u}\rangle|\varphi_0(0)|^2(2Z\alpha^2/2\pi)\\ &\times\int_{-1}^{1}\tfrac{1}{2}dv_1\int_{-1}^{1}\tfrac{1}{2}dv_2\int_0^1 du4u^{-\frac{1}{2}}\\ &\times\{-(1-u)\lambda_3^{-\frac{1}{2}}+(1-u)^2\Delta v(v_1+v_2)\lambda_3^{-\frac{1}{2}}\\ &-(1-u)^2\lambda_4^{-\frac{1}{2}}+(1-u)^2(\Delta v)^2\lambda_4^{-\frac{1}{2}}\}\\ &=\tfrac{2}{3}\mu_0\langle\boldsymbol{\sigma}\cdot\mathbf{u}\rangle|\varphi_0(0)|^2Z\alpha^2(5-12\ln 2).\end{aligned} \quad (5.11)$$

The sum of the three corrections is

$$\bar{M}=-\tfrac{2}{3}\mu_0\langle\boldsymbol{\sigma}\cdot\mathbf{u}\rangle|\varphi_0(0)|^2 \times\{(\alpha/2\pi)-\tfrac{1}{4}Z\alpha^2(13-4\ln 2)\}. \quad (5.12)$$

VI. VACUUM POLARIZATION

We shall now obtain the contribution of the vacuum polarization effects discussed in some detail in Sec. II. An equivalent to Eq. (2.14),

$$M^P=-e\int\bar{\psi}(\mathbf{r})\boldsymbol{\gamma}\cdot\mathbf{A}^P\psi(\mathbf{r})d\mathbf{r} \quad (6.1)$$

in conjunction with Eq. (2.19), permits direct utilization of the matrix elements calculated in Eqs. (4.16) and (4.17). The resultant expression,

$$\begin{aligned}M^P&=\tfrac{2}{3}\mu_0\langle\boldsymbol{\sigma}\cdot\mathbf{u}\rangle|\varphi_0(0)|^2(Z\alpha^2/2\pi)\\ &\times\int(2\pi)^{-3}d\tau d\mathbf{k}e^{i\mathbf{k}\cdot\mathbf{r}}(\tau k^2-2/\tau)m\\ &\times\int_0^1 dv\frac{v^2(1-\frac{1}{3}v^2)}{m^2+\frac{1}{4}k^2(1-v^2)},\end{aligned} \quad (6.2)$$

[17] Take, for example, the first term in C, Eq. (3.20f)
$\varphi_0^*(0)\Delta xJ^1\Delta xJ^1\varphi_0(0)\rightarrow|\varphi_0(0)|^2(4w^2(pJ^1)(pJ^1)+2iw(J^1J^1))$;
Now $J_\mu{}^BJ_\mu{}^M=0$ because $J^B=(\mathbf{0},J_0{}^B)$, $J^M=(\mathbf{J}^M,0)$; Further,
$(pJ^B(\mathbf{k}_1))(pJ^M(\mathbf{k}_2))\rightarrow p_0J_0{}^B(\mathbf{k}_1)\mathbf{p}\cdot\mathbf{J}^M(\mathbf{k}_2)$
$\rightarrow -mJ_0{}^B(\tfrac{1}{2}\Delta v\mathbf{k}_2\cdot\mathbf{J}^M(\mathbf{k}_2))=0.$

in which the expansion Eq. (2.22) has been made, includes Eq. (2.23) as the first contribution. The second one arises from the matrix element of the electric charge density. The substitution

$$[m^2+\tfrac{1}{4}k^2(1-v^2)]^{-1} = i\int_0^\infty ds\,\exp[-is(m^2+\tfrac{1}{4}k^2(1-v^2))] \quad (6.3)$$

brings Eq. (6.2) into a form corresponding precisely to Eq. (4.21). The space, momentum, and proper time integrations are carried out in exactly the same way as there. The final integral involves only the parameter v:

$$M^P=\tfrac{2}{3}\mu_0\langle\boldsymbol{\sigma}\cdot\mathfrak{y}\rangle|\,\varphi_0(0)\,|^2(Z\alpha^2/2\pi) \times\int_0^1 dv\,v^2(1-\tfrac{1}{3}v^2)[-4(1-v^2)^{-\frac{1}{2}}-4(1-v^2)^{-\frac{1}{2}}] =-\tfrac{2}{3}\mu_0\langle\boldsymbol{\sigma}\cdot\mathfrak{y}\rangle|\,\varphi_0(0)\,|^2\{\tfrac{3}{4}Z\alpha^2\}. \quad (6.4)$$

VII. SUMMARY

The two contributions to the Fermi formula are, Eqs. (5.12) and (6.4),

$$\bar{M}=-\tfrac{2}{3}\mu_0\langle\boldsymbol{\sigma}\cdot\mathfrak{y}\rangle|\,\varphi_0(0)\,|^2\{(\alpha/2\pi)+\tfrac{1}{4}Z\alpha^2(-13+4\ln 2)\}$$

and

$$M^P=-\tfrac{2}{3}\mu_0\langle\boldsymbol{\sigma}\cdot\mathfrak{y}\rangle|\,\varphi_0(0)\,|^2\{\quad+\tfrac{3}{4}Z\alpha^2\}.$$

Hence the Fermi formula Eq. (2.16) becomes[18]

$$\Delta E=-\tfrac{2}{3}\mu_0\langle\boldsymbol{\sigma}\cdot\mathfrak{y}\rangle|\,\varphi_0(0)\,|^2\{1+\alpha/2\pi-\tfrac{1}{4}Z\alpha^2(5-2\ln 2) -2.97\alpha^3/\pi^2\}(1+\tfrac{3}{4}(Z\alpha)^2)$$

when the fourth-order correction[2] to the magnetic moment is included.

With this change, the deduction of the value of the fine structure constant α from experimental quantities is modified. In terms of the notation of Dumond and Cohen,[5]

$$\Gamma=1.807\alpha^2+2\times10^{-6};$$
$$\delta(\alpha^{-1})=-0.880\alpha-1.5\times10^{-4}=-0.0065.$$

Hence

$$\alpha^{-1}=137.0364\pm0.0009.$$

Recent experimental and theoretical investigations of the deuteron[6,19] suggest that our treatment of the proton as a point magnetic dipole of infinite mass is inaccurate. An estimate of the necessary corrections is contained in reference 19.

It is a pleasure to acknowledge numerous stimulating and enlightening discussions with Julian Schwinger and with Norman M. Kroll.

[18] This result has been already reported by Karplus, Klein, and Schwinger, Phys. Rev. 84, 597 (1951). The same result has been obtained by a different method by N. M. Kroll and F. Pollock, Phys. Rev. 84, 594 (1951).

[19] F. E. Low and E. E. Salpteter, Phys. Rev. 83, 478 (1951).

Isotope Effect in the Imprisonment of Resonance Radiation

T. HOLSTEIN, D. ALPERT, AND A. O. MCCOUBREY
Westinghouse Research Laboratories, East Pittsburgh, Pennsylvania

(Received December 4, 1951)

On theoretical grounds it is expected that the decay time of imprisoned resonance radiation in the vapor of a single even isotope of mercury should be some six times larger than that observed with the natural samples of mixed isotopic constitution. To investigate this effect experimentally, decay measurements were carried out with samples of Hg^{199} (3 percent Hg^{199} and 0.1 percent Hg^{200}). For vapor densities $N \gtrsim 10^{14}$/cc, the predicted effect was verified. For $N > 10^{14}$/cc, the observed decay time drops below that predicted theoretically for pure Hg^{198}. This secondary effect is here attributed to the transfer of excitation from Hg^{198} to Hg^{199} and Hg^{200} by collisions of the second kind. Comparison of experimental data with an appropriately generalized theory permits estimation of the cross section for such collisions. The value so obtained is 10^{-12} cm², some twenty times the gas-kinetic cross section, and in order-of-magnitude agreement with theoretical expectations.

ACCORDING to theory,[1] the persistence of imprisoned resonance radiation in gases is strongly dependent upon the line shape of the radiation. In particular, it is found that a correct description of the phenomenon necessitates taking into account the hyperfine structure of the resonance line.[2] For example, the persistence time of the 2537A line of Hg, which in naturally occurring samples consists of five hyperfine components, is theoretically some six times smaller than that associated with a pure even isotope, which does not possess hyperfine structure. Measurements carried out with samples of Hg^{198} (3 percent contamination of Hg^{199}, 0.1 percent of Hg^{200}) not only confirm this marked difference, but also exhibit in a striking manner additional effects arising from small admixtures of isotopic impurities.

The measurements of the persistence time T of imprisoned radiation, as a function of vapor density N, were carried out in a manner previously described.[3] A special procedure[4] was required for the preparation of resonance tubes of Hg^{198} from two 2-milligram samples, kindly supplied to us by Dr. Meggers of the National Bureau of Standards. The experimental points are shown in Figs. 1(I) and 1(II) (black circles). By way of comparison, the corresponding data for natural mercury, presented in reference 3, are reproduced in both Figs. (black squares).

The dashed curves labeled "natural mercury," also reproduced from reference 3, represent upper and lower limits of the theoretical prediction for that case. The curves coincide in the region of Doppler broadening ($N < 10^{16}$/cc); in this region T is given analytically by the expression[3,5]

$$T = \tfrac{1}{8} k_0 R (\pi \log k_0 R)^{\frac{1}{2}} \tau, \qquad (1)$$

where τ, the lifetime of the isolated atom, is 1.08×10^{-7} sec, R is the radius of the resonance tube, and k_0 is the absorption coefficient at the center of the Doppler-broadened line. k_0 is given by the formula

$$k_0 = 2.19 \times 10^{-12} N/\theta^{\frac{1}{2}} \text{ cm}^{-1}, \qquad (2)$$

where θ is the absolute temperature. Equation (2) results from the assumption that the five hyperfine com-

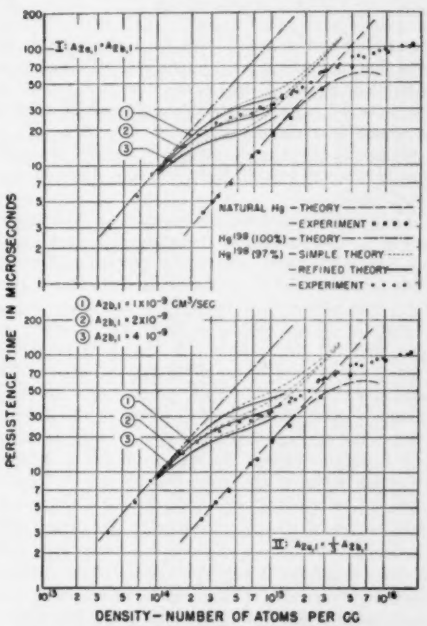
PERSISTENCE TIME IN MICROSECONDS
DENSITY – NUMBER OF ATOMS PER CC
NATURAL Hg – THEORY
– EXPERIMENT
Hg198 (100%) – THEORY
Hg198 (97%) – SIMPLE THEORY
– REFINED THEORY
– EXPERIMENT
I: A2a,1 = A2b,1
II: A2a,1 = ½ A2b,1

FIG. 1. Experimental and theoretical results on the imprisonment of resonance radiation in natural Hg, mono-isotopic Hg^{198}, and in a mixture of Hg^{198} (96.9 percent), Hg^{199} (3 percent), and Hg^{200} (0.1 percent). In the latter case the theoretical curves depend on the transfer coefficients, $A_{2a,1}$ and $A_{2b,1}$. Figure 1(I) is for the case $A_{2a,1} = A_{2b,1}$; Fig. 1(II) for the case $A_{2a,b} = \frac{1}{2} A_{2b,1}$.

[1] T. Holstein, Phys. Rev. **72**, 1212 (1947).
[2] Reference 1, Sec. 5.
[3] Alpert, McCoubrey, and Holstein, Phys. Rev. **76**, 1257 (1949). Footnote 7 of this reference contains the theoretical expression for T given in Eqs. (1) and (2) of the present paper. For the derivation of the result see T. Holstein, Phys. Rev. **83**, 1159 (1951).
[4] To be reported by D. Alpert and C. G. Matland in Rev. Sci. Instr.
[5] T. Holstein, Phys. Rev. **83**, 1159 (1951).

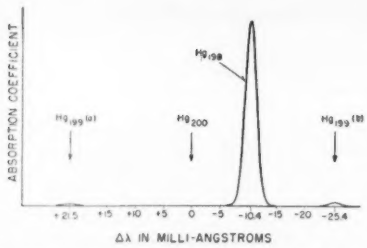

FIG. 2. Absorption spectrum of experimental Hg samples. On the scale of the figure the contribution of the Hg^{200} line is too small to be shown. In the case of Hg^{199} there are two hyperfine components, (a) and (b), corresponding to two excited states of total angular momentum $\frac{1}{2}$ and $\frac{3}{2}$, respectively.

ponents of the line are all of equal intensity; the more exact treatment,[2] which takes account of the actual intensity ratios of the different components, yields substantially the same result for T as (1) and (2).

The broken curve labeled "single isotope" is also given by an expression of the form of (1), in which, however, k_0 has to be multiplied by a factor of five, i.e.,

$$k_0 = 10.95 \times 10^{-12} N/\theta^{\frac{1}{2}}. \tag{2'}$$

The factor of five arises from the coalescence of the hyperfine components into the single line characteristic of Hg^{198}. It is immediately evident that for $N < 10^{14}$/cc the curve is in agreement with experiment. It will now be shown that the deviations for $N > 10^{14}$/cc can be explained in terms of nonradiative transfer of excitation between atoms of Hg^{198} and the other isotopic constituents.

The absorption spectrum of our samples is illustrated in Fig. 2. The maxima of the absorption lines are, in this case of Doppler broadening, proportional to the "line intensities," i.e., to the areas under the curves. Each line intensity, in turn, is proportional to the product of (a) the concentration of the absorbing isotope, and (b) the ratio of the statistical weights of excited and ground states of the line in question. The separations of the hyperfine components are large enough so that the absorption bands[3] of the different lines do not overlap; hence, radiative transfer of excitation between different isotopes or between different hyperfine states of the same isotope can be ignored. Then, at sufficiently low vapor densities, where nonradiative transfer is also absent, each line decays independently with its own characteristic persistence time. We may thus expect a very rapid decay[6] of the radiation from Hg^{199} and Hg^{200}, followed by a relatively long persistence of the Hg^{198} line. This is actually what is observed by visual examination of the oscillographic traces of light intensity *vs* time; the time constants given in Figs. 1(I) and 1(II) are taken from the terminal portion of these traces and hence represent the longest time constant, which is associated with Hg^{198}.

As the vapor density is increased, it becomes necessary to take into account collisions involving nonradiative transfer of excitation between the different hyperfine states. These collisions have essentially the effect of transferring excitation from the slowly decaying Hg^{198} line to the much more rapidly decaying lines of Hg^{199} and Hg^{200}, with the result that the over-all decay rate is speeded up.

A quantitative description of the phenomenon is afforded by the following set of equations for the time variation of the densities n_i of the different excited states:

$$dn_1/dt = -n_1/T_1 - n_1[A_{1,2a}N_2 + A_{1,2b}N_2 + A_{1,3}N_3] + [n_{2a}A_{2a,1} + n_{2b}A_{2b,1} + n_3A_{3,1}]N_1, \tag{4a}$$

$$dn_{2a}/dt = -n_{2a}/T_{2a} - n_{2a}A_{2a,1}N_1 + n_1A_{1,2a}N_2, \tag{4b}$$

$$dn_{2b}/dt = -n_{2b}/T_{2b} - n_{2b}A_{2b,1}N_1 + n_1A_{1,2b}N_2, \tag{4c}$$

$$dn_3/dt = -n_3/T_3 - n_3A_{3,1}N_1 + n_1A_{1,3}N_3. \tag{4d}$$

In these equations the subscripts 1, 2, 3 refer to isotopes Hg^{198}, Hg^{199}, and Hg^{200}; in the case of Hg^{199} the additional subscripts a and b are used to specify the two excited states of angular momentum $\frac{1}{2}$ and $\frac{3}{2}$, respectively. Terms of the form $-n_i/T_i$ describe the radiative decay of the ith excited state,[7] with time constants T_i characteristic of the isolated lines. Terms of the type $n_iA_{i,j}N_j$ represent the transfer of excitation from the ith to the jth excited state; each "transfer coefficient" $A_{i,j}$ is the gas-kinetic average of the cross section $Q_{i,j}$ for the process multiplied by the relative velocity of the colliding atoms.

Equations (4) are actually a simplified version of the more exact formulation which is given in the appendix of this paper. The simplification is twofold. Firstly, the radiative decay is not a straightforward emission process, as implied by the terms $-n_i/T_i$, but actually involves transport of radiation between different parts of the enclosure. Secondly, all excitation transfers among the isotopic impurities have been ignored; the collision terms in Eqs. (4) represent transfers either to or from Hg^{198}. The applicability of these simplifications to our problem is also discussed in the appendix.

Before solving Eqs. (4) we take advantage of the principle of detailed balancing to establish relationships between the different $A_{i,j}$. We consider the situation in which the enclosure is surrounded by perfectly reflecting walls. In this case both dn_i/dt and n_i/T_i are zero in

[6] For these lines, the values of k_0 to be inserted in (1) are smaller than (2') by factors of 50 to 1000.

[7] The subscripts i and j are here used primarily to enumerate the excited states, i.e., they take on the values 1, 2*a*, 2*b*, and 3. In the case of the isotopic densities N_i of normal atoms, however, the distinction between the notations 2*a* and 2*b* is meaningless; in this case, then, i and j assume the values 1, 2, and 3, which enumerate the isotopes.

Eqs. (4) and one obtains from (4b), (4c), (4d)

$$n_{2a}/n_1=(N_2/N_1)(A_{1,2a}/A_{2a,1}),$$
$$n_{2b}/n_1=(N_2/N_1)(A_{1,2b}/A_{2b,1}), \quad (5)$$
$$n_3/n_1=(N_3/N_1(A_{1,3}/A_{3,1}).$$

On the other hand, we have from general statistical considerations a kind of local thermodynamic equilibrium involving the ratios of the densities of the different excited states such that

$$n_1/N_1=Cw_1e^{-\epsilon_1/k\theta}, \quad n_{2a}/N_2=Cw_{2a}e^{-\epsilon_{2a}/k\theta},$$
$$n_{2b}/N_2=Cw_{2b}e^{-\epsilon_{2b}/k\theta}, \quad n_2/N_3=Cw_3e^{-\epsilon_3/k\theta}. \quad (6)$$

Here ϵ_i is the energy of the ith excited state and w_i its statistical weight relative to the ground state of the isotope involved. In the case at hand $w_1=w_3=3$, $w_{2a}=1$, and $w_{2b}=2$. Finally, C is a constant which, in the absence of complete thermodynamic equilibrium, is not determined.

Comparing Eqs. (5) and (6) and noting that, in the case at hand, $|\epsilon_i-\epsilon_j|\sim 10^{-4}$ ev$\ll k\theta$, we obtain

$$A_{1,2a}=\tfrac{1}{3}A_{2a,1}, \quad A_{1,2b}=\tfrac{2}{3}A_{2b,1}, \quad A_{1,3}=A_{3,1}. \quad (7)$$

The solution of Eqs. (4) is achieved by the standard technique of substituting $n_i=c_ie^{-t/T}$, where the c_i and T are constants to be determined. Elimination of the c_i then yields an algebraic equation of the fourth degree in T. The roots, T_α, of this equation characterize the "decay modes" of the n_i in the sense that each n_i, in general, can be written as a superposition of exponential decay terms $e^{-t/T\alpha}$. As pointed out in the text preceding Eqs. (4), the experimental observations refer to the terminal portion of the decay curve, for which the largest T_α is alone significant. For the case at hand, where N_2, $N_3\ll N_1$, the largest T_α (which we henceforth denote simply as T), may be approximated sufficiently accurately by the expression[8]

$$\frac{1}{T}=\frac{1}{T_1}+\frac{\frac{1}{3}(N_2/N_1)}{T_{2a}+1/(A_{2a,1}N_1)}+\frac{\frac{2}{3}(N_2/N_1)}{T_{2b}+1/(A_{2b,1}N_1)}+\frac{(N_3/N_1)}{T_3+1/(A_{3,1}N_1)}. \quad (8)$$

For low vapor densities such that $T_{2a}\ll 1/(A_{2a,1}N_1)$, $T_{2b}\ll 1/(A_{2b,1}N_1)$, and $T_3\ll 1/(A_{3,1}N_1)$, (8) reduces to a relation which with the use of (7) can be written as

$$1/T\cong 1/T_1+(A_{1,2a}+A_{1,2b})N_2+A_{1,3}N_3. \quad (8')$$

In this case the isotopic impurities act essentially as quenching agents; whatever excitation is transferred to them is for the most part radiated from the enclosure and hence constitutes a net loss.

At the other extreme of high densities such that

$$T_{2a}\gg 1/(A_{2a,1}N_1), \quad T_{2b}\gg 1/(A_{2b,1}N_1),$$

and $T_3\gg 1/(A_{3,1}N_1)$, we obtain

$$\frac{1}{T}\cong\frac{1}{T_1}+\frac{\frac{1}{3}(N_2/N_1)}{T_{2a}}+\frac{\frac{2}{3}(N_2/N_1)}{T_{2b}}+\frac{N_3/N_1}{T_3}. \quad (8'')$$

In this limit the predominance of the collision terms in Eqs. (4) gives rise to a thermodynamic equilibrium of the same type as described by (5) or (6). The right-hand side of (8'') may then be regarded as a weighted average of the decay rates, $1/T_i$, of the different excited states, each weighting factor being equal to the equilibrium fraction of excited atoms occupying the state in question.[8]

The first numerical calculations of T, based on (8) were carried out under the assumption that the 0.1 percent Hg^{200} impurity could be neglected. Results were obtained for various values of $A_{2a,1}$ and for different ratios[9] of $A_{2a,1}$ to $A_{2b,1}$; unity and $\frac{1}{3}$; they are represented by the light-dashed curves of Figs. 1(I) and 1(II), respectively. The behavior of these curves in the limits of high and low vapor density, in accordance with the remarks of the preceding paragraphs, is to be noted.

More recent computations have taken into account two refinements. Firstly, it was found that the presence of Hg^{200}, even in the small concentration of 0.1 percent, could not be ignored at densities (of the main isotope) $\sim 10^{15}$/cc. A second complication which manifests itself at high densities is the incipient effect of pressure broadening. Relegating the detailed calculation of this effect to the appendix (Sec. 4), we here write down the result. Namely, one adds to (8) the term

$$\Delta_p\equiv 1.01\times 10^{-10}N/(\theta\log k_0R)^{\frac{1}{2}}\ \text{sec}^{-1}. \quad (9)$$

The results obtained by the inclusion of these refinements are shown in Figs. 1(I) and 1(II) as solid curves for the cases of $A_{2a,1}/A_{2b,1}=1$ and $\frac{1}{3}$, respectively. The computations were performed only for vapor densities less than 10^{15}/cc; it was found by sample calculations that, for $N_1>10^{15}$/cc, the complicating effects of the overlap of the different hyperfine components rapidly become important. The limited results presented here, nevertheless, provide at least a qualitative understanding of the high density deviation of the experimental points from the simple theory as represented by the light-dashed curves.

[8] A simple way of deriving (8) is to assume that $T\gg T_{2a}, T_{2b}, T_3$. One may then take the left-hand sides of (4b), (4c), and (4d) equal to zero, thereby obtaining the appendix Eqs. (15A) for the ratios $n_{i\neq 1}/n_1$. Inserting the latter into (4a) and employing (7), we immediately arrive at (8). The assumption that $T\gg T_{i\neq 1}$ can then easily be justified *a posteriori* for the case of $N_{i\neq 1}/N_1\ll 1$ by inspection of (8''), which provides a lower limit for T.

[9] From the considerations of Sec. 5 of the appendix, the relative magnitudes of $A_{2a,1}$ and $A_{2b,1}$ are seen to depend upon the energy differences $|\epsilon_{2a}-\epsilon_1|$, and $|\epsilon_{2b}-\epsilon_1|$ of the excited levels involved in the excitation transfer. These are given in Table I of that section in wave-number units. Since $|\epsilon_{2a}-\epsilon_1|>|\epsilon_{2b}-\epsilon_1|$, the qualitative indication, based in Eq. (24A), is that $A_{2a,1}<A_{2b,1}$. Hence, the assumption $A_{2a,1}/A_{2b,1}=1$ doubtlessly represents an upper limit for the ratio. The other choice, namely $\frac{1}{3}$, appears to us, on the basis of Eq. (24A) and Table I, to be a reasonable lower limit.

Before proceeding further with the comparison of theory with experiment, we must point out that in the intermediate region of vapor densities ($\sim 5\times 10^{14}$/cc), for which $T_{2a}\sim 1/A_{2a,1}N_1$ and $T_{2b}\sim 1/A_{2b,1}$, the quantitative results are subject to some error. Namely, in this region it turns out that T_{2a} and T_{2b} are not much greater than the lifetime τ of the isolated atom; in other words, the lines of Hg^{199} are only moderately imprisoned. Unfortunately, our imprisonment formulas of the type of (1) are not quantitatively accurate for $T_i \cong 10\tau$. This inaccuracy is carried over, by virtue of (8), to the final values for T; some crude estimates indicate that the error thus incurred may be ~ 20 percent. With decreasing vapor densities, the errors in the T_i increase; however, as shown by (8′), T becomes essentially independent of the T_i.

With these considerations in mind, we have not attempted a detailed comparison of experiment with theory; it is nevertheless apparent that one can make an order of magnitude estimate for $A_{2b,1}$ which will give the best fit with the experimental points. Thus

$$A_{2b,1}\sim 2\times 10^{-9}\ \text{cm}^3/\text{sec}. \tag{9}$$

This estimate is not radically affected by different assumptions as to the ratio $A_{2a,1}/A_{2b,1}$.

Further comparison indicates that of the two choices for $A_{2a,1}/A_{2b,1}$ analyzed here, namely unity and $\frac{1}{3}$, the latter provides somewhat the better agreement with experimental facts. However, in view of the above remarks on the errors in the quantitative theory, we do not regard this indication as conclusive.

The order of magnitude of the transfer coefficient, as given by (9), deserves some comment. If we divide (9) by the mean relative velocity ($\sim 2\times 10^4$ cm/sec), we obtain an effective cross section,

$$Q\sim 10^{-13}\ \text{cm}^2, \tag{10}$$

which is some 20 to 30 times the gas-kinetic cross section (depending on the definition of the latter quantity). Actually, this result is not too surprising; in fact, cross sections for transfer of excitation can exceed gas-kinetic cross sections, especially when the energy levels of the colliding atoms are nearly coincident, as is the case with different isotopes of the same element.

An upper limit to $A_{2b,1}$ can be estimated by considering the transfer of excitation between identical atoms. For this case of exact resonance, the approximate theory presented in a paper by Furssov and Vlassov[10] may be employed. The calculation which is carried out in the appendix, Sec. V, yields the result

$$A_{2b,1}\sim 3.4\times 10^{-9}\ \text{cm}^3/\text{sec}, \tag{11}$$

which is in good order-of-magnitude agreement with (9).

There remains the question as to the effect of the energy-level discrepancy between Hg^{198} and Hg^{199}. The estimation of this effect, on the basis of a simplified theory of transfer of excitation, is also presented in Sec. V of the appendix; the conclusion therein reached is that the level discrepancy is too small to cause any order-of-magnitude diminution of $A_{2b,1}$ from the resonance value given in (11).

[10] W. Furssov and A. Vlassov, Physik. Z. Sowjetunion **10**, 378 (1936).

ACKNOWLEDGMENT

We take great pleasure in expressing our thanks to C. G. Matland for his active participation in the experimental work and for his assistance in the preparation of the manuscript.

APPENDIX

I. Formulation of the Decay Problem in Terms of Integro-Differential Equations

In this section, we seek a formulation which takes into account not only the collision-induced transfer of excitation in a given volume element (which is presented explicitly in Eqs. (4) of the text) but also the radiative transport of excitation between different volume elements of the enclosure. This goal is achieved by a straightforward generalization of the integro-differential Eq. (3.4) of reference 1,

$$\tau\partial n(\mathbf{r})/\partial t = -n(\mathbf{r}) + \int n(\mathbf{r}')G(\mathbf{r}',\mathbf{r})d\mathbf{r}', \tag{1A}$$

which describes the radiative transport of excitation for the case of a simple resonance state without hyperfine structure. In this equation the key quantity determining the time variation of the density of excited atoms, $n(\mathbf{r})$, is the kernel, $G(\mathbf{r}',\mathbf{r})$, of the integral term; it is defined as the probability that a resonance quantum emitted at $\mathbf{r}'$ is captured in a unit volume element centered at $\mathbf{r}$.

The required generalization to the case of present interest reads

$$\tau\partial n_i(\mathbf{r})/\partial t = -n_i(\mathbf{r}) + \int n_i(\mathbf{r})G_i(\mathbf{r}',\mathbf{r})d\mathbf{r}' + \tau\textstyle\sum_j [A_{j,i}N_i n_j(\mathbf{r}) - A_{i,j}N_j n_i(\mathbf{r})], \tag{2A}$$

where the subscripts i and j each take on the values 1, $2a$, $2b$, and 3. In these equations, the $G_i(\mathbf{r}',\mathbf{r})$ characterize the radiative transport for the different excited states. The relationship of Eqs. (2A) to Eqs. (4) of the text is treated in the following section.

II. Variational Treatment of the Basic Integro-Differential Transport Equations (2A)

For the purposes of the present paper we are interested in steady-state solutions, $n_i(\mathbf{r},t) = n_i(\mathbf{r})e^{-t/T}$, of (2A). For this case (2A) reduces to

$$-\tau n_i(\mathbf{r})/T = -n_i(\mathbf{r}) + \int n_i(\mathbf{r}')G_i(\mathbf{r}',\mathbf{r})d\mathbf{r}' + \tau\textstyle\sum_j [A_{j,i}N_i n_j(\mathbf{r}) - A_{i,j}N_j n_i(\mathbf{r})]. \tag{3A}$$

Now, by virtue of the text Eqs. (7), which are readily generalized to[11]

$$A_{i,j}=a_{ij}w_i, \tag{4A}$$

where

$$a_{ij}=a_{ji}, \tag{5A}$$

and, introducing the notation

$$F_i\equiv N_iw_i, \tag{6A}$$

we are able to establish the equivalence of (3A) to the following variational problem

$$\frac{\tau}{T}=1-\frac{\sum_i F_i^{-1}\int\int n_i(\mathbf{r}')G_i(\mathbf{r}',\mathbf{r})n_i(\mathbf{r})d\tau d\tau'}{\sum_i F_i^{-1}\int n_i^2(\mathbf{r})d\tau}+\tau\sum_{ij}a_{ij}\frac{F_jF_i^{-1}\int n_i^2(\mathbf{r})d\tau-\int n_i(\mathbf{r})n_j(\mathbf{r})d\tau}{\sum_i F_i^{-1}\int n_i^2(\mathbf{r})d\tau}; \tag{7A}$$

$$\delta(1/T)=0, \tag{8A}$$

as is easily verified.

The positive-definiteness of $1/T$ can be demonstrated by a procedure analogous to that used in reference 1, p. 1217. Namely, we can write (7A) in the alternate form

$$\frac{\tau}{T}=\frac{\sum_i F_i^{-1}\left[\int n_i^2(\mathbf{r})E_i(\mathbf{r})d\tau+\frac{1}{2}\int\int[n_i(\mathbf{r})-n_i(\mathbf{r}')]^2G(\mathbf{r},\mathbf{r}')d\tau d\tau'\right]}{\sum_i F_i^{-1}\int n_i^2(\mathbf{r})d\tau}$$

$$+\tfrac{1}{2}\sum_{ij}\tau A_{ij}\frac{\int[F_j^{\frac{1}{2}}F_i^{-\frac{1}{2}}n_i(\mathbf{r})-F_i^{\frac{1}{2}}F_j^{-\frac{1}{2}}n_j(\mathbf{r})]^2d\tau}{\sum_i F_i^{-1}\int n_i^2(\mathbf{r})d\tau}, \tag{9A}$$

where

$$E_i(\mathbf{r})=1-\int G_i(\mathbf{r},\mathbf{r}')d\tau'. \tag{10A}$$

In (9A) all the integrals are positive definite. The eigenvalues of $1/T$ can thus be arranged in a series of ascending positive numbers; the lowest of these, which is the one of interest to us, is an absolute minimum. Use of the Ritz variational procedure will therefore provide for $1/T$ an upper limit which will converge toward the true value as the number of adjustable parameters in the assumed functional forms for the $n_i(\mathbf{r})$ is increased.

We now choose

$$n_i(\mathbf{r})=n_if(\mathbf{r}), \tag{11A}$$

when n_i denotes the value of $n_i(\mathbf{r})$ at a convenient reference point in the enclosure. In the case of infinite cylinders we assume a parabolic form for $f(\mathbf{r})$:

$$f(\mathbf{r})=1-\rho^2/R^2, \tag{12A}$$

where ρ is the distance of the point $\mathbf{r}$ from the cylindrical axis; the reference point is, then, any point on the cylindrical axis.

Inserting (11A) into (9A), we obtain

$$\frac{1}{T}=\frac{\sum_i F_i^{-1}n_i^2/T_i}{\sum_i F_i^{-1}n_i^2}+\frac{1}{2}\frac{\sum_{ij}A_{ij}[F_j^{\frac{1}{2}}F_i^{-\frac{1}{2}}n_i-F_i^{\frac{1}{2}}F_j^{-\frac{1}{2}}n_j]^2}{\sum n_i^2F_i^{-1}}, \tag{13A}$$

where

$$\frac{1}{T_i}=\frac{1}{\tau}\frac{\int f^2(\mathbf{r})E_i(\mathbf{r})d\tau+\frac{1}{2}\int\int[f(\mathbf{r})-f(\mathbf{r}')]^2G_i(\mathbf{r},\mathbf{r}')d\tau d\tau'}{\int f^2(\mathbf{r})d\tau},$$

[11] w_i is the ratio of the statistical weight of the ith state divided by the statistical weight of the ground state, as employed in Eqs. (6) and subsequent text.

$1/T_i$ is actually the variational expression for the decay rate of an isolated line, as shown by comparison with Eq. (3.10) of reference 1.

An absolute minimum for (13A) is achieved by differentiation with respect to the n_i. The resulting equations are

$$n_i/T = n_i/\tau + \sum_j A_{ij}(F_j n_i - F_i n_j), \qquad (14A)$$

which, with the aid of (4A) and (6A), are seen to be just the equations one obtains by substituting the steady-state solutions

$$n_i(i) = n_i(0)e^{-t/T}$$

into Eqs. (4). In other words, our text procedure based on Eqs. (4) provides a variational approximation for $1/T$.

There remains the question as to how accurate a value of $1/T$ is obtained variationally by use of the $n_i(\mathbf{r})$ defined by (11A) and (12A). In this connection it should be pointed out that (a) the presence of the collision terms in (3A) or (7A) tends to equalize the spatial forms of the different $n_i(\mathbf{r})$; if, in particular, one passes to the high-density limit, where the collision terms dominate, the $n_i(\mathbf{r})$ bear constant ratios to each other [as given by the text Eqs. (5)] independent of position. (b) In the case of a single resonance state whose radiation is strongly imprisoned, reference 1 has shown that the assumption of a parabolic form for the density function yields a sufficiently accurate value for the decay time; in fact, Eq. (1) was derived[6] on this basis. (c) In the case of a weakly-imprisoned line, for which the parabolic function does not give good results, computational errors may be quite appreciable. These errors arise from the use of approximations, at various stages of the calculation, which are only asymptotically valid for the case of large optical opacities ($k_0R \gg 1$). It is these errors, in fact, which, as remarked in the second paragraph after Eq. (9), prevent us from achieving quantitative accuracy at intermediate vapor densities $\sim 5\times 10^{14}$/cc. Refinements in the variational treatment will not improve the situation unless they are accompanied by a reduction of the computational errors; this undertaking, however, promises to be exceedingly difficult and tedious.

III. Neglect of Collision Terms $A_{i,j}N_iN_j$, Where Neither i Nor j Are Equal to 1

In our treatment these terms are neglected relative to the terms $A_{i,1}n_1N_j$ and $A_{1,j}n_1N_j$; the reason is simply that both $N_{i\neq 1}/N_1 \ll 1$ and $n_{i\neq 1}/n_1 \ll 1$. The first inequality is valid "by construction," i.e., by virtue of the isotopic constitution of our samples. To demonstrate the validity of the second inequality, we observe the following: (a) In the limit of large vapor densities, where the collision terms become dominant, the ratios $n_{i\neq 1}/n_1$ are given by the text relations (6) which, apart from the weight factors and Boltzmann exponentials, are equal to the ratios $N_{i\neq 1}/N_1$, and are hence $\ll 1$. (b) In obtaining the approximate solution (8) of Eqs. (4) according to the prescription of reference 8, we find

$$n_{i\neq 1}/n_1 = A_{i,1}N_1/(1/T_i + A_{i,1}N_1), \qquad (15A)$$

which is even less than the high density limit as given by (6). Thus, in this case the inequality is *a fortiori* valid.

IV. Pressure-Broadening Effects

The initial manifestation of pressure broadening, with which we are alone concerned, have been treated in reference 1, pp. 1223–1224. In our case, we consider only the broadening of the Hg^{198} component and ignore the absorption of this line arising from the other hyperfine components. The effect of pressure broadening may then be represented quite simply by adding to the right-hand side of (8) the term

$$\Delta_p = 2a_p/\pi(\log k_0R)^{\frac{1}{2}}\tau; \qquad (16A)$$

(16A) is derived in much the same way as Eq. (5.14) of reference 1, which describes the effect of natural broadening in plane-parallel enclosures. The correspondence between the two expressions arises from the assumption that the pressure-broadened line shape is of the dispersion type $\sim[\frac{1}{4}\gamma_p^2+(\omega-\omega_0)^2]^{-1}$, which differs from the shape of the naturally broadened line, $\sim[\frac{1}{4}\tau^2+(\omega-\omega_0)^2]^{-1}$ only in the line width constant. The main differences between (16A) and (5.14) are (a) in the logarithmic factors, which are characteristic of enclosure geometries and (b) the replacement of the factor $a_N=(\lambda_0/4\pi)\tau(2R\theta/M)^{\frac{1}{2}}$ by $a_p=a_N\tau\gamma_p$; the absence of the factor $1/\tau$ from (5.14) is due to the circumstance that the time unit is there taken to be the natural lifetime of the isolated atom.

For γ_p we take the theoretical result of Furssov and Vlassov,[10] which, as shown in reference 1, p. 1224, may be written as

$$\gamma_p\tau = N\lambda_0^3/2\pi^2 = 0.83\times 10^{-15}N. \qquad (17A)$$

Combining (16A), (17A), and the expressions for a_p and a_N given above, and inserting numerical values, we obtain the text expression (9) for Δ_p.

V. Transfer of Excitation between Atoms

For the case of transfer of excitation between two identical atoms an approximate expression for the cross section may be derived from the results of Furssov and Vlassov.[10] These authors treated the case in which the atomic ground and excited states involved in the collision are S and P states. The expression which they obtain for the probability of excitation transfer in a binary encounter (Eq. 28 of their paper) may be written as

$$P(\rho) = \tfrac{2}{3}e^4f^2/m^2\omega_0^2\rho^4v^2. \qquad (18A)$$

Here, $P(\rho)$ (in the notation of Furssov and Vlassov, $\Delta|a|^2/|a|^2$) is a function of impact parameter ρ, the

frequency ω_0 associated with an optical transition from the excited level to the ground state—in our case the frequency of the resonance line—the oscillator strength f of the line, the relative velocity v of the colliding atoms and fundamental constants; the numerical factor, $\frac{3}{4}$, present in our version comes from the averaging of the quantity $\sin^2\gamma_1$ occurring in the original equation.

Equation (18A) holds only for ρ large enough so that $P(\rho)\ll 1$. We shall nevertheless apply it up to that impact parameter, ρ_1, such that $P(\rho_1)=\frac{1}{2}$. For $\rho<\rho_1$, $P(\rho)$ oscillates between zero and unity; we assume that its effective value is $\frac{1}{2}$. With these simplifications, the cross section for excitation transfer becomes

$$Q=\tfrac{1}{2}\pi\rho_1^2+2\pi\int_{\rho_1}^{\infty}P(\rho)\rho d\rho,$$

which is readily evaluated. The result is

$$Q=\pi\rho_1^2=(4/3)^{\frac{1}{2}}\pi e^2 f/m v\omega, \tag{19A}$$

or

$$A=Qv=(4/3)^{\frac{1}{2}}\pi e^2 f/m\omega,$$

which, by virtue of a well-known relationship[12] between f and the radiative lifetime of the excited state τ, may be written as

$$A=\sqrt{3}\lambda_0^3/8\pi^2\tau, \tag{20A}$$

where λ_0 is the wavelength of the atomic resonance line. Substituting appropriate numerical values, we find

$$A=3.4\times 10^{-9}\ \text{cm}^3/\text{sec},$$

as quoted in the text.

The foregoing considerations apply only to collisions between identical atoms. In the case of interest, however, we have to do with excitation exchange between different isotopes, and have therefore to take into account the effect of the energy level discrepancy of the colliding atoms. This problem has been investigated by Stückelberg[13] and, more recently, by Dr. Bernstein and one of the present authors (T.H.).[14] Both treatments employed a simplified model in which the excited and ground atomic states were assumed nondegenerate; the interaction responsible for excitation transfer was taken to be of the form K/R^3, suggestive of dipole-dipole coupling. It was found that the dependence of Q on the energy discrepancy ΔE between the excited states of the two colliding atoms is characterized by the parameter,

$$\delta=(\Delta E/\hbar)(R_c/v), \tag{21A}$$

where R_c, a "critical radius," is given by the formula

$$R_c=(2K/\Delta E)^{\frac{1}{3}}. \tag{22A}$$

[12] Reference 1, equation subsequent to (5.17). The right-hand side of this equation is incorrect; it should contain an extra factor of π in the numerator.

[13] E. G. G. Stückelberg, Helv. Phys. Acta **5**, 369 (1933).

[14] T. Holstein and I. B. Bernstein, Phys. Rev. **83**, 201 (1951); Bulletin of the Conference on Gaseous Electronics, November 3–5 (1949), paper D3.

TABLE I. Values of the parameter δ.

$\lvert\mu\rvert$	1	2
$\delta_{1,3_0}$	0.85	1.07
$\delta_{1,2_0}$	0.58	0.72

In our treatment of the problem the following results were obtained:

(a) for $\delta\ll 1$

$$Q=(\pi^2K/\hbar v)[1-(2\delta^3/\pi)(\log^2(\delta^3/2)+0.705\log(\delta^3/2)+48)], \tag{23A}$$

(b) for $\delta\ll 1$

$$Q=\pi^2K/\hbar v(3.2/\delta^2)e^{-1.133\delta}. \tag{24A}$$

These results, while qualitatively similar to those of Stückelberg, differ in quantitative detail.

One may conclude that in the region $\delta\gtrsim 1$ the order of magnitude of Q is that of the resonance value, $\pi^2K/\hbar v$. On the other hand, for $\delta>2$, Q lies appreciably below the resonance value and diminishes rapidly with increasing δ.

The difficulty in applying these results to the transfer of excitation between Hg isotopes (as well as to any other actual transfer problem) is that either the excited or ground states are degenerate. One of the consequences of this degeneracy is that the magnitude of the dipole-dipole coupling term is not constant, but depends upon the component of electronic angular momentum Ω parallel to the axis of figure. For example, if the two colliding atoms both possess ground and excited states with angular momenta zero and unity, respectively, the dipole-dipole interaction constant K is given by the expression[15]

$$K=\mu e^2 f\hbar/2m\omega_0, \tag{25A}$$

where $\mu=1$ or -2 for $\Omega=\pm 1$ or zero.

Despite this ambiguity, the theory should still be capable of yielding an order-of-magnitude estimate of the energy-discrepancy effect. We limit ourselves to the aforementioned case of angular momenta zero and unity for atomic ground and excited states; while this situation is not the one encountered in our most important reaction—excitation transfer between Hg^{198} and Hg^{199}—we believe that it is sufficiently illustrative for order-of-magnitude considerations.

Inserting (25A) into (21A), and utilizing the above-quoted[12] relation between f and τ, we obtain

$$\delta=(c/2v)\lambda_0(3\mu/\pi c\tau)^{\frac{1}{3}}(\Delta\bar{\nu})^{\frac{1}{3}}, \tag{26A}$$

where λ_0 is the wavelength of the composite resonance line, $\Delta\bar{\nu}$ is the wave-number discrepancy corresponding to the energy difference of the excited levels of the colliding atoms, and c the velocity of light. For Hg,

[15] H. Margenau and W. W. Watson, Revs. Modern Phys. **8**, 22 (1936), Sec. 5, Eq. (1).

taking $v=2\times10^4$ cm/sec, we obtain

$$\delta=2.8\mu^{\frac{1}{2}}(\Delta\bar{\nu})^{\frac{1}{2}}. \tag{27A}$$

Now the relevant wave-number separations in our case are (in the subscript notation of the excited states employed in the text)

$$\Delta\bar{\nu}_{L\,2a}=0.47\ \text{cm}^{-1},$$
$$\Delta\bar{\nu}_{L\,2b}=0.26\ \text{cm}^{-1}. \tag{28A}$$

The values of the δ's corresponding to (28A) and to the two different values of $|\mu|$ are given in Table I.

From these numbers and from the remarks subsequent to Eq. (25A) we arrive at the conclusion stated in the text subsequent to Eq. (11); namely, the energy-level discrepancy is too small to cause any order-of-magnitude diminution of the cross section from its resonance value.

PHYSICAL REVIEW VOLUME 85, NUMBER 6 MARCH 15, 1952

The Response of Anthracene Scintillation Crystals to High Energy μ-Mesons*†

THEODORE BOWEN AND FRANCIS X. ROSER‡
Department of Physics, University of Chicago, Chicago, Illinois
(Received December 7, 1951)

The response of an anthracene scintillation counter to high energy charged particles which lose only a small fraction of their energy in traversing the crystal was determined, using μ-mesons in the cosmic radiation at sea level with energies from 29 Mev to greater than 1 Bev. The light output was found to have a sizeable fluctuation for mesons of the same initial energy, due to ionization loss straggling. The scintillation efficiency of the phosphor was found to decrease for increasing specific ionization, in agreement with the work of others on electrons and protons. The response of the crystal showed no rise within 2 percent for relativistic meson energies, which agrees with calculations of the density effect reduction in ionization loss for anthracene.

THE light output of scintillation crystals has been shown to be approximately proportional to the total ionization energy loss for low energy particles which spend their entire range in the crystal.[1] Such proportionality between energy loss and light output would also be expected to be true for high energy charged particles which pass completely through the crystal and lose only a small fraction of their total energy by ionization in the crystal. It was the purpose of this work to find the light output of an anthracene crystal as a function of the energy of the traversing particle. Anthracene was used for this investigation because it has the largest light output of the known organic phosphors. μ-mesons from the cosmic radiation at sea level provided a good source of particles for such an experiment, because a wide range of energies is available and absorption by radiation losses and by nuclear collisions is negligibly small. The results which would be found for other charged particles should be the same as for μ-mesons, except for a simple change of scale.

I. THEORY

For the case of a charged particle traversing a thin absorber, a large fluctuation in the ionization energy loss is to be expected. This "straggling" has been calculated by Williams[2] and, later, more accurately by Landau[3] and Symon.[4] The straggling is essentially caused by the fact that large energy transfers to single electrons can occasionally occur. These electrons, which are seen as "δ-rays" in nuclear emulsions or as "knock-on electrons" in cosmic-ray work, lose their energy in the crystal in most cases; hence, the light output is increased. For high energy particles, where

$$W\gg\xi, \tag{1}$$

with

$$W\cong 2mc^2\beta^2/(1-\beta^2)\ \text{(mesons and protons)},$$
$$\xi=2\pi ne^4x/mc^2\beta^2, \tag{2}$$

the energy loss distribution approaches a form which can be expressed in terms of a universal function. Here n is the electron density, m is the electron mass, e is the electronic charge, c is the velocity of light, β is v/c for the incident particle, and x is the absorber thickness in cm. W is the maximum energy loss possible in a single collision, and ξ is a parameter with the dimensions of energy which is a measure of the thickness of the absorber. If the probability of an energy loss between ϵ and $\epsilon+d\epsilon$ is $P(\xi,\epsilon)d\epsilon$ in an absorber with a thickness parameter ξ, then it was shown by Landau[5] that

$$P(\xi,\epsilon)=\frac{1}{\xi}\phi\left(\frac{\epsilon-\epsilon_{\text{prob}}(\xi)}{\xi}\right). \tag{3}$$

* Assisted by the joint program of the ONR and AEC.
† Preliminary results of this investigation were reported in F. X. Roser and T. Bowen, Phys. Rev. **82**, 284 (1951) and T. Bowen and F. X. Roser, Phys. Rev. **83**, 689 (1951).
‡ Now at Universidad Catolica, Rio de Janeiro, Brazil.
[1] W. H. Jordan and P. R. Bell, Nucleonics **5**, 30 (1949); R. Hofstadter and J. McIntyre, Nucleonics **7**, 32 (1950); R. W. Pringle, Nature **166**, 11 (1950); and S. A. E. Johansson, Ark. Fys. **2**, 171 (1950).
[2] E. J. Williams, Proc. Roy. Soc. (London) **125**, 420 (1929).
[3] L. Landau, J. Phys. (U.S.S.R.) **8**, 201 (1944).
[4] K. R. Symon, Harvard University thesis (1948).
[5] See reference 3, Eq. (18).

The shape of ϕ is illustrated by the smooth curve in Fig. 4(c). This distribution function has the property that an average of several energy loss measurements is no more accurate than a single measurement. For this reason, one must not deal with average energy losses, which are given in the usual energy loss formulas, but with the most probable energy loss, which is that loss for which the curve of frequency *vs* energy loss is a maximum.

The most probable loss is always less than the average loss, but for low energy particles, or large thicknesses of absorber, where

$$W \ll \xi, \tag{4}$$

the two become practically equal. Thus, at low energies or large absorber thickness, the usual formulas give the most probable loss directly. For a particle with kinetic energy, E, which is less than about Mc^2, we may use the Bethe-Bloch formula[6] for the average loss

$$\bar{\epsilon} = \xi\left[\ln\frac{2mv^2W}{I^2(1-\beta^2)} - 2\beta^2\right], \tag{5}$$

where I is the average ionization potential of the absorber. At high energies or small thickness, where condition (1) holds, one simply replaces the quantity corresponding to W in the logarithm by $\xi \exp(0.37+\beta^2)$. Using formula (5) for the energy loss, we obtain[7]

$$\epsilon_{\text{prob}} = \xi\left[\ln\frac{2.90mv^2\xi}{I^2(1-\beta^2)} - \beta^2\right]. \tag{6}$$

Formulas (5) and (6) are not correct in the relativistic region because of the density effect, which was first calculated by Fermi[8] and later extended by Halpern and Hall,[9] Wick,[10] and Schönberg.[11] Fermi calculated the energy loss of a charged particle in a dispersive medium whose electrons had a single characteristic frequency. He showed that the loss at extreme relativistic energies was dependent only upon the electron density of the medium. The later calculations[9–11] made use of multifrequency models, which gave slightly varying results in the transition region from nonrelativistic to extreme-relativistic particle velocities, but all agreed with Fermi's fundamental result beyond the transition region. If I_K is the binding energy of a K-electron in the element with the highest atomic number in the absorber, and if

$$\frac{\beta}{(1-\beta^2)^{\frac{1}{2}}} \gg \frac{I_K}{(ne^2h^2/\pi m)^{\frac{1}{2}}}, \tag{7}$$

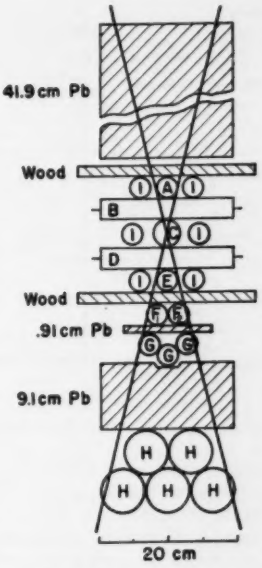

FIG. 1. Arrangement A for nonrelativistic meson energies.

then the most probable energy loss in an absorber satisfying Eq. (1) is given by[12]

$$\epsilon_{\text{prob}} = \xi \ln\left[\frac{2.9mv^2\xi}{(ne^2h^2/\pi m)}\right]. \tag{8}$$

For anthracene, condition (7) is equivalent to requiring that the energy of a μ-meson must be much greater than 1.7 Bev to make Eq. (8) valid.

II. EXPERIMENTAL ARRANGEMENT

The experiments to find the light output of the scintillation crystal as a function of meson energy and to check the validity of the theory outlined before were divided into two parts: nonrelativistic and relativistic meson energies.

The arrangement for the nonrelativistic energies (arrangement A) is shown in Fig. 1. Lead absorbers were used to select three ranges of meson energies, which were (a) 29 to 48 Mev, (b) 48 to 170 Mev, and (c) greater than 170 Mev.

A lead absorber above the apparatus caused μ-mesons to lose about 600 Mev before entering the scintillation crystal, which increased the number of low energy mesons passing through the crystal, since the peak in the meson spectrum at sea level is in the neighborhood of 600 Mev. Coincidence $ABDE$–I defined a narrow

[6] See B. Rossi and K. Greisen, Revs. Modern Phys. **13**, 247 (1941) Eq. (1.11) and for further references.
[7] See reference 3, Eq. (15).
[8] E. Fermi, Phys. Rev. **57**, 485 (1940).
[9] O. Halpern and H. Hall, Phys. Rev. **57**, 459 (1940); **73**, 477 (1948).
[10] G. C. Wick, Nuovo cimento (9), **1**, 302 (1943).
[11] M. Schönberg, Nuovo cimento **8**, No. 3 (1951).
[12] Equation (8) for the most probable loss was found by subtracting from Eq. (6) a correction term which is given, e.g., by Eq. (39) of reference (9), or by Eq. (22) of reference 10.

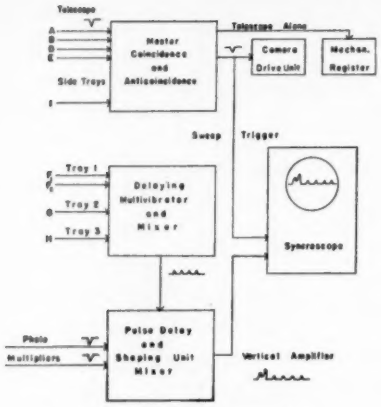

FIG. 2. Block diagram of recording circuits.

beam of particles which must traverse the anthracene scintillation crystal, C. The crystal was viewed by two 5819 photomultiplier tubes, one at each end of the cylindrical crystal (3-cm diam and 3 cm long). The remaining surface of the crystal was covered with aluminum foil to improve the light collection. Geiger counters F_1, F_2, G, and H covered the solid angle defined by $ABDE$. Counters I were for the detection of side showers, which were in anticoincidence with $ABDE$.

A fourfold coincidence of the crossed pairs of counters AB and DE with an anticoincidence of I resulted in a master pulse which initiated the sweep of an oscilloscope. The pulses from the two photomultiplier tubes were delayed and clipped to a width of 1.5 μsec by the use of delay line. One pulse was delayed by 4 μsec and the other by 7 μsec, so that they appeared independently at separate positions on the oscilloscope trace. Pulses from G-M counters F_1, F_2, G, and H were delayed with multivibrators by 15, 20, 25, and 30 μsec, respectively, and also appeared independently on the trace. The oscilloscope trace was photographically recorded by a camera which was equipped so that the master pulse automatically moved the film ahead for another event (see Fig. 2). This system made it possible to obtain the data for all three energy ranges during the same run of the equipment so that slow time variations in the apparatus could not affect the results in comparing the data for the various energy ranges.

Ordinarily, if only a single particle traversed the telescope, either F_1 or F_2, but not both, would fire. The presence of pulses from both F_1 and F_2 served as an additional indicator of showers and knock-on electrons, which were eliminated from the analysis. Only events in which the master coincidence $ABDE$-I was accompanied by pulses from counters (*a*) (F_1 or F_2)$-(GH)$, (*b*) (F_1 or F_2)$+G-H$, or (*c*) (F_1 or F_2)$+G+H$ were used, as these represent the three energy ranges for μ-mesons. Very few single electrons should have been present, as it was almost impossible for them to get through the large thickness of lead above the apparatus.

The arrangement for relativistic meson energies (arrangement B) is shown in Fig. 3. Lead absorbers determined three energy bands for μ-mesons from (*d*) 190 to 460 Mev, (*e*) 460 to 960 Mev, and (*f*) higher than 960 Mev. Coincidence $ABCD$ defined a beam of mesons which must pass through two separate, identical crystals, 1 and 2 (3-cm diam and 3 cm long). Each crystal was viewed at one end by a 5819 photomultiplier tube, which made possible two completely independent measurements of the ionization loss of a particular meson. The surfaces of the crystals, except for the ends used for viewing, were again covered with aluminum foil. Trays E, F, and G covered the solid angle defined by $ABCD$. The recording system was identical to that in arrangement A, with the master coincidence $ABCD$, and the delayed pulses from photomultipliers 1 and 2 and from counters E, F, G, and H.

Counters H detected events accompanied by side

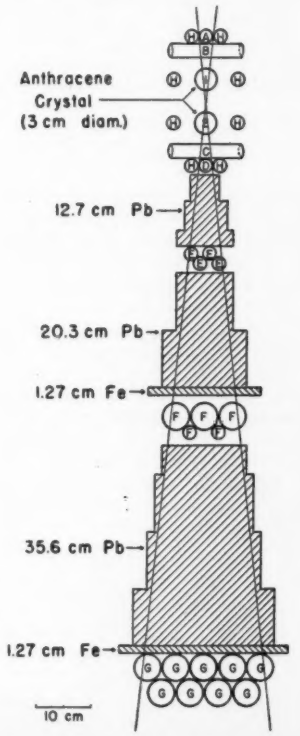

FIG. 3. Arrangement B for relativistic meson energies.

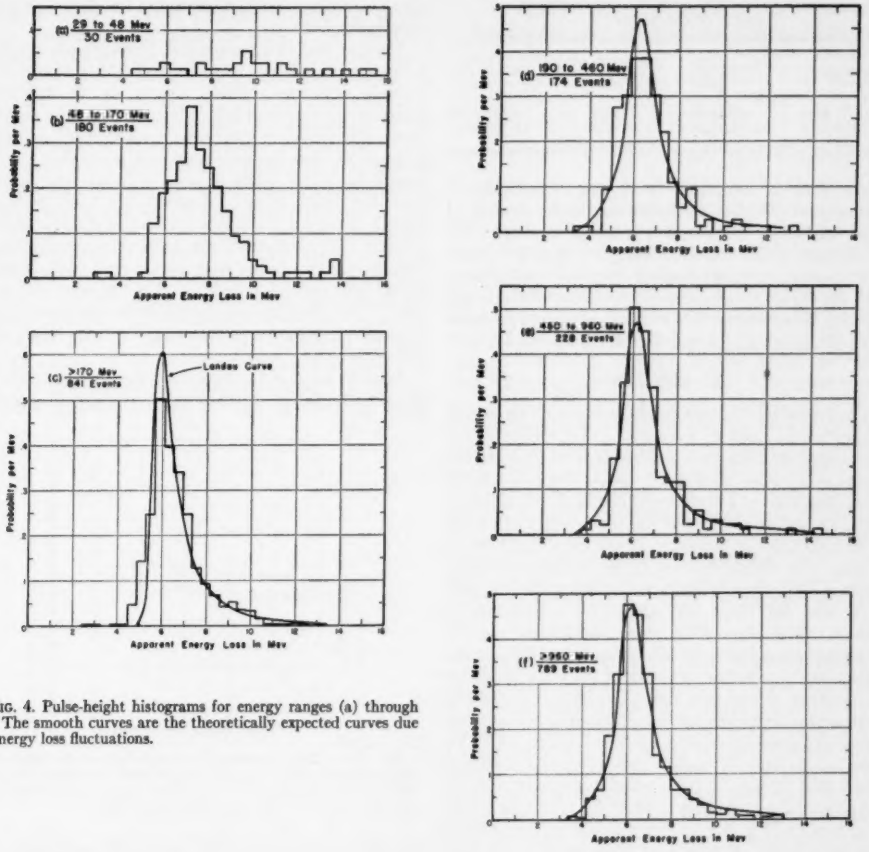

FIG. 4. Pulse-height histograms for energy ranges (a) through (f). The smooth curves are the theoretically expected curves due to energy loss fluctuations.

showers, which were eliminated from the analysis. Only those events in which the master coincidence $ABCD$ was accompanied by pulses from counters (*d*) $E-(FG)$, (*b*) $EF-G$, or (*f*) EFG were used, as these represent the three energy ranges for μ-mesons. Single electrons at sea level should have been stopped in the first 12.7 cm of lead, and therefore did not reach tray E.

Although energy loss fluctuations were important in the scintillation crystal, they resulted in only a 3 percent fluctuation in the range required to bring a meson to rest for the energies used in these experiments. Such a small variation could be completely neglected, since the ionization loss in the scintillation crystal was a slowly varying function of the energy. If high energy mesons were multiply scattered by the lead absorbers out of the solid angle covered by the G-M counter trays, then they would be counted as low energy particles and would affect the pulse-height distributions found for the low energy ranges. It was estimated from calculations of the multiple scattering and from the counting rates obtained that no range contained more than 25 percent of extraneous high energy particles, which may be tolerated for the purposes of these experiments.

It was assumed for the analysis of most of the data that the heights of the pulses from the photomultiplier tubes were proportional to the energies lost in the crystals. This assumption was based upon the evidence (see Table III) that the proportionality factor between light output and energy loss was a slowly varying function of the specific ionization, which was close to minimum for the μ-mesons and over most of the range of the electrons used for calibration.

The pulse-height scale with arrangement B was calibrated in units of energy loss (Mev) by comparison with the peak of the Compton electron distribution from the 2.62-Mev gamma-line of ThC″. The pulse-

TABLE I. The most probable pulse heights for energy ranges (a) and (b).

	Average energy	Pulse height (Mev)	Energy loss from theory (Mev)	Scintillation efficiency
(a)	38 Mev	9.7±0.7	11.6	0.84±0.06
(b)	109 Mev	7.2±0.3	7.4	0.97±0.03

height scale of arrangement A was normalized to arrangement B by the comparison of the distribution of pulse heights for $E>170$ Mev (range c) in A with the distribution of $E>190$ Mev (ranges d, e, and f) in B. This calibration made possible absolute comparisons with the theory to an estimated accuracy of about ±5 percent. However, relative comparisons could be made to within about ±2 percent for ranges d, e, and f.

III. RESULTS

The frequency *vs* pulse-height histograms for energy ranges (a), (b), and (c) are shown in Fig. 4(a), (b), (c). Although only a few events were obtained in range (a), a peak at 9.6 Mev is distinctly visible. The pulses below 8 Mev and above 12 Mev were probably due to knock-on electrons and small air showers, which might cause one or two electrons at minimum ionization to traverse the crystal. The distribution for range (b) has its peak at about 7 Mev, which is significantly higher than the peak at 6 Mev for range (c). Range (c) corresponds to mesons which, as will be shown below, all lose the minimum possible energy. The pulse-height distribution for range (b) is somewhat broader than that for range (c) because of the fact that there was a continuous decrease in energy loss throughout range (b). The energy loss distribution curve calculated by Landau, which has been normalized for equal areas under the histogram and curve, is seen to be in good agreement with the experimental distribution of losses for minimum ionization mesons [Fig. 4(c)]. The positions of the peaks in the pulse height distributions, together with the theoretical values, are given in Table I.

Three of the six distributions found for ranges (d), (e), and (f) of experiment B are shown in Fig. 4(d), (e), (f). They are all seen to be in agreement with the theoretically expected distribution. Corrections due to variations in path length made possible by the cylindrical shape of the crystals have been made to the theoretical curves. The positions of the peaks of the distribution curves are given in Table II. It can be seen that the most probable pulse heights are all equal within experimental error.

TABLE II. The most probable pulse heights for energy ranges (d), (e), and (f).

	Average energy	Counter 1	Counter 2	Average of 1 and 2
(d)	325 Mev	6.07±0.15	6.14±0.15	6.11±0.10
(e)	710	6.19±0.12	6.17±0.12	6.18±0.08
(f)	2700	6.15±0.07	6.15±0.07	6.15±0.05

The fact that in arrangement A two photomultiplier tubes viewed one crystal, whereas in B they viewed two entirely separate crystals, allows us to definitely establish the source of the distribution in pulse heights which was found. It was found in experiment A that a large pulse from one phototube was invariably accompanied by a large pulse of practically the same height from the other. Figure 5A shows the most probable height of pulse 1 for a given height of pulse 2. In the case of two photomultiplier tubes viewing the same crystal, the two pulses were highly correlated. Except for a small remaining fluctuation of the order of 5 percent, light collection and the photoelectron multiplying process are ruled out as sources of the pulse-height distributions which were found.

In experiment B, the height of pulse 1 was found to be almost completely unrelated to the height of pulse 2,

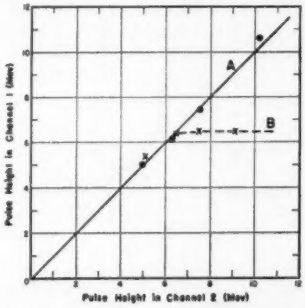

FIG. 5. A. The dependence of the height of the pulse from photomultiplier No. 1 upon the height from No. 2 when both are viewing the same crystal. B. Conditions similar to A, except that photomultipliers are viewing separate crystals.

as can be seen in Fig. 5B. Since both pulses were the result of the same high energy meson, this indicates that the fluctuation was primarily caused by the energy loss mechanism, and could not be due to a hypothetical large variation in the probable ionization with the meson energy. This is just what one would expect from the theory, as the probable ionizations of all high energy mesons should have been equal, and large fluctuations should have been present in the ionization loss in traversing thin absorbers. The slight dependence of the height of pulse 1 upon pulse 2 at small pulse-heights was probably caused by mesons which traverse unusually short paths in the cylindrical crystals. A particle which was close enough to the side of one crystal so as to appreciably shorten the path length must also have been close to the side in the other crystal, because of the G-M counters being some distance away from the crystals; hence a short path in one crystal implied a short one in the other, also.

A reduction in the scintillation efficiency of anthracene with increasing specific ionization is evident from an inspection of Table I, since the ionization loss theory must be regarded as well-verified for energies below the minimum ionization region. Table III compares these efficiencies with values found for electrons.[13] These results seem to indicate that the nonlinearity of the response of the scintillator is caused by a saturation effect which is a function only of the specific ionization and is independent of the type of particle.

The values found for the most probable energy losses for energy ranges (*a*), (*b*), (*d*), (*e*), and (*f*) are compared with the theoretically expected curve in Fig. 6. The points at (a) 38 and (b) 109 Mev were corrected for the loss in efficiency of the crystal, using the values for electrons listed in Table III, since the efficiencies must be taken from an independent source. The remaining three points are the averages from Table II. No scintillator efficiency correction was required for these points, since they were at minimum ionization. The density effect correction for anthracene was estimated to be a function similar in shape to those for carbon and water as found by Halpern and Hall[9] and Wick.[10] At nonrelativistic energies the correction was assumed to approach zero, and at extreme relativistic energies it was made so as to give a result in agreement with Eq. (8). The uncertainty of the ordinates of the theoretical curve with the density effect correction were estimated to be of the order of 2 or 3 percent. As a consequence of the low effective Z of anthracene, the calculated curve shows practically no relativistic rise in the probable ionization loss. Similar curves for higher Z absorbers generally would be expected to show some rise beyond the minimum before leveling off. The experimental points are seen to be in excellent agreement with the theoretical curve corrected for the density effect in anthracene, and indicate that between 300 and 3000 Mev there is no relativistic rise within 2 percent in the most probable ionization loss. The dashed curve calculated from the Bethe-Bloch formula (6) for the most probable loss without the density effect correction is seen to lie well outside the experimental points. These results appear to definitely establish the existence of the reduction in ionization loss due to the density effect.

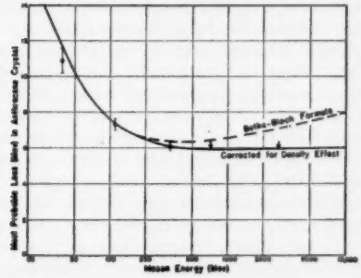

FIG. 6. The most probable energy loss in the anthracene crystal as a function of meson energy. Solid curve: theory with density effect correction. Dotted curve: Theory without density effect correction.

TABLE III. Scintillation efficiency of anthracene.

Specific ionization (Min ion = 1)	Scintillation efficiency Mesons	Electrons
1.00	1.00 (definition)	1.00
1.23	0.97±0.03	0.98
1.93	0.84±0.06	0.89

IV. CONCLUSIONS

The results of this work show that in dealing with scintillations caused by particles which lose only a small fraction of their energy in traversing the scintillator, one must necessarily have a sizeable fluctuation in light output because of straggling in the ionization energy loss. A reduction in the scintillation efficiency of anthracene with increasing specific ionization has been found for μ-mesons which is noticeable (0.84±0.06) even when the specific ionization is only double minimum ionization. The results for relativistic energies show no relativistic rise in ionization loss in anthracene, which can be regarded as a complete verification of the existence of the density effect.

The authors wish to express their appreciation to Professor Marcel Schein for his constant interest and guidance in this work.

[13] Data taken from graph in paper by Frey, Grim, Preston, and Gray, Phys. Rev. 82, 372 (1951), which was based on data in paper by J. I. Hopkins, Phys. Rev. 77, 406 (1950).

The Differential Range Spectrum of Cosmic-Ray Mesons at Sea Level*

CARL M. YORK, JR.†
Department of Physics, University of California, Berkeley, California
(Received October 24, 1951)

The low energy region of the differential range spectrum of cosmic-ray mesons at sea level has been investigated by means of a counter controlled cloud chamber. The results obtained in the region from 18 g/cm² to 76 g/cm² of air equivalent absorber have proved to be about 20 percent higher than predictions based upon similar measurements at greater absorber thicknesses. A possible explanation of this discrepancy lies in the consideration of the effect of multiple scattering of mesons in previous experiments. The present experiment employs a geometrical arrangement of the apparatus which minimizes the corrections to be applied to the data to allow for loss of mesons from the apparatus due to scattering. The earlier work in the field has not been corrected for scattering effects and can, as a result, be expected to give too low a value of the spectrum. The average differential intensity of mesons measured in the range interval mentioned above is 6.86×10^{-6} (particles/sec/sterad/g). The differential range spectrum of protons was also measured and is in good agreement with other work which measured the spectral values at somewhat higher energies than those encountered here. The proton intensity is 2.12×10^{-6} (particles/sec/sterad/g) in the region 16.5 to 42.3 g/cm² of air equivalent and 0.67×10^{-6} (particles/sec/sterad/g) in the region 42.5 to 63.3 g/cm² of air equivalent.

INTRODUCTION

THE differential range spectrum of cosmic-ray mesons has been studied extensively by a number of workers using a variety of experimental arrangements. In a recent review article Rossi[1] has classified the various methods of measurement into four categories. They are the coincidence, anticoincidence, delayed coincidence, and magnetic deflection methods. Of these the first is perhaps the most inaccurate method in that it cannot distinguish between protons, mesons, and multiple events and cannot easily be corrected for scattering. The anticoincidence method in the modified version used by Germain[2] avoids these difficulties. The present work employs an experimental arrangement similar to Germain's. The delayed coincidence method, which depends upon the decay properties of the μ-meson, cannot be used to obtain an accurate absolute value of the range spectrum because of the difficulties in evaluating the detection efficiency of the apparatus. Also, the geometrical arrangement of the apparatus used does not lend itself to any simple scattering correction. Usually the shape of the spectrum is measured with this method, and the resulting curve is normalized to an absolute value in some appropriate fashion. The magnetic deflection method is accurate for intermediate energies, but at very high and low energies serious difficulties are encountered in the measurements. At low energies the cone of acceptance of the apparatus plays an important role in the determination of the spectral values, while at high energies the magnetic deflections are too small to give accurate determinations of the energy.

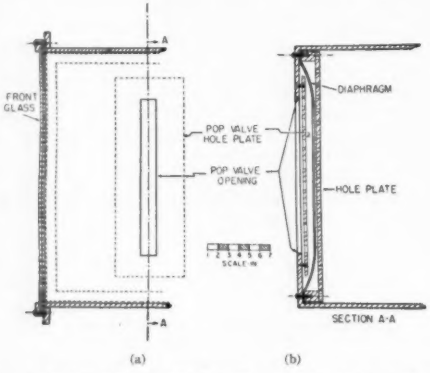

FIG. 1. Sectional views of the laterally expanding cloud chamber.

The only part of the range spectrum which has not been extensively studied lies in the low energy region below 100 g/cm² air equivalent of absorber. The present experiment is an investigation of this region and has been carried out by the anticoincidence method with the addition of a cloud chamber to discriminate between protons and mesons. The work was done at sea level and consisted of photographing the tracks of particles which stopped in the lead plates of the cloud chamber. The solid angle, through which particles entered the cloud chamber, was defined by a quadruple coincidence arrangement of Geiger counters. A bank of anticoincidence counters underneath the chamber prevented the apparatus from taking pictures of particles that went all the way through the chamber. To minimize the possibility of having particles scatter out of the solid angle of acceptance of the apparatus, no absorber was placed in this region. Because the rate at which the data could be collected was low, it was not feasible to acquire a statistical accuracy of greater than about 10 percent.

* Assisted by the joint program of the ONR and AEC.
† AEC Predoctoral Fellow, now at Manchester University, Manchester, England.
[1] B. Rossi, Revs. Modern Phys. **20**, 537 (1948).
[2] L. Germain, Phys. Rev. **80**, 616 (1950).

APPARATUS

As mentioned above, the apparatus used to measure the differential range spectrum in this experiment consisted of a counter controlled cloud chamber. The chamber had an active volume 16 in. by 24 in. by 20 in. The comparatively great depth of 20 in. made it necessary to use direct illumination and take advantage of the light scattering properties of water droplets at small angles of incidence. These properties have been investigated theoretically by Blumer[3] and experimentally by Webb,[4] and both pieces of work are in good agreement. To facilitate this direct illumination, the front and back surfaces of the chamber were made of glass, and the expansions were made laterally with the aid of valves mounted in the sides of the chamber. The pop-valves were of a shutter type first used by Brode and Merkle[5] and are not shown in the figure. Figure 1(b) is a sectional view of the chamber. The $\frac{1}{32}$-inch Neoprene rubber diaphragm acts as a gasket to give an airtight seal between the active volume of the chamber and the back volume. It was found necessary to augment the diaphragm with a gasket of $\frac{1}{16}$-inch gum rubber around the edges to give a satisfactory seal. The pop-valve hole plate is necessary to prevent the diaphragm from closing the pop-valve opening during a fast expansion.

The chamber was operated at 30 cm of Hg pressure of argon and a water-alcohol mixture of 1:3 gave tracks with an expansion ratio of about 9 percent. Alternately charged and grounded lead plates (mounted as shown in Fig. 2) provided a clearing field. The chamber was illuminated by two General Electric flash tubes mounted vertically, 19 in. from the rear glass and in such a position that the sides of the chamber obscure them from the direct view of the cameras. The lamps were energized by discharging a condenser bank of 200 mf charged to 2100 v through each lamp. Aluminum reflectors behind the tubes gave increased illumination in the direction of the chamber.

The camera was placed 6 feet from the front glass and took stereoscopic pictures with two f/4.5 Eastman Projection Anastigmat lenses of 135-mm focal length on Super XX film 1.75 in. wide. The lenses were stopped down to f/22. To reduce the amount of diffusely reflected light in the chamber the hole plates were covered with black velvet.

To minimize the distortion of the tracks due to the lateral expansion, the two pop valves were adjusted to open as nearly simultaneously as possible. The greatest measured difference in the opening times observed after adjustment was 0.002 sec, and the average of several measurements was 0.001 sec. Pads of forty layers of cheese cloth supported by wire matting were placed in the pop-valve openings to reduce the turbulence created by fast expansions.

[3] H. Blumer, Z. Physik **39**, 195 (1926).
[4] C. G. Webb, Phil. Mag. **19**, 927 (1935).
[5] R. B. Brode and T. C. Merkle, private communication.

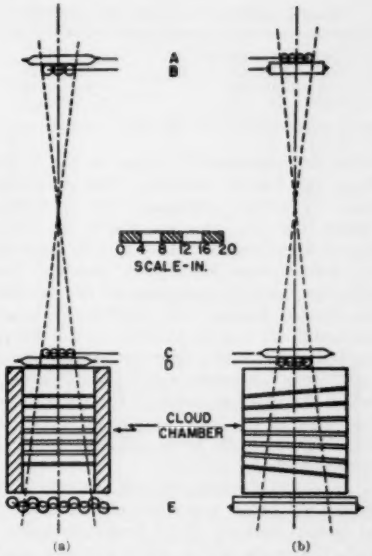

FIG. 2. Experimental arrangement used to measure the differential range spectrum.

A stereoscopic viewer was used to study the pictures. The actuating circuits used to cycle the chamber were of conventional design, with a dead time of 2 min 30 sec for each cycle of the chamber.

The coincidence circuits were of a standard type employing four coincidence channels and one anticoincidence channel. The Geiger counters used to trigger the coincidence unit were the external cathode type developed by MacKnight and Chasson.[6]

The room in which the chamber was housed was temperature controlled by means of a single heater-blower and thermostat. This simple arrangement proved very effective.

METHOD

The arrangement of the apparatus used to measure the differential range spectrum of mesons is indicated in Fig. 2. The counter trays *A*, *B*, *C*, and *D* define the solid angle of acceptance of particles into the cloud chamber. These trays are so arranged that the geometrical definition of the solid angle does not depend upon the effective length of the counters but instead upon their width. This arrangement has been used because the effective width of a cylindrical counter is a much more accurately defined quantity than its effective length. Because low energy particles tend to scatter through large angles, several precautions were

[6] M. L. MacKnight and R. L. Chasson, Rev. Sci. Instr. **22**, 700 (1951).

TABLE I. Values of the experimental parameters.

$A\Omega = 3.24$ sterad-cm²	$N_2 = 6579$
$t_1 = 14{,}029$ min	$\tau = 2.50$ min
$t_2 = 20{,}826$ min	$T_1 = 4039$ min
$N_1 = 3996$	$T_2 = 4379$ min

taken to minimize this effect upon the flux of particles through the counter telescope. The apparatus was covered by a thin aluminum roof of 0.151-g/cm² thickness. The only other material in the solid angle of the telescope was that of the counter walls and the ¼-in. plywood trays holding the counters. Particles entering the chamber must penetrate the ⅜-in. steel top of the chamber. Because of the small amount of material above and in the counter telescope, it will be assumed that all particles incident upon the telescope and within its solid angle will enter the chamber. However, after entering the chamber some of the particles will be scattered out of the active volume by the lead plates and will not contribute to the measured flux. A correction for this effect was made.

To check the determination of the solid angle the fourfold rate, *ABCD*, was measured and from this the total vertical intensity of the cosmic radiation determined. The result of this determination agreed with the value given by Rossi[1] to within the probable error of the measurements.

The particles stopping in the chamber are identified by their change in ionization as they slow down and stop. For accurate discrimination between protons and mesons it is useful to see at least three segments of the particle's track. For this reason, as well as to aid in the identification of electrons, the first two plates in the chamber were ¼ in. thick and only particles stopping in the third, fourth, fifth, and sixth plates were counted.

To distinguish between mesons and electrons, the shower producing properties of the latter were used. However, as pointed out in Appendix I, there is some possibility of confusing electrons and mesons stopping in the third and fourth plates of the chamber.

The stereoscopic photographs of the chamber include the images of a clock and a message register to give the time and number of each event. Although pictures of particles stopping in the chamber were desired, many pictures showed penetrating particles which triggered the apparatus due to the inefficiency of the anticoincidence tray, *E*. In addition, pictures of particles scattering out of the illuminated region of the chamber as well as a few low energy nuclear events were taken.

It was necessary to take the data in two parts. The first part, in which the low energy region of the spectrum was measured, made use of the lead plate arrangement in Fig. 2. The second part was performed to observe a higher energy region. A single plate 2 in. thick was placed at the position formerly occupied by the ¼-in. plates at the top of the chamber. This effectively moved the sixth plate of the first arrangement up to the position formerly occupied by the third plate and allowed more points on the spectrum at higher energies to be measured. This procedure also made it possible to check empirically the scattering correction applied to the sixth plate at the two different positions in the chamber. However, it must be borne in mind that mesons and protons stopping in the sixth plate in the second part of the experiment can no longer be distinguished by their ionizing characteristics, because all particles emerging from the 2-inch plate will be at minimum ionization on entering it. Thus, the ratio of mesons to protons found in the first part of the experiment must be used to determine the number of mesons stopping in this plate during the second part of the work. Hence, no very accurate check can be expected, but the two results should be reasonably consistent.

REDUCTION OF THE DATA

The differential range spectrum is given by the number of particles stopping per unit time per unit area from unit solid angle in a given thickness of absorber, plotted as a function of the total absorber traversed by the particles. This can be expressed by the equation

$$I_v(R) = [1/A\Omega d][N(R)/T],$$

where I_v is the vertical differential intensity under R, the total absorber traversed. A is the total area over which the particles are accepted; T is the total time during which the particles could be recorded by the apparatus; and $N(R)$ is the number of particles stopping in the absorber, d, in the time, T. Ω is the solid angle of acceptance of the apparatus. All ranges are expressed in units of grams per cm² air equivalent to simplify comparison with other data. The conversion from lead to air was made with the aid of the range-energy relations[8] of the two substances. Table I gives the values of the various quantities listed above which were used in this experiment. Table II gives the limits in total range, R, provided by the finite thickness, d, of each lead plate.

The total time, T, during which the apparatus could record the stopping particles is just equal to the running

TABLE II. The range limits of each plate and the corresponding number of stopped mesons in each interval. Total absorber above the chamber: 10.3 g/cm² (of air).

Plate	Range (in air) From	To	d (g/cm²)	$N(R)$
3	17.9	25.7	7.8	47
4	25.7	33.5	7.8	50
5	33.5	41.7	8.2	39
6	41.7	49.9	8.2	37 (53)
7	49.9	58.5	8.6	49
8	58.5	67.1	8.6	54
9	67.1	75.8	8.7	46

[8] D. J. X. Montgomery, *Cosmic Ray Physics* (Princeton University Press, Princeton, 1949), p. 349.

time, t, minus the total dead time of the machine. If τ is the dead time for each photograph, the total dead time is $N\tau$, where N is the total number of pictures taken. These numbers are included in Table II. In determining the total running time, t, it was necessary to decide upon a method of treatment of pictures which were unclear as a result of some failure of the apparatus. None of these pictures were counted, nor was the time associated with them. This time was chosen as the interval between the picture immediately preceding the one to be rejected and the rejected one. These times are not included in the values listed in Table II.

The errors associated with the time, T, are completely negligible. However, the determination of the other values, A, Ω, and d, have a total uncertainty of 1.6 percent associated with their values. Because this is a small uncertainty compared with the statistical inaccuracy of $N(R)$, it will not be included in the assignment of errors to the values of I_v.

RESULTS

The results of the measurements of the differential range spectrum at sea level are given in Table III with their associated probable errors. Table III also contains the differential intensity of protons. The number of protons observed was so small that the intensity has been calculated from the total number observed in each of the two phases of the experiment and the total range of lead used to stop them. The proton range curves calculated by Aaron *et al.*[9] were used to determine the ranges used.

The points of the differential spectrum of mesons are plotted in Fig. 3. The rectangles indicate the uncertainty in the range measurements in the horizontal direction and the statistical probable errors in the vertical direction. The solid curve drawn somewhat below the rectangles is the extrapolated curve given by Rossi.[1] The dotted rectangle is the value of the spectrum

TABLE III. Experimental values of the meson and proton intensities (the probable errors are indicated).

(a) Meson intensity	
Plate number	I_v (/sec/sterad/g) $\times 10^6$
3	7.69 $\pm$0.75
4	8.19 $\pm$0.77
5	6.06 $\pm$0.66
6	5.84 $\pm$0.66
6′	7.58 $\pm$0.70
7	6.70 $\pm$0.65
8	7.36 $\pm$0.67
9	6.20 $\pm$0.62
(b) Proton intensity	
Range (in g/cm² of air)	I_v (/sec/sterad/g) $\times 10^6$
16.5 to 42.3	2.12 $\pm$0.24
42.5 to 63.3	0.671$\pm$0.012

[9] Aaron, Hoffman, and Williams, Range-Energy Curves, Technical Information Division, ORE 675-A20779 (1950), Oak Ridge, Tennessee.

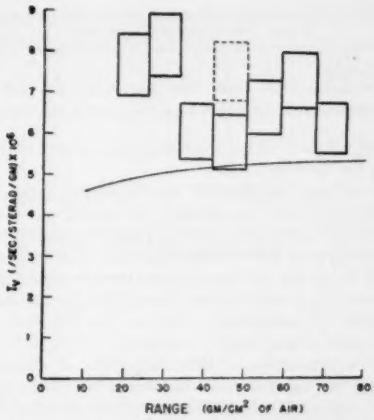

FIG. 3. Experimental results. (The solid curve is the extrapolation made by Rossi, see reference 1.)

obtained from the sixth plate in the second part of the experiment. The uncertainty in the vertical direction does not include the uncertainty in the ratio of protons to mesons which had to be used in the determination of the number of mesons from the total number of particles stopping in the sixth plate.

CONCLUSIONS

It is clear from Fig. 3 that the results of this experiment are not consistent with the extrapolated curve of Rossi. If, however, one ignores for the moment the two points at the lower energy limit of the data, the shape of Rossi's curve can be fitted to the data quite well by displacing the curve upward on the graph. The justification for ignoring the first two points lies in the consideration of the presence of electrons among the particles stopped in the first two lead plates. The detailed argument is given in Appendix I. The implication of having to move Rossi's curve upward is that the normalization point from which the curve was drawn is too low. This point was taken from the work of Sands[10] and depends for its absolute value upon the work of Greisen.[11] Greisen pointed out that his values of the flux of the penetrating component were not corrected for the effect of particles scattered out of the solid angle of his counter telescope. However, as seen in the work of Germain[2] and as is clear from the geometry of Greisen's apparatus, it is not justifiable to neglect this effect. Because the scattering correction is strongly energy dependent and because Greisen's experiment involves a large spread in energy values, it is difficult to make a meaningful correction to his result. However, it is clear that the net result is to cause

[10] M. Sands, Phys. Rev. **77**, 180 (1950).
[11] K. Greisen, Phys. Rev. **61**, 212 (1942).

TABLE IV. The calculated fraction of mesons lost by scattering in each plate (expressed in percent).

Plate number	3	4	5	6	6′	7	8	9
Percentage loss	0.34	0.6	0.9	1.0	0.23	0.5	1.0	1.7

Sands' values to be too small and hence Rossi's extrapolated curve to be too low.

As indicated in Appendix II, the present experiment is quite free from the necessity of making any sizable scattering corrections. Thus a possible explanation of the discrepancy between previous work and the present result lies in the fact that former measurements of the spectrum have not included corrections for the loss of particles by scattering in spite of the fact that they have used geometrical arrangements which make this effect appreciable. In this connection it should be mentioned that Germain[2] has made a mistake in his scattering calculations in the normalization factor of the distribution function of scattered angles that he used. This causes all of his corrected points to be too low by a factor of $(2\pi)^{\frac{1}{2}}$. When his results are corrected for this mistake, they are in good agreement with the present work.

The two values of the proton spectrum are based upon a small number of particles. However, the results are in very good agreement with the data of Mylroi and Wilson,[12] who have obtained the spectral values for protons of slightly higher energy than those observed in this experiment. However, there seems to be no agreement with the single spectral value given by Rochester and Bound[13] for protons with energy less than that observed in the present work. Indeed on the basis of this experiment there is no justification for a rapidly decreasing proton spectrum in the low energy region as Mylroi and Wilson have indicated in their work.

In conclusion the author wishes to express his indebtedness to Professor W. B. Fretter for his guidance throughout the course of the work and to Professor Robert B. Brode for his continued interest in the experiment.

APPENDIX I

The probability that an electron, which has sufficient energy to stop in the third plate of the chamber, can penetrate the steel top of the chamber and the first two lead plates without producing secondary electrons is calculated with the aid of the tables for shower theory given by Montgomery.[14] The Polya distribution can be used to estimate that 23.5 percent of the single electrons incident upon the chamber can penetrate to the third plate without producing another electron. This calculation underestimates the fraction of unaccompanied electrons because the energy loss in the first two plates is neglected. To allow for this effect one can say that the electron no longer has sufficient energy to shower when it reaches the second plate of the chamber. The fraction of particles which do not shower then becomes 41.5 percent.

To see how this might affect the meson spectrum, it is necessary to know the ratio of mesons to single electrons at the energies considered here. Lombardo and Hazen[15] have given an approximate value of 5 percent for this ratio. Thus the possible contribution to the meson spectrum is 5 percent of 41.5 percent, or 2 percent.

A similar correction for the fourth plate gives approximately the same result as that obtained above for the third plate. However, the corrections for the remaining points of the spectrum are much smaller than those just discussed.

It should be pointed out that in the above calculations we have required that more than one particle emerge from a plate. This criterion allows for a possible confusion in distinguishing an electron which is accompanied by another shower produced electron from a meson which is accompanied by a knock-on electron. If one repeats the above calculations and demands the appearance of three or more particles to identify an electron, one finds that about 10 percent of the particles stopping in the third plate and the same fraction stopping in the fourth plate could be electrons. An electron accompanied by only one other particle under one of the top plates would be erroneously called a meson with a knock-on electron.

As a possible check of this last point, the pictures of mesons stopping in the chamber were examined for the presence of knock-on electrons. It was found that of the mesons stopping in the fifth and sixth plates about 7 percent were accompanied by knock-on electrons. This is in good agreement with the results of Hazen.[16] However, of the mesons stopping in the third and fourth plates, 11 percent were accompanied by what appeared to be knock-on electrons. From this it seems reasonable to suppose that some of these latter events were indeed electrons which had only one additional shower produced electron accompanying them. Hence the points on the spectrum contributed by the third and fourth plates can be expected to be higher than they should be.

A very rough estimate of the contribution of electrons to these two points on the spectrum indicates that they should be about 10 percent too high. This is based upon the very poor statistics involved in the knock-on count mentioned above. Because this estimate is so crude, no attempt will be made to correct the results of Table III for this effect.

[12] M. G. Mylroi and J. G. Wilson, Proc. Phys. Soc. (London) **A64**, 404 (1951).
[13] G. D. Rochester and M. Bound, Nature **146**, 745 (1940).
[14] D. J. X. Montgomery, *Cosmic Ray Physics* (Princeton University Press, Princeton, 1949), pp. 63, 334, and 339.
[15] B. Lombardo and W. E. Hazen, Phys. Rev. **68**, 74 (1945).
[16] W. E. Hazen, Phys. Rev. **64**, 7 (1943).

APPENDIX II

The scattering corrections to the various points of the spectrum measured in this experiment were calculated with a modification of the method used by Germain.[2] Table IV summarizes the results of these calculations. In this table the fraction of mesons lost by scattering is expressed in percent. Because the corrections are so small, they have not been applied to the results in Table III. The author is indebted to Dr. S. Fernbach for an enlightening discussion of these calculations.

PHYSICAL REVIEW VOLUME 85, NUMBER 6 MARCH 15, 1952

Energy of a Bloch Wall on the Band Picture. I. Spiral Approach

CONYERS HERRING
Bell Telephone Laboratories, Murray Hill, New Jersey
(Received January 22, 1951)

It is shown that the band or itinerant electron model of a solid is capable of accounting for the "exchange stiffness" which determines the properties of the transition region, known as the Bloch wall, which separates adjacent ferromagnetic domains with different directions of magnetization. In this treatment the constant spin function usually assigned to each running electron wave is replaced by a variable spin function. At each point of space the spin of a moving electron is inclined at a small velocity-dependent angle to the mean spin direction of the other electrons, and this gives rise to an exchange torque which makes the spin direction of the given electron precess as it moves through the transition region, the precession rate being just sufficient to keep it in approximate alignment with the macroscopic magnetization. Physical insight into the mechanisms involved is provided by a rigorous solution of the wall problem for a ferromagnetic free electron gas in the Slater-Fock approximation, although it is known that the free electron gas is not likely to be ferromagnetic in higher approximations. Rough upper limits to the exchange stiffness constants for actual ferromagnetic metals can be calculated without using any empirical constants other than the saturation moment and the lattice constant. The results are only a few times larger than the observed values.

I. INTRODUCTION

IT has been shown by Bloch[1] and others that the change in the direction of magnetization of adjacent ferromagnetic domains takes place gradually, over a distance of the order of 10^{-5} cm; the transition layer is commonly known as the Bloch wall. The surface energy of this transition layer is a quantity of fundamental importance to the theory of ferromagnetic domains.[2] The occurrence of the transition layer represents a compromise between two tendencies, the tendency of the exchange effect to make the magnetization vector $\mathbf{M}$ vary as gradually as possible with position, and the tendency of anisotropy forces to force $\mathbf{M}$ into directions of easy magnetization. The former tendency can be described quantitatively by saying that when the spatial variation of the orientation of $\mathbf{M}$ is sufficiently gradual, it entails an increase ΔW in the energy per unit volume, given by

$$\Delta W = A|\nabla \mathbf{M}|^2/M^2, \tag{1}$$

where A is a numerical coefficient characteristic of the material. This coefficient A, which we shall refer to as the "Bloch wall coefficient," is also important in the theory of the temperature variation of the saturation magnetization at low temperatures (theory of spin waves),[3] and in the theory of the influence of skin effect on microwave resonance phenomena in ferromagnetics.[4]

In the papers cited under reference 1 the value of A is calculated on the Heitler-London or atomic model, according to which the electrons responsible for ferromagnetism are treated as localized on individual atoms of the crystal lattice. The calculation has not been carried out previously on the band or collective electron ferromagnetism model,[5] such as is employed in the work of Stoner and Slater, where the electrons are not localized, but are pictured as running waves moving through the lattice. In view of the well-known inadequacies of either model by itself it is rather unsatisfactory that the Bloch wall has not been treated on the running wave model, and it is with this gap that the present paper and a following one[6] are concerned. Specifically, we shall undertake to calculate A in the Slater-Fock approximation, i.e., assuming that the wave function of a crystal in which the spin direction varies slowly with position can be represented as a determinant of one-electron wave functions. Spin-orbit and other purely magnetic interactions will be neglected.

Two approaches to the problem of calculating A for

[1] F. Bloch, Z. Physik **74**, 295 (1932); L. Landau and E. Lifshitz, Physik Z. Sowjetunion **8**, 153 (1935); E. Lifshitz, J. Phys. U.S.S.R. **8**, 337 (1944); L. Néel, Cahiers phys. **25**, 1 (1944). For a summary of wall theory and other aspects of domain theory, see C. Kittel, Revs. Modern Phys. **21**, 541 (1949).

[2] C. Kittel, Phys. Rev. **70**, 965 (1946); Williams, Bozorth, and Shockley, Phys. Rev. **75**, 155 (1949).

[3] C. Herring and C. Kittel, Phys. Rev. **81**, 869 (1951).

[4] C. Kittel and C. Herring, Phys. Rev. **77**, 725 (1950).

[5] For a discussion of the various models used in ferromagnetism the following review articles are suggested: J. H. Van Vleck, Revs. Modern Phys. **17**, 27 (1945); W. Shockley, Bell System Tech. J. **18**, 645 (1939); E. C. Stoner, Rep. Prog. Phys. **11**, 43 (1946–47).

[6] C. Herring (to be published).

the running-wave model will be employed, and shown to give equivalent results, at least for one case which can be calculated rigorously by both methods. The first and more obvious approach is to calculate the energy of a block of crystal on which periodic boundary conditions are imposed, with the macroscopic **M** lying always in the x-y plane and having an orientation φ proportional to z, with a factor sufficient to make φ increase by a multiple of 2π in the fundamental period. This, which may be called the "spiral approach," is the one used in the present paper. The second approach, to be used in the forthcoming paper,[6] is to calculate the response of a crystal to an externally imposed force which exerts a small torque $\mathbf{M}\times\mathbf{R}\sin\kappa x$ per unit volume tending to create a sinusoidal variation of the orientation of **M** with a wavelength $2\pi/\kappa$ large compared with atomic dimensions. This "perturbation approach" has already been discussed in application to the more general problem of relating A to the energies of spin waves.[5] The spiral approach, though less powerful, is better adapted to giving an understanding of the problem in elementary physical terms, and it is for this reason that discussion of the more complicated perturbation approach is deferred to a separate paper.

II. REMARKS ON FOCK'S EQUATIONS FOR A MAGNETIC CRYSTAL

In the Slater-Fock-Dirac approximation[7] one seeks the set of one-electron wave functions ψ_i which will make the energy of the determinant $|\psi_i(\mathbf{r}_j, s_j)|$ a minimum. The functions of this set can be chosen in such a way as to satisfy the one-electron wave equations

$$(-\nabla^2+K+V-\mathfrak{A})\psi_i=\lambda_i\psi_i, \tag{2}$$

where the λ_i are constants, $-\nabla^2$ is the kinetic energy operator T in atomic units, K is the potential field caused by all external sources (nuclei of atoms, etc.), V is the Coulomb potential of the electrons themselves, and $\mathfrak{A}$ is their exchange operator. The energy in atomic units (rydbergs) is given by

$$\begin{aligned}E&=\sum_i(T_{ii}+K_{ii}+\tfrac{1}{2}V_{ii}-\tfrac{1}{2}\mathfrak{A}_{ii})\\&=\sum_i(i|-\nabla^2+K|i)+\tfrac{1}{2}\sum_{i,j}\left(ij\left|\frac{2}{|\mathbf{r}-\mathbf{r}'|}\right|ij\right)\\&\qquad-\tfrac{1}{2}\sum_{i,j}\left(ij\left|\frac{2}{|\mathbf{r}-\mathbf{r}'|}\right|ji\right).\end{aligned} \tag{3}$$

It can be shown that, if the external potential K is invariant under a group G of symmetry transformations, there will always exist solutions of the self-consistent field Eqs. (2) for which V and $\mathfrak{A}$ are also invariant under G, so that the ψ_i can be chosen to reduce G. For these solutions the determinant $|\psi_i(\mathbf{r}_j, s_j)|$ is taken into a multiple of itself by all transformations of the group. In the band theory of nonferromagnetic metals one usually assumes that the solution which reduces the space group and the group of spin rotations has in fact the lowest energy of all solutions of the self-consistent field equations. For a ferromagnetic metal this is obviously not true, since the total wave function is not taken into itself by all operations of the spin rotation group, but belongs instead to a representation of very high multiplicity; it is also obvious that the exchange operator $\mathfrak{A}$ will in this case not be invariant under spin rotations. It is reasonable to assume, however, that for a normal ferromagnetic crystal the lowest energy solutions include one which reduces the space group and the group of rotations of the spins about the z axis. Analogously, it will be equally reasonable to assume that if we wish to consider a ferromagnetic crystal with periodic boundary conditions and with **M** in the x-y plane with a constant $d\varphi/dz$, then the lowest energy solution of the self-consistent field equations will be one which reduces a group which is derived from the space group of the crystal by replacing each translation operation T by an operation TD_T where D_T is a spin rotation about the z axis through an angle $t_z d\varphi/dz$, where t_z is the z component of the vector describing the translation T. This is because the total wave function for this case is obviously invariant under this group. This fact will form the basis for the calculations of the present paper.

III. CORRELATION ENERGY

Since the calculations of the present paper are to be made using the Slater-Fock approximation, a few words on the limitations of this approximation are in place. In the Slater-Fock approximation the positions of the various electrons are statistically uncorrelated except for the correlations necessitated by the exclusion principle. In the ground state of a ferromagnetic crystal the ferromagnetic electrons will avoid each other fairly well, since the parallelism of their spins makes the probability of finding two of these electrons a distance r apart go to zero as $r\to 0$. In a state with varying spin direction, however, there will exist a nonzero probability density for finding two electrons of opposite spin at the same place. This probability of finding electrons of opposite spin close together will be greater for a determinantal wave function, where electrons of opposite spins are uncorrelated, than for the correct wave function, in which even electrons of opposite spins will avoid each other more than is possible in a determinantal wave function, and thereby lower their interaction energy. The difference between the energy of the true wave function and that of the determinantal solution of Fock's equations is called the "correlation energy"; from what has just been said it is clear that the correlation lowering will be greater for the state

[7] J. C. Slater, Phys. Rev. **35**, 210 (1930); V. Fock, Z. Physik **61**, 126 (1930); P. A. M. Dirac, Proc. Cambridge Phil. Soc. **26**, 376 (1930). An excellent summary is given by L. Brillouin, *Actualités Scientifiques et Industrielles* (Hermann et Cie., Paris, 1933–34), Nos. 71, 159, and 160.

with varying spin direction than for the state with constant spin direction. Therefore the methods of this paper and of reference 6 will lead to a value for the coefficient A in (1) which will be too large, at least if the calculations are carried out without the introduction of any empirical values for exchange integrals, etc.

It might therefore be supposed that almost any calculation made with wave functions of more general form than Slater determinants would give results superior to those obtainable by the Slater-Fock method. For example, Slater[8] has shown how the energy $E_{\mathbf{x}}$ of a spin wave of wave vector $\mathbf{x}$ can be calculated by solving a secular equation involving many determinantal wave functions, corresponding to the many possible states with a single reversed spin; since the Bloch wall coefficient A can be evaluated from a knowledge of $E_{\mathbf{x}}$, one might suppose that these calculations would provide a superior method of estimating A. However, this is not the case; as will be shown in the following paper, Slater's wave functions for the spin-wave state, though not of determinantal form, are related in a rather simple way to the determinantal wave functions used here, and the A values obtained by the two methods are the same.

IV. FORM OF THE WAVE FUNCTIONS

From what was said at the end of Sec. II it follows that the one-electron wave functions for the problem we wish to consider may be written in the form

$$\psi_{\mathbf{k}}=\exp(i\mathbf{k}\cdot\mathbf{r})u_{\mathbf{k}}(\mathbf{r})g_{\mathbf{k}}(\mathbf{r},s_z), \tag{4}$$

where $u_{\mathbf{k}}$ is a function with the periodicity of the lattice and where, for each point $\mathbf{r}$, $g_{\mathbf{k}}$ is a normalized spin function which is unchanged by all operators $TD_{\bar{\tau}}$, i.e.,

$$\sum_{s_z=\pm\frac{1}{2}}|g_{\mathbf{k}}(\mathbf{r},s_z)|^2=1 \tag{5}$$

$$g_{\mathbf{k}}(\mathbf{r})=\exp[it_z(d\varphi/dz)(\sigma_z/2)]g_{\mathbf{k}}(\mathbf{r}-\mathbf{t}), \tag{6}$$

where in the last line $g_{\mathbf{k}}$ is to be visualized as a two-row matrix and where σ_z is the Pauli spin matrix, the exponential being merely the operator $D_{\bar{\tau}}$ rotating the spin through the angle $t_z d\varphi/dz$.

Several qualitative properties of the wave function (4) are worth noting here.

(1) Whatever the form of $g_{\mathbf{k}}$, there will exist at each point $\mathbf{r}$ some direction along which the component of spin has the eigenvalue $+\frac{1}{2}$; $g_{\mathbf{k}}$ may therefore be described by the polar angles $\theta_{\mathbf{k}}(\mathbf{r})$, $\varphi_{\mathbf{k}}(\mathbf{r})$ of this direction, and by a phase factor which, though the same for both values of the argument s_z, may depend in any way on $\mathbf{r}$. Different choices of this phase factor merely imply use of different functions $u_{\mathbf{k}}$.

(2) For singly-occupied levels[9] $\mathbf{k}$, the deviations of $\theta_{\mathbf{k}}$, $\varphi_{\mathbf{k}}$ from the macroscopic spin direction $\theta=\pi/2$, $\varphi=\bar{\varphi}$, must be $O(d\bar{\varphi}/dz)$ as $d\bar{\varphi}/dz\to 0$. One consequence of this is that at a given point of space the angle between the directions $\theta_{\mathbf{k}}$, $\varphi_{\mathbf{k}}$, and $\theta_{\mathbf{k}'}$, $\varphi_{\mathbf{k}'}$ is $O(d\bar{\varphi}/dz)$ whenever $\mathbf{k}$ and $\mathbf{k}'$ correspond to two different singly-occupied levels.

(3) The functions $u_{\mathbf{k}}$ can be taken to be of the form $u_{\mathbf{k}}^{(0)}+O(d\bar{\varphi}/dz)$, where $u_{\mathbf{k}}^{(0)}$ are the solutions of the self-consistent field problem for constant spin direction. This specifies the phases of the $g_{\mathbf{k}}$ to within terms of order $d\bar{\varphi}/dz$.

In the sections immediately following, we shall assume the spin function $g_{\mathbf{k}}$ going with any particular direction $\theta_{\mathbf{k}}$, $\varphi_{\mathbf{k}}$ (direction of quantization of the spin) to be defined by

$$g_{\mathbf{k}}=\begin{pmatrix}\exp(-i\varphi_{\mathbf{k}}/2)\cos\frac{1}{2}\theta_{\mathbf{k}}\\ \exp(i\varphi_{\mathbf{k}}/2)\sin\frac{1}{2}\theta_{\mathbf{k}}\end{pmatrix}. \tag{7}$$

It will be verified below that the choice of the phase factor in (7) causes the $u_{\mathbf{k}}$ to coincide with the $u_{\mathbf{k}}^{(0)}$ to within terms of order $(d\bar{\varphi}/dz)^2$. Using (7), the spin distribution is completely described by the set of functions $\theta_{\mathbf{k}}(\mathbf{r})$, $\varphi_{\mathbf{k}}(\mathbf{r})$, or equivalently by

$$\xi_{\mathbf{k}}(\mathbf{r})=\theta_{\mathbf{k}}(\mathbf{r})-\pi/2 \tag{8}$$

and

$$\eta_{\mathbf{k}}(\mathbf{r})=\varphi(\mathbf{r})-\bar{\varphi}(\mathbf{r}), \tag{9}$$

where $\bar{\varphi}$ is a linear function of position defined so that $d\bar{\varphi}/dz=$ the macroscopic $d\varphi/dz$ and so that the average of $\eta_{\mathbf{k}}$ over a unit cell, weighted with the charge density $|u_{\mathbf{k}}|^2$, vanishes when summed over all occupied states. The quantities $\xi_{\mathbf{k}}$, $\eta_{\mathbf{k}}$ thus measure the deviation, in distance on the unit sphere, of the local spin direction from the mean direction $(\pi/2,\bar{\varphi})$. These quantities must obviously be periodic with the periodicity of the lattice; this follows mathematically from (6).

V. TERMS IN THE ENERGY

Let the function $\psi_{\mathbf{k}}$ given by (4) be written as

$$\psi_{\mathbf{k}}=\chi_{\mathbf{k}}(\mathbf{r})g_{\mathbf{k}}(\mathbf{r},s_z), \tag{10}$$

where now $g_{\mathbf{k}}$ is given by (7). The mean kinetic energy of $\psi_{\mathbf{k}}$ is, in atomic units,

$$\begin{aligned}T_{\mathbf{kk}}&=\sum_{s_z}\int|\nabla\chi_{\mathbf{k}}|^2d\tau\\&=\int[|\nabla\chi_{\mathbf{k}}|^2+2\,\mathrm{Re}\chi_{\mathbf{k}}^*\nabla\chi_{\mathbf{k}}(\nabla g_{\mathbf{k}},g_{\mathbf{k}})\\&\qquad+|\chi_{\mathbf{k}}|^2(\nabla g_{\mathbf{k}},\nabla g_{\mathbf{k}})]d\tau,\end{aligned} \tag{11}$$

where the expressions in parentheses are spin scalar products at a given position $\mathbf{r}$. A straightforward

[8] J. C. Slater, Phys. Rev. **52**, 198 (1937).

[9] Strictly speaking it is not possible to separate the one-electron states of a ferromagnetic crystal into singly- and doubly-occupied levels, because the electrons of the two spins move in different exchange fields, and this makes the orbital parts of their wave functions slightly different. However, the distinction is obviously only of significance in calculations much more refined than those considered here.

calculation based on (7) and using (8) gives, to the second order in $d\bar{\varphi}/dz$ (i.e., to the second order in ξ_k and η_k),

$$(\nabla g_k, g_k) = -(i/2)\xi_k \nabla \varphi_k \tag{12}$$

$$(\nabla g_k, \nabla g_k) = \tfrac{1}{4}[|\nabla \xi_k|^2 + |\nabla \varphi_k|^2]. \tag{13}$$

Insertion of these into (11) gives T_{kk} in terms of χ_k, ξ_k, and φ_k or η_k.

Since the charge density for the state ψ_k is simply $|\chi_k|^2$ and is independent of ξ_k and φ_k, the Coulomb energy in the presence of a spin gradient will depend on the χ_k in the same way as for the case of constant spin direction. The exchange energy, however, will be different, unless ξ_k and φ_k happen to be independent of $\mathbf{k}$. For the $\mathbf{k}\mathbf{k}'$ contribution to the exchange energy is the self-energy of the distribution

$$\chi_{k'}^* \chi_k (g_{k'}, g_k), \tag{14}$$

and we have from (7), to the second order in $d\bar{\varphi}/dz$,

$$(g_{k'}, g_k) = 1 - (i/4)(\eta_{k'} - \eta_k)(\xi_{k'} + \xi_k) - \tfrac{1}{8}(\eta_{k'} - \eta_k)^2 - \tfrac{1}{8}(\xi_{k'} - \xi_k)^2. \tag{15}$$

The total exchange energy of the ferromagnetic electrons, which we shall not attempt to write down explicitly, is obtained by substituting (15) into (14), evaluating the self-energy, and summing over $\mathbf{k}$ and $\mathbf{k}'$. Electronic states having the minority spin direction could be taken into account if necessary, by assigning to them spin functions of the form (7) but with (θ, φ) close to $(\frac{1}{2}\pi, \bar{\varphi}+\pi)$ instead of to $(\frac{1}{2}\pi, \bar{\varphi})$; spin scalar products of states with nearly opposite spins would then have to be evaluated, as well as those of the type (15).

The total energy is made up of kinetic, potential, Coulomb, and exchange contributions, and it is now clear that each of these contributions either is exactly the same function of the χ_k as when the spin direction is constant, or else equals this function plus something that is second order in the ξ's and η's, i.e., second order in the macroscopic $d\bar{\varphi}/dz$. Thus, as far as terms of the second order in $d\bar{\varphi}/dz$ are concerned, any change in χ_k would increase the energy, and so in the problem of minimizing the total energy by proper choice of the χ_k, ξ_k, and η_k we can assume the χ_k to be of the same form as when the spin direction is constant, and vary only the ξ_k and η_k. However, even the variational problem involved in finding the ξ_k and η_k which minimize the energy is quite a formidable once in the general case, and we shall here apply the approach just described to only two simplified cases:

(1) The free electron case. The simplification here arises, as will be shown below, from the fact that each ξ_k and η_k is independent of position, and from the related fact that cross terms between the ξ's and η's disappear from the exchange energy.

(2) The case where ξ_k and η_k are arbitrarily constrained to be independent of $\mathbf{k}$. Though this assumption does not give as low an energy as when the ξ's and η's are unrestricted, it probably gives the right order of magnitude for the Bloch wall coefficient, and it is particularly simple because the exchange energy reduces to the same value as for constant spin direction, so that only the kinetic energy term need be considered. This case will be discussed in Secs. VIII and IX below. In the forthcoming paper[6] it will be shown that other, less drastic, simplifying assumptions can be used to make the problem tractable when the perturbation approach is used. However, I have not discovered any way of carrying through corresponding simplifications using the spiral approach.

VI. THE PROBLEM OF THE FREE ELECTRON GAS

Bloch[10] has shown that an assembly of free electrons moving in a volume pervaded by a uniform density of positive charge will be ferromagnetic, in the approximation of determinantal wave functions, if its density is sufficiently low. This case provides a convenient illustration of the physical principles involved in the Bloch wall problem, and, since the solution for this case can be obtained without any approximations beyond those involved in the use of determinantal wave functions, it offers an opportunity to assess the accuracy of various methods of calculation which involve additional simplifications. The utility of the free electron example is somewhat marred by the fact that the correlation energy for free electrons, which Wigner[11] has calculated, is so large that it will probably prevent a free electron gas of any density from being ferromagnetic.[12] Nevertheless, it is interesting to compare the results of different methods of estimating the Bloch wall coefficient for free electrons, starting from the (false) assumption that the ground state is a determinant of plane waves with parallel spins.

One such method is that based on the atomic approximation[13] as used in Heisenberg's theory of ferromagnetism, Bloch's theory of spin waves,[14] and previous theories of the Bloch wall.[1] The determinant of plane waves which approximates the ferromagnetic state for the free electron gas can be approximated by a determinant of "atomic" functions defined by Wannier's transformation[15]

$$w(\mathbf{r}-\mathbf{R}_n) = \sum_k [\exp(-i\mathbf{k}\cdot\mathbf{R}_n)/N^{\frac{1}{2}}][\exp(i\mathbf{k}\cdot\mathbf{r})/\Omega^{\frac{1}{2}}], \tag{16}$$

where Ω is the fundamental volume associated with the periodic boundary conditions and N is the number of electrons, and where the points $\mathbf{R}_n$ may refer to any arbitrary lattice of points in space. The quantity in brackets is a unitary matrix on the indices $\mathbf{k}$ and n if $\mathbf{k}/2\pi$ is allowed to run over a unit cell (Brillouin zone) in the lattice reciprocal to that of the $\mathbf{R}_n$. Since suitable

[10] F. Bloch, Z. Physik **57**, 545 (1929).
[11] E. Wigner, Phys. Rev. **46**, 1002 (1934).
[12] E. Wigner, Trans. Faraday Soc. **34**, 678 (1938).
[13] See, for example, the review by J. H. Van Vleck, Revs. Modern Phys. **17**, 27 (1945).
[14] F. Bloch, Z. Physik **61**, 206 (1931).
[15] G. H. Wannier, Phys. Rev. **52**, 191 (1937).

choice of this lattice will make the Brillouin zone nearly spherical, it is reasonable to try to estimate the value of the Bloch wall coefficient either by assuming the occupied $\mathbf{k}$ values to fill a Brillouin zone, or by assuming them to fill a sphere and ignoring the correction due to the fact that the w's defined by (16) will in the latter case not be exactly orthonormal. In this approximation the procedure used in previous theories of the Bloch wall corresponds to assuming the state with varying spin direction to consist of a determinant of w's, each with a spin function g_n which corresponds to eigenvalue $+\frac{1}{2}$ for the component of spin along a direction in the x-y plane and making an angle $\varphi_n = Z_n d\varphi/dz$ with the x axis, where Z_n is the z component of $\mathbf{R}_n$. Evaluating the contributions to the energy in (3), we see that the kinetic, potential, and Coulomb terms are the same as in the ground state, while the exchange term is numerically smaller. A rough estimation of this change in the exchange energy, given in Appendix I, indicates that the Bloch wall coefficient computed in this way has a value

$$A = \beta/r_s^2 \tag{17}$$

rydbergs per Bohr unit, where r_s is the radius in Bohr units of the sphere whose volume equals the volume per electron, and where β is a constant which is certainly greater than 0.026, perhaps by as much as a factor of two or so. A more accurate estimate of β could be made, but would hardly be worth while, since we shall see presently that the atomic approximation is a very poor one.

VII. APPLICATION OF THE SPIRAL APPROACH TO THE FREE ELECTRON GAS

We now return to the approach of Sec. V. For a free electron gas we may choose any vectors we please for the fundamental translations of the "crystal lattice"; the requirement that the ξ_k and η_k defined by (8) and (9) be periodic therefore implies that they must be independent of position. Therefore, the $(g_{k'}, g_k)$ in (14) is a constant, and the $\mathbf{kk}'$ contribution to the exchange energy is just $|(g_{k'}, g_k)|^2$ times the corresponding contribution for the case of constant spin direction. Thus using (15) and ignoring terms of higher order than the second in the ξ's and η's,

exchange contribution to energy (3)

$$= -\frac{1}{\Omega}\sum_{k,k'} \frac{4\pi}{|\mathbf{k}-\mathbf{k}'|^2}\left[1 - \frac{(\eta_{k'}-\eta_k)^2}{4} - \frac{(\xi_{k'}-\xi_k)^2}{4}\right], \tag{18}$$

where Ω is the fundamental volume associated with the periodic boundary conditions. From (11), (12), and (13) we have

$$\text{kinetic energy} = \sum_k [k^2 + (d\bar{\varphi}/dz)k_z\xi_k + (d\bar{\varphi}/dz)^2]. \tag{19}$$

The constants ξ_k, η_k must be chosen to minimize the sum of (18) and (19).

It is obvious from inspection that the proper choice of η_k is a value independent of $\mathbf{k}$, and since the mean of all the η_k must vanish, as specified under Eq. (9), we must take $\eta_k = 0$. The Euler equation for the ξ_k reduces to

$$\frac{d\bar{\varphi}}{dz}k_z + \frac{1}{\Omega}\sum_{k'} \frac{4\pi}{|\mathbf{k}-\mathbf{k}'|^2}(\xi_k - \xi_{k'}) = 0 \tag{20}$$

with the auxiliary condition that $\sum_k \xi_k = 0$. Since the possible values of $\mathbf{k}'$ are almost continuously distributed over the occupied sphere in $\mathbf{k}$-space, this is really an integral equation of the Fredholm type. It may be placed in a form convenient for computation by making the substitutions

$$\mathbf{y} = \mathbf{k}/k_{\max}, \quad \sum_{\mathbf{k}} \rightarrow (3N/4\pi)\int_{S_1} dy,$$

where N is the total number of electrons in the fundamental volume Ω, supposed all to have the same spin when $d\varphi/dz = 0$, and where the region S_1 of integration is the unit sphere. The result is

$$\int_{S_1} \frac{[\xi(\mathbf{y}) - \xi(\mathbf{y}')]}{|\mathbf{y}-\mathbf{y}'|^2} d\mathbf{y}' = -2\pi^2 \frac{d\bar{\varphi}}{dz} y_z, \tag{21}$$

where, it must be remembered, $d\bar{\varphi}/dz$ is to be evaluated in atomic units.

The integral Eq. (21) and its solution have a simple physical interpretation. Suppose that an electron moving with a given z component of velocity has a spin direction which at each point of space differs from the mean spin direction of the electrons to which it is coupled by the exchange effect. Then these other electrons will exert a torque on the spin of the given electron, in such direction as to tend to bring its spin into coincidence with theirs. Since the spin behaves gyroscopically, this torque will cause it to precess on the surface of the unit sphere in a direction at right angles to the line joining it to the mean spin direction of its fellows. An observer traveling with the moving electron would observe a constant magnitude for the discrepancy between his spin and that of the neighborhood, and would observe his own spin to precess in a very flat cone on the unit sphere, with a velocity proportional to $d\bar{\varphi}/dz$ times his z component of velocity. This is essentially the right of (21); the left of (21) corresponds to the suitably weighted average of the torques exerted by the various other electrons on the given one, each term in the average being proportional to the difference in the spin orientation of the two electrons concerned and to the strength of the exchange coupling between them. The equation thus expresses the proportionality of precessional velocity to torque. We shall see in the forthcoming paper[6] that the same integral equation results when the free electron problem is attacked by the perturbation method.

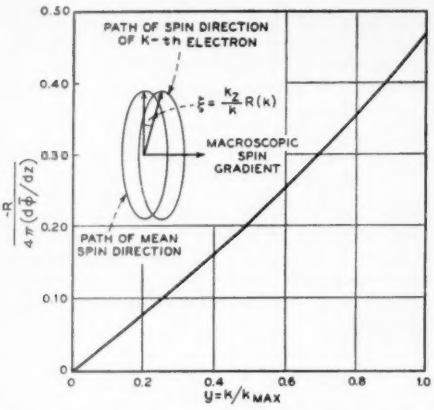

FIG. 1. Deviation of spin orientation from the mean orientation for free electrons, plotted as a function of wave number for electrons moving in the direction of the macroscopic gradient of spin direction.

The solution of (21) which has mean value zero is obviously of the form

$$\xi(\mathbf{y}) = (y_z/y)R(y), \tag{22}$$

since the spherical symmetry of the kernel causes each term in an expansion of ξ in spherical harmonics to be transformed into a term with the same angular dependence. A variational calculation, described in Appendix II, gives for R the approximate form shown in Fig. 1, *viz.*, the polynomial

$$R(y) = \gamma[-(243/610)y - (9/122)y^3], \tag{23}$$

where

$$\gamma = 4\pi d\bar{\varphi}/dz. \tag{24}$$

The increase in total energy, as compared with the state with all spins parallel, is the sum of (18) and (19) with the first term of each omitted. It thus consists of a term in $(d\bar{\varphi}/dz)^2$, one linear in ξ and $d\bar{\varphi}/dz$, and one quadratic in ξ; if the scale of ξ is so chosen as to minimize the sum of these three terms, this sum can be replaced by the term in $d\bar{\varphi}/dz$ plus half the term linear in ξ. Thus the energy increase is

$$E - E_0 = \tfrac{1}{2}(d\bar{\varphi}/dz)\textstyle\sum_k k_z\xi_k + (N/4)(d\bar{\varphi}/dz)^2. \tag{25}$$

Combining (22), (23), and (25) gives

$$\begin{aligned} E - E_0 &= (N/4)(d\bar{\varphi}/dz)^2(1 - 0.72169\pi k_{\max}) \\ &= (N/4)(d\bar{\varphi}/dz)^2(1 - 5.4851/r_s), \end{aligned} \tag{26}$$

which by (1) and with $4\pi r_s^3/3 = \Omega/N$ gives for the Bloch wall coefficient

$$\begin{aligned} A &= (E - E_0)/\Omega(d\bar{\varphi}/dz)^2 \\ &= (3/16\pi r_s^2)(1 - 5.4851/r_s). \end{aligned} \tag{27}$$

The values (26) and (27), being obtained from a rigorous solution of the self-consistent field equations, may be expected to be lower than the energy or A value obtained by any other method based on determinantal wave functions. This is exemplified by the comparison of (27) with the value (17) obtained from the atomic approach, as illustrated in Fig. 2. It is clear that in spite of the uncertainty in the value of β in (17) the present value (27) is much the smaller. The simplification to be discussed in the next section, that of assuming all the spin functions the same, corresponds to replacing the last factor in (27) by unity; the resulting value of A is shown as the middle curve in Fig. 2.

According to (27), ferromagnetism should cease when the electron density exceeds the value for which $r_s = 5.4851$ Bohr units, even when only wave functions of determinantal form are considered. Bloch,[10] considering only determinants of plane waves each with constant spin direction, found that ferromagnetism should cease when r_s becomes less than $(2\pi/5)(9\pi/4)^{\frac{1}{3}} \times (2^{\frac{1}{3}}+1) = 5.4531$. Thus (27) gives a slightly more stringent criterion for ferromagnetism than Bloch's. (Improvement of the approximate solution (23) would merely increase the critical r_s, and probably only by a very small amount.) It is surprising that the critical r_s given by (27) comes so close to Bloch's value, since the former is the condition for stability with respect to a very gradual alteration of direction of magnetization with position, spin parallelism being preserved locally, while the latter is the condition for stability with respect to reversal of half the spins at every point of space. On Bloch's model the state with all spins parallel is stable with respect to removing a single electron at the top of the Fermi distribution and inserting it in the

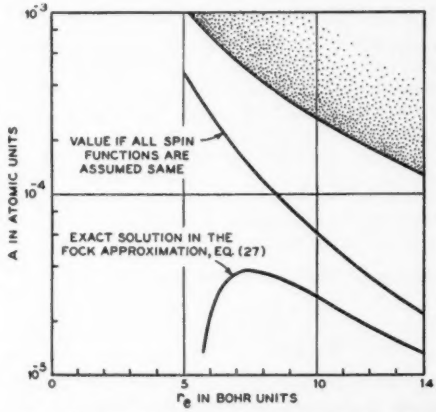

FIG. 2. Values of the Bloch wall coefficient A for a free electron gas, as computed by various methods of approximation. Bottom curve: best possible approximation using determinantal wave functions, as given by Eq. (27). Middle curve: approximation assuming all electrons to have the same spin function, given by replacing parentheses by unity in (27). Top curve: lower limit to value calculable from the atomic model, as given by Eq. (17).

state $k=0$ with reversed spin, whenever

$$r_s > 2^{-\frac{1}{3}}\pi(9\pi/4)^{\frac{1}{3}} = 3.8002.$$

VIII. APPROXIMATION OF ASSUMING ALL SPIN FUNCTIONS THE SAME

Although Fig. 2 shows that the correct value of A may be considerably less than that computed on the assumption that all electrons have the same spatially varying spin function, it does show that for free electrons the latter value is at least of the same order of magnitude as the best value that can be computed from determinantal wave functions, except near the critical density where ferromagnetism disappears. Moreover, the error is of course always in the direction of making the computed A too large. It therefore seems worth while to expend a little effort toward computing A for narrow bands of itinerant electrons, using this assumption that at each point of space all the ferromagnetic electrons $\mathbf{k}$ have the same spin orientation, i.e., the same $\theta_k(\mathbf{r})$, $\varphi_k(\mathbf{r})$, or the same $\eta_k(\mathbf{r})$, $\xi_k(\mathbf{r})$, in the notation of Sec. IV. With this assumption the exchange energy as well as the Coulomb energy is the same in the presence of a gradient of spin direction as when the spin direction is constant; this can be seen from the fact that the exchange charge density (14) reduces to $\chi_{k'}{}^*\chi_k$ if the ξ's and η's are the same for all $\mathbf{k}$.

Thus only the kinetic energy (11) needs to be considered; using (12) and (13) we have for the energy increase over the state with uniform spin direction

$$E-E_0 = -\int \xi \nabla\varphi \cdot \sum_k \mathrm{Re}[i\chi_k{}^*\nabla\chi_k]d\tau$$

$$+\frac{1}{4}\int[|\nabla\xi|^2+|\nabla\varphi|^2]\sum_k|\chi_k|^2 d\tau. \quad (28)$$

Here the summations extend over the singly filled orbitals: we shall suppose in the present section that the remaining electrons are paired off with two electrons of opposite spin to each orbital, and shall assume the latter levels to be unperturbed by the fact that the direction of magnetization is spatially varying. Now since we are neglecting spin-orbit interaction, the wave equation for each χ_k contains only real operators, and there will therefore be another orbital, with wave vector $-\mathbf{k}$, which is a multiple of $\chi_k{}^*$ and which has the same energy parameter λ_k in the one-electron wave equation (2). Thus for each $\mathbf{k}$

$$\chi_k{}^*\nabla\chi_k + \chi_{-k}{}^*\nabla\chi_{-k} = \nabla|\chi_k|^2$$

and is real; grouping the terms of the first integral of (28) in pairs in this way, the whole integral can be seen to vanish. We are left merely with the problem of choosing $\xi(\mathbf{r})$ and $\varphi(\mathbf{r})$ so as to minimize the second integral of (28) subject to the condition that the space average of $d\varphi/dz$ be fixed; obviously ξ must be chosen zero, while the variational equation for φ gives

$$\nabla\cdot\rho\nabla\varphi = 0, \quad (29)$$

where $\rho=\sum|\chi_k|^2$ is the charge density of the ferromagnetic electrons in atomic units.

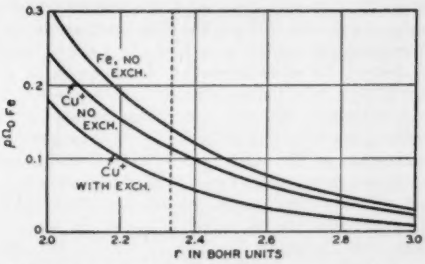

FIG. 3. Charge distributions for the $3d$ electrons of free atoms of Fe and Cu^+. The ordinate is the product of the $3d$ charge density ρ by the atomic volume Ω_0 of iron. The top curve is taken from the calculations of Manning and Goldberg (see reference 18) for Fe, made without exchange. The middle curve is taken from the calculations of Hartree (see reference 19) for Cu^+, without exchange, and the bottom curve from those of Hartree and Hartree for Cu^+, with exchange. The vertical dotted line is at the half-distance between nearest neighbors for Fe, which is also the same as that for Ni.

Although our primary concern in this paper is with the itinerant electron model, it is worth noting that the approximation of the present section, as represented by Eqs. (28) and (29), can be applied equally well to the atomic model. One has merely to assign to each atomic orbital a spatially varying spin function which is the same function of position for all atoms, instead of using spatially constant spin functions which are different for neighboring atoms, as is done in the conventional treatment, and as Fig. 2 shows, this may give a considerably lower energy. The results of this and the following section are in fact independent of whether an itinerant or an atomic model is used.

Equation (29) is the same as that for the electrostatic potential in a medium of variable dielectric constant ρ, when the mean field $\bar{\delta}$ is $-d\bar{\varphi}/dz$. The problem of determining the Bloch wall coefficient A in the present approximation is therefore identical with that of determining the gross dielectric constant $\bar{\kappa}$ of an inhomogeneous medium, and it is in fact easy to show that

$$A = \bar{\kappa}/4 \text{ rydbergs per Bohr unit.} \quad (30)$$

While the exact calculation of $\bar{\kappa}$ from any given periodic density function $\rho(r)$ is difficult,[16] it is obvious that $\bar{\kappa}$ satisfies the inequalities[17]

$$\rho_{\min} < \bar{\kappa} < \bar{\rho}, \quad (31)$$

[16] The problem of estimating gross dielectric constants, permeabilities, etc., for inhomogeneous media has received considerable attention in the literature. A comprehensive review has been given by K. Lichtenecker, Physik. Z. 27, 115 (1926).

[17] Note that the upper limit to A given by (30) and (31) is identical with that given in Eq. (44) of reference 3.

where $\rho_{\min}$ is the minimum value of the electron density ρ over a unit cell, and $\bar{\rho}$ is the mean electron density. More elaborate inequalities satisfied by $\bar{\kappa}$ can of course be derived. Of more interest to us, however, is the general picture of the variation of φ with position. If, as is doubtless the case, the charge density of the ferromagnetic electrons is much smaller in between the atoms than in the region well within an atomic cell, φ will be nearly constant over most of each atomic cell and will vary rapidly with position near the half-way point between nearest neighbor atoms. In fact, the closer the charge density hugs the atoms, the more nearly correct it is, in the approximation of this section, to picture each atomic cell as having its own constant spin orientation, different from that of its neighbors. We shall show in the next section how this fact makes possible a simple quantitative estimate of $\bar{\kappa}$, and hence of A.

IX. ESTIMATES FOR ACTUAL METALS, ASSUMING ALL SPIN FUNCTIONS THE SAME

To carry out the rough estimation of the Bloch wall coefficient outlined in the preceding section one must first make a reasonable guess at the charge density $\rho(\mathbf{r})$ of the ferromagnetic electrons. Figure 3 shows the d shell charge density calculated for the free iron atom by Manning and Goldberg[18] by the Hartree method. To illustrate the order of magnitude of the correction which might be introduced if exchange were included, charge densities calculated for Cu^+ by Hartree and Hartree[19] both with and without exchange are also shown.

Although the charge distributions in atom and metal certainly differ and although the decrease of d electron charge density at large distances from the nucleus is not overwhelmingly rapid, it will suffice for the present crude estimate to use an expression for the gross dielectric constant $\bar{\kappa}$ which can be derived by assuming that near the midpoint between two nearest neighbor atoms

$$\rho \propto \exp(-\lambda r_1)+\exp(-\lambda r_2),$$

where r_1 and r_2 are the distances from the two nuclei and λ is a very large constant. A little calculation based on this assumption gives

$$\bar{\kappa} \approx (3/2)^{\frac{1}{3}}\rho_0$$

for the body-centered cubic lattice, and twice this for the face-centered lattice, where ρ_0 is the charge density of ferromagnetic electrons at the midpoint between nearest neighbors. Substitution of this into (30) with a ρ_0 estimated by combining Fig. 3 with the known number of ferromagnetic electrons per atom gives values of A for Fe and Ni which are three or four times larger than the observed values of 2×10^{-6} ergs/cm for Fe,[20,21] and 8×10^{-7} ergs/cm for Ni.[20]

When it is remembered that the calculations of the present section overestimate A, both by using the assumption that all spin functions are the same, and by neglecting correlation, this agreement to within a factor of 3 or 4 is about all that can be expected. Crude though it is, the agreement is gratifying in that no empirical magnetic constants except the saturation magnetization have been used in the present calculation. The ratio of A to the saturation moment has been estimated from h, m, e, and the lattice constant of iron, by use of a very simple physical model. However, the limitations of the model used in this section are severe; for example, it would be very risky to try to predict relative values of A for different metals from their respective values of ρ_0, since the correction factor corresponding to the expression in parentheses in the free electron Eq. (27) may vary considerably from one metal to another. The forthcoming paper[6] will present an alternative approach which throws some light on how this correction factor can be calculated.

I am very much indebted to Dr. C. Kittel for bringing this problem to my attention and for many helpful discussions in the course of the work, and to Dr. G. H. Wannier for suggestions on the calculations of Appendix II.

APPENDIX I. VALUE OF A FOR FREE ELECTRONS ON THE ATOMIC MODEL

We assume the wave function to be a determinant of functions of the form (16), each multiplied by a spin function g_n of the form (7) with $\theta_n=\pi/2$, $\varphi_n=Z_n d\varphi/dz$, where Z_n is the z component of the coordinate vector $\mathbf{R}_n$ of the nth lattice site. Using the subscript 0 for the state where all spins are parallel the contribution of the m, n pairs of w's to the exchange energy is

$$\left(mn\left|\frac{2}{|\mathbf{r}-\mathbf{r}'|}\right|nm\right)=\left(mn\left|\frac{2}{|\mathbf{r}-\mathbf{r}'|}\right|nm\right)_0|(g_m,g_n)|^2$$

$$|(g_m,g_n)|^2=\cos^2\tfrac{1}{2}(\varphi_m-\varphi_n)\sim 1-\tfrac{1}{4}(Z_m-Z_n)^2(d\varphi/dz)^2.$$

Taking the origin of coordinates at one of the lattice sites we have for an assembly of N electrons, to order $(d\varphi/dz)^2$,

$$E-E_0=\frac{N}{8}\sum_n\left(0n\left|\frac{2}{|\mathbf{r}-\mathbf{r}'|}\right|n0\right)_0 Z_n^2\left(\frac{d\varphi}{dz}\right)^2. \quad \text{(I.1)}$$

The exchange integrals $(0n|(2/|\mathbf{r}-\mathbf{r}'|)|n0)_0$ are messy to evaluate; however, they undoubtedly decrease with increasing $|\mathbf{R}_n|$, and their sum (including the term

[18] M. F. Manning and L. Goldberg, Phys. Rev. **53**, 662 (1938).
[19] D. R. Hartree, Proc. Roy. Soc. (London) **A141**, 282 (1937); D. R. Hartree and W. Hartree, Proc. Roy. Soc. (London) **A157**, 490 (1936).
[20] M. Fallot, Ann. phys. **6**, 305 (1936); see also C. Kittel, Revs. Modern Phys. **21**, 541 (1949).
[21] Williams, Bozorth, and Shockley, Phys. Rev. **75**, 155 (1949).

$n=0$) satisfies

$$\sum_n \left(0n\left|\frac{2}{|\mathbf{r}-\mathbf{r}'|}\right|n0\right)_0 = \frac{1}{N}\sum_{\mathbf{k}\mathbf{k}'}\left(\mathbf{k}\mathbf{k}'\left|\frac{2}{|\mathbf{r}-\mathbf{r}'|}\right|\mathbf{k}'\mathbf{k}\right)_0 \quad \text{(I.2)}$$

$$= 2.31/r_s \text{ rydbergs},$$

where r_s is the radius in Bohr units of the sphere whose volume equals the volume per electron.[22]

It can be verified that the term $n=0$ contributes only a little over half of this sum. For by (16)

$$\left(00\left|\frac{2}{|\mathbf{r}-\mathbf{r}'|}\right|00\right)$$

$$= \text{self energy of } (\Omega N)^{-1}\sum_{\mathbf{k}\mathbf{k}'}\exp[i(\mathbf{k}-\mathbf{k}')\cdot\mathbf{r}]$$

$$= (8\pi/\Omega N)\sum_{\mathbf{k}\mathbf{k}'} G(|\mathbf{k}-\mathbf{k}'|)/|\mathbf{k}-\mathbf{k}'|^2,$$

where $NG(|k-k'|)$ is the number of pairs of occupied states $\mathbf{k}, \mathbf{k}'$ which have a given value of $(\mathbf{k}-\mathbf{k}')$. A simple geometrical calculation gives

$$G(k) = 1-(3k/4k_{\max})+(k^3/16k_{\max}^3).$$

When this is inserted into the preceding equation the double integrations can all be carried out analytically, and give the result

$$\left(00\left|\frac{2}{|\mathbf{r}-\mathbf{r}'|}\right|00\right) = 66k_{\max}/35\pi = 1.45/r_s. \quad \text{(I.3)}$$

Since all the terms in (I.1) are positive, we underestimate $(E-E_0)$ if we assume that the entire difference between (I.2) and (I.3) is due to those terms in whose $\mathbf{R}_n$ are nearest neighbors to the origin site. Therefore

$$A = \frac{E-E_0}{\Omega(d\bar{\varphi}/dz)^2} \geq \frac{N\bar{Z}_n^2}{8\Omega}\left(\frac{0.86}{r_s}\right), \quad \text{(I.4)}$$

where $\bar{Z}_n^2$ is the mean square distance of nearest neighbors in the z direction. For body-centered and face-centered cubic lattices the right of (I.4) has the values $0.026/r_s^2$ and $0.028/r_s^2$, respectively.

[22] See, for example, F. Seitz, *Modern Theory of Solids* (McGraw-Hill Book Company, Inc., New York, 1940), No. 75.

APPENDIX II. SOLUTION OF THE INTEGRAL EQUATION (21)

Equation (21) was derived by minimizing an expression equivalent to

$$\int_{S_1}\int_{S_1}\frac{(\xi-\xi')^2}{|\mathbf{y}-\mathbf{y}'|^2}dydy'+8\pi^2\frac{d\bar{\varphi}}{dz}\int_{S_1}\xi\cdot\mathbf{y}dy, \quad \text{(II.1)}$$

the ξ of (21) being merely the z component of the ξ of (II.1). Equation (22) becomes $\xi=R(y)\mathbf{y}/y$. The first integral in (II.1), which we may call I, is equal to twice the corresponding integral taken over the region of $\mathbf{y}\mathbf{y}'$ space where $y\leq y'$. Throughout this region we may expand $1/|\mathbf{y}-\mathbf{y}'|$ as a series in Legendre functions of the cosine of the angle θ between $\mathbf{y}$ and $\mathbf{y}'$. Squaring this series and inserting it in I, only terms in P_n^2 and $P_nP_{n\pm1}$ will give a nonvanishing result after integration on θ. The result is

$$I = 32\pi^2\sum_{n=0}^{\infty}\left[\frac{2}{(2n-1)(2n+3)}\int_0^1 R^2y^3dy\right.$$

$$-\frac{1}{(4n^2-1)}\int_0^1 R^2y^{2n+2}dy-\frac{2(2n+2)}{(2n+1)(2n+3)}$$

$$\left.\times\int_0^1\int_0^{y'} RR'(y^{2n+3}/y'^{2n+1})dydy'\right]. \quad \text{(II.2)}$$

Inserting a trial function of the form $R=ay+by^3$ into (II.1) and (II.2) there results a quadratic expression in a and b, with coefficients which are infinite series of terms containing products of factors of the type $(2n+s)$ in the denominator. These series can be summed by decomposing the general term into partial fractions. The choice of a and b which minimizes the quadratic resulting from (II.1) is $a=-243\gamma/610$, $b=-9\gamma/122$, where γ is given by (24). Since, as Fig. 1 shows, the cubic term in R is rather small compared to the linear one, and since an independent calculation using a linear trial function $R=a'y$ gives almost the same value for (II.1) as when the cubic term is included, it is likely that this approximate solution is quite close to the true one. The evaluation of I assuming $R=a'y$, or $\xi=a'y$, is very easy, of course, since the integrand becomes unity and $I=(4\pi/3)^2$.

Neutron Capture γ-Rays from Phosphorus, Sulfur, Chlorine, Potassium, and Calcium

B. B. KINSEY, G. A. BARTHOLOMEW, AND W. H. WALKER*
Division of Atomic Energy, National Research Council of Canada, Chalk River, Ontario, Canada
(Received November 30, 1951)

The prominent capture γ-rays from phosphorus, sulfur, chlorine, potassium, and calcium have been studied with the aid of a pair spectrometer. The neutron binding energies obtained for P^{32}, S^{33}, Cl^{36}, and K^{40} are 7.94 ± 0.03, 8.64 ± 0.02, 8.56 ± 0.03, and 7.77 ± 0.03 Mev. Neutron capture in phosphorus produces a complicated spectrum in which the ground-state γ-ray is weak. Most of the captures in sulfur occur in S^{32} and produce S^{33} in a cascade process involving the fifth excited state near 3.2 Mev. The direct transition to the ground state in S^{33} is weak. In chlorine the ground state γ-ray and those produced by transitions from the capturing state to the first six excited states in Cl^{36} are of comparable intensity. In potassium there are relatively strong transitions to the ground state and to the second excited state of K^{40}. Some of the γ-rays produced by potassium can be identified with transitions in K^{42}, the excited state at 2.3 Mev being favored above all others. Three very weak γ-rays have been detected with energies above that to be expected from capture in K^{39} and K^{41}. These γ-rays do not appear to be due to impurities. It is possible that they arise from the capture of neutrons by K^{40} and, if this hypothesis is correct, that isotope must have a large capture cross section for thermal neutrons. In calcium the greater part of the γ-ray spectrum can be fitted into the energy level system of Ca^{41}. No γ-ray corresponding to the ground-state transition in Ca^{41} was detected.

I. INTRODUCTION

THE present paper contains the results of a study of the neutron capture γ-rays produced by a group of adjacent elements, *viz.*, phosphorus, sulfur, chlorine, potassium, and calcium. Because of the technical difficulties involved, no attempt has been made to study the neutron capture γ-rays produced by argon. A pair spectrometer has been used in these investigations; a description of the experimental arrangement is given in an earlier paper.[1] The relative intensities of the γ-rays from a particular sample were determined from the peak coincidence counting rates by using a calculated curve for the variation with energy of the counting efficiency of the spectrometer. For each spectrum the absolute intensity of one of the strong γ-rays was measured by comparing its peak coincidence counting rate with that of the 9.0-Mev γ-ray produced by neutron capture in nickel, using an intimate mixture of weighed amounts of the sample material and nickel sesquioxide. The absolute intensity of the nickel γ-ray in photons per capture was determined in a separate experiment. A more detailed description of the intensity measurements is given in the previous paper,[1] where the results indicate that the intensities of the γ-rays between 3 and 6 Mev are overestimated by this method. It seems probable that the theoretical counting efficiency may be incorrect in this energy range. A full description of the method of energy measurement will be published elsewhere.

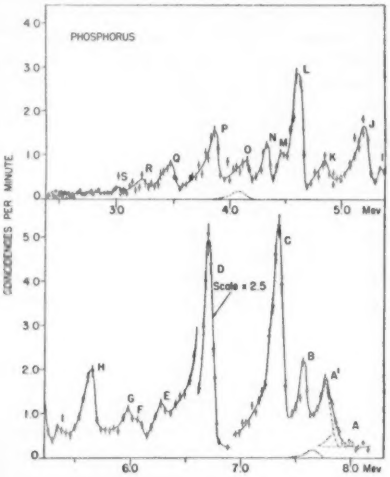

FIG. 1. Coincidence spectrum produced by phosphorus. Line width: 130 kev. The dotted lines represent the contribution to the spectrum from bismuth and aluminum radiations arising from the experimental arrangement.

II. PHOSPHORUS

The phosphorus source consisted of 940 grams of chemically pure red phosphorus enclosed in a container with Bakelite ends. The coincidence spectrum was studied from 2.5 to 10.0 Mev. The results up to 8.0 Mev are shown in Fig. 1. No coincidences were recorded above the background counting rate between 8.0 and 10.0 Mev. In this and the other coincidence spectra presented in this paper the abscissas of the curves are scaled so that the extrapolated end points of the peaks correspond to the energies of the γ-rays.

The end point of the peak of highest energy is at 7.94 ± 0.03 Mev. This γ-ray was not detected in a preliminary study[2] because the peak was masked by unwanted aluminum radiations. Its energy is in agreement with the binding energy of P^{32} calculated from the Q value of the $P^{31}(d,p)P^{32}$ reaction. The width of this peak and the slope of the high energy edge suggest that two γ-rays contribute to it. In an unresolved peak produced by two γ-rays of very nearly equal energies, the position of the end point of the higher

* Now at McMaster University, Hamilton, Ontario.
[1] Kinsey, Bartholomew, and Walker, Phys. Rev. **83**, 519 (1951).
[2] Kinsey, Bartholomew, and Walker, Phys. Rev. **78**, 481 (1950).

TABLE I. Energies and intensities of the phosphorus capture γ-rays.

γ-ray	Energy in Mev	Intensity in photons per 100 captures
A	7.94±0.03	0.5
A'	7.85 0.05	1.5
B	7.62 0.03	2
C	7.42 0.03	7
D	6.76 0.03	24
E	6.33 0.03	0.7
F	6.14 0.03	1.5
G	6.02 0.04	1.5
H	5.71 0.03	6
I	5.41 0.03	2
J	5.27 0.03	8
K	4.92 0.03	4
L	4.68 0.03	26
M	4.49 0.03	4
N	4.38 0.03	11
O	4.20 0.03	7
P	3.92 0.03	25
Q	3.55 0.03	22
R	3.28 0.04	9
S	3.04 0.04	7

energy γ-ray will not be appreciably affected by the presence of the other γ-ray, and the separate contributions of the peaks to the observed coincidence spectrum can usually be estimated. The extrapolated end point of a homogeneous peak in this energy region falls approximately 80 kev above the energy corresponding to the maximum counting rate, and the peak width at half-maximum is approximately 130 kev. These values were used to determine the shape of peak *A*, and peak *A'* was obtained by subtraction. The background counting rate underlying the two peaks is derived mainly from the tails of the peaks *B* and *C* and is due to scattering of electrons by the walls of the spectrometer. It has a shape close to that shown by the almost horizontal broken line. The end point of peak *A'* falls at 7.85±0.05 Mev and, as shown below, corresponds to a transition from the capturing state to the first excited state of P^{32}. The energies and absolute intensities of the γ-rays are given in Table I. The absolute intensities were determined by the nickel method[1] by comparison of the intensity of the 9.0-Mev nickel γ-ray with that of the γ-ray *D*, assuming that the capture cross section of phosphorus for thermal neutrons is 193±7 mb;[3] the absolute intensities of the other γ-rays were determined relative to that of *D*. The corrected γ-ray spectrum is shown in Fig. 2. The ordinates $\nu(E)$, representing the number of photons produced per capture per unit energy range, were obtained by application of Eq. (3), reference 1.

The $P^{31}(d,p)P^{32}$ reaction was studied by Allen and Rall[4] who found the *Q* value of the most energetic proton group to be 5.52±0.10 Mev. With the deuteron binding energy of 2.226±0.003 Mev[5] it follows that the binding energy of P^{32} is 7.75±0.10 Mev. A more recent value for the energy balance has been obtained by Strait and his collaborators;[6] it is 5.704±0.008 Mev, whence the corresponding binding energy of P^{32} is 7.930±0.009 Mev. The energy of the γ-ray *A* is in excellent agreement with the latter value.

Some of the γ-rays have been fitted to the level scheme shown in Fig. 3. This is drawn to conform to the results of Van Patter and Endt[7] which are in good agreement with earlier measurements by Allen and Rall. In this diagram γ-rays for which the assignment seems certain have been drawn as full lines. Those for which the position in the scheme is uncertain or ambiguous are drawn in broken lines. Strong γ-rays are drawn in heavy lines. The level at 3.141 Mev is drawn as a dotted line because the existence of a level at this energy is indicated but not definitely established by the measurements on the (d,p) reaction. The level energies on the right are the results of Van Patter and Endt; those on the left are obtained by subtracting the γ-ray energies from Table I from the 7.930±0.009-Mev binding energy.

The identification of the γ-rays *A* and *A'* has already been discussed. The difference between the binding energy and the energy of the strong γ-ray *D* is 1.17 ±0.03 Mev in agreement with the energy of the third excited state found by Van Patter and Endt. The equally intense γ-ray *L* appears to lead to an excited state at 3.25±0.03 Mev and may be in cascade with the ill-defined γ-ray *R*, since the sum of their energies is 7.96±0.05 Mev. The intensity of *R* is only one-third of that of *L*; the excitation of the 3.25-Mev state, therefore, is more frequent than the emission of the γ-ray *R*, and consequently, softer radiation must also be emitted producing excited states at lower energies. The difference energy corresponding to the γ-ray *P* is 4.01±0.03 Mev which suggests that it corresponds to a transition to the fourteenth excited state. Among the weaker radiations the γ-ray *C* clearly corresponds to a

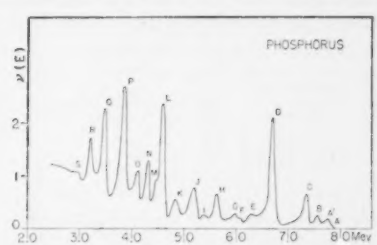

FIG. 2. Corrected γ-ray spectrum from phosphorus.

[3] F. C. W. Colmer and D. J. Littler, Proc. Phys. Soc. (London) **63**, 1175 (1950); H. Pomerance, Phys. Rev. **83**, 641 (1951), has obtained the value 0.15 barn (±10 percent). We choose the result with the lowest quoted error.

[4] R. C. Allen and W. Rall, Phys. Rev. **81**, 60 (1951).

[5] R. C. Mobley and R. A. Laubenstein, Phys. Rev. **80**, 309 (1950).

[6] Strait, Van Patter, Buechner, and Sperduto, Phys. Rev. **81**, 747 (1951).

[7] We are indebted to Dr. D. M. Van Patter and Dr. P. Endt for the privilege of quoting these results before publication.

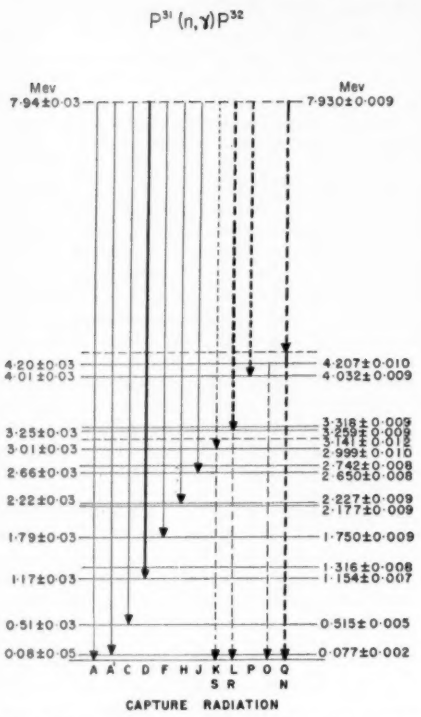

FIG. 3. Decay scheme for phosphorus. The energy levels are drawn to scale according to the results of Van Patter and Endt right-hand figures (see reference 7). The energies of these levels, obtained by subtracting the γ-ray energies from the neutron binding energy, are given on the left.

transition to the second excited state at 0.515 Mev and, the energy of H is equal to that of a transition to the 2.227-Mev level. The γ-ray J seems to correspond to a transition to the eighth excited state at 2.650 Mev. The

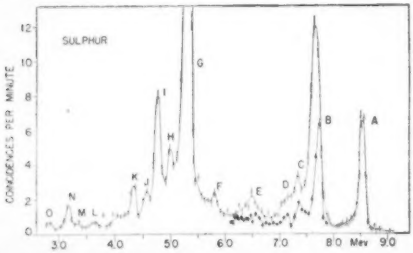

FIG. 4. Coincidence spectrum produced by sulfur. Line width: 130 kev. The results obtained using a container with Dural end walls are shown by open circles; those obtained in similar conditions with a container with Bakelite ends are shown by full circles.

difference between the binding energy and the energy of the γ-ray K is 3.01±0.03 Mev which is equal to the energy of the tenth excited state. The γ-ray S, the existence of which is not well established in the coincidence spectrum, may correspond to a transition from this state to the ground state in cascade with K. The difference energy for the γ-ray F is 1.79±0.03 Mev, and this suggests that F is emitted in a transition from the capturing state to the fifth excited state. The energy of the γ-ray O agrees with the energy of the fifteenth excited state. The strong γ-rays N and Q have a total energy of 7.93±0.04 Mev and may be in cascade. The weaker γ-rays B, E, G, I, and M cannot be identified with transitions from the capturing state to any of the known states of P^{32}. The γ-ray B may be due to a transition from a higher level to the ground state.

Both the γ-rays J and L in Fig. 3 correspond to transitions from the capturing state to the lowest

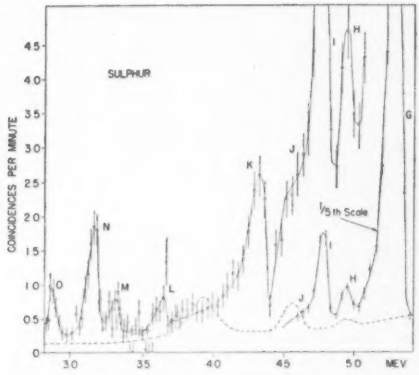

FIG. 5. Detail of coincidence spectrum from sulfur between 2.7 and 5.3 Mev. The contribution of the Dural container to this spectrum is shown by the dotted line.

member of a pair of levels. The doublet separation for the levels corresponding to J is 92 kev which is less than the resolution of the apparatus. The peak J in Fig. 1 is wider than that expected for a homogeneous γ-ray, and this fact suggests that a γ-ray corresponding to a transition to the higher level of the pair may be present. Referring now to the γ-ray L, it is not possible to determine whether a γ-ray is present which corresponds to a transition to the higher component of the doublet, *viz.*, the level at 3.318 Mev, for the separation of the level doublet is only about 60 kev. The peak H may also be complex since the 50-kev separation of the 2.227 and 2.177-Mev levels is small. There is no evidence for a transition to the level at 1.316 Mev though a weak γ-ray may be obscured by the tail of peak D.

If the numbers of photons per capture, which have been ascribed to γ-rays emitted by the capturing state,

are added together, it will be seen that the total exceeds unity by about 40 percent. If the product of the intensities and the energies of the γ-rays listed in Table I are added together, the result (8.2 Mev) is higher than the binding energy of P^{32}. A lower value is to be expected because low energy γ-rays are certainly radiated in the capture process and are not detected. An even higher value (11 Mev) is obtained by integrating the γ-ray spectrum of Fig. 2. Such discrepancies are probably caused by an overestimate of the intensities of γ-radiation between 3 and 6 Mev and have been discussed in a previous paper.[1]

III. SULFUR

The spectrum of sulfur was originally investigated using a sample consisting of 920 grams of chemically pure sulfur cast into a Dural container with Dural end walls. Under these conditions the spectrum was surveyed between 2.7 and 12.0 Mev. A portion of this

TABLE II. Energies and intensities of sulfur capture γ-rays.

γ-ray	Energy in Mev	Intensity in photons per 100 captures
A	8.64±0.02	3
B	7.78 0.03	4
C	7.42 0.03	0.7
D	7.19 0.03	0.5
E	6.64 0.03	0.7
F	5.97 0.06	1
G	5.43 0.02	84
H	5.03 0.06	5
I	4.84 0.06	20
J	4.60 0.06	5
K	4.38 0.03	13
L	3.69 0.05	5
M	3.36 0.05	7
N	3.21 0.03	30
O	2.94 0.05	19

spectrum is shown in Fig. 4 (open circles). No coincidence counting rate above that of the background was found above 9.0 Mev. In addition, the spectrum was examined in detail between 2.7 and 5.3 Mev (Fig. 5). In Fig. 4, the coincidence peak *B* includes a contribution from the 7.72-Mev γ-ray produced by the aluminum in the container. In order to obtain a more accurate measurement of the sulfur spectrum near 7 Mev, further measurements were made using a container with Bakelite ends and the results of these measurements are also plotted in Fig. 4 (full circles). The two curves in Fig. 4 have been adjusted using peak *G*, so that they represent the same neutron capturing rate for the two samples; the difference between them near 7 Mev, therefore, represents the contribution from the spectrum of the Dural container. The contribution of the container to the spectrum at lower energies, which is shown by the broken curve in Fig. 5, was determined in separate measurements with an empty container.[1]

The energies and intensities of the sulfur capture γ-rays are listed in Table II. The absolute intensity of

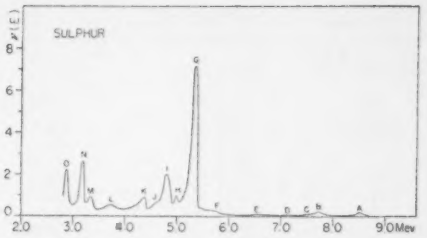

FIG. 6. Corrected γ-ray spectrum from sulfur.

the γ-ray *G* was determined by the nickel method, and the intensities of the remaining γ-rays were determined relative to that of *G*. The capture cross section of sulfur was assumed to be 0.49 barn.[3] The corrected γ-ray spectrum of sulfur is given in Fig. 6.

The most energetic γ-ray *A* is produced in a direct transition to the ground state when a neutron is captured in S^{32}. The energy of this γ-ray, 8.64±0.02 Mev, is in agreement with the neutron binding energy of S^{33}, a quantity which may be deduced from the energy balance of the $S^{32}(d,p)S^{33}$ reaction. For the *Q* of this reaction Davison[8] obtained 6.48±0.11 Mev. More recently Strait and his collaborators[6] have obtained 6.422±0.011 Mev which corresponds to a neutron binding energy of 8.648±0.012 Mev in good agreement with the energy of the γ-ray *A*.

For the *Q* of the $S^{33}(d,p)S^{34}$ reaction Davison[8] found 8.67±0.25 Mev whence the binding energy of S^{34} is 10.90±0.25 Mev. The binding energy of the other isotopes of sulfur can be calculated from the mass values collected by Low and Townes.[9] These binding energies together with the abundances and contributions[10] to the total absorption cross section for the sulfur isotopes are summarized in Table III.

Neither the direct transition to the ground state in S^{34} nor the transition to the excited state at 0.82 Mev[6] was detected for, as already mentioned, no coincidence

TABLE III. Abundances, cross sections, and neutron binding energies of the sulfur isotopes.

Target nucleus	Abundance percent	Contribution to total cross section in barns	Reference	Binding energy of product nucleus in Mev		Reference
S^{32}	95.1	0.49	a	8.648±0.012		d
S^{33}	0.74			10.90	0.25	e
S^{34}	4.2	0.011	b	7.16	0.45	f
S^{36}	0.016	2×10^{-5}	c	5.78	0.60	f

[a] See reference 3.
[b] See reference 10.
[c] *Nuclear Data* (National Bureau of Standards Circular No. 499, Washington, D. C., 1950).
[d] See reference 6.
[e] See reference 8.
[f] See reference 9.

[8] P. W. Davison, Phys. Rev. **75**, 757 (1949).
[9] W. Low and C. H. Townes, Phys. Rev. **80**, 608 (1950).
[10] Seren, Friedlander, and Turkel, Phys. Rev. **72**, 888 (1947).

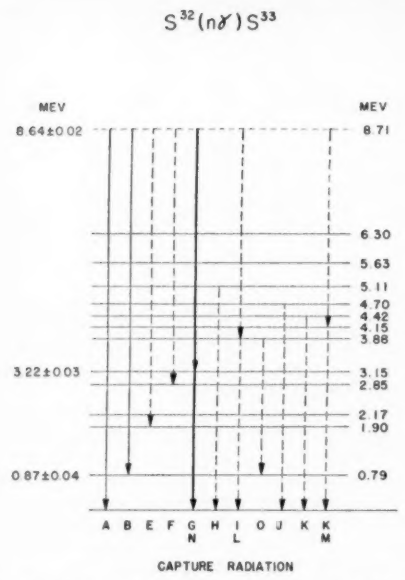

FIG. 7. Decay scheme for sulfur. The figures on the right are the positions of the energy levels determined by Davison (see reference 8); those on the left were obtained from the subtraction of the γ-ray energies from the neutron binding energy.

peaks were observed above 9 Mev. Alburger[11] has measured the γ-radiation emitted in the reaction $P^{31}(\alpha,p)S^{34}$ and found γ-rays with energies of 2.55 and 4.1 Mev. If these energies are those of two of the excited states in S^{34}, we might expect neutron capture γ-rays with energies of 8.3 and 6.8 Mev. No positive identification of such radiation can be made with any of the γ-rays of Table II.

The weak γ-rays C and D both have energies which fall within the probable error of the binding energy of S^{35} given in Table III and, therefore, either one may represent the ground state transition in that isotope. Until more accurate values of the γ-ray energies and of the binding energy of S^{35} are determined or until sulfur enriched in S^{34} is available, it will not be possible to determine if either of these γ-rays are produced by that isotope.

In view of the very small fraction of the total cross section contributed by S^{36} a 5.8-Mev ground-state γ-ray from S^{37} would not be detected in the presence of stronger γ-rays in its vicinity.

Some of the γ-rays listed in Table III can be explained in terms of capture by S^{32}, and an attempt has been made to fit most of them into a decay scheme in Fig. 7, which has been derived from the level energies obtained by Davison.[8] Those γ-rays whose positions in the scheme are subject to little doubt are indicated by full lines while those whose assignment is only tentative are shown by broken lines. The level energies found by Davison are given on the right of the decay scheme. The level energies on the left are obtained by subtracting γ-ray energies in Table II from the neutron binding energy in S^{33}, *viz.*, 8.648±0.012 Mev.

The two strongest γ-rays G and N appear to be in cascade, for their energies add up to 8.64±0.04 Mev in excellent agreement with the energy of the γ-ray A. In addition, their intensities, which are comparable, suggest that they are related in this manner. The energy of N is very close to that of the 3.15-Mev level in S^{33}, and it seems probable that N represents the transition between this state and the ground state. However, the γ-ray G is stronger than N, and this indicates that softer radiations also are emitted in transitions between the 3.15-Mev level and the levels lying between it and the ground state.

It is worth noting that the 3.15-Mev level, which is strongly excited in the neutron capture process, is also one of the levels most strongly excited in the (d,p) reaction. In a previous paper[1] we have noted that a similar phenomenon occurs in Si^{29}.

The assignment of the γ-ray B is clear for its energy corresponds to the formation of an excited state at 0.87±0.04 Mev, in fair agreement with Davison's first excited state at 0.79 Mev.

The remaining γ-rays are less certainly identified. Of the stronger γ-rays I, O, and L can be connected with the excited state near 3.88 Mev in the way shown in Fig. 7. Peak L is not well defined and may correspond to more than one γ-ray. The width of the peak at K is also large and several γ-rays may contribute

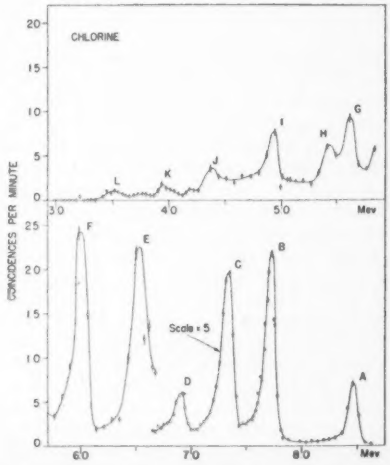

FIG. 8. Coincidence spectrum produced by chlorine. Line width: 130 kev.

[11] D. E. Alburger, Phys. Rev. **73**, 1014 (1948).

to it. A part of K could represent a transition to the level at 4.15 Mev or again another from the level at 4.42 Mev to the ground state.

Of the weaker γ-rays C and D, if they belong to S^{33}, must arise from hitherto unknown excited states at 7.42 and 7.19 Mev, respectively. Alternatively, they may arise from capture in S^{32}, for little is known about the excited states of S^{34}, or as we have already mentioned, one of them might represent the ground state transition in S^{35}. The γ-rays E and F apparently are complex, and as they are assigned in Fig. 7, their emission produces the excited states at 2.00±0.04 and 2.68±0.07 Mev, respectively, in rather poor agreement with Davison's values of 1.90 and 2.85 Mev. A very weak γ-ray corresponding to a transition to the level at 2.17 Mev may be present in the tail of the peak E. Peak J may be due entirely to radiation from the Dural container.

The total energy radiated from sulfur, according to the results of Table II, is 8.7 Mev which is equal to the binding energy of S^{33}. As in the case of phosphorus, a value lower than the binding energy is to be expected. The value obtained from the integral of the γ-ray spectrum (Fig. 6) is 13 Mev.

IV. CHLORINE

The chlorine sample consisted of 810 grams of chemically pure hexachlorobenzene (C_6Cl_6) enclosed in a Dural container with Dural ends. The neutron capture cross section of chlorine (32 barns) is much greater than that of carbon so that the carbon capture γ-rays do not appreciably affect the chlorine spectrum. The γ-rays caused by neutron capture in the Dural of the sample container are negligible for the same reason. Furthermore, since the contribution to the total cross section by Cl^{37} is only 0.14 barn,[10] the γ-ray spectrum observed is due largely to capture in the single isotope Cl^{35}. A sample consisting of a mixture of weighed amounts of hexachlorobenzene and nickel sesquioxide was used in an additional experiment to obtain the absolute intensities of the chlorine γ-rays.

The coincidence spectrum was measured from 2.5 to 9.5 Mev with a resolution of 130 kev. No γ-rays were detected below 3.3 Mev or above 8.6 Mev. The results

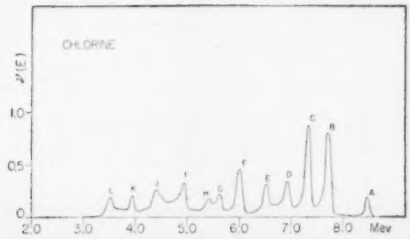

FIG. 9. Corrected γ-ray spectrum from chlorine.

TABLE IV. Energies and intensities of chlorine capture γ-rays.

γ-ray	Energy in Mev	Intensity in photons per 100 captures
A	8.56±0.03	3
B	7.77 0.03	10
C	7.42 0.03	8
D	6.98 0.03	1
E	6.62 0.06	4
F	6.12 0.03	6
G	5.72 0.03	2
H	5.51 0.03	1
I	5.01 0.03	4
J	4.46 0.04	2
K	4.06 0.04	3
L	3.62 0.05	2

obtained are shown in Fig. 8. The corrected γ-ray spectrum is given in Fig. 9.

The neutron binding energy of Cl^{36}, determined from the results of Shrader and Pollard[12] on the energy balance of the (d,p) reaction, is 8.54 Mev. This figure is in agreement with that derived from recent work by Ennis,[13] *viz.*, 8.49 Mev. Both are in agreement with the energy of the most energetic γ-ray at 8.56±0.03 Mev (peak A), which can therefore be identified as the ground-state γ-ray in Cl^{36}.

Shrader and Pollard also report the presence of two levels at 0.96 and 4.81 Mev. The positions of other excited states in Cl^{36} have been observed by Ennis.[14] No other information concerning the excited states of Cl^{36} is available, and consequently, the positions of some of the capture γ-rays in the decay scheme cannot be determined with certainty. The energies of the γ-rays and their intensities determined by the nickel calibration method are given in Table IV. A tentative decay scheme for some of these radiations is given in Fig. 10. The level energies given on the left of the diagram are derived from the γ-ray measurements with the help of the results obtained by Ennis. The energies of the γ-rays B and C correspond to transitions from the capturing state to low-lying states at 0.79 and 1.14 Mev. These values bracket the 0.96-Mev energy level obtained by Shrader and Pollard. The γ-rays D, E, F, and G have energies which show that they correspond to transitions to the third, fourth, fifth, and sixth excited states found by Ennis, and H could be the γ-ray emitted by his tenth state. The total energy of γ-rays K and J is 8.52±0.06 Mev; this quantity is close to the binding energy of Cl^{36} and suggests that these γ-rays may be in cascade. As indicated in Fig. 10, the order of their emission is unknown. The γ-ray I corresponds to a transition to an excited state at 3.55 Mev. The γ-rays I and L may be in cascade for the sum of their energies is 8.63±0.06 Mev.

For the reaction $Cl^{37}(d,p)Cl^{38}$ Shrader and Pollard[12] found Q values of 4.02, 3.02, and 2.10 Mev. We might

[12] E. F. Shrader and E. Pollard, Phys. Rev. **59**, 277 (1941).
[13] W. W. Ennis, Phys. Rev. **82**, 304 (1951).
[14] We are indebted to Dr. W. W. Ennis for sending us these later results before publication.

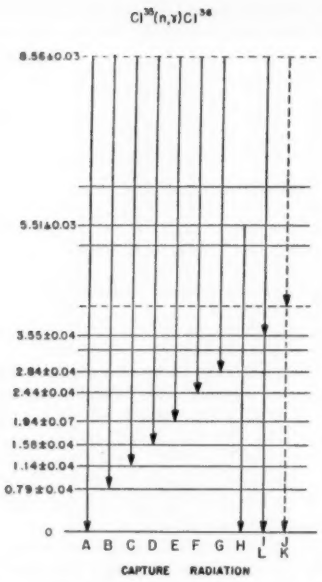

FIG. 10. Decay scheme for chlorine. The figures on the left are the positions of the energy levels of Cl^{36} obtained by subtracting the energies of the γ-rays from the neutron binding energy.

expect to observe, therefore, a ground-state γ-ray with an energy of 6.25 Mev and two others with energies of 5.25 and 4.33 Mev. The first has an energy close to that of the γ-ray F, but the intensity of that γ-ray is much greater than the neutron capture rate of Cl^{37}, and most of this peak therefore is a result of capture by Cl^{35}. Even if all the captures in Cl^{37} produced the ground-state γ-ray, its peak intensity[15] would be only some 3 percent of that of F. The other two γ-rays, if present, might be discernable in the spectrum between the peaks K and H if a much higher resolution were available.

The total energy radiated in the γ-rays listed in Table IV is only 3.0 Mev. This small amount, less than half of the binding energy, is surprising in view of the much larger values obtained for lighter elements. The integrated energy emitted is 5.8 Mev which again is much lower than the binding energy. As pointed out above, our estimates for these quantities are, for instrumental reasons, usually too high. Probably less energetic γ-rays are emitted in cascading processes which, on account of their low energy, escape detection. If this is the correct explanation, it is in accord with the measurements of Muehlhause[16] on the multiplicity of neutron capture γ-rays; for chlorine he obtains 3.1 γ-rays per capture, a rather high result for elements in this part of the periodic table. Numerous low energy γ-rays have been detected recently by Hamermesh and Hummel,[17] but their significance in relation to the decay scheme is not clear.

V. POTASSIUM

In the first survey experiments with potassium, the source consisted of one kilogram of the anhydrous carbonate enclosed in a Dural container. In more recent measurements a similar quantity of the carbonate was placed in a Dural container with Bakelite ends. The results of the latter measurements, obtained with a resolution of 170 kev, are shown in Figs. 11 and 12, and the energies and intensities of the γ-rays are listed in Table V. The absolute intensities were obtained by comparing the intensity of the 9.0-Mev nickel γ-ray with that of the γ-ray F, using a separate sample of potassium carbonate mixed with nickel sesquioxide. The corrected γ-ray spectrum is shown in Fig. 13.

Potassium possesses two stable isotopes K^{39} and K^{41} for which the abundances are 93.2 and 6.8 percent. According to Colmer and Littler[3] the total capture cross section is 1.89 ± 0.06 barns, and the contribution to this cross section caused by K^{41} is 67 mb.[10] The naturally occurring radioactive isotope K^{40} is present in ordinary potassium only to the extent of 0.01 percent, and its contribution to the cross section is unknown.

The positions of the excited states of the potassium isotopes K^{40} and K^{42} have been determined by Sailor[18] from a study of the (d,p) reaction using the separated isotopes K^{39} and K^{41} as targets. The Q value of the highest energy group of protons from the reaction $K^{39}(d,p)K^{40}$ was found to be 5.48 ± 0.08 Mev, whence, if this group produces the ground state, it follows that the binding energy of a neutron in K^{40} is 7.71 ± 0.08 Mev. The energy of the γ-ray B is 7.77 ± 0.03 Mev and is in good agreement with this value. It does not follow that this γ-ray should be identified with the direct transition to the ground state in K^{40} for γ-rays with a

TABLE V. Energies and intensities of potassium capture γ-rays.

γ-ray	Energy in Mev	Intensity in photons per 100 captures
A''	9.28 ± 0.05	0.2
A'	8.48 0.05	0.2
A	8.03 0.05	0.5
B	7.77 0.03	11
C	7.20 0.07	0.5
D	6.98 0.03	2
E	6.30 0.05	0.5
F	5.75 0.03	18
G	5.38 0.03	6
H	5.01 0.03	6
I	4.39 0.03	10
J	4.18 0.05	6
K	3.92 0.05	5
L	3.67 0.05	8

[15] In another communication, reference 2, we have incorrectly identified the γ-ray F with this ground state γ-ray.
[16] C. O. Muehlhause, Phys. Rev. **79**, 277 (1950).
[17] B. Hamermesh and V. Hummel, Phys. Rev. **83**, 663 (1951).
[18] V. L. Sailor, Phys. Rev. **77**, 794 (1950).

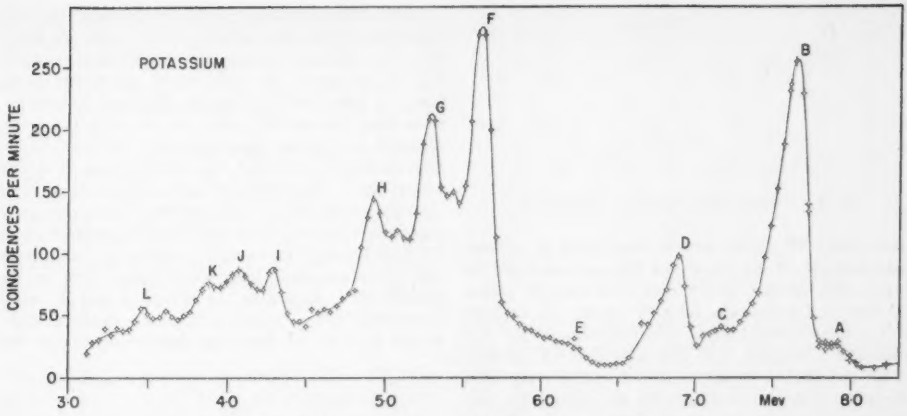

FIG. 11. Coincidence spectrum produced by potassium. Line width: 170 kev.

greater energy have been detected (Fig. 12). However, an independent check on the neutron binding energy of K^{40} in agreement with these values can be obtained from recent mass-spectrographic results and the energy of the β-decay of that isotope. From the results of Nier and Roberts,[19] we have 0.32 ± 0.08 mmu for the mass difference $Ca^{40}-A^{40}$. For the energy of the decay of K^{40} we take the mean value 1.35 ± 0.02 Mev,[20] which is equivalent to 1.45 ± 0.03 mmu for the mass difference $K^{40}-Ca^{40}$. Hence, the difference $K^{40}-A^{40}$ is 1.77 ± 0.09 mmu. The mass of A^{40} is 39.97524 ± 0.00003 amu.[21] Therefore the mass of K^{40} is 39.97701 ± 0.00010 amu. For K^{39} Collins, Nier, and Johnson[22] obtained a packing fraction of $-6.12\pm0.02\times10^{-4}$ which corresponds to a mass of 38.97613 ± 0.00008 amu. With the neutron mass of 1.008982 ± 0.000003 amu given by Li, Whaling, Fowler, and Lauritsen,[23] we calculate the neutron binding energy of K^{40} to be 8.10 ± 0.14 mmu or 7.54 ± 0.13 Mev. This result agrees with that obtained from the (d,p) reaction within the combined probable errors.

The highest Q value found by Sailor for the reaction $K^{41}(d,p)K^{42}$ is 5.12 ± 0.10 Mev, whence if we assume that the ground-state group was observed, it follows that the neutron binding energy of K^{42} is 7.35 ± 0.10 Mev. This result can also be checked by calculation from mass-spectrographic values. From the results of Collins *et al.*[22] the mass of K^{41} is 40.97499 ± 0.00008 amu, and the mass of Ca^{42} is 41.97228 ± 0.00008 amu. From the β-decay of K^{42} we have $K^{42}-Ca^{42}=3.83\pm0.20$ mmu.[24] Hence we calculate the mass of K^{42} to be 41.97611 ± 0.00022 amu and the neutron binding energy of K^{42} to be 7.86 ± 0.24 amu or 7.32 ± 0.22 Mev in good agreement with that derived from the results of Sailor. The energy of the partially resolved peak at C, Fig. 11, is 7.20 ± 0.07 Mev and may represent therefore the ground-state transition in K^{42}.

From the mass values aforementioned we can also calculate the neutron binding energy of K^{41}. It is 10.24 ± 0.13 Mev.

Figure 12 contains clear evidence for a γ-ray A at 8.03 ± 0.05 Mev and for two others: A' at 8.48 ± 0.05 Mev and A'' at 9.28 ± 0.05 Mev. The width of A' is excessive, and this γ-ray is certainly complex. All of these γ-rays have energies which exceed the neutron binding energies of K^{40} and K^{42} calculated above by a margin considerably greater than the combined probable errors, and none of them correspond to the γ-rays emitted by any of the forty-odd elements which we have studied and which could possibly be present as impurities. A spectroscopic analysis indicated that the sample material contained Ca, Cu, and Mg in concentrations of only one part per million and no other detectable impurities. It seems possible, therefore, that these γ-rays are caused by capture in K^{40}, for if the isotopic capture cross section of K^{40} for thermal neu-

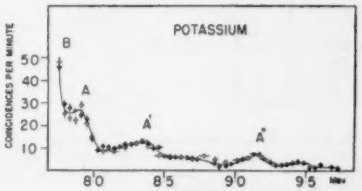

FIG. 12. Upper part of the coincidence spectrum of potassium. The full and open circles represent the results of two separate experiments.

[19] A. O. Nier and T. R. Roberts, Phys. Rev. **81**, 507 (1951).
[20] D. E. Alburger, Phys. Rev. **79**, 236 (1950); Bell, Weaver, and Cassidy, Phys. Rev. **77**, 399 (1950); L. Feldman and C. S. Wu, Phys. Rev. **81**, 298 (1950).
[21] A. O. Nier, Phys. Rev. **81**, 624 (1951).
[22] Collins, Nier, and Johnson, Phys. Rev. **83**, 228 (1951).
[23] Li, Whaling, Fowler, and Lauritsen, Phys. Rev. **83**, 512 (1951).
[24] K. Siegbahn, Arkiv Mat. Astron. Fysik **34B**, No. 4 (1947).

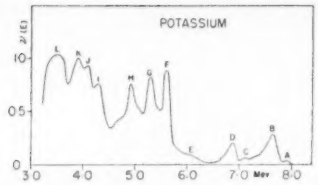

FIG. 13. Corrected γ-ray spectrum from potassium.

trons were 100 times greater than that of natural potassium, about one percent of the captures would be due to this isotope, and γ-rays with energies above 8.0 Mev and intensities above 10 percent per capture in K^{40} might be detected. Excited states of K^{41} are known at 1.34±0.15, 3.10, and 4.40 Mev.[25] If capture in K^{40} occurred to an appreciable extent, a γ-ray with an energy 1.34 Mev less than the binding energy, i.e., 8.9±0.2 Mev, might be observed. This energy is close to that of the γ-ray A''. However, such an assignment is not very convincing in view of the large probable errors associated with both the binding energy of K^{41} and the energy of the γ-ray A''. Although the coincidence spectrum has been explored up to 11 Mev, no evidence was found for the emission of a γ-ray near 10.3 Mev produced by the excitation of the ground state transition in K^{41}.

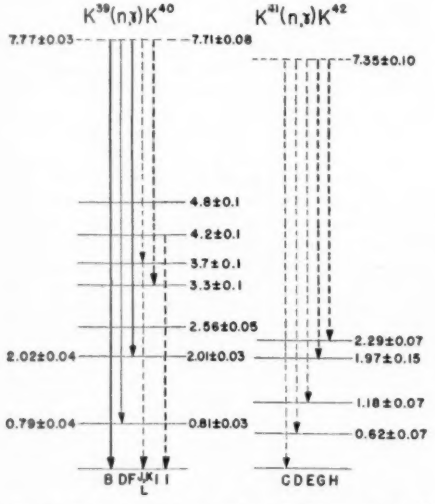

FIG. 14. Decay scheme for potassium. The figures on the right are the positions of the energy levels found by Sailor (see reference 18); those on the left were obtained by subtracting the γ-ray energy from the neutron binding energy.

[25] Bleuler, Boltmann, and Zünti, Helv. Phys. Acta **19**, 419 (1946); D. C. Worth, Phys. Rev. **78**, 378 (1950).

Most of the remaining γ-rays can be identified with transitions from the capturing state to energy levels found by Sailor. A tentative decay scheme is shown in Fig. 14, in which the positions of the energy levels found by Sailor are shown on the right and those calculated from the capture γ-rays, on the left. The γ-ray D, which is complex, corresponds to a transition to the first excited state of K^{40}, the strong γ-ray F to the second state. This state is again among those most strongly excited in the (d,p) reaction. The γ-ray I may represent a transition to the fourth excited state at 3.3 Mev although its energy is also in agreement with that of a transition from the 4.2-Mev state to the ground state. Either of the γ-rays J and K could correspond to the transition from the capturing state to the level at 3.7 Mev. As already mentioned, the

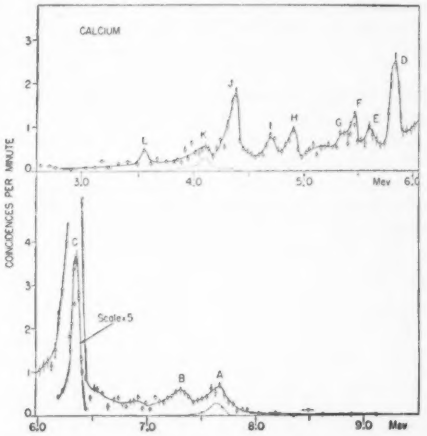

FIG. 15. Coincidence spectrum produced by calcium. Line width: 130 kev. The dotted lines represent the contributions caused by bismuth and aluminum radiations.

γ-ray C may be produced in the ground-state transition in K^{42}. The γ-ray E, 6.30±0.05 Mev, is in rough agreement with the energy difference 6.17±0.18 Mev between the capturing state and the second excited state in K^{42}. The γ-rays G and H are in good agreement with the transition energies from the capturing state to the third and fourth excited states of K^{42}. The γ-ray representing the transition to the first excited state of K^{42} is probably responsible for part, at least, of the excessive width of the peak D.

The γ-rays listed in Table V and shown in Fig. 14 only account for a fraction of the total captures in potassium. The sum of the intensities of the γ-rays which are probably radiated from the capturing state, i.e., all except I and L, amount to 60 percent of the rate of neutron capture and the total energy radiated per capture by the γ-rays of Table V is 3.8 Mev. These

low values merely indicate that the γ-rays, which appear resolved distinctly in Fig. 11, form only a part of the total radiation emitted, for when the unresolved radiations are taken into account by integration, the result is 10.1 Mev which is somewhat higher than the binding energy in K^{40}.

The γ-rays, which have been assumed to follow capture in K^{41}, account for about 13 percent of the total neutron capture rate. This fraction is three times greater than that to be expected from the ratio of the capture cross sections of the two isotopes. The discrepancy suggests that part of the poorly resolved peaks at *G* and *H*, which have been assigned to capture by K^{41}, must in fact be produced by capture in K^{39}.

VI. CALCIUM

The calcium capture γ-rays were obtained from a sample of pure calcium oxide contained in a Dural container with Bakelite ends. The spectrum was investigated up to 11 Mev with a resolution of 130 kev. No γ-ray was found with an energy greater than 7.83 Mev.

TABLE VI. Energies and intensities of calcium capture γ-rays.

γ-ray	Energy in Mev	Intensity in photons per 100 captures
A	7.83±0.05	1
B	7.43 0.05	1.4
C	6.42 0.03	83
D	5.89 0.03	11
E	5.66 0.06	3
F	5.49 0.05	4
H	4.95 0.03	8
I	4.76 0.03	6
J	4.45 0.05	30
L	3.62 0.05	16

The results are shown in the coincidence spectrum of Fig. 15, and the energies and intensities of the γ-rays are listed in Table VI. The corrected γ-ray spectrum is shown in Fig. 16. The absolute intensities of the γ-rays were determined by a comparison of the intensity of the strong γ-ray *C* with that of the 9.0-Mev nickel γ-ray, assuming that the capture cross section for thermal neutrons in calcium is 0.40 barn.[3]

The abundances and the thermal neutron capture cross sections of the calcium isotopes, so far as they are known, are listed in Table VII. The binding energy of Ca^{41} may be obtained from the *Q* value of the reaction $Ca^{40}(d,p)Ca^{41}$. For this quantity Sailor[26] obtained the value 6.17±0.05 Mev, whence the neutron binding energy is 8.40±0.05 Mev. This result is consistent with that which may be calculated from mass data and the *Q* of the reaction $K^{41}(p,n)Ca^{41}$. For the latter quantity Richards, Smith, and Browne[27] obtain −1.22 ±0.02 Mev from which we obtain $Ca^{41}-K^{41}=0.47$ ±0.02 mmu. With the mass of K^{41} referred to above, *viz.*, 40.97499±0.00008 amu, we obtain 40.97546 0.00008 amu for the mass of Ca^{41}. With the $Ca^{40}-A^{40}$ mass difference and the mass of A^{40} also quoted above, we obtain 39.97556±0.00009 amu for the mass of Ca^{40}. From these results it follows that the neutron binding energy of Ca^{41} is 8.45±0.10 Mev in agreement with the result obtained from the (d,p) reaction. The packing fractions given by Collins *et al.*[22] for Ca^{42}, Ca^{43}, and Ca^{44} may be used to calculate a neutron binding energy of 8.02±0.13 Mev for Ca^{43} and 11.50±0.13 Mev for Ca^{44}. There is insufficient information to enable one to determine the neutron binding energies of Ca^{45}, Ca^{47}, or Ca^{49} in the same way; these quantities may be estimated by means of the Bohr-Wheeler formula and are given in parentheses in Table VII. The γ-rays due to capture in Ca^{46} would be difficult to detect unless the capture cross section of that isotope were exceptionally large. The activity of the product nucleus Ca^{47} seems not to have been observed.

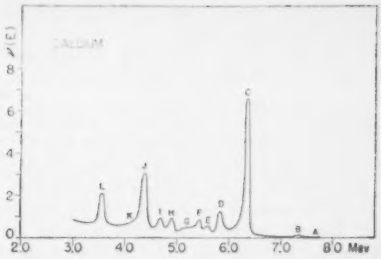

FIG. 16. Corrected γ-ray spectrum from calcium.

The excited states of Ca^{41} have been observed by Sailor[26] in a study of the $Ca^{40}(d,p)Ca^{41}$ reaction. The positions of these levels are shown on the right-hand side in Fig. 17. An excited state at about 0.4 Mev[28] has been observed in Ca^{43} from the β-decay of K^{43}. Another level near 1 Mev is excited in the decay of Sc^{42}, for a γ-ray with an energy at 1.0 Mev has been reported by Walke[29] and at 1.65 Mev by Hibdon, Pool, and Kurbatov.[30] From the decay of Sc^{44}, γ-rays of 0.52 and 1.25 Mev have been observed,[30] but the position of the excited states in Ca^{44} is not clear. No other data is

TABLE VII. Abundances, cross sections, and binding energies of the calcium isotopes.

Target nucleus	Abundance percent	Contribution to cross section in mb	Binding energy of product nucleus in Mev
Ca^{40}	96.9		8.40±0.05
Ca^{42}	0.64	386±30	8.02±0.13
Ca^{43}	0.14		11.50±0.13
Ca^{44}	2.1	13	(5.8)
Ca^{46}	0.0032	...	(4.6)
Ca^{48}	0.18	1	(3.7)

[26] V. L. Sailor, Phys. Rev. **75**, 1836 (1949).
[27] Richards, Smith, and Browne, Phys. Rev. **80**, 524 (1950).
[28] Overstreet, Jacobson, and Stout, Phys. Rev. **75**, 231 (1949).
[29] H. Walke, Phys. Rev. **57**, 163 (1940).
[30] Hibdon, Pool, and Kurbatov, Phys. Rev. **67**, 289 (1945); A. Bruner and M. Langer, Phys. Rev. **79**, 236 (1950).

available on the energy levels of the calcium isotopes relevant to the present work.

An inspection of Table VI and Fig. 17 will show that the γ-rays A and B cannot be produced in transitions to any of the known low-lying levels of Ca^{41}. It is possible that A and B arise from transitions to the ground state from highly excited states in Ca^{41} lying near the capturing state, but it is more probable that they are produced in the decay of Ca^{43} and Ca^{44}. The energy of the γ-ray A agrees with the binding energy of Ca^{43} though the probable errors involved are too great for this identification to be made with certainty.

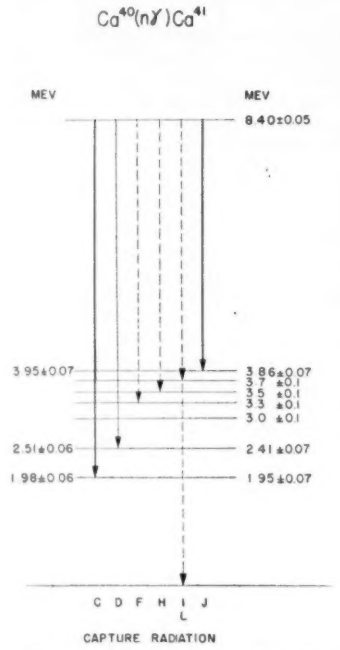

FIG. 17. Decay scheme for calcium. The figures on the right are the positions of the energy levels found by Sailor (see reference 26); those on the left were obtained by subtracting the γ-ray energies from the neutron binding energy.

However, as shown below, it is unlikely theoretically, that such a transition should be detected. A γ-ray corresponding to a transition from the capturing state to the 0.4-Mev level in Ca^{43} would have an energy of 7.6 Mev, and it is possible that γ-ray B is produced in this transition.

The origin of the remaining capture γ-rays cannot be determined with certainty because of the lack of information concerning the separate cross sections of Ca^{40}, Ca^{42}, and Ca^{43}. However, it will be shown below that the majority of these γ-rays can be fitted to the level scheme of Ca^{41}. Moreover, such an assignment for the strong γ-rays C and J seems very probable because of the high abundance of Ca^{40}. It will be noted that the γ-ray C could be fitted to the decay of Ca^{42}. For if the value of 1.65 Mev for the second excited state of this isotope is correct, the difference between this energy and the binding energy of Ca^{43} is 6.3 Mev in agreement with the energy of C. However, if the γ-ray C is produced by capture in Ca^{42}, that nucleus would require an isotopic capture cross section of at least 50 barns. While such a cross section is quite possible, it seems much more probable that C is a result of a transition in Ca^{41} between the capturing state and the first excited state at 1.95 Mev.

The γ-ray D very probably produces the second excited state at 2.41 Mev. The γ-rays F, H, and I probably represent transitions to the fourth, fifth, and sixth excited states. The strong γ-ray J corresponds to a transition to the seventh excited state. The existence of the γ-ray L in Fig. 15 is demonstrated by only one point; however, earlier measurements made with a Dural container indicate unmistakeably the presence of a γ-ray at this energy. L appears to be in cascade with I for the sum of the energies of L and I is 8.38 ± 0.07 Mev in agreement with the neutron binding energy of Ca^{41}. The peak K, however, is probably caused by the bismuth background.[1] Assuming then that C and J are due to Ca^{41}, that isotope is another example of the correspondence already noted between the frequency of excitation of nuclear states in the neutron capture and in the (d,p) process. In this instance, both the first and the seventh excited states are favored.

The γ-ray E and a background of unresolved radiation between H and F remain unaccounted for in the scheme of Fig. 17. The total energy represented by the radiations of Table VI amounts to 9.2 Mev. The integrated energy of the spectrum of Fig. 16 is much higher (15 Mev). These estimates, however, in view of the instrumental difficulties already discussed, are not unreasonable.

VII. DISCUSSION

According to the current shell structure theories, no parity change should be produced in a direct radiative transition to the ground state following the addition of any neutron between the ninth and the twentieth. No parity change is expected to be produced, therefore, in the ground-state transitions in P^{32}, S^{33}, or Cl^{36}. The spin of P^{32} has not been measured; it has been variously stated as 1 or 2. The ground-state transition in this nucleus therefore should be of the electric quadrupole or magnetic dipole type. In sulfur the state responsible for thermal neutron capture must have a spin of $\frac{1}{2}$, for the spin of S^{32} is zero. The spin of the product nucleus S^{33} is $\frac{3}{2}$, and the ground-state γ-ray in this case can radiate one or two units. The spin of Cl^{35} is $\frac{3}{2}$ and that of the radioactive nucleus Cl^{36} has been found to be 2 units. Although the capture of slow neutrons by

chlorine has been carefully investigated by Hibdon and Muehlhause,[21] the spin of the compound nucleus produced by thermal neutron capture, as a result of a resonance at negative energy, has not definitely been established. It follows that either one or two units of angular momentum must be radiated in this γ-ray. In all three nuclei the ground-state γ-rays are probably of the second order, and they are all relatively weak.

The addition of the odd neutron to the nuclei Cl^{37}, K^{39}, K^{41}, and Ca^{40} should produce a change in parity, for according to shell structure theories, this neutron will occupy an $f_{7/2}$ state. The β-decay of both Cl^{38} and K^{42} are of the first forbidden type and if, as would seem probable, the spins of these nuclei are both 2 units, the ground-state γ-rays are of the electric dipole type. Of these two γ-rays we have already noted that the one due to capture in Cl^{37} is obscured by the γ-ray *F* produced by capture in Cl^{35}. If the γ-ray *C* is indeed the ground-state γ-ray in K^{42}, its intensity is such that about one-sixth of the captures in K^{41} produce it.

The ground-state γ-ray in K^{40} is of unusual interest for the spin of K^{39} is $\frac{3}{2}$ and that of K^{40} in its ground state is 4 units. However, there is at present no slow neutron data nor fast neutron scattering data which can be used to determine the spin of the compound nucleus responsible for capture by K^{39}. If the odd neutron in K^{40} is in an $f_{7/2}$ state, the emission of the ground-state γ-ray is accompanied by a change in parity. This γ-ray will be of the electric octopole or magnetic quadrupole type according to whether the spin of the state responsible for capture is 1 or 2 units. If this γ-ray is identified with the γ-ray *B* in the potassium spectrum, it is surprising that its intensity is as great as it appears. In calcium the intensity of the ground-state γ-ray in Ca^{41} may be less than one photon per 500 captures, and the failure to detect it is to be expected. The spin of Ca^{41} has not been measured, but we should anticipate a spin of 7/2 from shell structure theory, and this value seems to be consistent with the very long life of this nucleus.[22] Since Ca^{40} has no spin, the ground-state γ-ray must be of the electric octopole type.

It would be interesting if the absolute, rather than the relative, rate of emission of these radiations were known. If the radiative width of the state responsible for capture is known, the partial widths for the various γ-rays emitted by this state can be obtained immediately by multiplying the total radiation width by the absolute intensities. For S^{33} a rough estimate of the total radiation width can be computed from neutron scattering data on the assumption that the observed thermal neutron capture cross section is caused entirely by the lowest *S* state which appears in the spectrum of the scattering cross section. Such a computation ignores the effect on the thermal neutron cross section states lying below the neutron binding energy, and the value obtained represents an upper limit for the width. For S^{33} the total width obtained in this way is about 20 volts, and the partial width of the ground-state transition is therefore about one volt. The fast neutron scattering data for the other elements considered in this paper are not sufficiently precise for the calculation of radiation widths.

The scattering and absorption of slow neutrons in chlorine[31] appears to be caused by a resonance at −75 ev with a radiation width of 0.3 volt. The low value of this resonance energy suggests that the level concerned is indeed the one responsible for the majority of the thermal neutron captures, and it follows that the radiation widths corresponding to the more energetic γ-rays in the chlorine spectrum have widths of the order of 10 millivolts. This result is very much less than that expected on the basis of current theoretical formulas[33] for magnetic dipole or electric quadrupole radiations.

[21] C. T. Hibdon and C. O. Muehlhause, Phys. Rev. **79**, 44 (1950).

[31] Brown, Hanna, and Yaffe, Phys. Rev. **84**, 1243 (1951).

[33] See the formulas quoted by M. Goldhaber and A. W. Sunyar, Phys. Rev. **83**, 906 (1951).

Proton-Proton Scattering at 240 Mev by a Magnetic Deflection Method*

O. A. Towler, Jr.†‡
University of Rochester, Rochester, New York
(Received November 14, 1951)

Differential cross sections for proton-proton scattering have been measured at eight angles ranging from 171.3° to 108.1° center of mass by magnetically deflecting protons scattered by hydrocarbon and carbon targets into photographic plates placed inside the tank of the Rochester 130″ cyclotron. The incident beam was monitored by the beta-activity induced in the target by the reaction $C^{12}(p,pn)C^{11}$, the absolute value of the cross section being based on a 49±3 mb carbon cross section. The measured cross section is isotropic within statistical errors from 108° to 167°, with an average value of 4.66±0.39 millibarns/steradian, and increases sharply to a value of 15.8±1.6 mb at 171.3°. The average value of the cross section agrees with that of Oxley and Schamberger, but is in disagreement with the value obtained by Chamberlain, Segrè, and Wiegand.

I. INTRODUCTION

DETERMINATIONS of proton-proton scattering cross sections at 240 Mev were undertaken by a method differing from the coincidence counter measurements of Oxley and Schamberger[1] of this laboratory in the method of counting the scattered protons. The reasons were to provide a check on the counter experiment and to extend the angular range of the measurements. The measurement of the differential scattering cross section has been extended to 8.7° c.m.[2]

The experimental method, which has been described briefly before,[3] was to use the magnetic field of the cyclotron to deflect protons scattered by a hydrocarbon target into photographic plates placed in the cyclotron tank. When properly shielded nuclear track sensitive photographic plates are inserted in the cyclotron tank near the lower pole tip of the magnet, a part of the protons scattered from the internal circulating beam by the protons in a hydrocarbon target describe helical paths and enter the plates at an angle directly related to the scattering angle. These protons enter in a well-collimated group, while those scattered by the carbon nuclei arrive uncollimated. The number of protons scattered by protons is obtained from the difference in the number entering a plate in a certain range of entrance angle when scattered by a hydrocarbon and a carbon target. The beam incident on the target is monitored by the radioactivity induced in the carbon of the target.

The laboratory cross section, $\sigma(\theta)$, is given by

$$\sigma(\theta)=\frac{N_P(\theta)\sigma_C C/H}{N_C\Delta\Omega(\theta)}, \tag{1}$$

where $N_P(\theta)$ is the number of protons scattered by protons at an angle θ into the solid angle $\Delta\Omega(\theta)$, σ_C the production cross section for C^{11} at 240 Mev, C/H the ratio of carbon to hydrogen atoms in the target, and N_C the number of C^{11} atoms produced at the time of exposure of the plates.

The C:H ratio in the polyethylene $(CH_2)_n$ targets was determined by Wichers and Paulson of the National Bureau of Standards to be 1:2 within 0.2 percent. The production cross section of C^{11} was taken to be 49±3 mb[4] at 240 Mev. The incident proton energy, 240 Mev, was determined by range measurements in copper and by consideration of the geometry and expected entrance angle for proton-proton collisions in the apparatus to be described. The determination of the other factors in Eq. (1) will now be considered in some detail.

II. APPARATUS

A. General Description

A plan view of the apparatus showing the target at the 58.5-inch radius used, plate holder positions, and shielding is given in Fig. 1. The target holder probe was inserted in the median plane of the tank, while the plate holder probe was inserted 4.21″ below the median plane through one of two flanges, making different angles with the radius to the target. The flanges could be moved horizontally to permit the use of several positions of the plate holder relative to the target, since no one position of the plate holder probe was suitable for the entire angular scattering range. Position 1 was used for laboratory angles 45° to 55°, position 2 for 55° to 75°, and position 3 for 75° to 87.5°. The projection of the helical path of a typically scattered proton is also shown.

* This work has been supported by the joint program of the ONR and AEC.

† This work is part of a dissertation submitted to the Graduate School of the University of Rochester in partial fulfillment of the requirements for the degree of Doctor of Philosophy.

‡ Present address: E. I. du Pont de Nemours and Company, Argonne National Laboratory, Chicago, Illinois.

[1] C. L. Oxley and R. D. Schamberger, Phys. Rev. **85**, 416 (1952).

[2] In the remainder of this paper all c.m. scattering angles will be designated by the more commonly used supplementary scattering angle of the conjugate proton, although all measurements were actually done with the lower energy backward scattered particle.

[3] O. A. Towler, Jr., Phys. Rev. **84**, 1262 (1951). Also O. A. Towler, Jr., and C. L. Oxley, Phys. Rev. **78**, 326 (1950); Oxley, Schamberger, and Towler, Phys. Rev. **82**, 295 (1951).

[4] Aamodt, Petersen, and Phillips, University of California Radiation Laboratory Report-526 (1949).

B. Target Holder and Targets

The target holder was made in the form of a "*C*" from a thin piece of aluminum rod. All dimensions of the "*C*" were made as large as posssible to reduce scattering from the target holder to a negligible amount. The ends of the target holder were turned to reduce the effective thickness of the target for the low energy scattered protons.

The polyethylene targets were cut in narrow strips 0.32 by 7.3 cm from commercially available polyethylene film. The surface densities ranged from 7.1 to 0.71 mg/cm².

For measurements involving high energy scattered protons, the carbon targets used were milled to 17 mg/cm² from nearly pure graphite (less than 0.5 percent residue). For scattered proton energies of 15 to 30 Mev, 6 mg/cm² carbon targets were employed. These uniform films were prepared by drying a water solution of colloidal graphite (Aquadag). Targets thus prepared had a residue of about 1 percent and a hydrogen content less than 1 percent.

For the very large angle scattering, where the energy of the scattered proton was 10 Mev or less, thin polystyrene $(CH)_n$ targets, 0.3 mg/cm², were used for comparison with the polyethylene. These were made by dissolving polystyrene in benzene and floating the film out on water.

C. Plate Holder and Plates

The plate holder was made from solid cylindrical aluminum stock, a quarter section of which had been cut out to provide a flat base for six 1-in. by 3-in. photographic plates. The plates were exposed horizontally with the emulsion side up. Spring clamps held one long edge of the plates to a machined edge of the plate holder and left fiducial marks on the emulsion which enabled accurate determination of the distance of the plate from some known point. The side of the plate which fitted to the machined edge was later the same side which determined the alignment of the plate on the microscope stage. The light shield fitting over the plate holder was provided with a 1.16 mg/cm² aluminum window.

The photographic plates were Eastman NTB-3, NTB, or NTA, depending on the energy of the scattered proton. These were developed by standard procedure, maintaining the emulsions horizontal to reduce deformation.

D. Shielding

During an exposure large numbers of nuclear particles, mostly protons, were traveling in the vicinity of the plates near the floor of the tank. The main shielding (Fig. 1) was placed along the axis of the plate holder to prevent protons traveling in the general direction of the beam from striking the plates. This shielding was elevated to prevent protons scattered in the target from

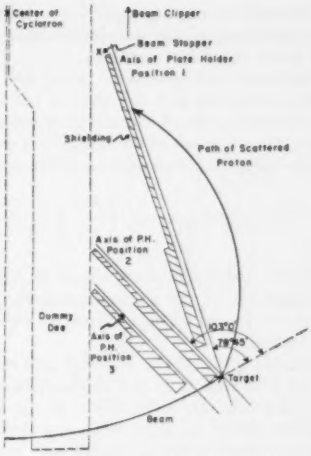

FIG. 1. Arrangement in cyclotron tank.

making more than half a revolution before entering the plates.

A *C*-shaped beam clipper with a 1-inch aperture, introduced in the median plane with the jaws extending to the 59.25-in. radius, was used to reduce the beam height and decrease the number of traversals through the target.

In some of the exposures it was expedient to insert thin vertical strips of copper in the plate holder itself to shadow portions of the plates from low energy protons coming from spurious sources. The direction of these tracks was such as to make them a nonconfusable background, but their deletion made the scanning easier.

An electromagnetically actuated beam stopper was placed at the 13-in. radius to prevent exposure of the plates while the operation of the cyclotron was stabilized.

III. CALCULATION OF SCATTERING ANGLE AND SOLID ANGLE

The determination of the scattering angle can proceed in one of several different ways. The method used was chosen because it was most direct. The general procedure was to measure the mean entrance angle λ_P for proton-proton scattering in a plate at a given distance x, measured in the horizontal plane, from the target. Knowing the vertical separation of the plates and the beam center and the plate holder position, the horizontal and vertical components of the scattering angle θ can be obtained. The radius of curvature of the scattered proton can then be calculated from (1) the scattering angle, the incident proton energy, the energy-scattering angle relationship for p-p collisions, and the magnetic field constants, or (2) geometrical considerations involving λ_P, x, the vertical separation, and the plate holder position. These two independent calcula-

tions of the radius of curvature provide a check on the internal consistency of the calculations and measurements of probe and target positions.

The solid angle was calculated, taking into account relativistic corrections and the effect of the magnetic field on the trajectories of the scattered protons. The solid angle $\Delta\Omega$ subtended at the target by a small area $\Delta a \Delta b$ in the horizontal plane of the emulsion is given by

$$\Delta\Omega = \cos\beta \Delta\beta \Delta\gamma = \cos\beta J\left(\frac{\beta, \gamma}{a, b}\right)\Delta a \Delta b,$$

where β and γ are, respectively, the vertical and horizontal components of the scattering angle θ. The calculation of the Jacobian is rather involved and will not be given here.

The focusing action of the magnetic field tending to return ions scattered from the median plane is negligible in this case, as is the effect on the scattered proton trajectories of the slight increase of the magnetic field from the target to the plate position.

Ideally, the protons scattered by protons in the hydrocarbon target should enter a given position on a plate at only one angle, λ_P. However, a large number of factors tend to spread out the entrance angle. These are the energy spread in the incident beam, the vertical spread of the beam on the target, the energy spread of the scattered protons due to absorption in the target, the angular divergencies in the beam caused by radial and vertical oscillations, the dimensions of the area scanned on the plate, the observer's error in measuring the track angle, and multiple scattering in the target, aluminum window, and emulsion. These effects were estimated and calculated for various scattering angles. The observed entrance angle spread is accounted for largely by factors other than the incident beam energy spread. There is some indication, however, that the energy spread is of the order of 20-Mev full width.

The energy loss per traversal in the targets was small (3 to 10 kev), and it was thought that such particles would be removed by the clipper before the energy loss became considerable. This was borne out by the fact that the entrance angle distributions in the proton-proton peak were not skewed in a manner that would show a rather large lower energy component in the incident beam. Also, the calculated entrance angle agreed very well with the mean of the observed. The fraction of protons striking the target a distance 1.1 in. removed from the median plane, and hence the fraction making large vertical oscillations, was measured by observing the activity in the ends of the strip targets which had been exposed vertically. This fraction varied between 0.01 and 0.03 from run to run. This effect, as well as the radial oscillations, decreases the angular resolution of this method.

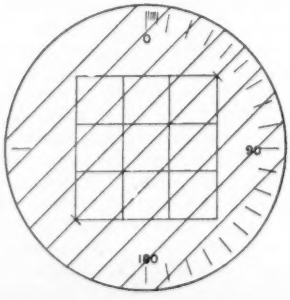

FIG. 2. Protractor eyepiece reticules.

IV. MEASUREMENT OF THE C^{11} ACTIVITY

The C^{11} activity was measured with the calibrated beta-counter described by Oxley and Schamberger.[1] A pertinent point to be stressed is that one of the calibrating sources of the counter had been used by Aamodt, Petersen, and Phillips[4] as a secondary standard in their measurement of the C^{11} production cross section.

V. PHOTOGRAPHIC METHOD

A. Scanning Procedure

The protons which are scattered by protons in the hydrocarbon target enter the plate at certain definite angles which are determined by the energy-scattering angle relation for proton-proton scattering. The protons scattered by the carbon nuclei have no such energy-angle relationship; therefore these carbon scattered protons enter the plate with an angular spread of five to ten times the spread observed for the proton-proton collisions. The scanning problem then is to obtain an angular distribution at a given point on a plate for those protons scattered by a hydrocarbon target, and another angular distribution at the same point on a plate for those scattered by a carbon target. From an exposure to a hydrocarbon target, one would expect to see:

(1) A small number of protons entering the plate at angles far removed from the entrance angle λ_P expected for p-p collisions. These presumably come from other scatterings in the cyclotron tank. (2) A larger number of protons, scattered by the carbon, entering at angles around λ_P. (3) A large number of protons entering at λ_P, which are the protons from the p-p collisions in the target. From a carbon target, one expects only the effects (1) and (2).

Almost all of the scanning was done using a 43× fluorite oil immersion objective and 15× eyepieces. The right eyepiece of the microscope was fitted with a special protractor device by which the angles of the tracks were measured. In the focal plane of the eyepiece lenses were two reticules, one fixed and the other rotatable (Fig. 2).

Etched on the fixed reticule were a square, divided into nine smaller squares, and degree marks, going from

0° to 180°, each degree divided into 20 minutes of arc. The area of the large square, which defined the solid angle, was calibrated with a Bausch and Lomb micrometer disk. The division into nine smaller squares facilitated the counting. On the rotatable reticule were etched a group of parallel lines, the center line of which was diametric and distinguished by two small intersecting lines. This center line read the entrance angle when a proton track was aligned with one of the parallel lines.

We will now consider the criteria used in the selection of tracks. A track, to be counted, must begin in the surface of the emulsion and within the area described by the large square. A track must have a dip angle that is close to the calculated one to be counted. Tracks which dived steeply or just skimmed the surface of the emulsion were not counted, because these could not have come directly from the target. There were a few very heavy thick tracks which were obviously (from the delta-ray density) particles with $Z \geq 2$. These were not counted, as well as some low energy proton tracks which ended in the emulsion. An exception to this last rule occurred when observations were made on scattered protons expected to end in the emulsion. All other tracks were counted.

When it was decided that a track was to be counted, and if the track entered at an angle plus or minus 5° from λ_P, the microscope field was moved slightly to place the track directly beneath one of the parallel lines. Then the angle was recorded and the field moved back to its original setting. This was done by taking certain grains or tracks intersecting the lines of the squares as fiducial marks and not by the verniers on the stage. Tracks which entered at angles beyond the plus or minus 5° mentioned above were not lined up by moving the field, but by setting the closest parallel line parallel to the track. An experienced observer could do this within 20 minutes of the real angle of entrance of the track. To reduce the labor involved, only certain ranges of entrance angle were measured for each area.

Three observers collected the final data. Frequent spot checks were made between the author and the other two observers. Since it was impractical to rematch all the fields scanned by one observer, areas within the same coordinates were scanned by different observers to determine any differences in the method of counting or measuring the tracks. In these checks, the number of tracks per degree of entrance angle counted by each observer agreed to within 3 percent, which was better than allowed by the statistical fluctuations.

B. Determination of the Number of Scattered Protons

When the entrance angle distribution is obtained for the protons scattered by a hydrocarbon target, the effect due to the proton-proton collisions is quite obvious, as is the effect due to carbon collisions. One may make a fair estimate in determining the number of proton-scattered protons by counting those in the peak above a smooth curve drawn to fit the distribution for carbon scattering outside the peak. However, the actual shape under the p-p peak of the proton distribution from carbon collisions is of some importance, and therefore proton distributions were obtained from carbon targets. They were matched to the hydrocarbon distributions by correcting for the incident beam in the two exposures. The actual number of protons scattered by protons was obtained by subtracting the number of tracks given by the carbon data under the peak, using a smoothed curve, from the actual number of tracks in the peak of the hydrocarbon data.

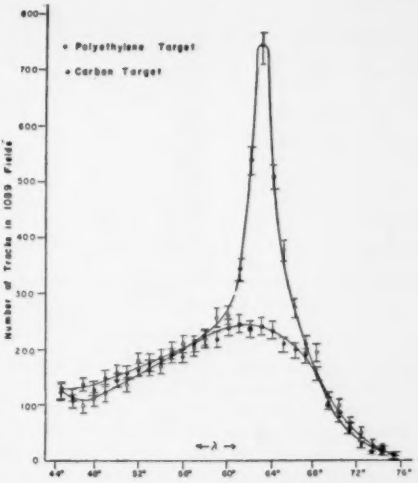

FIG. 3. Entrance angle distribution for $\theta = 52.4°$.

The proton distributions from the carbon collisions in the two targets matched very well in absolute value and shape for all angles except one ($\theta = 70.6°$), and in this one case an additional factor had to be applied to the carbon target distribution in order to match the absolute value of the distribution for the hydrocarbon target. This is perhaps justified by the fact that spurious sources and beam distribution may change over a short period of time, which might affect the actual number scattered into this one plate. Other plates exposed in the same runs as the one in which the discrepancy occurred produced good agreement between the polyethylene and carbon data, and it is difficult to see that the number of protons in the proton-proton peak could be affected except by a small amount due to the shape of the corrected carbon distribution under the peak.

The distributions obtained for the scattering angles 52.4°, 83.1° and 85.4° are shown in Figs. 3, 4, and 5. The distributions for the other five scattering angles observed are similar to that shown in Fig. 3.

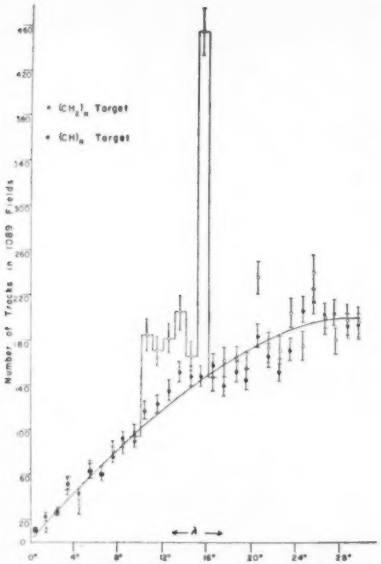

FIG. 4. Entrance angle distribution for $\theta = 83.1°$.

For the two large scattering angles, 83.1° and 85.4°, data were taken for polyethylene $(CH_2)_n$ and polystyrene $(CH)_n$ targets. Any pure carbon target that could be made, inserted, and removed from the tank was still too thick for the energies of the protons involved. The polystyrene distribution was taken mainly to check the shape of the proton spectrum from carbon on sides adjacent to the proton-proton peak. In these two cases, a smooth curve was drawn through the sides adjacent to the peak and this curve was used for subtraction purposes. A cross section could be obtained from the polystyrene data alone, using the same subtraction process, but the statistical errors are very large. (However, the cross sections obtained from the two types of hydrocarbon targets agreed within the errors.)

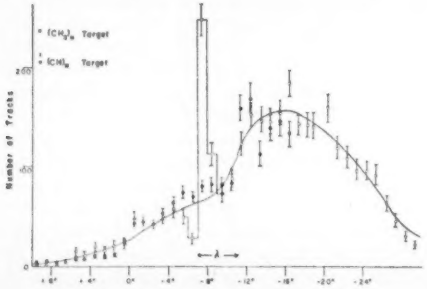

FIG. 5. Entrance angle distribution for $\theta = 85.4°$.

TABLE I. Number of proton scattered protons for each scattering angle.

θ	N_{CH_2}	N_C	N_P	Mean error (%)
52.4°	3682	2174	1508	5.07
66.1°	1133	384	749	5.27
70.6°	992	343[a]	649	5.64
75.0°	3435	1888	1547	4.72
75.6°	647	293	354	8.67
80.1°	2492	1560	932	6.83
83.1°	1359	750[b]	609	7.50
85.4°	360	135[b]	225	9.90

N_{CH_2} = number of protons from polyethylene.
N_C = number of protons from carbon.
[a] Number of tracks corrected by 38 percent to match sides of CH_2 peak.
[b] N_C taken from smooth curves drawn through base of peak, based on CH_2 and CH data.

The number of proton-scattered protons, N_P, is shown in Table I. The error assigned to N_P is the mean statistical error considering the background subtraction.

Data for the scattering angles 70.6° and 75.0° were obtained from the same exposure and probe position for both the polyethylene and carbon target. The polyethylene data for the angles 75.6°, 80.1°, 83.1°, and 85.4° were obtained from the same exposure and probe position, as were the carbon data for the first two of these angles and the polystyrene data for the last two. The first two scattering angles in Table I were measured with probe position 1, the second two angles with probe position 2, and all the others with position 3. A check of the consistency of the cross sections obtained in different runs at different probe positions is provided by the agreement of the cross sections at laboratory angles 75.0° and 75.6°.

VI. DIFFERENTIAL CROSS SECTION

The experimental results and the cross sections are given in Table II, and the cross section in the center-of-mass system is plotted in Fig. 6.

The errors assigned to the cross section are the relative mean errors in the determination of N_P. These errors are valid for the relative values of the cross sec-

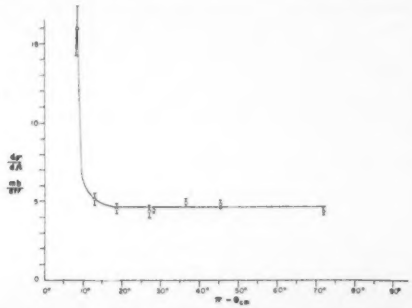

FIG. 6. Differential scattering cross section at 240 Mev. The assigned errors are the statistical errors only.

TABLE II. Experimental results.

$\pi-\theta_{c.m.}$	$\theta_{c.m.}$	θ	N_P	N_C	$\Delta\Omega$	Lab cross section mb/sterad	$\frac{\Delta\Omega}{\Delta\Omega_{c.m.}}$	c.m. cross section mb/sterad	Resolution (c.m.)
71.9°	108.1°	52.4°	1508	9.033×10^{8}	4.002×10^{-6}	10.22	0.4241	4.33±0.22	1.6°
45.2°	134.8°	66.1°	749	5.852	4.376	7.165	0.6713	4.81±0.25	1.3°
36.6°	143.4°	70.6°	649	2.931	9.187	5.905	0.8293	4.90±0.28	1.3°
28.3°	151.7°	75.0°	1547	2.931	31.33	4.129	1.072	4.43±0.21	1.2°
27.2°	152.8°	75.6°	354	2.413	9.183	3.837	1.119	4.38±0.38	1.2°
18.6°	161.4°	80.1°	932	2.413	33.72	2.807	1.636	4.59±0.31	1.5°
13.0°	167.0°	83.1°	609	2.413	28.01	2.207	2.336	5.16±0.39	2.1°
8.7°	171.3°	85.4°	225	2.413	5.038	4.535	3.482	15.8±1.6	2.4°

tions in this experiment. The absolute value of the cross section depends upon the calibration of the beta-counter, the $C^{12}(p,pn)C^{11}$ cross section, calibration of the microscope field areas, relative position of the target and plate holder probes, the incident energy and perhaps unknown systematic errors. The error in the calibration of the beta-counter is 4 percent, and in the $C^{12}(p,pn)C^{11}$ cross section 6 percent. The error due to the other factors mentioned above is estimated to be 6 percent, giving a total error in the absolute value of the cross section of 9 percent.

The experimental cross section exhibits the previously observed flat behavior down to a c.m. angle of about 15°, and then increases by a factor 3.5 over the isotropic average at 8.7°. The laboratory cross section increases by a factor two in going from a scattering angle of 83° to 85°. The sharp increase at 8.7° is certainly due to Coulomb effects, while the extreme flatness in the region preceding this is probably due to interference terms.

The averaged value of the observed cross section in the center-of-mass system (excluding the value for 8.7°) is 4.66±0.39 mb. This assigned error includes the absolute errors mentioned above and a 2.3 percent statistical error, based on the observation of 21,132 tracks for the seven angles.

The angular resolution of this method depends upon the area of the plate scanned, the energy spread of the incident beam, the vertical spread of the beam on the target, the energy loss in the target, the angular divergence of the beam, and the multiple scattering of the recoil proton in the target. The resolution for each of the eight angles measured is given in Table II.

VII. COMPARISON OF RESULTS

The agreement between this experiment and that of Oxley and Schamberger[1] at the same energy is good. Their average value of the cross section, measured from 27.5° to 90°, is 4.97±0.43 mb/sterad. When the mutual errors in the $C^{12}(p,pn)C^{11}$ cross section and the calibration of the beta-counter are subtracted, the relative error in both of these experiments is 0.22 mb. The combined value for the isotropic portion of the cross section obtained by these two experiments is 4.81±0.38 mb/sterad.

These results are higher by about 30 percent than the value of 3.6±0.2 mb/sterad obtained by Chamberlain, Segrè, and Wiegand.[5] We have done some work at this laboratory in determining the p-p scattering cross section using carbon detectors throughout and referring only to the slope of the C^{11} production cross section curve. Preliminary results favor the higher values of the cross section.

VIII. ACKNOWLEDGMENTS

I wish to thank Professor C. L. Oxley, who originally suggested this method of attacking the problem, for many helpful suggestions during the course of this work. I also wish to express appreciation to Miss Evelyn Kohn for her work at the microscope, and to the cyclotron crew under the direction of Mr. Hugo Logemann.

[5] Chamberlain, Segrè, and Wiegand, Phys. Rev. **83**, 923 (1951).

Some Experiments on Flow in the Unsaturated Helium II Film

EARL LONG AND LOTHAR MEYER
Institute for the Study of Metals, University of Chicago, Chicago, Illinois
(Received November 30, 1951)

The mass flow in adsorbed layers of helium has been measured. Superfluidity occurs at all temperatures below the λ-temperature of the bulk liquid down to 1¼ statistical layers. The bearings of these results on the thermodynamics of transition HeI—HeII in adsorbed layers is discussed.

THE existing data on multilayer adsorption of helium at temperatures below 4.2°K,[1] show that adsorbed layers of helium exhibit unusual properties, as compared to the behavior of other adsorption systems.

The first adsorbed monolayer is very highly compressed,[1] the density varying from about twice that of the bulk liquid at 4.2° to almost four times the liquid density at temperatures below 2.19°. The properties of this first layer resemble those of solid helium under high pressure.[2]

The adsorption in the He II region, below 2.19°K, is anomalously high, and only slightly temperature-dependent, so that the heat of adsorption is not much different from the heat of vaporization of the bulk liquid, even at fairly low coverage.

In the course of the work of Long and Meyer,[1] some measurements on the distribution of He^3 between adsorbed film and vapor at various temperatures and saturations indicated that, as in the bulk liquid case,[3] He^3 was extremely difficult to remove by evaporation from the condensed phase at temperatures below the lambda-point; above this temperature, the distributions between gas and condensed phase were normal. Also, in the measurement of the adsorption isotherms in this work, it was noticed that the observed speed of approach to equilibrium was quite different above and below T_λ.

The early work of Ganz[4] on heat propagation in helium II included some experiments in which a metal tube containing adsorbed film was used for measuring the velocity of transmission of heat. Ganz was apparently able to detect weak heat pulses through the adsorbed He II film, and concluded that thermal energy can be transmitted through the film at quite high velocities.

Finally, the careful measurements of Frederikse[1] on the specific heats of adsorbed He II films of varying thickness showed that the adsorbed layers were undergoing some sort of excitation process which could reasonably be assumed to have some features in common with that which produces the well-known peak in the specific heat curve of the bulk liquid.[5]

It therefore seemed probable that the unsaturated He II film should exhibit some of the unusual features of the behavior of bulk liquid He II. The flow properties seemed the most easily and reliably investigated; a number of experiments were devised, in order to detect, in the unsaturated film, the most striking property of He II, i.e., superfluidity, and, if possible, to evaluate its behavior.

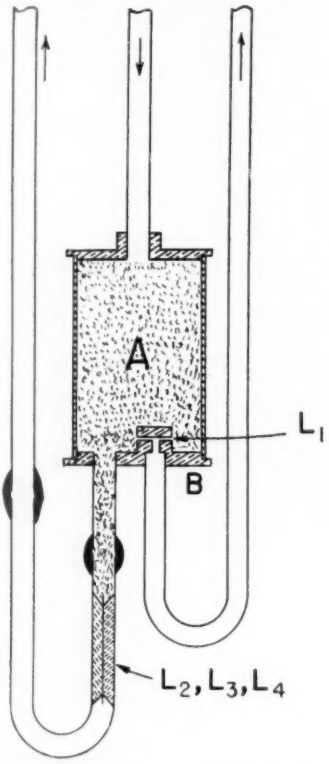

FIG. 1. Apparatus for measuring mass flow in adsorbed layers of helium resulting from pressure gradients.

[1] Schaeffer, Smith, and Wendell, J. Am. Chem. Soc. **71**, 863 (1949); H. P. R. Frederikse, thesis, Leiden (1950); E. Long and L. Meyer, Phys. Rev. **76**, 440 (1949).

[2] See comment by W. Band, Phys. Rev. **76**, 441 (1950).

[3] See Taconis, Beenakker, Nier, and Aldrich, Physica **15**, 733 (1949).

[4] E. Ganz, Proc. Cambridge Phil. Soc. **36**, 127 (1940).

[5] See W. H. Keesom, *Helium* (Elsevier Publishing Company, Amsterdam, 1942), pp. 211–219.

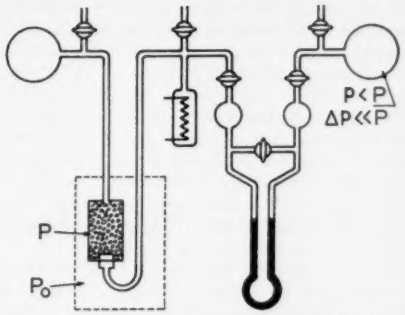

FIG. 2. Measuring system for determining mass flow in adsorbed layers of helium.

In order to measure superflow in the adsorbed film, it is of course necessary to provide a flow system with channels so narrow that ordinary gas flow is negligibly small compared to the film flow itself. Therefore, a technique similar to that used to measure the flow of liquid helium II through narrow channels[6] was adopted, as shown in the apparatus of Fig. 1. A copper chamber, A, containing 75 grams of adsorbent (Fe_2O_3) was sealed at the bottom with a thick stainless steel plate B, through which several narrow channels ("superleaks") L-1, L-2 of varying geometry were connected to the chamber.

Leak L-1 was made by pressing together two optically flat stainless steel circular plates of one-cm diameter, the bottom plate having a central exit channel 0.08-cm diam. Leaks L-2 and L-3 were made by sealing 2.5-cm lengths of 0.013-cm and 0.008-cm diam, respectively, platinum wire into Pyrex glass. Leak, L-4, was similar to L-2 and was mounted in the same manner, but without adsorbent in A. All connecting tubes to the leaks and the adsorbent chamber were 4.8-mm. o.d. $\times$0.13-mm wall copper-nickel tubing. The whole assembly was immersed directly in the liquid helium bath of the cryostat.

The widths of the leak channels were determined from gas flow measurements under known pressure gradients at 4.2°K. They varied from 1 to 9×10^{-5} cm. The calculation of the channel widths neglected the fact that one dimension of the channels is smaller than the mean free path of the gas, but not the others, a case which is between "Knudsen" gas flow and ordinary viscous flow, and which seems not to have treated at the present time. With channel widths of these dimensions. it seemed that the gas flow would be sufficiently small for the purposes of the experiment.

The adsorption chamber and superleaks were connected to a reservoir and measuring systems, as shown in the schematic diagram of Fig. 2.

[6] See Giauque, Stout, and Barieau, J. Am. Chem. Soc. **61**, 654 (1939); and Osborne, Weinstock, and Abraham, Phys. Rev. **75**, 988 (1949).

The measurements were carried out in two ways. The adsorption chamber was loaded with a constant pressure P of helium gas, always lower than the bath pressure P_0 at temperature T. P/P_0 represents the saturation, and, at any given temperature T, is a measure of the number of adsorbed layers, provided of course that the adsorption isotherms are known.

In method I, at temperature T and saturation P/P_0 in the adsorption chamber, high vacuum was initially pumped on the exit side of the superleak being investigated, then the stopcock leading to the vacuum pump was closed and the pressure rise in a known volume was measured for a given period of time, usually ten minutes, using a Pirani gauge the calibration of which was frequently checked by comparison with a McLeod gauge.

The results of this series of measurements were quite striking. Superfluidity was observed, but the "onset" temperatures for superflow varied from 1.39° at $P/P_0\sim0.485$ to 2.04° at $P/P_0\sim0.986$, as contrasted to 2.186°K for the start of superflow in the bulk liquid case. The results for eleven different saturations are shown in Fig. 3, in which the flow rate in cc(STP)/min is plotted against the temperature. The number of adsorbed layers varies from $\sim$2 at 0.485 to $\sim$18 at 0.986.[7] All data shown in Fig. 3 were taken using leak L-2. It will be noted that for each saturation, the onset of superflow is quite sharp, about 0.001°; these onset

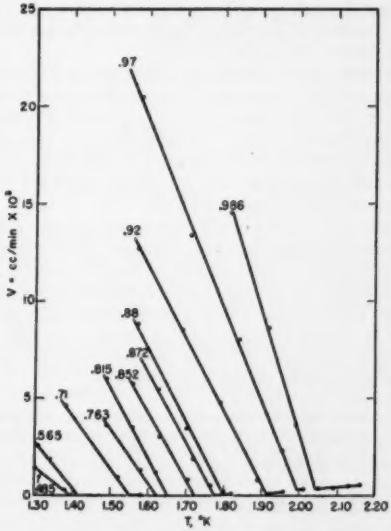

FIG. 3. Flow rate through superleaks as a function of temperature for different saturations.

[7] As determined from unpublished adsorption isotherms of A. J. Strauss, this laboratory, using the same adsorbent as in these experiments.

temperatures were very reproducible. All the leaks gave the same variation of onset temperature with saturation. Since the leaks must have differed greatly in detailed geometry, it is concluded that these onset temperatures are therefore independent of geometry, for the range of channel sizes used in the experiment. The only determining factors seem to be the number of adsorbed layers, the temperature, and possibly the pumping speed at the exit of the leak.

The fact that in this experiment superflow starts at a temperature which is evidently determined by the number of adsorbed layers is, at the present time, unexplained. However, there seems to be no apparent relationship to the fundamental properties of the film itself, as shown by the experiments of method II.*

In method II, it was reasoned that high vacuum on the exit of the leak would reduce the film thickness near the exit to less than a monolayer. Since the first monolayer of adsorbed helium is so dense that it behaves rather like a solid, it must be considered as immobile. So long as high vacuum is maintained at the exit, film flow is therefore only possible because of a lack of equilibrium between film and vapor which allows the surface of the leak, at least temporarily, to be covered with more layers than correspond to the pressure in the gas phase under the equilibrium conditions given by the adsorption isotherm. This evidently cannot occur until, at some lower temperature, the mobility becomes sufficiently high for the film flow to overcome the pumping rate, permitting the film to flow into the larger connecting tube and evaporate there, rather than in the narrow channel itself.

Therefore, an alternative measuring system was used, as shown in Fig. 2. Instead of initial high vacuum at the leak exit, helium gas was admitted to a pressure p, such that $p<P$, however, $\Delta p \ll P$. Consequently, at least one statistical monolayer was present at all times, and usually the whole leak was covered by practically the same number of layers throughout.

The flow was investigated under these conditions, by balancing the initial pressure p through an oil manometer M against a buffer volume of large capacity, also at p, initially. Thus, measurements of the oil manometer heights as a function of time provide the necessary data for rate of flow through the leak under conditions of essentially constant Δp. The pressure readings were made with a Wild precision cathetometer.

In this manner, flow measurements were made over a wide range of saturations and temperatures. Quite different results from those of method I were obtained; for all saturations above $P/P_0=0.15$ ($\sim 1\frac{1}{2}$ statistical layers) superflow was observed at all temperatures below the lambda-temperature of the bulk liquid.

The superflow observed in method II was extremely sensitive to slight variations of the bath temperature. A normal rate of flow from the adsorption vessel to the measuring system was either greatly increased or even reversed by raising or lowering the bath temperature by a few ten-thousandths of a degree.[8]

This dependence of the flow rate and direction of flow on rapid temperature changes was most pronounced with leak L-1, which permitted the highest flow rate, but was also observed with all the other leaks. The magnitude of the effect was greatest at the highest saturations and the higher temperatures in the He II region. No effect was observed below $P/P_0 \sim 0.15$. Furthermore the magnitude was greatest with the smallest values of Δp across the leak; for values of Δp greater than about 10-mm oil, the effect was almost insensitive to Δp, until, with initial high vacuum at the leak exit, the effect disappeared completely.

It was realized that the relatively high thermal capacities of the adsorbent vessel A and the leak assemblies L-1 and L-2 did not permit the system to follow rapid changes of temperature; thus, the system was unable to stay in phase with fluctuations of the bath temperature, so that a temperature gradient was set up across the leak. This, though representing a nonsteady state, is just the condition for thermomechanical effects to occur in the film. Qualitatively, the observed flow behavior was quite analogous to the fountain effect in bulk-liquid helium II.

It was at first thought[8] that the large effects here observed were of about the same magnitude and significance as those of the steady-state measurements on bulk liquid,[9] but later considerations[10] have shown that the thermomechanical effect in adsorbed layers can contribute a ΔP in the gas phase for a given ΔT which is only about 10 percent of the vapor pressure change, whereas in bulk-liquid helium the hydrostatic head resulting from the fountain effect is *ca* ten times the vapor pressure change. It is therefore probable that the phenomenon here observed is a rather severe case of nonequilibrium flow under transient temperature gradients. It is, moreover, true that considerable net mass transfer in either direction can be effected by such temperature gradients in the experiments herein described on the unsaturated film.

Cooling Experiments

Following these studies, it seemed desirable to investigate the flow under more easily controlled and de-

* *Note added in proof:* However, new evidence has cast doubt on the arguments given to explain the different results of Method I and Method II. Experiments are now being carried out in this laboratory on the heat transport of unsaturated He-II films, using an apparatus similar in principle to that of Bowers, Brewer, and Mendelssohn (Proc. Int. Conference on Low Temperature Physics, Oxford, 1951, p. 75). At any given saturation P/P_0, the contribution of the adsorbed film to the heat transport appears sharply at a temperature which coincides with the onset temperature of Method I, Fig. 3. Since the gradients of pressure and temperature in the heat transport experiment are very small, the explanation of onset temperatures given above cannot be applied to this case. The measurements are being continued; a more detailed report will be submitted to this journal.

[8] See E. Long and L. Meyer, Phys. Rev. **79**, 1031 (1950) for a more detailed description.

[9] See L. Meyer and J. H. Mellink, Physica **13**, 197 (1947).

[10] L. Meyer and E. Long, Phys. Rev. **84**, 551 (1951).

finable gradients of both pressure and temperature. For this purpose, the apparatus shown in Fig. 4 was used. An adsorbent chamber A, containing 25 grams of Fe_2O_3, was connected by a 2.5-cm length of thin-walled stainless-steel capillary L, 1.5-mm i.d., to a much smaller chamber B, containing 3.5 grams of Fe_2O_3. The connecting tube was tightly packed with Fe_2O_3 powder, thus constituting an effective superleak, of channel size *ca* the same as the previous leaks, but of much greater flow capacity. Chambers A and B were connected to the external measuring systems by the stainless steel capillaries C-1 and C-2, of 1.5-mm i.d., which were thermally insulated from the bath by enclosure in the pumping lead P. The apparatus was provided with vacuum insulation by means of the container D, which was sealed to chamber A as shown, so that A was always in direct contact with the bath, whereas chamber B and the superleak L were insulated by high vacuum, as were the connecting leads C-1 and C-2. This arrangement eliminated any effect of accidental fluctuations of the bath temperature on the flow rate.

Carbon thermometers Th-1 and Th-2 were arranged in good thermal contact with chambers A and B, respectively, and a heater H was wound around B. Chambers A and B were of copper, and thus known temperature gradients could be set up along the superleak L.

The capillaries C-1 and C-2 were connected to a system of oil manometers, arranged so that the pressures in each chamber were read independently, and the pressure difference between A and B could be measured directly.

A typical cooling experiment was carried out as follows: With the cryostat bath and whole assembly initially at 2.08°K, chamber A was filled with helium to $P/P_0=0.74$ (~3 layers), and chamber B to P/P_0 0.45 (~2 layers). Then, by means of heater H chamber B was heated to 2.5°; the system was held with A at 2.08° and B at 2.5° until a steady state was attained. Under these conditions the pressure in B was 90 percent of that in A, but the number of adsorbed layers was of course lower. Then the heater was turned off, and with chamber A still at 2.08°, readings of the pressure in A, the temperature of A, the pressure in B, and thete mperature of B were taken as a function of time. Over a period of about one hour, B cooled from 2.5° to 2.12°.

Without superflow, the rate of fall of the pressure in B would be approximately logarithmic, following the temperature of B. However, if superflow starts at any given temperature, film will flow from A into B, and a break in the $\log P_B$ *vs* time curve should appear. This does happen, as is shown in Fig. 5, in which $\log P_B$ and T_B are plotted against time. There is a distinct break at 27 minutes, at which time the temperature of chamber B was 2.19±0.01°K, as read from the time-temperature curve.

A number of these cooling experiments, with different saturations ranging from P/P_0~0.40 to P/P_0~0.85, and and with varying initial temperatures in chamber B gave the same result, though not as accurately at the lower saturations. Thus, superfluidity is again seen to start at the normal lambda-point, in agreement with the flow measurements of method II, described previously.

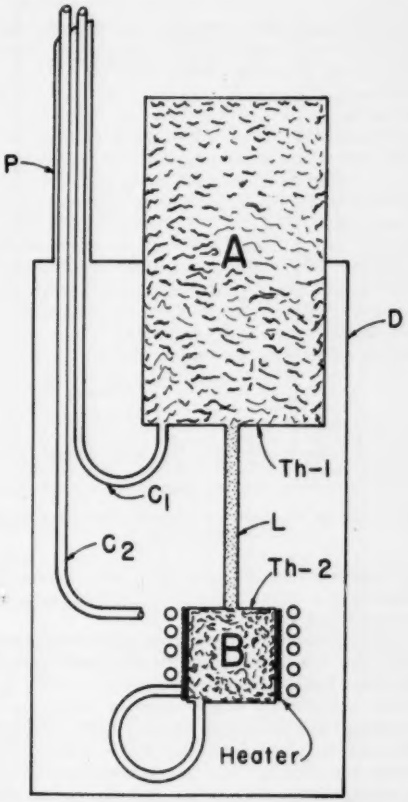

FIG. 4. Apparatus for measuring mass flow in adsorbed layers of helium resulting from temperature gradients.

These measurements do not exclude the possibility of the superflow starting at temperatures a few thousandths of a degree above the normal λ-point for the following reasons: (1) It is extremely difficult to perform measurements immediately above the normal λ-temperature. Below T_λ the temperature in the bath is completely homogeneous because of the high heat conductivity of He II. Above T_λ however, the temperature in the lower parts of the bath—where the apparatus usually is situated—is higher than on the top because the liquid is boiling under the hydrostatic pressure head of the bath itself. This amounts to about 0.001° per cm liquid helium. Even with a good stirrer

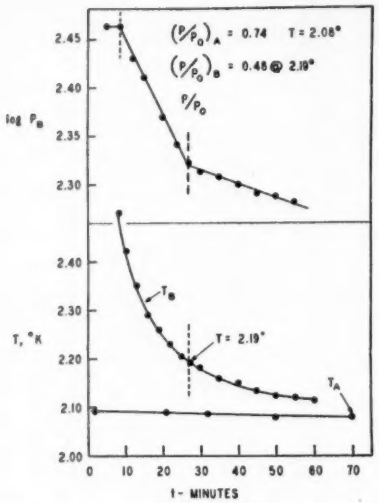

FIG. 5. Changes of pressure and temperature as a function of time in the apparatus of Fig. 4.

it is almost impossible to avoid a jump of some thousandths of a degree in the lower parts of the cryostat when passing T_λ.

(2) It is known from the flow measurements performed with the film in contact with saturated vapor (the so-called Rollin film) that the critical velocity up to which superfluidity occurs decreases rapidly on approaching the λ-point. It is therefore quite possible that the real onset of superfluidity in the case of surface layers in equilibrium with unsaturated vapor occurs at a slightly higher temperature than T_λ, and its effects only reach the threshold of our observations below T_λ.

Possibility of Capillary Condensation

Several arguments can be applied to show that capillary condensation cannot be responsible for these flow results: (1) The adsorption isotherms measured on the adsorbent used in these experiments[11] are typical of multi-layer adsorption, and show no sign of capillary condensation.[12] (2) Capillary condensation, if present, would actually lead to entirely different results. Assume that the equilibrium pressure over the adsorbent is not reduced by adsorption, but by capillary condensation; then the well-known Kelvin relation for the vapor pressure over curved surfaces can be applied:

$$RT \log(P/P_0) = 2\gamma V/r, \qquad (1)$$

where γ is the surface tension, V the molar volume of the liquid, and r is the radius of curvature, i.e., the radius of the capillary in which condensation occurs. This yields, for 60 percent saturation and 2.18°K, $r \sim 10^{-7}$ cm. In a capillary of this size, the condensed liquid would be under a pressure of *ca* 3 atmospheres; the corresponding λ-temperature is about 0.04° below that of the liquid under vapor pressure,[13] which exceeds by a factor of ten the estimated error of the present experiments on the start of superflow; in this work, no such lowering of the λ-temperature has been observed (3) The appearance of superfluidity has been determined dynamically. If the helium is not distributed by more or less uniform adsorption over the whole surface of the superleak and adsorption system, but is confined by capillary condensation to certain very narrow cavities; these cavities must connect in a continuous path in order to permit superflow. It seems difficult to conceive that the system provides for all measured saturations just the right size cavities, interconnected so as to form a continuous path.

It is indeed an open and interesting question whether capillary condensation is ever possible in a He II system, because of the influence of the thermomechanical effect in the small temperature gradients which are inevitably present.

Relationship to Thermodynamic Data

Aside from the adsorption isotherms, previously discussed, the specific heat measurements of Frederikse[1] are of interest in connection with these flow measure-

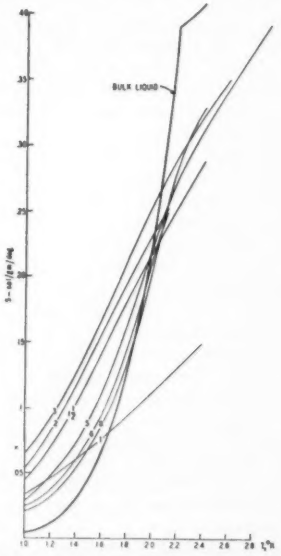

FIG. 6. Entropy of adsorbed layers of helium.

[11] See reference 1, and unpublished data of A. J. Strauss, this laboratory.

[12] See H. Brunauer, *The Adsorption of Gases and Vapors* (Princeton University Press, Princeton, 1945), where the two types of isotherms are discussed in detail.

[13] See reference 5, p. 256.

ments. Frederikse found that the maximum in the specific heat-temperature curve, which for bulk liquid helium coincides with the temperature at which superflow appears, namely T_λ, appears also in adsorbed layers, but is broadened and moves to lower temperatures the thinner the coverage, i.e., the lower the saturation. For a coverage of $1\frac{1}{2}$ statistical layers, the specific heat maximum occurs at 1.45°K, whereas the onset of superflow at this coverage is at 2.19°K, the λ-point of the bulk liquid.

These data are not necessarily inconsistent, for it is thermodynamically not required, and even improbable, that the specific heat maxima define the highest temperatures at which the special properties of He II appear (they were indeed not so identified by Frederikse).

It is known that the entropy of adsorbed He is higher than that of the bulk liquid below 2.19°K,[1] as contrasted to the usual case (including He I) for which adsorbed layers possess an entropy lower than that of bulk liquid.[14] An estimate of these entropy relationships is shown in Fig. 6, in which the entropy of bulk liquid He is compared with that of the unsaturated films as computed by the present authors from the specific heat data of Frederikse.[15] It is seen that the entropy-temperature curves of the adsorbed layers do not show the breaks or kinks which appear in first or second order transitions; the specific heat maxima appear here only as points of inflection. The form of these curves can probably be explained as the result of the competition between two processes: (1) The He II phenomenon, dominant below T_λ (2.186°K), and (2) the ordering process in space, because of the usual van der Waals' forces responsible for adsorption, dominant above T_λ. Thus a sigmoid form of the entropy-temperature curve is produced, and the occurrence of superfluidity in the films at temperatures higher than those of the specific heat maxima is not surprising.

[14] Compare C. Kemball, *Advances in Catalysis* (Academic Press, New York, 1950), Volume II, p. 233.

[15] For this calculation it was necessary to extrapolate the specific heat data to 0°K, thus introducing a relatively serious error in the absolute values of S; this, however, does not affect the qualitative features of Fig. 1, since the contribution to the total entropy in the extrapolated region is comparatively small.

PHYSICAL REVIEW VOLUME 85, NUMBER 6 MARCH 15, 1952

Phase Transitions in Adsorbed Films

LOTHAR MEYER AND EARL LONG
Institute for the Study of Metals, University of Chicago, Chicago, Illinois
(Received November 30, 1951)

A thermodynamic treatment of first- and second-order transitions in adsorbed layers is given. The results are compared with the experimental evidence for the melting of argon and the transition He I–He II in adsorbed layers.

A THERMODYNAMIC treatment of transitions for the case in which a condensed phase does not exist in bulk but as adsorbed layers is of interest, since experimental data have recently become available for two examples of such systems: 1. The transition He I–He II (λ-transition).[1–3] 2. The melting point of argon.[4] In the following the effect of surface energies on the melting process (as an example of a first-order transition) and the λ-transition (as an example of a second-order transition) will be treated thermodynamically.

First, consider the case of a first-order transition in a one-component system. From the equality of the chemical potentials in phases 1 and 2 (solid and liquid, respectively) we have, neglecting surface energies, the well-known Clapeyron equation,

$$d\mu_1 = -S_1 dT + V_1 dP = d\mu_2 = -S_2 dT + V_2 dP, \quad (1a)$$

$$(dP/dT)_{equ} = (S_2 - S_1)/(V_2 - V_1), \quad (1b)$$

where S is the molar entropy, V the molar volume, T the temperature, and P the pressure.

If the surface effects cannot be neglected—as in adsorbed layers—a surface energy term must be added to (1a):

$$d\mu_1 = -S_1 dT + V_1 dP - A_1 d\gamma = d\mu_2 = -S_2 dT + V_2 dP - A_2 d\gamma. \quad (2a)$$

where A is the surface area per mole adsorbed and γ the surface tension.[5] Equation (1b) is changed to,[6]

$$(dP/dT)_{equ} = (S_2 - S_1)/(V_2 - V_1) + (A_2 - A_1)/(V_2 - V_1)(d\gamma/dT)_{equ}. \quad (2b)$$

However, this equation is not directly useful, since $(d\gamma/dT)_{equ}$ is not easily evaluated from experimental data. The surface tension γ is not an independent variable; for a given adsorbent and a given surface

[1] H. P. R. Frederikse, Physica, **15**, 860 (1949), thesis, Leiden, 1950.
[2] E. Long and L. Meyer, Phys. Rev. **76**, 440 (1949); Phys. Rev. **79**, 1031 (1950).
[3] S. V. R. Mastrangelo, J. Chem. Phys. **18**, 846 (1950).
[4] J. A. Morrison and N. E. Drain, J. Chem. Phys. **19**, 1063 (1950).

[5] Compare E. A. Guggenheim, *Thermodynamics* (Amsterdam-New York, 1949), pp. 38–39.
[6] For adsorbed films of even a one component system, S, V, and A are not purely extensive properties, but should be treated as partial molal quantities. As there is no ambiguity in the present case, special notation has been omitted.

area, P and T uniquely determine the amount adsorbed per unit area ($1/A$) and herewith γ. The equation which enables us to replace the surface tension term in (2b) is supplied by the condition that an adsorbed phase is in equilibrium with the vapor,

$$d\mu_a = -S_a dT + V_a dP - A d\gamma = d\mu_g = -S_g dT + V_g dP, \quad (3a)$$

where the subscripts a and g denote the adsorbed phase and gas phase, respectively; or, neglecting the volume of the adsorbed phase with respect to that of the gas,[7]

$$-A d\gamma = (S_a - S_g) dT + V_g dP. \quad (3b)$$

Also,

$$(d\gamma/dT)_{\text{equ}} = (\partial\gamma/\partial T)_P + (\partial\gamma/\partial P)_T (dP/dT)_{\text{equ}}, \quad (4)$$

and from Eq. (3b),

$$(\partial\gamma/\partial T)_P = (S_g - S_a)/A \quad (5a)$$

and[8]

$$(\partial\gamma/\partial P)_T = -V_g/A. \quad (5b)$$

Substitution of (5a) and (5b) in (4) yields

$$(d\gamma/dT)_{\text{equ}} = (S_g - S_a)/A - V_g/A (dP/dT)_{\text{equ}}. \quad (6)$$

At equilibrium, not only the total free energy but also the surface free energies themselves must be equal, i.e., γ and therefore, $d\gamma/dT$ are the same for both condensed phases 1 and 2. Then using Eq. (6) for either phase 1 or 2 and inserting into Eq. (2b) leads to[9]

$$(dP/dT)_{\text{equ}} = 1/V_g [S_g + A_1 S_2/(A_2 - A_1) - A_2 S_1/(A_2 - A_1)]. \quad (7a)$$

This may be rewritten as[10]

$$RT(d \log P/dT)_{\text{equ}} = S_g + A_1 S_2/(A_2 - A_1) - A_2 S_1 (A_2 - A_1), \quad (7b)$$

or, if $(A_2 - A_1) \ll A$,

$$RT(d \log P/dT)_{\text{equ}} = S_g + (S_2 - S_1) A/(A_2 - A_1). \quad (7c)$$

THE MELTING CURVE OF ARGON

Applied to a typical first-order process, such as the melting curve, Eqs. (7) have the following meaning: If the melting curve (the change of melting temperature with pressure) crosses the vapor pressure curve to values of $P < P_0$, then the slope is radically different from that at pressures higher than the vapor pressure P_0 of the bulk phase. This is because at P_0 and lower pressures the two condensed phases are in equilibrium not only with each other, but also with the gas phase, thus introducing the term $1/V_g$ in Eqs. (7).

Since V_g is generally large, $(dP/dT)_{\text{equ}}$ is correspondingly reduced, and the change of melting temperature with pressure is thus greater below P_0 than above. However, comparison of Eqs. (7) and (1b) leads to the conclusion that the sign of $(dP/dT)_{\text{equ}}$ must be the same above and below the vapor pressure curve. The phase stable at higher temperatures must have the higher entropy in adsorbed layers as well as in bulk liquid (or solid), so that $(S_2 - S_1)$ cannot change sign. Also $(A_2 - A_1)$ is of the same sign as $(V_2 - V_1)$, since the spacing of atoms or simple molecules in adsorption is usually very nearly the same as that of the bulk liquid or solid, especially for the case of multi-layer adsorption.[11]

Equation (7c) may be tested by the recent results of Morrison and Drain (reference 4) who measured the specific heat of adsorbed argon in the neighborhood of the melting point.[12] The values used for checking Eq. (7c) were

Number of layers	T_m, °K	p, atmospheres
∞	83.7	0.68
4.3	82.0	0.47
3.5	81.7	0.42
2.3	81.0	0.30

A-liquid was computed from the liquid spacing (4.04A)[13] to be 9.9×10^8 cm²/mole per layer. A-solid was likewise derived from the solid spacing (3.86A)[14] to be 9.0×10^8 cm²/mole per layer, assuming as usual that the spacing in the adsorbed layers is the same as in the bulk phase. S_g was calculated from the Sackur-Tetrode equation,

$$S_g = R[(3/2) \log M + (5/2) \log T - \log P - 2.298].$$

From these values Eq. (7c) yields $\Delta T_m/\Delta P = +6$ deg/atmos.[15] The value of $\Delta T/\Delta P$ for the bulk phases above P_0 is +0.024 deg/atmos as measured by Bridgman,[16] or as calculated from Eq. (1b), using a heat of fusion of 280 cal/mole and a volume change of 3.5 cm³/mole (reference 13). This illustrates the strong change in slope of the melting curve on crossing the vapor pressure curve; however, the sign remains unchanged, as already shown by the experimental evidence of Morrison and Drain. The melting process observed by Morrison and Drain does not occur at one single temperature, as in the bulk liquid-solid transition, but is spread over a range of 5°–15°, depending on the thickness of the adsorbed film. For comparison with the calculated melting temperatures we choose the high temperature end of

[7] See reference 5, Eq. (4-72-3).

[8] Eliminating V_g from (5b) by the ideal gas law leads to

$$\partial\gamma = -RT \partial \log P,$$

the familiar form of Gibb's adsorption isotherm.

[9] Equation (7a) can be derived directly from Eq. (6) without the use of Eq. (2b) by the condition that $(d\gamma/dT)_{\text{equ}}$ must be the same for phases 1 and 2.

[10] Equation (7b) is equivalent to Eq. (104) in Terell L. Hill, J. Chem. Phys. **17**, 520 (1949).

[11] Even in the case of helium (reference 2) only the spacing of the first statistical layer can be markedly different from that of the liquid; the succeeding layers must rapidly approach the liquid spacing.

[12] We are indebted to Dr. J. A. Morrison for communicating to us the adsorption isotherm corresponding to the conditions of the specific heat measurements.

[13] Compare O. K. Rice, J. Chem. Phys. **14**, 324 (1946).

[14] Compare O. K. Rice, J. Chem. Phys. **14**, 321 (1946).

[15] In using the values of A_{liquid} and A_{solid} given above in Eq. (7c), it is assumed that even in multilayer adsorption the numbers of statistical layers for phase 1 and 2 in equilibrium are essentially the same, and that the spacing of the atoms determines the area per mole.

[16] P. W. Bridgman, Proc. Am. Acad. Sci. **70**, 1 (1935).

the specific heat anomaly (Fig. 2, reference 4) instead of the temperature of the maximum, for the following reason: An adsorbed phase is—because of the field of force of the wall—a highly inhomogenous phase. The temperature which corresponds to the thermodynamic calculation of the melting point is the highest temperature at which the solid phase appears in equilibrium with the liquid phase, just as the melting point of a solution is the highest temperature at which the solid phase appears. In adsorbed layers, the freezing is not completed at this temperature, presumably because the layers nearer to the wall must form more and more distorted lattices because of the mismatch with the substrate; in the case of argon this would reduce the melting temperature. Under this assumption, we obtained the values of T_m tabulated above, as read from Fig. 2 of reference 4. The experimental value of $\Delta T_m/\Delta P$ is 6–8 deg/atmosphere, in excellent agreement with the value calculated from Eq. (7c); considering the approximation necessary to evaluate the quantities of (7c), not much more than an order of magnitude agreement could be expected.

THE λ-TRANSITION IN HELIUM

The transition He I—He II is second order; instead of Eq. (2b) we must use the equivalent of the Ehrenfest equations:

$$\left(\frac{dp}{dT}\right)_\lambda = \frac{\dfrac{\partial S_2}{\partial T}-\dfrac{\partial S_1}{\partial T}}{\dfrac{\partial V_2}{\partial T}-\dfrac{\partial V_1}{\partial T}} + \frac{\dfrac{\partial A_2}{\partial T}-\dfrac{\partial A_1}{\partial T}}{\dfrac{\partial V_2}{\partial T}-\dfrac{\partial V_1}{\partial T}}\left(\frac{d\gamma}{dT}\right)_\lambda$$

$$= \frac{\dfrac{\partial S_2}{\partial P}-\dfrac{\partial S_1}{\partial P}}{\dfrac{\partial V_2}{\partial P}-\dfrac{\partial V_1}{\partial P}} + \frac{\dfrac{\partial A_2}{\partial P}-\dfrac{\partial A_1}{\partial P}}{\dfrac{\partial V_2}{\partial P}-\dfrac{\partial V_1}{\partial P}}\left(\frac{d\gamma}{dT}\right)_\lambda . \quad (8)$$

From the same argument, which leads from (2b) to (7) we derive from (8)

$$\left(\frac{dP}{dT}\right)_\lambda = \frac{1}{V_g}\left\{S_g - S_a + A\frac{\partial S_2/\partial T - \partial S_1/\partial T}{\partial A_2/\partial T - \partial A_1/\partial T}\right\}$$

$$= \frac{1}{V_g}\left\{S_g - S_a - A\frac{\partial V_2/\partial T - \partial V_1/\partial T}{\partial A_2/\partial P - \partial A_1/\partial P}\right\} . \quad (9)$$

It would be of interest to apply Eq. (9) to the data of Frederikse (reference 1) who measured the specific heat and adsorption isotherms of unsaturated helium films in the region of the transition He I—He II. However—even though the data represent a considerable experimental achievement—it seems at present impossible to evaluate with sufficient accuracy the second-order terms in Eq. (9) for comparison with experiment as was done for Eq. (7). But the qualitative features remain the same, as may be seen from an examination of (9): The slope of the λ-curve must change strongly on passing the vapor pressure curve to values $P<P_0$, but the sign should not change as long as the second order terms in Eq. (9) are dominant.[17] Thus since $\Delta T/\Delta P$ is negative above P_0, the transition in adsorbed films is expected to occur at temperatures above the λ-temperature of the bulk liquid. The effect should be very small, since the vapor pressure of the liquid at the λ-point is only 0.05 atmosphere and the total available pressure range 0.04 atmos.

The data of Frederikse show that the specific heat anomaly resulting from the He I—He II transition in adsorbed layers is smeared out in a manner similar to the melting point of argon. If again the first appearance of an anomalous thermal effect on cooling the system is chosen as the temperature characteristic for the transition, the specific heat curves are in agreement with these conclusions; the anomalous rise in specific heat always occurs between 2.2° and 2.3°K.

The superfluid properties of bulk liquid helium disappear above the λ-point. The fact that superflow is observed in unsaturated films at all temperatures below the normal λ-temperature[18] is another confirmation of these considerations, showing that the transition temperature in these films is practically the same as T_λ.[19]

[17] An order of magnitude estimate can be derived under the following admittedly rather crude assumptions which might be somewhat justified for more than several statistical layers and a saturation P/P_0 just slightly smaller than 1: The value of $(\partial S_2/\partial T)-(\partial S_1/\partial T)=\Delta c/T$ (c being the specific heat) equals that of the bulk liquid. The spacing in the adsorbed layers is the same as in the bulk liquid so that $(1/A)dA/dT=\frac{1}{3}(1/V)dV/dT$. Using $\Delta c=-7.6$ cal/mole deg and $\Delta(1/V)(dV/dT)=0.065$ deg^{-1} as given by Keesom [see W. H. Keesom, *Helium* (Elsevier Publishing Company, Amsterdam, 1942), p. 256] the third term inside the brackets of (9) is about 160 cal/mole deg, compared with 10 cal/mole deg for S_g-S_a, the entropy of adsorption. These assumptions lead to $(\Delta T/\Delta P)=-0.45$ deg/atmosphere compared with -0.012 deg/atmosphere above P_0.

[18] See reference 2 and E. Long and L. Meyer, Phys. Rev. **85**, 1030 (1952) [preceding article].

[19] Mastrangelo (reference 3) has recently discussed the specific heat maxima of unsaturated helium films and has attempted a correlation of these maxima with the shift of the λ-temperature in bulk liquid with pressure. It should therefore be emphasized that the pressure entering thermodynamic relationships concerning unsaturated films is the pressure of the gas phase in equilibrium with the film, which is always smaller than P_0, the vapor pressure. The pressures which Mastrangelo assumes in his treatment have no relationship to the thermodynamic pressure.

Letters to the Editor

PUBLICATION of brief reports of important discoveries in physics may be secured by addressing them to this department. The closing date for this department is five weeks prior to the date of issue. No proof will be sent to the authors. The Board of Editors does not hold itself responsible for the opinions expressed by the correspondents. Communications should not exceed 600 words in length.

The Exchange Integral in the 3*d* Shell

HARVEY KAPLAN
*Department of Physics, University of California, Berkeley, California**
(Received January 23, 1952)

DURING the past twenty years there has been considerable speculation as to the sign of the Heitler-London exchange integral,

$$J=2\int\psi_m^*(1)\psi_n^*(2)\left[\frac{1}{r_{mn}}+\frac{1}{r_{12}}-\frac{1}{r_{1m}}-\frac{1}{r_{1n}}\right]\psi_n(1)\psi_m(2)d\tau_1 d\tau_2$$

for the known ferromagnetic elements. The question arises in connection with Heisenberg's theory of ferromagnetism,[1] which requires this integral to have a positive sign. In 1930, Slater[2] argued that two atoms having large internuclear separation and unfilled inner shells (both of which requirements are fulfilled for the ferromagnetics) should have a positive J. The argument was extended somewhat further by Bethe,[3] who stressed the importance of the angular dependence of the electronic wave functions. Since that time doubt as to the positive sign of J has been expressed by Slater[4] and more recently by Zener.[5]

Not much has been done in the way of actually computing exchange integrals. Bartlett[6] showed that 2 atoms each having one $2p$ electron would be most strongly bound in the triplet state, each electron having a space function with a node on the line joining the atoms,

$$\psi(r,\theta)=cr\exp(-r/2r_0)\cos\theta.$$

The positive sign he obtained for the exchange integral was an aid in explaining the paramagnetism of the oxygen molecule.

Wohlfarth[7] calculated J for iron, using spherically symmetric wave functions. In view of the predominant importance of angular dependence,[3,6] the negative sign he obtained for J is of little significance.

The purpose of the present letter is to report the result of a calculation of the exchange integral for two atoms each having one $3d$ electron. The wave function used was of the form

$$\psi(r,\theta)=cr^2\exp(-r/2r_0)P_2(\cos\theta).$$

Bartlett's[6] method of calculation was used throughout. In order to find the total energy of the state the Coulomb integral

$$C=2\int|\psi_m(1)|^2|\psi_n(2)|^2\left[\frac{1}{r_{mn}}+\frac{1}{r_{12}}-\frac{1}{r_{1n}}-\frac{1}{r_{2m}}\right]d\tau_1 d\tau_2$$

was also calculated. The $3d$ binding energy is $E=(J-C)/S$, where $S=\int\psi_m^*(1)\psi_n(1)d\tau_1$. Both J and C appear as functions of $\alpha=R/r_0$, where R is the internuclear separation. C and J were tabulated for various values of α using Bartlett's tables of $f_l(m,\alpha)$ and $A_m(l,\alpha)$. Because of enormous subtraction effects, the accuracy of the results, particularly for J, was severely limited; for example, at $\alpha=6$, $Jr_0=0.004\pm0.002$ (atomic units) probable error. However, since the accuracy of C was not quite so poor and $|C|\gg|J|$ it was possible to determine the general variation of E with α. There is maximum binding for α between 5 and 6 of about $0.2/r_0$ atomic units. At $\alpha=10$, E has fallen to about forty percent of its maximum value. This is a less rapid decrease than that obtained by Bartlett for $2p$ electrons, which is reasonable since the $3d$ function are more sharply concentrated between the nuclei.

In order to remove any uncertainty as to the sign of J, it was recalculated after first extending Bartlett's tables a few places and making a few minor corrections. This was done only for $\alpha=6$ (maximum binding) since the work is tedious. The final value obtained is $J=0.00552/r_0$ atomic units or $0.150/r_0$ ev. If the value 0.25 is used for r_0, corresponding to a reasonable fit to the $3d$ iron function, $J=0.60$ ev. This value is a factor of ten larger than ferromagnetic exchange integrals.

Although the present calculation serves to support the Heisenberg theory of ferromagnetism, several qualifications of its significance must be mentioned. The radial function used is a poor approximation to a true $3d$ function. Furthermore, at maximum binding the reasonable one-exponential fit $r_0=0.25$ corresponds to the very small internuclear separation of $\sim$0.75 Angstroms. The rough calculation indicates that J almost certainly remains positive out to about twice this separation ($\alpha=10$), but this is still considerably short of the nearest neighbor spacing in ferromagnetics. The $4s$ electrons have been neglected. The effect of the other nearest neighbor atoms has been neglected also.

I wish to thank Professor C. Kittel for suggesting this problem and for constant encouragement during its progress. I am indebted to Mr. F. Keffer for checking some of the calculations. Part of this work was done during the tenure of a James Sutton Fellowship at the University of California.

* This research has been assisted in part by the ONR.

[1] W. Heisenberg, Z. Physik **49**, 619 (1928).
[2] J. C. Slater, Phys. Rev. **36**, 57 (1930).
[3] A. Sommerfeld and H. Bethe, *Elektronentheorie der Metalle*, Handbuch der Physik (Verlag. Julius Springer, Berlin, Germany, 1933), Vol. **24**, pt. II, p. 595.
[4] J. C. Slater, Phys. Rev. **49**, 537 (1936).
[5] C. Zener, Phys. Rev. **81**, 440 (1951); **82**, 403 (1951); **83**, 299 (1951).
[6] James H. Bartlett, Jr., Phys. Rev. **37**, 507 (1931).
[7] E. P. Wohlfarth, Nature **163**, 57 (1949).

Radioactivity of $Eu^{152,154}$

ROBERT KATZ AND MILFORD R. LEE
Kansas State College, Manhattan, Kansas
(Received January 28, 1952)

ALTHOUGH the spectrographic analysis accompanying several enriched samarium isotopes from Oak Ridge contained $\leq$0.6 percent europium, some of the more intense internal conversion lines attributed to the disintegration of europium[1] have been found photographically with neutron-activated samarium isotopes in a 180° focusing β-ray spectrograph. Conversion lines of some gamma-rays designated by Cork *et al.*[1] as 122.0 (K, L, M), 244.3 (K, L), and 343.8 (K, L) kev were found on spectrograms of neutron-irradiated Sm^{150}, while conversion lines of these three gamma-rays, together with the K conversion line of the 123.2-kev gamma-ray, were found associated with neutron-irradiated Sm^{154}. Our energies for these gamma-rays were 121.2, 243.8, 343.8, and 122.4 kev, respectively. The spectrograph was calibrated with Cs^{137}. Assuming that the europium impurity was enriched in nearly the same way as the samarium, the abundance ratio of Eu^{151}:Eu^{153} would be markedly different in the two samples, being 6:1 in the Sm^{150} enrichment and 1:16 in the Sm^{154} enrichment. In addition to these long lived conversion electrons, hard gamma-rays (half-life$>$1 yr) of energy 990 kev in the Sm^{150} sample and 1170 kev in the Sm^{154} sample were found by absorption, in lead, in a geometry calibrated with Cs^{137} and Co^{60}.

The recently revised gamma-ray assignments in Eu^{152} and Eu^{154} by Keller and Cork,[2] insofar as they refer to the transfer of the highest energy (1116 kev) gamma-ray to Eu^{154} and of the 344-kev gamma-ray to Eu^{152}, are in good agreement with our data. These results appear to be in disagreement with Fowler and Schreffler[3] who have reported finding coincidences between conversion electrons from the 123- and 344-kev gamma-rays. Our data indicate that the 122-, 244-, and 344-kev gamma-rays are associated with the disintegration of Eu^{152} while the 123-kev gamma-ray appears to be associated with the disintegration of Eu^{154}.

It seems clear that the long lived activity assigned to Sm^{146} by Cork, Fowler, and Schreffler[4] consisting of gamma-rays of energy 950 and 242 kev (and listed under Sm^{149} in both the latest Seaborg table and National Bureau of Standards circular 499)[5] was the result of europium contamination. We have found conversion electrons of the 242-kev gamma-ray and/or the "950-kev" gamma-ray (Pb absorber) in nearly the same intensity in pile irradiated Sm^{149}, Sm^{150}, and Sm^{152}. The high energy gamma-ray was considerably weaker in a source of pile-irradiated unenriched samarium, further indicating that this activity was because of an impurity.

[1] Cork, Keller, Rutledge, and Stoddard, Phys. Rev. **77**, 848 (1950).
[2] H. B. Keller and J. M. Cork, Phys. Rev. **84**, 1079 (1951).
[3] C. M. Fowler and R. G. Schreffler, Rev. Sci. Instr. **21**, 740 (1950).
[4] Cork, Fowler, and Schreffler, Phys. Rev. **74**, 240 (1948).
[5] K. Way (private communication) stated that this long lived activity was listed as Sm^{149} in National Bureau of Standards Circular 499 (1950), since Sm^{149} was reported to be short lived.

Masses of Pb^{208}, Th^{232}, U^{234}, U^{235}, and U^{238}

GEORGE S. STANFORD*
Wesleyan University, Middletown, Connecticut
HENRY E. DUCKWORTH†
Wesleyan University, Middletown, Connecticut, and McMaster University, Hamilton, Ontario, Canada
AND
BENJAMIN G. HOGG AND JAMES S. GEIGER‡
McMaster University, Hamilton, Ontario, Canada
(Received January 10, 1952)

MASS spectrographic mass values have been obtained for five of the isotopes of lead, thorium, and uranium, namely Pb^{207}, Pb^{208}, Th^{232}, U^{234}, and U^{238}. Since these masses are related to one another through more or less known disintegration data, they have been considered as a group, and the individual masses adjusted to secure a mutually consistent set of values.

Pb^{207} and Pb^{208}.—The doublet formed by triply-charged Pb^{207} and doubly-charged Ba^{138} was photographed at mass number 69, and from this the Pb^{207}-Ba^{138} packing fraction difference[1] was found to be $\Delta f = 5.62 \pm 0.05$. This datum combined[2] with $Ba^{138} = 137.9510 \pm 8$ AMU leads to the mass $Pb^{207} = 207.0429 \pm 16$ AMU. Recent precise transmutation work[3–6] has shown that Pb^{208}-$Pb^{207} = 1.00106 \pm 4$ AMU, whence $Pb^{208} = 208.0440 \pm 16$ AMU. Meanwhile the mass of Pb^{208} determined from the Pb^{208}-Pd^{104} doublet ($\Delta f = 8.055 \pm 0.02$)[7] is 208.0409 ± 13 AMU. There are, thus, two independent mass spectrographic values for the mass of Pb^{208}, giving a mean of 208.0421 ± 12 AMU.

Th^{232}.—Values for the mass of Th^{232} have been obtained by photographing the Th^{232}-Sn^{116} and Th^{232}-Fe^{56} doublets. The packing fraction differences found for these doublets are Th^{232}-Sn^{116}: $\Delta f = 10.058 \pm 0.03$, and Th^{232}-Fe^{56}: $\Delta f = 13.17 \pm 0.05$. From the former, assuming $Sn^{116} = 115.93761 \pm 48$ AMU, one deduces $Th^{232} = 232.1086 \pm 10$ AMU, and from the latter, assuming $Fe^{56} = 57.95106 \pm 25$ AMU, $Th^{232} = 232.1102 \pm 17$ AMU, giving a weighted mean of 232.1092 ± 10 AMU. The mass of Sn^{116} given here is based on $Si^{28} = 27.98579 \pm 4$ AMU,[8] Si^{29}-$Si^{28} = 0.99988 \pm 2$ AMU,[9] Si^{30}-Ni^{58}: $\Delta f = 3.086 \pm 0.02$,[10] and Sn^{116}-Ni^{58}: $\Delta f = 2.647 \pm 0.015$.[11] The mass of Fe^{56} was deduced from $Co^{59} = 58.95160 \pm 12$ AMU, using the 10.25 ± 0.20 Mev $Co^{59}(\gamma, n)$ threshold,[6] and the mass difference Co^{56}-$Fe^{56} = 0.00247$ AMU.[12] The mass of Co^{59} was deduced from $Ni^{60} = 59.94923 \pm 15$ AMU,[13] knowing that Co^{60}-$Co^{59} = 1.00070 \pm 5$ AMU[4,13–15] and Co^{60}-$Ni^{60} = 0.00302$ AMU;[12] and from $Ni^{58} = 57.95354 \pm 23$ AMU using Ni^{60}-$Ni^{58} = 0.99930 \pm 3$ AMU,[4,13] and Ni^{59}-$Co^{59} = 0.00116$ AMU.[16] The Th^{232}-Sn^{116} packing fraction difference of 10.058 ± 0.03 agrees well with Dempster's value of 10.14 ± 0.1.[17]

U^{234}.—From the U^{234}-Sn^{117} doublet we have obtained the packing fraction difference $\Delta f = 10.008 \pm 0.025$. Assuming $Sn^{117} = 116.93957 \pm 45$ AMU, one deduces $U^{234} = 234.1133 \pm 11$ AMU. The mass of Sn^{117} is based on $\Delta f = 2.99 \pm 0.02$ for the Sn^{118}-Co^{59} doublet and $Q = 7.14 \pm 0.2$ Mev for the $Sn^{117}(d, p)$ reaction.[4]

U^{238}.—The study of U^{234}-Sn^{119} doublet has given $\Delta f = 10.187 \pm 0.025$. Assuming $Sn^{119} = 118.94048 \pm 43$ AMU, one deduces $U^{238} = 238.1234 \pm 10$ AMU. The mass of Sn^{119} was obtained from Sn^{118} using 6.50 ± 0.15 Mev for the $Sn^{119}(\gamma, n)$ threshold.[18] Studies of the U^{238}-Sn^{119} doublet made in Dempster's laboratory on two different occasions[17,19] have given for the U^{238}-Sn^{119} doublet $\Delta f = 10.41 \pm 0.1$ and 10.12 ± 0.09, in satisfactory agreement with the present value.

Adjusted mass values.—The masses of Pb^{208}, Th^{232}, U^{234}, and U^{238} given above have been adjusted in the standard manner by imposing upon them the conditions that U^{238}-$Pb^{208} = 30.0834 \pm 15$ AMU,[20] U^{238}-$Th^{232} = 6.0148 \pm 6$ AMU,[20] and U^{238}-$U^{234} = 4.0112 \pm 2$ AMU.[20] The adjusted values so obtained are

$$Pb^{208} = 208.0416 \pm 10 \text{ AMU},$$
$$Th^{232} = 232.1093 \pm 10 \text{ AMU},$$
$$U^{234} = 234.1129 \pm 10 \text{ AMU},$$
$$U^{238} = 238.1241 \pm 10 \text{ AMU}.$$

The mass of U^{235} can be computed from Th^{232} using 4.64 ± 0.3 Mev for the energy[21] of the α-particle emitted by U^{235} plus the energy of the recoiling nucleus, and 6.0 ± 0.15 Mev for the $Th^{232}(\gamma, n)$ threshold.[22] The resulting mass is $U^{235} = 235.1156 \pm 10$ AMU.

Comparison with other measurements.—Dempster in his pioneer work with thorium and uranium gave the masses[23] $Th^{232} = 232.12$, $U^{235} = 235.125$, and $U^{238} = 238{:}132$: these are not inconsistent with the present values. Very recently the mass of Pb^{208} has been determined[24] by Richards, Hays, and Goudsmit to be 208.0412 ± 15 AMU, a value which is in excellent agreement with the present one, an especially gratifying situation since their work has been done with a completely different type[25] of mass spectrograph.

The authors appreciate the cooperative interest shown in these experiments by Glenn T. Seaborg. They are also grateful to Katherine Way, A. H. Wapstra, and A. C. Pappas for critical comments and to S. A. Goudsmit, J. Halpern, H. Ewald, and J. J. G. McCue for prepublication data which have aided us in this work. The U^{234} measurement required a sample of uranium greatly enriched in U^{235}, kindly secured for us by E. B. Meservey. It is a pleasure to acknowledge that this work was made possible by financial help from the AEC, the Research Corporation, the National Research Council of Canada, and the Ontario Research Council.

* Now at Sloane Laboratory of Physics, Yale University, New Haven, Connecticut.
† Now at McMaster University, Hamilton, Canada.
‡ Holder of an Ontario Research Council Scholarship.
[1] Throughout the letter the factor $\times 10^{-4}$ will be understood and not written in expressing the numerical value of the packing fraction.
[2] Duckworth, Kegley, Olson, and Stanford, Phys. Rev. **83**, 1114 (1951). In this and in other references to our own work the masses quoted may differ slightly from those given originally. These differences arise in part from the use of the subtandards $H^1 = 1.008142 \pm 3$ and $C^{12} = 12.003804 \pm 17$ [Li *et al.*, Phys. Rev. **83**, 512 (1951)] and in part from the results of recent unpublished work.
[3] Kinsey, Bartholomew, and Walker, Phys. Rev. **82**, 380 (1951).
[4] J. A. Harvey, Phys. Rev. **81**, 353 (1951).
[5] Sher, Halpern, and Mann, Phys. Rev. **84**, 387 (1951).
[6] H. Palevsky and A. O. Hanson, Phys. Rev. **79**, 242 (1950).
[7] B. G. Hogg and H. E. Duckworth, unpublished result.
[8] H. Ewald, Z. Naturforsch. **6a**, 293 (1951).
[9] Endt, Van Patter, and Buechner, Phys. Rev. **81**, 317 (1951).
[10] Duckworth, Johnson, Preston, and Woodcock, Phys. Rev. **78**, 386 (1950); plus unpublished work.
[11] H. E. Duckworth and R. S. Preston, Phys. Rev. **79**, 402 (1950); plus unpublished work.
[12] A. C. G. Mitchell, Revs. Modern Phys. **22**, 36 (1950).
[13] Kinsey, Bartholomew, and Walker, Phys. Rev. **78**, 481 (1950).
[14] H. E. Kubitschek and S. M. Dancoff, Phys. Rev. **76**, 531 (1949).
[15] W. O. Bateson and E. Pollard, Phys. Rev. **79**, 241 (1950).
[16] J. J. G. McCue and W. M. Preston, Phys. Rev. **84**, 384 (1951).
[17] A. J. Dempster, Phys. Rev. **53**, 64 (1938).
[18] Hanson, Duffield, Knight, Diven, and Palevsky, Phys. Rev. **76**, 578 (1949).
[19] A. C. Graves, Phys. Rev. **55**, 863 (1939).
[20] G. T. Seaborg, private communication.
[21] A. H. Wapstra, Physica **16**, 33 (1950).
[22] R. W. Parsons and C. H. Collie, Proc. Phys. Soc. (London) **63**, 839 (1950).
[23] A. J. Dempster, Phys. Rev. **53**, 869 (1938).
[24] Richards, Hays, and Goudsmit, Phys. Rev. **85**, 630 (1952).
[25] Hays, Richards, and Goudsmit, Phys. Rev. **84**, 824 (1951).

The M_5 and M_4 X-Ray Absorption Edges of Tantalum

DONALD D. DOUGHTY* AND J. W. MCGRATH
Kent State University, Kent, Ohio
(Received February 5, 1952)

MOST of the M edges of 20 of the heavier elements have been measured. The study of tantalum is a logical extension of the work of others. Its M_5, M_4, and M_3 edges have been measured by Whitmer,[1] but some repetition in the initial stages of investigation seemed desirable.

The vacuum spectrograph[2] is of the Siegbahn type. The focal circle radius was 13.94 cm. The x-ray tube, which had a copper target, was operated on dc at about 3300 volts and a current of about 120 ma. Exposure times for emission and absorption spectrograms were about 2½ hours and 50 hours, respectively.

Tantalum absorbing films were produced on very thin, soft glass by evaporation in a vacuum. The film thickness was about 4×10^{-5} cm which is near the optimum value.

Wavelengths of the edges were determined by interpolation using a formula developed by Whitmer.[1] Reference lines were the tungsten emission lines M_α (6969 X.U.), M_β (6743 X.U.), and the silicon K edge (6705 X.U.). Five successful spectrograms were obtained for the M_5 edge and four for the M_4 edge. Comparison to emission spectrograms and to a glass-absorption spectrogram showed that the observed absorption fluctuation was truly due to tantalum.

Values obtained are shown in Table I. Quoted experimental

TABLE I. M edge values.

Edge	Wavelength (X.U.)	r/R	Observed energy (ev)	Energy computed from L lines (ev)	Discrepancy (ev)
M_5	7033±5	129.3±0.1	1760±2	1730	+30
M_4	6845±5	132.8±0.1	1808±2	1788	+20

errors do not take into account errors in the wavelengths of the reference lines and in the gypsum crystal spacing (7586 X.U.). Whitmer's values are 6997±10 X.U. for the M_5 edge and 6773 ±10 X.U. for the M_4 edge.

The M_5 edge energy was computed by subtracting the energy difference for the tantalum $L_{\alpha1}$ line from the tantalum L_3 edge energy. The M_4 edge energy was computed by the equation $M_4=L_3-L_{\alpha2}$. Discrepancies between observed and computed values for the M_5 and M_4 edges appear in 14 of the 19 elements studied. The discrepancies are positive as is usually the case.

The differences between Whitmer's values and ours are significant. The origin of the differences is unclear. He stated that the M_5 and M_4 edges were so close to the tungsten M_α and M_β lines on his spectrograms that the lines, when present, masked the edges. To avoid this difficulty this procedure was used: The absorption spectrograms were taken when there was no tungsten on the target and while using a molybdenum x-ray tube filament. Then the molybdenum filament was replaced by a tungsten filament, a horizontal slit 5 mm tall was placed in the x-ray beam, and a ten-minute emission exposure was superimposed on the absorption exposure. Thus the spectrogram, which was about 3 cm tall, showed the tungsten lines for only a 5-mm height. There were no absorption discontinuities as close to the tungsten lines as would be required by Whitmer's values. The M_5 edge was 0.135 cm from the tungsten M_α line, and the M_4 edge was 0.210 cm from the tungsten M_β line. The observed tantalum edges were diffuse and did not exhibit great contrast; they were, however, clear.

It has been suggested and fairly well established by Siegbahn,[3] Phelps,[4] and McGrath[5] that the M edge discrepancies (see Table I, last column) arise because atomic electrons may not all go to the same final valence or crystal lattice level in an absorption edge transition. If there are assigned to the low lattice levels the l quantum numbers which the parent optical levels have in free atoms, there are preferred edge-giving transitions which are often described by the selection rule $\Delta l=\pm1$. On this basis L_3 electrons in tantalum may go to the $O_{4,5}$ level which is only partially filled. The M_5 and M_4 electrons, however, must go to a level or levels about 30 to 20 ev higher. This lattice level may be the one which originates from the $P_{2,3}$ level in the free tantalum atom.

* Now at Westinghouse Research Laboratories, Pittsburgh, Pennsylvania.

[1] C. A. Whitmer, Phys. Rev. **38**, 1164 (1931).
[2] J. W. McGrath, Rev. Sci. Instr. **11**, 396 (1940).
[3] M. Siegbahn, Z. Physik **67**, 567 (1931).
[4] W. D. Phelps, Phys. Rev. **46**, 357 (1934).
[5] J. W. McGrath, Phys. Rev. **56**, 137 (1939).

Electromagnetic Effects Due to Spin-Orbit Coupling

J. HANS D. JENSEN*
University of Wisconsin, Madison, Wisconsin
AND
M. GOEPPERT-MAYER
Argonne National Laboratory, Chicago, Illinois
(Received January 30, 1952)

THE existence of strong spin-orbit coupling in the single-particle model of the nucleus implies the existence of a term

$$-f(r)(\boldsymbol{\sigma}\cdot\mathfrak{L})=-f(r)(\boldsymbol{\sigma}\cdot[\mathbf{r}\times\mathbf{p}]) \quad (1)$$

in the single-particle Hamiltonian. This gives rise to an interaction of charged nucleons with external electromagnetic fields with vector potentials $\mathbf{A}$. Replacing the momentum in the Hamiltonian by $\mathbf{p}-(e/c)\mathbf{A}$, we obtain from the spin-orbit coupling term the interaction energy,

$$(e/c)f(r)\cdot(\boldsymbol{\sigma}\cdot[\mathbf{r}\times\mathbf{A}]). \quad (2)$$

One consequence of this effect is that the magnetic moments of odd-proton nuclei should deviate from the Schmidt lines.[1] In a constant magnetic field with $\mathbf{A}=\frac{1}{2}[\mathbf{H}\times\mathbf{r}]$ the interaction term (2) becomes,

$$(e/2c)f(r)(\boldsymbol{\sigma}\cdot[\mathbf{r}\times[\mathbf{H}\times\mathbf{r}]]) = (e/2c)f(r)\{r^2(\boldsymbol{\sigma}\cdot\mathbf{H})-(\mathbf{r}\cdot\boldsymbol{\sigma})(\mathbf{r}\cdot\mathbf{H})\}. \quad (3)$$

For a state with orbital angular momentum l, total angular momentum $j=l\pm\frac{1}{2}$, and magnetic quantum number m_j, the expectation value of the interaction energy is,

$$\pm\frac{e}{2c}\langle r^2f(r)\rangle_{Nl}\frac{2j+1}{2j+2}\frac{m_j}{j}H, \quad (4)$$

with the positive sign for $j=l+\frac{1}{2}$, the negative sign for $j=l-\frac{1}{2}$. The factor in front of H, for $m_j=j$, is the negative additional magnetic moment. The effect consequently places the magnetic moments between the Schmidt lines, as is experimentally observed. Taking the spin-orbit splitting energy, $\langle f(r)\rangle_{Nl}(2l+1)\hbar$, to be about 2 Mev at $l=4$, $A=100$, we estimate the magnitude of the additional magnetic moment to be $0.25(2j+1)/(2j+2)$ nuclear magnetons, which is too small to explain the observed deviations. If we assume[2] $\langle f(r)\rangle_{Nl}$ to be proportional to $A^{-\frac{1}{3}}$, then $\langle r^2f(r)\rangle_{Nl}$ and consequently the additional magnetic moment are independent of A.

Another consequence of (2) are additional radiative transition probabilities which are important only in cases where the ordinary transitions have vanishing matrix elements. For example, in transitions from a state with $j=l-\frac{1}{2}$ to a state with $j'=l'+\frac{1}{2}$, the interaction (2) gives a nonvanishing matrix element for magnetic L-pole transitions with $\Delta j=L$ and $\Delta l=L+1$, which otherwise would be forbidden. As a special example we mention the transition $d\frac{3}{2}\rightarrow S\frac{1}{2}$ for which we calculated for the magnetic dipole radiation a transition probability which corresponds to the radiation of an oscillating classical magnetic dipole with an amplitude of 0.25 nuclear magnetons. The electric transitions turn out not to be affected by (2), in agreement with a general theorem given by Sachs and Austern.[3]

As stated above, both effects are present for odd protons only. They are closely connected with the more general "interaction moments" as defined and discussed by Sachs,[3] which according to Sachs might give additional moments of a somewhat greater magnitude than those discussed in this paper, and of equal character for odd neutrons and odd protons. We wish to express our thanks to R. G. Sachs for helpful discussions.

* On leave of absence from the University of Heidelberg, Heidelberg, Germany.
[1] The fact that velocity dependent two-body forces give rise to additional moments has been pointed out by Blanchard, Avery, and Sachs, Phys. Rev. **78**, 292 (1950).
[2] M. Goeppert-Mayer, Phys. Rev. **78**, 16 (1950).
[3] R. G. Sachs and N. Austern, Phys. Rev. **81**, 705 (1951).

Polarization of the 6.13-Mev Gamma-Rays Emitted in the Reaction $F^{19}(p,\alpha)O^{16*}(\gamma)O^{16}$

A. P. FRENCH AND J. O. NEWTON*
Cavendish Laboratory, Cambridge, England
(Received January 29, 1952)

THE angular correlation between the γ-rays from the 6.13-Mev level of O^{16} and the corresponding α-particles in the $F^{19}(p,\alpha)$ reaction (Arnold[1] and Barnes *et al.*[2]) indicates that (i) the intermediate state formed in Ne^{20} at 340-kev proton energy has spin 1 and is formed by s-protons and (ii) the spin of the excited state in O^{16} is 3, so that it decays by emission of octupole gamma-radiation. In order to find the parity of this state in O^{16} we decided to investigate the polarization of the γ-rays at an angle of 118° to the α-particles. For this particular angle the octupole γ-rays should be plane polarized. Since the polarization directions for electric and magnetic radiations of the same type differ by a right angle,[3] such a measurement determines the parity of the emitting state relative to that of the ground state of O^{16}, which is certainly even.

If plane polarized γ-rays suffer Compton scattering, the scattered intensity is a maximum in the plane perpendicular to the direction of the electric vector **E** of the incident rays.[4] Thus a measurement of scattered intensity in the two possible polarization planes gives the direction of **E**. This has been done by Metzger and Deutsch[5] for low energy γ-rays. At higher energies it becomes more difficult, because the Compton scattering is predominantly in the forward direction, and the ratio of scattered intensities parallel and perpendicular to **E** approaches unity;[4] also scintillation counters become less efficient. Nevertheless we adopted this method.

The γ-rays were detected by two scintillation counters of volume 350 cc, made from solutions of terphenyl in xylene. One counter was used as a scatterer, and the other, which could be rotated about the first, was arranged so as to be as sensitive as possible to the angular variation of scattered intensity, subject to the need to secure a measurable coincidence rate. The α-particles were detected in a proportional counter. Triple coincidences between the detectors were recorded; the movable γ-counter was set alternately in the two principal positions, changing every 5 minutes or less to eliminate drift. Double coincidence counts and single counts were also recorded so that corrections for mechanical asymmetries and random coincidences could be made. A total of 166 readings was taken, corresponding to about 450 true triple coincidences in each position.

If the α-particles leading to the 6.13-Mev level in O^{16} have orbital momentum 3, as is most probable,[2] the ratio of scattered intensities expected with our geometrical arrangement is 1.19 for electric octupole and 0.84 for magnetic octupole radiation. Our experimental result was 1.14 ± 0.06, which makes it seem very unlikely that the transition is magnetic, and one may conclude that the parity of this state is odd. It then follows that the ground state of F^{19} and the excited state in Ne^{20} have even parity. The absence of long range α-particle emission from this Ne^{20} level to the ground state of O^{16} is then accounted for, since conservation of both angular momentum and parity in such a transition becomes impossible.

It has been suggested by Dr. D. H. Wilkinson that the polarization direction might be established more conclusively from the photodisintegration of deuterium. This, in contrast to Compton scattering, is a nonrelativistic effect, and observation of the photoprotons should reveal a much larger ratio of intensities parallel and perpendicular to **E**. Though this advantage is partly offset by the low (γ,p) cross section, we hope to repeat the experiment (in collaboration with Dr. Wilkinson and Mr. J. H. Carver) by this method.

* Now at A.E.R.E., Harwell, England.
[1] W. R. Arnold, Phys. Rev. **80**, 34 (1950).
[2] Barnes, French, and Devons, Nature **166**, 145 (1950).
[3] W. Heitler, Proc. Cambridge Phil. Soc. **32**, 112 (1936).
[4] W. Heitler, *The Quantum Theory of Radiation* (Oxford University Press, London, 1944), chapter III.
[5] F. Metzger and M. Deutsch, Phys. Rev. **78**, 551 (1950).

Dielectric Constant and Permeability of Various Ferrites in the Microwave Region

TOSHIHIKO OKAMURA, TADAO FUJIMURA, AND MUNEYUKI DATE
Research Institute for Scientific Measurements, Sendai, Japan
(Received January 18, 1952)

THE dielectric constant ϵ and permeability μ of ferrites have already been studied at the audiofrequencies,[1,2] but they have scarcely been measured in the microwave region.[3,4]

We determined ϵ and μ with various polycrystalline specimens of magnesium, copper, cobalt, nickel, and manganese ferrites, both quenched and annealed, at a wavelength of 6.6 cm and at room temperature. We measured the changes in Q and the cavity frequency shift when a thin disk-shaped specimen, 20 mm in diameter and 1.5 mm in thickness, attached to a support, was inserted in a rectangular cavity (TE_{104} mode), in the positions of maximum E and H.

From these measurements the real and imaginary parts of ϵ and μ were determined by the following formulas derived by expanding the field in the cavity in the orthogonal functions introduced by Slater:[5]

Put $\epsilon=\epsilon_0(\epsilon_1-j\epsilon_2)$ and $\mu=\mu_0(\mu_1-j\mu_2)$; then

$$-2\frac{\Delta\omega_a}{\omega}=(\epsilon_1-1)\int_{\Delta V}E_a^2dv,$$

$$\frac{1}{Q_\epsilon}=\frac{\sigma}{\omega}\int_{\Delta V}E_a^2dv+\epsilon_2\int_{\Delta V}E_a^2dv, \tag{1}$$

$$-2\frac{\Delta\omega_a'}{\omega}=(\mu_1-1)\int_{\Delta V}H_a^2dv,$$

$$\frac{1}{Q_\mu}=\mu_2\int_{\Delta V}H_a^2dv, \tag{2}$$

where $\Delta\omega_a$ and $\Delta\omega_a'$ are the frequency shifts caused by inserting the specimen at the positions of the electric and magnetic field maxima, respectively, in the cavity. The experimental results thus obtained are shown in Table I, in which ϵ_1, ϵ_2, and μ_1, μ_2 respectively represent real and imaginary parts of ϵ and μ.

From Table I, we found that the values of ϵ and μ were of the order of 10 and 1.5, respectively, in the case of simple ferrites, that ϵ of the quenched Ni-ferrite was comparatively larger than that of the other ferrites, and also that $\tan\delta$ of Co-ferrite was the smallest of all. As the half-width of the Q-curve in the experiment on annealed Co-ferrite did not change, within the limits of error, ϵ_2 could not be determined in this case.

It was noticed that the dc resistance of all the specimens was of the order of $10^6\Omega$/cm; therefore the skin depth at 4500 Mc is 2 cm and the high frequency field in the specimen may be treated

TABLE I. Dielectric constant, permeability and $\tan\delta_{\epsilon,\mu}$ of various ferrites at a wavelength of 6.6 cm; thickness of the specimen is 1.5 mm.

Ferrite	ϵ_1	ϵ_2	$\tan\delta_\epsilon$	μ_1	μ_2	$\tan\delta_\mu$
$MgOFe_2O_3$ quenched from 1200°C	9.66	0.174	0.018	1.20	0.974	0.812
$MgOFe_2O_3$ slow cooled	8.53	0.132	0.016	2.84	0.341	0.120
$CuOFe_2O_3$ quenched from 1000°C	9.29	0.520	0.056	1.94	1.240	0.639
$CuOFe_2O_3$ slow cooled	8.65	0.089	0.010	1.38	0.740	0.543
$CoOFe_2O_3$ quenched from 1200°C	9.49	0.045	0.047	1.57	0.211	0.138
$CoOFe_2O_3$ slow cooled	9.00			1.90	0.116	0.061
$NiOFe_2O_3$ quenched from 1200°C	13.40	3.520	0.260	1.74	0.460	0.264
$NiOFe_2O_3$ slow cooled	8.88	0.155	0.017	1.47	2.377	1.620
$MnOFe_2O_3$ quenched from 1200°C	9.30	0.475	0.051	2.31	2.040	0.883

as uniform. The same experiment was also made with a specimen of different size, 1 mm in thickness and 20 mm in diameter, but no effect of the thickness could be observed in the present experiment.

Details will be published in the Scientific Reports of the Research Institute of Tohoku University.

The writers would like to express their thanks to Mr. Y. Torizuka for discussions concerning the theoretical and experimental aspects of the problem.

[1] C. G. Koops, Phys. Rev. **83**, 121 (1950).
[2] K. Kamiyoshi, Phys. Rev. **84**, 374 (1951).
[3] W. H. Hewitt, Phys. Rev. **73**, 1118 (1948).
[4] D. W. Healy, Jr., Cruft Laboratory, Harvard University, Technical Report No. 135 (1951).
[5] J. C. Slater, Revs. Modern Phys. **18**, 441 (1946).

The Closing of the Proton Sub-Shell at Z 58

G. P. DUBE AND S. JHA*
Physics Department, Science College, Patna, India
(Received February 1, 1952)

NUCLEI containing 2, 8, 20, 28, 50, 82, and 126 neutrons and protons are particularly stable. The extra stability of these nuclei is attributed to the completion of the neutron or proton shells at these numbers. Of the various schemes[1-4] suggested to explain this, the one due to Mayer[5] and Jensen *et al.*[4] seems to fit the data best. They explain the occurrence of these magic numbers on a single particle model with a strong spin-orbit coupling, and the levels responsible for the aforementioned magic numbers are $1s_{1/2}$, $1p_{3/2,1/2}$, $2s_{1/2}$, $1f_{1/2}$, $1g_{9/2}$, $1h_{11/2}$, and $1i_{13/2}$ [Mayer[6]].

There is some dispute about the closing of the shells at N or $Z=20$.[6] On the other hand, there is evidence to show that there is a closing of the shell at N or $Z=40$.[7] On Mayer's scheme, this can happen by the filling up of the sub-shells $2p_{3/2,1/2}$; but with considerations like this, one would expect the systems with 58, 68, 70, 92, 106, 112, 138, and 156 neutrons or protons, in addition to the usual magic number isotopes, to be specially stable because of the filling up of $1g_{7/2}$, $2d_{5/2,3/2}$, $3s_{1/2}$, $1h_{9/2}$, $2f_{7/2,5/2}$, $3p_{3/2,1/2}$, and $1i_{11/2}$, respectively. Besides these, Feenberg and Hammack[8] have suggested, on the basis of the nonoccurrence of stable isotopes with N or $Z=61$, that perhaps there is a closing of the shells $4d$ at N or $Z=60$, giving rise to an extra stable configuration. It seems to us that instances like β-stable $_{51}$Sb and $_{84}$Ac C'^{211} show that a magic number configuration is not necessarily followed by an unstable one. It seems to us that one should expect the occurrence of extra stable configurations only if the building up of the nucleus of the isotope in question is as regular as, say, the Mayer scheme. An examination of the table of spins and magnetic moments[6] shows that this is not always so. In this connection it is worthwhile emphasizing what Mayer has pointed out, that in the region between N or $Z=50$ and 82, the last odd proton, in contrast to the last odd neutron, is usually found in an orbit of high angular momentum, perhaps due to the Coulomb repulsion tending to concentrate the charge on the periphery of the nuclei. So far as the neutron shells are concerned, the examination of the neutron binding energy values[9] and the results of the mass spectrometer studies[7] suggest the closing of the neutron shells at $N=60$ and 70.

Although it is difficult to say what happens at the neutron numbers 58, 68, 92, 106, 112, and others mentioned above, one can readily say that there is no closing of the proton shell at $Z=92$, and the protons between $Z=83$ and 91 are not filled in the level $1h_{9/2}$; this is based on the fact that the spin of $_{91}Pa^{231}$ is $3/2$[9] and that of $_{89}Ac^{227}$ is $3/2$.[10] In the case of the closing of the shell there, the spin of at least $_{91}Pa^{231}$ (which would in that case be a nucleus with a hole in the level $1h_{9/2}$) should have been 9/2 as in the case of $_{83}Bi^{209}$.

The case of the element cerium ($Z=58$) is different. In this region the heavier of the two stable isotopes of $_{51}$Sb and $_{53}$I, and the even N isotopes of $_{55}$Cs and $_{57}$La have all spin 7/2, pointing to the fact that the level $2g_{7/2}$ is regularly filled; and after the completion of this sub-shell, the protons start filling the shell $2d_{5/2}$ as is shown by the occurrence of spin 5/2 in $_{59}Pr^{141}$ and $_{63}Eu^{151,153}$.[8]

What one can thus surmise on this point from the evidences of the spin values is corroborated by the results of the mass spectrometer measurements. Duckworth *et al.*[11] have shown, by plotting the average nucleon binding energy (calculated from the packing fraction values) *vs* the mass number, that there is a kink in the curve wherever the nucleus is doubly magic; the kink is interpreted as being caused by a sudden fall in the average nucleon binding energy in the isotopes that follow. This they first showed for $_{14}Si^{30}$, $_{28}Ni^{60}$, $_{40}Zr^{90}$, $_{50}Sn^{120}$, and $_{82}Pb^{208}$; and recently they have shown this for $_{58}Ce^{140}$. We have approached the problem more directly. Instead of relying on the average binding energy, we have sought to calculate the binding energy of the last proton.

On the single particle model one can think of the β^- decay as the neutron in the topmost ground-state level emitting an electron and a neutrino, being converted into a proton, and then making a transition to the proton level, energetically permitted and most allowed. In case the allowed level is not the ground state, there is a subsequent emission of gamma-radiation. Similarly, the positron emission can be thought of as the proton emitting a positive electron and a neutrino, being converted into a neutron, and then making a transition to the neutron level energetically permitted and most allowed. On this basis then, we can write for the maximum energy of the beta-emission (including any gamma-radiation emitted in cascade)[12,13]

$$E_{\beta^-}=B_p(Z+1,A)-B_n(Z,A)-0.75 \text{ Mev}$$
$$E_{\beta^+}=B_n(Z+1,A)-B_p(Z,A)-1.77 \text{ Mev}$$
$$E_K=B_n(Z+1,A)-B_p(Z,A)-0.75 \text{ Mev},$$

where $B_p(Z,A)$ and $B_n(Z,A)$ are the binding energy of the last proton and the last neutron respectively in the isotope (Z,A). B_n and B_p values in the region of Pb have been given by Way,[14] Kinsey *et al.*,[15] and Harvey.[9] By making use of their values and the above formulas, the maximum energies of the betas can be calculated quite accurately. In the region of cerium no proton binding energies are experimentally known; but the neutron binding energies in the following have been measured:

B_n in $_{56}Ba^{137,138,139}$	7.1,[15] 8.7,[16] 5.2[9] Mev, respectively
$_{57}La^{139}$	8.8 or 9.8[16] Mev
$_{58}Ce^{140,142}$	8.7, 6.7 Mev, respectively[16]
$_{59}Pr^{141}$	9.4 or 9.8 Mev.[9]

From these values and the beta-decay data[17] we can calculate with the help of the above formula the B_p values in some of the

isotopes in this region. They come out as given below:

B_p in $_{57}La^{137,139}$ ~7 Mev
$_{58}Ce^{140,142}$ ~8 Mev
$_{59}Pr^{140,142}$ = 4.5 and 6 Mev, respectively
$_{60}Nd^{141}$ ~7 Mev.

The sudden drop in the binding energy values is exactly what is observed for the 51st and the 83rd neutrons and protons, and for the 127th neutron. One can feel, therefore, that the occurrence of a similar situation for the 59th proton is a very strong evidence in favor of the view, suggested from other considerations also, that there is a completion of the proton sub-shell $1g_{7/2}$ at $Z=58$ making $_{58}Ce^{140}$ a doubly magic isotope.

* Now at the Tata Institute of Fundamental Research for the work of the AEC.

[1] Maria G. Mayer, Phys. Rev. **74**, 235 (1948).
[2] E. Feenberg and K. C. Hammack, Phys. Rev. **75**, 1877 (1949).
[3] L. W. Nordheim, Phys. Rev. **75**, 1894 (1949).
[4] Haxel, Jensen, and Suess, Phys. Rev. **75**, 1766 (1949).
[5] M. G. Mayer, Phys. Rev. **78**, 16 (1950).
[6] W. Low and C. H. Townes, Phys. Rev. **80**, 608 (1950).
[7] H. E. Duckworth and R. S. Preston, Phys. Rev. **82**, 468 (1951).
[8] J. E. Mack, Revs. Modern Phys. **22**, 64 (1950).
[9] J. A. Harvey, Phys. Rev. **81**, 353 (1951).
[10] Tomkins, Fred, and Meggers, Phys. Rev. **84**, 168 (1951).
[11] Duckworth, Kegley, Olson, and Stanford, Phys. Rev. **83**, 1114 (1951).
[12] S. Jha, thesis, Edinburgh University, 1950.
[13] S. Jha and G. P. Dube, Indian J. Phys. (to be published).
[14] Katharine Way, Phys. Rev. **75**, 1448 (1949).
[15] Kinsey, Bartholomew, and Walker, Phys. Rev. **82**, 380 (1951).
[16] Sher, Halpern, and Stephens, Phys. Rev. **81**, 154 (1951).
[17] G. T. Seaborg and I. Perlman, Revs. Modern Phys. **20**, 585 (1948).

The Ionization Loss of Energy of Relativistic Mu-Mesons in Argon*

J. E. Kupperian, Jr., and E. D. Palmatier
Department of Physics, University of North Carolina, Chapel Hill, North Carolina

(Received January 30, 1952)

SINCE recent observations with mu-mesons[1] in dispersed media indicate an absence of the relativistic rise in the ionization loss of these particles, we have studied the variation with energy of the ionization loss of cosmic-ray mu-mesons in proportional counters filled to 1.6 atmospheres with a mixture of 97 percent argon and 3 percent CO_2.

Two proportional counters, located one above the other, were employed as an aid in the analysis of the data. A series of Geiger counter telescopes selected those vertically incident mesons which traversed at least 10 cm of Pb and both proportional counters. No path length in the proportional counters deviated from the mean path length (3.75 inches) by more than 1.5 percent. The mesons were divided into four range groups (Table I) by means of Pb absorbers and coincident counter trays, the arrangement of the various components being similar to that of Bowen and Roser.[2] The output of each proportional counter channel was displayed on a meter and photographed along with a system of lights which indicated the range tray coincidences. An important feature is the concurrent registration of data on all four range groups.

Several runs have been taken to date, all with similar results. In the table are given the final results for that run in which the greatest amount of Pb absorber was used and the greatest number of particles observed (897). We have compared the mean observed energy loss with that to be expected on the basis of a correction to allow for off scale meter readings from high energy loss fluctuations. This latter correction necessitated that we use the Landau[3] distribution.

Assuming a constant relationship between energy loss and number of ion pairs produced, we conclude that within the limits of accuracy of our measurements, the Bethe,[4] Bloch,[5] and Williams[6] theory of energy loss, as extended by Landau to account for fluctuations in the energy loss, predicts quite accurately our observed rise in energy loss with increasing energy of mu-mesons. This result for an argon-CO_2 mixture, which has previously been obtained for mu-mesons in hydrogen by shamos and Hudes with low efficiency Geiger counters containing hydrogen,[7] is quite contrary to the observations of Goodman, Nicholson, and Rathgeber who used an argon-ethylene mixture. A full report of this work is in preparation.

TABLE I. Mean energy loss of four energy groups.

Range in Pb (cm)	Energy limits (Mev)	Counter	Mean energy loss (kev) Calc.	Exptal.[a]
10.3- 30.1	160- 400	Upper	29.9	29.9±0.5[b]
		Lower	30.3	30.3±0.5[b]
30.1- 63.2	400- 840	Upper	31.3	31.7±0.4
		Lower	31.5	32.3±0.5
63.2-130.2	840-1800	Upper	33.1	33.2±0.4
		Lower	33.6	34.7±0.4
130.2-	1800-	Upper	37.3	36.7±0.4
		Lower	37.9	37.9±0.3

[a] Standard deviation.
[b] Normalized to calculated value of mean energy loss.

* Supported by the AEC.

[1] Goodman, Nicholson, and Rathgeber, Proc. Phys. Soc. (London) **A64**, 96 (1951).
[2] T. Bowen and F. X. Roser, Phys. Rev. **83**, 689 (1951).
[3] L. Landau, J. Phys. (U.S.S.R.) **8**, 201 (1944).
[4] H. Bethe, Z. Physik **76**, 293 (1932).
[5] F. Bloch, Z. Physik **81**, 363 (1933).
[6] E. J. Williams, Proc. Roy. Soc. (London) **139**, 163 (1933).
[7] M. H. Shamos and I. Hudes, Phys. Rev. **84**, 1056 (1951).

Transmission and Spectral Response of Lead Sulfide and Lead Telluride*

M. A. Clark and R. J. Cashman
Northwestern University, Evanston, Illinois

(Received January 28, 1952)

THE spectral response of lead sulfide and lead telluride photoconductive films has been known for some time. These compounds, as well as thallous sulfide and lead selenide, have been found to produce photoconductive layers with sensitivity in the

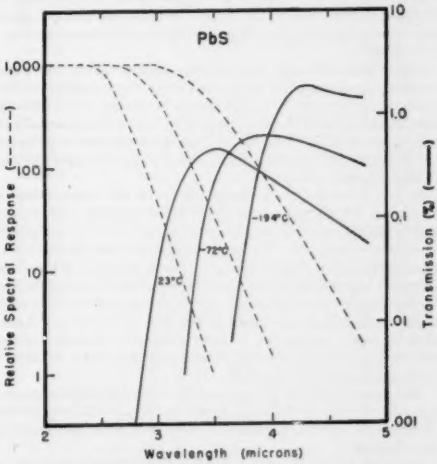

FIG. 1. Transmission of lead sulfide crystal, thickness 0.48 mm. Relative spectral response of lead sulfide photocells.

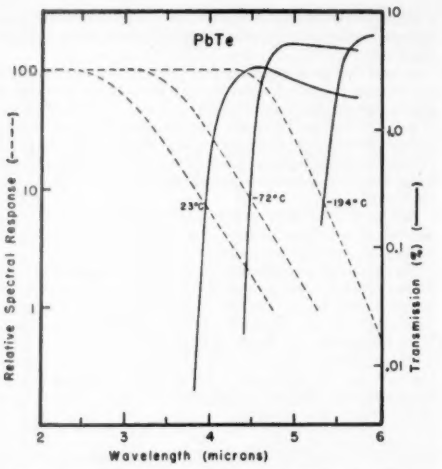

FIG. 2. Transmission of lead telluride crystal, thickness 0.11 mm. Relative spectral response of lead telluride photocells.

near infrared region greatly exceeding that attainable by any other means.

The spectral response of all these compounds is characterized by a fairly sharp edge defining a long wavelength threshold energy. Until recently these edges had not been correlated with any other property of the materials. Conductivity *versus* temperature plots have indicated thermal activation energies at high temperatures considerably greater than the threshold energies of the photoconductivity.[1] Since the Franck-Condon principle requires that the thermal activation energies be no greater than the optical activation energies, the thermal activation energies that have been observed must relate to energy levels other than those excited by photons with energy near the spectral response edge. Absorption data[1] for the photoconductive films do not show an abrupt change in absorption at the wavelength at which the spectral response is changing rapidly. Absorption edges do appear at shorter wavelengths, and these may correspond to the reported thermal activation energies.

Transmission through natural lead sulfide (galena) at room temperature showing an absorption edge corresponding to the spectral response edge of the photoconductive layers has recently been reported.[2] Recent measurements of the optical constants of bulk galena and lead telluride confirm the absorption edge found in the layers but do not include the wavelength region of the photoconductive threshold.[3]

In Fig. 1 we show our measurements of the transmission of galena for various temperatures of a typical sample. The characteristic spectral response of photoconductive layers of lead sulfide or of photovoltaic point contacts on galena are given at the corresponding temperatures for reference. The dependence of threshold energy on temperature is the same but a threshold is more sharply defined by the transmission experiment. Measurements have been made on numerous samples of galena and synthetic lead sulfide single crystals. At present it appears that the absorption edges and corresponding photoconductive thresholds shown in Figs. 1 and 2 are caused by impurities.

The transmission of a single crystal of lead telluride prepared here by Mr. N. S. Dallas is shown in Fig. 2. Here again the characteristic spectral response of photoconductive layers is given for reference.

For both the lead sulfide and the lead telluride the shift of threshold energy is about $+3.8\times10^{-4}$ ev/deg K. This is a little less than has been determined previously from the spectral response. Shifts of the same order of magnitude but opposite in sign are found for silicon and germanium.

A complete report of this research is in preparation.

[*] This work was sponsored by the Department of the Navy, Bureau of Ships, Washington 25, D. C.
[1] R. P. Chasmar and E. H. Putley, Conference on Semi-Conducting Materials, edited by H. K. Henisch (Butterworth's Scientific Publications, London, 1951), p. 208.
[2] Paul, Jones, and Jones, Proc. Phys. Soc. (London) **B64**, 528 (1951).
[3] D. G. Avery, Proc. Phys. Soc. (London) **B64**, 1087 (1951).

Critical Velocity of Superflow in Liquid Helium II

H. M. FRIED[*] AND P. R. ZILSEL
University of Connecticut, Storrs, Connecticut
(Received December 21, 1951)

IT is generally known that the limit on the validity of a linear description of stationary flow through narrow slits or capillaries in helium II may be expressed, within experimental accuracy, by a limiting condition on the superflow velocity,

$$v_s d < 10^{-4} - 10^{-3}\ \text{cm}^2/\text{sec}, \tag{1}$$

where d = width (radius) of the slit (capillary). For v_s much larger than the limit given by (1), both the heat current and the fountain pressure are proportional to $(\Delta T)^4$ instead of to (ΔT).

Gorter[1] has proposed to account for this situation by introducing *ad hoc* a mutual friction term between the normal and the superfluid proportional to v^3 (v = relative velocity of the two fluids) into otherwise linear equations of motion of the two fluid model. This conception involves dissipation of the superflow and is, therefore, in contradiction to basic ideas on the nature of the superfluid state expressed by Landau[2] and London.[3]

It appears, however, that from the nonlinear equations of motion derived by Zilsel[4] the condition (1) can be understood without the introduction of any additional terms, except for the ordinary linear viscous friction of the normal fluid. For the case of stationary heat flow one has, eliminating grad$P$ from Eqs. (2.18) and (2.20′) of reference 4,

$$\rho S\ \text{grad}T = -\eta_n[\text{curl curl}\mathbf{v}_n - (4/3)\ \text{grad div}\mathbf{v}_n] - \tfrac{1}{2}\rho_n\ \text{grad}v^2 - v\Gamma + \rho_n[(\mathbf{v}_s\cdot\text{grad})\mathbf{v}_s - (\mathbf{v}_n\cdot\text{grad})\mathbf{v}_n], \tag{2}$$

where η_n is the coefficient of viscosity of the normal fluid. In the limit of small velocities the solution was obtained by London and Zilsel,[5] giving for a slit of width d (flow in the z direction; slit width in the x direction)

$$v_n = \tfrac{3}{2}v_n(1-4x^2/d^2), \quad v_n = -\frac{d^2}{12}\frac{\rho S}{\eta_n}\frac{\partial T}{\partial z}. \tag{3}$$

After substituting this into (2) one sees that the z component of (2) balances but that the term gradv^2 has an x component indicating a breakdown of the linear approximation. Using the condition of no total flow, $\rho_n v_n + \rho_s v_s = 0$, one finds for the average absolute value of this term

$$\tfrac{1}{2}\left\langle \rho_n \left|\frac{\partial v^2}{\partial x}\right| \right\rangle_{Av} = \frac{\rho S}{4\eta_n}\left|\frac{\partial T}{\partial z}\right|(\rho - \tfrac{1}{2}\rho_s)v_s d. \tag{4}$$

To estimate the effect of (4) we introduce a $\partial T/\partial x$ to balance Eq. (2):

$$\left\langle \left|\frac{\partial T}{\partial x}\right| \right\rangle_{Av} = \left|\frac{\partial T}{\partial z}\left(\frac{\rho - \tfrac{1}{2}\rho_s}{4\eta_n}\right)v_s d\right|. \tag{5}$$

The magnitude of (5) is a measure of flow perpendicular to the z direction; we can expect the linear approximation to be valid as long as $|\langle\partial T/\partial x\rangle_{Av}/(\partial T/\partial z)| < 1$, or

$$v_s d < 4\eta_n/(\rho - \tfrac{1}{2}\rho_s) \approx 5\times10^{-4}\ \text{cm}^2/\text{sec}. \tag{6}$$

We see that the limiting condition arises from the gradv^2 term in the equations of motion, the existence of which was first pointed out by Landau.[2]

Detailed calculations for the supracritical region are in progress. We are indebted to the Research Corporation for financial support.

* Frederick Gardner Cottrell Fellow.
[1] C. J. Gorter, Physica **15**, 523 (1949).
[2] L. Landau, J. Phys. U.S.S.R. **5**, 71 (1941).
[3] F. London, Phys. Soc. Cambridge Conference Report (1947), p. 1.
[4] P. R. Zilsel, Phys. Rev. **79**, 309 (1950).
[5] F. London and P. R. Zilsel, Phys. Rev. **74**, 1148 (1948).

A Test for the Charge-Symmetry Hypothesis

RICHARD L. GARWIN
Institute for Nuclear Studies, University of Chicago, Chicago, Illinois
(Received January 31, 1952)

YANG has recently suggested[1] an experiment to test the charge-symmetry hypothesis in the coupling of mesons to nucleons. The proposed experiment is to study the following pair of reactions

$$p+p\rightarrow d+\pi^+ \tag{1a}$$
$$n+p\rightarrow d+\pi^0. \tag{1b}$$

These reactions have the advantage over those studied so far in that only one isotopic spin state of the nucleons in the initial state can contribute to the reactions if isotopic spin is conserved, i.e., if it is a good quantum number. The simple argument here is that since a nucleon in the theory of isotopic spin is defined by four variables (position, momentum, spin S, and isotopic spin I) and is a fermion, then the total wave function of a pair of nucleons must be antisymmetric. Now, since the deuteron has an even space wave function and a symmetric spin function, the isotopic spin function must be antisymmetric. The only odd isotopic spin function for two isotopic spins $\frac{1}{2}$ is that one with total $I=0$. Therefore, the final state of (1a) has $I=1$ (that of the pion, with $I_z=+1$ for π^+, 0 for π^0, and -1 for π^-) and $I_z=+1$. Thus the two protons in the initial state have total $I=1$ and $I_z=+1$. Likewise in (1b) the two nucleons have $I=1$, $I_z=0$. Since the statistical probabilities of these total spin orientations are equal, these two reactions (granting the charge-symmetry hypothesis) must have the same angular distributions, and cross sections differing exactly by a factor 2 (since only half of the state $n+p$ is the required isotopic triplet).[2]

It is the purpose of this note to point out two other reactions which give as good a test of charge-symmetry, are probably considerably easier experimentally, and in addition measure the interaction of pions and mesons in states of total isotopic spin $\frac{1}{2}$—a question in which there is considerable interest as the result of recent scattering measurements[3] which have been interpreted[4] as interactions through a resonance state of total isotopic spin $\frac{3}{2}$. The two reactions are really the two branches of the reaction

$$p+d\rightarrow d+n+\pi^+ \tag{2a}$$
$$p+d\rightarrow d+p+\pi^0. \tag{2b}$$

These reactions are the two possible breakups of a proton catalyzed by the presence of the deuteron which absorbs the extra momentum.

Here again the deuteron with $I=0$ forces the initial state to have $I=\frac{1}{2}$, $I_z=+\frac{1}{2}$, as must the final state. Therefore the odd nucleon and the pion must be in a state with $I=\frac{1}{2}$, $I_z=+\frac{1}{2}$, instead of the usual variety of states available to a nucleon and a pion. So we see that the branching ratio should be 2:1, with identical angular distributions, etc. The factor 2 comes again from the fact that the interaction leads only to a final state $I=\frac{1}{2}$, $I_z=+\frac{1}{2}$. Thus, the square of the matrix elements must be reduced to the fraction of $I=\frac{1}{2}$ contained in the ordinary $I_z=+\frac{1}{2}$ state. This is $\frac{2}{3}$ for $n+\pi^+$ and $\frac{1}{3}$ for $p+\pi^0$.

Since there are three particles in the final state one must investigate not only the angle of emission of the π^+ or p, but the energy also (or the angles of the light charged particle and the deuteron also). In a cloud chamber with magnetic field, one of the easiest things to do is to measure the energy spectrum of deuterons accompanied by positive pions in (2a) or by inelastically scattered protons as in (2b).

[1] C. N. Yang, unpublished communication to C. Richman.
[2] See also the general paper by K. M. Watson and K. A. Bruechner, Phys. Rev. **83**, 1 (1951).
[3] H. L. Anderson, Bull. Am. Phys. Soc. **26**, No. 6, 33 (1951).
[4] K. A. Brueckner, Bull. Am. Phys. Soc. **27**, No. 1, 51 (1952).

A Proposed Test of the Nuclear Shell Model

H. A. BETHE AND S. T. BUTLER
Laboratory of Nuclear Studies, Cornell University, Ithaca, New York
(Received February 5, 1952)

IN this note we wish to suggest certain experiments which should give direct information concerning the accuracy of the independent particle model of nuclear structure[1] in ascribing definite orbital angular momentum states to nucleons in a nucleus.

Interpretation of the angular distributions from (d, p) and (d, n) nuclear reactions[2] has shown these reactions to proceed mainly by means of a stripping process, the angular distribution of the outgoing particle in any one case being characterized by the orbital angular momentum l with which the captured particle can be accepted into the appropriate final state. The angular distributions all show a pronounced peak at small angles, this maximum lying directly forward if $l=0$, but moving progressively towards larger angles as l is increased. Also, if more than one value of l is allowed by the selection rules in a particular case, and if the initial nucleus should be indifferent as to which of these values it accepts, then it is found that the maximum in the angular distribution which is nearest the forward direction, i.e., which results from the smallest allowed l, is of much larger magnitude than the others; there is, in fact, an order of magnitude decrease in the heights of the maxima as l is increased by 2 (the allowed values of l in any one case being either all even or all odd).

According to the shell model, however, the initial nucleus will accept a particle only in a certain definite orbital angular momentum state. Although the lowest allowed l usually coincides with the value required by the shell model, there are some instances where the reverse is true, i.e., where the shell model l value is 2 units higher than the lowest value allowed by the selection rules. It is in these latter cases that we are interested. If the shell model were precise, the experimental angular distributions for such cases should show no evidence of the maximum nearest the forward direction which would be expected to be present on the grounds of selection rules alone; on the other hand, there has to be only a very small deviation from the shell model before this peak in the angular distribution is as large as the following one. The angular distributions will therefore effectively amplify by a factor $\sim$10 any admixture of the lower orbital angular momentum state in the wave function of the final nucleus, as well as any admixture of states in the initial nucleus which allow the low orbital angular momentum transfer. Such angular distributions should, therefore, provide a sensitive measure of the accuracy with which a nucleon in a nucleus can be ascribed a definite orbital angular momentum.

Some examples of reactions which satisfy the above requirements, and for which therefore it would be very desirable to have experimental angular distributions, are given in Table I. These refer to formation of the final nuclei in ground states only, since the shell model cannot be expected to give the precise ordering of excited states. In choosing such examples it is, of course, important that the lowest allowed angular momentum does not correspond to an independent particle level which is so very little separated from the predicted ground level that the two could very easily cross. Such a state of affairs occurs, for example, in the shell with neutron or proton numbers between 8 and 20 where the ordering of levels is in general $d_{3/2}$, $s_{1/2}$, $d_{5/2}$, but where the $d_{3/2}$ and $s_{1/2}$ levels are very little separated and are known in fact to

TABLE I. Some examples of stripping reactions whose angular distributions should give direct information concerning the accuracy of the independent particle model of nuclear structure.

Reaction	Spin and parity Initial	Final	Required by shell model	l Allowed values
(1) $P^{31}(d, p)P^{32}$	1/2+	1+	2	0 and 2
(2) $Cl^{36}(d, p)Cl^{38}$	3/2+	2+	2	0, 2, and 4
(3) $Cl^{37}(d, p)Cl^{38}$	3/2+	2−	3	1 and 3
(4) $K^{40}(d, p)K^{42}$	3/2+	2−	3	1 and 3
(5) $Sc^{46}(d, p)Sc^{48}$	7/2−	4+	3	1, 3, 5, and 7
(6) $V^{51}(d, p)V^{52}$	7/2−	2 or 3+	3	1, 3, 5 (and 7)

cross on a number of occasions. In the region where the $d_{5/2}$ levels are being filled, therefore, if a reaction which is expected on the shell model to require an orbital momentum transfer of $l=2$ in fact shows strong evidence of an $l=0$ change, the reason might well be merely that for the case considered the $d_{5/2}$ and $s_{1/2}$ levels have crossed.

Near the end of the shell just discussed, however, when the $d_{5/2}$ and $s_{1/2}$ levels have all been filled, there should be no such difficulty, and it is in this region that our first two examples lie. These should be particularly good cases for our purpose since the next $s_{1/2}$ orbits on the independent particle model lie very much higher in energy than the ground state $d_{3/2}$ levels. Examples (3), (4), and (5) correspond to filling the $f_{7/2}$ shell in the region $20<N\leqslant 28$, and the aim of the experiments would be to detect any p admixture in the predicted $f_{7/2}$ orbital states. These again should be clear-cut cases, since the next p levels occur in a higher shell. The last example, however, lies in the region $28<N<38$ where the $f_{5/2}$ and $p_{3/2}$ levels have about the same energy, and this case must therefore be considered as doubtful. On Nordheim's rule[3] it is perhaps more likely that a spin of 2 or 3 for V^{52} be produced by a combination of the $f_{7/2}$ state for the odd proton with an $f_{5/2}$ rather than a $p_{3/2}$ state for the odd neutron, but this is of course not certain.

In order that, in the angular distributions, there be appreciable separation between the peaks of interest, the most favorable incident deuteron energy is probably about 10–15 Mev. For these energies, the transition $l=2$ in our first two examples will produce a maximum at about 20–30 degrees from the forward direction, whereas that for the $l=0$ transition will lie directly forward; in the other cases the $l=3$ transition will produce a peak at about 35–45 degrees, while the maximum resulting from $l=1$ will be at angles of about 5–15 degrees. Moreover, if the probability of the smaller angular momentum transfer be only 1/10th the probability of the transfer required by the shell model, the two resulting maxima will be of approximately the same height.

We are indebted to Dr. Maurice Goldhaber for supplying us with information concerning the spins of the odd-odd nuclei employed in our examples.

[1] Maria Goeppert Mayer, Phys. Rev. **78**, 22 (1950).
[2] S. T. Butler, Phys. Rev. **80**, 1095 (1950); and Proc. Roy. Soc. (London) **A208**, 559 (1951).
[3] L. W. Nordheim, Phys. Rev. **78**, 294 (1950).

Radiations of Rh^{99}, Rh^{101}, Rh^{105}, and Ru^{105}

C. L. SCOVILLE,* S. C. FULTZ,† AND M. L. POOL
Ohio State University, Columbus, Ohio
(Received January 9, 1952)

RUTHENIUM metal of high purity was bombarded with 6.3-Mev protons and 10-Mev deuterons and the spectra of the activities obtained were examined in a 180° beta-ray spectrometer. The spectrometer sources consisted of the activated metal spread out evenly on thin Zapon foil ribbons. The source and backing had a thickness of about 15 mg/cm². The spectra were scanned in the spectrometer at suitable intervals of time. By correcting for decay the component spectra were separated.

Both the positron and negatron spectra were examined when the ruthenium metal was bombarded with protons. The positron spectra of 4.5-hour Rh^{99} and 19-hour Rh^{100} were observed. A Kurie plot of the corrected positron spectrum of Rh^{99} indicated that the spectrum is allowed and probably simple, having an end-point energy of 0.74±0.01 Mev, for which the log(ft) value is 4.95. No gamma-rays of 4.5-hour half-life were observed. The intensity of the Rh^{100} positrons was not sufficiently high to give a reliable Kurie plot. Examination of the negatron spectrum showed the presence of several well-defined internal conversion peaks, decaying with a half-life of 4.5 days. These peaks were attributed to K and L conversion electrons from gamma-rays of Rh^{101}. The energies of the corresponding gamma-rays are 0.148±0.005 and 0.300±0.005 Mev. The former value is in fair agreement with 0.13 Mev previously reported[1] from beta-ray spectrograph measurements, and the latter roughly agrees with the value 0.35 Mev reported from lead-absorption measurements.[2]

With deuteron bombardment of ruthenium two negatron spectra with half-lives of 4.5 hours and 36 hours were observed. The 4.5-hour activity is attributed to Ru^{105} which is obtained by a (d, p) reaction on Ru^{104}. A Kurie plot of the corrected Ru^{105} negatron spectrum indicated a simple spectrum of allowed shape. The end-point energy is 1.15±0.02 Mev. The 36-hour activity was attributed to Rh^{105} obtained by the reaction $Ru^{104}(d, n)Rh^{105}$ and by negatron decay of Ru^{105}. A Kurie plot of the corrected Rh^{105} spectrum indicated a simple spectrum also of allowed shape. The end-point energy is 0.57±0.01 Mev. The above results for Ru^{105} and Rh^{105} spectra are in agreement with those obtained by Duffield and Langer.[3] High internal conversion peaks at 1140 and 1250 gauss-cm with half-life of less than 6 hours were found superposed on the negatron spectra. These peaks are believed to be K and L conversion lines from a gamma-ray of Rh^{105}.[3] The corresponding energy of the gamma-ray is 0.127±0.005 Mev.

* Major, U.S.A.F. Now at Washington, D. C. Research under auspices of USAFIT, Wright Patterson Air Force Base, Dayton, Ohio.
† Fellow, National Cancer Institute, National Institutes of Health, Federal Security Agency.
[1] D. Eggen and M. L. Pool, Phys. Rev. **75**, 1464 (1949).
[2] B. M. Lindner and I. Perlman, Phys. Rev. **73**, 1202 (1948).
[3] R. B. Duffield and L. M. Langer, Phys. Rev. **81**, 203 (1951).

Energy Absorption During Twin Formation in Zinc Single Crystals*

E. I. SALKOVITZ
Electric and Magnetic Alloys Branch, Metallurgy Division, Naval Research Laboratory, Washington, D. C.
(Received December 3, 1951)

THE energy absorbed during the formation of twins in single crystals of 99.999 percent pure zinc was measured by means of ballistic pendulums in a manner first used by Chalmers[1] to measure the twinning energy in tin. The method was also used by the present author in measuring the energy absorbed during kink formation in zinc and cadmium.[2] It should be noted that in the very early stages of the latter work the kinks were thought to be twins and were erroneously reported as such.[3]

The single crystals were grown in a vacuum using a Bridgeman-type furnace. In order to study twin formation by impact it is necessary to have the (0001) plane nearly normal to the specimen axis. Using the Bridgeman technique the author had previously found that most of the crystals grew with the (0001) plane nearly parallel to the specimen axis.[3] In the current work, however, it has been possible to produce crystals with the (0001) plane nearly normal to the specimen axis by making short right angle bends in the Pyrex crucibles just beyond the seed point of the crucible. The crystals grown in this manner were rods 15 to 30 cm long and about 6 mm in diameter with the basal plane (0001) within 16° of the normal to the specimen axis. These rods were sectioned into lengths of about 2.5 cm for the twinning experiments.

As indicated in metallurgical literature, twins when produced in compression in pure zinc are rather narrow and frequently do not

extend completely across the diameter of the specimen. The twins obtained in the first few crystals tested were extremely fine in size and did not extend very far below the surface. Data were obtained, however, on several succeeding crystals for which the volumes of the twins produced could be measured to an accuracy of approximately 25 percent. The results are compiled in Table I.

TABLE I. Energy absorbed per unit volume of twins. ϕ = angle between specimen axis and the normal to the basal plane.

Temp.	Crystal	ϕ	Energy absorbed per unit volume of twins, in ergs/cc
20°C	*FF*-1	15½°	38×10^6
20°C	*FF*-2	15½°	27×10^6
−180°C	*GG*-3	7°	38×10^6
20°C	*GG*-1	7°	5×10^6
20°C	*GG*-2	7°	2×10^6
200°C	*GG*-4	7°	$<1\times10^6$

The first two specimens were cut from the same single crystal, while the last four were cut from another. The tests were run at the temperatures indicated. At 200°C, unfortunately, an extremely large number of fine twins were produced whose volume could not be measured. Nevertheless, the indication was that less energy per unit volume of twin was absorbed at this temperature.

The data taken on crystals *FF*-1 and *FF*-2 at 20°C agree well within an order of magnitude; the same is true for crystals *GG*-1 and *GG*-2. It is therefore believed that the differences in the values of energy absorbed per unit volume of twins for the two orientations are significant and the following conclusions may be drawn:

(1) At room temperature the energy absorbed in twins produced by impact is less, the closer the basal plane approaches being normal to the specimen axis.

(2) As the temperature is decreased the energy absorbed seems to increase. This would agree with the work of Davidenkov *et al.*,[4] who showed that the resistance to twinning under tension increased with decreasing temperature. Obviously there are insufficient data to indicate the exact relationship.

I wish to thank Mr. F. W. VonBatchelder for determining the orientations of the above crystals.

* The opinions expressed in this paper are those of the author, and not necessarily the Navy Department.

[1] B. Chalmers, Proc. Phys. Soc. (London) **47**, 733 (1935).
[2] E. I. Salkovitz, Summer (1950) Meeting, American Crystallographic Association (to be submitted to Journal of Applied Physics).
[3] E. I. Salkovitz and J. S. Koehler, Phys. Rev. **77**, 749 (1950).
[4] Davidenkov, Kolsnikov, and Fedorov, J. Exptl. Theoret. Phys. (U.S.S.R.) **3**, 350 (1933).

Zeeman Effect and Hyperfine Splitting of Positronium*

MARTIN DEUTSCH AND SANBORN C. BROWN
Department of Physics, Laboratory for Nuclear Science and Engineering, and Research Laboratory of Electronics, Massachusetts Institute of Technology, Cambridge, Massachusetts

(Received February 6, 1952)

THE effect of a magnetic field on the ground state doublet of positronium may be calculated from the Breit-Rabi formula. The result, first published by Berestetskii,[1] is illustrated in Fig. 1. The hyperfine splitting ΔW, here of the order of the fine structure, can be obtained from the frequencies of transitions between the magnetic levels as in the case of the other hydrogen isotopes.[2] Because of the high rate of annihilation the lines are wide and rf fields of several gauss are required to obtain observable transition rates. Therefore, the transitions with $\Delta F=1$ which occur near 200,000 Mc/sec are beyond the power of established techniques. We have observed the line $(1,\pm1)\rightarrow(1,0)$ in a field of about 9000 gauss at a frequency of 3000 Mc/sec. According to Fig. 1 this frequency is given by $\nu=(\Delta W/2h)((1+x^2)^{\frac{1}{2}}-1)$, where $x=4\mu_0 H/\Delta W$.

The transition was detected by the increase, at resonance, of two-photon annihilation relative to the three-photon process.

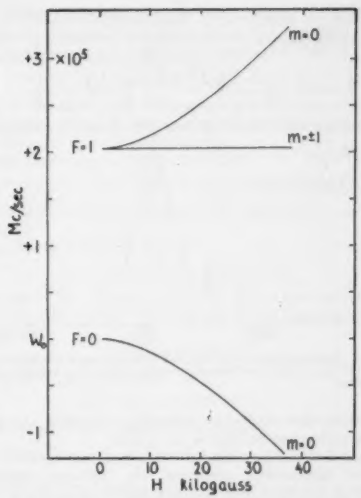

FIG. 1. Positronium levels in a magnetic field. The energies of the levels with respect to the unperturbed singlet state are given by: $W-W_0=(\Delta W/2)[1+mx\pm(1-2mx+x^2)^{1/2}]$; where $x=4\mu_0 H/\Delta W$.

In a magnetic field of the magnitude used, there is sufficient admixture of singlet component to the (1, 0) level to make two-quantum decay predominant. The states (1, 1) and (1, −1) always decay into three photons. This quenching by the magnetic field was discussed in an earlier communication.[2] Induced transitions from (1, ±1) to (1, 0) will result in additional quenching. To an accuracy sufficient for our purpose, the fraction ϕ of the (1, ±1) atoms quenched at resonance by an rf field of amplitude H' perpendicular to H is given by $\phi\cong(\mu_0 H'/\pi h)^2\lambda_0/\lambda_p$, where λ_0 and λ_p are the unperturbed decay rates of the ortho- and para-states, respectively. For $H'=5$ gauss, $\phi\cong0.1$. The fractional width of the line due to the annihilation process is $\gamma/\nu\cong\lambda_p h/2\pi\Delta W=6.2\times10^{-9}$. In our experiments H is varied rather than ν. The observed width should then be $\Delta H/H=\gamma/2\nu=3.1\times10^{-9}$. These expressions for ϕ and γ are also valid for the transitions with $\Delta F=1$. More exact expressions will be given in a more extensive later communication. There we shall also discuss reasons for believing that other causes of line width should be small compared with the annihilation width.

A source of a few millicuries of Cu^{64} was electroplated at the center of one of the end plates of a cylindrical high Q cavity driven in the $TM(110)$ mode. The cavity was placed with its axis parallel to the magnetic field which confined the positrons to a beam of about 3 cm diameter. Extensive lead collimation assured that the gamma-ray detector used counted only radiation from annihilations occurring in the gas near the center of the cavity. In this region the magnetic field deviated no more than ±10 gauss from its value at the center. Most of the rf transitions probably occurred near the middle of this region where the field is very uniform. The quenching was observed by measuring the gamma-ray scintillation spectrum as in the experiments of Deutsch and Dulit,[3] and in one run also by the gamma-ray coincidence rate at 180°. Under our experimental conditions the former method proved more sensitive. A statistically significant run could be obtained in about two hours. An unexpected complication arose from the fact that the high rf fields (about 1000 v/cm) used increase the amount of positronium formed, probably by accelerating some slow positrons to the energy required for electron capture. In argon, where the energy required for inelastic scatter-

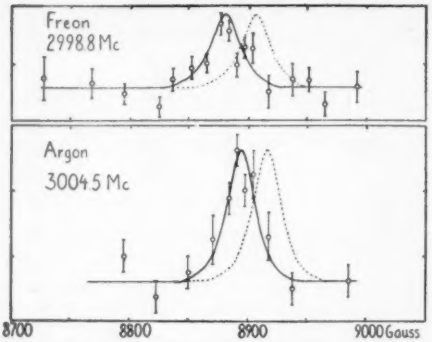

FIG. 2. Radiofrequency quenching of three-quantum annihilation. The dotted curves indicate the theoretical position of the line without radiative corrections.

ing is above that required for positronium formation, the amount of positronium was doubled by the rf field.

Figure 2 shows the results of two typical runs obtained under different experimental conditions. The ordinates represent a parameter extracted from the data roughly proportional to the amount of two-quantum annihilation. The solid curves are drawn with the theoretical width with the location and height of the peak fitted to the data. The height, corresponding to $\phi=0.06$, is slightly less than expected but within the uncertainty of the estimate; the observed width, although very uncertain, does not seem to be much larger than the theoretical value. From the average of five runs like those shown in Fig. 2 we calculate the hyperfine splitting $\Delta W/h=2.032\pm0.003\times10^9$ Mc/sec. This compares with the value 2.044×10^9 Mc/sec calculated from the expression $\Delta W=7\mu_0^2/3a_0^3$ given by Pirenne[4] and Berestetskii.[1] The dotted curves in Fig. 2 show the expected location of the line for this value of ΔW. First results of a new and fairly complex experiment may always be affected by unsuspected systematic errors but it seems very probable that the observed shift of -1200 ± 300 Mc/sec is at least partly real. Both ΔW and the magnetic energy are subject to corrections of the order of α/π. Ferrell[5] has calculated some of the corrections to ΔW and the interaction with the field must be corrected at least by multiplying μ_0 in the expression for x above by $(1+\alpha/2\pi)$. When all known corrections are thus considered the line is shifted by about -4 gauss compared with an observed shift of -27 ± 7 gauss. Other corrections of comparable magnitude still remain to be calculated, however.

Improvements in field homogeneity, higher rf power and provision for circular polarization will be used to extend our results and to search for the structure of excited states. We wish to thank Professor F. Bitter for permission to use the large magnet.

* Supported in part by the AEC, ONR, the Signal Corps, and the Air Materiel Command.
[1] V. B. Berestetskii and L. D. Landau, J. Exptl. Theoret. Phys. (U.S.S.R.) **19**, 673, 1130 (1949).
[2] J. E. Nafe and E. B. Nelson, Phys. Rev. **73**, 718 (1948).
[3] M. Deutsch and E. Dulit, Phys. Rev. **84**, 601 (1951).
[4] J. Pirenne, Arch. sci. phys. et nat. **29**, 207 (1947).
[5] R. A. Ferrell, thesis, Princeton University, Princeton, New Jersey (1951).

Multiple Gamma-Ray Scattering in Lead

J. O. ELLIOT, R. T. FARRAR, R. D. MYERS, AND C. F. RAVILIOUS
Electricity Division, Naval Research Laboratory, Washington, D. C.
(Received January 28, 1952)

SPENCER and Fano[1] have published solutions of the general transport equation for the propagation of gamma-rays through an infinite medium. Their method of solution depends upon the fact that the moments $b_{ln}(\lambda)$ of the photon distribution can be found by a chainwise solution of a set of integral equations, which for a point isotropic source are

$$(2l+1)^{-1}[(l+1)(l-n)b_{l+1,n-1}(\lambda)-l(l+n+1)b_{l-1,n-1}(\lambda)] = -\mu(\lambda)b_{ln}(\lambda)+\int_0^\lambda d\lambda' k(\lambda',\lambda)P_l(1-\lambda+\lambda')b_{ln}(\lambda') + \text{source term.} \quad (1)$$

A knowledge of the $b_{ln}(\lambda)$ enables one to calculate the energy distribution of photons as a function of the distance from the source.

This approach was used with success by Spencer and Fano[2] to explain the data of White[3] for the case of a point isotropic Co^{60} source in water.

In the present work, calculations have been made by this method to obtain the distribution function in lead in order to check the consistency of the theoretical predictions with experimental build-up factors measured in lead. A cylindrical pellet (1 cm in diameter and 1 cm in length) containing 2.74 curies of Co^{60} was used as a source in the experiment. The scattering medium was composed of antimony-hardened lead bricks; chemical analysis of the bricks showed an average of 2.89 percent antimony present. Du Pont 552 x-ray film was used as a detector; the blackening of this film per roentgen is known[4,5] to be the same for all photon energies from the Co^{60} primary energies down to approximately 0.2 Mev. The experimental build-up factor, defined as the ratio of the total film blackening to that expected from narrow-beam absorption coefficient calculations, was measured at various distances from the source; the results of two such runs are shown in Fig. 1.

To simplify the source term for the numerical integrations required in Eq. (1), the photons were separated into two classes in the following manner:

$$N(r,u_r,\lambda)=N'(r,u_r,\lambda)+\sum_i \frac{e^{-\mu(\lambda)r}}{4\pi r^2}\frac{\delta(1-u_r)}{2\pi}\delta(\lambda-\lambda_i), \quad (2)$$

where $N'(r,u_r,\lambda)$ represents those photons which have been scattered at least once and the remaining term is the direct beam. This separation leads to

$$(2l+1)^{-1}\{(l+1)(l-n)b_{l+1,n-1}'(\lambda)-l(l+n+1)b_{l-1,n-1}'(\lambda)\} = -\mu(\lambda)b_{ln}'(\lambda)+\int_0^\lambda d\lambda' k(\lambda,\lambda')P_l(1-\lambda+\lambda')b_{ln}(\lambda') + \sum_i \frac{n!}{\mu^{n+1}(\lambda_i)}k(\lambda,\lambda_i)P_l(1-\lambda+\lambda_i), \quad (3)$$

where the $b_{ln}'(\lambda)$ now represent the moments of the photons scattered at least once.

For the present experiment the distribution function for scattered photons at a distance r, including photons arriving in all directions, was computed using the first four moments $b_{0n}'(\lambda)$.

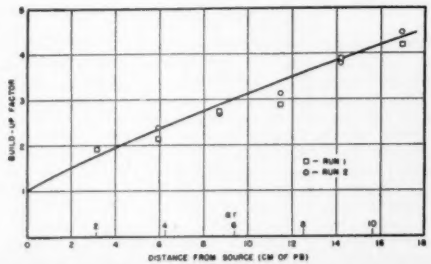

FIG. 1. Build-up factor in lead for a Co^{60} point isotropic source as measured by duPont 552 photographic film. The solid curve represents the calculated build-up factor.

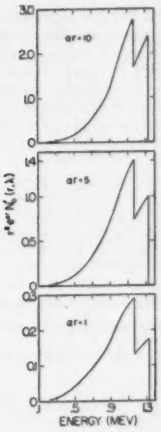

FIG. 2. Energy distribution of scattered photons in lead for a Co^{60} point isotropic source.

The numerical integrations were carried out, using the trapezoidal rule, from 0.384 Compton units (1.33 Mev) to 2.384 Compton units (approximately 213 kev) in twenty equal wavelength steps. The values of $\mu(\lambda)$ in Eq. (3) were obtained from an experimental curve based on available data[5-8] for gamma-ray scattering in lead; in addition, these values were corrected to take into account the stated antimony content. The distribution functions thus calculated are shown for three different distances in Fig. 2.

The build-up factor for the scattered radiation as measured by the photographic film can be obtained from Fig. 1 by

$$B'(r)=\int Q(\lambda)N_0'(r,\lambda)d\lambda \Big/ \sum_i \left[Q(\lambda_i)\frac{e^{-\mu_i r}}{4\pi r^2}\right], \tag{4}$$

where $Q(\lambda)$ is the blackening of the film per photon. The total build-up factor measured by the film is then

$$B(r)=1+B'(r); \tag{5}$$

this calculated build-up factor is shown as the solid curve in Fig. 1.

[1] L. V. Spencer and U. Fano, J. Research Natl. Bur. Standards **46**, 446 (1951).
[2] L. V. Spencer and U. Fano, Phys. Rev. **81**, 464 (1951).
[3] G. R. White, Phys. Rev. **80**, 154 (1950).
[4] L. S. Taylor, Brit. J. Radiology **24**, 67 (1951).
[5] E. Storm, Los Alamos Report 1220 (1951).
[6] S. A. Colgate, private communication of unpublished data.
[7] C. M. Davisson, Phys. Rev. **81**, 404 (1951).
[8] M. T. Jones, Phys. Rev. **50**, 110 (1936).

Bernoulli's Theorem for Viscous Fluids

J. J. VAN DEEMTER
Koninklijke/Shell-Laboratorium, Amsterdam, Netherlands
(Received January 21, 1952)

WITH reference to the papers of Truesdell,[1] and Etkin and Szebehely,[2] I should like to draw attention to another form of Bernoulli's theorem for viscous fluids.

Bernoulli's theorem for a nonviscous, no-heat conducting fluid may be deduced in two ways, viz., by putting the impulse equation into a proper form, or by taking the dot product of the impulse equation by $\mathbf{v}$ thus forming an energy equation.

The former method has been extended to a viscous fluid by the aforementioned authors. The latter method has been followed by Madelung[3] and to some extent by Lohr.[4] Madelung, however, confines himself to steady flow and moreover neglects extraneous forces and heat conductivity. In the present paper the derivation of Madelung is extended to any motion of a general viscous fluid.

We start from the general impulse equation

$$\rho D\mathbf{v}/Dt=\rho\mathbf{f}-\nabla p+\nabla\cdot(2\mu\,\mathrm{def}\mathbf{v}+\lambda I\nabla\cdot\mathbf{v}), \tag{1}$$

where ρ is the density, p is the pressure, $\mathbf{f}$ is the extraneous force per unit mass, $\mathrm{def}\mathbf{v}$ is the deformation tensor, I is the unit tensor, and λ and μ are coefficients of viscosity.

Taking the dot product of (1) by $\mathbf{v}$ gives

$$\rho D(\tfrac{1}{2}\mathbf{v}^2)/Dt=\rho\mathbf{v}\cdot\mathbf{f}-\mathbf{v}\cdot\nabla p+\nabla\cdot(2\mu\mathbf{v}\cdot\mathrm{def}\mathbf{v}+\lambda\mathbf{v}\nabla\cdot\mathbf{v})-\Phi, \tag{2}$$

where $\Phi=2\mu(\nabla\mathbf{v}):(\mathrm{def}\mathbf{v})+\lambda(\nabla\cdot\mathbf{v})^2$ is the dissipation of energy by viscosity.

According to the energy equation

$$\Phi-\nabla\cdot\mathbf{q}=\rho Du/Dt+\rho pD(1/\rho)/Dt, \tag{3}$$

where $\mathbf{q}$ is the flow of heat by conduction and u is the intrinsic energy per unit of mass. With the aid of the equation of continuity,

$$D\rho/Dt+\rho\nabla\cdot\mathbf{v}=0, \tag{4}$$

Eq. (3) can be put in the form

$$\Phi-\nabla\cdot\mathbf{q}=\rho Du/Dt+p\nabla\cdot\mathbf{v}. \tag{5}$$

By eliminating Φ from (2) and (5) we obtain

$$\rho D(\tfrac{1}{2}\mathbf{v}^2+u)/Dt-\rho\mathbf{v}\cdot\mathbf{f}+\nabla\cdot(\mathbf{v}p-2\mu\mathbf{v}\cdot\mathrm{def}\mathbf{v}-\lambda\mathbf{v}\nabla\cdot\mathbf{v}+\mathbf{q})=0, \tag{6}$$

or, alternatively,

$$\frac{\partial}{\partial t}[\rho(\tfrac{1}{2}\mathbf{v}^2+u)]-\rho\mathbf{v}\cdot\mathbf{f}+\nabla\cdot\left[\rho\mathbf{v}\left(\tfrac{1}{2}\mathbf{v}^2+u+\frac{p}{\rho}\right)-2\mu\mathbf{v}\cdot\mathrm{def}\mathbf{v}-\lambda\mathbf{v}\nabla\cdot\mathbf{v}+\mathbf{q}\right]=0. \tag{7}$$

Assuming that the extraneous force is conservative, $\mathbf{f}=-\nabla\psi$, and further that $u=c_vT$ and $\mathbf{q}=-k\nabla T$, Eq. (7) can be brought in a noteworthy form in two important special cases:

1. Steady flow of a perfect gas

$$\nabla\cdot[\rho\mathbf{v}(c_pT+\tfrac{1}{2}\mathbf{v}^2+\psi)-2\mu\mathbf{v}\cdot\mathrm{def}\mathbf{v}+\tfrac{2}{3}\mu\mathbf{v}\nabla\cdot\mathbf{v}-k\nabla T]=0. \tag{8}$$

2. Steady flow of an incompressible fluid

$$\nabla\cdot[\rho\mathbf{v}(c_vT+\tfrac{1}{2}\mathbf{v}^2+\psi+p/\rho)-2\mu\mathbf{v}\cdot\mathrm{def}\mathbf{v}-k\nabla T]=0. \tag{9}$$

It follows from (8) and (9) that the classical Bernoulli "constant" alters along a streamline due to the flow of heat by conduction and to the flow of dynamical energy caused by viscous forces. In the case of zero viscosity and zero heat conductivity (8) and (9) reduce to the well-known classical forms.

Equation (8) shows that the Prandtl number $\mu c_p/k$ plays a part in the discussion of heat effects in flowing gases. This fact is well known for the thermometer problem. Neglecting heat conductivity, as has been done by Madelung, therefore leads to incorrect results.

An article by the author covering the application of a modification of Eq. (8) to the flow in the Ranque-Hilsch vortex tube will be published in *Applied Scientific Research A*.

[1] C. Truesdell, Phys. Rev. **77**, 535 (1950).
[2] B. Etkin and V. G. Szebehely, Phys. Rev. **80**, 767 (1950).
[3] E. Madelung, Ann. Phys. **43**, 417 (1943).
[4] E. Lohr, *Vektor- und Dyadenrechnung für Physiker und Techniker* (Walter de Gruyter and Company, Berlin, 1939), p. 310ff.

The Natural Scintillations from Uranyl Nitrate Crystals

S. G. COHEN AND Y. FEIGE
Department of Physics, The Hebrew University, Jerusalem, Israel
(Received January 24, 1952)

IT is well known that pure hydrated crystals of the uranyl salts fluoresce strongly when excited by ultraviolet radiation. Decay times of about a millisecond have been observed,[1] but the possi-

bility of much faster fluorescent components is not excluded. It is reasonable to expect that fluorescence in these crystals should be excited by fast ionizing particles, and in particular, by the radiations accompanying the natural radioactive decay of the uranium isotopes and their disintegration products, which are present in the crystals. The authors have, therefore, looked for fast fluorescent light pulses from pure hydrated uranyl nitrate crystals using an E.M.I. photomultiplier.

Scintillations were detected, although the amplitude of the pulses obtained were small and close to the thermionic background of the multiplier. An amplifier of rise time 0.5 μsec and clipping time 3 μsec was used. The crystal could quickly be moved away from the photocathode and back again so that an accurate comparison of the discriminator bias curves with and without the crystal near the photocathode could be obtained. Typical bias curves are shown in Fig. 1. These curves were taken when using a crystal whose approximate dimensions were 3×4×8 mm. It is seen, for example, that at a bias of 13 volts, the number of pulses from the crystal is about twice the background. The pulses which

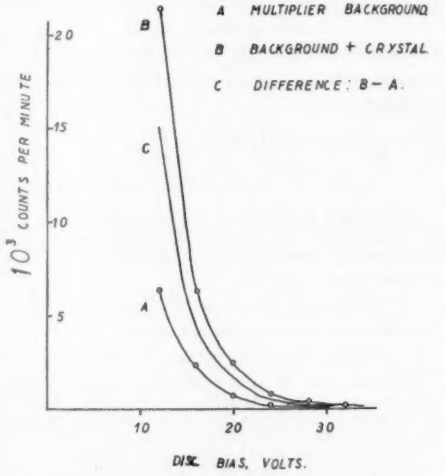

FIG. 1. Discriminator bias curves obtained with and without uranyl nitrate crystal near photocathode of multiplier.

were obtained in the presence of the crystal were not the effect of nuclear radiation impinging directly on the elements of the photomultiplier tube, since practically all the pulses were removed by interposing a very thin aluminium foil (0.37 mg/cm²) between the crystal and the photocathode. It was also shown that the results cannot be explained in terms of a long period phosphorescence of the crystals, because similar results were obtained with crystals which were freshly recrystallized from aqueous solutions in the dark, and placed in the multiplier housing using a dark room red light.

Further experiments using small crystals indicate that the bias curve flattens out at a sufficiently low bias, where the scintillation rate approximately equals the calculated disintegration rate of α-particles from U I and U II. This shows that, as may be expected, the α-particles on the average produce much larger scintillations than the β-particles or secondary electrons from γ-rays. In general, however, the detection of the smaller pulses is difficult because of the multiplier background. It is hoped to overcome these difficulties using two multipliers in coincidence.

If a measure of proportionality exists between the amount of fluorescence and the energy of the individual ionizing particles up to high energies, it should be possible to detect scintillations induced by fission fragments. Such a detector might have a useful application in the study of cosmic rays, e.g., for the measurement of star energies, since an internal calibration of fluorescence as a function of energy would be provided. Experiments are being carried out to see whether neutron induced and spontaneous fission scintillations can be detected in large crystals.

The fluorescence excited by a 5 millicurie source of radium which is placed close to a large crystal of uranyl nitrate can easily be seen by a moderately dark adapted eye.

It is also interesting to note that these results provide a possible interpretation of some of the apparently unexplained observations of Becquerel[2] during his classical experiments on radioactivity, which he claimed show that the newly discovered radiations from uranium salts possess some of the properties of visible light.

[1] J. T. Randall and M. H. F. Wilkins, Proc. Roy. Soc. (London) **184**, 347 (1945).
[2] H. Becquerel, Compt. rend. **122** (1896).

Magic Numbers and the Isotope Shift in Atomic Spectra of Heavy Elements

P. BRIX AND H. KOPFERMANN
II. *Physikalisches Institut der Universität Göttingen, Göttingen, Germany*
(Received January 25, 1952)

IN a letter to this journal Murakawa and Ross[1] have recently reported a rise in the isotope shift at the magic neutron number 82. This conclusion had already been reached by us from a systematic study[2] of the isotope shift constants.[3,2] Measurements on $Ce^{140}-Ce^{142}$ substantiated this view.[4]

More recently[5] it has been possible to show, from the isotope shift of RaD (Pb^{210}) relative to the stable lead isotopes, that a corresponding, though less pronounced, rise exists at the magic neutron number $N=126$.

At $N=50$ the values of the isotope shift constants are considerably more uncertain because of the great influence of mass dependent effects, but there is some indication[3] of a rise at this magic number, too.

The discontinuities at the magic neutron numbers may be seen from Fig. 1 where we have plotted, as a function of the neutron number N, the experimental isotope shifts divided by those calculated from Breit's theory of the nuclear volume effect.[6] This kind of diagram gives a better representation of the nuclear properties as derived from isotope shifts than the plot given by

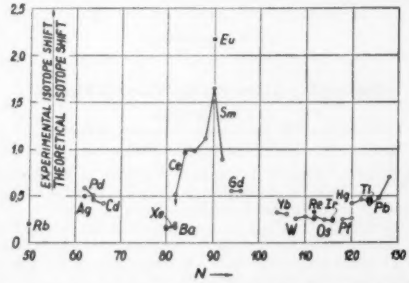

FIG. 1. Ratio of experimental to theoretical isotope shift for heavy elements as a function of the neutron number N. (Points are drawn for isotopic pairs with $N-2$ and N neutrons, and only for even N.) Black circles: Z odd. The measured shifts have been corrected for mass dependent effects; the theoretical values were calculated for homogeneously charged spherical nuclei with radii equal to $1.4A^{1/3}\times10^{-13}$ cm.

Murakawa and Ross, where the influence of the respective atomic electrons has not been eliminated.

The fact that most of the ratios in Fig. 1 are much smaller than unity can be explained by the assumption[2,7,8] that the addition of neutrons to a nucleus usually does not cause a uniform expansion of the nuclear charge distribution proportional to $A^{1/3}$ and that the added neutrons are mainly in the outer region of the nucleus. The exceptionally high points for $Eu^{151}-Eu^{153}$ and $Sm^{150}-Sm^{152}$ at $N=90$ have been related[2,7] to the quadrupole moments of europium.

Figure 1 also shows, as has been mentioned before,[2] that the values obtained for different isotopic pairs of the same element[9] show a tendency to follow the general trend of the values for different elements. The measurement of Murakawa and Ross[1] on the isotope shift $Ce^{139}-Ce^{140}$ can be considered an instructive example of this fact.

[1] K. Murakawa and J. S. Ross, Phys. Rev. **83**, 1272 (1951).
[2] P. Brix and H. Kopfermann, Z. Physik **126**, 344 (1949).
[3] P. Brix and H. Kopfermann, Festschrift Akad. Wiss. Göttingen, Math.-physik. Kl., p. 17 (1951).
[4] P. Brix and H. Frank, Z. Physik **127**, 289 (1950).
[5] Brix, Buttlar, Houtermans, and Kopfermann, Nachr. Akad. Wiss. Göttingen, Math.-physik. Kl., Nr. 7 (1951).
[6] For detailed discussion, accuracy (on the average about 10–20 percent) and literature see reference 3. The points for cerium 138–140 (only upper limit known) and lead 208–210 have been added. The new values for Pd are from Steudel (to be published), the relative shifts of the osmium isotopes have been corrected according to Suwa [Phys. Rev. **83**, 1258 (1951)].
[7] P. Brix and H. Kopfermann, Nachr. Akad. Wiss. Göttingen, Math.-physik Kl., p. 31 (1947).
[8] M. F. Crawford and A. L. Schawlow, Phys. Rev. **76**, 1310 (1949).
[9] The corresponding points have been connected by full lines in Fig. 1.

An Attempt to Produce Nuclear Orientation in Mercury Vapor*

FRANCIS BITTER AND JEAN BROSSEL
Research Laboratory of Electronics, Massachusetts Institute of Technology, Cambridge, Massachusetts
(Received January 21, 1952)

THE absorption of polarized resonance radiation by a vapor produces unequal populations of the magnetic sublevels of the excited state, and also of the ground state after re-emission. Kastler[1] has suggested that, as a consequence of these facts, polarized light may be used to orient nuclei. An experimental demonstration of this effect was attempted, and yielded a negative result.

A sample of mercury enriched in the isotope with mass number 199 and spin $\frac{1}{2}$ was supplied by the Atomic Energy Commission. The level structure of this isotope is shown in Fig. 1. The sample was placed in a quartz resonance lamp in a magnetic field of a few hundred gauss and illuminated by circularly polarized resonance radiation incident in a direction parallel to the field. Atoms in the ground state with $m=\frac{1}{2}$ can be excited only to the $^3P_1$ level with $F=\frac{3}{2}$ and $m=\frac{3}{2}$, and, in the absence of collisions, can return only to the ground state sublevel from which they came. On the other hand, atoms originally in the ground state sublevel with $m=-\frac{1}{2}$ are excited exclusively to levels with $m=+\frac{1}{2}$, and may return by radiating to either of the two ground levels. The net result is an optical "pumping" as Kastler suggests, from $m=-\frac{1}{2}$ to $m=+\frac{1}{2}$, or a tendency in the direction of nuclear orientation. This is in competition with a disorienting tendency caused by collisions.

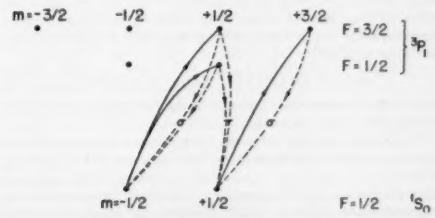

FIG. 1. Optically induced transitions in Hg^{199}.

If an appreciable degree of preferred nuclear orientation is produced, the intensity of the π-component of the resonance radiation with $\Delta m=0$ is less than for a disoriented vapor because fewer atoms are in the $m=-\frac{1}{2}$ ground level. This criterion was used to detect nuclear orientation. A radiofrequency field, of such frequency as to induce transitions between the ground state magnetic sublevels, was applied to the resonance lamp. We estimate that when the magnetic resonance condition $\omega=\gamma H$ is fulfilled, a change in the intensity of the π component of the optical resonance radiation should be observed if the polarized light has produced an excess of $m=\frac{1}{2}$ over $m=-\frac{1}{2}$ of at least a few percent. No such effects were observed.

Further experimentation is under way in an attempt to isolate the reasons for the negative results reported.

* This work has been supported in part by the Signal Corps, the Air Materiel Command, and the ONR.
[1] A. Kastler, J. phys. et radium **11**, 255 (1950).

The Scattering of 9.6-Mev Protons by Carbon, Aluminum, and Magnesium

C. J. BAKER, J. N. DODD, AND D. H. SIMMONS
Department of Physics, The University, Birmingham, England
(Received January 22, 1952)

A REMOTELY controlled scattering chamber, which will be described in detail later, has been used to investigate the scattering of 9.6-Mev protons by some light nuclei. The source of protons was the extracted beam of the Birmingham 60-in. cyclotron. The beam passes through a steering magnet which brings it to a focus just in front of the chamber. After collimation to $\frac{1}{2}°$ by rectangular slits, the beam passes through a scattering foil and is collected in a Faraday cup. The foils were about 4 mg/cm² in thickness, and the proton currents varied between 1 and 5×10^{-9} amp.

The scattered particles were detected by a counter telescope consisting of three proportional counters which fed a flexible coincidence or anticoincidence circuit. A set of fifty graded aluminum absorbers before counter 1, and a further set of five between counters 2 and 3, could be used to measure the ranges of the scattered particles. The proton current entering the Faraday cup was passed through a high resistance, and the resulting dc potential integrated electronically to give an absolute measure of the charge collected during a run.

Differential range curves were taken by observing coincidences between pulses in the first two counters for different thicknesses of absorber in front of counter 1. Counter 1 was biased low enough to count all particles which traversed it, while counter 2 was biased high so as to count only those particles which stopped in counter 2. This arrangement was insensitive to the large background of pulses because of fast neutron recoils in the counter gas. Figure 1 shows a range distribution curve for 9.6-Mev protons scattered through 60° (lab. angle) by a magnesium foil of normal isotopic constitution, set so that the normal to the foil bisected the scattering angle.

The three large peaks correspond, respectively, to elastic scattering and to excitation of the 1.38- and 4.14-Mev levels of Mg^{24}. The widths of these peaks are only slightly greater than those to be expected from range straggling in the absorber alone, so that the effects of energy spread of the incident beam, thickness of the scattering foil, range of energies accepted by counter 2, and the spread in scattering angle are small, as anticipated from detailed calculations.

Particle ranges in aluminum, corrected for energy loss in the scattering foil and the counter, were converted to energies by

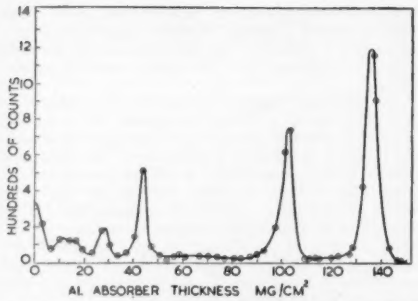

FIG. 1. Range distribution curve for 9.6-Mev protons scattered through 60° (lab. angle) by magnesium of normal isotopic constitution.

means of a range-energy relation which is an experimentally corrected version (to be described later) of the figures of Smith.[1]

The 1.38- and 4.14-Mev levels in Mg^{24} are well known,[2] and were used to estimate the accuracy of the determination of nuclear excitation energies by the present method. Measurements at four angles gave mean values of 1.34 and 4.17 Mev for these two levels. A further check was made by measuring the scattering from carbon, in which the first excited state of C^{13} is at an energy of 4.44±0.01 Mev.[3,4] Carbon foils prepared by burning filter paper were used, and measurements at five angles gave a mean value of 4.40 Mev for this level. From these results, the accuracy of the determinations of excitation energies is estimated to be 0.05 Mev for well resolved peaks.

For aluminum, observations at six angles yielded the levels of Al^{27} shown in Table I. The probable errors have been assigned on an appraisal of the resolution of the peaks, and the spread between observations at different angles.

In these experiments, no certain evidence was found for the 0.8- or 2.78-Mev levels. The levels at 3.93, 4.39, 4.66, and 5.46 Mev have not previously been reported from studies of the inelastic scattering of protons, but a level at 3.83±0.07 Mev has been found independently by this method.[6,7] In the magnesium curves, three peaks have been found which correspond to excitation energies higher than 4.14 Mev. One of these yields a level at 6.38±0.08 Mev which may be assigned to Mg^{24} on the basis of a level at 6.3 Mev found from studies of the inelastic scattering of deuterons by separated Mg^{24}.[8]

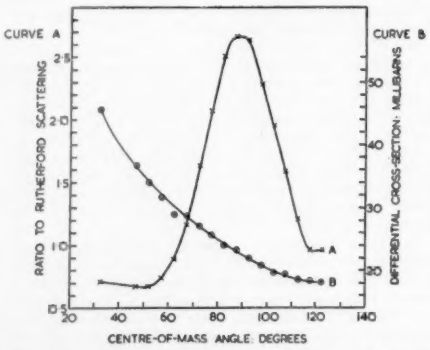

FIG. 2. Angular distributions for 9.6-Mev protons scattered by magnesium. Curve *A*: absolute ratio to Rutherford scattering for protons elastically scattered. Curve *B*: absolute differential cross sections (corrected to center-of-mass) for protons scattered inelastically (1.38-Mev level of Mg^{24}).

TABLE I. Energy levels in Al^{27}.

Observed level Mev	Reported level[a] Mev	Observer reference No.
	0.804	(2)
0.99±0.05	1.02	(2)
1.72±0.15	1.85	(2)
2.22±0.08	2.15	(2)
	2.78	(2)
3.00±0.05	3.03	(2)
3.63±0.12	3.65±0.07	(5)
3.93±0.10	3.83±0.07	(6)
4.39±0.12	4.33±0.07	(5)
4.66±0.10		
5.46±0.08	5.32±0.07	(5)

[a] See reference 7.

Absolute cross sections and angular distributions were measured by observing coincidences between counters 1 and 2, both biased low enough to count all particles which traversed them. The reliability of the system in this condition was checked by measuring the elastic scattering from gold, for which the absolute cross sections found agreed within 3 percent with those calculated on the assumption of Rutherford scattering. Figure 2 shows the ratio of measured to Rutherford scattering for 9.6-Mev protons elastically scattered by magnesium (Curve *A*), and absolute differential cross sections (corrected to center-of-mass) for one group of inelastically scattered protons (1.38-Mev level of Mg^{24}) (Curve *B*). The elastic scattering of protons by carbon and aluminium gave curves which are similar in shape to Curve *A* of Fig. 2: the ratio to Rutherford scattering at the peak is higher, and the peak is shifted to larger angles for the lighter nuclei.

We wish to acknowledge our indebtedness to Mr. H. I. S. Allwood and Dr. C. H. Westcott for the large part they played in the original design of the scattering chamber.

[1] J. Smith, Phys. Rev. **71**, 32 (1947).
[2] D. E. Alburger and E. M. Hafner, Revs. Modern Phys. **22**, 373 (1950).
[3] $N^{15}(p, \alpha)C^{12}$ reaction. Hornyak, Lauritsen, Morrison, and Fowler, Revs. Modern Phys. **22**, 291 (1950).
[4] R. Malm and W. W. Buechner, Phys. Rev. **81**, 519 (1951).
[5] Swann, Mandeville, and Whitehead, Phys. Rev. **79**, 598 (1950).
[6] G. W. Greenlees (private communication).
[7] Since this work was completed there has appeared an abstract by Reilley, Allen, Arthur, Bender, Ely, and Hausman, Bull. Am. Phys. Soc. **26**, No. 6, 8 (1951), listing 22 energy levels in Al^{27} which have been found by the magnetic analysis of the inelastic scattering of 8.0-Mev protons from Al.
[8] MIT Progress Report, July, 1950, p. 174.

The Elastic Scattering of Deuterons by Deuterons

RICHARD J. RUNGE
Department of Physics, University of New Mexico, Albuquerque, New Mexico
(Received September 10, 1951)

AN analytical solution of the problem of the elastic scattering of deuterons by deuterons is obtained for the case of an interaction between nucleons of the type,[1]

$$V_{ij} = -(g_1 + MP_{ij} + g_2 Q_{ij} + gP_{ij}Q_{ij})W_0 \exp(-\mu^2 r_{ij}^2), \quad (1)$$

where $M = 1 - g - g_1 - g_2$. In addition, a Coulomb repulsion between the two protons of the system is included. The deuteron ground state is assumed to be a ^3S state,[1,2] described by the Gaussian wave function,

$$\psi_0(r) = a \exp(-\lambda^2 r^2), \quad \text{where} \quad a^2 = 2\lambda^3/\pi^{\frac{3}{2}}; \quad (2)$$

that is, the ^3D state is not included in the calculation. In addition polarization of the deuterons is neglected.

The procedure employed in the calculation is to set up the wave equation, including the total interaction between the four nucleons of the system, express it in suitable coordinates in the center-of-mass system and then proceed to a solution of the properly symmetrized wave function which describes the elastic scattering. This solution obeys the Pauli principle with respect to exchanges

of spin and coordinates of like particles. The treatment is essentially that of Wu and Ashkin[2] in their work on the three-body problem, extended to four nucleons. The Born approximation is used to obtain the asymptotic form of the angular dependence of the scattering in center-of-mass system. This involves reducing 64 integrals in the wave equation down to 5 distinct types after calculating the effects of spin and coordinate exchange operators on the integrands of expressions involving the total nuclear interaction on the system. The Coulomb interaction introduces four integrals. The spin states are introduced by means of nine spin wave functions, χ_s^m, where $s=2$, 1, 0 for the quintet, triplet, and singlet states, respectively. The author used these spin wave functions directly in the calculation rather than the spur theory. Since the procedure of calculation was standard, the details are here omitted. It was easily shown that for an interaction of the type (1), the spin was a constant of the motion, i.e., a state χ_s^m was always scattered into a state $\chi_{s'}^{m'}$ where $s=s'$ and $m=m'$. If we denote by $U_1\cdots U_9$ the functions,

$$U_1=(a_1K_0/\mu^2)\exp[-k^2(4\lambda^2+\mu^2)\sin^2\tfrac{1}{2}\theta/4\lambda^2\mu^2],$$
$$U_2=(a_1K_0/\mu^2)\exp[-k^2(4\lambda^2+\mu^2)\cos^2\tfrac{1}{2}\theta/4\lambda^2\mu^2],$$
$$U_3=[a_2K_0/(\mu^2+\lambda^2)^2]\exp[-k^2\{1+(\mu^2/\lambda^2)\sin^2\tfrac{1}{2}\theta\}/4(\mu^2+\lambda^2)],$$
$$U_4=[a_2K_0/(\mu^2+\lambda^2)^2]\exp[-k^2\{1+(\mu^2/\lambda^2)\cos^2\tfrac{1}{2}\theta\}/4(\mu^2+\lambda^2)],$$
$$U_5=-4K_1\exp[-k^2(\mu^2+2\lambda^2)/2\lambda^2(3\mu^2+4\lambda^2)],$$
$$U_6=(K_2/4k^3)\csc^2\tfrac{1}{2}\theta\exp[-k^2\sin^2\tfrac{1}{2}\theta/4\lambda^2],$$
$$U_7=(K_2/4k^3)\sec^2\tfrac{1}{2}\theta\exp[-k^2\cos^2\tfrac{1}{2}\theta/4\lambda^2],$$
$$U_8=-(K_2/\lambda k)\exp(-k^2/4\lambda^2)\csc\tfrac{1}{2}\theta F(k\sin\tfrac{1}{2}\theta/2\lambda),$$
$$U_9=-(K_2/\lambda k)\exp(-k^2/4\lambda^2)\sec\tfrac{1}{2}\theta F(k\cos\tfrac{1}{2}\theta/2\lambda),$$

we can then express the amplitudes $f_Q(\theta)$, $f_T(\theta)$, and $f_S(\theta)$ of the asymptotic form of the scattered waves for the quintet, triplet, and singlet scattering (where θ is the scattering angle in the center-of-mass system) in terms of these functions. They are

$$\text{Quintet: } f_Q(\theta)=U_1+U_2+U_3+U_4+U_5+U_6+U_7+U_8+U_9,$$
$$\text{Triplet: } f_T(\theta)=U_1-U_2+U_3-U_4+U_5-U_7,$$
$$\text{Singlet: } f_S(\theta)=U_1+U_2+U_3+U_4-\tfrac{1}{2}U_5+U_6+U_7-\tfrac{1}{2}U_8-\tfrac{1}{2}U_9.$$

In the above expressions we have,

$$K_0=W_0\pi^{7/2}a^4m/16\lambda^6\hbar^2,$$
$$K_1=W_0\pi^{5/2}a^4m/4\lambda^6(3\mu^2+4\lambda^2)^{5/2}\hbar^2,$$
$$K_2=-\pi^2e^2a^4m/4\lambda^6\hbar^2,\quad k=(2mE_0)^{1/2}/\hbar,$$
$$F(x)=\int_0^x e^{t^2}dt,$$

$$\text{(Quintet): } a_1=6g_1+6g_2-2,\qquad a_2=4-6g_1-6g_2,$$
$$\text{(Triplet): } a_1=4g_1-2g,\qquad a_2=4-4g-4g_1-6g_2,$$
$$\text{(Singlet): } a_1=1+3g_1-3g-3g_2,\quad a_2=4-6g-3g_1-6g_2.$$

The quantities W_0, μ, and λ are defined in (1) and (2), m is the proton rest mass, e is the fundamental electronic charge and E_0 is the kinetic energy of the two deuterons in the center-of-mass system at infinite separation. The differential cross section, $d\sigma$, is then,

$$d\sigma=I(\theta)d\Omega,$$

where

$$I(\theta)=(5|f_Q(\theta)|^2+3|f_T(\theta)|^2+|f_S(\theta)|^2)/9,$$

for an unpolarized incident beam of deuterons. Inspection of these results shows that the quintet and singlet amplitudes behave like even Legendre polynomials (symmetry about $\theta=90°$) or S, D, etc., waves while the triplet amplitude behaves like an odd Legendre polynomial (antisymmetry about $\theta=90°$), that is, like a P, F, etc., wave. These symmetry properties follow from certain symmetry properties of the nine spin wave functions used to describe the scattering under exchanges of spin and coordinates of the like particles of the system. The function $I(\theta)$ itself is always symmetrical about $\theta=90°$.

The scattering formulas show that as θ increases from 0° to 90°, $I(\theta)$ is at first extremely large ($I(0)=\infty$) and reflects the Coulomb contribution to the scattering. $I(\theta)$ decreases very quickly with increasing θ, showing a minimum because of phase cancellation between the Coulomb repulsion and the nuclear attraction for small values of θ. A rise in $I(\theta)$ then occurs and a finite maximum is then attained. Then a steady drop of $I(\theta)$ out to $\theta=90°$ occurs. The magnitude of this drop to a finite minimum at 90° is not large, especially at low energies.

By using values of g, g_1, and g_2 suggested by other authors,[3] a calculation of $I(\theta)$ was made for $2E_0=10.8$ Mev. The well depth, W_0, was taken to be 45 Mev following Bethe.[4] Comparison of the theoretical values so obtained with the experimental results of Allred *et al.*[5] showed the theoretical values to be too high by a factor of three. However, an investigation of the criterion for the validity of the Born approximation shows that for such a low energy this approximation would be invalid, the amplitude of the scattered wave in the vicinity of the scatterer being quite large. The author was unable to find any experimental data for higher energies. At higher energies, it would seem that the tensor interaction and the ^3D state of the deuteron would have to be included. This leads to a quite complicated problem since the spin is no longer a constant of the scattering.

[1] L. Motz and J. Schwinger, Phys. Rev. **58**, 26 (1940).
[2] T. Y. Wu and J. Ashkin, Phys. Rev. **73**, 986 (1948).
[3] R. Buckingham and H. S. W. Massey, Proc. Roy. Soc. (London) **A179**, 123 (1941).
[4] H. Bethe and R. F. Bacher, Revs. Modern Phys. **8**, 82 (1936).
[5] Allred, Erickson, Fowler, and Stovall, Phys. Rev. **76**, 1430 (1949).

Absorption Experiment to Detect the Cosmic-Ray Albedo at High Altitudes*

J. R. WINCKLER
University of Minnesota, Minneapolis, Minnesota
(Received January 7, 1952)

MEASUREMENTS of the cosmic-ray intensity at the top of the atmosphere with balloons[1] or outside the atmosphere with rockets[2] using counting telescopes show that there is a considerable east-west asymmetry. Its magnitude, however, is much too small to agree with the value predicted from the latitude variation of the vertical flux and the geomagnetic theory of the allowed cone. The disagreement is most pronounced at geomagnetic latitudes of about 40°, where at a 60° zenith angle the predicted asymmetry is 300 percent of the observed.[1] It is possible that the apparent asymmetry of the primary radiation is reduced by an upward component of secondaries projected into the easterly direction, where the primary intensity should be low, by the much larger flux of primaries incident from the west. A measurement of particle direction at high altitude could establish the magnitude of this effect.

As a preliminary approach to the problem, several measurements have been made by balloon techniques with the apparatus shown in Fig. 1. The three-fold Geiger telescope was inclined at a fixed zenith angle of 60°. A large lead block 6.5 in. thick, weighing 105 pounds and completely covering the telescope solid angle is placed below the telescope. This block is periodically moved from position A to position B relative to the telescope. (In actuality the telescope is moved upwards away from the block.) The black circles in the figure represent counters connected in a 4-fold arrangement to give information about shower events. One experiment was conducted with a one-inch block of lead F in the tele-

TABLE I. Observed counting rates for different experimental conditions.

	Position of large block	Telescope rate	4-fold rate
Without lead	A	0.928 ±0.017	0.182 ±0.007
Block F	B	0.916 ±0.017	0.089 ±0.005
With lead	A	0.735 ±0.014	0.237 ±0.008
Block F	B	0.698 ±0.014	0.181 ±0.007

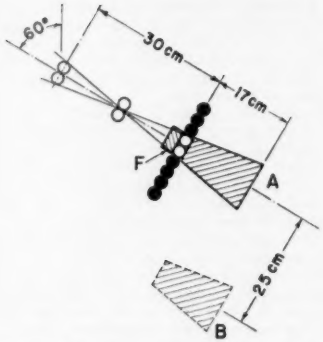

FIG. 1. Geiger counter telescope fixed at zenith angle of 60°. Lead can be placed at F and A and moved periodically from A to B.

scope. This was removed for a second flight. Both flights were carried by "Skyhook" plastic balloons and remained level at about 80,000 feet (27 g/cm²) for several hours. Data from the level portions are summarized in Table I.

If one compares the telescope counting rates to determine the upward flux subtracted out by the lead block, one finds no significant difference between the "A" and "B" rates in either experiment. The large lead block has a stopping power corresponding to 200-Mev μ-mesons or 400-Mev protons.

In interpreting the results one must consider that although the large block is capable of removing certain albedo particles generated in the atmosphere, it in turn generates an albedo effect proportional to the number of energetic nucleons or other interacting particles incident on the block from top and sides. If this albedo generation is detected as 4-fold events, the shower counter rate should increase monotonically to the top of the atmosphere. The observed 4-fold events, on the other hand, follow the telescope flux, and when the 3-fold counting rate passed a peak as the balloon passed through the region of the Pfotzer maximum for the telescope at 60° (without F), the shower rate also passed a maximum and then decreased.

The small lead block F contributes a large fraction of the shower events when present in the telescope, and in this case the Pfotzer maximum is not observed in either telescope or showers. The shower rate is considerably higher in position "A" than "B," and reaches 20 percent of the telescope rate. Despite the negative result of this experiment and the arguments given above, there is a chance that the true albedo effect is obscured by these showers. The apparatus, in principle, gives no information about the albedo effect for particles more energetic than a few hundred Mev. The balloon flights for the above experiments and those described in the following letter were made at Minneapolis.

* This work supported by the joint program of the AEC and ONR.
[1] Winckler, Stix, Dwight, and Sabin, Phys. Rev. **79**, 656 (1950).
[2] J. D. Van Allen and A. V. Gangnes, Phys. Rev. **79**, 51 (1950).

Application of Čerenkov Radiation to the Cosmic-Ray Albedo Problem*

J. R. WINCKLER
University of Minnesota, Minneapolis, Minnesota
(Received January 7, 1952)

THE Čerenkov light[1] from fast charged particles is emitted in a cone about the particle direction with the ray direction inclined to the particle direction at an angle θ given by $\cos\theta = 1/\beta n$, where n is the index of refraction of the medium. It has been shown both experimentally[2] and theoretically[3] that the angular dependence is a δ-function in θ for particles of equal β. The apparatus shown in Fig. 1 makes use of this behavior of the Čerenkov light to establish the direction of motion of a cosmic-ray particle. The Geiger counters form a telescope whose solid angle between the tubes is filled by the 15 cm long lucite block. Čerenkov light from downward particles is internally reflected and reaches the end-window photomultiplier (E.M.I. type 5311) which is optically sealed to a slant face of the lucite block. Light emitted by upward moving particles is internally reflected upwards and is absorbed by the black upper surface of the lucite. This absorbing surface is increased by slots as shown.

The behavior of the apparatus when detecting cosmic-ray particles is summarized in Table I. Pulse-height distributions for the photomultiplier pulses in coincidence with the counter telescope were obtained at sea level in a basement room under 4 feet of concrete, and at various atmospheric depths using balloon techniques. The tabular values give the ratio (Čerenkov-telescope counts)/(total telescope counts), for various relative bias values. n_1 refers to the apparatus oriented upwards as shown in the figure, and n_2 to the apparatus rotated 180° about axis A–A.

TABLE I. Čerenkov counting efficiency.

Bias		0	10	15	20	25	30
Sea level 0° zenith	n_1	0.94	0.90	0.86	0.80	0.62	0.33
	n_2	0.21	0.16	0.13	0.077	0.060	0.038
	n_2/n_1	0.23	0.18	0.15	0.098	0.096	0.12
120–150 g/cm² 0° zenith	n_1	0.70	0.66	0.64	0.60	0.54	0.43
	n_2	0.16	0.15	0.11	0.10	0.07	0.05
0° zenith	n_1	0.93	0.92	0.91	0.89	0.86	0.77
	n_2	0.18	0.16	0.13	0.11	0.09	0.07
17 g/cm² 60° zenith	n_1	0.69	0.66	0.62	0.57	0.44	0.25
	n_2	0.16	0.14	0.13	0.11	0.11	0.08
60° relativistic albedo at 17 g/cm²		0.03 ±0.02	0.03 ±0.02	0.04 ±0.02	0.05 ±0.02	0.06 ±0.02	0.07 ±0.02

At sea level 94 percent of the cosmic-ray particles give detectable light pulses. The reverse efficiency n_2 for the same bias is 21 percent. With higher bias values the back-front ratio, n_2/n_1, decreases to a minimum of 10 percent, which approximately agrees with data obtained by Jelly[4] using a water cell. Part of the "back" efficiency can be explained by side showers, but the major part is the result of other causes which are being investigated.

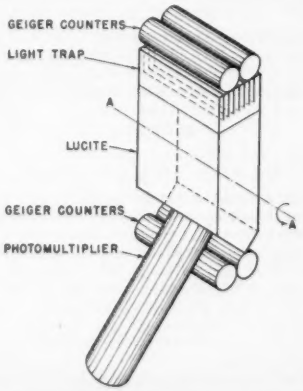

FIG. 1. Geometric arrangement of Čerenkov radiation detector as applied to cosmic-ray albedo experiment.

At 120–150 g/cm² atmospheric depth (about the depth of the Pfotzer maximum) the efficiency drops to 70 percent with bias "0." This is interpreted as being caused by particles of velocity below the Čerenkov threshold ($\beta=0.7$ for lucite) which trigger the telescope but do not give a detectable Čerenkov pulse. Analysis shows that these particles must be protons, as mesons or electrons having the 25 g/cm² range necessary to traverse the detector would be well above the threshold. Comparison with the sea-level data shows that between 24 percent and 30 percent of the particles at the Pfotzer maximum having a range of 25 g/cm² or greater must be these protons, of energy between 185 and 400 Mev. The absolute flux is 0.07 ± 0.01 particle cm^{-2} sec^{-1} sterad^{-1}.

At 17 g/cm² atmospheric depth the vertical efficiency is 93 percent, indicating that, as in the basement laboratory, all or nearly all particles are relativistic with β well above 0.7. At 60° zenith angle, however, the nonrelativistic or backward flux increases, and the efficiency drops to 69 percent. If one assumes that the relativistic vertical backward flux at sea level or at 17 g/cm² is negligible, then one can calculate the 60° zenith backward relativistic flux from the relation

$$\text{Albedo}=\frac{\text{relativistic up}}{\text{total down}+\text{up}}=\frac{n_2'n_1-n_1'n_2}{n_1^2-n_2^2},$$

where n_1' and n_2' are the observed Čerenkov efficiencies at 60° zenith angle, and n_1 and n_2 the efficiencies for the same bias at sea level. Calculated albedo values are given in the last line of the table. These data have poor statistical accuracy because of the subtraction process and insufficient data at high altitude.

The apparatus in principle gives no albedo data on nonrelativistic particles, and in its present crude form, requires two measurements differing by 180° in zenith to determine the backward flux. It appears, however, that with further development this type of detector will have a number of applications in cosmic-ray research.

Acknowledgment is made to C. L. Critchfield for the initial suggestion of applying Čerenkov radiation to this problem, and to Mr. Baskin and Mr. Mitchell for valuable assistance with the experiment.

* This work supported by the joint program of the AEC and ONR.

[1] P. A. Čerenkov, Compt. rend. acad. sci. URSS 2, 451 (1934).
[2] R. L. Mather, Phys. Rev. 84, 181 (1951).
[3] I. Frank and I. Tamm, Compt. rend. acad. sci. URSS 14, 109 (1937).
[4] J. V. Jelly, Harwell Nuclear Physics Conference (September, 1950).

A Second γ-Transition ($d_{\frac{1}{2}}\rightarrow s_{\frac{1}{2}}$) in Xe^{129m}

S. Thulin and I. Bergström
Nobel Institute for Physics, Stockholm, Sweden
(Received February 4, 1952)

EARLIER we have reported a new isomer of Xe^{129}.[1] It was found that the ratio of the intensities of the K and L conversion electrons of Xe^{129m} was close to that of Xe^{131m}, indicating

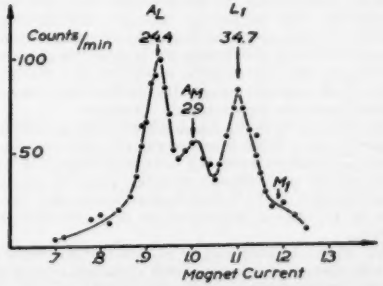

FIG. 1. Low energy electron lines of Xe^{129m}.

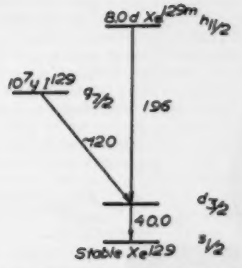

FIG. 2. Decay scheme of I^{129} and Xe^{129m}.

that the isomeric transitions are of the same type. The spins of the ground states of Xe^{129} and Xe^{131} are known to be 1/2 and 3/2 respectively. The experiments then favored the spins 9/2 and 11/2 for the isomeric states. However, the strong spin-orbit coupling model suggests the spin 11/2 also for the isomeric state of Xe^{129}. In order to obtain agreement with the theory, it is necessary to postulate a second γ-ray in the decay of Xe^{129m}. We have remeasured Xe^{129m} with a stronger sample and found a γ-ray of the energy 40.0 kev.

Figure 1 shows the low energy electron lines of an electromagnetically separated Xe^{129m} sample. In addition to the K and $L+M$ conversion lines of the 196-kev isomeric γ-ray and the two strongest Auger lines, there is a line at the energy 34.7 kev, which for the following reason must be interpreted as the L line of a 40.0-kev γ-ray. Earlier experiments[2] on Xe^{131m} have shown that the intensity ratio of the Auger lines and the isomeric K conversion line is 0.16 ± 0.02 (fluorescence yield of $Xe=0.84\pm0.02$). From Fig. 1, however, we find that this ratio is about twice the expected value. This means that Auger electrons must also be due to another K conversion line, having an intensity comparable to that of the K line (K_1) of the isomeric γ-ray. The intensity of the 34.7-kev line, however, is only ~0.15 of that of the K_1 line. It must therefore be concluded that the 34.7-kev line is an L line of a γ-ray of the energy 40.0 kev. The corresponding K line at 5.4 kev cannot be detected with the GM-window, which we used.

Borkowski and Brosi[3] have reported a 39-kev γ-ray in the decay of I^{129}. This γ-ray is certainly identical with that found by us. The decay scheme of Xe^{129m} and I^{129} is presented in Fig. 2. Thus Xe^{129m} is now in excellent agreement with the predictions of the strong spin-orbit coupling model.

It should be pointed out that we have not been able to observe the crossover transition. $E5$ radiation is thus in this case much less probable than $M4$ radiation, which is in contradiction to older theories. Hill[4] has reached similar conclusions for some of the Te isomers.

[1] I. Bergström, Nature 167, 634 (1951).
[2] I. Bergström, Arkiv. Fys. (to be published).
[3] C. J. Borkowski and A. R. Brosi, Oak Ridge National Laboratory Report No. 607 (1950).
[4] R. D. Hill, Phys. Rev. 81, 470 (1951).

Probing the Space-Charge Layer in a p-n Junction

G. L. Pearson, W. T. Read, and W. Shockley
Bell Telephone Laboratories, Murray Hill, New Jersey
(Received January 25, 1952)

ACCORDING to theory, the rectifying junctions of semiconductor art involve space-charge layers. These layers contain relatively small densities of holes and electrons and acquire their charge density from ions, donors, and acceptors. Evidence for the presence of these layers has been obtained from capacity measurements of rectifying diodes biased in the reverse

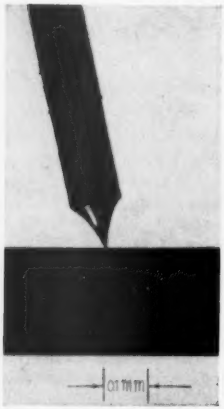

FIG. 1. Tungsten point for probing $p-n$ junctions.

directions. Schottky and his colleagues,[1] who devised the theory and made the first measurements for metal-semiconductor contacts, found that the predicted $V \propto C^{-2}$ relationship generally held.

For $p-n$ junctions with linear concentration gradients the relationship[2] should be $V \propto C^{-3}$, a prediction found to agree with experiment for many $p-n$ junctions studied.[3] If the transition from uniform n-type to uniform p-type is abrupt, the Schottky $V \propto C^{-2}$ relationship should again apply.[3] Underlying these relationships is the theory that the capacity per unit area is

$$C = K/(4\pi W), \tag{1}$$

with W the width of the space-charge layer, C the capacity per unit area, and K the dielectric constant. So far as we are aware relationship (1) has not previously been verified by direct measurement of the width W of the space-charge layer.

We have investigated the extent and potential distribution in the space-charge region in a germanium $p-n$ junction[4] by measuring the zero-current potential of a tungsten probe pressed against the space-charge layer where it comes to the surface of a specimen of square cross section cut parallel to the x-axis. The probe, a photograph of which is shown in Fig. 1, was pointed by an electrolytic etch.[5] The space-charge layer is wide compared to the area of contact of the point and may be thought of as a region of dielectric. If the point is at the natural potential of the dielectric, the voltage between the point and the semiconductor is relatively small; on the other hand if the point has a potential applied to it externally, a strong local field will be set up. Since there are relatively few holes or electrons to extract, the current which the point carries should consist predominantly of injected carriers. This is observed to be the case: with fixed voltage between the n- and p-terminals; making the point positive in respect to the floating potential results in a positive current from point to semiconductor which shows up almost entirely in an equal added current in the p-terminal lead, and mutatis mutandis the same for negative potentials. This experimental result may be taken as evidence that at the zero-current condition, the point is floating substantially at the space-charge potential. Furthermore, since the dielectric constant is 16.1, the fringing effects will be small and the potential distribution on the surface will be of nearly the same form as in the interior.

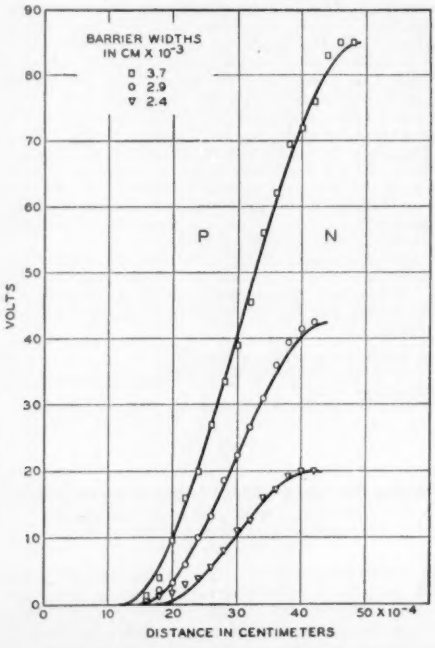

FIG. 2. Voltage *vs* distance through space-charge barrier.

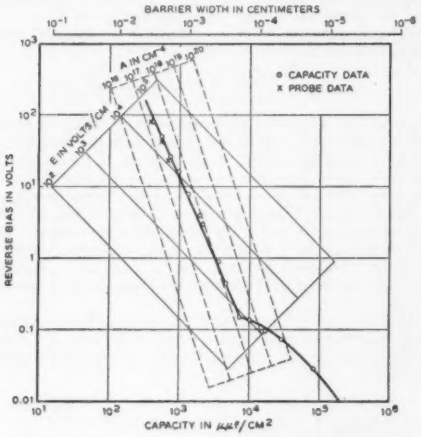

FIG. 3. Capacity and barrier width as functions of reverse bias. E = average field. A = impurity concentration gradient.

The point was moved by dragging it with light pressure in the x-direction with a Hilger interferometer movement and the zero current potentials measured as a function of distance. A typical set of data for three different potentials across the junction is shown by points in Fig. 2. Within experimental error, the same curve for 45 volts was obtained on the other three sides of the specimen.

The curves are cubics used to estimate the locations of zero-potential gradient and thus the width of the space-charge layer. The relationship (1) between W and C is tested in Fig. 3 by

plotting W *vs* V and C *vs* V, using Briggs' infrared value[6] $K=n^2=16.1$ to relate the C and W scales. On the basis of this procedure the points agree, and within this accuracy the experiment confirms that n^2 at infrared equals K at 1000 cps. Unfortunately, the junction studied has neither a linear concentration gradient nor an abrupt transition as evidenced by the approach of the data to $C\propto V^{-2}$ and in fact the curves of Fig. 2 can be equally well fitted by parabolas. This introduces an uncertainty in the W estimate of about 30 percent, which we hope to eliminate by future studies of other junctions.

We are indebted to E. Buehler, M. Sparks, and G. K. Teal, who prepared the single crystal $p-n$ junction and to W. L. Bond, P. W. Foy, and H. R. Moore for help with the measurements.

[1] W. Schottky and E. Spenke, Wiss. Veröff. Siemens-Werk. **18**, 1 (1939); see also S. J. Angello, Elec. Eng. **68**, 865 (1949).
[2] W. Shockley, Bell System Tech. J. **28**, 435 (1949).
[3] McAffee, Ryder, Shockley, and Sparks, Phys. Rev. **83**, 650 (1951); and Goucher, Pearson, Sparks, Teal, and Shockley, Phys. Rev. **81**, 637 (1951).
[4] This junction is the same as that investigated by Goucher *et al.* (reference 3).
[5] The technique employed is that of W. G. Pfann, Trans. Am. Inst. Mining and Metall. Engrs. **175**, 606 (1948).
[6] H. B. Briggs, Phys. Rev. **77**, 287 (1950).

Electron Interferometer*

L. MARTON
National Bureau of Standards, Washington, D. C.
(Received January 28, 1952)

THIS brief report contains the basic principles of an interferometer operating with electron beams. The possibility of building such an interferometer may have occurred to many, but in the absence of any publications on this subject some elementary considerations may not be misplaced.

It is rather simple to conceive an interferometer operating with electron beams based on the equivalent light optical experiment of Young. In principle, the double slit method could be employed but simple calculations, based on light optical analogies, indicate that the dimensions and complexities of such an instrument are rather undesirable. Because of the short wavelength, the source size, the size of the slits and their separation, and the separation of the fringes becomes so small that a major experimental effort may be needed for coping with them. In view of these difficulties it is worthwhile to explore the possibilities of a wide beam interferometer instead of a narrow beam instrument. In principle a wide beam interferometer of, let us say, the Michelson or the Jamin type is possible provided an efficient beam splitter is available. Such a good beam splitting mechanism exists for electrons, although not in the customary sense of light optics. Diffraction from thin crystal lamellae offers an excellent mechanism for carrying out such an interferometer experiment. Several lamellar crystals are needed in the manner indicated in Fig. 1. Let us assume an incident parallel beam of electrons passes through a thin crystal in the manner indicated by Fig. 1(a). Part of the beam is transmitted and part of it is diffracted. At a certain distance a second crystal is placed. Part of the original beam again is transmitted and part of it is diffracted as indicated. The same applies to the beam diffracted on the first crystal. The same phenomenon is repeated again on a third crystal placed at equal distance. By placing convenient limiting apertures we can select two diffracted beams out of the multitude of all the beams indicated on Fig. 1(a) and have a total path indicated on Fig. 1(b). The resulting trajectories correspond roughly to the equivalent of the Mach-Zehnder type interferometer. Figure 1(b) indicates the optical path for zero-path difference. A field gradient across the two paths will produce a path difference which can be observed by means of the shifting of the fringes localized at infinity.

To convince ourselves that the proposed scheme is feasible, we carried out light optical analog experiments. They consisted in reproducing the optical path indicated on Fig. 1(b) by means of transmission-type grating replicas. It was found that while such a system does not offer any particular advantages as compared to the conventional interferometer, it constitutes a perfectly good light optical interferometer and it helped us to compute some of the design characteristics of the electron beam instrument. Further proof for the soundness of the idea is furnished by the electron microscope observations of interference fringes published by Mitsuishi, Nagasaki, and Uyeda.[1] Similar observations have been reported also by Rees[2] from Australia and also by Hillier.[3] Observations in all three places indicate that the type of interference necessary for the operation of an electron interferometer is produced on lamellar thin crystals.

Calculations have been carried out to determine the tolerances for misalignment of the elements of an electron beam interferometer. These calculations will be reported later by J. Arol Simpson. Anticipating this report it may be mentioned that the dimensional and other tolerances of the instrument are well within experimental possibilities.

The crystals required for carrying out such experiments can be either selected from natural crystals or grown for the purpose.

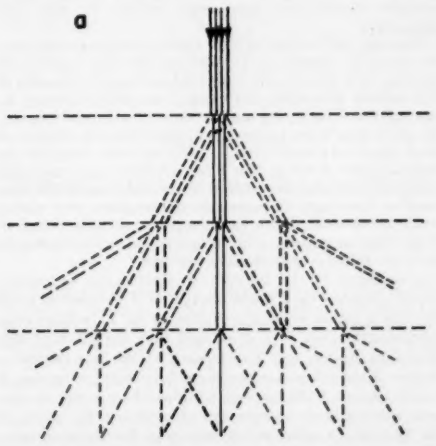

FIG. 1(a). Schematic representation of rays passing through three crystals.

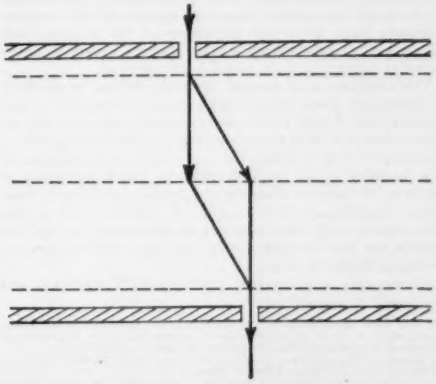

FIG. 1(b). Rays as limited by apertures.

It has been shown in the past by numerous observers that epitaxy offers a good way for the production of thin lamellar crystals. Experiments have been carried out in this laboratory by O. G. Engel, J. A. Simpson, J. Suddeth, and T. McCraw, and thin films of different metals having thicknesses of the order of 100 to 200A have been produced with the required characteristics. While the produced films may not be single crystals in the true sense of the word, electron diffraction patterns indicate that if they are constituted by smaller crystals all the constituent crystals are so well aligned that the conditions for the interferometer experiment are fulfilled. Details about these experiments will also be contained in later publications.

In principle, the optics of such a wide beam interferometer could be simplified, to contain only one thin crystal, as shown in Fig. 2. In this case the incident beam is deflected at right angles by a first magnet A to impinge on a thin crystal. The incident beam again is partly transmitted and partly diffracted. The transmitted beam is intercepted by a conveniently located stop. The two diffracted beams are deflected by the magnets B_1, B_2, C_1, C_2 in the manner shown on the figure and are reunited by the crystal to form an emerging beam proceeding in the opposite direction from the incident one. Magnet A deflects then this emerging beam in a direction coincident with the original one of the incident beam.

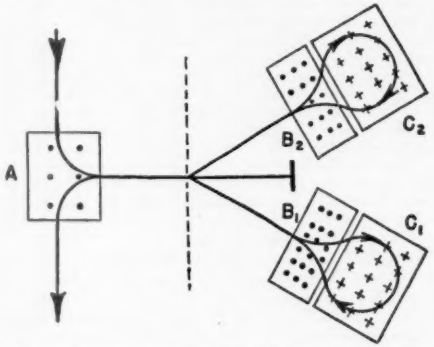

FIG. 2. Interferometer arrangement with one crystal and magnetic field.

A number of other possible combinations with varying number of crystals and fields could be listed. It is conceivable that Bragg reflection on thicker crystals could also be used. The geometries which reduce the number of crystals merely shift the required tolerances from the crystal alignments to the magnetic field alignments. No estimates have been made up to now as to the degree of accuracy required in this latter operation.

The usefulness of an electron interferometer can be manifold. As mentioned above, fringe displacement is produced by a field gradient and therefore such an instrument constitutes an extremely sensitive device for measuring gradients of magnetic or electrostatic fields. By producing large differences of optical paths it is intended to use the instrument for the determination of the limit of coherence of an electron beam. In analogy to interference spectroscopy of light optics it could be used for the determination of the band structure of electron emitters. Another possible use may be indicated by applying it to the study of internal potentials in solids.

Construction of an electron interferometer is underway and results will be reported later.

* This work was done as part of a cooperative program of research and development in basic instrumentation sponsored jointly by the National Bureau of Standards, ONR, Office of Air Research, and the AEC.

[1] Mitsuishi, Nagasaki, and Uyeda, Proc. Japan Acad. **27**, 86 (1951).

[2] Private communication from Dr. Rees.

[3] Reported at the National Bureau of Standards Electron Physics Symposium.

Stopping Power of Heavier Substances

J. LINDHARD AND M. SCHARFF
Institute for Theoretical Physics, Copenhagen, Denmark
(Received February 11, 1952)

IN recent years a considerable number of experiments have been performed on the stopping of swift particles of low charge. The results have been discussed on the basis of the treatments by Bethe and by Bloch. The purpose of the present note is to point out a simple way in which to compare the experimental data for substances of fairly high atomic numbers.

When the dynamics of atoms is described on classical lines on the basis of the Thomas-Fermi model a striking similarity appears in the behavior of different atoms for the following reason. In the dynamics of a Fermi gas of density ρ there enters directly a frequency, namely the classical resonance frequency $\omega_0=(4\pi\rho e^2/m)^{1/2}$, involving the interaction of the electrons. In the statistical model of the atom, where the common unit of length is proportional to $Z^{-1/3}$, the scale serving as a norm for the frequencies ω_0 is proportional to Z. Similarly, since the velocities involved behave as $\rho^{1/3}$ or $Z^{1/3}$, the scale measuring frequencies of revolution ω_r in the atom is also proportional to Z. This gives the characteristics of the dynamics of heavy atoms on the classical approach, in which the motion is shared by many electrons.

Consider now the process of slowing-down of a swift atomic particle of low charge, z, so that the energy transfer is proportional to z^2. The effects of the particle are then completely specified by its velocity v, corresponding to a frequency $\omega_{\max}=2mv^2/\hbar$. The stopping will be determined by the relative value of the frequencies in the atom measured in terms of $\omega_{\max}$. One then finds for dimensional reasons that the specific energy loss as a function of v and Z, may be written $(4\pi z^2e^4/mv^2)\cdot N\cdot Z$ times a dimensionless function of $(\omega_0$ or $\omega_r)/\omega_{\max}\propto Z/v^2$, and one may write

$$\frac{1}{N}\frac{dE}{dR}\cdot\frac{mv^2}{4\pi z^2e^4Z}=L=L(Z/v^2), \tag{1}$$

where L is a so far unspecified function, determined by the distribution of the proper frequencies in the atom. When relativistic effects are of importance, the familiar quantity $\log(1-v^2/c^2)+v^2/c^2$ is to be added on the left hand side. But corrections for K-shells are not to be introduced in a statistical description of atoms of the kind considered here.

By using a simplified classical hydrodynamical treatment of the motion of a Fermi gas, Bloch has obtained a formula of the type (1) with $L=\log(2mv^2/Z\cdot I_0)$, I_0 being a constant. This expression should have approximate validity for very high velocities v.

The considerations leading to (1) may be given a more quantitative form. It is here useful to note that for a free Fermi gas of electrons the frequency giving the adiabatic limit for a particle of high velocity is precisely the classical resonance frequency ω_0. Averaging over the density distribution in the atom and including the above frequencies of revolution, one obtains the formula of Bloch for a very swift particle, while for lower velocities the stopping power of the medium is found to be nearly proportional to $Z^{1/3}/v$. The constants obtained are in both cases of the right order of magnitude. Moreover, it can be shown that similar results are obtained directly from the general stopping formula of Bethe when one introduces the frequencies and oscillator strengths of the individual atomic transition processes.

According to Eq. (1) the data on stopping may be approximately described by a single function of Z/v^2 common to all elements of not too low atomic number. In Fig. 1 are shown some experimental values of L determined from the left hand side of (1); the abscissa used is $x=(v/v_0)\cdot Z^{-1/2}$. We have included a number of absolute measurements on the stopping of protons of energy between 1–200 kev and 340 Mev,[1-3] for metals ranging from uranium to the extreme case of beryllium. The points on the figure show a rather well-defined curve. The placing of other elements may be obtained from the numerous relative measure-

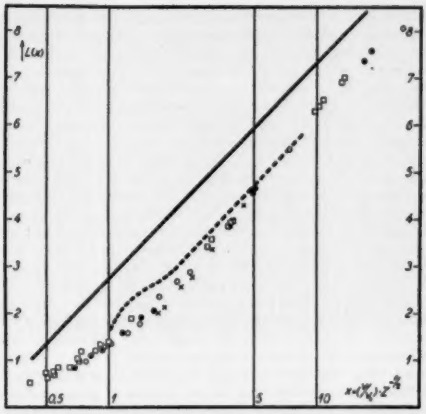

FIG. 1. The points represent experimental values of the quantity L given by Eq. (1). The abscissa is the variable $x=(v/v_0)\cdot Z^{-1/3}$ in a logarithmic scale, where $v_0=e^2/\hbar$. The crosses are for elements with $Z<10$ (only Be). The open circles correspond to $10<Z<20$. The black dots: $20<Z<40$, and the squares: $40<Z$. For low values of x the points nearly correspond to $L=$const. $\cdot x$. The dotted line is the curve of Bethe for air, and the straight full-drawn line gives the inclination corresponding to Bloch's asymptotic formula.

ments, which indicate that substances like air or the noble gases do not deviate appreciably from the metals. However, the curve obtained from the absolute measurements is not in agreement with that given by Bethe[4] for air, supported by range measurements and indicated by the dotted line on the figure. Still, independently of the way in which such systematic deviations may be explained, the measurements do indicate that L is a well-defined function of Z/v.

Arguments similar to those above may be applied in the case of straggling in energy loss and for the stopping of electrons penetrating matter. A closer discussion of these and related questions will be published in the Kgl. Danske Videnskab. Selskab, Mat.-Fys. Medd.

We are much indebted to Professor N. Bohr and to Aage Bohr for illuminating discussions.

[1] S. D. Warshaw, Phys. Rev. **76**, 1759 (1949).
[2] C. B. Madsen and T. Huus, Phys. Rev. **76**, 323 (1949); C. B. Madsen and P. Venkateswarlu, Phys. Rev. **74**, 648 (1948); C. B. Madsen, to be published in Kgl. Danske Videnskab. Selskab, Mat.-Fys. Medd.
[3] D. C. Sachs and J. R. Richardson, Phys. Rev. **83**, 834 (1951). C. J. Bakker and E. Segrè, Phys. Rev. **81**, 489 (1951).
[4] H. A. Bethe and M. S. Livingston, Revs. Modern Phys. **9**, 245 (1937); see also H. A. Bethe, Revs. Modern Phys. **22**, 213 (1950).

Electromagnetic Interference Effects in Charged Meson-Proton Scattering*

M. F. KAPLON
University of Rochester, Rochester, New York
(Received January 30, 1952)

BETHE and Wilson[1] have recently pointed out that the sign of the scattering amplitude for meson-nucleon scattering depends on the charge of the meson and the specific meson theory employed. One is reminded of proton-proton scattering in which the interference effects between the nuclear and electromagnetic scattering were used to determine the sign of the nuclear amplitude. In the meson scattering it turns out that it is also feasible in principle to use the interference between nuclear and electromagnetic scattering by protons to determine the sign of the nuclear scattering amplitude for a given meson charge.[2]

In order to estimate these effects one must use a given model. Although it is not expected that weak coupling theory will give a quantitatively correct account of meson interactions, it is thought that the qualitative predictions of the theory may have some interest, particularly in the nonrelativistic region.[3] It is with this basic qualification that the interference effects are calculated to lowest order in the weak coupling approximation.

Since the present evidence strongly favors the pseudoscalar theory,[4] we restrict ourselves to this theory and consider both the direct and derivative couplings. Two Feynman diagrams are needed to calculate either process I: $(\pi^++P\to\pi^++P)$ or process II: $(\pi^-+P\to\pi^-+P)$, one for the nuclear and one for the electromagnetic scattering. The matrix elements are (primed quantities refer to the $PS(PS)$ theory):

$$\mathbf{M}_{\mathrm{I}}=-\frac{f^2}{\mu^2}\left\langle \mathbf{I}\left|\left[\frac{2Mqq_o}{\mu^2-2p_o\cdot q}+q\right]\right|\mathbf{F}\right\rangle-\frac{2e^2\langle\mathbf{I}|q|\mathbf{F}\rangle}{(p_o-p)^2}$$

$$\mathbf{M}_{\mathrm{I}}'=-\langle\mathbf{I}|q|\mathbf{F}\rangle\left[\frac{g^2}{\mu^2-2p_o\cdot q}+\frac{2e^2}{(p_o-p)^2}\right]$$

$$\mathbf{M}_{\mathrm{II}}=-\frac{f^2}{\mu^2}\left\langle \mathbf{I}\left|\left[\frac{2Mq_oq}{\mu^2+2p_o\cdot q_o}-q\right]\right|\mathbf{F}\right\rangle+\frac{2e^2\langle\mathbf{I}|q|\mathbf{F}\rangle}{(p_o-p)^2}$$

$$\mathbf{M}_{\mathrm{II}}'=\langle\mathbf{I}|q|\mathbf{F}\rangle\left[\frac{g^2}{\mu^2+2p_o\cdot q_o}+\frac{2e^2}{(p_o-p)^2}\right].$$

The notation is that of Feynman,[5] the letters p and q referring respectively to the proton and the meson and the subscript o denoting the initial state.

We note first, a feature already pointed out by Bethe and Wilson,[1] that the signs of the nuclear scattering amplitudes for processes I and II are the same for the $PS(PS)$ theory. Therefore, if constructive interference is observed for one process (I) this theory would then predict destructive interference for the other (II). On the other hand, the $PS(PV)$ theory behaves like the $PS(PS)$ theory only at extremely low meson energies. At meson energies greater than approximately five to ten Mev and for reasonable angles, the nuclear amplitude changes sign[6] for process I but does not do so for process II. Hence, under the usual experimental conditions, destructive interference should be observed for both processes I and II for the $PS(PV)$ theory in contrast to the $PS(PS)$ theory.

In order to demonstrate the nature of the interference effects, we have calculated the differential cross section in the center-of-mass system for process I on the basis of the $PS(PV)$ theory (this seems to be the more promising; see reference 3) for three different energies of the π^+ meson in the laboratory system. The results are shown in Figs. 1 and 2 for two different coupling constants to indicate the dependence on the strength of the π meson-nucleon coupling. It is seen that a smaller coupling constant shifts the minima in the scattering cross section to higher angles. It would therefore seem possible to differentiate experimentally between the two types of coupling of the pseudoscalar theory. In

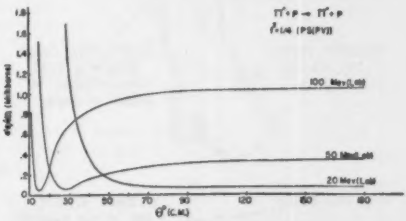

FIG. 1. Differential scattering cross section in the center-of-mass system for the reaction $\pi^++P\to\pi^++P$ including electromagnetic effects for the $PS(PV)$ theory. The π meson-nucleon coupling constant $f^2=\frac{1}{4}$. The curves are labeled according to the π-meson kinetic energy in the laboratory system.

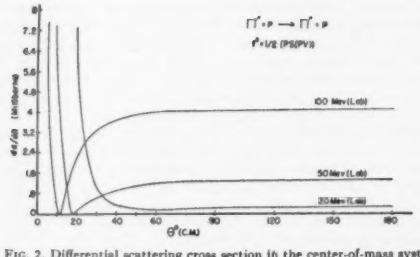

FIG. 2. Differential scattering cross section in the center-of-mass system for the reaction $\pi^+ + P \rightarrow \pi^+ + P$ including electromagnetic effects for the $PS(PV)$ theory. The π meson-nucleon coupling constant $f^2 = \frac{1}{2}$. The curves are labeled according to the π-meson kinetic energy in the laboratory system.

any event, one should be able to obtain useful information concerning the meson-nucleon scattering amplitude by observations on the interference effects with the electromagnetic scattering.

The consideration of this problem arose from a discussion with Professor R. E. Marshak and Mr. A. Messiah. I am indebted to Professor Marshak for further discussion.

* This research supported by the AEC.
[1] H. A. Bethe and R. R. Wilson, Phys. Rev. **83**, 690 (1951).
[2] These interference effects have also been considered by Dr. M. H. Johnson as a possibility of distinguishing between the various spin 0-meson theories (private communication from Dr. M. H. Johnson).
[3] R. E. Marshak, Revs. Modern Phys. **23**, 137 (1951).
[4] Clark, Roberts, and Wilson, Phys. Rev. **83**, 649 (1951).
[5] R. P. Feynman, Phys. Rev. **76**, 749 (1949).
[6] At higher meson energies the sign of the nuclear scattering amplitude is determined by the second term of the nuclear matrix element, while at very low meson energies the nuclear amplitude for both processes I and II is $\sim +1/2M$. The change of sign of the amplitude for process I occurs at such low meson energies that it is probably not experimentally detectable due to the extremely large electromagnetic scattering in this energy region.

The Velocity of 170-Mev Gamma-Rays*

DAVID LUCKEY AND JOHN W. WEIL†
Cornell University, Ithaca, New York
(Received January 31, 1952)

As a test of a high resolution coincidence circuit for experiments utilizing monoenergetic gamma-rays selected from bremsstrahlung,[1] we have measured the velocity of 170-Mev gamma-rays. A bremsstrahlung gamma-ray is counted in delayed coincidence with the electron producing it. 310-Mev electrons in the circulating beam of the Cornell synchrotron strike a thin target and are analyzed after radiation by the magnetic guide field (Fig. 1). A stilbene crystal is located so as to intercept electrons of about 140 Mev. The energy spectrum of the gamma-rays in coincidence with these electrons was measured by use of the Cornell pair spectrometer[2] and was found to correspond to a peak at 170 Mev with a full width at half-maximum of twenty percent or less.[1] The velocity of the coincident gamma-rays was determined by measurement of relative delay time *versus* position of a movable, external, scintillation counter. Transit time differences were measured for four positions (extreme positions had a separation of thirteen meters) using a coincidence circuit with a resolving time of 4×10^{-9} second. The peak of the resolution curve at each position could be determined within 2×10^{-10} second. Cable delay times were calibrated by observing their resonant frequencies under shorted termination in the frequency range from 10 to 500 megacycles.[3] The error in cable calibration is of the order of one-half percent. A plot of distance *versus* transit time gives a straight line whose slope is the velocity of the 170-Mev gamma-rays. A least squares fit gives a value of 2.974×10^{10} cm/sec, with estimated probable error of one percent. This agrees within the experimental uncertainties with the value of c obtained for 0.5-Mev gamma-rays,[3] and with the most probable value of c obtained from measurements at lower frequencies to be 2.998×10^{10} cm/sec.[4]

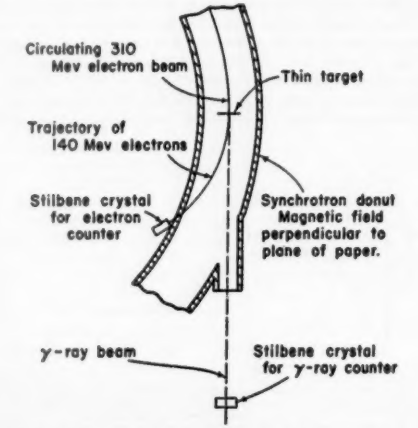
Circulating 310 Mev electron beam
Thin target
Trajectory of 140 Mev electrons
Stilbene crystal for electron counter
Synchrotron donut Magnetic field perpendicular to plane of paper.
γ-ray beam
Stilbene crystal for γ-ray counter

FIG. 1. Experimental arrangement for velocity measurement.

We wish to thank Professor B. D. McDaniel for his helpful advice and encouragement.

* Supported in part by the ONR.
† AEC Predoctoral Fellow.
[1] J. W. Weil and B. D. McDaniel, Bull. Am. Phys. Soc. **27**, No. 1, 7 (1952).
[2] DeWire, Ashkin, and Beach, Phys. Rev. **83**, 505 (1951).
[3] M. R. Cleland and P. S. Jastram, Phys. Rev. **84**, 271 (1951).
[4] J. W. DuMond and E. R. Cohen, Phys. Rev. **82**, 555 (1951).

Elastic and Plastic Properties of Very Small Metal Specimens

CONYERS HERRING AND J. K. GALT
Bell Telephone Laboratories, Murray Hill, New Jersey
(Received January 29, 1952)

THE elastic and plastic behavior of bulk tin has been investigated by several workers. As a result, quite detailed data are available on the yield stress and creep rate. The yield stress varies, of course, with the crystal plane across which stress is applied and its direction in that plane, but the values for the principal cases of interest are all shears of approximately 0.15 kg/mm²[1] resolved shear stress. From the elastic constants of tin we are thus led to a maximum yield strain of about 10^{-4} before slip occurs in a simple tension experiment. The minimum creep rates observed are about 2×10^{-6}/sec at tensions of about 0.1 kg/mm².[2] This behavior is usually explained in terms of the motion of imperfections, especially of dislocations, since on any reasonable model of a perfect crystal one expects the yield strain[3] to be of the order of 10^{-1}.

It has often been presumed[4] that specimens of very small dimensions ought to have a much larger range of elastic strain than the bulk metal, either because they are free of dislocations, or because the few dislocations present cannot multiply sufficiently to give an observable amount of slip. It occurred to us that this hypothesis could be tested by performing experiments on the thin whiskers which have been observed to grow out from the surfaces of a number of low-melting-point metals.[5] We have therefore made observations on some tin whiskers grown from a tin-plated surface by Mr. S. M. Arnold of these laboratories. Electron microscope observations of many such whiskers, carried out by Mr. C. J. Calbick, of these laboratories, have shown their diameters to be

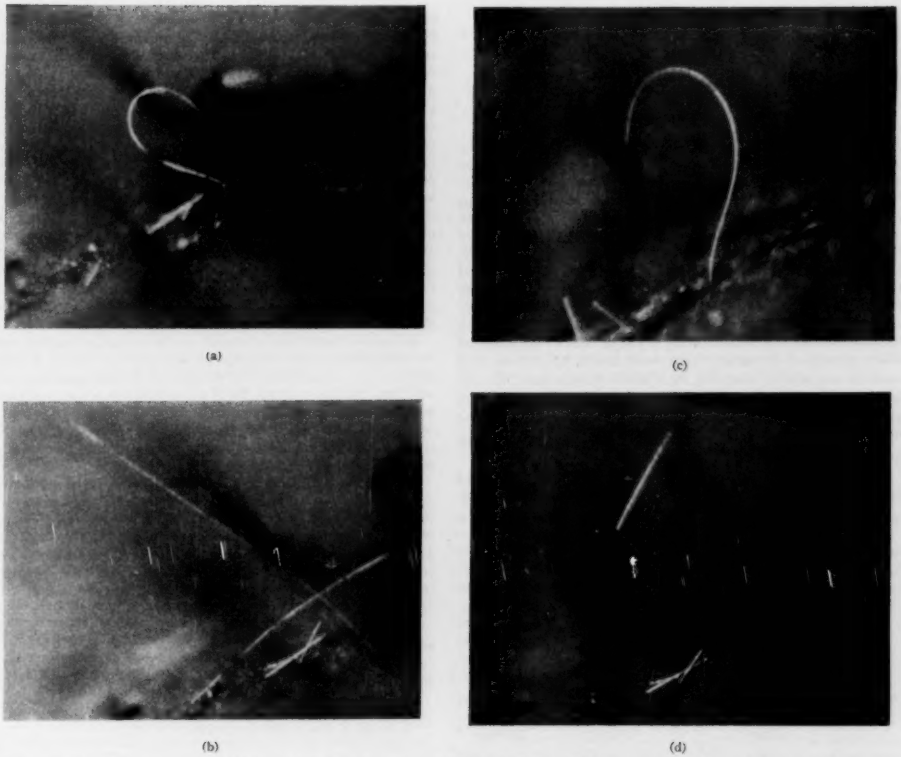

(a) (c)

(b) (d)

FIG. 1. Bending and recovery of tin whiskers. (a) Radius of curvature 0.009 cm. (b) Same whisker after removal of constraining probe. (c) Creep experiment, radius of curvature 0.015 cm. (d) Typical bend produced by excessive stress. In all pictures the whiskers have been manipulated to be in the plane of the picture or close enough to it so that angles and radii of curvature may be read with reasonable accuracy from the pictures.

remarkably uniform and equal to $1.8\pm0.1\times10^{-4}$ cm. They range up to several millimeters in length. Our experiments have consisted in bending a number of these whiskers; the results indicate an elastic and plastic behavior not far different from that to be expected from a truly perfect crystal.

In the first place, very large strains can be tolerated in these whiskers without slip. Figure 1(a) shows a whisker bent sharply (radius of curvature $r_c=0.009$ cm) about a No. 44 formex copper wire (running perpendicular to the plane of the picture and only in focus over a short part of its length) by a 0.010-in. music wire probe. Figure 1(b) shows the same crystal straightened out (running upward from right to left). The strain varies across the cross section from a large positive value at the outer surface through zero to a large negative value on the inner surface of the curved whisker. The maximum strain in Fig. 1(a) is thus the ratio of whisker radius to radius of curvature, or 10^{-2}.

These whiskers also sustain large strains without creep. Figure 1(c) shows a whisker bent to a radius of curvature $r_c=0.015$ cm. The strain is thus 6×10^{-3}. After a week in this position, this whisker straightened out perfectly, as nearly as we were able to tell, when the restraining probe was removed. From the minimum strain which we could observe, we deduce that the strain rate in this experiment was certainly less than 5×10^{-10} sec^{-1}. In comparing this value with the value given above for the minimum creep rate in tin it should be borne in mind that the stresses occurring in our experiment are much higher. From the product of strain and elastic constant we deduce that stresses of the order of tens of kg/mm^2 were present in our sample.

When these whiskers are bent until the maximum strain in them is about 2 or 3 percent they do deform, but in a rather unusual way. A bend which seems to be perfectly sharp occurs in the whisker. Such a bend is shown in Fig. 1(d). It should be emphasized that the whisker has considerable strength at these bends. This has been determined by manipulating them, and by observing the fact that the part of the whisker beyond the bend can be supported by them. Other bend angles have been observed, but values near the one shown in Fig. 1(d) seem to be the most common.

We wish to express our gratitude to Mr. S. M. Arnold for providing us with samples, and to Mr. H. G. Hopper for technical assistance.

[1] J. Obinata and E. Schmid, Z. Physik **82**, 224 (1933); K. Bausch, Z. Physik **93**, 479 (1935).
[2] B. Chalmers, Proc. Roy. S. (London) **A156**, 427 (1936).
[3] L. Bragg and W. M. Lomer, Proc. Roy. Soc. (London) **A196**, 171 (1949); W. M. Lomer, Proc. Roy. Soc. (London) **A196**, 182 (1949).
[4] See for example C. Herring, Chap. 8 of *The Physics of Powder Metallurgy*, edited by W. E. Kingston (McGraw-Hill Book Company, Inc., New York, 1951).
[5] Compton, Mendizza, and Arnold, Corrosion **7**, 327 (1951).

The Pure Nuclear Electric Quadrupole Resonance of N^{14} in Three Molecular Solids*

G. D. WATKINS AND R. V. POUND
Harvard University, Cambridge, Massachusetts
(Received January 28, 1952)

BY using an rf spectrometer[1] of the regenerative type, the pure quadrupole resonance of N^{14} has been observed in three solids: cyanogen iodide, cyanogen bromide, and hexamethylenetetramine. An "on-off" square wave of magnetic field at 280 cps was applied to the sample. In this way, the resonance was smeared out for half of the modulation period and 280 cps modulation of the absorption resulted. A narrow band amplifier, a phase sensitive detector, and an integrating output circuit were used and the signal was displayed on a recording meter. Figure 1 shows the recorded signal in $(CH_2)_6N_4$ at room temperature. The amplitude ratio of signal-to-noise in BrCN and ICN is only about one-tenth as large as this, as a result mainly, of longer relaxation times and lower density of nitrogen. A ten-times longer integration time constant was used in observing these lines to compensate partially for the loss in signal intensity. Defining the width of an absorption as $[g_{max}(\nu)]^{-1}$, where $g(\nu)$ is the normalized shape function of the line, the observed widths are 1.05 kcps, 760 cps, and 1.08 kcps for ICN, BrCN, and $(CH_2)_6N_4$, respectively.

The frequencies were measured at room, ice, dry ice, and liquid N_2 temperatures and these data are given in Table I.

TABLE I. Frequency (Mcps) *vs* temperature.

Temperature	$(CH_2)_6N_4$	BrC≡N	IC≡N
−196°C	3.4076 ∓0.0001	(1) 2.5109∓0.0001 (2) 2.5203∓0.0001	—
− 74°C	3.3560 ∓0.0001	(1) 2.4910∓0.0002 (2) 2.4963∓0.0002	2.5512∓0.0002
0°C	3.31990∓0.00005	2.4734∓0.0002	2.5451∓0.0002
Room temp.	3.3062 ∓0.0001	(1) 2.4650∓0.0002 (2) 2.4627∓0.0002	2.5424∓0.0002
	(26.6°C)	(24.2°C)	(26.8°C)

A search over the range 2.52–2.57 Mcps failed to detect the absorption in ICN at liquid N_2 temperature. While warming up from this temperature, the crystal grains appeared to fracture violently just below dry ice temperature, possibly evidence of a phase change, and associated strains may have so broadened the line that it was undetectable. In BrCN, two lines of approximately equal intensity were observed. They have different temperature dependences and cross at 0°C. This could result if there were two nonequivalent molecules per unit cell or if there were a temperature dependent asymmetry factor $\eta=[(\partial^2V/\partial x^2)-(\partial^2V/\partial y^2)]/(\partial^2V/\partial z^2)$. For $I=1$, departure from axial symmetry would remove the $m_I=\pm1$ degeneracy and two lines would result. No data on crystal structure for BrCN has been found in the literature. Neither of the above sources of doubling of the N^{14} resonance would be present if the unit cell were similar to the unimolecular rhombohedral cell of ICN.[3] Information on this point could be obtained by observation of the Zeeman pattern in a single crystal.[5] In the gas state, quadrupole coupling constants e^2qQ/h of 3.83 ±0.08 and 3.80 Mcps are reported for BrCN[4] and ICN[3], respectively. For $I=1$, the resonance is at $\nu=\frac{1}{4}e^2qQ/h$ and the coupling constants are thus about 12 percent smaller in the solid than in the gaseous state.

Relaxation times were measured by the saturation method and for ICN, BrCN, and $(CH_2)_6N_4$ they are, at 0°C, 7.4 sec, 2.7 sec, and 0.17 sec, respectively. For samples of the size used (2.5 cm³) and these relaxation times, the rf voltages at the coil for optimum signal-to-noise are 0.19 v(rms), 0.26 v(rms), and 1.6 v(rms), respectively. At these levels, the noise figure of the spectrometer is low,[1] and little could be gained by the use of more complicated detection systems.

The relaxation time in $(CH_2)_6N_4$ was found to be 1.7 sec at −74°C and 11 sec at −196°C. If we assume the model of Bayer,[6] in which the relaxation mechanism arises from the torsional oscillations of the molecule as a whole, a dependence $T_1\sim\tau_a T^{-1}$ is predicted, where τ_a is the average lifetime of the various states of torsional oscillation. This is not compatible with the rapid temperature dependence of T_1 that is observed unless τ_a varies with temperature.

* This work was partially supported by the joint program of the ONR and AEC.
[1] G. D. Watkins and R. V. Pound, Phys. Rev. **82**, 343 (1951).
[3] R. W. G. Wyckoff, *Crystal Structures I* (Interscience Publishers, Inc., New York, 1948).
[4] C. Dean, Bull. Am. Phys. Soc. **27**, No. 1, 32 (1952).
[5] Townes, Holden, and Merrit, Phys. Rev. **74**, 1113 (1948).
[6] Smith, Ring, Smith, and Gordy, Phys. Rev. **73**, 633 (1948).
[6] H. Bayer, Z. Physik **130**, 227 (1951).

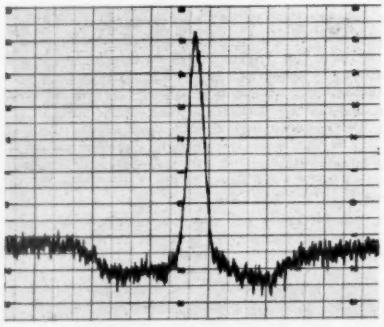

FIG. 1. Pure quadrupole absorption of N^{14} in $(CH_2)_6N_4$. The negative deflections in the wings correspond to the absorption when the modulating magnetic field is on. Each of the two cascaded *RC* integrating circuits has a time constant of 2 sec.

The Photodissociation of the Deuteron by High Energy Gamma-Rays

SEISHI KIKUCHI
Radiation Laboratory, Department of Physics, University of California, Berkeley, California
(Received January 23, 1952)

AN analysis was made of proton tracks found in photographic emulsions exposed to the secondary particles from a high pressure deuterium gas target bombarded by the synchrotron bremsstrahlung gamma-rays of maximum energy 320 Mev,[1] with the object of investigating the photodissociation of the deuteron in the high energy region. The secondary particles were collimated by slit systems in such a manner that we could analyze the protons at emission angles of approximately 45, 90, and 135 degrees.

The minimum energy required for a proton to penetrate through the walls of the target chamber to reach the plates was 70 Mev at 45 and 135 degrees and 60 Mev at 90 degrees. This circumstance excluded the possibility of recoil protons ejected by the photomeson producing process from reaching the plates. The energy of the proton was computed from the thickness of the absorbing material between the end point of the proton and the target.

In the case of the photo-dissociation of a deuteron into a proton and a neutron, there is a relation $k=2T[1-(T/M)(P\cos\theta/M)]^{-1}$ between the energy T and momentum P of the proton of mass M,

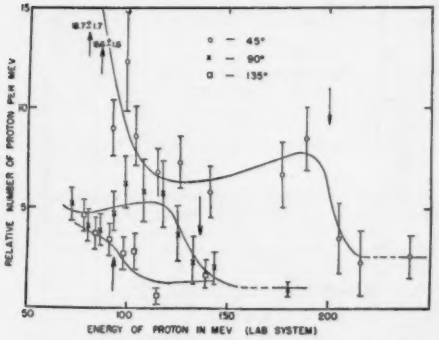

FIG. 1. Differential cross section per photon for the photodissociation, as a function of the photon energy.

the angle θ between the direction of the ejection and the incident beam, and the energy k of the photon which caused the dissociation.

Putting $k=320$ Mev in this relation we get 93, 136, and 200 Mev for the maximum energy of protons at 45, 90, and 135 degrees, respectively.

The energy spectra obtained are shown in Fig. 1. These spectra show well defined cutoffs at the proton energies 95, 135, and 200 Mev, coinciding closely with the expected values. This seems to indicate that these protons are actually the photoprotons produced by the splitting of a deuteron into a proton and a neutron by the absorption of a photon.

Assuming the bremsstrahlung spectrum to be proportional to $1/E$, we can compute from the results shown in Fig. 1, the differential cross section per photon for the photodissociation as a function of the photon energy. The result is given in Table I.[2] In

TABLE I. Differential cross section as a function of photon energy in the laboratory system.

	Energy of photon in Mev	Diff. cross sec in microbarns		Energy of photon in Mev	Diff. cross sec in microbarns
45°	133	14.4 ±1.8	90°	158	2.7 ±0.6
	144	12.8 ±1.9		178	2.4 ±0.7
	152	6.6 ±1.8		194	2.4 ±0.7
	162	10.7 ±3.0		211	3.4 ±1.0
	170	6.9 ±2.2		226	5.1 ±1.3
	189	5.4 ±2.1		248	5.2 ±1.7
	205	6.5 ±2.3		272	5.5 ±1.3
	228	5.0 ±2.6			
	285	8.0 ±3.8	135°	250	0.99 ±0.27
	304	12.3 ±4.0		272	0.99 ±0.35

the 45-degree case one can see the dependence of the cross section on photon energy in a fairly wide range. Below 150 Mev it decreases rather steeply with increasing energy, and at about 150 Mev it begins to flatten out and then starts to increase again with increasing energy.

The angular distribution in laboratory system shows a fairly strong forward asymmetry. The same trend can be seen in the center-of-mass system.

The total cross section was roughly estimated by multiplying the differential cross section at 90° by 4π. Below 150 Mev, where no data for 90° was available, the cross section was assumed to be proportional to the differential cross section at 45°. Table II shows the results. The errors indicated are those referred to the relative values. Referring to the absolute value, the error might be as large as a factor of 3. Comparing with Schiff's theoretical values given in Table II, one should rather consider that the

TABLE II. Total cross section as a function of photon energy.

Energy of photon in lab. system	Energy of photon in c.m. system	Total cross section in 10^{-29} cm²	Theoretical value (Schiff), in 10^{-29} cm²
133	125	6.2 ±0.5	2.3
158	146	3.4 ±0.8	1.6
178	163	3.0 ±0.8	
194	176	3.0 ±0.9	
211	191	4.3 ±1.2	
226	202	6.4 ±1.7	
248	220	6.6 ±2.2	
272	239	6.9 ±1.7	

experimental values are compatible with the theoretical values below 150 Mev, which is the upper limit of the validity of the theory set by Schiff himself. Above 150 Mev the cross section does not decrease as the straightforward extrapolation of Schiff's curve does. Recently, Gilbert and Rose[3] at this Laboratory studied the photodissociation of the deuteron in nearly the same energy range as the present work, using a counter technique. For the dissociation at photon energies of 200 and 250 Mev in the c.m. system, they obtained total cross sections which are about twice as large as the present values. Because of the relatively large error involved in both experiments, the results should be regarded as in agreement with each other.

The increase of the photodissociation cross section above 150 Mev may be explained by the increasing importance of the absorption of a photon with emission and reabsorption of a virtual meson in the energy range above the meson threshold. It is hoped that the experimental evidence given here may provide a more direct and more stringent test for the different types of meson theory, than has been the case with experiments in the low energy region, where the comparison of the theory with the experiments was made more or less indirectly, as far as the meson theory is concerned.

The author wishes to thank Professors McMillan and Helmholz, and R. S. White and W. S. Gilbert for discussions as well as for their generosity in placing their plates at the author's disposal.

[1] The exposure had been made originally by R. S. White and others of this laboratory to investigate the photomeson production in deuterium [Bull. Am. Phys. Soc. **26**, No. 8, 22 (1951)].
[2] The relatively large error in the 45° case compared to the other cases came from the ambiguity involved in the background.
[3] W. S. Gilbert and J. W. Rose, Phys. Rev. (to be published).

Silver-Activated Alkali Halides

H. W. ETZEL, J. H. SCHULMAN, R. J. GINTHER, AND E. W. CLAFFY
Crystal Branch, Metallurgy Division, Naval Research Laboratory, Washington, D. C.

(Received February 4, 1952)

THE earliest investigation of the silver-activated alkali halides appears to have been made by Smakula.[1] His data show a single sharp absorption band peaking at 2100A in NaCl:Ag. The most recent study of these phosphors is evidently by Kato,[2] who investigated the emission as well as the absorption spectra. Kato's absorption data agree very well with Smakula's. He observes that excitation into the characteristic silver ion absorption band in NaCl:Ag produces two emission bands, one peaking at 2490A and a second at 4000A.

We have found, as shown in Fig. 1, that three absorption bands appear in NaCl upon the introduction of ionic silver. These bands lie at 2095A, 2170A, and 2295A. The absorption measurements were made with a split-beam, frequency selective, single detector, automatic recording spectrophotometer[3] on single crystals grown by the Kyropoulos technique from NaCl-AgCl melts. Figure 2 is a photograph of the emission of the NaCl:Ag upon excitation into each of the three absorption bands. For this measurement

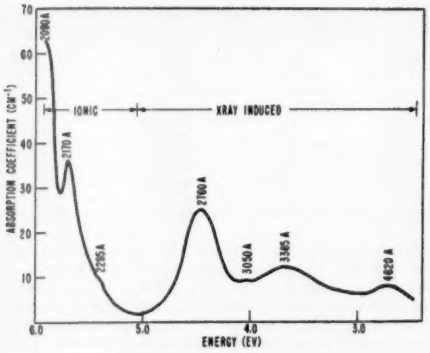

FIG. 1. Spectral absorption of x-rayed NaCl:Ag.

the output of a quartz envelope H-4 mercury lamp was monochromatized by a Gaertner quartz monochromator. The monochromatic light then impinged upon a plaque of powdered NaCl:Ag, the fluorescence of which was photographed with a Gaertner quartz spectrograph. Excitation with ultraviolet light of 2100A wavelength and below produced only the 2500A emission; excitation with 2170A light produced predominantly 2500A emission but also some 4000A emission, while 2270A excitation produced a stronger emission of 4000A light than of 2500A light.

In order to determine whether the observed emissions were caused by different excited states of the same center or to two or more types of centers, absorption measurements were made on a series of single crystals containing varying amounts of ionic silver. Figure 3 shows a plot of the observed absorption coefficient for the 2170A and the 2295A bands plotted against the mole ratio of silver to sodium. Superimposed on this graph is a plot of the number of paired silver ions, calculated on the assumption of a random distribution of these ions. The shape of the 2295A curve agrees well enough with the calculated curve for pairs to indicate that this absorption and resulting emission at 4000A are due to pairs. The 2170A absorption is apparently not due to pairs but to individual silver ions.

The above data are a part of a more extensive study of Ag-activated alkali halide systems. It has been found[4,5] that these systems are radio-photoluminescent, i.e., NaCl:Ag luminesces under near ultraviolet light after exposure to x-rays or gamma-

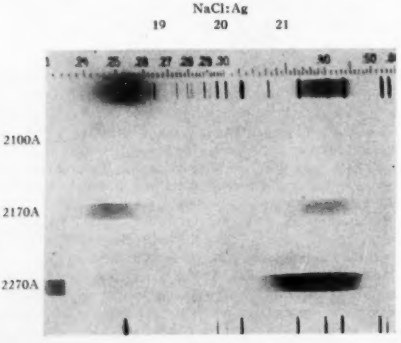

FIG. 2. Emission spectra of NaCl:Ag under various exciting wavelengths.

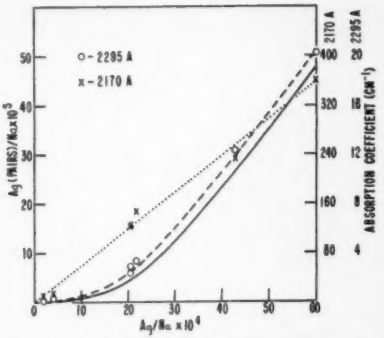

FIG. 3. Ratio of Ag pairs to Na (calculated) vs ratio of Ag to Na (experimental): solid curve. Measured absorption coefficient vs ratio of Ag to Na (experimental): dotted curves.

rays. The new absorption bands observed after x-raying NaCl:Ag are shown in Fig. 1 (at 2760A, 3050A, 3365A) together with the *F*-band at 4620A. A more complete study of this system will be reported in a forthcoming paper.

[1] A. Smakula, Z. Physik **45**, 1 (1927).
[2] M. Kato, Sci. Papers Inst. Phys. Chem. Research (Tokyo) **41**, 113 (1943).
[3] H. W. Etzel (to be published).
[4] Weyl, Schulman, Evans, and Ginther, J. Electrochem. Soc. Japan **95**, 70 (1944).
[5] Schulman, Ginther, and Evans, "X-ray sensitive screen," U. S. Patent No. 2,524,839 (October 10, 1950).

Errata

The Corbino Effect and the Change of Resistance in a Magnetic Field, K. M. KOCH AND L. HALPERN [Phys. Rev. **82**, 460 (1951)]. The name of the second author was inadvertently omitted from the manuscript of the above-cited paper.

Relativistic Corrections to the Lamb Shift, MICHEL BARANGER [Phys. Rev. **84**, 866 (1951)]. The last published experimental value was erroneously stated to be 1061±2. It should have been 1062±5 Mc.

Radiative Corrections to the Intensities for Hydrogen-Like Atoms, T. TATI [Phys. Rev. **84**, 150 (1951)]. In the letter of the above title, I stated that if one takes into account the higher order field reaction, the transition probability between very near levels would become quite large. However, this conclusion was obtained by an incorrect neglect of terms[1] having the same order of magnitude as the fourth term of Eq. (2). If one adds these neglected contributions, one finds a vanishing matrix element for the process in the leading order.[2]

[1] This error was pointed out by Professor S. Tomonaga.
[2] This vanishing of the matrix element was pointed out by Dr. S. D. Drell in a private communication.

Absorption Spectrum of GaCl, FRANKLYN K. LEVIN AND J. G. WINANS [Phys. Rev. **84**, 431 (1951)]. On page 433, line 31, first column, the sentence beginning "The (0, 0) and (1, 0) bands of the 2440 to . . ." should read "The (0, 0) and (0, 1) bands of the 2440 to . . . ." On page 435, second column, the equation "$G(v+\frac{1}{2})=365.3(v''+\frac{1}{2})$ . . ." should

read "$G(v)=365.3(v''+\frac{1}{2})$ . . . ." On page 439, second column, the caption of Fig. 4 should read "Plot of $\Delta_2F(J)/(J+\frac{1}{2})$ *versus* $(J+\frac{1}{2})^2$ . . . ."

***P−N* Transition of an Oxide-Coated Cathode,** Y. ISHIKAWA, T. SATO, K. OKUMURA, AND T. SASAKI [Phys. Rev. **84**, 371 (1951)]. The first sentence of the third paragraph of the above Letter should read: "The activation energies of the conductivity are 16 kcal in high vacuum and 23 kcal in oxygen at high pressure."

Computation of Photonuclear Resonance Curves from Relative Activity Curves Monitored by Induced Radioactivity, R. SAGANE [Phys. Rev. **84**, 586 (1951)]. It has been found that a poor choice was made of the theoretical formula to represent the energy distribution of the bremsstrahlung, as used in Fig. 3 in the letter of the above title. The author had simply assumed Eq. (1) of Schiff,[1] with the substitution $x=0$, to be the best approximation for the x-ray spectrum produced by the Iowa State College synchrotron.

From a recent conversation with Dr. Schiff, it appears clear to the author that Eq. (3) of Schiff's paper or the curves given by Bethe and Heitler would represent a better approximation than Schiff's Eq. (1) with $x=0$. This is because the mean scattering angle is expected to be more than several times larger than mc^2/E, in the case of a tungsten target 0.005 in. thick and an electron energy between 20 and 65 Mev. Furthermore, due to the use of the Born approximation, a systematic error of about 10 percent has been found to arise with heavy target materials.[2]

Although the argument given in the recent letter by the present author is affected very little by the choice of the theory, the author felt it best to point out at this time the desirability of using a modified bremsstrahlung spectrum. The author is very grateful to Dr. Schiff for information concerning this point.

[1] L. I. Schiff, Phys. Rev. **83**, 252 (1951).
[2] DeWire, Ashkin, and Beach, Phys. Rev. **83**, 505 (1951), Fig. 5.

A Phenomenological Derivation of the 'First- and Second-Order Magnetostriction and Morphic Effects for a Nickel Crystal,' W. P. MASON [Phys. Rev. **82**, 715 (1951)]. It has been pointed out to the writer by Dr. F. G. Fumi of the Institute of Physics of Milan, that the numbering system used in the 6th rank magnetostrictive tensor $N_{ijmnop}T_{ij}I_mI_nI_oI_p$ of the above paper is inconsistent with the method used to derive it, namely reduction from the R_{ijklmn} tensor for which i can be interchanged with j, k with l, n with o, and ij with kl. To use this method of reduction the magnetostrictive tensor has to be written in the form

$$N_{mnopij}I_mI_nI_oI_pT_{ij}.$$

Then since m, n, o, and p can all be interchanged, there are three relations between the $9R$ coefficients of Appendix I, and the independent terms are N_{111}, N_{112}, $N_{121}=N_{211}$; $N_{122}=N_{441}$; $N_{144}=N_{455}$, and N_{155}.

The h constants of Eqs. (8) and (14) become

$$\begin{aligned}
h_1&=[\tfrac{1}{3}(M_{11}-M_{12})I_0^2+3(N_{121}-N_{122})I_0^4]\\
h_2&=[2M_{44}I_0^2+2N_{155}I_0^4]\\
h_3&=[\tfrac{1}{3}(N_{111}+2N_{112})-(N_{122}+2N_{121})]I_0^4\\
h_4&=[N_{111}-N_{112}+3(N_{122}-N_{121})]I_0^4\\
h_5&=[4N_{144}-2N_{155}]I_0^4.
\end{aligned} \tag{14}$$

No numerical results are involved.

Mass Measurements with a Magnetic Time-of-Flight Mass Spectrometer, E. E. HAYS, P. I. RICHARDS, AND S. A. GOUDSMIT [Phys. Rev. **84**, 824 (1951)]. A preliminary value was given for the mass of I^{127} based on a recalculation from data obtained by an inadequate early measuring technique. An improved technique gives for this mass $I^{127}=126.946\pm0.001$. This value was obtained by measuring the time of flight for ions of I and ICH_3 using as standards CF_3 and C_3F_8, with $C^{12}=12.003895$ and $F^{19}=19.00445$. The improved technique does not change any of the other mass values reported in our paper. The new measurement of I^{127} agrees with the preliminary value recently reported by R. E. Halstead [Phys. Rev. **85**, 726 (A) (1952)].

Author Index to Volume 85

References with (A) are to abstracts of papers presented at meetings of the American Physical Society, and those with (T) designate title only. References with (L) are to Letters to the Editor.

Abell, D. F. and W. D. Knight. Nuclear magnetic resonance in metallic Rb and Cs—762(A)
Abraham, B. M. (see Osborne, D. W.)—715(A)
—— (see Weinstock, B.)—158(L)
Adair, R. K. Evidence for strong spin orbit coupling from the low states of light nuclei—722(T)
Adams, E. N., II. Motion of an electron in a perturbed periodic potential—41
Adelman, Frank L. Fast protons from the capture of π^- mesons in photographic emulsions—249
Ahlert, R. H. (see Rittner, E. S.)—390(A)
Alburger, David E. Decay of Rh^{106}—734(A)
Alexander, W. R. (see Seagondollar, L. W.)—713(A)
Allen, A. J. (see Arthur, James S.)—704(A)
—— (see Ely, Ralph, Jr.)—704(A)
—— (see Reilley, E. M.)—704(A)
—— (see Sun, K.-H.)—942(L)
Allen, K. W. (see Pepper, T. P.)—155(L)
Allen, R. G., C. P. Stanford, T. E. Stephenson, and S. Bernstein. Slow neutron crystal spectrometer—767(A)
Allen, William A. and Clyde L. McCrary. Transient waves through steel produced by impulsive loading—769(A)
Allison, H. W. and George E. Moore. Production of Sr metal in the reduction of SrO by methane—388(A)
—— (see Moore, George E.)—389(A)
Allison, S. K. Experiments on light nuclei and on atomic beams —739(T)
Almqvist, E. (see Pepper, T. P.)—155(L)
Alpert, D. (see Holstein, T.)—985
Alvarez, L. W. (see Jenkins, F. A.)—763(A)
Anderson, C. D. Report on *V*-particles—744(T)
Anderson, Herbert L. Interaction of π-mesons with protons—729(T)
——, **E. Fermi, E. A. Long, R. Martin, and D. E. Nagle.** Total cross sections of negative pions in hydrogen—934(L)
——, **E. Fermi, E. A. Long, and D. E. Nagle.** Total cross sections of positive pions in hydrogen—936(L)
—— (see Fermi, E.)—935(L)
—— (see Martin, R. L.)—486(L)
Anderson, P. W. Approximate quantum theory of the antiferromagnetic ground state—714(A)
Anderson, Roger E. and Robert B. Duffield. Photofission of uranium—728(A)
Andrew, Kenneth L. and K. W. Meissner. Arc spectrum of germanium—716(A)
Antal, John J. and A. H. Weber. Tracer method for measurement of evaporated Bi film thicknesses—710(A)
Anthony, Romuald. Atmospheric absorption of solar infrared radiation—674(L)
Arfken, G. B. (see Rose, M. E.)—5
Arizumi, T. and S. Narita. Application of Nijboer's theory to the semiconducting emitters, and its modification—388(A)
Arnold, J. T. Chemical effects in nuclear induction—763(A)
Arthur, James S., A. J. Allen, R. S. Bender, R. L. Ely, H. J. Hausman, L. A. Page, and E. M. Reilley. Precision scattering project—704(A)
—— (see Ely, Ralph, Jr.)—704(A)
—— (see Reilley, E. M.)—704(A)
Asaro, Frank, Fred L. Reynolds, and I. Perlman. Complex alpha-structure of the heavy elements—758(A)
Ashburn, Edward V. Determination of the height and the diurnal variation of the night airglow—767(A)
Ashkin, J. and G. C. Wick. Comment on the "impulse approximation"—686(L)
—— (see Wolfenstein, L.)—947
Atkinson, W. R., R. G. Fowler, L. W. Marks, and G. W. Charles. Spectroscopic investigations of pulsed gas discharges—706(A)
Austern, N. Angular distribution in the high energy deuteron photoeffect—283
—— Quadrupole radiation in πD capture—147(L)
Avery, Eugene (see Smaller, Bernard)—766(A)
Axel, P. and J. C. Bowe. Radioactive decay of Te^{125m}—734(A)
—— (see Bowe, J. C.)—734(A), 858

Babiskin, Julius. Magnetic properties of a hollow superconducting lead sphere—104
Backman, Marvin E. Some experiments confirming the existence of electrical phenomena during the freezing of dilute aqueous solutions—759(A)
Baggett, L. M. and S. J. Bame, Jr. Disintegration of lithium by deuteron bombardment—434; 741(A)
Bair, J. K., H. B. Willard, C. W. Snyder, T. M. Hahn, J. D. Kington, and F. P. Green. Proton bombardment of lithium —946(L)
—— (see Hahn, T. M.)—934(L)
—— (see Willard, H. B.)—849
Baker, A. N., Jr. (see Webber, D. S.)—755(A)
Baker, C. J., J. N. Dodd, and D. H. Simmons. Scattering of 9.6-Mev protons by carbon, aluminum, and magnesium—1051(L)
Balfour, J. G. (see Insch, G. M.)—805
Bame, S. J., Jr. (see Baggett, L. M.)—434; 741(A)
Bandtel, Kenneth C. (see Madey, Richard)—771(A)
Bannerman, R. C. and S. C. Curran. Radiations of RaD—134(L)
Baranger, Michel. Erratum: Relativistic corrections to the Lamb shift—1064(L)
Barber, W. C., G. E. Becker, and E. L. Chu. Electron-electron scattering at 6.1 Mev—774(A)
Barghausen, W. B. (see Jen, C. K.)—717(A)
Barkas, Walter H., (see Giles, Peter C.)—756(A)
—— (see Heckman, Harry H.)—771(A)
—— (see Oliver, A. J.)—756(A)
—— (see Rankin, Bayard)—754(A)
—— (see Sherman, D. F.)—771(A)
—— (see Smith, F. M.)—771(A)
—— (see Violet, Charles E.)—756(A)
Barkofsky, Ernest (see Bennett, Arthur L.)—774(A)
Barnes, R. G. (see Harrick, N. J.)—716(A)
Barrett, P. H. and Y. Eisenberg. Diurnal variations in high energy cosmic-ray intensities—674(L)
Bartholomew, G. A. (see Kinsey, B. B.)—1012
Bauer, E. Dissociation of hydrogen molecules by vibrational excitation and three-body recombination coefficient. II—277
—— Excitation and de-excitation of the vibrational motion of hydrogen molecules by slow hydrogen atoms—707(A)
Beach, A. L. (see Lander, J. J.)—389(A)
Beattie, J. W. (see Laughlin, J. S.)—725(A)
—— (see Ovadia, J.)—725(A)
Becker, G. E. (see Barber, W. C.)—774(A)
Becker, J. A. Use of field emission in the study of the absorption of Ba on W—391(A)
Becker, M., H. Y. Fan, and K. Lark-Horovitz. Infrared absorption of nucleon bombarded silicon. I—730(A); II, H. Y. Fan—730(A)
Bederson, Benjamin (see Eisinger, Joseph T.)—716(A)

Belinfante, Frederik J. Gauge-independent quantized Bopp theory—722(A)
—— Phenomenological theory of Lamb shift—735(A)
—— Problems connected with the prohibition of self-interactions in integro-causal quantum field-theory—468
—— (see Caplan, D. K.)—721(A)
Bell, P. R. (see McGowan, F. K.)—152(L)
Bender, R. S. (see Arthur, James S.)—704(A)
—— (see Ely, Ralph, Jr.)—704(A)
—— (see Reilley, E. M.)—704(A)
Benedict, T. S. and W. M. Woodward. High energy photodisintegration of the deuteron—924(L)
Bengston, J. (see Yovits, M. C.)—540
Bennett, Arthur L., Ivar Highberg, Ernest Barkofsky, and Lucien M. Biberman. Aeroballistics Laboratory of the U. S. Naval Ordnance Test Station—774(A)
Bergström, I. (see Thulin, S.)—1055(L)
Berman, Arthur I. Absorption cross sections for 19.5-Mev quanta—774(A)
—— (see Harris, John N.)—765(A)
Bernardini, G., E. T. Booth, and S. J. Lindenbaum. Interactions of high energy nucleons with nuclei—826
Bernstein, S. (see Allen, R. G.)—767(A)
Bernstein, William and A. W. Schardt. Activation of LiI crystal phosphors—919(L)
—— **and A. W. Schardt.** Scintillation neutron detector—711(A)
—— (see Schardt, A. W.)—712(A)
Berry, Clifford E. Ion trajectories in the omegatron—765(A)
Bertini, H. W. (see Guier, W. H.)—426
Bethe, H. A. and S. T. Butler. Proposed test of the nuclear shell model—1045(L)
—— (see Levinger, J. S.)—577; 742(A)
Bianco, D. R. (see Massey, J. T.)—717(A)
Biberman, Lucien M. (see Bennett, Arthur L.)—774(A)
Biedenharn, L. C. (see Rose, M. E.)—5
Birge, Ann C. Aluminum-24, a delayed heavy-particle emitter—753(A)
Birge, Robert W. New type Čerenkov counter—766(A)
Birnbaum, W. (see Smith, F. M.)—771(A)
Bitter, Francis and Jean Brossel. Attempt to produce nuclear orientation in mercury vapor—1051(L)
Blake, N. W., D. S. McClure, and H. Winston. Electronic states of molecular crystals—754(A)
Bleaney, B., J. M. Daniels, M. A. Grace, H. Halban, N. Kurti, and F. N. H. Robinson. Determination of the nuclear magnetic moment of Co^{60}, using the method of nuclear alignment—688(L)
Blewitt, T. H. and R. R. Coltman. Effect of neutron irradiation on metallic diffusion—384(L)
Block, M. M., S. Passman, and W. W. Havens, Jr. Charged π-meson production in D and Pb at 90° from a 381-Mev proton beam—718(A)
—— (see Passman, S.)—370(L)
Bloembergen, N. and R. W. Damon. Relaxation effects in ferromagnetic resonance—699
Blois, Marsden S., Jr. Structure and stability of thin evaporated metallic films—764(A)
Bloom, Arnold L. Inelastic and total scattering of 190-Mev deuterons by protons—752(A)
Bloom, Stanley and Henry Margenau. Ion clustering—670
—— **and Henry Margenau.** Pressure-broadening of absorption lines—717(A)
—— (see Margenau, Henry)—735(A)
Bockelman, C. K. (see Miller, D. W.)—704(A)
Boehmer, H. W. and H. S. Bridge. Mean free path of neutral penetrating shower-producing radiation—863
Bohm, David. Suggested new interpretation of the quantum theory in terms of "hidden" variables. I—166; II—180
—— (see Pines, David)—338
Bolef, D. I. and H. J. Zeiger. Molecular beam magnetic resonance spectra of $Rb^{87}F$ and $Rb^{87}Cl$ at zero field—799
—— (see Zeiger, H. J.)—788
Bonet, J. V. and A. V. Bushkovitch. Calculations of the diamagnetic susceptibility of N_2—707(A)
Bonner, Norman A. (see Wahl, Arthur C.)—570
Bonner, T. W. Research at Rice Institute using 14-Mev monoenergetic neutrons—739(T)
—— (see Famularo, K.)—742(A)
—— (see Shalek, R. J.)—739(A)
Booth, E. T. (see Bernardini, G.)—826
Borst, L. B. and V. L. Sailor. Crystal spectrometer for neutrons—711(A)
Bowe, J. C. and P. Axel. Decay of Te^{125m}—858
—— **and P. Axel.** Second transition in the decay of Sn^{119m}—734(A)
—— (see Axel, P.)—734(A)
Bowen, Theodore and Francis X. Roser. Response of anthracene scintillation crystals to high energy μ-mesons—992
Bowman, D. W. Physics in general education—160(T)
Bowman, F. E. and M. Tarpinian. Measurement of Young's modulus and internal friction in metal specimens suitable for uniform cyclotron irradiation—769(A)
Bozorth, R. M. (see Williams, H. J.)—713(A)
Bramson, H. J., A. M. Seifert, and W. W. Havens. Photographic study of $\pi \rightarrow \mu \rightarrow \beta$-decay—719(A)
Brand, Frank (see Jacobs, Harold)—441
Branscomb, L. M. (see Shalek, R. J.)—739(A)
Branyan, C. E. (see Cork, M. M.)—386(L)
Bray, P. J. (see Harrick, N. J.)—716(A)
Breit, G. and W. W. Clendenin. Effect of intrinsic moment of electron on spectroscopic isotope shift—689(L)
—— (see Yovits, M. C.)—540
Bridge, Herbert, Hans Courant, and Bruno Rossi. Nuclear interactions of the decay products of a neutral V-particle—159(L)
Bridge, H. S. (see Boehmer H. W.)—863
Brightsen, R. A. (see Coryell, C. D.)—732(A)
Brinkman, J. A. Considerations of the elastic constants of copper—768(A)
Brinton, Robert K. (see Volman, David H.)—707(A)
Brix, P. and H. Kopfermann. Magic numbers and the isotope shift in atomic spectra of heavy elements—1050(L)
Brode, W. R. Address of welcome—388(T)
Broida, H. P. Rotational temperatures of OH in several flames—755(A)
Brossel, Jean (see Bitter, Francis)—1051(L)
Brown, Fielding, R. R. Rau, and George T. Reynolds. Combination cloud-ion chamber using cylindrical geometry—712(A)
Brown, H. Dean and M. Dresden. Positional correlations in interacting fields—748(A)
—— (see Dresden, M.)—748(A)
Brown, L. M. and R. P. Feynman. Radiative corrections to Compton scattering—231
Brown, Robert R. Mean free path of the high energy nuclear component—773(A)
Brown, S. Leroy. Pulse analysis with the aid of a mechanical synthesizer-analyzer—753(A)
—— (see Schwetman, Herbert D.)—740(A)
Brown, Sanborn C. (see Deutsch, Martin)—1047(L)
Browne, Charles I. and I. Perlman. L x-rays and low energy gamma-radiation in the decay of Am^{241}—758(A)
——, **John O. Rasmussen, Joseph P. Surls, and Donald F. Martin.** Decay series $Nd^{140}-Pr^{140}-Ce^{140}$—146(L)
Broyles, C. D. and S. K. Haynes. K-auger yield for Ba—733(A)
Buechner, W. W. (see Van Patter, D. M.)—142(L)
Buehler, Robert J. and Joseph O. Hirschfelder. Bipolar expansion of Coulombic potentials, addenda—149(L)

Burke, W. H. and J. R. Risser. p-γ angular correlation in the reaction $Li^6(d,p)Li^{7*}$ at low energy—741(A)
—— (see Risser, J. R.)—742(A)
Burson, S. B. (see Rutledge, W. C.)—734(A)
Burstein, E., J. J. Oberly, and J. W. Davisson. Effect of pressure on the position of the F-band in alkali halides—729(A)
Bushkovitch, A. V. (see Bonet, J. V.)—707(A)
Butler, J. W. Neutrons from the deuteron bombardment of F^{19}—743(A)
Butler, S. T. (see Bethe, H. A.)—1045(L)
Byfield, H., J. Kessler, and L. Lederman. Interactions of pi-mesons in carbon—718(A)
—— (see Lederman, L.)—719(A)

Callen, E., W. F. Love, and F. C. Nix. Meissner effect in alloys of In-Tl and Sn-Bi—715(A)
Callen, Herbert B. Adiabatic thermomagnetic effects—16
Campbell, Edward C. (see Goodrich, Max)—742(A)
Caplan, D. I. and F. J. Belinfante. Do Coulomb fields signal faster than light?—721(A)
Carlson, R. O., C. A. Lee, and B. P. Fabricand. Molecular beam electric resonance method study of thallium monochloride—784
Carlson, Thomas and W. S. Koski. Some polystyrene solid solutions as scintillation counters—697(L)
Carnap, R. Inductive logic and science—735(T)
Carr, W. J. Intrinsic magnetization in alloys—590
Carroll, Paul E. and E. A. Coomes. Photoelectric emission from BaO in an accelerating field—389(A)
Carroll, Thomas' J. Propagation of short radio waves well beyond the horizon—732(A)
Cashman, R. J. (see Clark, M. A.)—1043(L)
Chalmers, Bruce (see Martius, Ursla, M.)—713(A)
Chamberlain, Owen. High energy proton-deuteron scattering —763(T)
Chang, Chia-hua and C. Sharp Cook. Measurements of the relative transmission of beta-particles through Geiger-Müller counter windows—724(A)
Chang, C. S. Wang (see Uhlenbeck, G. E.)—684(L)
Chang, W. Y. (see Grodzins, L.)—719(A)
Charles, G. W. (see Atkinson, W. R.)—706(A)
Chasson, R. L. Two cosmic-ray decreases associated with the geomagnetic storms and sunspot activity of May and June, 1951—719(A)
Chatterjee, S. D. and R. N. Olcott. Absence of spontaneous emission of neutrons from samarium—147(L)
—— (see Mandeville, C. E.)—193; 725(A)
Chen, S. C. (see Present, R. D.)—447
Ch'en, Shang-yi (see Clayton, Eugene D.)—68
Cheston, W. B. Interaction of charged π-mesons with the deuteron—718(A); 952
Chew, Geoffrey and Gian Carlo Wick. Impulse approximation —636
Chikazumi, Sōshin. Origin of high permeability in permalloy —918(L)
Chivers, E. (see Danielson, G. C.)—711(A)
Chodorow, M. Space charge phenomena in high density electron beams—752(T)
Christy, Robert F. Energy loss of fast particles—763(T)
Chu, E. L. (see Barber, W. C.)—774(A)
Chubb, T. (see Friedman, H.)—705(A)
Church, E. L. (see Mihelich, J. W.)—733(A); 690(L)
Cladis, J. B., W. Hess, and B. J. Moyer. Internal momentum distributions from scattering experiments—766(A)
—— (see Hess, W.)—757(A)
Claffy, E. W. (see Etzel, H. W.)—1063(L)
Clark, Donald L., Arthur Roberts, and Richard Wilson. Disintegration of the deuteron by π^+ mesons and the spin of the π^+ meson—523
Clark, J. S. (see Feld, B. T.)—680(L)
Clark, M. A. and R. J. Cashman. Transmission and spectral response of lead sulfide and lead telluride—1043(L)
Clarke, Edward N. and H. E. Farnsworth. Observations on the photoelectric work functions and low speed electron diffraction from thin films of silver on the (100) face of a silver single crystal—484(L)
Clay, Forrest P. and Frank L. Hereford. Scattering of 0.5-Mev circularly polarized photons in magnetized iron—675(L)
Clayton, Eugene D. and Shang-yi Ch'en. Pressure effects of argon and helium on the resonance lines of silver—68
Cleland, J. W. (see Crawford, J. H., Jr.)—730(A)
Clement, J. (see Jensen, Erling N.)—112
Clement, J. R. and E. H. Quinnell. Atomic heat of lead in the region of its transition to superconductivity—502(L)
Clendenin, W. W. (see Breit, G.)—689(L)
—— (see Luke, P. J.)—401
—— (see Meyerott, R. E.)—393
Cleveland, Forrest F. (see Davis, Abram)—730(A)
Cohen, M. H. Theory of the nuclear quadrupole interaction of Nb^{93} in $KNbO_3$—762(A)
Cohen, S. G. and Y. Feige. Natural scintillations from uranyl nitrate crystals—1049(L)
Cohen, Victor W., C. Kikuchi, and John Turkevich. Anisotropy in paramagnetic resonance absorption of picryl-n-amino carbazyl—379(L)
Cohn, Marius. Theory of dielectric dispersion—708(A)
Collins, Edward M. Course in physical science as general education at Denison—160(T)
Collins, T. L., A. O. Nier, and W. H. Johnson, Jr. Atomic masses of titanium, vanadium, and chromium—726(A)
Coltman, R. R. (see Blewitt, T. H.)—384(L)
Compton, Karl T. Title to be announced—702(T)
Condit, Richard I. Interactions of shock waves in air with three-dimensional surfaces—769(A)
—— (see Graves, J. D.)—752(A)
Condon, E. U. The atom—702(T)
Connell, L. F. and R. L. Seale. Electrical properties of rutile single crystals—745(A)
Conner, J. P. and J. R. Smith. Preparation of thin zirconium tritium targets—741(A)
Cook, Charles F. and J. Richard Smith. Differential cross section of $H^2(d,p)T^3$ at low energy—741(A)
Cook, C. Sharp (see Chang, Chia-hua)—724(A)
—— (see Porter, Fred T.)—733(A)
Coomes, E. A. Interpretation of periodic deviation data for highly refractory metals—392(A)
—— (see Carroll, Paul E.)—389(A)
Coon, J. B. Structural constants of ClO_2—746(A)
Coppola, P. P. (see Hughes, R. C.)—388(A)
Corak, W. S. (see Wexler, A.)—85
Cork, J. M., D. W. Martin, J. M. LeBlanc, and C. E. Branyan. Radioactive decay of Hg^{197} and Hg^{203}—386(L)
—— (see Rutledge, W. C.)—734(A)
Coryell, C. D., R. A. Brightsen, and A. C. Pappas. Empirical analysis of nuclear shell effects in β-energetics—732(A)
Courant, Hans (see Bridge, Herbert)—159(L)
Coutu, A. (see Duckworth, H. E.)—929(L)
Cowie, Dean B. (see Heydenburg, N. P.)—742(A)
—— (see Phillips, G. C.)—742(A)
Craig, D. N. (see Sommer, H.)—740(A)
Craig, H. Measurements on the I, F, and A lines of thorium by a new method—688(L)
Crandall, W. E., K. Crowe, B. J. Moyer, W. K. H. Panofsky, R. Phillips, and D. Walker. Analysis of neutral meson gamma-ray spectra from carbon—771(A)
Crawford, J. H., Jr., J. W. Cleland, K. Lark-Horovitz, J. C. Pigg, and F. W. Young, Jr. Evidence of hole traps in Ge produced by fast neutron bombardment—730(A)
Critchfield, C. L., E. P. Ney, and Sophie Oleksa. Soft radiation at balloon altitudes—461

Crouch, Marshall F. and Robert D. Sard. Distribution of multiplicities of neutrons produced by cosmic-ray μ-mesons captured in lead—120
Crowe, K. (see Crandall, W. E.)—771(A)
Curl, G. W. and G. C. Danielson. Rectification effects in diamond—729(A)
Curran, S. C. (see Bannerman, R. C.)—134(L)
—— (see Insch, G. M.)—805
Curtiss, L. F. and P. S. Gill. Variation of intensity of fast cosmic-ray neutrons with altitude—309
Cwilong, B. M. and M. H. Edwards. Sublimation threshold —a new physical constant—380(L)

Daitch, P. B. and J. B. French. High energy nucleon-deuteron scattering—695(L)
Damon, R. W. (see Bloembergen, N.)—699
Danforth, W. E. Electrolysis of thorium dioxide. II. Observations with homogeneous crystalline specimens.—390(T)
Daniels, J. M. (see Bleaney, B.)—688(L)
Danielson, G. C. and E. Chivers. Optical properties of sodium tungsten bronze—711(A)
—— (see Curl, G. W.)—729(A)
—— (see Sidles, P. H.)—710(A)
Danielson, W. E. (see Shenfil, L.)—739(A)
Darrow, K. K. Physics as science and art—702(T)
Date, Muneyuki (see Okamura, Toshiko)—1041(L)
Davidson, Jack P. Magnetic moments of even-odd nuclei—432
Davis, Abram, Forrest F. Cleveland, and Arnold G. Meister. Raman and infrared spectral data, force constants, and thermodynamic properties for dibromodichloromethane—707(A)
Davisson, J. W. (see Burstein, E.)—729(A)
Day, Robert B. and Torben Huus. Low-lying levels in Be^{7} and B^{10}—761(A)
—— **and R. L. Walker.** Reaction $Be^{9}(p,\alpha\gamma)Li^{6}$—582
—— (see Huus, Torben)—761(A)
—— (see Tollestrup, A. V.)—760(A)
—— (see Woodbury, H. H.)—760(A)
De Benedetti, S. and G. H. Minton. Fine structure and angular correlation in Po^{210}—944(L); 726(A)
—— **and H. J. Richings.** Half-life of positrons in condensed materials—377(L)
—— **and R. Siegel.** Three-quantum annihilation and positronium—371(L)
Debs, R. J. (see Labitt, M.)—713(A)
Decius, J. C. Relations between the vibrational intensities of isotopic molecules—755(A)
Dedrick, K. G. Theory of the angular width of Čerenkov radiation from a particle undergoing multiple scattering—765(A)
Deeds, W. Edward. Vibrational analysis of chain molecules—160(A)
Dekker, A. J. and A. van der Ziel. Wave-mechanical foundation of Baroody's theory of secondary emission—391(A)
Del Castillo, G. (see Grodzins, L.)—719(A)
Demos, P. T. (see Labitt, M.)—713(A)
—— (see Winhold, E. J.)—728(A)
de Oyarzabal, Juan. Fourth-order effects in vacuum polarization—748(A)
Depocas, F. and B. G. Harvey. Preparation of Ra^{229} and Ac^{229}—499(L)
der Mateosian, E. (see Scharff-Goldhaber, G.)—734(A)
Derr, V. E. and M. D. Earle. Properties of powdered $BaTiO_3$ —384(L)
Deutsch, Martin and Sanborn C. Brown. Zeeman effect and hyperfine splitting of positronium—1047(L)
—— (see Sunyar, A. W.)—734(A)
Deutsch, Robert W. (see Violet, Charles E.)—756(A)
DeVore, H. B. Photoconductivity study of activation of barium oxide—390(A)
Dewan, J. T. (see Pepper, T. P.)—155(L)
DeWitt, Bryce Seligman. Point transformations in quantum mechanics—653
DeWitt, T. W. (see Morrisson, T. E.)—708(A)
Dexter, D. L. Conductivity of cold-worked metals—936(L)
—— **and W. R. Heller.** Quantum theory of the internal field in an idealized crystal—723(A)
Dharmatti, S. S. and H. E. Weaver, Jr. Magnetic moment of Zn^{67}—927(L)
Dicke, R. H. (see Pond, T. A.)—489(L)
Dijkstra, L. J. and U. Martius. Strain induced curvature of Bloch walls in silicon iron—714(A)
Dixon, W. R. Build-up factors for transmission of Co^{60} gamma-rays through concrete and lead—498(L)
Dodd, E. E. Spray electrification of liquid drops—759(A)
Dodd, J. N. (see Baker, C. J.)—1051(L)
Dohne, C. F. (see Hoover, J. I.)—58
Donnelly, F. K., H. J. Engebretson, J. E. Henderson, T. J. Morgan, F. H. Schmidt, and J. F. Streib. University of Washington 60-in. cyclotron—767(A)
Donoghue, J. J. (see McClelland, J. D.)—768(A)
Doughty, Donald D. and J. W. McGrath. M_3 and M_4 x-ray absorption edges of tantalum—1040(L)
Drahmann, John B. (see Rouse, Arthur G.)—739(A)
Dresden, M. and H. Dean Brown. Classical quantum electrodynamics of interacting fields—748(A)
—— (see Brown, H. Dean)—748(A)
Dube, G. P. and S. Jha. Closing of the proton subshell at Z58—1042(L)
Duborg, R. W. (see Schoenfeld, W. A.)—873
Duckworth, Henry E., R. F. Woodcock, G. S. Stanford, A. Coutu, and R. L. Stearns. Limits of isotopic abundance for hafnium and platinum—929(L)
—— (see Stanford, George S.)—1039(L)
Duffield, Robert B. (see Anderson, Roger E.)—728(A)
Duller, N. M. (see Walker, W. D.)—773(A)
DuMond, J. W. M. (see Shenfil, L.)—739(A)
Dunlap, W. C., Jr. Zinc as an acceptor in germanium—945(L)
Dunlavey, Dean C. and Glenn T. Seaborg. Alpha-activity in Bi^{203} as detected with nuclear emulsions—757(A)
Dyke, W. P. Field emission; a comparison between theory and experiment including pulsed emission at large densities—752(T); **and J. K. Trolan**—391(A)
Dyson, F. J. Divergence of perturbation theory in quantum electrodynamics—631

Earle, M. D. (see Derr, V. E.)—384(L)
Earle, T. T. (see Riess, Karlem)—741(A)
Easterday, Harry T. (see Medicus, Heinrich A.)—735(A)
Eatherly, W. P. Theoretical and experimental investigation of high temperature graphitization—768(A)
Edwards, John E. Curved quartz crystal x-ray spectrometer —160(A)
Edwards, M. H. (see Cwilong, B. M.)—380(L)
Edwards, P. D. Calorimetric calibration of a secondary standard for 150–317 Mev bremsstrahlung—725(A)
Eguchi, Tetsuo. Radiative π-μ decay—943(L)
Eisenberg, Y. (see Barrett, P. H.)—674(L)
Eisenstein, Julian. Spin-spin relaxation in a simple system —603
Eisinger, Joseph T. and Benjamin Bederson. Nuclear moment and hyperfine structure anomaly of K^{40}—716(A)
Eisner, Melvin. Scattering of strongly coupled pseudovector mesons—748(A)
—— (see Hudson, P. A.)—746(A)
Ekstein, H. Scattering by bound particles with short-range interaction force—703(A)
Elder, F. K., Jr., and R. E. McDonald. Distribution of components of ternary isotopic mixture along Clusius-Dickel column—500(L)

Elliot, J. O., R. T. Farrar, R. D. Myers, and C. F. Ravilious. Multiple gamma-ray scattering in lead—1048(L)
Elliott, L. G. Half-life of the 1.3-Mev excited state in K^{41}—942(L)
Ellis, J. W. Molecular and atomic spectra associated with the solid state—756(T)
Elsasser, W. M. Quantum measurement as an amplifying process—735(T)
Elsken, R. H. (see Shaw, T. M.)—708(A); 762(A)
El-Sum, Hussein M. A. and Paul Kirkpatrick. Microscopy by reconstructed wave-fronts—763(A)
Ely, Ralph, Jr., A. J. Allen, J. S. Arthur, R. S. Bender, H. J. Hausman, and E. M. Reilley. Inelastic scattering of protons from nickel—704(A)
—— (see Arthur, James S.)—704(A)
—— (see Reilley, E. M.)—704(A)
Emigh, C. R. Relative pair production cross section in the region 50 to 300 Mev—719(A)
Emmerich, W. S. and J. D. Kurbatov. Disintegration of the ground-state Sr^{85} and metastable energy level of 514 kev in Rb^{85}—149(L)
—— **and J. D. Kurbatov.** 514-kev energy level of rubidium 85—733(A)
Enatsu, H. Self-energies of nucleons and the mass spectra of heavy particles—483(L)
Endt, P. M. (see Van Patter, D. M.)—142(L)
Enge, H. A. (see Van Patter, D. M.)—142(L)
Engebretson, H. J. (see Donnelly, F. K.)—767(A)
English, W. N. Further measurements of electron drift velocities in a grid ionization chamber—759(A)
Erickson, R. A. Antiferromagnetic structure of manganese dioxide by neutron diffraction—745(A)
Eriksen, V. O. and G. Jenssen. Studies on the linearity of a scintillation gamma-ray spectrometer—150(L)
Errett, D. D. and F. F. Rieke. Drift velocity of electrons in pure gases—706(A)
—— (see Rieke, F. F.)—706(A)
Eshbach, J. R., R. E. Hillger, and M. W. P. Strandberg. Nuclear magnetic moment of S^{33} from microwave spectroscopy—532
—— **and M. W. P. Strandberg.** Rotational magnetic moments of $^1\Sigma$ molecules—24
Estermann, I. and S. A. Friedberg. Specific heats of several metals and semiconductors between 1.8 and 4.2°K—715(A)
—— (see Friedberg, S. A.)—375(L)
Etzel, H. W., J. H. Schulman, R. J. Ginther, and E. W. Claffy. Silver-activated alkali halides—1063(L)
Evans, H. T. (see Hughes, R. C.)—388(A)
Eyges, L. Interpretation of photonuclear experiments—741(A)

Fabricand, B. P. (see Carlson, R. O.)—784
Famularo, K., L. C. Thompson, and T. W. Bonner. Study of the 1435-kev resonance of carbon bombarded by deuterons—742(A)
Fan, H. Y. Infrared absorption of nucleon-bombarded silicon. II—730(A)
—— (see Becker, M.)—730(A)
Farnsworth, H. E. (see Clarke, Edward N.)—484(L)
—— (see Ying, Chung Fu)—485(L)
Farrar, R. T. (see Elliot, J. O.)—1048(L)
Faust, W. R. (see Hoover, J. I.)—58
Feenberg, E. Nuclear shell structure—739(T)
Feige, Y. (see Cohen, S. G.)—1049(L)
Feinstein, J. Condition for radiation from a solar plasma—145(L)
Feld, B. T., D. H. Frisch, I. L. Lebow, L. S. Osborne, and J. S. Clark. Photomeson production in carbon and hydrogen—680(L)
—— (see Lebow, I. L.)—681(L)
Feldman, G. (see Pope, N. K.)—703(A)
Ferguson, E. E. (see Smith, D. C.)—739(A)
Fermi, Enrico. The nucleus—702(T)
——, **H. L. Anderson, A. Lundby, D. E. Nagle, and G. B. Yodh.** Ordinary and exchange scattering of negative pions by hydrogen—935(L)
—— (see Anderson, H. L.)—934(L); 936(L)
Feuer, Paula and Hubert M. James. Electronic states in crystals under large over-all perturbations—723(A)
Feynman, R. P. (see Brown, L. M.)—231
Fields, R. E. (see Miller, D. W.)—704(A)
Fisher, Thomas F. Cathodic sputtering as a sectioning method in diffusion studies—709(A)
Fletcher, Harvey. Acoustics—702(T)
Fonger, W. (see Simpson, J. A.)—366(L); 720(A)
—— (see Trieman, S. B.)—364(L)
Fosdick, L. D. and H. M. James. Approximate treatment of order-disorder transitions in the triangular Ising lattice—714(A)
Fournet, Gérard. Theory of cooperative phenomena—692(L)
Fowler, C. M. (see Hein, R. E.)—138(L)
Fowler, E. C. (see Thorndike, A. M.)—929(L)
Fowler, Richard G. and Robert J. Lee. Synchronized rotating mirror system—732(A)
—— (see Atkinson, W. R.)—706(A)
Fowler, W. B. (see Thorndike, A. M.)—929(L)
Fowler, William Alfred (see Woodbury, Eric John)—51
Fox, I. D. and James R. Wilson. Classical meson fields—772(A)
Fox, R. E., W. M. Hickam, T. Kjeldaas, Jr., and D. J. Grove. Direct measurement of ionization probability and appearance potential using a mass spectrometer—707(A)
Francis, N. C. and R. E. Marshak. Elastic photoproduction of π^0 mesons in deuterium—496(L)
Frank, P. Philosophical interpretations of modern physics—735(T)
Frank, Wilson J. (see Madey, Richard)—771(A)
Fraser, J. S. Angular distribution of prompt neutrons in the fission of Pu^{239}—726(A)
Fraser, Ronald. UNESCO and international cooperation in the physics sciences—729(T)
Frazer, B. C. and R. Pepinsky. Structural changes in the ferroelectric transition of KH_2PO_4—479(L)
Frei, E. H. Measurements of components of stress produced by shearing strain—708(A)
Freier, George (see Heusinkveld, M.)—80
French, A. P. and J. O. Newton. Polarization of the 6.13-Mev gamma-rays emitted in the reaction $F^{19}(p,\alpha)O^{16*}(\gamma)O^{16}$—1041(L)
French, J. B. (see Daitch, P. B.)—695(L)
Fretter, W. B. and M. M. May. Angular distribution of the decay tracks of neutral V-particles—773(A)
Frey, S. C. (see Sternglass, E. J.)—391(A)
Fried, H. M. and P. R. Zilsel. Critical velocity of superflow in liquid helium II—1044(L)
Friedberg, S. A., I. Estermann, and J. E. Goldman. Electronic specific heat in chromium and magnesium—375(L)
—— (see Estermann, I.)—715(A)
Friedman, H., T. Chubb, and D. A. Patterson. Photoelectric thresholds in photon counters containing electronegative quenching gases—705(A)
Frisch, D. H. (see Feld, B. T.)—680(L)
—— (see Lebow, I. L.)—681(L)
Fristrom, Robert M. Microwave spectrum of a slightly aspherical top—the structure and dipole moment of sulfuryl fluoride—717(A)
Fry, W. F. Phenomena associated with negative μ-mesons stopped in photographic emulsions—676(L)
Fujimura, Tadao (see Okamura, Tosihiko)—1041(L)

Fuller, C. S., H. C. Theuerer, and W. van Roosbroeck. Properties of thermally produced acceptors in germanium —678(L)
Fultz, S. C. (see Scoville, C. L.)—1046(L)
Furst, Milton and Hartmut Kallmann. High energy induced fluorescence in organic liquid solutions (energy transport in liquids). III—816

Gabillard, R. Steady-state transient technique in nuclear resonance—694(L)
Galt, John K. Motion of a ferromagnetic domain wall in Fe_3O_4—664
—— (see Herring, Conyers)—1060(L)
Gambling, W. A. Striations in the hydrogen glow discharge—677(L)
Gardner, J. W. Connection between $\gamma-\gamma$ and internal conversion angular correlations—137(L)
Garfunkel, M. P. and B. Serin. Formation of a boundary between normal-conducting and superconducting metal—834
Garrison, Gerald (see Miller, C. E.)—773(A)
Garwin, Richard L. Test for the charge-symmetry hypothesis —1045(L)
Geballe, Ronald and Melvin A. Harrison. Negative ion formation in oxygen—372(L)
Geiger, James S. (see Stanford, George S.)—1039(L)
Gellman, H., B. A. Griffith, and J. P. Stanley. Internal conversion in the *L*-shell—944(L)
Geltman, S. (see Meyerott, R. E.)—393
Gerjuoy, E. and David S. Saxon. Variational calculation of scattering cross sections—939(L)
—— (see Saxon, David)—704(A)
Germer, L. H. and J. L. Smith. Arcing at electrical contacts on closure. III. Development of the arc—392(A)
Geschwind, S., G. R. Gunther-Mohr, and G. Silvey. Spin and quadrupole moment of O^{17}—474
Ghiorso, Albert (see James, Ralph A.)—369(L)
—— (see Meinke, W. W.)—429
—— (see Street, K., Jr.)—135(L)
—— (see Thompson, S. G.)—758(A)
Gilbert, D. A. Nuclear spin of Cl^{36} from the microwave spectrum of $C^{13}H_3Cl^{36}$—716(A)
Gilbert, F. C. (see Violet, Charles E.)—756(A)
Gilbert, W. S. and J. W. Rose. Photodisintegration of the deuteron—766(A)
—— (see Rose, J. W.)—766(A)
Gilchrist, Lachlan. Distribution of potential in an electrically excited nonhomogeneous medium—731(A)
Giles, Peter C. and Walter H. Barkas. Electron pickup by fast C^{12} nuclei in emulsion—756(A)
Gill, P. S. (see Curtiss, L. F.)—309
Gilmore, E. H. and R. H. Knipe. Relative spectral sensitivity calibration of electron multiplier phototubes in the 2500A–3500A region—764(A)
Ginther, R. J. (see Etzel, H. W.)—1063(L)
Givens, M. Parker and Walter P. Siegmund. Absorption of selenium in the soft x-ray region—313
Glenn, William E. Design and operation of a high geometry electrostatic time-of-flight mass spectrograph—763(A)
Goldberg, Leo, Robert R. McMath, Orren C. Mohler, and A. Keith Pierce. Abundance of CO in the sun and in the earth's atmosphere—481(L)
——, **Robert R. McMath, Orren C. Mohler, and A. Keith Pierce.** Identification of CO in the solar atmosphere—140(L)
Goldhaber, M. (see Sunyar, A. W.)—734(A)
Goldman, J. E. Saturation magnetic moment of alloys on the collective electron theory—375(L)
—— (see Friedberg, S. A.)—375(L)
Goldstein, Louis. Critical state of normal fluids—35
Good, R. H., Jr. Generalization of the WKB method to radial wave equations—754(A)
Good, W. M. (see Moak, C. D.)—929(L)
Goodman, Clark (see Schoenfeld, W. A.)—873
Goodrich, Max and Edward C. Campbell. Radioactivity of Ag^{108}—742(A)
Gossick, Ben R. Resolution of fast neutron energy measurements using proton recoils from a thin radiator—711(A)
—— (see Pizzaro, R.)—711(A)
Goudsmit, S. A. (see Hays, E. E.)—1065(L)
—— (see Richards, P. I.)—630
Gove, H. E. and A. Hedgran. Angular correlation between inelastically scattered protons and gamma-rays from the 1.4-Mev level in Mg^{24}—727(A)
Gow, K. V. (see Martius, Ursula M.)—713(A)
Grace, M. A. (see Bleaney, B.)—688(L)
Grannis, F. H. (see Sternglass, E. J.)—391(A)
Grattidge, W. and H. John. Electronic properties of barium sulfide—389(A)
Graves, E. Scattering of 30-Mev alpha-particles by helium—703(A)
Graves, J. D. and Richard I. Condit. Locating buried radioactive sources—752(A)
Green, F. P. (see Bair, J. K.)—946(L)
—— (see Hahn, T. M.)—934(L)
—— (see Willard, H. B.)—849
Green, H. S. and H. Messel. Lateral spread of cosmic-ray showers in air and lead—679(L)
Green, John R. Knock-on secondaries from penetrating particles in carbon—774(A)
Green, Louis C., Marjorie M. Mulder, C. W. Ufford, E. Slaymaker, Eleanor Krawitz, and R. T. Mertz. Superposition of configurations in the ground state of He I—65
Greifinger, P. S. Limits of stability of the heavy elements and the effects of nuclear shell structure—253
Griffith, B. A. (see Gellman, H.)—944(L)
Grodzins, L., G. Del Castillo, and W. Y. Chang. Study of penetrating showers produced in Be, carbon, and lead at sea level—719(A)
Groetzinger, Gerhart, Watts Humphrey, Jr., and Fred L. Ribe. Study of the multiple scattering of fast charged particles in a gas. II. (Negative and positive beta-particles.)—78
Grove, D. J. (see Fox, R. E.)—707(A)
Grove, G. R. Energy levels of the S^{32} nucleus—160(A)
Guier, W. H., H. W. Bertini, and J. H. Roberts. Energy levels in C^{13} from $Be^9(\alpha,n)C^{13}$—426
Gunther-Mohr, G. R. (see Geschwind, S.)—474

Hadley, J. (see Hess, W.)—757(A)
Hagstrum, H. D. Ejection of electrons by ion impact—752(T)
—— Ejection of electrons from molybdenum by helium ions —392(A)
Hahn, E. L. and D. E. Maxwell. Spin-echo measurements of nuclear spin-spin coupling—762(A)
Hahn, T. M., C. W. Snyder, H. B. Willard, J. K. Bair, E. D. Klema, J. D. Kington, and F. P. Green. Neutrons and gamma-rays from the proton bombardment of beryllium—934(L)
—— (see Bair, J. K.)—946(L)
—— (see Willard, H. B.)—849
Halban, H. (see Bleaney, B.)—688(L)
Hales, R. W., R. H. Hildebrand, N. Knable, and B. J. Moyer. Yield of neutral mesons from proton bombardment of light nuclei—373(L)
Halpern, I. (see Labitt, M.)—713(A)
—— (see Winhold, E. J.)—728(A)
Halpern, L. (see Koch, K. M.)—1064(L)
Halpern, Otto. Production and detection of circularly polarized gamma-rays—747(A)
Halsted, R. E. Atomic masses of xenon, iodine, and some isotopes of tin—726(A)

Hamermesh, Bernard. Recent experiments in neutron physics: neutron-proton capture cross section; neutron-electron interaction; total cross sections in the kev region; capture gamma-rays—722(T)
Hamermesh, M., G. R. Ringo, and A. Wattenberg. Measurement of the electron-neutron interaction—483(L)
Hanai, Tetsuya (see Shimizu, Sakae)—290
Hanson, William B. (see Pellam, John R.)—216
Hardy, W. A., G. Silvey, and C. H. Townes. Spin and quadrupole moment of Se^{79}—494(L)
Harker, Kenneth James. LSM_LM_S eigenfunctions of an atom—753(A)
Harrick, N. J., R. G. Barnes, and P. J. Bray. Quadrupole moment of the electron distribution in the hydrogen molecule—716(A)
Harris, John N. and Arthur I. Berman. Precision measurement of uniformity of materials by gamma-ray transmission—765(A)
Harrison, D. E. (see Margenau, Henry)—707(A)
Harrison, Melvin A. (see Geballe, Ronald)—372(L)
Hart, H. E. (see Hatcher, R. D.)—703(A)
Harvey, B. G. α-half-life of Am^{241}—482(L)
—— (see Depocas, F.)—499(L)
Hatcher, R. D. and H. E. Hart. Regular meson type potentials in proton-proton scattering—703(A)
Hausman, H. J. (see Arthur, James S.)—704(A)
—— (see Ely, Ralph, Jr.)—704(A)
—— (see Reilley, E. M.)—704(A)
Havas, Peter. Classical meson theory and action at a distance—720(A)
Havens, W. W., Jr. (see Block, M. M.)—718(A)
—— (see Bramson, H. J.)—719(A)
—— (see Passman, S.)—370(L)
Hayashi, I. (see Kumagai, H.)—925(L)
Hayes, J. W. (see Wildhack, W. A.)—731(A)
Haynes, J. R. and W. C. Westphal. Drift mobility of electrons in silicon—680(L)
Haynes, S. K. (see Broyles, C. D.)—733(A)
Hays, E. E., P. I. Richards, and S. A. Goudsmit. Erratum: Mass measurement with a magnetic time-of-flight mass spectrometer—1065(L)
—— (see Richards, P. I.)—630
Hayward, Raymond W. Decay of Ag^{105} and Ag^{106}—760(A)
Hazen, W. E. Air-shower cores—455
Heaps, C. W. (see Scales, John)—743(A)
Heath, R. L. (see Schenck, James)—923(L)
Heckman, Harry H. and Walter H. Barkas. Scattering of negative π-mesons in aluminum, copper, and lead—771(A)
—— (see Sherman, D. F.)—771(A)
Heckrotte, W., L. R. Henrich, and J. V. Lepore. Photoproduction of neutral mesons from deuterium—490(L)
Hedgran, A. (see Gove, H. E.)—727(A)
Hein, R. E., C. M. Fowler, and R. H. McFarland. Search for long-lived Nb^{94}—138(L)
Heller, William R. (see Dexter, D. L.)—723(A)
Henderson, J. E. (see Donnelly, F. K.)—767(A)
—— (see Miller, C. E.)—773(A)
—— (see Wilfong, T. C., Jr.)—765(A)
Henley, Ernest M. Nonlinear pseudoscalar meson theory—772(A)
—— π-meson production by protons on nuclei—204
Henrich, L. R. (see Heckrotte, W.)—490(L)
Henry, Warren E. Spin paramagnetism of Cr^{+++} at liquid helium temperatures and high magnetic fields—487(L)
Hensley, E. B. Electrical properties of porous semiconductors—388(A)
Hereford, Frank L. (see Clay, Forrest P.)—675(L)
—— (see Lodge, John I.)—725(A)
Herring, Conyers. Atomistic theory of the metallic surface—388(T)
—— Energy of a Bloch wall on the band picture—1003
—— **and J. K. Galt.** Elastic and plastic properties of very small metal specimens—1060(L)
Hess, W., J. B. Cladis, and J. Hadley. Fast protons from 270-Mev $n-d$ scattering—757(A)
—— (see Cladis, J. B.)—766(A)
Hesthal, C. E. Course of general education in physics and astronomy at Ohio State University—160(T)
Heusinkveld, M. and George Freier. Production of polarized protons and the inversion of energy levels of the $P_{1/2}-P_{3/2}$ doublet in Li^8—80
Heydenburg, N. P., G. C. Phillips, and Dean B. Cowie. Inelastic scattering of protons from light nuclei—742(A)
—— (see Hudspeth, Emmett L.)—742(A)
—— (see Phillips, G. C.)—742(A)
Hibdon, Carl T., Alexander Langsdorf, Jr., and Robert E. Holland. Neutron transmission cross sections in the kilovolt region—595
Hickam, W. M. (see Fox, R. E.)—707(A)
Hidalgo, John (see Riess, Karlem)—741(A)
Hiedemann, E. A. Photoelastic analysis of ultrasonic waves—729(T)
Highberg, Ivar (see Bennett, Arthur L.)—774(A)
Hildebrand, R. H. (see Hales, R. W.)—373(L)
Hill, R. D. Systematics of isomer energy levels—722(T)
Hillger, R. E. (see Eshbach, J. R.)—532
Hine, G. J. "Effective" atomic numbers of materials for various γ-ray interactions—725(A)
Hipple, J. A. and H. Sommer. Combination crossed-field and time-of-flight mass spectrometer—712(A)
—— (see Sommer, H.)—740(A)
Hirsch, J. and R. B. McQuistan. Pulse-heating of bulk semiconductors—723(A)
Hirschfelder, Joseph O. (see Buehler, Robert)—149(L)
Hirsh, F. R., Jr. Auger enhancement of the $M\alpha$ x-ray satellite lines—685(L)
Hoffman, J. I. (see Sommer, H.)—740(A)
Hofstadter, Robert and Alvin M. Hudson. Energy loss of cosmic-ray μ-mesons—773(A)
Hogg, Benjamin G. (see Stanford, George S.)—1039(L)
Holland, Robert E. (see Hibdon, Carl T.)—595
Holstein, T., D. Alpert, and A. O. McCoubrey. Isotope effect in the imprisonment of resonance radiation—985
Hooper, James R. Microwave propagation through an electronic space charge in a magnetic field—705(A)
Hoover, J. I., W. R. Faust, and C. F. Dohne. Polarization of scattered quanta—58
Horton, C. W. Propagation of Rayleigh waves on the surface of a visco-elastic solid—744(A)
Houston, Robert E. and Robert H. Noble. Electromagnetic field measurements in the plane of a circular aperture—732(A)
Houston, W. V. Temperature dependence of electrical conductivity—743(A)
Howell, Lynn G. Wave propagation ducts in geophysics—744(A)
Hsieh, Yü-Chang. Calculation of the specific heat of Ge—730(A)
Hubbard, E. L. and K. R. MacKenzie. Range of 18-Mev protons in aluminum—107
Hudson, Alvin M. (see Hofstadter, Robert)—773(A)
Hudson, P. A. and M. Eisner. Investigations on the Debye-Frenkel theory of ultrasonic absorption—746(A)
Hudson, R. P. Magnetic threshold field curve of a superconductor—382(L)
Hudspeth, Emmett L., William B. Rose, and N. P. Heydenburg. Delayed γ-emission from decay of C^{15}—742(A)
Hughes, D. S. Elastic constants of rocks at high pressures and temperatures—744(T)
Hughes, R. C., P. P. Coppola, and H. T. Evans. Chemical reactions in barium oxide on tungsten emitters—388(A)

Hughes, Richard H. Microwave spectrum and structure of ozone—717(A)
Hull, M. H., Jr. (see Yovits, M. C.)—540
Humphrey, Watts, Jr. (see Groetzinger, Gerhart)—78
Hurst, C. A. Graphs for the kernel of the Bethe-Salpeter equation—920(L)
Huus, Torben and Robert B. Day. Investigation of the reaction $B^{11}(p,\gamma)C^{12}$—761(A)
—— (see Day, Robert B.)—761(A)

Inglis, D. R. Two-model interpretation of a nuclear spectrum—492(L)
Insch, G. M., J. G. Balfour, and S. C. Curran. Beta-spectrum of RaD—805
Isaacs, P., A. Sachs, and J. Steinberger. Elastic scattering of negative pions in carbon—718(A)
——, **A. M. Sachs, and J. Steinberger.** Total cross sections of 6-Mev mesons in hydrogen and deuterium—803
Ishikawa, Y., T. Sato, K. Okumura, and T. Sasaki. Erratum: $P-N$ transition of an oxide-coated cathode—1065(L)
Itoh, J. (see Kanda, T.)—938(L)

Jacobs, Donald H. and Seymour Scholnick. Development of ultra compact, ultra high speed digital computers, II—731(A)
Jacobs, Harold, Jack Martin, and Frank Brand. Secondary emission from composite surfaces—441
Jaffé, George. Diffusion of thermal neutrons—747(A)
—— Theory of conductivity of semiconductors—354
—— (see Rider, John A.)—746(A)
Jakobson, Mark J., Alvin G. Schulz, and R. Stephen White. Production of photomesons from helium—772(A)
—— (see White, R. Stephen)—770(A)
James, Hubert M. (see Feuer, Paula)—723(A)
—— (see Fosdick, L. D.)—714(A)
James, Ralph A., Albert Ghiorso, and Donald Orth. L-electron capture and alpha-decay in Np^{238}—369(L)
Jastrow, R. and J. E. Roberts. Nuclear cross sections for high energy neutrons and protons—757(A)
Jauch, J. M. Radiative correction for the collision loss of fast particles—950
Jaumot, Frank E., Jr. (see Nix, Foster C.)—709(A)
Jeffries, C. D., H. Loeliger, and H. H. Staub. Nuclear magnetic resonance of titanium and arsenic—478(L)
Jen, C. K., J. W. B. Barghausen, and R. W. Stanley. Sign determination of molecular magnetic moments—717(A)
Jenkins, F. A. and L. W. Alvarez. Use of successive diffractions to double or quadruple the resolving power of a grating—763(A)
Jenkins, William A. and Glenn T. Seaborg. Production and assignment of Ra^{230} and Ac^{230}—758(A)
Jennings, B. (see Sun, K.-H.)—726(A)
Jensen, Erling N., R. T. Nichols, J. Clement, and A. Pohm. Beta-spectra of P^{32} and P^{33}—112
Jensen, J. Hans D. and M. Goeppert Mayer. Electromagnetic effects due to spin-orbit coupling—1040(L)
Jenssen, G. (see Eriksen, V. O.)—150(L)
Jha, S. (see Dube, G. P.)—1042(L)
John, G. (see Lin-sheng, Cheng)—487(L)
John, H. (see Grattidge, W.)—389(A)
Johnson, C. H., G. P. Robinson, and C. D. Moak. Capture gamma-rays from 277-kev protons on N^{14}—931(L); ——, **C. D. Moak, and G. P. Robinson**—727(A)
Johnson, H. R. Resolution and sensitivity of microwave spectrographs—764(A)
—— **and M. W. P. Strandberg.** Beam system for reduction of Doppler broadening of a microwave absorption line—503(L)
Johnson, J. B. and K. G. McKay. Secondary electron emission from germanium—390(A)
Johnson, M. H. Annihilation radiation from μ^+ mesons—719(A)
Johnson, S. J. and T. F. Rogers. Magnetically induced ultrasonic velocity changes in polycrystalline nickel—714(A)
Johnson, V. A. and F. L. Shipley. Comparison of the adiabatic and isothermal Hall effects—724(A)
—— (see Martin, B.)—714(A)
—— (see Whitesell, W. J.)—724(A)
Johnson, W. H., Jr. (see Collins, T. L.)—726(A)
Jones, F. Llewellyn. Cold emission of electrons in spark gaps—392(A)
Jones, John W. and Truman P. Kohman. Search for natural radioactivity of calcium 48—941(L)
Jones, Lawrence W. and Kent M. Terwilliger. Comparison of total photoneutron yield from 160- and 320-Mev bremsstrahlung—686(L)
Jonker, J. L. H. Angular distribution of secondary electrons from nickel—390(A)
Jossem, E. L. (see Parratt, L. G.)—729(A)

Kalkstein, Marvin I. and W. F. Libby. Investigation of the double beta-decay of $_{50}Sn^{124}$—368(L)
Kallmann, Hartmut (see Furst, Milton)—816
Kamefuchi, Susumu (see Umezawa, Hiroomi)—505
Kanda, T., Y. Masuda, R. Kusaka, Y. Yamagata, and J. Itoh. Gyromagnetic ratios of Li^7, Na^{23}, Al^{27}, and P^{31}—938(L)
Känzig, W. and M. Peter. Critical domain size in ferroelectrics—940(L)
Kaplan, Harvey. Exchange integral in the $3d$ shell—1038(L)
Kaplon, M. F. Electromagnetic interference effects in charged meson-proton scattering—1059(L)
—— Multiple meson production at extremely high energies—744(T)
——, **B. Peters, and D. M. Ritson.** Emulsion cloud-chamber study of a high energy interaction in the cosmic radiation—900
——, **B. Peters, H. L. Reynolds, and D. M. Ritson.** Energy spectrum of primary cosmic radiation—295
—— **and D. M. Ritson.** Extremely high energy nuclear interactions—932(L)
——, **D. M. Ritson, and Edythe P. Woodruff.** Primary flux of high energy protons and α-particles—933(L)
Karp, Ira L. Influence of well shape on the pickup process in deuterium—754(A)
Karplus, Robert and Abraham Klein. Electrodynamic displacement of atomic energy levels. I. Hyperfine structure—972
Katz, E. Splitting of bands in solids—495(L)
Katz, Robert and Milford R. Lee. Radioactivity of $Eu^{152,154}$—1038(L)
Kauffman, John and David Lazarus. Effect of plastic deformation on anelastic properties of alpha-brass—710(A)
Keck, James C. Energetic protons from nuclei exposed to 300-Mev Bremsstrahlung—410
Keesom, P. H. and Norman Pearlman. Atomic heat of silicon and germanium at very low temperatures—730(A)
Keffer, F. and C. Kittel. Theory of antiferromagnetic resonance—329
Kelly, W. C. Internal conversion in Pr^{144}, In^{114}, Ba^{137}, and Cd^{110}—101
Kern, H. E. (see Lander, J. J.)—389(A)
Kessler, J. (see Byfield, H.)—718(A)
—— (see Lederman, L.)—719(A)
Kikuchi, C. (see Cohen, Victor W.)—379(L)
Kikuchi, Seishi. Photodissociation of deuteron by high energy gamma-rays—753(A); 1062(L)
Killeen, John (see Rankin, Bayard)—754(A)
Kim, Y. (see Salvini, G.)—921(L)
King, Gilbert W. Biased random walks in classical, statistical, and quantum mechanics—708(A)
Kington, J. D. (see Bair, J. K.)—946(L)
—— (see Hahn, T. M.)—934(L)
—— (see Willard, H. B.)—849

Kinsey, B. B., G. A. Bartholomew, and W. H. Walker. Neutron capture γ-rays from phosphorus, sulfur, chlorine, potassium, and calcium—1012
Kirkpatrick, Paul (see El-Sum, Hussein M. A.)—763(A)
Kittel, C. (see Keffer, F.)—329
Kjekdaas, T., Jr. (see Fox, R. E.)—707(A)
Klein, Abraham (see Karplus, Robert)—972
Klema, E. D. (see Hahn, T. M.)—934(L)
—— (see McGowan, F. K.)—152(L)
Klick, Clifford C. Experimentally derived configurational coordinate curves for phosphors—154(L); 723(A)
Knable, N. (see Hales, R. W.)—373(L)
Knight, W. D. Properties of transition metals V and Nb by nuclear magnetic resonance—762(A)
—— (see Abell, D. F.)—762(A)
Knipe, R. H. (see Gilmore, E. H.)—764(A)
Kobayashi, Koichi. Heat capacity and lattice defect of silver chloride—150(L)
Koch, K. M. and L. Halpern. Erratum: Corbino effect and the change of resistance in a magnetic field—1064(L)
Koehler, J. S. Production of large tensile stresses by dislocations—480(L)
Koehler, W. C. and E. O. Wollan. Coherent neutron scattering cross section of C^{12}—490(L)
Koester, Louis J., Jr. Classification of energy levels in Al^{25}—643; 704(A)
Kohman, Truman P. Pairing effect in nuclei and the beta-labile elements—530
—— (see Jones, John W.)—941(L)
—— (see Mulholland, George I.)—144(L)
Kojima, Yūzo (see Okamura, Tosihiko)—690(L); 693(L)
Kopfermann, H. (see Brix, P.)—1050(L)
Koski, W. S. (see Carlson, Thomas)—697(L)
Kraushaar, J. J. Angular correlation of Rh^{104}—727(A)
Krawitz, Eleanor (see Green, Louis C.)—65
Kriessman, C. J., Jr. and T. R. McGuire. Magnetic susceptibility of uranium—71
—— (see McGuire, T. R.)—452
Kristensen, P. and C. Møller. Convergent *S*-matrix formalism with correspondence to ordinary quantum mechanics—928(L)
Kumagai, H., K. Ono, and I. Hayashi. Line width of paramagnetic resonance and exchange interaction in salts containing Mn^{++} and Fe^{+++}—925(L)
Kunkel, Wulf B. (see Leob, Leonard B.)—493(L)
Kunsman, C. H. (see Shaw, T. M.)—708(A)
Kunz, W. E. (see Moak, C. D.)—928(L)
Kupperian, J. E., Jr., and E. D. Palmatier. Ionization loss of energy of relativistic mu-mesons in argon—1043(L)
Kurbatov, J. D. (see Emmerich, W. S.)—149(L); 733(A)
—— (see Lin-sheng, Cheng)—487(L)
Kurti, N. (see Bleaney, B.)—688(L)
Kusaka, R. (see Kanda, T.)—938(L)
Kusch, P. (see Ochs, S. A.)—145(L)

Labitt, M., R. J. Debs, I. Halpern, and P. T. Demos. Operating current and energy of the MIT linear electron accelerators—713(A)
Lamb, Willis E., Jr. Fine structure of the hydrogen atom. III—259
Land, Edwin H. Optics—702(T)
Lander, J. J., H. E. Kern, and A. L. Beach. Solubility and diffusion coefficient of carbon in nickel—389(A)
Lander, Richard L. and C. E. Nielsen. Scattering of light from small drops—712(A)
Langer, R. M. Beer's law generalized and applied to the Herzberg continuum in oxygen gas—740(A)
Langer, Lawrence M. Beta spectra—722(T)
Langsdorf, Alexander, Jr. (see Hibdon, Carl T.)—595
Laporte, Otto. Recent experiments with the University of Michigan shock tube—723(T)
Lark-Horovitz, K. (see Becker, M.)—730(A)
—— (see Crawford, J. H., Jr.)—730(A)
—— (see Roth, L. M.)—724(A)
Lathrop, Arthur L. Studies of superconductivity with a torsion pendulum—743(A)
Lauer, Eugene J. Positive wire corona mechanisms in hydrogen and argon—759(A)
Laughlin, J. S., J. W. Beattie, and J. Ovadia. Calorimetric determination of the roentgen for 400-kv x-rays—725(A)
—— (see Ovadia, J.)—725(A)
Law, R. R. Decay time of secondary electron emission—391(A)
Lax, Melvin. Dipole lattice in the spherical model—744(A)
—— Multiple scattering of waves. II. Effective field in dense systems—621
Lazarus, David (see Kauffman, John)—710(A)
LeBlanc, J. M. (see Cork, J. M.)—386(L)
Lebow, I. L., B. T. Feld, D. H. Frisch, and L. S. Osborne. Photomeson production from deuterium—681(L)
—— (see Feld, B. T.)—680(L)
Lederman, L., H. Byfield, and J. Kessler. Lifetime of the pi-meson—719(A)
—— (see Byfield, H.)—718(A)
Lee, C. A. (see Carlson, R. O.)—784
Lee, Milford R. (see Katz, Robert)—1038(L)
Lee, Robert J. (see Fowler, Richard G.)—732(A)
Leenov, Daniel. Electromagnetic properties of spin one particles—841
Lehovec, K. Influence of field on temperature saturated emissions from semiconducting cathodes—705(A)
LeLevier, R. E. Photoproduction of negative pions from deuterium—771(A)
Lennard-Jones, John E. Some contributions to the theory of molecular structure—702(T)
Lepore, J. V. (see Heckrotte, W.)—490(L)
Leverenz, H. W. and D. O. North. Interactions of remote impurity centers in phosphors—930(L)
Leverton, W. F. and W. G. Shepherd. Use of radioactive isotopes in the study of the evaporation from thermionic cathodes—389(A)
Levin, Franklyn K. and J. G. Winans. Erratum: Absorption spectrum of GaCl—1064(L)
Levinger, J. S. and H. A. Bethe. Neutron yield from the nuclear photoeffect—577; 742(A)
Levy, Harris B. and I. Perlman. Isomeric states of Bi^{210}—758(A)
Lewis, H. W. Range straggling of a nonrelativistic charged particle—20
Leyshon, W. E. (see Walchli, H. E.)—922(L)
Liang, C. Y. (see Nielsen, J. Rud)—740(A)
Libby, W. F. (see Kalkstein, Marvin I.)—368(L)
—— (see Wolfgang, Richard L.)—437
Liebowitz, B. Relation between Planck's constant and the gravitational constant—722(A)
Lindenbaum, S. J. (see Bernardini, G.)—826
Lindhard, J. and M. Scharff. Stopping power of heavier substances—1058(L)
Lin-sheng, Cheng, G. John, and J. D. Kurbatov. Beta-spectra of cerium 144 and praseodymium 144—487(L)
Lipkin, Harry J. Nuclear scattering of 1-Mev electrons and positrons—517
Livingston, Ralph (see Walchli, Harold)—479(L)
Livingston, Robert S. Oak Ridge 86-in. cyclotron—713(A)
Lloyd, Stuart P. Angular correlation of two successive nuclear radiations—904
Lockenvitz, Arthur E. and Kenneth H. Ribe. Time rate of transformation of amorphous selenium into another form as a function of temperature—746(A)
—— (see Murphy, John)—745(A)
Lodge, John I. and Frank L. Hereford. Energy loss of monoenergetic electrons in carbon and water—725(A)

Loeb, Leonard B. and Wulf B. Kunkel. Interpretation of observed pressure-dependent recombination coefficients—493(L)
Loeliger, H. (see Jeffries, C. D.)—478(L)
Long, E. A. (see Anderson, H. L.)—934(L); 936(L)
Long, Earl and Lothar Meyer. Some experiments on flow in the unsaturated helium II film—1030
—— (see Meyer, Lothar)—1035
Long, John K. and M. L. Pool. Radioactive Pm^{148} and Pm^{150}—137(L)
Long, R. W. and I. A. Robertson. Reduction of temperature coefficient of magnetic moment for a bar magnet—746(A)
Lord, R. C. Far infrared transmission of silicon and germanium—140(L)
Love, W. F. Some observations on the superconductive transition in pure metals—715(A)
—— (see Callen, E.)—715(A)
Lovington, J. A., J. J. G. McCue, and W. M. Preston. (p,n) reaction on separated isotopes of chromium—585
Luckey, David and John W. Weil. Velocity of 170-Mev gamma-rays—1060(L)
Luke, P. J., R. E. Meyerott, and W. W. Clendenin. Wave function of ionized lithium—401
—— (see Meyerott, R. E.)—393
Lundby, A. (see Fermi, E.)—935(L)
Luyet, B. Supercooling of water—746(A)

Macdonald, J. Ross. Photocontrolled low frequency dielectric dispersion—381(L)
Mack, J. E. Long forbidden $s-ns$ series in RbI—716(A)
MacKenzie, K. R. (see Hubbard, E. L.)—107
Madey, Richard, Kenneth C. Bandtel, and Wilson J. Frank. Photoproduction of negative mesons from deuterium—771(A)
Malenka, B. J. Nonlinearities due to vacuum polarization in meson-nucleon interactions—686(L)
Mandeville, C. E., C. P. Swann, S. D. Chatterjee, and D. M. Van Patter. Neutrons from the disintegration of the separated isotopes of silicon by deuterons—193; ——, **C. P. Swann, and S. D. Chatterjee**—725(A)
Mann, Ralph W. Thermal coefficients applying to deflection of springs—740(A)
Manring, Edward R. (see Weatherly, Thomas L.)—717(A)
Margenau, Henry and Stanley Bloom. Clustering of ions—735(A)
—— **and D. E. Harrison.** Van der Waals forces in magnetic fields—707(A)
—— (see Bloom, Stanley)—717(A); 670
Marks, Graham W. and Lester A. Monson. Effect of certain group IV oxides on the permittivity and loss tangent of barium titanate—723(A)
Marks, L. W. (see Atkinson, W. R.)—706(A)
Marple, D. T. F. (see Trischka, J. W.)—136(L)
Marshak, R. E. (see Francis, N. C.)—496(L)
—— (see Petschek, A. G.)—698(L)
Martin, B., D. Ter Haar, and V. A. Johnson. Statistics of the three-dimensional ferromagnet—714(A)
Martin, Donald F. (see Browne, Charles I.)—146(L)
Martin, D. W. (see Cork, J. M.)—386(L)
Martin, Jack (see Jacobs, Harold)—441
Martin, R. L., H. L. Anderson, and G. Yodh. Nuclear cross sections for negative pions of energy 109 and 133 Mev—486(L)
Martin, R. (see Anderson, H. L.)—934(L)
Martin, William J. (see Walchli, Harold)—479(L)
Martius, Ursula M., K. V. Gow, and Bruce Chalmers. Ferromagnetic domain structure of single crystals and bicrystals of nickel—713(A)
—— (see Dijkstra, L. J.)—714(A)
Marton, L. Electron interferometer—1057(L)
Mason, W. P. Erratum: Phenomenological derivation of the first- and second-order magnetostriction and morphic effects for a nickel crystal—1065(L)
Massey, J. T. and D. R. Bianco. Microwave absorption spectrum of H_2O_2—717(A)
Masuda, Y. (see Kanda, T.)—938(L)
Matossi, Frank. Computation of infrared intensities—708(A)
Matthias, B. T. Isotope effect in RbD_2PO_4—723(A)
—— Phase transition of $ND_4D_2PO_4$—141(L)
May, M. M. (see Fretter, W. B.)—773(A)
Mayer, M. Goeppert (see Jensen, J. Hans D.)—1040(L)
Mayfield, Earle B. Time-resolved spectroscopy of the incandescence associated with ultraspeed pellets—769(A)
Maxwell, D. E. (see Hahn, E. L.)—762(A)
Maze, R. Absence of secondary maxima in the transition curve for electronic showers—697(L)
McAfee, K. B., W. Shockley, and M. Sparks. Pressure dependence of Zener current in germanium—730(A)
McClelland, J. D. and J. J. Donoghue. Magnetic susceptibility of polycrystalline anisotropic materials, and observations on artificial graphites—768(A)
McClure, D. S. (see Blake, N. W.)—754(A)
—— (see Schnepp, O.)—755(A)
McClure, J. W. Magnetic susceptibility of zinc at liquid nitrogen temperatures—715(A)
McCoubrey, A. O. (see Holstein, T.)—985
McCrary, Clyde L. (see Allen, William A.)—769(A)
McCue, J. J. C. (see Lovington, J. A.)—585
McDonald, R. E. (see Elder, F. K., Jr.)—500(L)
McFarland, R. H. (see Hein, R. E.)—138(L)
McGowan, F. K. Lifetime of an excited state of $_{68}Dy^{169}$ and upper limits for some other nuclei—142(L)
—— Measurements of some K-shell internal conversion coefficients—151(L)
——, **E. D. Klema, and P. R. Bell.** Classification of the γ-radiation of Hf^{177}—152(L)
McGrath, J. W. (see Doughty, Donald D.)—1040(L)
McGuire, T. R. and C. J. Kriessman. Magnetic susceptibility of chromium—452
—— (see Kriessman, C. J.)—71
McKay, C. D. (see Scheidegger, A. E.)—376(L); 721(A)
McKay, K. G. (see Johnson, J. B.)—390(A)
McMahon, Brien. Title to be announced—702(T)
McMath, Robert R. (see Goldberg, Leo)—140(L); 481(L)
McQuistan, R. B. (see Hirsch, J.)—723(A)
Medicus, Heinrich A. and Harry T. Easterday. Mass designation of the 51.5-min Tc isomer—735(A)
Meinke, W. W., A. Ghiorso, and G. T. Seaborg. Further work on heavy collateral radioactive chains—429
Meissner, K. W. and W. F. Miller. Influence of irradiation on the characteristic of a glow discharge in pure rare gases—706(A)
—— (see Andrew, Kenneth L.)—716(A)
—— (see Roth, L. M.)—724(A)
Meister, Arnold G. (see Davis, Abram)—707(A)
Mertz, R. T. (see Green, Louis C.)—65
Messel, H. (see Green, H. S.)—679(L)
Metzger, Franz R. Gamma-gamma coincidences in "Cs^{127}" and Fe^{59}—727(A)
Meyer, Lothar and Earl Long. Phase transitions in adsorbed films—1035
—— (see Long, Earl)—1030
Meyerott, R. E., P. J. Luke, W. W. Clendenin, and S. Geltman. Numerical variational method—393
—— (see Luke, P. J.)—401
Mihelich, J. W. and E. L. Church. Low energy γ-ray transitions in some rare earth isotopes—690(L)
—— **and E. L. Church.** Relative internal conversion in the L subshells—733(A)
—— (see Scharff-Goldhaber, G.)—734(A)
—— (see Sunyar, A. W.)—734(A)

Miller, B. L. and W. C. Porter. Secondary electron emission under high energy electron bombardment—391(A)
Miller, C. E., J. E. Henderson, Gerald Garrison, and Wayne Sandstrom. Zenith angle effects for cosmic-ray protons and mesons—773(A)
Miller, D. W., R. E. Fields, and C. K. Bockelman. Total cross sections of heavy nuclei for fast neutrons—704(A)
Miller, P. H., Jr. X-ray study of lattice imperfections—709(A)
Miller, W. C. (see Noyes, J. C.)—727(A)
Miller, W. F. (see Meissner, K. W.)—706(A)
Milligan, W. O. and Harry B. Whitehurst. Diamagnetic properties of adsorbed gases—746(A)
Milne, Edmund A. (see Warters, William D.)—761(A)
Minton, G. H. (see De Benedetti, S.)—726(A); 944(L)
Mitchell, Allan C. G. and Alan B. Smith. Isomeric transition in Ge^{77}—153(L)
Mizushima, Masataka and Minoru Umezawa. Nuclear magnetic moment and $j-j$ coupling shell model—37
Moak, C. D., W. M. Good, and W. E. Kunz. Reaction $Li^6(t,p)Li^8$—928(L)
—— (see Johnson, C. H.)—727(A); 931(L)
Mohler, Orren C. (see Goldberg, Leo)—140(L); 481(L)
Møller, C. (see Kristensen, P.)—928(L)
Molmud, Paul. Equation of motion of the Landé electron—139(L)
Monson, Lester A. (see Marks, Graham W.)—723(A)
Moore, George E. and H. W. Allison. BaSrO cathode supported on an insulator—389(A)
—— (see Allison, H. W.)—388(A)
Morgan, T. J. (see Donnelly, F. K.)—767(A)
Morrison, H. L. Successive approximations in a theory for critical stability of fluids—770(A)
Morrisson, T. E. and T. W. DeWitt. Apparatus for creep and low frequency dynamic studies on polymers—708(A)
Moshinsky, Marcos. Time dependent description of resonance reactions—748(A)
Motz, Henry T. Beta-activity of Si^{31} and the masses of the Al and Si isotopes—501(L)
Moyer, B. J. (see Cladis, J. B.)—766(A)
—— (see Crandall, W. E.)—771(A)
—— (see Hales, R. W.)—373(L)
Mrozowski, S. Semiconductivity and diamagnetism of polycrystalline graphite and condensed ring systems—609
Muehlhause, C. O. and G. E. Thomas. Slow neutron liquid scintillation detector—926(L)
Mulder, Marjorie M. (see Green, Louis C.)—65
Mulholland, George I. and Truman P. Kohman. Possible natural radioactivity of neodymium—144(L)
Muller, D. E. Recent results with the curved-crystal gamma-ray spectrometer—739(T)
Müller, E. W. Observations with the field emission microscope—392(A)
Munesue, Seiji (see Sakurai, Takemaro)—921(L)
Murakawa, Kiyoshi and Shigeki Suwa. Hyperfine structure in the spectrum of erbium—683(L)
—— (see Ross, John S.)—559
Murphy, John and Arthur E. Lockenvitz. Time rate of transformation of α-monoclinic selenium into hexagonal as a function of the temperature—745(A)
Myers, R. D. (see Elliot, J. O.)—1048(L)

Nagle, D. E. (see Anderson, H. L.)—934(L); 936(L)
—— (see Fermi, E.)—935(L)
Narita, S. (see Arizumi, T.)—388(A)
Neher, H. V., Vincent Z. Peterson, and Edward A. Stern. Latitude effect of cosmic rays between geomagnetic latitudes 54° and 88°N—772(A)
Nereson, Norris. Fission neutron spectrum of U^{235}—600
Neuman, Maurice. Eigenvalue problem in quantum electrodynamics—129
Newkirk, Lester L. New technique for the determination of photonuclear cross sections—767(A)
Newton, J. O. (see French, A. P.)—1041(L)
Ney, E. P. (see Critchfield, C. L.)—461
Nichols, M. H. Growth of single crystals of tantalum and their surface structure—769(A)
Nichols, R. T. (see Jensen, Erling N.)—112
Nielsen, C. E. (see Lander, Richard L.)—712(A)
Nielsen, J. Rud. Vibrational spectra of fluorinated hydrocarbons—739(T)
——, **C. Y. Liang, and D. C. Smith.** Infrared and Roman spectra and calculated thermodynamical properties of $CF_2=CHCl$—740(A)
—— (see Smith, D. C.)—739(A)
Nier, A. O. (see Collins, T. L.)—726(A)
Nieset, Robert. Recent work in the biophysics laboratory at Tulane University—741(T)
Nijboer, B. R. A. and L. Van Hove. Radial distribution function of a gas of hard spheres and the superposition approximation—777
Nix, Foster C. and Frank E. Jaumot, Jr. Experimental evidence for the vacancy mechanism for diffusion in metals and alloys—709(A)
—— (see Callen E.)—715(A)
Noble, Robert H. (see Houston, Robert E.)—732(A)
North, D. O. (see Leverenz, H. W.)—930(L)
Norton, Francis J. Ions of mass 19 from water—154(L)
Nowak, W. B. Temperature dependence of internal friction at 44 kc—710(A)
Noyes, J. C., J. E. Van Hoomissen, W. C. Miller, and B. Waldman. Photodisintegration thresholds of beryllium and deuterium—727(A)
Nuckolls, R. G. and L. J. Rueger. Stabilized synchronous amplifier—731(A)
Nystrom, Robert F. (see Yankwich, Peter E.)—753(A)

Oberly, J. J. (see Burstein, E.)—729(A)
Ochs, S. A. and P. Kusch. Hyperfine structure anomaly of the Rb isotopes—145(L)
O'Dell, Francis W. (see Stiller, Bertram)—712(A)
Odencrantz, F. K. (see Rogers, Marguerite)—756(A)
Okamoto, Sunao (see Shimizu, Sakae)—290
Okamura, Tosihiko, Tadao Fujimura, and Muneyuki Date. Dielectric constant and permeability of various ferrites in the microwave region—1041(L)
—— **and Yûzo Kojima.** Ferromagnetic resonance in single crystals of cobalt-zinc ferrite—690(L)
——, **Kojima, and Yosiharu Torizuka.** Temperature dependence of the line half-width of ferromagnetic resonance in single crystals of zinc-manganese ferrite—693(L)
Okumura, K. (see Ishikawa, Y.)—1065(L)
Olcott, R. N. (see Chatterjee, S. D.)—147(L)
Oleksa, Sophie (see Critchfield, C. L.)—461
Oliver, A. J. and Walter H. Barkas. Physical measurements on nuclear photographic emulsion—756(A)
Ono, K. (see Kumagai, H.)—925(L)
O'Rourke, R. C. Multiple Compton scattering of low energy gamma-radiation—881
Orth, Donald (see James, Ralph A.)—369(L)
Osborne, D. W., B. M. Abraham, and B. Weinstock. Melting curve of He^3—715(A)
—— (see Weinstock, B.)—158(L)
Osborne, L. S. (see Feld, B. T.)—680(L)
—— (see Lebow, I. L.)—681(L)
Ovadia, J., J. W. Beattie, and J. S. Laughlin. Ranges of high energy electrons in water—725(A)
—— (see Laughlin, J. S.)—725(A)
Owen, G. E. Physics, a part of general education at Harvard—160(T)

Oxley, C. L. and R. D. Schamberger. Proton-proton scattering at 240 Mev—416

Page, L. A. (see Arthur, James S.)—704(A)
Pake, G. E., J. Townsend, and S. I. Weissman. Hyperfine structure in the paramagnetic resonance of the ion $(SO_3)_2NO^{--}$—682(L)
Palmatier, E. D. (see Kupperian, J. E., Jr.)—1043(L)
Palmer, K. J. (see Shaw, T. M.)—708(A)
Palmer, W. F. (see Van Dyke, K. S.)—745(A)
Panofsky, W. K. H. (see Crandall, W. E.)—771(A)
Pappas, A. C. (see Coryell, C. D.)—732(A)
Parratt, L. G. and E. L. Jossem. Energy levels in KCl—729(A)
Parzen, P. Effect of the thermal velocity distribution upon the behavior of diodes at microwave frequencies—704(A)
Passman, S., M. M. Block, and W. W. Havens, Jr. Charged π-meson production from deuterium—370(L)
—— (see Block, M. M.)—718(A)
Pattee, H. H., Jr. Compound x-ray microscope—764(A)
Patterson, D. A. (see Friedman, H.)—705(A)
Pearlman, Norman (see Keesom, P. H.)—730(A)
Pearson, G. L., W. T. Read, and W. Shockley. Probing the space-charge layer in a $p-n$ junction—1055(L)
Pearson, John and John S. Rinehart. Deformation and fracturing of thick-walled steel cylinders under explosive attack—768(A)
—— (see Rinehart, John S.)—768(A)
Peaslee, D. C. Neutron scattering lengths—555
Pecjak, F. A. (see Sun, K.-H.)—726(A); 942(L)
Pellam, John R. Experiments on second sound in liquid helium II—741(T)
—— **and William B. Hanson.** Thermal Rayleigh disk measurements in liquid helium II—216
Pepinsky, R. (see Frazer, B. C.)—479(L)
Pepper, T. P., K. W. Allen, E. Almqvist, and J. T. Dewan. Protons and deuterons from Li^6+T reactions—155(L)
Perkins, W. D. and M. Kent Wilson. Vibrational spectrum of dinitrogen tetroxide—755(A)
Perlman, I. (see Asaro, Frank)—758(A)
—— (see Browne, C. I.)—758(A)
—— (see Levy, Harris B.)—758(A)
Perls, T. A. (see Wildhack, W. A.)—731(A)
Perry, Alfred M., Jr. Inelastic cross sections for 240-Mev protons—497(L)
Peter, M. (see Känzig, W.)—940(L)
Peters, B. (see Kaplon, M. F.)—295; 900
Peterson, Vincent Z. (see Neher, H. V.)—722(A)
Petschek, A. G. and R. E. Marshak. β-decay of radium E and the pseudoscalar interaction—698(L)
Phillips, G. C., N. P. Heydenburg, and D. B. Cowie. Angular correlation studies of $(d;p,\gamma)$ processes of the target nuclei Li^6, B^{10}, and O^{16}—742(A)
—— (see Heydenburg, N. P.)—742(A)
Phillips, R. (see Crandall, W. E.)—771(A)
Pickup, E. (see Voyvodic, L.)—91
Pierce, A. Keith (see Goldberg, Leo)—140(L); 481
Pigg, J. C. Automatic multirange recording device for measuring varying potentials—731(A)
—— (see Crawford, J. H., Jr.)—730(A)
Pines, David. Stopping power of a metal for charged particles—931(L)
—— **and David Bohm.** Collective description of electron interactions: II. Collective *vs* individual particle aspects of the interactions—338
Pirenne, J. C. Covariant theory of damping—721(A)
Pizzaro, R. and B. Gossick. Design of extensometer for creep studies—711(A)
Plain, G. J. (see Rogers, Marguerite)—756(A)
Plass, Gilbert N. and Douglas Warner. Infrared absorption by asymmetrical spectral lines—708(A)
Pohm, A. (see Jensen, Erling N.)—112
Pollock, H. C. High energy electron and x-ray beams from the 80-Mev synchrotron—739(T)
Pond, T. A. Formation of triplet positronium in gases—489(L)
—— **and R. H. Dicke.** Fine structure splitting in the ground state of positronium—489(L)
Pool, M. L. (see Long, John K.)—137(L)
—— (see Scoville, C. L.)—1046(L)
Pope, N. K. and G. Feldman. Theory of neutron scattering by gases—703(A)
Porter, Fred T. and C. Sharp Cook. Beta-spectra of Ce^{144} and Pr^{144}—733(A)
Porter, W. C. (see Miller, B. L.)—391(A)
Poss, H. L., E. O. Salant, and L. C. L. Yuan. Total cross sections of carbon and hydrogen for 14-Mev neutrons—703(A)
Pound, R. V. (see Watkins, G. D.)—1062(L)
Present, R. D. and S. C. Chen. Nuclear disintegration by positron-K electron annihilation—447
Preston, W. M. (see Lovington, J. A.)—585
—— (see Schoenfeld, W. A.)—873
Price, Edward W. One-dimensional flow with mass addition—769(A)
Prieto C., Fernando E. Anomalous magnetic moments of nucleons—747(A)
Primakoff, H. Angular correlation of electrons in double beta-decay—888
Purcell, E. M. (see Ramsey, N. F.)—143(L)
Putnam, T. M. Differential cross section for the scattering of 9.5-Mev protons from helium—774(A)

Quinnell, E. H. (see Clement, J. R.)—502(L)

Racah, Guilio. $L(L+1)$ correction in the spectra of the iron group—381(L)
Ramachandran, G. M. New method of obtaining focused images with x-rays—378(L)
Ramsey, Norman F. Long range proton-proton tensor force—937(L)
—— Theory of molecular hydrogen and deuterium in magnetic fields—60
—— Use of HD for experiments on the proton-deuteron magnetic moment ratio—688(L)
—— **and E. M. Purcell.** Interactions between nuclear spins in molecules—143(L)
Randolph, Burton. Temperature dependence of the resistivity of deuteron irradiated and annealed molybdenum—710(A)
Rankin, Bayard, John Killeen, and Walter H. Barkas. Some differential analyzer methods for orbit problems in the cyclotron—754(A)
Rasmussen, John O. Semiempirical correlation of alpha-decay rates—758(A)
—— (see Browne, Charles I.)—146(L)
—— (see Thompson, S. G.)—758(A)
Rau, R. R. (see Brown, Fielding)—712(A)
Ravilious, C. F. (see Elliot, J. O.)—1048(L)
Read, W. T. (see Pearson, G. L.)—1055(L)
Reff, Israel. Anti-proton annihilation—379(L)
Reilley, E. M., A. J. Allen, J. S. Arthur, R. S. Bender, R. L. Ely, and A. J. Hausman. Energy levels in Al^{37}—704(A)
—— (see Arthur, James S.)—704(A)
—— (see Ely, Ralph, Jr.)—704(A)
Reynolds, C. A. (see Serin, B.)—938(L)
Reynolds, Fred L. (see Asaro, Frank)—758(A)
Reynolds, George T. (see Brown, Fielding)—712(A)
Reynolds, H. L. (see Kaplon, M. F.)—295
Reynolds, John H. Surface ionization of lanthanum—770(A)
Ribe, Fred L. (see Groetzinger, Gerhart)—78
Ribe, Kenneth H. (see Lockenvitz, Arthur E.)—746(A)

Richards, P. I., E. E. Hays, and S. A. Goudsmit. Masses of lead and bismuth—630
—— (see Hays, E. E.)—1065(L)
Richings, H. J. (see DeBenedetti, S.)—377(L)
Richman, C., M. Weissbluth, and H. A. Wilcox. Production cross sections for π^+- and π^--mesons by 340-Mev protons on carbon and lead at 90° to the beam—161
—— (see Whitehead, Marian)—772(A)
Riddell, R. J., Jr. Theory of condensation of gases—760(A)
Rider, John A. and George Jaffé. Polarization in electrolyte solutions—746(A)
Rieke, F. F. and D. D. Errett. Drift velocity of electrons in gas mixtures—706(A)
—— (see Errett, D. D.)—706(A)
Rieser, L. M., Jr. Reflection of x-rays and the x-ray microscope—764(A)
Riess, Karlem, T. T. Earle, and John Hidalgo. Tracer studies on alligator weed using 2,4-D-C^{14}—741(A)
Rinehart, John S. and John Pearson. Some tensile fractures generated in metals by impulsive compressional loading—768(A)
—— (see Pearson, John)—768(A)
Ringo, G. R. (see Hamermesh, M.)—483(L)
Risser, J. R. and W. H. Burke. Evidence for stripping in the $B^{10}(d,n)C^{11}$ reaction at low deuteron energies—742(A)
—— (see Burke, W. H.)—741(A)
Ritow, Herman. Electric current between flashes of the intermittent glow discharge in H_2—706(A)
Ritson, D. M. (see Kaplon, M. F.)—295; 900; 932(L); 933(L)
Rittner, E. S. Diffusion phenomena in the oxide cathode—389(A)
—— **and R. H. Ahlert.** $I-V$ characteristics of the "L-cathode"—390(A)
Rivier, D. C. Extension of the classical infinitesimal group of canonical transformations—721(A)
Robba, Wm. A. 800-kc Cockroft-Walton generator—741(A)
Roberts, Arthur (see Clark, Donald L.)—523
Roberts, J. E. (see Jastrow, R.)—757(A)
Roberts, J. H. (see Guier, W. H.)—426
Roberts, Shepard. Adiabatic study of the 128°C transition in barium titanate—925(L)
Robertson, I. A. (see Long, R. W.)—746(A)
Robinson, F. N. H. (see Bleaney, B.)—688(L)
Robinson, G. P. (see Johnson, C. H.)—931(L); 727(A)
Roever, W. L. Experimental laboratory studies of elastic wave propagation—744(A)
Rogers, F. T., Jr. Variational approach to a theory for critical stability of a fluid—770(A)
Rogers, Marguerite, F. K. Odencrantz, and G. J. Plain. Neutron spectrum from $B^{10}(\alpha,n)N^{13}$, N^{13*}—756(A)
Rogers, T. F. (see Johnson, S. J.)—714(A)
Rogosa, G. L. K-excitation potentials of the elements—716(A)
Rollosson, George W. Penetrating cosmic-ray showers in water—774(A)
Rose, J. W. and W. S. Gilbert. High energy photoprotons from carbon—766(A)
—— (see Gilbert, W. S.)—766(A)
Rose, M. E., L. C. Biedenharn, and G. B. Arfken. Internal conversion angular correlations—5
Rose, William B. (see Hudspeth, Emmett L.)—742(A)
Rosen, A. Z. Protons and mesons at 9000 feet—773(A)
Rosen, Nathan and Herbert B. Rosenstock. Force between particles in a nonlinear field theory—257
Rosenblum, E. S., E. F. Shrader, and R. M. Warner. Gamma-ray absorption coefficients in the 5–10 Mev energy range—728(A)
Rosenstock, Herbert B. (see Rosen, Nathan)—257
Roser, Francis X. (see Bowen, Theodore)—992
Ross, John S. and Kiyoshi Murakawa. Hyperfine structure and isotope shift in the spectrum of tellurium—559
Ross, Marc. Contribution of interaction moments to nuclear magnetic moments—721(A)
Rossi, Bruno (see Bridge, Herbert)—159(L)
Roth, L. M., K. W. Meissner, and K. Lark-Horovitz. Optical and electrical behavior of lanarkite—724(A)
Rothstein, Jerome. Information and thermodynamics—135(L)
—— Information, logic, and physics—722(A)
Rouse, Arthur G. and John B. Drahmann. Cathodoluminescence of commercial oxide coated cathodes—739(A)
Ruark, Arthur E. Electrodynamics as a basis for special relativity—770(A)
Ruderman, M. Decay of the π-meson—157(L)
Rueger, L. J. (see Nuckolls, R. G.)—731(A)
Runge, Richard J. Elastic scattering of deuterons by deuterons—1052(L)
Russell, Paul. Study of evaporated films of BaO using electron diffraction techniques—705(A)
Rutledge, W. C., J. M. Cork, and S. B. Burson. Clarification of the radioactivity of Nd^{151} and Pm^{151}—734(A)

Sachs, A. M. (see Isaacs, P. J.)—803; 718(A)
Sagane, Ryokichi. Erratum: Computation of photonuclear resonance curves from relative activity curves monitored by induced radioactivity—1065(L)
—— Relative probabilities of diverse photonuclear reactions from Zn^{64} and Fe^{54}—926(L)
Sailor, V. L. (see Borst, L. B.)—711(A)
Sakurai, Takemaro and Seiji Munesue. Resistivity of evaporated tellurium films—921(L)
Salant, E. O. (see Poss, H. L.)—703(A)
Salkovitz, E. I. Energy absorption during twin formation in zinc single crystals—1046(L)
Salvini, G. and Y. Kim. Production cross section and energy spectrum of the neutral mesons in cosmic rays—921(L)
Sampson, M. B. (see Toops, E. C.)—280
Sandstrom, Wayne (see Miller, C. E.)—773(A)
Sard, Robert D. (see Crouch, Marshall F.)—120
Sasaki, T. (see Ishikawa, Y.)—1065(L)
Sato, T. (see Ishikawa, Y.)—1065(L)
Satten, Robert A. Eigenfunctions and Landé interval factors for terms of f^3 electrons—775(A)
—— Spectrum of Nd^{+++} in crystals—755(A)
Saunders, R. A. (see Smith, D. C.)—739(A)
Saur, A. J. and H. M. Schwartz. Proposed methods for determining K-capture partial lifetimes—733(A)
Savitt, J. and R. H. Stresau, Jr. Velocities of ionized air shocks near detonating explosives—732(A)
Saxon, David S. and E. Gerjuoy. Calculation of high energy scattering cross sections using variational methods—704(A)
—— (see Gerjuoy, E.)—939(L)
Scales, John and C. W. Heaps. Resistance variation of MnSe at low temperatures—743(A)
Schamberger, Robert D. 240-Mev proton-deuteron scattering—424
—— (see Oxley, C. L.)—416
Schamp, H. W., Jr. Anionic self-diffusion and electrical conduction in sodium bromide—729(A)
Schardt, A. W. and William Bernstein. Performance of 5819 photomultipliers in scintillation spectrometers—712(A)
—— (see Bernstein, William)—713(A); 919(L)
Scharff, M. (see Lindhard, J.)—1058(L)
Scharff-Goldhaber, G., E. der Mateosian, and J. W. Mihelich. Disintegration scheme of Lu^{176m}—734(A)
—— (see Sunyar, A. W.)—734(A)
Scheibner, E. J. Electron microscope and diffraction study of the aging of evaporated metal films—709(A)
Scheidegger, A. E. and C. D. McKay. Relativistic modification of Bose and Fermi statistics—376(L)
—— **and C. D. McKay.** Thermodynamics of fields—721(A)

Schein, Marcel and Victor H. Yngve. Absorption curve of the cosmic radiation in the stratosphere—607
—— (see Weaver, A. B.)—719(A)
Scheitlin, F. M. (see Walchli, H. E.)—922(L)
Schenck, James and R. L. Heath. Tin activation of LiI—923(L)
Schiff, Daniel. Gamma-gamma coincidence absorption and angular correlation of I^{131}—727(A)
Schiff, L. I. Neutral V-particle decay and the negative proton—374(L)
—— Radiative corrections to the distribution of nuclear recoils from electron scattering—754(A)
Schindler, Mark and G. L. Weissler. Positive ion energies in a point-to-plane corona—759(A)
Schmidt, F. H. (see Donnelly, F. K.)—767(A)
Schmitt, Roland W. Adiabatic thermal changes in barium titanate ceramic at low temperatures—1
—— **and R. T. Swim.** Adiabatic thermal changes in barium titanate ceramic and strontium titanate at low temperatures—743(A)
Schnepp, O. and D. S. McClure. Vibrational analysis of the fluorescence of naphthalene vapor—755(A)
Schoenfeld, W. A., R. W. Duborg, W. M. Preston, and C. Goodman. Reaction $Cl^{37}(p,n)A^{37}$; excited states in A^{38}—873
Scholnick, Seymour (see Jacobs, Donald H.)—731(A)
Schremp, E. J. Geometry of the group-space of the proper Lorentz group—721(A)
Schulman, J. H. (see Etzel, H. W.)—1063(L)
Schulz, Alvin G. (see Jakobson, Mark J.)—772(A)
—— (see White, R. Stephen)—770(A)
Schwartz, H. M. Atomic binding energy considerations in negative beta-decay—733(A)
—— (see Saur, A. J.)—733(A)
Schwetman, Herbert D. and S. Leroy Brown. Application of the Laplace transformation and a mechanical harmonic synthesizer in the analysis of electric circuits—740(A)
Scott, W. T. Mean-value calculations for projected multiple scattering—245
Scoville, C. L., S. C. Fultz, and M. L. Pool. Radiations of Rh^{99}, Rh^{101}, Rh^{105}, and Ru^{105}—1046(L)
Seaborg, Glenn T. Mechanism of fission—157(L); 757(A)
—— (see Dunlavey, Dean C.)—757(A)
—— (see Jenkins, William A.)—758(A)
—— (see Meinke, W. W.)—429
Seagondollar, L. W., R. K. Smith, W. R. Alexander, and J. W. Teener. University of Kansas Van de Graaf generator—713(A)
Seagrave, John D. Radiative capture of protons by C^{12}—197
Seale, R. L. (see Connell, L. F.)—745(A)
Secrest, E. Leigh. Quadrature method for computing neutron distributions in two dimensions—747(A)
Seifert, A. M. (see Bramson, H. J.)—719(A)
Seliger, Howard H. Absolute backscattering coefficients for positrons and electrons—724(A)
Serin, B. and C. A. Reynolds. Experiments with audiofrequencies on superconductors—938(L)
—— (see Garfunkel, M. P.)—834
Shaefer, D. L. and J. E. White. Physical processes in the "L" cathode—390(A)
Shalek, R. J., T. W. Bonner, and L. M. Branscomb. Emission spectra of nitrogen bombarded by high energy protons—739(A)
Shapiro, Edward. Electrolysis of thorium dioxide. I. Oxygen evolution from operating cathodes—390(T)
Shapiro, Maurice M. (see Stiller, Bertram)—712(A)
Sharma, J. Color centers and thermoluminescence in alkali halides—692(L)
Shaw, T. M., R. H. Elsken, and C. H. Kunsman. Proton magnetic resonance absorption and water content of biological materials—708(A)
——, **R. H. Elsken, and K. J. Palmer.** Nuclear magnetic resonance absorption in glycine—762(A)
Shenfil, L., W. E. Danielson, and J. W. M. DuMond. Point focusing monochromator for low angle x-ray diffraction—739(A)
Shepherd, W. G. (see Leverton, W. F.)—389(A)
Sherman, D. F., Harry H. Heckman, and Walter H. Barkas. Capture of μ-mesons in nuclear emulsions—771(A)
Shimizu, Sakae, Tetsuya Hanai, and Sunao Okamoto. Absorption of gamma-rays from Co^{60}—290
Shipley, F. L. (see Johnson, V. A.)—724(A)
Shockley, W. (see McAfee, K. B.)—730(A)
—— (see Pearson, G. L.)—1055(L)
Shrader, E. F. (see Rosenblum, E. S.)—728(A)
Shutt, R. P. (see Thorndike, A. M.)—929(L)
Sidles, P. H. and G. C. Danielson. Thermal conductivity of metals—710(A)
Siegel, R. (see DeBenedetti, S.)—371(L)
Siegmund, Walter P. (see Givens, M. Parker)—313
Sillars, R. W. Light emission from silicon carbide—136(L)
Silverman, Richard A. Fermi energy of metallic lithium—227
Silvey, G. (see Geschwind, S.)—474
—— (see Hardy, W. A.)—494(L)
Simmons, D. H. (see Baker, C. J.)—1051(L)
Simpson, J. A., W. Fonger, and L. Wilcox. Solar component of the primary cosmic radiation—366(L); 720(A)
Slater, J. C. Solid state—702(T)
Slaymaker, E. (see Green, Louis C.)—65
Smaller, Bernard and Eugene Avery. Long-lived phosphorescence of potassium iodide-thallium iodide—766(A)
Smart, J. Samuel. Generalizations of the Weiss molecular field theory of antiferromagnetism—714(A)
Smith, Alan B. (see Mitchell, Allan C. G.)—153(L)
Smith, D. C., R. A. Saunders, J. Rud Nielsen, and E. E. Ferguson. Infrared and Raman spectra and calculated thermodynamical properties of CH_3-CH_2F and CH_3-CHF_2—739(A)
—— (see Nielsen, J. Rud)—740(A)
Smith, F. M., W. Birnbaum, and W. H. Barkas. Range straggle of μ^+-mesons—771(A)
Smith, J. L. (see Germer, L. H.)—392(A)
Smith, J. R. (see Conner, J. P.)—741(A)
Smith, J. Richard (see Cook, Charles F.)—741(A)
Smith, Lincoln G. Recent developments with the mass synchrometer—767(A)
Smith, R. K. (see Seagondollar, L. W.)—713(A)
Smith, R. L. (see Yovits, M. C.)—540
Smith, Warren H. $Cu(\gamma,d):(\gamma,p)$ ratio—728(A)
Smoluchowski, R. Statistical theory of properties of solid solutions—710(A)
Snow, A. I. Neutron diffraction investigation of the atomic magnetic moment orientation in the antiferromagnetic compound CrSb—365(L)
Snow, George. Analysis of 14-Mev $n-p$ scattering—703(A)
Snyder, C. W. (see Bair, J. K.)—946(L)
—— (see Hahn, T. M.)—934(L)
—— (see Willard, H. B.)—849
Sommer, H., D. N. Craig, J. I. Hoffman, and J. A. Hipple. Effect of recent mass measurements on the Faraday—740(A)
—— (see Hipple, J. A.)—712(A)
Sommers, Henry. Experimental investigations of liquid mixtures of helium 3 and helium 4—741(T)
Sorrells, J. D. (see Walker, W. D.)—773(A)
Sparks, I. L. Retarding potential method of measuring the electrical conductivity of oxide coated cathodes—705(A)
Sparks, M. (see McAfee, K. B.)—730(A)
Spencer, L. V. and Fannie Stinson. Further calculations of x-ray diffusion in an infinite medium—662
Sperduto, A. (see Van Patter, D. M.)—142(L)
Squire, C. F. Results from low temperature studies at Rice Institute—741(T)

Stanford, George S., Henry E. Duckworth, Benjamin G. Hogg, and James S. Geiger. Masses of Pb^{208}, Th^{232}, U^{234}, U^{235}, and U^{238}—1039(L)
—— (see Duckworth, H. E.)—929(L)
Stanford, P. (see Allen, R. G.)—767(A)
Stanley, J. P. (see Gellman, H.)—944(L)
Stanley, R. W. (see Jen, C. K.)—717(A)
Staub, H. H. (see Jeffries, C. D.)—478(L)
Stearns, R. L. (see Duckworth, H. E.)—929(L)
Steigert, F. E. (see Toops, E. C.)—280
Stein, Robert P. Electrical fields in the Crooke's dark space of flow pressure glow discharges by electron beam probes—759(A)
Steinberger, J. (see Isaacs, P. J.)—803; 718(A)
Stephens, William E. (see Toms, M. Elaine)—728(A)
Stephenson, T. E. (see Allen, R. G.)—767(A)
Stern, Edward A. (see Neher, H. V.)—772(A)
Stern, Martin O. Elastic scattering of 190-Mev deuterons by protons—752(A)
Sternglass, E. J., S. C. Frey, and F. H. Grannis. Backscattering of low energy electrons—391(A)
Stiller, Bertram, Maurice M. Shapiro, and Francis W. O'Dell. Special techniques for processing thick nuclear emulsions—712(A)
Stinson, Fannie (see Spencer, L. V.)—662
Stivers, Edward C. (see Yankwich, Peter E.)—753(A)
Stout, Virgil L. Luminescence of BaO—390(A)
Strandberg, M. W. P. (see Eshbach, J. R.)—24; 532
—— (see Johnson, H. R.)—503(L)
Street, K., Jr., A. Ghiorso, and S. G. Thompson. Slow neutron fission of Am^{242}, Am^{242m}, and Am^{243}—135(L)
Streib, J. F. (see Donnelly, F. K.)—767(A)
Stresau, R. H., Jr. (see Savitt, J.)—732(A)
Sun, K.-H., F. A. Pecjak, B. Jennings and A. J. Allen. New medium mass α-emitters—726(A)
——, **F. A. Pecjak, and A. J. Allen.** Tetraneutron—942(L)
Sunyar, A. W., J. W. Mihelich, G. Scharff-Goldhaber, M. Deutsch, and M. Goldhaber. Isomerism of Sr^{86}—734(A)
Surls, Joseph P. (see Browne, Charles I.)—146(L)
Suwa, Shigeki (see Murakawa, K.)—683(L)
Swann, C. P. (see Mandeville, C. E.)—193; 725(A)
Swartz, Clifford. High energy neutron collisions with helium—73
Swim, R. T. (see Schmitt, R. W.)—743(A)

Takagi, Yutaka. Ferroelectricity and antiferroelectricity of a crystal containing rotatable polar molecules—315
Takahashi, Yasushi (see Umezawa, Hiroomi)—505
Tarpinian, M. (see Bowman, F. E.)—769(A)
Tati, T. Erratum: Radiative corrections to the intensities for hydrogen-like atoms—1064(L)
Teener, J. W. (see Seagondollar, L. W.)—713(A)
Ter Haar, D. (see Martin, B.)—714(A)
Terwilliger, Kent M. (see Jones, Lawrence W.)—686(L)
Tessman, Jack R. Anisotropy energy in a cubic lattice of spin dipoles—752(A)
Theuerer, H. C. (see Fuller, C. S.)—678(L)
Thomas, G. E. (see Muehlhause, C. O.)—926(L)
Thomas, L. H. Relativistic dynamics of a system of particles interacting at a distance—868
Thompson, L. C. (see Famularo, K.)—742(A)
Thompson, S. G., J. O. Rasmussen, and A. Ghiorso. Alpha-radioactivity in elements below lead—758(A)
—— (see Street, K., Jr.)—135(L)
Thompson, T. J. Effect of chemical structure on stopping powers for high energy protons—765(A)
Thorndike, A. M., E. C. Fowler, W. B. Fowler, and R. P. Shutt. Scattering of 50-Mev positive pions by helium—929(L)
Thulin, S. and I. Bergström. Second γ-transition ($d_{3/2} \rightarrow s_{1/2}$) in Xe^{129m}—1055(L)
Tobias, Cornelius A. Acceleration of multiply charged nuclei—764(A)
Tollestrup, A. V., R. B. Day, and H. H. Woodbury. New gamma-ray from $C^{13}+p$—760(A)
—— (see Woodbury, H. H.)—760(A)
Toms, M. Elaine and William E. Stephens. Photoprotons from bismuth—728(A)
Toops, E. C., M. B. Sampson, and F. E. Steigert. Investigation of alpha-particle groups from $Al^{27}(d,\alpha)Mg^{25}$—280
Torizuka, Yosiharu (see Okamura, Tosihiko)—693(L)
Torrey, H. C. Nutational resonance—365(L)
Towler, O. A., Jr. Proton-proton scattering at 240 Mev, by a magnetic deflection method—1024
Townes, C. H. (see Hardy, W. A.)—494(L)
Townsend, J. (see Pake, G. E.)—682(L)
Trainor, Lynne E. H. Symmetry effects on nuclear dipole radiation with application to a bound excited state of $_2He^4$—962
Trees, R. E. $L(L+1)$ correction to the Slater formulas for the energy levels—382(L)
Treiman, S. B. Analysis of the nucleonic component using neutron latitude variations—720(A)
—— **and W. Fonger.** Transition effect for neutron production in lead—364(L)
Trischka, J. W., D. T. F. Marple, and A. White. Production of halogen negative ions at the surface of a thoriated tungsten filament—136(L)
Trolan, J. K. (see Dyke, W. P.)—391(A)
Turkevich, John (see Cohen, Victor W.)—379(L)
Twersky, Vic. Multiple scattering theory of the grating and the Wood anomalies—715(A)

Ufford, C. W. (see Green, Louis C.)—65
Uhlenbeck, G. E. and C. S. Wang Chang. Is there a neutral μ-meson?—684(L)
Umezawa, Hiroomi, Yasushi Takahashi, and Susumu Kamefuchi. Mesonic proper-field—505
Umezawa, Minoru (see Mizushima, Masataka)—37

Vallarta, M. S. Energy spectrum of primary cosmic radiation as determined from neutron intensities—748(A)
—— Recent research in cosmic radiation and radio waves emitted by the sun—744(T)
van Deemter, J. J. Bernoulli's theorem for viscous fluids—1049(L)
Vanderberg, R. M. Unusual dispersion aspects of gypsum in the near infrared—755(A)
van der Ziel, A. Space charge suppression of Flicker effect—392(A)
—— (see Dekker, A. J.)—391(A)
Van Dilla, M. A. Liquid-filled ionization chambers—705(A)
Van Dyke, K. S. and W. F. Palmer. Experimental studies on quartz resonators—745(A)
Van Hoomissen, J. E. (see Noyes, J. C.)—727(A)
Van Horn, David D. Solid-state diffusion in cylindrical geometry—709(A)
Van Hove, L. (see Nijboer, B. R. A.)—777
Van Patter, D. M., A. Sperduto, P. M. Endt, W. W. Buechner, and H. A. Enge. Nuclear reaction energies—142(L)
—— (see Mandeville, C. E.)—193
Van Roosbroeck, W. (see Fuller, C. S.)—678(L)
Vineyard, George H. Geometrical optics and the theory of small angle scattering—633
Violet, Charles E., F. C. Gilbert, Robert W. Deutsch and Walter H. Barkas. High energy electron-electron scattering—756(A)
Volman, David H. and Robert K. Brinton. Decomposition of di-*t*-butyl peroxide and kinetics of the gas phase reactions of *t*-butoxy radicals in the presence of ethylenimine—707(A)
Votruba, V. Charge-symmetrical interaction between nucleons and leptons—141(L)

Voyvodic L. and E. Pickup. Multiple scattering of fast particles in photographic emulsions—91

Wahl, Arthur C. and Norman A. Bonner. Genetic relationships and fission yields of members of the mass-115 decay chain—570
Walchli, Harold E., W. E. Leyshon, and F. M. Scheitlin. Nuclear gyromagnetic ratio of V^{50} and measurements on Rb^{85} and Cl^{35}—922(L)
——, **Ralph Livingston, and William J. Martin.** Nuclear magnetic moment of Tc^{99}—479(L)
Waldman, B. (see Noyes, J. C.)—727(A)
Walker, D. (see Crandall, W. E.)—771(A)
Walker, R. L. (see Day, R. B.)—582
Walker, W. D., N. M. Duller, and J. D. Sorrells. Cloud-chamber study of penetrating showers in light and heavy elements—773(A)
Walker, W. H. (see Kinsey, B. B.)—1012
Warner, Douglas (see Plass, Gilbert N.)—708(A)
Warner, R. M. (see Rosenblum, E. S.)—728(A)
Warters, William D. and Edmund A. Milne. Elastic scattering of Li^7+p and $C^{12}+p$—761(A)
Waser, Jürg. Modification functions in the Fourier inversion of diffraction data—745(A)
—— (see Wieland, K.)—385(L)
Watanabe, Satosi. Fundamental reversibility and the phenomenological irreversibility—721(A)
Watkins, G. D. and R. V. Pound. Pure nuclear electric quadrupole resonance of N^{14} in three molecular solids—1062(L)
Watson, Kenneth M. Hypothesis of charge independence for nuclear phenomena—852
Wattenberg, A. (see Hamermesh, M.)—483(L)
Weatherly, Thomas L., Edward R. Manring, and Dudley Williams. Further studies of *l*-type doubling transitions in HCN and DCN—717(A)
Weaver, A. B. and Marcel Schein. Penetrating showers under hydrogen and heavier elements observed in a cloud chamber at sea level—719(A)
Weaver, H. E., Jr. (see Dharmatti, S. S.)—927(L)
Webber, D. S. and A. N. Baker, Jr. Structure of the 3μ-band of $NaBr \cdot 2H_2O$—755(A)
Weber, A. H. (see Antal, John J.)—710(A)
Weil, John W. (see Luckey, David)—1060(L)
Weinstock, B., B. M. Abraham, and D. W. Osborne. Melting pressure of He^3—158(L)
Weissbluth, M. (see Richman, C.)—161
Weissler, G. L. (see Schindler, Mark)—759(A)
Weissman, S. I. (see Pake, G. E.)—682(L)
Wenzel, W. A. and Ward Whaling. Cross section of the $D(d,p)H^3$ reaction—761(A)
—— (see Whaling, Ward)—761(A)
West, W. Photochemistry of condensed systems as illustrated by the optical sensitization of the photographic emulsion—707(T)
Westphal, W. C. (see Haynes, J. R.)—680(L)
Wexler, A. and W. S. Corak. Superconductivity of vanadium—85
Whaling, Ward and W. A. Wenzel. Stopping cross section of ice—761(A)
—— (see Wenzel, W. A.)—761(A)
Wheelon, Albert D. Gravitational deflection of photons with non-vanishing rest mass—383(L)
White, A. (see Trischka, J. W.)—136(L)
White, J. E. (see Shaefer, D. L.)—390(A)
White, R. Stephen, Mark J. Jakobson, and Alvin G. Schulz. Photomesons from deuterium—770(A)
—— (see Jakobson, Mark J.)—772(A)
Whitehead, Marian and Chaim Richman. Angular distribution of π^+-mesons produced in $P-P$ collisions—772(A)
Whitehurst, Harry B. (see Milligan, W. O.)—746(A)
Whitesell, W. J., II, and V. A. Johnson. Magnetoresistive effect in impurity semiconductors—724(A)
Wick, Gian Carlo (see Ashkin, J.)—686(L)
—— (see Chew, Geoffrey)—636
Wieland, K. Absorption spectra of simple radicals in thermal equilibrium—756(T)
—— **and Jürg Waser.** Molecular spectrum of iodine excited in the presence of an inert gas—385(L)
Wilcox, H. A. (see Richman, C.)—161
Wilcox, L. (see Simpson, J. A.)—366(L); 720(A)
Wildhack, W. A., T. A. Perls, and J. W. Hayes. Critical-flow pneumatic hygrometer—731(A)
Wilfong, T. C., Jr., and J. E. Henderson. Čerenkov radiation from positrons—765(A)
Wilkening, M. H. Monitor for natural radioactivity in the atmosphere—712(A)
Willard, H. B., J. K. Bair, J. D. Kington, T. M. Hahn, C. W. Snyder, and F. P. Green. Yield of gamma-rays and neutrons from the proton bombardment of fluorine—849
—— (see Bair, J. K.)—946(L)
—— (see Hahn, T. M.)—934(L)
Williams, Dudley (see Weatherly, Thomas L.)—717(A)
Williams, H. J. and R. M. Bozorth. Effect of stress on the curvature of domain boundaries—713(A)
Wilson, H. A. Magnetic moments of nuclei—747(A)
Wilson, James R. (see Fox, I. D.)—772(A)
Wilson, M. Kent (see Perkins, W. D.)—755(A)
Wilson, Richard. Proton bremsstrahlung at 140 Mev—563
—— (see Clark, Donald L.)—523
Winans, J. G. (see Levin, Franklyn K.)—1064(L)
Winckler, J. R. Absorption experiment to detect the cosmic-ray albedo at high altitudes—1053(L)
—— Application of Čerenkov radiation to the cosmic-ray albedo problem—1054(L)
Winhold, E. J., P. T. Demos, and I. Halpern. Angular distribution of photofission fragments from thorium—728(A)
Winston, H. (see Blake, N. W.)—754(A)
Winter, Rolf G. Search for double beta-decay in palladium—687(L)
Witmer, Enos E. Nuclear masses as integral multiples of a natural unit of mass—748(A)
Wolfenstein, L. and J. Ashkin. Invariance conditions on the scattering amplitudes for spin $\frac{1}{2}$ particles—947
Wolff, Peter A. Nuclear momentum distributions—766(A)
Wolfgang, Richard L. and W. F. Libby. Absolute excitation function of the $Be^9(d,t)$ reaction—437
Wollan, E. O. (see Koehler, W. C.)—490(L)
Woodbury, Eric John and William Alfred Fowler. Cross section for the radiative capture of protons by C^{13} at 129 kev—51
Woodbury, H. H., R. B. Day, and A. V. Tollestrup. Measurement of gamma-rays in the reaction $C^{13}(p,\gamma)N^{14}$—760(A)
—— (see Tollestrup, A. V.)—760(A)
Woodcock, R. F. (see Duckworth, H. E.)—929(L)
Woodruff, Edythe P. (see Kaplon, M. F.)—933(L)
Woodward, W. M. (see Benedict, T. S.)—924(L)
Wouters, L. F. Detection of azimuthal polarization in double $n-p$ scattering at 150 Mev—757(A)

Yafet, Y. Calculation of the *g* factor of metallic sodium—478(L); 762(A)
Yagoda, Herman. Emission of slow positive and negative mesons from nuclear disruptions produced by cosmic radiation—891
—— Heavy metal cosmic-ray primaries—720(A)
Yamagata, Y. (see Kanda, T.)—938(L)
Yang, C. N. Spontaneous magnetization of a two-dimensional Ising model—808

Yankwich, Peter E., Edward C. Stivers, and Robert F. Nystrom. Isotope effects in the decarboxylation of malonic acids—753(A)
Yennie, D. R. Angular momentum in non-local field theory—877
Yevick, George J. Quantum theory for a finite-sized electron. I—911
Ying, Chung Fu and H. E. Farnsworth. Changes in work functions of vacuum distilled gold films—485(L)
Yngve, Victor H. (see Schein, Marcel)—607
Yodh, G. B. (see Fermi, E.)—935(L)
—— (see Martin, R. L.)—486(L)
York, Carl M., Jr. Differential range spectrum of cosmic-ray mesons at sea level—998
Young, F. W., Jr. (see Crawford, J. H., Jr.)—730(A)
Young, J. R. Electrical conductivity and thermoelectric power of (BaSr)O and BaO—388(A)
Yovits, M. C., R. L. Smith, Jr., M. H. Hull, Jr., J. Bengston, and G. Breit. Meson tail effect and treatment of proton-proton scattering data—540
Yuan, L. C. L. (see Poss, H. L.)—703(A)

Zeiger, H. J. and D. I. Bolef. Molecular beam magnetic resonance spectra of $TlCl^{35}$ and $TlCl^{37}$ at zero field—788
—— (see Bolef, D. I.)—799
Zener, C. Interaction between the *d*-shells in the transition metals. IV. Intrinsic antiferromagnetic character of iron—324
Zilsel, P. R. (see Fried, H. M.)—1044(L)
Zimm, Bruno H. Theory of the critical point—702(T)

PHYSICAL REVIEW VOLUME 85, NUMBER 6 MARCH 15, 1952

Analytic Subject Index to Volume 85

References with (A) are to abstracts of papers presented at meetings of the American Physical Society. References with (L) are to Letters to the Editor.

Absorption of radiation
Absorption cross sections for 19.5-Mev quanta, Arthur I. Berman—774(A)
Absorption of γ-rays from Co^{60}, Sakae Shimizu, Tetsuya Hanai, and Sunao Okamoto—290
Absorption of Se in soft x-ray region, M. Parker Givens and Walter P. Siegmund—313
Atmospheric absorption of solar infrared radiation, Romuald Anthony—674(L)
γ-ray absorption coefficients in 5–10 Mev energy range, E. S. Rosenblum, E. F. Shrader, and R. M. Warner—728(A)
Acoustics
Debye-Frenkel theory of ultrasonic absorption, P. A. Hudson and M. Eisner—746(A)
Elastic wave propagation, W. L. Roever—744(A)
Magnetically induced ultrasonic velocity changes in polycrystalline Ni, S. J. Johnson and T. F. Rogers—714(A)
Adsorption
Diamagnetic properties of adsorbed gases, W. O. Milligan and Harry B. Whitehurst—746(A)
Flow in unsaturated helium II film, Earl Long and Lothar Meyer—1030
Phase transitions in adsorbed films, Lothar Meyer and Earl Long—1035
Aerodynamics (see also **Hydrodynamics**)
One-dimensional flow with mass addition, Edward W. Price—769(A)
Alloys (see **Crystalline states**)
Annihilation (see **Pair production and annihilation**)
Antiferroelectric phenomena (see **Ferroelectric and antiferroelectric phenomena**)
Antiferromagnetism (see **Magnetic properties**)
Arcs (see **Discharge of electricity in gasses**)
Astrophysics
Abundance of CO in sun and in earth's atmosphere, Leo Goldberg, Robert R. McMath, Orren C. Mohler, and A. Keith Pierce—481(L)
Identification of CO in solar atmosphere, Leo Goldberg, Robert R. McMath, Orren C. Mohler, and A. Keith Pierce—140 (L)
Atmosphere (see **Meteorology**)
Atomic and molecular beams
Molecular beam electric resonance method study of TlCl, R. O. Carlson, C. A. Lee, and B. P. Fabricand—784
Theory of H_2 and D_2 in magnetic fields, Norman F. Ramsey—60
Atomic mass (see **Isotopes; Mass spectroscopy**)

Biophysics
Proton magnetic resonance absorption and water content of biological materials, T. M. Shaw, R. H. Elsken, and C. H. Kunsman—708(A)
Tracer studies on alligator weed using 2,4-D-C^{14}, Karlem Riess, T. T. Earle, and John Hidalgo—741(A)
Bremsstrahlung (see **Radiation**)
Broadening of spectral lines
Beam system for reduction of Doppler broadening of microwave absorption line, H. R. Johnson and M. W. P. Strandberg—503(L)
Pressure-broadening of absorption lines, Stanley Bloom and Henry Margenau—717(A)
Pressure effects of A and He on resonance lines of Ag, Eugene D. Clayton and Shang-yi Ch'en—68

Chemical reactions
In BaO on W emitters, R. C. Hughes, P. P. Coppola, and H. T. Evans—388(A)
Decomposition of di-*t*-butyl peroxide and kinetics of gas phase reactions of *t*-butoxy radicals in presence of ethylenimine, David H. Volman and Robert K. Brinton—707(A)
Isotope effects in decarboxylation of malonic acids, Peter E. Yankwich, Edward C. Stivers, and Robert F. Nystrom—753(A)
Production of Sr metal in reduction of SrO by CH_4, H. W. Allison and George E. Moore—388(A)
Cold emission (see **Field currents**)
Compton effect (see **Scattering of radiation**)
Conductivity, electrical (see **Electrical conductivity; Discharge of electricity in gases; Semiconductors; Superconductivity**)
Conductivity, thermal (see **Thermal conductivity**)
Constants, physical standards
Calorimetric calibration of a secondary standard for 150–317 Mev bremsstrahlung, P. D. Edwards—725(A)

Calorimetric determination of the roentgen for 400-kv x-rays, J. S. Laughlin, J. W. Beattie, and J. Ovadia—725(A)
Effect of recent mass measurements on the Faraday, H. Sommer, D. N. Craig, J. I. Hoffman, and J. A. Hipple—740(A)
Nuclear masses as integral multiples of a natural unit, Enos E. Witmer—748(A)
Relation between Planck's constant and gravitational constant, B. Liebowitz—722(A)

Cosmic radiation
Absence of secondary maxima in transition curve for electronic showers, R. Maze—697(L)
Absorption curve in stratosphere, Marcel Schein and Victor H. Yngve—607
Absorption experiment to detect cosmic-ray albedo at high altitudes, J. R. Winckler—1053(L)
Air-shower cores, W. E. Hazen—455
Analysis of nucleonic component using neutron latitude variations, S. B. Treiman—720(A)
Angular distribution of decay tracks of V^0-particles, W. B. Fretter and M. M. May—773(A)
Application of Čerenkov radiation to cosmic-ray albedo problem, J. R. Winckler—1054(L)
Differential range spectrum of mesons at sea level, Carl M. York, Jr.—998
Diurnal variations in high energy cosmic-ray intensities, P. H. Barrett and Y. Eisenberg—674(L)
Emulsion cloud-chamber study, M. Kaplon, B. Peters, and D. M. Ritson—900
Energy loss of μ-mesons, Robert Hofstadter and Alvin M. Hudson—773(A)
Energy spectrum of primary radiation, M. F. Kaplon, B. Peters, H. L. Reynolds, and D. M. Ritson—295; M. S. Vallarta—748(A)
Extremely high energy nuclear interactions, M. F. Kaplon and D. M. Ritson—932(L)
Heavy metal cosmic-ray primaries, Herman Yagoda—720(A)
Ionization loss of energy of relativistic μ-mesons in A, J. E. Kupperian, Jr., and E. D. Palmatier—1043(L)
Knock-on secondaries from penetrating particles in C, John R. Green—774(A)
Lateral spread of showers in air and Pb, H. S. Green and H. Messel—679(L)
Latitude effect between geomagnetic latitudes 54° and 88°N, H. V. Neher, Vincent Z. Peterson, and Edward A. Stern—772(A)
Mean free path of high energy nuclear component, Robert R. Brown—773(A)
Mean free path of neutral penetrating shower-producing radiation, H. W. Boehmer and H. S. Bridge—863
Multiplicities of neutrons produced by μ-mesons in Pb, Marshall F. Crouch and Robert D. Sard—120
Neutral V particle decay and negative proton, L. I. Schiff—374(L)
Nuclear interactions of decay products of V^0-particle, Herbert Bridge, Hans Courant, and Bruno Rossi—159(L)
Penetrating showers in Be, C, and Pb at sea level, L. Grodzins, G. Del Castillo, and W. Y. Chang—719(A)
Penetrating showers in H_2O, George W. Rollosson—774(A)
Penetrating showers in light and heavy elements, W. D. Walker, N. M. Duller, and J. D. Sorrells—773(A)
Penetrating showers under hydrogen and heavier elements observed in cloud chamber at sea level, A. B. Weaver and Marcel Schein—719(A)
Primary flux of high energy protons and α-particles, M. F. Kaplon, D. M. Ritson, and Edythe P. Woodruff—933(L)
Production cross section and energy spectrum of neutral mesons, G. Salvini and Y. Kim—921(L)
Protons and mesons at 9000 feet, A. Z. Rosen—773(A)
Slow mesons produced by cosmic radiation, Herman Yagoda—891
Soft radiation at balloon altitudes, C. L. Critchfield, E. P. Ney, and Sophie Oleksa—461
Solar component of primary cosmic radiation, J. A. Simpson, W. Fonger, and L. Wilcox—366(L); 720(A)
Transition effect for neutron production in Pb, S. B. Treiman, and W. Fonger—364(L)
Two cosmic-ray decreases associated with geomagnetic storms and sunspot activity of May and June, 1951, R. L. Chasson—719(A)
Variation of intensity of fast cosmic-ray neutrons with altitude, L. F. Curtiss and P. S. Gill—309
Zenith angle effects for cosmic-ray protons and mesons, C. E. Miller, J. E. Henderson, Gerald Garrison, and Wayne Sandstrom—773(A)

Cross section, measurements, theory (see also **Scattering of electrons, mesons, neutrons, protons, and ions**)
Differential cross section of $H^3(d,p)T^2$ at low energy, Charles F. Cook and J. Richard Smith—741(A)
High energy scattering cross sections using variational methods, David S. Saxon and E. Gerjuoy—704(A)
Inelastic cross sections for 240-Mev protons, Alfred M. Perry, Jr.—497(L)
Neutron transmission cross sections in kev region, Carl T. Hibdon, Alexander Langsdorf, Jr., and Robert E. Holland—595
Nuclear cross sections for high energy neutrons and protons, R. Jastrow and J. E. Roberts—757(A)
Nuclear cross sections for negative pions of energy 109 and 133 Mev, R. L. Martin, H. L. Anderson, and G. Yodh—486(L)
For radiative capture of protons by C^{13} at 129 kev, Eric John Woodbury and William Alfred Fowler—51
Of 6-Mev mesons in H and D, P. J. Isaacs, A. M. Sachs, and J. Steinberger—803
Stopping cross section of ice, Ward Whaling and W. A. Wenzel—761(A)
Theory of neutron scattering by gases, N. K. Pope and G. Feldman—703(A)
Total cross sections of C and H for 14-Mev neutrons, H. L. Poss, E. O. Salant, and L. C. L. Yuan—703(A)
Total cross sections of heavy nuclei for fast neutrons, D. W. Miller, R. E. Fields, and C. K. Bockelman—704(A)
Total cross sections of negative pions in H, H. L. Anderson, E. Fermi, E. A. Long, R. Martin, and D. E. Nagle—934(L)
Total cross sections of positive pions in H, H. L. Anderson, E. Fermi, E. A. Long, and D. E. Nagle—936(L)
Variational calculation of scattering cross sections, E. Gerjuoy and David S. Saxon—939(L)

Crystal counters (see **Methods and instruments**)

Crystal structure
Antiferromagnetic structure of MnO_2 by neutron diffraction, R. A. Erickson—745(A)
Ferromagnetic domain structure of single crystals and bicrystals of Ni, Ursula M. Martius, K. V. Gow, and Bruce Chalmers—713(A)
Growth of single crystals of Ta and their surface structure, M. H. Nichols—769(A)

Crystalline state
Adiabatic study of 128° transition in $BaTiO_3$, Shepard Roberts—925(L)
Adiabatic thermal changes in $BaTiO_3$ ceramic and $SrTiO_3$ at low temperatures, R. W. Schmitt and R. T. Swim—743(A)
Anisotropy energy in cubic lattice of spin dipoles, Jack R. Tessman—952(A)
Collective *vs* individual particle aspects of electron interactions, David Pines and David Bohm—338

Crystalline state (continued)
Color centers and thermoluminescence in alkali halides, J. Sharma—692(L)
Conductivity of cold-worked metals, D. L. Dexter—936(L)
Critical domain size in ferroelectrics, W. Känzig and M. Peter—940(L)
Dielectric constant and permeability of various ferrites in microwave region, Tosihiko Okamura, Tadao Fujimura, and Muneyuki Date—1041(L)
Dipole lattice in spherical model, Melvin Lax—744(A)
Effect of plastic deformation on anelastic properties of α-brass, John Kauffman and David Lazarus—710(A)
Effect of pressure on position of F band in alkali halides, E. Burstein, J. J. Oberly, and J. W. Davisson—729(A)
Effect of stress on curvature of domain boundaries, H. J. Williams and R. M. Bozorth—713(A)
Elastic and plastic properties of very small metal specimens, Conyers Herring and J. K. Galt—1060(L)
Electrical properties of rutile single crystals, L. F. Connell and R. L. Seale—745(A)
Electronic specific heat in Cr and Mg, S. A. Friedberg, I. Estermann, and J. E. Goldman—375(L)
Electronic states in crystals under large perturbations, Paula Feuer and Hubert M. James—723(A)
Electronic states of molecular crystals, N. W. Blake, D. S. McClure, and H. Winston—754(A)
Energy absorption during twin formation in Zn single crystals, E. I. Salkovitz—1046(L)
Energy levels in KCl, L. G. Parratt and E. L. Jossem—729(A)
Energy of Bloch wall on band picture, Conyers Herring—1003
Experimental evidence for vacancy mechanism for diffusion in metals and alloys, Foster C. Nix and Frank E. Jaumot, Jr.—709(A)
Experimentally derived configurational coordinate curves, Clifford C. Klick—154(L); 723(A)
Ferromagnetic domain structure of single crystals and bicrystals of Ni, Ursula M. Martius, K. V. Gow, and Bruce Chalmers—713(A)
Ferromagnetic resonance in single crystals of Co-Zn ferrite, Tosihiko Okamura and Yûzo Kojima—690(L)
Growth of single crystals of Ta and their surface structure, M. H. Nichols—769(A)
Heat capacity and lattice defect of AgCl, Koichi Kobayashi—150(L)
High temperature graphitization, W. P. Eatherly—768(A)
Interactions of remote impurity centers in phosphors, H. W. Leverenz and D. O. North—930(L)
Intrinsic magnetization in alloys, W. J. Carr—590
Light emission from SiC, R. W. Sillars—136(L)
Line width of paramagnetic resonance and exchange interaction in salts containing Mn^{++} and Fe^{+++}, H. Kumagai, K. Ono, and I. Hayashi—925(L)
Magnetic susceptibility of polycrystalline anisotropic materials, and observations on artificial graphites, J. D. McClelland and J. J. Donoghue—768(A)
Magnetically induced ultrasonic velocity changes in polycrystalline Ni, S. J. Johnson and T. F. Rogers—714(A)
Modification functions in Fourier inversion of diffraction data, Jürg Waser—745(A)
Optical properties of sodium tungsten bronze, G. C. Danielson and E. Chivers—711(A)
Order-disorder transitions in triangular Ising lattice, L. D. Fosdick and H. M. James—714(A)
Origin of high permeability in permalloy, Sōshin Chikazumi—918(L)
Phase transition of $ND_4D_2PO_4$, B. T. Matthias—141(L)
Production of large tensile stresses by dislocations, J. S. Koehler—480(L)
Quantum theory of internal field in idealized crystal, D. L. Dexter and W. R. Heller—723(A)
Quartz resonator studies, K. S. Van Dyke and W. F. Palmer—745(A)
Resistance variation of MnSe at low temperatures, John Scales and C. W. Heaps—743(A)
Saturation magnetic moment of alloys on collective electron theory, J. E. Goldman—375(L)
Semiconductivity and diamagnetism of polycrystalline graphite and condensed ring systems, S. Mrozowski—609
Solubility and diffusion coefficient of C in Ni, J. J. Lander, H. E. Kern, and A. L. Beach—389(A)
Spectrum of Nd^{+++} in crystals, Robert A. Satten—755(A)
Splitting of bands in solids, E. Katz—495(L)
Statistical theory of properties of solid solutions, R. Smoluchowski—710(A)
Stopping power of metal for charged particles, David Pines—931(L)
Strain induced curvature of Bloch walls in Si iron, L. J. Dijkstra and U. Martius—714(A)
Temperature dependence of electrical conductivity, W. V. Houston—743(A)
Temperature dependence of internal friction at 44 kc, W. B. Nowak—710(A)
Temperature dependence of resistivity of deuteron irradiated and annealed Mo, Burton Randolph—710(A)
Theory of cooperative phenomena, Gérard Fournet—692(L)
Time rate of transformation of α-monoclinic Se into hexagonal as function of temperature, John Murphy and Arthur E. Lockenvitz—745(A)
Time rate of transformation of amorphous Se into another form as function of temperature, Arthur E. Lockenvitz and Kenneth H. Ribe—746(A)
X-ray study of lattice imperfections, P. H. Miller, Jr.—709(A)

Diamagnetism (see **Magnetic properties**)
Dielectrics and dielectric properties
Adiabatic thermal changes in $BaTiO_3$ ceramic at low temperatures, Roland W. Schmitt—1; Roland W. Schmitt and R. T. Swim—743(A)
Effect of certain group IV oxides on permittivity and loss tangent of $BaTiO_3$, Graham W. Marks and Lester A. Monson—723(A)
Of ferrites in microwave region, Tosihiko Okamura, Tadao Fujimura, and Muneyuki Date—1041(L)
Isotope effect in RbD_2PO_4, B. T. Matthias—(723A)
Photocontrolled low frequency dielectric dispersion, J. Ross Macdonald—381(L)
Properties of powdered $BaTiO_3$, V. E. Derr and M. D. Earle—384(L)
Theory of dielectric dispersion, Marius Cohn—708(A)
Diffraction of electrons (see **Electron diffraction**)
Diffraction of neutrons (see **Neutron diffraction**)
Diffraction of radiation
Modification functions in Fourier inversion of diffraction data, Jürg Waser—745(A)
Use of successive diffractions to double or quadruple resolving power of a grating, F. A. Jenkins and L. W. Alvarez—763(A)
Diffusion (see also **Thermal diffusion**)
Anionic self-diffusion and electrical conduction in NaBr, H. W. Schamp, Jr.—729(A)
Biased random walks in classical, statistical, and quantum mechanics, Gilbert W. King—708(A)
Of C in Ni, J. J. Lander, H. E. Kern, and A. L. Beach—389(A)
Cathodic sputtering as sectioning method in diffusion studies, Thomas F. Fisher—702(A)
Effect of neutron irradiation on metallic diffusion, T. H. Blewitt and R. R. Coltman—384(L)

Evidence for vacancy mechanism for diffusion in metals and alloys, Foster C. Nix and Frank E. Jaumot, Jr.—709(A)
In oxide cathode, E. S. Rittner—389(A)
Solid-state diffusion in cylindrical geometry, David D. Van Horn—709(A)
Of thermal neutrons, George Jaffé—747(A)
X-ray diffusion in infinite medium, L. V. Spencer and Fannie Stinson—662

Discharge of electricity in gases
Arcing at electrical contacts on closure. III. Development of arc, L. H. Germer and J. L. Smith—392(A)
Drift velocity of electrons in gas mixtures, F. F. Rieke and D. D. Errett—706(A); in pure gases, D. D. Errett and F. F. Rieke—706(A)
Electric current between flashes of intermittent glow discharge in H_2, Herman Ritow—706(A)
Electrical fields in Crooke's dark space of low pressure glow discharges by electron beam probes, Robert P. Stein—759(A)
Electron drift velocities in a grid ionization chamber, W. N. English—759(A)
Height and diurnal variation of night airglow, Edward V. Ashburn—767(A)
Influence of irradiation on glow discharge in pure rare gases, K. W. Meissner and W. F. Miller—706(A)
Negative ion formation in O_2, Ronald Geballe and Melvin A. Harrison—372(L)
Positive ion energies in point-to-plane corona, Mark Schindler and G. L. Weissler—759(A)
Positive wire corona mechanism in H_2 and A, Eugene J. Lauer—759(A)
Pressure-dependent recombination coefficients, Leonard B. Loeb and Wulf B. Kunkel—493(L)
Spectroscopic investigations of pulsed gas discharges, W. R. Atkinson, R. G. Fowler, L. W. Marks, and G. W. Charles—706(A)
Striations in hydrogen glow discharge, W. A. Gambling—677(L)

Disintegration and excitation of nucleus (see also **Radioactivity; Photodisintegration**)
Al^{24}, delayed heavy-particle emitter, Ann C. Birge—753(A)
$Al^{27}(d,\alpha)Mg^{25}$ α-particle groups, E. C. Toops, M. B. Sampson, and F. E. Steigert—280
Angular correlation between inelastically scattered protons and γ-rays from 1.4-Mev level in Mg^{24}, H. E. Gove and A. Hedgran—727(A)
Angular correlation studies of $(d;\ p,\gamma)$ processes of target nuclei Li^6, B^{10}, and O^{16}, G. C. Phillips, N. P. Heydenburg, and D. B. Cowie—742(A)
Angular distribution of π^+-mesons produced in $p-p$ collisions, Marian Whitehead and Chaim Richman—772(A)
Be^7 and B^{10} low-lying levels, Robert B. Day and Torben Huus—761(A)
$Be^9(d,t)$ absolute excitation function, Richard L. Wolfgang and W. F. Libby—437
$Be^9(p,\alpha)Li^6$, R. B. Day and R. L. Walker—582; Richard L. Wolfgang and W. F. Libby—437
$B^{11}(P,\gamma)C^{12}$, Torben Huus and Robert B. Day—761(A)
Capture γ-rays from protons on N^{14}, C. H. Johnson, C. D. Moak, and G. P. Robinson—727(A); C. H. Johnson, G. P. Robinson, and C. D. Moak—931(L)
C^{12} energy levels from $Be^9(\alpha,n)C^{12}$, W. H. Guier, H. W. Bertini, and J. H. Roberts—426
$C^{13}(p,\gamma)N^{14}$ γ-rays, H. H. Woodbury, R. B. Day, and A. V. Tollestrup—760(A)
Charged π-meson production from deuterium, S. Passman, M. M. Block, and W. W. Havens, Jr.—370(L)
$Cl^{37}(p,n)A^{37}$; excited states in A^{38}, W. A. Schoenfeld, R. W. Duborg, W. M. Preston, and C. Goodman—873
$D(d,p)H^3$ cross section, W. A. Wenzel and Ward Whaling—761(A)
Disintegration of deuteron by π^+ mesons and spin of π^+ meson, Donald L. Clark, Arthur Roberts, and Richard Wilson—523
Disintegration of Li by deuterons, L. M. Baggett and S. J. Bame, Jr.—434
Energy levels in Al^{27}, E. M. Reilley, A. J. Allen, J. S. Arthur, R. S. Bender, R. L. Ely, and A. J. Hausman—704(A)
Energy levels of S^{33}, G. R. Grove—160(A)
Extremely high energy nuclear interactions, M. F. Kaplon and D. M. Ritson—932(L)
Fast protons from capture of π^- mesons in photographic emulsions, Frank L. Adelman—249
Fast protons from 270-Mev $\pi-d$ scattering, W. Hess, J. B. Cladis, and J. Hadley—757(A)
γ-ray and neutron yield from proton bombardment of F, H. B. Willard, J. K. Bair, J. D. Kington, T. M. Hahn, C. W. Snyder, and F. P. Green—849
High energy neutron collisions with He, Clifford Swartz—73
$H^3(d,p)T^3$, differential cross section at low energy, Charles F. Cook, and J. Richard Smith—741(A)
Inelastic and total scattering of 190-Mev deuterons by protons, Arnold L. Bloom—752(A)
Inelastic cross sections for 240-Mev protons, Alfred M. Perry, Jr.—497(L)
Inelastic scattering of protons from light nuclei, N. P. Heydenburg, G. C. Phillips, and Dean B. Cowie—742(A)
Inelastic scattering of protons from Ni, Ralph Ely, Jr., A. J. Allen, J. S. Arthur, R. S. Bender, H. J. Hausman, and E. M. Reilley—704(A)
Influence of well shape on pick-up process in D, Ira L. Karp—754(A)
Interaction of charged π-mesons with deuteron, W. B. Cheston—718(A); 952
Interactions of high energy nucleons with nuclei, G. Bernardini, E. T. Booth, and S. J. Lindenbaum—826
Li disintegration by deuteron bombardment, L. M. Baggett and S. J. Bame, Jr.—741(A)
$Li^6(t,p)Li^8$, C. D. Moak, W. M. Good, and W. E. Kunz—928(L)
μ-mesons stopped in photographic emulsions, W. F. Fry—676(L)
Neutral mesons from proton bombardment of light nuclei, R. W. Hales, R. H. Hildebrand, N. Knable, and B. J. Moyer—373(L)
Neutron spectrum from $B^{10}(\alpha,n)N^{13}$, N^{14}, Marguerite Rogers, F. K. Odencrantz, and G. J. Plain—756(A)
Neutrons and γ-rays from proton bombardment of Be, T. M. Hahn, C. W. Snyder, H. B. Willard, J. K. Bair, E. D. Klema, J. D. Kington, and F. P. Green—934(L)
Neutrons from deuteron bombardment of F^{19}, J. W. Butler—743(A)
Neutrons from disintegration of separated Si isotopes by deuterons, C. E. Mandeville, C. P. Swann, S. D. Chatterjee, and D. M. Van Patter—193; C. E. Mandeville, C. P. Swann, and S. D. Chatterjee—725(A)
New γ-ray from $C^{13}+p$, A. V. Tollestrup, R. B. Day, and H. H. Woodbury—760(A)
Nuclear cross sections for high energy neutrons and protons, R. Jastrow and J. E. Roberts—757(A)
Nuclear disintegration by positron-K electron annihilation, R. D. Present and S. C. Chen—447
Nuclear reaction energies, D. M. Van Patter, A. Sperduto, P. M. Endt, W. W. Buechner, and H. A. Enge—142(L)
1435-kev resonance of C bombarded by deuterons, K. Famularo, L. C. Thompson, and T. W. Bonner—742(A)
π-meson interactions in C, H. Byfield, J. Kessler, and L. Lederman—718(A)
π-meson production by protons on nuclei, Ernest M. Henley—204

Disintegration and excitation of nucleus (continued)
Polarization of 6.13-Mev γ-rays emitted in reaction $F^{19}(p,\alpha)O^{16*}(\gamma)O^{16}$, A. P. French and J. O. Newton—1041(L)
Production cross sections for π^+ and π^- mesons by 340-Mev protons on C and Pb at 90° to the beam, C. Richman, M. Weissbluth, and H. A. Wilcox—161
Production of polarized protons and inversion of energy levels of the $P_{1/2}$ doublet in Li^8, M. Heusinkveld and George Freier—80
Proton bombardment of Li, J. K. Bair, H. B. Willard, C. W. Snyder, T. M. Hahn, J. D. Kington, and F. P. Green—946(L)
$p-\gamma$ angular correlation in $Li^8(d,p)Li^{9*}$ at low energy, W. H. Burke and J. R. Risser—741(A)
(p,n) reaction on separated Cr isotopes, J. A. Lovington, J. J. G. McCue, and W. M. Preston—585
Protons and deuterons from Li^6+t, T. P. Pepper, K. W. Allen, E. Almqvist, and J. T. Dewan—155(L)
Radiative capture of protons by C^{13}, John D. Seagrave—197
Radiative capture of protons by C^{13} at 129 kev, Eric John Woodbury and William Alfred Fowler—51
Scattering of 9.6-Mev protons by C, Al, and Mg, C. J. Baker, J. N. Dodd, and D. H. Simmons—1051(L)
Slow mesons produced by cosmic radiation, Herman Yagoda—891
Stripping in $B^{10}(d,n)C^{11}$ at low deuteron energies, J. R. Risser and W. H. Burke—742(A)
Tetraneutron, K.-H. Sun, F. A. Pecjak, and A. J. Allen—942(L)
Total cross sections of heavy nuclei for fast neutrons, D. W. Miller, R. E. Fields, and C. K. Bockelman—704(A)
Dissociation
Of H_2 by vibrational excitation, E. Bauer—277
Doppler effect
Beam system for reduction of Doppler broadening of microwave absorption line, H. R. Johnson and M. W. P. Strandberg—503(L)

Elasticity
Of Cu, J. A. Brinkman—768(A)
Production of large tensile stresses by dislocations, J. S. Koehler—480(L)
Thermal coefficients applying to deflection of springs, Ralph W. Mann—740(A)
Of very small metal specimens, Conyers Herring and J. K. Galt—1060(L)
Young's modulus and internal friction in metal specimens, F. E. Bowman and M. Tarpinian—769(A)
Electrical circuits (see **Methods and instruments**)
Electrical conductivity and resistance (see also **Semiconductors; Superconductivity**)
Of (BaSr)O and BaO, J. R. Young—388(A)
Of cold-worked metals, D. L. Dexter—936(L)
Corbino effect and change of resistance in magnetic field, erratum, K. M. Koch and L. Halpern—1064(L)
Of oxide-coated cathodes by retarding potential method, I. L. Sparks—705(A)
$P-N$ transition of oxide-coated cathode, erratum, Y. Ishikawa, T. Sato, K. Okumura, and T. Sasaki—1065(L)
Rectification effects in diamond, G. W. Curl and G. C. Danielson—729(A)
Resistance variation of MnSe at low temperatures, John Scales and C. W. Heaps—743(A)
Resistivity of evaporated Te films, Takemaro Sakurai and Seiji Munesue—921(L)
In NaBr, H. W. Schamp, Jr.—729(A)
Temperature dependence, W. V. Houston—743(A)
Temperature dependence of resistivity of deuteron irradiated and annealed Mo, Burton Randolph—710(A)

Electrodynamics (see **Electromagnetic theory**)
Electrolysis
Polarization in electrolyte solutions, John A. Rider and George Jaffé—746(A)
Electromagnetic theory (see also **Quantum electrodynamics**)
Condition for radiation from solar plasma, J. Feinstein—145(L)
Differential analyzer methods for cyclotron orbit problems, Bayard Rankin, John Killeen, and Walter H. Barkas—754(A)
Distribution of potential in electrically excited nonhomogeneous medium, Lachlan Gilchrist—731(A)
Do Coulomb fields signal faster than light?, D. I. Caplan and F. J. Belinfante—721(A)
Electrodynamics as basis for special relativity, Arthur E. Ruark—770(A)
Electromagnetic field measurements in plane of circular aperture, Robert E. Houston and Robert H. Noble—732(A)
Ion trajectories in omegatron, Clifford E. Berry—765(A)
Landé electron, equation of motion, Paul Molmud—139(L)
Propagation through electronic space charge in magnetic field, James R. Hooper—705(A)
Electron diffraction
Changes in work functions of vacuum distilled Au films, Chung Fu Ying and H. E. Farnsworth—485(L)
Electron microscope and diffraction study of aging of evaporated metal films, E. J. Scheibner—709(A)
Study of evaporated films of BaO using electron diffraction, Paul Russell—705(A)
From thin films of Ag on (100) face of Ag single crystal, Edward N. Clarke and H. E. Farnsworth—484(L)
Electron optics
Electron interferometer, L. Marton—1057(L)
Electronic tubes
Effect of thermal velocity distribution upon behavior of diodes at microwave frequencies, P. Parzen—704(A)
Relative spectral sensitivity calibration of electron multiplier phototubes in 2500A–3500A region, E. H. Gilmore and R. H. Knipe—764(A)
Space charge suppression of Flicker effect, A. van der Ziel—392(A)
Electrons (see also **Positrons; E/m**)
Collective *vs* individual particle aspects of electron interactions, David Pines and David Bohm—338
Effect of intrinsic moment of electron on spectroscopic isotope shift, G. Breit and W. W. Clendenin—689(L)
Relative transmission through Geiger-Müller counter windows, Chia-hua Chang and C. Sharp Cook—724(A)
Electrons in metals
Collective *vs* individual particle aspects of electron interactions, David Pines and David Bohm—338
Conductivity of cold-worked metals, D. L. Dexter—936(L)
Fermi energy of metallic Li, Richard A. Silverman—227
Motion of electron in perturbed periodic potential, E. N. Adams, II—41
Electrons, scattering of
Absolute backscattering coefficients for positrons and electrons, Howard H. Seliger—724(A)
Backscattering of low energy electrons, E. J. Sternglass, S. C. Frey, and F. H. Grannis—391(A)
High energy electron-electron scattering, Walter H. Barkas, Robert W. Deutsch, F. C. Gilbert, and Charles E. Violet—756(A)
Multiple scattering of fast charged particles in gas. II. β^- and β^+, Gerhart Groetzinger, Watts Humphrey, Jr., and Fred L. Ribe—78
Nuclear scattering of 1-Mev electrons and positrons, Harry J. Lipkin—517
Radiative corrections to distribution of nuclear recoils from electron scattering, L. I. Schiff—754(A)

Electrons, secondary
Angular distribution of secondary electrons from Ni, J. L. H. Jonker—390(A)
Decay time of emission, R. R. Law—(391A)
Ejection of electrons from Mo by He ions, H. D. Hagstrum —392(A)
Emission under high energy electron bombardment, B. L. Miller and W. C. Porter—391(A)
Secondary electron emission from Ge, J. B. Johnson and K. G. McKay—390(A)
Secondary emission from composite surfaces, Harold Jacobs, Jack Martin, and Frank Brand—441
Wave-mechanical foundation of Baroody's theory of secondary emission, A. J. Dekker and A. van der Ziel—391(A)
Electrons, thermionic (see **Thermionic emission**)
Electrostatics
Bipolar expansion of Coulombic potentials, addenda, Robert J. Buehler and Joseph O. Hirschfelder—149(L)
Energy loss of particles (see **Range and energy loss of particles**)
Energy states of atoms (see **Spectra, atomic**)
Energy states of molecules (see **Molecular structure and constants; Spectra, molecular**)
Energy states of nucleus (see **Disintegration and excitation of nucleus; Nuclear spectra; Nuclear structure**)
Equations of state
Sublimation threshold, B. M. Cwilong and M. H. Edwards —380(L)
Errata
Absorption spectrum of GaCl, Franklyn K. Levin and J. G. Winans—1064(L)
Computation of photonuclear resonance curves from relative activity curves monitored by induced radioactivity, R. Sagane—1065(L)
Corbino effect and change of resistance in magnetic field, K. M. Koch and L. Halpern—1064(L)
Mass measurements with magnetic time-of-flight spectrometer, E. E. Hays, P. I. Richards, and S. A. Goudsmit—1065(L)
Phenomenological derivation of first- and second-order magnetostriction and morphic effects for Ni crystal, W. P. Mason—1065(L)
$P-N$ transition of oxide-coated cathode, Y. Ishikawa, T. Sato, K. Okumura, and T. Sasaki—1065(L)
Radiative corrections to the intensities for hydrogen-like atoms, T. Tati—1064(L)
Relativistic corrections to Lamb shift, Michel Baranger—1064(L)
Evaporation
Sublimation threshold, B. M. Cwilong and M. H. Edwards —380(L)
Use of radioactive isotopes in study of evaporation from thermionic cathodes, W. F. Leverton and W. G. Shepherd —389(A)
Excitation of atoms and molecules
Emission spectra of nitrogen bombarded by high energy protons, R. J. Shalek, T. W. Bonner, and L. M. Branscomb—739(A)
Excitation and de-excitation of vibrational motion of hydrogen molecules by slow hydrogen atoms, E. Bauer —707(A)
Excitation of nuclei (see **Disintegration and excitation of nucleus; Nuclear spectra; Nuclear structure**)
Explosion phenomena (see also **Shock waves**)
Deformation and fracturing of thick-walled steel cylinders under explosive attack, John Pearson and John S. Rinehart—768(A)
Tensile fractures generated in metals by impulsive compressional loading, John S. Rinehart and John Pearson —768(A)
Time-resolved spectroscopy of the incandescence associated with ultraspeed pellets, Earle B. Mayfield—769(A)
Transient waves through steel produced by impulsive loading, William A. Allen and Clyde L. McCrary—769(A)
Velocities of ionized air shocks near detonating explosives, J. Savitt and R. H. Stresau, Jr.—732(A)

Ferroelectric and antiferroelectric phenomena
Adiabatic study of 128°C transition in $BaTiO_3$, Shepard Roberts—925(L)
Adiabatic thermal changes in $BaTiO_3$ ceramic and $SrTiO_3$ at low temperatures, R. W. Schmitt and R. T. Swim—743(A)
Critical domain size in ferroelectrics, W. Känzig and M. Peter—940(L)
Ferroelectricity and antiferroelectricity of crystal containing rotatable polar molecules, Yutaka Takagi—315
Isotope effect in RbD_2PO_4, B. T. Matthias—723(A)
Properties of powdered $BaTiO_3$, V. E. Derr and M. D. Earle—384(L)
Structural changes in ferroelectric transition of KH_2PO_4, B. C. Frazer and R. Pepinsky—479(L)
Ferromagnetism (see **Magnetic properties**)
Field currents
Cold emission of electrons in spark gaps, F. Llewellng Jones—392(A)
Comparison between theory and experiment includiny pulsed emission at large densities, W. P. Dyke and J. K. Trolan—391(A)
Observations with field emission microscope, E. W. Müller —392(A)
Use in study of absorption of Ba on W, J. A. Becker—391(A)
Field theory (see also **Quantum electrodynamics**)
Angular momentum in nonlocal field theory, D. R. Yennie —877
Anomalous magnetic moments of nucleons, Fernando E Prieto C.—747(A)
Antiproton annihilation, Israel Reff—379(L)
Charge-symmetrical interaction between nucleons and leptons, V. Votruba—141(L)
Classical meson fields, I. D. Fox and James R. Wilson—772(A)
Classical meson theory and action at a distance, Peter Havas—720(A)
Classical quantum electrodynamics of interacting fields, M. Dresden and H. Dean Brown—748(A)
Convergent S matrix formalism with correspondence to ordinary quantum mechanics, P. Kristensen and C. Møller—928(L)
Covariant theory of damping, J. C. Pirenne—721(A)
Electromagnetic interference effects in charged meson-proton scattering, M. F. Kaplon—1059(L)
Electromagnetic properties of spin-one particles, Daniel Leenov—841
Force between particles in nonlinear field theory, Nathan Rosen and Herbert B. Rosenstock—257
Gauge-independent quantized Bopp theory, Frederik J. Belinfante—722(A)
Graphs for kernel of Bethe-Salpeter equation, C. A. Hurst —920(L)
Interaction of charged π-mesons with deuteron, W. B. Cheston—718(A); 952
Mesonic proper-field, Hiroomi Umezawa, Yasushi Takahashi, and Susumu Kamefuchi—505
Nonlinear pseudoscalar meson theory, E. M. Henley—772(A)
Nonlinearities due to vacuum polarization in meson-nucleon interactions, B. J. Malenka—686(L)
Positional correlations in interacting fields, H. Dean Brown and M. Dresden—748(A)

Field theory (continued)
Prohibition of self-interactions in integro-causal quantum field-theory, Frederik J. Belinfante—468
Scattering of strongly coupled pseudovector mesons, Melvin Eisener—748(A)
Self-energies of nucleons and mass spectra of heavy particles, H. Enatsu—483(L)
Test for charge-symmetry hypothesis, Richard L. Garwin—1045(L)
Thermodynamics of fields, A. E. Scheidegger and C. D. McKay—721(A)
Films, properties of
Changes in work functions of vacuum distilled Au films, Chung Fu Ying and H. E. Farnsworth—485(L)
Electron microscope and diffraction study of aging of evaporated metal films, E. J. Scheibner—709(A)
Evaporated Bi film thicknesses by tracer method, John J. Antal and A. H. Weber—710(A)
Flow in unsaturated He II film, Earl Long and Lothar Meyer—1030
Phase transitions in adsorbed films, Lothar Meyer and Earl Long—1035
Photoelectric work functions and low speed electron diffraction from thin films of Ag on (100) face of Ag single crystal, Edward N. Clarke and H. E. Farnsworth—484(L)
Resistivity of evaporated Te films, Takemaro Sakurai and Seiji Munesue—921(L)
Structure and stability of thin evaporated metallic films, Marsden S. Blois, Jr.—764(A)
Study of evaporated films of BaO using electron diffraction, Paul Russell—705(A)
Fine structure (see **Spectra, etc.; Hyperfine structure**)
Fission of nucleus (see also **Disintegration and excitation of nucleus**)
Of Am^{242}, Am^{242m}, and Am^{243} by slow neutrons, K. Street, Jr., A. Ghiorso, and S. G. Thompson—135(L)
Angular distribution of photofission fragments from Th, E. J. Winhold, P. T. Demos, and I. Halpern—728(A)
Angular distribution of prompt neutrons in fission of Pu^{239}, J. S. Fraser—726(A)
Fission neutron spectrum of U^{235}, Norris Nereson—600
Genetic relationships and fission yields of members of mass-115 decay chain, Arthur C. Wahl and Norman A. Bonner—570
Mechanism, Glenn T. Seaborg—157(L); 757(A)
Photofission of U, Roger E. Anderson and Robert B. Duffield—728(A)
Fluctuation phenomena
Range straggle of μ^+ mesons, F. M. Smith, W. Birnbaum, and W. H. Barkas—771(A)
Range straggling of nonrelativistic charged particle, H. W. Lewis—20
Space charge suppression of Flicker effect, A. van der Ziel—392(A)
Fluid dynamics (see also **Hydrodynamics; Aerodynamics**)
Bernoulli's theorem for viscous fluids, J. J. van Deemter—1049(L)
Successive approximations in theory for critical stability of fluids, H. L. Morrison—770(A)
Variational approach to theory for critical stability of fluids, F. T. Rogers, Jr.—770(A)
Fluorescence (see also **Luminescence**)
High energy induced fluorescence in organic liquid solutions, Milton Furst and Hartmut Kallmann—816
Of naphthalene vapor, O. Schnepp and D. S. McClure—755(A)
Friction
Temperature dependence of internal friction at 44 kc, W. B. Nowak—710(A)
Galvanomagnetic effects (see **Thermomagnetic effects**)
Gamma-rays (see also **Disintegration and excitation of nucleus; Nuclear spectra; Radiation; Radioactivity**)
Absorption of γ-rays from Co^{60}, Sakae Shimizu, Tetsuya Hanai, and Sunao Okamoto—290
Build-up factors for transmission of Co^{60} γ-rays through concrete and Pb, W. R. Dixon—498(L)
Circularly polarized γ-rays, Otto Halpern—747(A)
"Effective" atomic numbers of materials for various γ-ray interactions, G. J. Hine—725(A)
γ-ray absorption coefficients in 5–10 Mev energy range, E. S. Rosenblum, E. F. Shrader, and R. M. Warner—728(A)
Linearity of scintillation γ-ray spectrometer, V. O. Eriksen and G. Jenssen—150(L)
Measurement of uniformity of materials by γ-ray transmission, John N. Harris and Arthur I. Berman—765(A)
Multiple Compton scattering of low energy γ-radiation, R. C. O'Rourke—881
Multiple γ-ray scattering in Pb, J. O. Elliot, R. T. Farrar, R. D. Myers, and C. F. Ravilious—1048(L)
Polarization of scattered quanta, J. I. Hoover, W. R. Faust, and C. F. Dohne—58
Velocity of 170-Mev γ-rays, David Luckey and John W. Weil—1060(L)
Gases (see also **Kinetic theory**)
Diamagnetic properties of adsorbed gases, W. O. Milligan and Harry B. Whitehurst—746(A)
Theory of condensation of gases, R. J. Riddell, Jr.—760(A)
Van der Waals forces in magnetic fields, Henry Margenau and D. E. Harrison—707(A)
Geophysics
Height and diurnal variation of night airglow, Edward V. Ashburn—767(A)
Propagation of Rayleigh waves on surface of viscoelastic solid, C. W. Horton—744(A)
Wave propagation ducts in geophysics, Lynn G. Howell—744(A)
Gravitation
Gravitational deflection of photons with nonvanishing rest mass, Albert D. Wheelon—383(L)
Relation between Planck's constant and gravitational constant, B. Liebowitz—(722A)

Hall effect
Comparison of adiabatic and isothermal Hall effects, V. A. Johnson and F. L. Shipley—724(A)
Heat conduction (see **Thermal conductivity**)
Helium, liquid
Critical velocity of superflow in liquid He II, H. M. Fried and P. R. Zilsel—1044(L)
Flow in unsaturated He II film, Earl Long and Lothar Meyer—1030
Melting pressure curve of He^3, D. W. Osborne, B. M. Abraham, and B. Weinstock—715(A); B. Weinstock, B. M. Abraham, and D. W. Osborne—158(L)
Thermal Rayleigh disk measurements in liquid He II, John R. Pellam and William B. Hanson—216
Hyperfine structure (see also **Nuclear moments and spin**)
Hfs and isotope shift in spectrum of Te, John S. Ross and Kiyoshi Murakawa—559
Hfs anomaly of Rb isotopes, S. A. Ochs and P. Kusch—145(L)
Hfs in paramagnetic resonance of $(SO_3)_2NO^{--}$, G. E. Pake, J. Townsend, and S. I. Weissman—682(L)
Hfs in spectrum of Er, Kiyoshi Murakawa and Shigeki Suwa—683(L)
Nuclear moment and hfs anomaly of K^{40}, Joseph T. Eisinger and Benjamin Bederson—716(A)
Zeeman effect and hyperfine splitting of positronium, Martin Deutsch and Sanborn C. Brown—1047(L)

Instruments (see **Methods and instruments**)
Internal conversion (see **Nuclear spectra**)
Ionization
Calorimetric determination of the roentgen for 400-kv x-rays, J. S. Laughlin, J. W. Beattie, and J. Ovadia—725(A)
Direct measurement of ionization probability and appearance potential using a mass spectrometer, R. E. Fox, W. M. Hickam, T. Kjeldaas, Jr., and D. J. Grove—707(A)
Electrical phenomena during freezing of dilute aqueous solutions, Marvin E. Backman—759(A)
Ionization loss of energy of relativistic μ-mesons in A, J. E. Kupperian, Jr., and E. D. Palmatier—1043(L)
Liquid-filled ionization chambers, M. A. Van Dilla—705(A)
Spray electrification of liquid drops, E. E. Dodd—759(A)
Stopping power of heavier substances, J. Lindhard and M. Scharff—1058(L)
Surface ionization of La, John H. Reynolds—770(A)
Ions
Clustering of ions, Henry Margenau and Stanley Bloom—735(A); 670
Ejection of electrons from Mo by He ions, H. D. Hagstrum—392(A)
Halogen negative ions at surface of thoriated W filament, J. W. Trischka, D. T. F. Marple, and A. White—136(L)
Of mass 19 from H_2O, Francis J. Norton—154(L)
Negative ion formation in oxygen, Ronald Geballe and Melvin A. Harrison—372(L)
Isomers, nuclear (see also **Nuclear structure; Radioactivity**)
Bi^{210} isomeric states, Harris B. Levy and I. Perlman—758(A)
Ge^{77} isomeric transition, Allan C. G. Mitchell and Alan B. Smith—153(L)
Lu^{176m} disintegration scheme, G. Scharff-Goldhaber, E. der Mateosian, and J. W. Mihelich—734(A)
Mass designation of 51.5-min Tc isomer, Heinrich A. Medicus and Harry T. Easterday—735(A)
Second γ-transition ($d_{3/2} \rightarrow s_{1/2}$) in Xe^{129m}, S. Thulin and I. Bergström—1055(L)
Second transition in decay of Sn^{119m}, J. C. Bowe and P. Axel—734(A)
Sr^{85} isomerism, A. W. Sunyar, J. W. Mihelich, G. Scharff-Goldhaber, M. Deutsch, and M. Goldhaber—734(A)
Te^{125m} decay, P. Axel and J. C. Bowe—734(A); J. C. Bowe and P. Axel—858
Isotopes and atomic masses
Atomic masses of Ti, V, and Cr, T. L. Collins, A. O. Nier, and W. H. Johnson, Jr.—726(A)
Atomic masses of Xe, I, and some isotopes of Sn, R. E. Halsted—726(A)
Effect of intrinsic moment of electron on spectroscopic isotope shift, G. Breit and W. W. Clendenin—689(L)
Hfs and isotope shift in spectrum of Te, John S. Ross and Kiyoshi Murakawa—559
Isotope effect in imprisonment of resonance radiation, T. Holstein, D. Alpert, and A. O. McCoubrey—985
Isotope effects in decarboxylation of malonic acids, Peter E. Yankwich, Edward C. Stivers, and Robert F. Nystrom—753(A)
Limits of isotopic abundance for Hf and Pt, H. E. Duckworth, R. F. Woodcock, G. S. Stanford, A. Coutu, and R. L. Stearns—929(L)
Magic numbers and isotope shift in atomic spectra of heavy elements, P. Brix and H. Kopfermann—1050(L)
Mass measurements with magnetic time-of-flight mass spectrometer, erratum, E. E. Hays, P. I. Richards, and S. A. Goudsmit—1065(L)
Masses of Al and Si isotopes, Henry T. Motz—501(L)
Masses of Pb and Bi, P. I. Richards, E. E. Hays, and S. A. Goudsmit—630
Masses of Pb^{208}, Th^{232}, U^{234}, U^{235}, and U^{238}, George S. Stanford, Henry E. Duckworth, Benjamin G. Hogg, and James S. Geiger—1039(L)
Nuclear masses as integral multiples of a natural unit, Enos E. Witmer—748(A)
Production and assignment of Ra^{230} and Ac^{230}, William A. Jenkins and Glenn T. Seaborg—758(A)

Kinetic theory
Clustering of ions, Henry Margenau and Stanley Bloom—735(A); 670

Liquids (see also **Hydrodynamics**)
Critical state of normal fluids, Louis Goldstein—35
Supercooling of H_2O, B. Luyet—746(A)
Low temperature phenomena (see also **Helium, liquid**)
Adiabatic thermal changes in $BaTiO_3$ ceramic at low temperatures, Roland W. Schmitt—1; Roland W. Schmitt and R. T. Swim—743(A)
Phase transitions in adsorbed films, Lothar Meyer and Earl Long—1035
Resistance variation of MnSe at low temperatures, John Scales and C. W. Heaps—743(A)
Luminescence (see also **Fluorescence, Phosphorescence**)
Of BaO, Virgil L. Stout—390(A)
Cathodoluminescence of commercial oxide coated cathodes, Arthur G. Rouse and John B. Drahmann—739(A)

Magnetic properties (see also **Nuclear moments and spin; Crystal structure; Magnetic resonance absorption**)
Anisotropy energy in cubic lattice of spin dipoles, Jack R. Tessman—752(A)
Antiferromagnetic structure of MnO_2 by neutron diffraction, R. A. Erickson—745(A)
Approximate quantum theory of antiferromagnetic ground state, P. W. Anderson—714(A)
Corbino effect and change of resistance in magnetic field, erratum, K. M. Koch and L. Halpern—1064(L)
Diamagnetic properties of adsorbed gases, W. O. Milligan and Harry B. Whitehurst—746(A)
Diamagnetic susceptibility of N_2, J. V. Bonet and A. V. Bushkovitch—707(A)
Effect of stress on curvature of domain boundaries, H. J. Williams and R. M. Bozorth—713(A)
Energy of Bloch wall on band picture, Conyers Herring—1003
Exchange integral in the 3*d* shell, Harvey Kaplan—1038(L)
Ferromagnetic domain structure of single crystals and bicrystals of Ni, Ursula M. Martius, K. V. Gow, and Bruce Chalmers—713(A)
First- and second-order magnetostriction and morphic effects for Ni crystal, erratum, W. P. Mason—1065(L)
Generalizations of Weiss molecular field theory of antiferromagnetism, J. Samuel Smart—714(A)
Of hollow superconducting lead sphere, Julius Babiskin—104
Intrinsic antiferromagnetic character of Fe, C. Zener—324
Intrinsic magnetization in alloys, W. J. Carr—590
Magnetic susceptibility of Cr, T. R. McGuire and C. J. Kriessman—452
Magnetic susceptibility of polycrystalline anisotropic materials and observations on artificial graphites, J. D. McClelland and J. J. Donoghue—768(A)
Magnetic susceptibility of U, C. J. Kriessman, Jr., and T. R. McGuire—71
Magnetic susceptibility of Zn at liquid nitrogen temperatures, J. W. McClure—715(A)
Motion of ferromagnetic domain wall in Fe_3O_4, John K. Galt—664
Neutron diffraction investigation of atomic magnetic moment orientation in the antiferromagnetic compound CrSb, A. I. Snow—365(L)

Magnetic properties (continued)
Origin of high permeability in permalloy, Sōshin Chikazumi—918(L)
Reduction of temperature coefficient of magnetic moment for bar magnet, R. W. Long and I. A. Robertson—746(A)
Saturation magnetic moment of alloys on collective electron theory, J. E. Goldman—375(L)
Scattering of 0.5-Mev circularly polarized photons in magnetized Fe, Forrest P. Clay and Frank L. Hereford—675(L)
Semiconductivity and diamagnetism of polycrystalline graphite and condensed ring systems, S. Mrozowski—609
Spin paramagnetism of Cr^{+++} at liquid He temperatures and high magnetic fields, Warren E. Henry—487(L)
Spin-spin relaxation in simple system, Julian Eisenstein—603
Spontaneous magnetization of two-dimensional Ising model, C. N. Yang—808
Statistics of three-dimensional ferromagnet, B. Martin, D. Ter Haar, and V. A. Johnson—714(A)
Strain induced curvature of Bloch walls in Si iron, L. J. Dijkstra and U. Martius—714(A)
Magnetic resonance absorption (see also **Nuclear moments and spin**)
Anisotropy in paramagnetic resonance absorption of picryl-π-amino carbazyl, Victor W. Cohen, C. Kikuchi, and John Turkevich—379(L)
Calculation of g factor of metallic Na, Y. Yafet—478(L)
Chemical effects in nuclear induction, J. T. Arnold—763(A)
Ferromagnetic resonance in single crystals of Co-Zn ferrite, Tosihiko Okamura and Yūzo Kojima—690(L)
In glycine, T. M. Shaw, R. H. Elsken, and K. J. Palmer—762(A)
Gyromagnetic ratios of Li^7, Na^{23}, Al^{27}, and P^{31}, T. Kanda, Y. Masuda, R. Kusaka, Y. Yamagata, and J. Itoh—938(L)
Interactions between nuclear spins in molecules, N. F. Ramsey and E. M. Purcell—143(L)
Line width of paramagnetic resonance and exchange interaction in salts containing Mn^{++} and Fe^{+++}, H. Kumagai, K. Ono, and I. Hayashi—925(L)
Magnetic resonance spectra of $Rb^{87}F$ and $Rb^{87}Cl$ at zero field, D. I. Bolef and H. J. Zeiger—799
Magnetic resonance spectra of $TlCl^{35}$ and $TlCl^{37}$ at zero field, H. J. Zeiger and D. I. Bolef—788
In metallic Rb and Cs, D. F. Abell and W. D. Knight—762(A)
Nuclear gyromagnetic ratio of V^{50} and measurements on Rb^{85} and Cl^{35}, H. E. Walchli, W. E. Leyshon, and F. M. Scheitlin—922(L)
Nuclear magnetic resonance of Ti and As, C. D. Jeffries, H. Loeliger, and H. H. Staub—478(L)
Nutational resonance, H. C. Torrey—365(L)
Properties of transition metals V and Nb by nuclear magnetic resonance, W. D. Knight—762(A)
Proton magnetic resonance absorption and water content of biological materials, T. M. Shaw, R. H. Elsken, and C. H. Kunsman—708(A)
Pure nuclear electric quadrupole resonance of N^{14} in three molecular solids, G. D. Watkins and R. V. Pound—1062(L)
Quadrupole moment of electron distribution in H_2 molecule, N. J. Harrick, R. G. Barnes, and P. J. Bray—716(A)
Relaxation effects in ferromagnetic resonance, N. Bloembergen and R. W. Damon—699
Spin-echo measurements of nuclear spin-spin coupling, E. L. Hahn and D. E. Maxwell—762(A)
Steady-state transient technique in nuclear resonance, R. Gabillard—694(L)
Temperature dependence of line half-width of ferromagnetic resonance in single crystals of Zn-Mn ferrite, Tosihiko Okamura, Yuzo Kojima, and Yosiharu Torizuka—693(L)
Theory of antiferromagnetic resonance, F. Keffer and C. Kittel—329
Magnetostriction (see **Magnetic properties**)
Mass spectroscopy
Combination crossed-field and time-of-flight mass spectrometer, J. A. Hipple and H. Sommer—712(A)
High geometry electrostatic time-of-flight mass spectrograph, William E. Glenn—763(A)
Mass measurements with magnetic time-of-flight mass spectrometer, erratum, E. E. Hays, P. I. Richards, and S. A. Goudsmit—1065(L)
Of mass 19 from H_2O, Francis J. Norton—154(L)
Masses of Pb and Bi, P. I. Richards, E. E. Hays, and S. A. Goudsmit—630
Masses of Pb^{208}, Th^{232}, U^{234}, U^{235}, and U^{238}, George S. Stanford, Henry E. Duckworth, Benjamin G. Hogg, and James S. Geiger—1039(L)
Mathematical Methods (see **Methods and instruments**)
Measurements (see **Methods and instruments**)
Mechanics, quantum—atomic structure and spectra
Eigenfunctions and Landé interval factors for terms of f^3 electrons, Robert A. Satten—775(A)
$L(L+1)$ correction in spectra of Fe group, Guilio Racah—381(L)
$L(L+1)$ correction to Slater formulas for energy levels, R. E. Trees—382(L)
Li^+ wave function, P. J. Luke, R. E. Meyerott, and W. W. Clendenin—401
LSM_LM_S eigenfunctions of an atom, Kenneth James Harker—753(A)
Numerical variational method, R. E. Meyerott, P. J. Luke, W. W. Clendenin, and S. Geltman—393
Radiative corrections to the intensities for hydrogen-like atoms, erratum, T. Tati—1064(L)
Superposition of configurations in ground state of He I, Louis C. Green, Marjorie M. Mulder, C. W. Ufford, E. Slaymaker, Eleanor Krawitz, and R. T. Mertz—65
Mechanics, quantum—general
Biased random walks in classical, statistical, and quantum mechanics, Gilbert W. King—708(A)
Extension of classical infinitesimal group of canonical transformations, D. C. Rivier—721(A)
Fundamental reversibility and phenomenological irreversibility, Satosi Watanabe—721(A)
Generalization of WKB method to radial wave equations, R. H. Good, Jr.—754(A)
New interpretation of quantum theory in terms of "hidden" variables. I, D. Bohm—166; II—180
Point transformations, Bryce Seligman DeWitt—653
Mechanics, quantum—molecular structure and spectra
Computation of infrared intensities, Frank Matossi—708(A)
Rotational magnetic moments of $^1\Sigma$ molecules, J. R. Eshbach and M. W. P. Strandberg—24
Theory of H_2 and D_2 in magnetic fields, Norman F. Ramsey—60
Van der Waals forces in magnetic fields, Henry Margenau and D. E. Harrison—707(A)
Vibrational analysis of chain molecules, W. Edward Deeds—160(A)
Mechanics, quantum—nuclear
Angular correlation of electrons in double β-decay, H. Primakoff—888
Angular correlation of two successive nuclear radiations, Stuart P. Lloyd—904
Angular distribution in high energy deuteron photoeffect, N. Austern—283

β-decay of RaE and the pseudoscalar interaction, A. G. Petschek and R. E. Marshak—698(L)
Charge independence for nuclear phenomena, Kenneth M. Watson—852
Contribution of interaction moments to nuclear magnetic moments, Marc Ross—721(A)
Elastic photoproduction of π^0 mesons in D, N. C. Francis and R. E. Marshak—496(L)
Elastic scattering of deuterons by deuterons, Richard J. Runge—1052(L)
Electromagnetic effects due to spin-orbit coupling, J. Hans D. Jensen and M. Goeppert Mayer—1040(L)
$\gamma-\gamma$ and internal conversion angular correlations, J. W. Gardner—137(L)
High energy nucleon-deuteron scattering, P. B. Daitch and J. B. French—695(L)
Impulse approximation, Geoffrey Chew and Gian Carlo Wick—636; J. Ashkin and G. C. Wick—686(L)
Influence of well shape on pick-up process in D, Ira L. Karp—754(A)
Internal conversion angular correlations, M. E. Rose, L. C. Biedenharm, and G. B. Arfken—5
Internal conversion in the L-shell, H. Gellman, B. A. Griffith, and J. P. Stanley—944(L)
Invariance conditions on scattering amplitudes for spin $\frac{1}{2}$ particles, L. Wolfenstein and J. Ashkin—947
Long range $p-p$ tensor force, Norman F. Ramsey—937(L)
Nuclear magnetic moment and $j-j$ coupling shell model, Masataka Mizushima and Minoru Umezawa—37
Nuclear momentum distributions, Peter A. Wolff—766(A)
Quadrupole radiation in πD capture, N. Austern—147
Symmetry effects on nuclear dipole radiation with application to bound excited state of $_2He^4$, Lynne E. H. Trainor—962
Time dependent description of resonance reactions, Marcos Moshinsky—748(A)

Mechanics, quantum—of solid bodies

Anisotropy energy in cubic lattice of spin dipoles, Jack R. Tessman—752(A)
Approximate quantum theory of antiferromagnetic ground state, P. W. Anderson—714(A)
Energy of Bloch wall on band picture, Conyers Herring—1003
Exchange integral in 3d shell, Harvey Kaplan—1038(L)
Fermi energy of metallic Li, Richard A. Silverman—227
g factor of metallic Na, Y. Yafet—478(L); 762(A)
Generalizations of the Weiss molecular field theory of antiferromagnetism, J. Samuel Smart—714(A)
Heat capacity and lattice defect of AgCl, Koichi Kobayashi—150(L)
Intrinsic antiferromagnetic character of Fe, C. Zener—324
Intrinsic magnetization in alloys, W. J. Carr—590
Motion of electron in perturbed periodic potential, E. N. Adams, II—41
Multiple scattering of waves. II. Effective field in dense systems, Melvin Lax—621
Quantum theory of internal field in idealized crystal, D. L. Dexter and W. R. Heller—723(A)
Saturation magnetic moment of alloys on collective electron theory, J. E. Goldman—375(L)
Spin-spin relaxation in simple system, Julian Eisenstein—603
Splitting of bands in solids, E. Katz—495(L)
Spontaneous magnetization of two-dimensional Ising model, C. N. Yang—808
Statistics of three-dimensional ferromagnet, B. Martin, D. Ter Haar, and V. A. Johnson—714(A)
Theory of nuclear quadrupole interaction of Nb^{93} in $KNbO_3$, M. H. Cohen—762(A)

Mechanics, statistical

Critical state of normal fluids, Louis Goldstein—35
Radial distribution function of gas of hard spheres and superposition approximation, B. R. A. Nijboer and L. Van Hove—777
Relativistic modification of Bose and Fermi statistics, A. E. Scheidegger and C. D. McKay—376
Theory of condensation of gases, R. J. Riddell, Jr.—760(A)

Mesons (see also **Cosmic radiation**)

Angular distribution of decay tracks of V^0-particles, W. B. Fretter and M. M. May—773(A)
Angular distribution of π^+ mesons produced in $p-p$ collisions, Marian Whitehead and Chaim Richman—772(A)
Annihilation radiation from μ^+ mesons, M. H. Johnson—719(A)
Capture of μ-mesons in nuclear emulsions, D. F. Sherman, Harry H. Heckman, and Walter H. Barkas—771(A)
Charged π-meson production from D, S. Passman, M. M. Block, and W. W. Havens, Jr.—370(L)
Charged π-meson production in D and Pb at 90° from a 381-Mev proton beam, M. M. Block, S. Passman, and W. W. Havens, Jr.—718(A)
Cross sections of 6-Mev mesons in H and D, P. J. Isaacs, A. M. Sachs, and J. Steinberger—803
Differential range spectrum of cosmic-ray mesons at sea level, Carl M. York, Jr.—998
Disintegration of deuteron by π^+ mesons and spin of π^+ meson, Donald L. Clark, Arthur Roberts, and Richard Wilson—523
Elastic photoproduction of π^0 mesons in D, N. C. Francis and R. E. Marshak—496(L)
Elastic scattering of negative pions in C, P. Isaacs, A. Sachs, and J. Steinberger—718(A)
Electromagnetic interference effects in charged meson-proton scattering, M. F. Kaplon—1059(L)
Emulsion cloud-chamber study of a high energy interaction, M. Kaplon, B. Peters, and D. M. Ritson—900
Energy loss of cosmic-ray μ-mesons, Robert Hofstadter and Alvin M. Hudson—773(A)
Extremely high energy nuclear interactions, M. F. Kaplon and D. M. Ritson—932(L)
Fast protons from capture of π^- mesons in photographic emulsions, Frank L. Adelman—249
Interaction of charged π-mesons with deuteron, W. B. Cheston—718(A); 952
Ionization loss of energy of relativistic μ-mesons in A, J. E. Kupperian, Jr., and E. D. Palmatier—1043(L)
Is there a neutral μ-meson?, G. E. Uhlenbeck and C. S. Wang Chang—684(L)
Lifetime of π-meson, L. Lederman, H. Byfield, and J. Kessler—719(A)
Multiplicities of neutrons produced by cosmic-ray μ-mesons captured in Pb, Marshall F. Crouch and Robert D. Sard—120
μ^- mesons stopped in photographic emulsions, W. F. Fry—676(L)
Neutral meson γ-ray spectra from C, W. E. Crandall, K. Crowe, B. J. Moyer, W. K. H. Panofsky, R. Phillips, and D. Walker—771(A)
Neutral mesons from proton bombardment of light nuclei, R. W. Hales, R. H. Hildebrand, N. Knable, and B. J. Moyer—373(L)
Nonlinearities due to vacuum polarization in meson-nucleon interactions, B. J. Malenka—686(L)
Nuclear cross sections for negative pions of energy 109 and 133 Mev, R. L. Martin, H. L. Anderson, and G. Yodh—486(L)
Ordinary and exchange scattering of negative pions, H. E. Fermi, H. L. Anderson, A. Lundby, D. E. Nagle, and G. B. Yodh—935(L)

Mesons (continued)
Photographic study of $\pi \to \mu \to \beta$-decay, H. J. Bramson, A. M. Seifert, and W. W. Havens—719(A)
Photomesons from D, R. Stephen White, Mark J. Jakobson, and Alvin G. Schulz—770(A)
Photomesons from He, Mark J. Jakobson, Alvin G. Schulz, and R. Stephen White—772(A)
Photoproduction of negative mesons from D, Richard Madey, Kenneth C. Bandtel, and Wilson J. Frank—771(A)
Photoproduction of negative pions from D, R. E. LeLevier—771(A)
Photoproduction of neutral mesons from D, W. Heckrotte, L. R. Henrich, and J. V. Leport—490(L)
π-meson decay, M. Ruderman—157(L)
π-meson interactions in C, H. Byfield, J. Kessler, and L. Lederman—718(A)
π-meson production by protons on nuclei, Ernest M. Henley—204
Production cross section and energy spectrum of neutral mesons in cosmic rays, G. Salvini and Y. Kim—921(L)
Production cross sections for π^+ and π^- mesons by 340-Mev protons on C and Pb at 90° to the beam, C. Richman, M. Weissbluth, and H. A. Wilcox—161
Protons and mesons at 9000 feet, A. Z. Rosen—773(A)
Radiative π-μ decay, Tetsuo Eguchi—943(L)
Range straggle of μ^+ mesons, F. M. Smith, W. Birnbaum, and W. H. Barkas—771(A)
Regular meson type potentials in $p-p$ scattering, R. D. Hatcher and H. E. Hart—703(A)
Response of anthracene scintillation crystals to high energy μ-mesons, Theodore Bowen and Francis X. Roser—992
Scattering of 50-Mev positive pions by He, A. M. Thorndike, E. C. Fowler, W. B. Fowler, and R. P. Shutt—929(L)
Scattering of negative π-mesons in Al, Cu, and Pb, Harry H. Heckman and Walter H. Barkas—771(A)
Scattering of strongly coupled pseudovector mesons, Melvin Eisner—748(A)
Self-energies of nucleons and mass spectra of heavy particles, H. Enatsu—483(L)
Slow mesons produced by cosmic radiation, Herman Yagoda—891
Total cross sections of negative pions in H, H. L. Anderson, E. Fermi, E. A. Long, R. Martin, and D. E. Nagle—934(L)
Zenith angle effects for cosmic-ray protons and mesons, C. E. Miller, J. E. Henderson, Gerald Garrison, and Wayne Sandstrom—773(A)
Metals (see **Crystalline state**)
Meteorology
Monitor for natural radioactivity in atmosphere, M. H. Wilkening—712(A)
Methods and instruments
Acceleration of multiply charged nuclei, Cornelius A. Tobias—764(A)
Aeroballistics Laboratory of U. S. Naval Ordnance Test Station, Arthur L. Bennett, Ivar Highberg, Ernest Barkofsky, and Lucien M. Biberman—774(A)
Apparatus for creep and low frequency dynamic studies on polymers, T. E. Morrisson and T. W. DeWitt—708(A)
Application of Laplace transformation and mechanical harmonic synthesizer in analysis of electric circuits, Herbert D. Schwetman and S. Leroy Brown—740(A)
Automatic multirange recording device for measuring varying potentials, J. C. Pigg—731(A)
Beam system for reduction of Doppler broadening of microwave absorption line, H. R. Johnson and M. W. P. Strandberg—503(L)
Cathodic sputtering as sectioning method in diffusion studies, Thomas F. Fisher—709(A)
Čerenkov counter, Robert W. Birge—766(A)
Combination cloud-ion chamber using cylindrical geometry, Fielding Brown, R. R. Rau, and George T. Reynolds—712(A)
Combination crossed-field and time-of-flight mass spectrometer, J. A. Hipple and H. Sommer—712(A)
Compound x-ray microscope, H. H. Pattee, Jr.—764(A)
Critical-flow pneumatic hygrometer, W. A. Wildhack, T. A. Perls, and J. W. Hayes—731(A)
Crystal spectrometer for neutrons, L. B. Borst and V. L. Sailor—711(A)
Curved quartz crystal x-ray spectrometer, John E. Edwards—160(A)
Differential analyzer methods for orbit problems in the cyclotron, Bayard Rankin, John Killeen, and Walter H. Barkas—754(A)
800-kc Cockroft-Walton generator, Wm. A. Robba—741(A)
Electron interferometer, L. Marton—1057(L)
Extensometer for creep studies, R. Pizzaro and B. Gossick—711(A)
High geometry electrostatic time-of-flight mass spectrograph, William E. Glenn—763(A)
Ion trajectories in omegatron, Clifford E. Berry—765(A)
Linearity of scintillation γ-ray spectrometer, V. O. Eriksen and G. Jenssen—150(L)
Liquid-filled ionization chambers, M. A. Van Dilla—705(A)
Mass synchrometer, Lincoln G. Smith—767(A)
Measurement of uniformity of materials by γ-ray transmission, John N. Harris and Arthur I. Berman—765(A)
Microscopy by reconstructed wave fronts, Hussein M. A. El-Sum and Paul Kirkpatrick—763(A)
Monitor for natural radioactivity in atmosphere, M. H. Wilkening—712(A)
Multiple scattering theory of grating and Wood anomalies, Vic Twersky—715(A)
New method of obtaining focused images with x-rays, G. M. Ramachandran—378(L)
New technique for photonuclear cross sections, Lester L. Newkirk—767(A)
Numerical variational method, R. E. Meyerott, P. J. Luke, W. W. Clendenin, and S. Geltman—393
Oak Ridge 86-in. cyclotron, Robert S. Livingston—713(A)
Operating current and energy of M.I.T. linear electron accelerators, M. Labitt, R. J. Debs, I. Halpern, and P. T. Demos—713(A)
Performance of 5819 photomultipliers in scintillation spectrometers, A. W. Schardt and William Bernstein—712(A)
Photoelectric thresholds in photon counters containing electronegative quenching gases, H. Friedman, T. Chubb, and D. A. Patterson—705(A)
Point focusing monochromator for low angle x-ray diffraction, L. Shenfil, W. E. Danielson, and J. W. M. DuMond—739(A)
Polystyrene solid solutions as scintillation counters, Thomas Carlson and W. S. Koski—697(L)
Precision scattering project, James S. Arthur, A. J. Allen, R. S. Bender, R. L. Ely, H. J. Hausman, L. A. Page, and E. M. Reilley—704(A)
Preparation of thin Zr-Tr targets, J. P. Conner and J. R. Smith—741(A)
Processing thick nuclear emulsions, Bertram Stiller, Maurice M. Shapiro, and Francis W. O'Dell—712(A)
Production of halogen negative ions at surface of thoriated W filament, J. W. Trischka, D. T. F. Marple, and A. White—136(L)
Pulse analysis with aid of mechanical synthesizer-analyzer, S. Leroy Brown—753(A)
Relative spectral sensitivity calibration of electron multiplier phototubes in 2500A–3500A region, E. H. Gilmore and R. H. Knipe—764(A)

Resolution and sensitivity of microwave spectrographs, H. R. Johnson—764(A)
Resolution of fast neutron energy measurements using proton recoils from thin radiator, Ben R. Gossick—711(A)
Response of anthracene scintillation crystals to high energy μ-mesons, Theodore Bowen and Francis X. Roser—992
Retarding potential method of measuring electrical conductivity of oxide coated cathodes, I. L. Sparks—705(A)
Scintillation neutron detector, William Bernstein and A. W. Schardt—711(A)
Slow neutron crystal spectrometer, R. G. Allen, C. P. Stanford, T. E. Stephenson, and S. Bernstein—767(A)
Slow neutron liquid scintillation detector, C. O. Muehlhause and G. E. Thomas—926(L)
Stabilized synchronous amplifier, R. G. Nuckolls and L. J. Rueger—731(A)
Steady-state transient technique in nuclear resonance, R. Gabillard—694(L)
Synchronized rotating mirror system, Richard G. Fowler and Robert J. Lee—732(A)
Tracer method for measurement of evaporated Bi film thicknesses, John J. Antal and A. H. Weber—710(A)
Ultracompact, ultra-high speed digital computers. II, Donald H. Jacobs, and Seymour Scholnick—731(A)
University of Kansas Van de Graaf generator, L. W. Seagondollar, R. K. Smith, W. R. Alexander, and J. W. Teener—713(A)
University of Washington 60-in. cyclotron, F. K. Donnelly, H. J. Engebertson, J. E. Henderson, T. J. Morgan, F. H. Schmidt, and J. F. Streib—767(A)
Use of successive diffractions to double or quadruple resolving power of a grating, F. A. Jenkins and L. W. Alvarez—763(A)

Microwaves (see also **Electromagnetic theory; Electronic tubes; Spectra, microwave**)
Electromagnetic field measurements in plane of circular aperture, Robert E. Houston and Robert H. Noble—732(A)
Propagation through electronic space charge in magnetic field, James R. Hooper—705(A)

Molecular beams (see **Atomic and molecular beams**)

Molecular structure and constants (see also **Spectra, molecular; Raman spectra**)
Interactions between nuclear spins in molecules, N. F. Ramsey and E. M. Purcell—143(L)
Of ozone, Richard H. Hughes—717(A)
Structural constants of ClO_2, J. B. Coon—746(A)
TlCl, molecular beam electric resonance method study, R. O. Carlson, C. A. Lee, and B. P. Fabricand—784
Vibrational analysis of chain molecules, W. Edward Deeds—160(A)

Moments, of molecules
Quadrupole moment of electron distribution in H_2 molecule, N. J. Harrick, R. G. Barnes, and P. J. Bray—716(A)
Rotation magnetic moments of $^1\Sigma$ molecules, J. R. Eshbach and M. W. P. Strandberg—24
Sign determination of molecular magnetic moments, C. K. Jen, J. W. B. Barghausen, and R. W. Stanley—717(A)

Neutron diffraction
Antiferromagnetic structure of MnO_2 by neutron diffraction, R. A. Erickson—745(A)
Crystal spectrometer for neutrons, L. B. Borst and V. L. Sailor—711(A)
Slow neutron crystal spectrometer, R. G. Allen, C. P. Stanford, T. E. Stephenson, and S. Bernstein—767(A)

Neutrons
Diffusion of thermal neutrons, George Jaffé—747(A)
Measurement of electron-neutron interaction, M. Hamermesh, G. R. Ringo, and A. Wattenberg—483(L)
Neutron transmission cross sections in kv region, Carl T. Hibdon, Alexander Langsdorf, Jr., and Robert E. Holland—595
Quadrature method for computing neutron distributions in two dimensions, E. Leigh Secrest—747(A)
Resolution of fast neutron energy measurements using proton recoils from thin radiator, Ben R. Gossick—711(A)
Scintillation neutron detector, William Bernstein and A. W. Schardt—713(A)
Slow neutron liquid scintillation detector, C. O. Muehlhause and G. E. Thomas—926(L)
The tetraneutron, K.-H. Sun, F. A. Pecjak, and A. J. Allen—942(L)
Theory of neutron scattering by gases, N. K. Pope and G. Feldman—703(A)

Nuclear induction (see **Magnetic resonance absorption; Nuclear moments and spin**)

Nuclear moments and spin (see also **Hyperfine structure**)
Anomalous magnetic moments of nucleons, Fernando E. Prieto C.—747(A)
Attempt to produce nuclear orientation in Hg vapor, Francis Bitter and Jean Brossel—1051(L)
Cl^{36} spin from microwave spectrum of $C^{13}H_3Cl^{36}$, D. A. Gilbert—766(A)
Contribution of interaction moments to nuclear magnetic moments, Marc Ross—721(A)
Hfs and isotope shift in spectrum of Te, John S. Ross and Kiyoshi Murakawa—559
Interactions between nuclear spins in molecules, N. F. Ramsey and E. M. Purcell—143(L)
Magnetic moment of Co^{60} using nuclear alignment, B. Bleaney, J. M. Daniels, M. A. Grace, H. Halban, N. Kurti, and F. N. H. Robinson—688(L)
Magnetic moments of even-odd nuclei, Jack P. Davidson—432
Magnetic moments of nuclei, H. A. Wilson—747(A)
Nuclear magnetic moment and $j-j$ coupling shell model, Masataka Mizushima and Minoru Umezawa—37
Nuclear moment and hfs anomaly of K^{40}, Joseph T. Eisinger and Benjamin Bederson—716(A)
O^{17} spin and quadrupole moment, S. Geschwind, G. R. Gunther-Mohr, and G. Silvey—474
Se^{79} spin and quadrupole moment, W. A. Hardy, G. Silvey, and C. H. Townes—494(L)
Spin-echo measurements of nuclear spin-spin coupling, E. L. Hahn and D. E. Maxwell—762(A)
Spin of π^+ meson, Donald L. Clark, Arthur Roberts, and Richard Wilson—523
S^{33} magnetic moment from microwave spectroscopy, J. R. Eshbach, R. E. Hillger, and M. W. P. Strandberg—532
Tc^{99} magnetic moment, Harold Walchli, Ralph Livingston, and William J. Martin—479(L)
Theory of nuclear quadrupole interaction of Nb^{93} in $KNbO_3$, M. H. Cohen—762(A)
Use of HD for experiments on $p-d$ magnetic moment ratio, Norman F. Ramsey—688(L)
Zn^{67} magnetic moment, S. S. Dharmatti and H. E. Weaver, Jr.—927(L)

Nuclear reactions (see **Disintegration and excitation of nucleus**)

Nuclear spectra (see also **Disintegration and excitation of nucleus**)
Angular correlation of electrons in double β-decay, H. Primakoff—888
Angular correlation of two successive nuclear radiations, Stuart P. Lloyd—904
Be^7 and B^{10} low-lying levels, Robert B. Day and Torben Huus—761(A)
β-decay of RaE and pseudoscalar interaction, A. G. Petschek and R. E. Marshak—698(L)

Nuclear spectra (continued)
Capture γ-rays from protons on N^{14}, C. H. Johnson, C. D. Moak, and G. P. Robinson—727(A); C. H. Johnson, G. P. Robinson, and C. D. Moak—931(L)
C^{12} energy levels from $Be^9(\alpha,n)C^{12}$, W. H. Guier, H. W. Bertini, and J. H. Roberts—426
$C^{13}(p,\gamma)N^{14}$ γ-rays, H. H. Woodbury, R. B. Day, and A. V. Tollestrup—760(A)
Ce^{144} and Pr^{144} β-spectra, Cheng Lin-sheng, G. John, and J. D. Kurbatov—487(L); Fred T. Porter and C. Sharp Cook—733(A)
Classification of levels in Al^{25}, L. J. Koester—704(A)
Decay series $Nd^{140}-Pr^{140}-Ce^{140}$, Charles I. Browne, John O. Rasmussen, Joseph P. Surls, and Donald F. Martin—146(L)
Delayed γ-emission from decay of C^{15}, Emmett L. Hudspeth, William B. Rose, and N. P. Heydenburg—742(A)
Disintegration of ground-state Sr^{85} and metastable energy level of 514 kev in Rb^{85}, W. S. Emmerich and J. D. Kurbatov—149(L)
Energy levels in Al^{27}, E. M. Reilley, A. J. Allen, J. S. Arthur, R. S. Bender, R. L. Ely, and A. J. Hausman—704(A)
Of $Eu^{153,154}$, Robert Katz and Milford R. Lee—1038(L)
Fine structure and angular correlation in Po^{210}, S. De Benedetti and G. H. Minton—944(L)
Fine structure of α-particles of Po^{210}, S. De Benedetti and G. H. Minton—726(A)
$\gamma-\gamma$ and internal conversion angular correlations, J. W. Gardner—137(L)
$\gamma-\gamma$ coincidence absorption and angular correlation of I^{131}, Daniel Schiff—727(A)
$\gamma-\gamma$ coincidences in "Cs^{137}" and Fe^{59}, Franz R. Metzger—727(A)
Hf^{177} γ-ray classification, F. K. McGowan, E. D. Klema, and P. R. Bell—152(L)
Half-life of 1.3-Mev excited state in K^{41}, L. G. Elliott—942(L)
Internal conversion angular correlations, M. E. Rose, L. C. Biedenharn, and G. B. Arfken—5
Internal conversion in L-shell, H. Gellman, B. A. Griffith, and J. P. Stanley—944(L)
K-Auger yield for Ba, C. D. Broyles and S. K. Haynes—733(A)
K-capture partial lifetimes, A. J. Saur and H. M. Schwartz—733(A)
K-shell internal conversion coefficients, F. K. McGowan—151(L)
L x-rays and low energy γ-radiation in decay of Am^{241}, C. I. Browne and I. Perlman—758(A)
Lifetime of excited state of $_{66}Dy^{160}$ and upper limits for some other nuclei, F. K. McGowan—142(L)
Low energy γ-ray transitions in some rare earth isotopes, J. W. Mihelich and E. L. Church—690(L)
Lu^{176m} disintegration scheme, G. Scharff-Goldhaber, E. der Mateosian, and J. W. Mihelich—734(A)
Of Hg^{197} and Hg^{203}, J. M. Cork, D. W. Martin, J. M. LeBlanc, and C. E. Branyan—386(L)
Of Nd^{151} and Pm^{151}, W. C. Rutledge, J. M. Cork, and S. B. Burson—734(A)
Neutral meson γ-ray spectra from C, W. E. Crandall, K. Crowe, B. J. Moyer, W. K. H. Panofsky, R. Phillips, and D. Walker—771(A)
Neutron capture γ-rays from P, S, Cl, K, and Ca, B. B. Kinsey, G. A. Bartholomew, and W. H. Walker—1012
Neutron spectrum from $B^{10}(\alpha,n)N^{13}$, N^{139}, Marguerite Rogers, F. K. Odencrantz, and G. J. Plain—756(A)
New γ-ray from $C^{13}+p$, A. V. Tollestrup, R. B. Day, and H. H. Woodbury—760(A)
P^{32} and P^{33} β-spectra, Erling N. Jensen, R. T. Nichols, J. Clement, and A. Pohm—112
Polarization of 6.13-Mev γ-rays emitted in the reaction $F^{19}(p,\alpha)O^{16*}(\gamma)O^{16}$, A. P. French and J. O. Newton—1041(L)
Pr^{144}, In^{114}, Ba^{137}, and Cd^{110}, internal conversion, W. C. Kelly—101
Production of polarized protons and inversion of energy levels of the $P_{1/2}-P_{3/2}$ doublet in Li^5, M. Heusinkveld and George Freier—80
Of RaD, R. C. Bannerman and S. C. Curran—134(L)
RaD β-spectrum, G. M. Insch, J. G. Balfour, and S. C. Curran—805
Of Rh^{99}, Rh^{101}, Rh^{105}, and Ru^{106}, C. L. Scoville, S. C. Fultz, and M. L. Pool—1046(L)
Relative internal conversion in the L subshells, J. W. Mihelich and E. L. Church—733(A)
Rh^{100} angular correlation, J. J. Kraushaar—727(A)
Rh^{106} decay, David E. Alburger—734(A)
Rb^{85}, 514-kev energy level, W. S. Emmerich and J. D. Kurbatov—733(A)
Second γ-transition ($d_{3/2}\rightarrow s_{1/2}$) in Xe^{129m}, S. Thulin and I. Bergström—1055(L)
Second transition in decay of Sn^{119m}, J. C. Bowe and P. Axel—734(A)
Si^{31} β-activity and masses of Al and Si isotopes, Henry T. Motz—501(L)
Of Ag^{108}, Max Goodrich and Edward C. Campbell—742(A)
Ag^{105} and Ag^{106} decay, Raymond W. Hayward—760(A)
Sr^{85} isomerism, A. W. Sunyar, J. W. Mihelich, G. Scharff-Goldhaber, M. Deutsch, and M. Goldhaber—734(A)
Te^{126m} decay, P. Axel and J. C. Bowe—734(A); J. C. Bowe and P. Axel—858
Two-model interpretation of a nuclear spectrum, D. R. Inglis—492(L)

Nuclear structure (see also **Disintegration and excitation of nucleus; Nuclear spectra; Radioactivity**)
Closing of proton subshell at Z 58, G. P. Dube and S. Jha—1042(L)
Electromagnetic effects due to spin-orbit coupling, J. Hans D. Jensen and M. Goeppert Mayer—1040(L)
Empirical analysis of nuclear shell effects in β-energetics, C. D. Coryell, R. A. Brightsen, and A. C. Pappas—732(A)
Influence of well shape on the pick-up process in deuterium, Ira L. Karp—754(A)
Interpretation of photonuclear experiments, L. Eyges—753(A)
Limits of stability of heavy elements and effects of nuclear shell structure, P. S. Greifinger—253
Magic numbers and isotope shift in atomic spectra of heavy elements, P. Brix and H. Kopfermann—1050(L)
Magnetic moments of even-odd nuclei, Jack P. Davidson—432
Nuclear magnetic moment and $j-j$ coupling shell model, Masataka Mizushima and Minoru Umezawa—37
Nuclear momentum distributions, Peter A. Wolff—766(A)
Pairing effect in nuclei and β-labile elements, Truman P. Kohman—530
Proposed test of nuclear shell model, H. A. Bethe and S. T. Butler—1045(L)
Symmetry effects on nuclear dipole radiation with application to bound excited state of $_1He^4$, Lynne E. H. Trainor—962
Tetraneutron, K.-H. Sun, F. A. Pecjak, and A. J. Allen—942(L)
Two-model interpretation of a nuclear spectrum, D. R. Inglis—492(L)

Nucleons
Interactions of high energy nucleons with nuclei, G. Bernardini, E. T. Booth, and S. J. Lindenbaum—826
Self-energies of nucleons and mass spectra of heavy particles, H. Enatsu—483(L)

Optical constants and properties
Optical and electrical behavior of lanarkite, L. M. Roth, K. W. Meissner, and K. Lark-Horovitz—724(A)
Optical properties of sodium tungsten bronze, G. C. Danielson and E. Chivers—711(A)
Optical instruments (see **Methods and instruments**)
Optical theory
Geometrical optics and theory of small angle scattering, George H. Vineyard—633

Pair production and annihilation
Antiproton annihilation, Israel Reff—379(L)
Half-life of positrons in condensed materials, S. De Benedetti and H. J. Richings—377(L)
Nuclear disintegration by positron-K electron annihilation, R. D. Present and S. C. Chen—447
Relative pair production cross section in region 50 to 300 Mev, C. R. Emigh—719(A)
Three-quantum annihilation and positronium, S. De Benedetti and R. Siegel—371(L)
Philosophy of physics
Information, logic, and physics, Jerome Rothstein—722(A)
Phosphorescence (see also **Luminescence**)
Activation of LiI crystal phosphors, W. Bernstein and A. W. Schardt—919(L)
Experimentally derived configurational coordinate curves for phosphors, Clifford C. Klick—154(L); 723(A)
Interactions of remote impurity centers in phosphors, H. W. Leverenz and D. O. North—930(L)
Long-lived phosphorescence of KI-TlI, Bernard Smaller and Eugene Avery—766(A)
Sn activation of LiI, James Schenck and R. L. Heath—923(L)
Photoconductivity
Optical and electrical behavior of lanarkite, L. M. Roth, K. W. Meissner, and K. Lark-Horovitz—724(A)
Photoconductivity study of activation of BaO, H. B. DeVore—390(A)
Photocontrolled low frequency dielectric dispersion, J. Ross Macdonald—381(L)
Transmission and spectral response of PbS and PbTe, M. A. Clark and R. J. Cashman—1043(L)
Photodisintegration
Angular distribution in high energy deuteron photoeffect, N. Austern—283
Angular distribution of photofission fragments from Th, E. J. Winhold, P. T. Demos, and I. Halpern—728(A)
Comparison of total photoneutron yield from 160- and 320-Mev bremsstrahlung, Lawrence W. Jones and Kent M. Terwilliger—686(L)
Cu$(\gamma,d):(\gamma,p)$ ratio, Warren H. Smith—728(A)
Of deuteron, W. S. Gilbert and J. W. Rose—766(A)
Of deuteron by high energy γ-rays, Seishi Kikuchi—753(A); 1062(L)
Elastic photoproduction of π^0 mesons in D, N. C. Francis and R. E. Marshak—496(L)
Energetic protons from nuclei exposed to 300-Mev bremsstrahlung, James C. Keck—410
High energy photodisintegration of deuteron, T. S. Benedict and W. M. Woodward—924(L)
High energy photoprotons from C, J. W. Rose and W. S. Gilbert—766(A)
Interpretation of photonuclear experiments, L. Eyges—741(A)
Neutron yield from nuclear photoeffect, J. S. Levinger and H. A. Bethe—577; 742(A)
New technique for photonuclear cross sections, Lester L. Newkirk—767(A)
Photofission of U, Roger E. Anderson and Robert B. Duffield—728(A)
Photomeson production from D, I. L. Lebow, B. T. Feld, D. H. Frisch, and L. S. Osborne—681(L); R. Stephen White, Mark J. Jakobson, and Alvin G. Schulz—770(A)
Photomeson production in C and H, B. T. Feld, D. H. Frisch, I. L. Lebow, L. S. Osborne, and J. S. Clark—680(L)
Photomesons from He, Mark J. Jakobson, Alvin G. Schulz, and R. Stephen White—772(A)
Photonuclear resonance curves from relative activity curves monitored by induced radioactivity, erratum, R. Sagane—1065(L)
Photoproduction of negative mesons from D, Richard Madey, Kenneth C. Bandtel, and Wilson J. Frank—771(A); R. E. LeLevier—771(A)
Photoproduction of neutral mesons from D, W. Heckrotte, L. R. Henrich, and J. V. Lepore—490(L)
Photoprotons from Bi, M. Elaine Toms and William E. Stephens—728(A)
Relative probabilities of diverse photonuclear reactions from Zn^{64} and Fe^{54}, Ryokichi Sagane—926(L)
Thresholds of Be and D, J. C. Noyes, J. E. Van Hoomissen, W. C. Miller, and B. Waldman—727(A)
Photoelectric effect and properties; Cells
Photoelectric emission from BaO in accelerating field, Paul E. Carroll and E. A. Coomes—389(A)
Photoelectric work functions for thin films of Ag on (100) face of Ag single crystal, Edward N. Clarke and H. E. Farnsworth—484(L)
Photography (see also **Methods and instruments**)
Physical measurements on nuclear photographic emulsion, A. J. Oliver and Walter H. Barkas—756(A)
Processing thick nuclear emulsions, Bertram Stiller, Maurice M. Shapiro, and Francis W. O'Dell—712(A)
Piezoelectric effect
Quartz resonator studies, K. S. Van Dyke and W. F. Palmer—745(A)
Plasticity
Effect of plastic deformation on anelastic properties of α-brass, John Kauffman and David Lazarus—710(A)
Of very small metal specimens, Conyers Herring and J. K. Galt—1060(L)
Polarization, electrical (see also **Dielectrics and dielectric properties**)
Polarization in electrolyte solutions, John A. Rider and George Jaffé—746(A)
Polarization of radiation
Circularly polarized γ-rays, Otto Halpern—747(A)
Polarization of 6.13-Mev γ-rays emitted in the reaction $F^{19}(p,\alpha)O^{16*}(\gamma)O^{16}$, A. P. French and J. O. Newton—1041(L)
Polymerization, properties of polymers
Apparatus for creep and low frequency dynamic studies on polymers, T. E. Morrisson and T. W. DeWitt—708(A)
Measurements of components of stress produced by shearing strain, E. H. Frei—708(A)
Positrons
Absolute backscattering coefficients, Howard H. Seliger—724(A)
Čerenkov radiation from positrons, T. C. Wilfong, Jr., and J. E. Henderson—765(A)
Fine structure splitting in ground state of positronium, T. A. Pond and R. H. Dicke—489(L)
Half-life of positrons in condensed materials, S. De Benedetti and H. J. Richings—377(L)
Relative transmission through G-M counter windows, Chia-hua Chang and C. Sharp Cook—724(A)
Three-quantum annihilation and positronium, S. De Benedetti and R. Siegel—371(L)
Triplet positronium in gases, T. A. Pond—489(L)
Zeeman effect and hyperfine splitting of positronium, Martin Deutsch and Sanborn C. Brown—1047(L)

Proceedings of the American Physical Society
Meeting at Chicago, Illinois (Bull. Am. Phys. Soc. **26**, No. 6), October 24–27, 1951—700
Meeting of the Division of Electron Physics, National Bureau of Standards, Washington, D. C., November 1–3, 1951—388
Ohio Section Meeting, Yellow Springs, Ohio, November 10, 1951—160
Meeting at Houston, Texas (Bull. Am. Phys. Soc. **26**, No. 7), November 30 and December 1, 1951—738
Meeting at Berkeley, California (Bull. Am. Phys. Soc. **26**, No. 8), December 27–29, 1951—751

Protons
Antiproton annihilation, Israel Reff—379(L)
Production of polarized protons and inversion of energy levels of the $P_{1/2}-P_{3/2}$ doublet in Li^8, M. Heusinkveld and George Freier—80

Quantum electrodynamics (see also **Field theory**)
Classical quantum electrodynamics of interacting fields, M. Dresden and H. Dean Brown—748(A)
Covariant theory of damping, J. C. Pirenne—721(A)
Divergence of perturbation theory, F. J. Dyson—631
Do Coulomb fields signal faster than light?, D. I. Caplan and F. J. Belinfante—721(A)
Eigenvalue problem, Maurice Neuman—129
Electrodynamic displacement of atomic energy levels. I. Hyperfine structure, Robert Karplus and Abraham Klein—972
Fourth-order effects in vacuum polarization, Juan de Oyarzabal—748(A)
Phenomenological theory of Lamb shift, Frederik J. Belinfante—735(A)
Quantum theory for finite-sized electron. I, George J. Yevick—911
Radiative corrections to intensities for hydrogen-like atoms, erratum, T. Tati—1064(L)
Relativistic corrections to Lamb shift, erratum, Michel Baranger—1064(L)

Quantum mechanics (see **Mechanics, quantum**)

Radiation (see also **Thermal radiation**)
Absorption cross sections for 19.5-Mev quanta, Arthur I. Berman—774(A)
Application of Čerenkov radiation to cosmic-ray albedo problem, J. R. Winckler—1054(L)
Atmospheric absorption of solar infrared radiation, Romuald Anthony—674(L)
Calorimetric calibration of secondary standard for 150—317 Mev bremsstrahlung, P. D. Edwards—725(A)
Calorimetric determination of the roentgen for 400-kev x-rays, J. S. Laughlin, J. W. Beattie, and J. Ovadia—725(A)
Čerenkov radiation from positrons, T. C. Wilfong, Jr., and J. E. Henderson—765(A)
Condition for radiation from solar plasma, J. Feinstein—145(L)
Energetic protons from nuclei exposed to 300-Mev bremsstrahlung, James C. Keck—410
Propagation of short radio waves well beyond the horizon, Thomas J. Carroll—732(A)
Proton bremsstrahlung at 140 Mev, Richard Wilson—563
Theory of angular width of Čerenkov radiation from particle undergoing multiple scattering, K. G. Dedrick—765(A)

Radio (see also **Ionosphere; Radiation**)
Propagation of short radio waves well beyond horizon, Thomas J. Carroll—732(A)

Radioactivity (see also **Disintegration and excitation of nucleus; Nuclear spectra**)
Absence of spontaneous emission of neutrons from Sm, S. D. Chatterjee and R. N. Olcott—147
α-radioactivity in elements below Pb, S. G. Thompson, J. O. Rasmussen, and A. Ghiorso—758(A)
Al^{24}, delayed heavy-particle emitter, Ann C. Birge—753(A)
Am^{241} α-half-life, B. G. Harvey—482(L)
Atomic binding energy considerations in negative β-decay, H. M. Schwartz—733(A)
β-decay of RaE and pseudoscalar interaction, A. G. Petschek and R. E. Marshak—698(L)
Bi^{203} α-activity, Dean C. Dunlavey and Glenn T. Seaborg—757(A)
Bi^{210} isomeric states, Harris B. Levy and I. Perlman—758(A)
Ca^{48} natural radioactivity, John W. Jones and Truman P. Kohman—941(L)
Ce^{144} and Pr^{144} β-spectra, Cheng Lin-sheng, G. John, and J. D. Kurbatov—487(L); Fred T. Porter and C. Sharp Cook—733(A)
Complex α-structure of heavy elements, Frank Asaro, Fred L. Reynolds, and I. Perlman—758(A)
Decay series $Nd^{140}-Pr^{140}-Ce^{140}$, Charles I. Browne, John O. Rasmussen, Joseph P. Surls, and Donald F. Martin—146(L)
Delayed γ-emission from decay of C^{16}, Emmett L. Hudspeth, William B. Rose, and N. P. Heydenburg—742(A)
Disintegration of ground-state Sr^{88} and metastable energy level of 514 kev in Rb^{88}, W. S. Emmerich and J. D. Kurbatov—149(L)
Of $Eu^{152,154}$, Robert Katz and Milford R. Lee—1038(L)
Fine structure and angular correlation in Po^{210}, S. De Benedetti and G. H. Minton—944(L)
Fine structure of α-particles of Po^{210}, S. De Benedetti and G. H. Minton—726(A)
Genetic relationships and fission yields of members of the mass-115 decay chain, Arthur C. Wahl and Norman A. Bonner—570
Half-life of 1.3-Mev excited state in K^{41}, L. G. Elliott—942(L)
Heavy collateral radioactive chains, W. W. Meinke, A. Ghiorso, and G. T. Seaborg—429
I, *F*, and *A* lines of ThC, H. Craig—688(L)
L x-rays and low energy γ-radiation in decay of Am^{241}, C. I. Browne and I. Perlman—758(A)
Lifetime of excited state of $_{66}Dy^{160}$ and upper limits for some other nuclei, F. K. McGowan—142(L)
Limits of stability of heavy elements and effects of nuclear shell structure, P. S. Greifinger—253
Locating buried radioactive sources, J. D. Graves and Richard I. Condit—752(A)
Lu^{176m} disintegration scheme, G. Scharff-Goldhaber, E. der Mateosian, and J. W. Mihelich—734(A)
Mass designation of 51.5-min Tc isomer, Heinrich A. Medicus and Harry T. Easterday—735(A)
Of Hg^{197} and Hg^{203}, J. M. Cork, D. W. Martin, J. M. LeBlanc, and C. E. Branyan—386(L)
Monitor for natural radioactivity in the atmosphere, M. H. Wilkening—712(A)
Natural scintillations from uranyl nitrate crystals, S. G. Cohen and Y. Feige—1049(L)
Nd, possible natural radioactivity, George I. Mulholland and Truman P. Kohman—144(L)
Of Nd^{151} and Pm^{151}, W. C. Rutledge, J. M. Cork, and S. B. Burson—734(A)
Np^{235}, *L*-electron capture and α-decay, Ralph A. James, Albert Ghiorso, and Donald Orth—369(L)
New medium mass α-emitters, K.-H. Sun, F. A. Pecjak, B. Jennings, and A. J. Allen—726(A)
P^{32} and P^{33} β-spectra, Erling N. Jensen, R. T. Nichols, J. Clement, and A. Pohm—112
Production and assignment of Ra^{230} and Ac^{230}, William A. Jenkins and Glenn T. Seaborg—758(A)
Of Pm^{146} and Pm^{150}, John K. Long and M. L. Pool—137(L)
Of RaD, R. C. Bannerman and S. C. Curran—134(L)

Ra^{220} and Ac^{220} preparation, F. Depocas and B. G. Harvey—499(L)
Of Rh^{99}, Rh^{101}, Rh^{105}, and Ru^{105}, C. L. Scoville, S. C. Fultz, and M. L. Pool—1046(L)
Rh^{106} decay, David E. Alburger—734(A)
Search for double β-decay in Pd, Rolf G. Winter—687(L)
Search for long-lived Nb^{94}, R. E. Hein, C. M. Fowler, and R. H. McFarland—138(L)
Second transition in decay of Sn^{119m}, J. C. Bowe and P. Axel—734(A)
Si^{31} β-activity and masses of Al and Si isotopes, Henry T. Motz—501(L)
Ag^{105} and Ag^{106} decay, Raymond W. Hayward—760(A)
Of Ag^{108}, Max Goodrich and Edward C. Campbell—742(A)
Sr^{88} isomerism, A. W. Sunyar, J. W. Mihelich, G. Scharff-Goldhaber, M. Deutsch, and M. Goldhaber—734(A)
Te^{125m} decay, P. Axel and J. C. Bowe—734(A)
Semiempirical correlation of α-decay rates, J. O. Rasmussen—758(A)
Sn^{126}, double β-decay, Marvin I. Kalkstein and W. F. Libby—368(L)

Raman spectra
Of CBr_2Cl_2, Abram Davis, Forrest F. Cleveland, and Arnold G. Meister—707(A)
Of $CF_2{=}CHCl$, J. Rud Nielsen, C. Y. Liang, and D. C. Smith—740(A)
Of CH_3CH_2F and $CH_3{-}CHF_2$, D. C. Smith, R. A. Saunders, J. Rud Nielsen, and E. E. Ferguson—739(A)

Range and energy loss of particles
Effect of chemical structure on stopping powers for high energy protons, T. J. Thompson—765(A)
Electron pick-up by fast C^{13} nuclei in emulsion, Peter C. Giles and Walter H. Barkas—756(A)
Energy loss of monoenergetic electrons in C and H_2O, John I. Lodge and Frank L. Hereford—725(A)
Ionization loss of energy of relativistic μ-mesons in A, J. E. Kupperian, Jr., and E. D. Palmatier—1043(L)
Physical measurements on nuclear photographic emulsion, A. J. Oliver and Walter H. Barkas—756(A)
Radiative correction for collision loss of fast particles, J. M. Jauch—950
Raman and infrared spectral data, force constants, and thermodynamic properties for CBr_2Cl_2, Abram Davis, Forrest F. Cleveland, and Arnold G. Meister—707(A)
Range of 18-Mev protons in Al, E. L. Hubbard and K. R. MacKenzie—107
Range of high energy electrons in H_2O, J. Ovadia, J. W. Beattie, and J. S. Laughlin—725(A)
Range straggle of μ^+ mesons, F. M. Smith, W. Birnbaum, and W. H. Barkas—771(A)
Range straggling of nonrelativistic charged particle, H. W. Lewis—20
Relative transmission of β-particles through G-M counter windows, Chia-hua Chang and C. Sharp Cook—724(A)
Stopping cross section of ice, Ward Whaling and W. A. Wenzel—761(A)
Stopping power of heavier substances, J. Lindhard and M. Scharff—1058(L)
Stopping power of metal for charged particles, David Pines—931(L)

Recombination
Dissociation of H_2 by vibrational excitation and three-body recombination coefficient. II, E. Bauer—277
Pressure-dependent recombination coefficients, Leonard B. Loeb and Wulf B. Kunkel—493(L)

Rectifier (see **Electrical conductivity and resistance; Semiconductors**)

Relativity
Electrodynamics as basis for special relativity, Arthur E. Ruark—770(A)
Geometry of group-space of proper Lorentz group, E. J. Schremp—721(A)
Gravitational deflection of photons with nonvanishing rest mass, Albert D. Wheelon—383(L)
Relativistic dynamics of system of particles, L. H. Thomas—868

Resistance, electrical (see **Electrical conductivity and resistance**)

Resonance radiation
Isotope effect in imprisonment of resonance radiation, T. Holstein, D. Alpert, and A. O. McCoubrey—985

Scattering of electrons, mesons, neutrons, protons, deuterons, and ions (see also **Electron diffraction; Cross section, measurements, theory**)
Absolute backscattering coefficients for positrons and electrons, Howard H. Seliger—724(A)
Analysis of 14-Mev $n-p$ scattering, George Snow—703(A)
Angular correlation between inelastically scattered protons and γ-rays from 1.4-Mev level in Mg^{24}, H. E. Gove and A. Hedgran—727(A)
Backscattering of low energy electrons, E. J. Sternglass, S. C. Frey, and F. H. Grannis—391(A)
By bound particles with short range interaction force, H. Ekstein—703(A)
Coherent neutron scattering cross section of C^{13}, W. C. Koehler and E. O. Wollan—490(L)
Detection of azimuthal polarization in double $n-p$ scattering at 150 Mev, L. F. Wouters—757(A)
Differential cross section for scattering of 9.5-Mev protons from He, T. M. Putnam—774(A)
Elastic scattering of deuterons by deuterons, Richard J. Runge—1052(L)
Elastic scattering of Li^7+p and $C^{13}+p$, William D. Warters and Edmund A. Milne—761(A)
Elastic scattering of negative pions in C, P. Isaacs, A. Sachs, and J. Steinberger—718(A)
Elastic scattering of 190-Mev deuterons by protons, Martin O. Stern—752(A)
Electron-electron scattering at 6.1 Mev, W. C. Barber, G. E. Becker, and E. L. Chu—774(A)
Electron-neutron interaction, M. Hamermesh, G. R. Ringo, and A. Wattenberg—483(L)
Energy levels in Al^{27}, E. M. Reilley, A. J. Allen, J. S. Arthur, R. S. Bender, R. L. Ely, and A. J. Hausman—704(A)
Fast protons from 270-Mev $n-d$ scattering, W. Hess, J. B. Cladis, and J. Hadley—757(A)
Of 50-Mev positive pions by He, A. M. Thorndike, E. C. Fowler, W. B. Fowler, and R. P. Shutt—929(L)
Geometrical optics and theory of small angle scattering, George H. Vineyard—633
High energy electron-electron scattering, Charles E. Violet, F. C. Gilbert, Robert W. Deutsch, and Walter H. Barkas—756(A)
High energy neutron collisions with He, Clifford Swartz—73
High energy nucleon-deuteron scattering, P. B. Daitch and J. B. French—695(L)
High energy scattering cross sections using variational methods, David S. Saxon and E. Gerjuoy—704(A)
Impulse approximation, Geoffrey Chew and Gian Carlo Wick—636; J. Ashkin and G. C. Wick—686(L)
Inelastic and total scattering of 190-Mev deuterons by protons, Arnold L. Bloom—752(A)
Inelastic cross sections for 240-Mev protons, Alfred M. Perry—497(L)
Inelastic scattering of protons from light nuclei, N. P. Heydenburg, G. C. Phillips, and Dean B. Cowie—742(A)
Inelastic scattering of protons from Ni, Ralph Ely, Jr., A. J. Allen, J. S. Arthur, R. S. Bender, H. J. Hausman, and E. M. Reilley—704(A)

Scattering of electrons, mesons, neutrons, protons, deuterons, and ions (continued)
Interaction of charged π-mesons with deuteron, W. B. Cheston—718(A); 952
Internal momentum distributions from scattering experiments, J. B. Cladis, W. Hess, and B. J. Moyer—766(A)
Invariance conditions on scattering amplitudes for spin $\frac{1}{2}$ particles, L. Wolfenstein and J. Ashkin—947
Mean-value calculations for projected multiple scattering, W. T. Scott—245
Meson tail effect and treatment of $p-p$ scattering data, M. C. Yovits, R. L. Smith, Jr., M. H. Hull, Jr., J. Bengston, and G. Breit—540
Multiple scattering of fast charged particles in a gas. II. β^- and β^+, Gerhart Groetzinger, Watts Humphrey, Jr., and Fred L. Ribe—78
Multiple scattering of fast particles in photographic emulsions, L. Voyvodic and E. Pickup—91
Of negative π-mesons in Al, Cu, and Pb, Harry H. Heckman and Walter H. Barkas—771(A)
Neutron scattering lengths, D. C. Peaslee—555
Of 9.6-Mev protons by C, Al, and Mg, C. J. Baker, J. N. Dodd, and D. H. Simmons—1051(L)
Nuclear scattering of 1-Mev electrons and positrons, Harry J. Lipkin—517
Ordinary and exchange scattering of negative pions by H, E. Fermi, H. L. Anderson, A. Lundby, D. E. Nagle, and G. B. Yodh—935(L)
Precision scattering project, James S. Arthur, A. J. Allen, R. S. Bender, R. L. Ely, H. J. Hausman, L. A. Page, and E. M. Reilley—704(A)
$p-d$ scattering at 240 Mev, Robert D. Schamberger—424
$p-p$ scattering at 240 Mev, C. L. Oxley and R. D. Schamberger—416; O. A. Towler, Jr.—1024
Radiative correction for collision loss of fast particles, J. M. Jauch—950
Radiative corrections to distribution of nuclear recoils from electron scattering, L. I. Schiff—754(A)
Range of 18-Mev protons in Al, E. L. Hubbard and K. R. MacKenzie—107
Range straggling of nonrelativistic charged particle, H. W. Lewis—20
Regular meson type potentials in $p-p$ scattering, R. D. Hatcher and H. E. Hart—703(A)
Scattering of strongly coupled pseudovector mesons, Melvin Eisner—748(A)
Theory of angular width of Čerenkov radiation from particle undergoing multiple scattering, K. G. Dedrick—765(A)
Theory of neutron scattering by gases, N. K. Pope and G. Feldman—703(A)
Of 30-Mev α-particles by He, E. Graves—703(A)
Time dependent description of resonance reactions, Marcos Moshinsky—748(A)
Total cross sections of negative pions in H, H. L. Anderson, E. Fermi, E. A. Long, R. Martin, and D. E. Nagle—934(L)
Total cross sections of positive pions in H, H. L. Anderson, E. Fermi, E. A. Long, and D. E. Nagle—936(L)
Variational calculation of scattering cross sections, E. Gerjuoy and David S. Saxon—939(L)
Scattering of radiation (see also **Raman spectra**)
Multiple Compton scattering of low energy γ-radiation, R. C. O'Rourke—881
Multiple γ-ray scattering in Pb, J. O. Elliot, R. T. Farrar, R. D. Myers, and C. F. Ravilious—1048(L)
Multiple scattering of waves. II. Effective field in dense systems, Melvin Lax—621
Multiple scattering theory of grating and Wood anomalies, Vic Twersky—715(A)
Of 0.5-Mev circularly polarized photons in magnetized Fe, Forrest P. Clay and Frank L. Hereford—675(L)
Polarization of scattered quanta, J. I. Hoover, W. R. Faust, and C. F. Dohne—58
Radiative corrections to Compton scattering, L. M. Brown and R. P. Feynman—231
Scattering of light from small drops, Richard L. Lander and C. E. Nielsen—712(A)
Scintillation counters (see **Methods and instruments**)
Secondary electrons (see **Electrons, secondary**)
Semiconductors (see also **Electrical conductivity and resistance**)
Application of Nijboer's theory to semiconducting emitters, T. Arizumi and S. Narita—388(A)
Atomic heat of Si and Ge at very low temperatures, P. H. Keesom and Norman Pearlman—730(A)
Automatic multirange recording device for measuring varying potentials, J. C. Pigg—731(A)
Calculation of specific heat of Ge, Yü-Chang Hsieh—730(A)
Comparison of adiabatic and isothermal Hall effects, V. A. Johnson and F. L. Shipley—724(A)
Drift mobility of electrons in Si, J. R. Haynes and W. C. Westphal—680(L)
Electrical properties of porous semiconductors, E. B. Hensley—388(A)
Electrical properties of rutile single crystals, L. F. Connell and R. L. Seale—745(A)
Evidence of hole traps in Ge produced by fast neutron bombardment, J. H. Crawford, Jr., J. W. Cleland, K. Lark-Horovitz, J. C. Pigg, and F. W. Young, Jr.—730(A)
Far infrared transmission of Si and Ge, R. C. Lord—140(L)
Influence of field on temperature saturated emissions from semiconducting cathodes, K. Lehovec—705(A)
Infrared absorption of nucleon bombarded Si. I, M. Becker, H. Y. Fan, and K. Lark-Horovitz—730(A); II, H. Y. Fan—730(A)
Magnetoresistive effect in impurity semiconductors, W. J. Whitesell, II, and V. A. Johnson—724(A)
Of polycrystalline graphite and condensed ring systems, S. Mrozowski—609
Pressure dependence of Zener current in Ge, K. B. McAfee, W. Shockley, and M. Sparks—730(A)
Probing the space-charge layer in $p-n$ junction, G. L. Pearson, W. T. Read, and W. Shockley—1055(L)
$P-N$ transition of oxide-coated cathode, erratum, Y. Ishikawa, T. Sato, K. Okumura, and T. Sasaki—1065(L)
Pulse-heating of bulk semiconductors, J. Hirsch and R. B. McQuistan—723(A)
Specific heats of several metals and semiconductors between 1.8 and 4.2°K, I. Estermann and S. A. Friedberg—715(A)
Theory of conductivity of semiconductors, George Jaffé—354
Thermally produced acceptors in Ge, C. S. Fuller, H. C. Theuerer, and W. van Roosbroeck—678(L)
Zn as acceptor in Ge, W. C. Dunlap, Jr.—945(L)
Shock waves (see also **Explosion phenomena; Supersonics**)
Interactions of shock waves in air with three-dimensional surfaces, Richard I. Condit—769(A)
Velocities of ionized air shocks near detonating explosives, J. Savitt and R. H. Stresau, Jr.—732(A)
Solid state (see **Crystalline state; Mechanics, quantum—of solid bodies**)
Sound (see **Acoustics**)
Spallation (see **Disintegration and excitation of nucleus**)
Specific heat
Atomic heat of Pb in region of transition to superconductivity, J. R. Clement and E. H. Quinnell—502(L)
Atomic heat of Si and Ge at very low temperatures, P. H. Keesom and Norman Pearlman—730(A)
Calculation for Ge, Yü-Chang Hsieh—730(A)
Electronic specific heat in Cr and Mg, S. A. Friedberg, I. Estermann, and J. E. Goldman—375(L)

Heat capacity and lattice defect of AgCl, Koichi Kobayashi —150(L)
Of several metals and semiconductors between 1.8 and 4.2°K, I. Estermann and S. A. Friedberg—715(A)
Spectra, absorption (see also **Absorption of radiation; Spectra, general; Spectra, microwave; Spectra, molecular**)
Beer's law generalized and applied to Herzberg continuum in oxygen gas, R. M. Langer—740(A)
Of GaCl, erratum, Franklyn K. Levin and J. G. Winans—1064(L)
Infrared absorption by asymmetrical spectral lines, Gilbert N. Plass and Douglas Warner—708(A)
Infrared absorption of nucleon bombarded Si. I, M. Becker, H. Y. Fan, and K. Lark-Horovitz—730(A); II, H. Y. Fan—730(A)
Long forbidden $s-ns$ series in RbI, J. E. Mack—716(A)
Pressure-broadening of absorption lines, Stanley Bloom and Henry Margenau—717(A)
Ag activated alkali halides, H. W. Etzel, J. H. Schulman, R. J. Ginther, and E. W. Claffy—1063(L)
Structure of 3μ-band of $NaBr \cdot 2H_2O$, D. S. Webber and A. N. Baker, Jr.—755(A)
Spectra, atomic
Effect of intrinsic moment of electron on spectroscopic isotope shift, G. Breit and W. W. Clendenin—689(L)
Eigenfunctions and Landé interval factors for terms of f^3 electrons, Robert A. Satten—775(A)
Fine structure of H_2 atom. III, Willis E. Lamb, Jr.—259
Fine structure splitting in ground state of positronium, T. A. Pond and R. H. Dicke—489(L)
Ge arc spectrum, Kenneth L. Andrew and K. W. Meissner—716(A)
$L(L+1)$ correction in spectra of Fe group, Guilio Racah—381(L)
$L(L+1)$ correction to Slater formulas for energy levels, R. E. Trees—382(L)
Magic numbers and isotope shift in atomic spectra of heavy elements, P. Brix and H. Kopfermann—1050(L)
Pressure effects of A and He on resonance lines of Ag, Eugene D. Clayton and Shang-yi Ch'en—68
Radiative corrections to intensities for hydrogen-like atoms, erratum, T. Tati—1064(L)
Superposition of configurations in ground state of He I, Louis C. Green, Marjorie M. Mulder, C. W. Ufford, E. Slaymaker, Eleanor Krawitz, and R. T. Mertz—65
Spectra, general
CO in solar atmosphere, Leo Goldberg, Robert R. McMath, Orren C. Mohler, and A. Keith Pierce—140(L)
Emission spectra of nitrogen bombarded by high energy protons, R. J. Shalek, T. W. Bonner, and L. M. Branscomb—739(A)
Far infrared transmission of Si and Ge, R. C. Lord—140(L)
Raman and infrared spectral data, force constants, and thermodynamic properties for CBr_2Cl_2, Abram Davis, Forrest F. Cleveland, and Arnold G. Meister—707(A)
Spectrum of Nd^{+++} in crystals, Robert A. Satten—755(A)
Structure of 3μ-band of $NaBr \cdot 2H_2O$, D. S. Webber and A. N Baker, Jr.—755(A)
Time-resolved spectroscopy of incandescence associated with ultraspeed pellets, Earle B. Mayfield—769(A)
Unusual dispersion aspects of gypsum in the near infrared, R. M. Vanderberg—755(A)
Spectra, microwave
Beam system for reduction of Doppler broadening of microwave absorption line, H. R. Johnson and M. W. P. Strandberg—503(L)
Cl^{35} spin from microwave spectrum of $C^{12}H_3Cl^{35}$, D. A. Gilbert—716(A)
Fine structure of H_2 atom. III, Willis E. Lamb, Jr.—259
Of H_2O_2, J. T. Massey and D. R. Bianco—717(A)
Of ozone, Richard H. Hughes—717(A)
Resolution and sensitivity of microwave spectrographs, H. R. Johnson—764(A)
Of a slightly aspherical top—structure and dipole moment of SO_2F_2, Robert M. Fristrom—717(A)
S^{33} magnetic moment from microwave spectroscopy, J. R. Eshbach, R. E. Hillger, and M. W. P. Strandberg—532
Spectra, molecular (see also **Molecular structure and constants; Spectra absorption**)
Computation of infrared intensities, Frank Matossi—708(A)
Infrared absorption by asymmetrical spectral lines, Gilbert N. Plass and Douglas Warner—708(A)
l-type doubling transitions in HCN and DCN, Thomas L. Weatherly, Edward R. Manring, and Dudley Williams —717(A)
Molecular spectrum of I_2 excited in presence of inert gas, K. Wieland and Jürg Waser—385(L)
Relations between vibrational intensities of isotopic molecules, J. C. Decius—755(A)
Rotational temperatures of OH in flames, H. P. Broida—755(A)
Vibrational analysis of fluorescence of naphthalene vapor, O. Schnepp and D. S. McClure—755(A)
Vibrational spectrum of N_2O_4, W. D. Perkins and M. Kent Wilson—755(A)
Spectra, nuclear (see **Nuclear spectra**)
Spectra, x-ray (see **X-rays, spectra**)
Spectroscopy, technique
Use of successive diffractions to double or quadruple the resolving power of grating, F. A. Jenkins and L. W. Alvarez—763(A)
Standards (see **Constants, physical standards**)
Statistical mechanics (see **Mechanics, statistical**)
Superconductivity (see also **Electrical conductivity and resistance; Low temperature phenomena**)
Atomic heat of Pb in region of transition to superconductivity, J. R. Clement and E. H. Quinnell—502(L)
Experiments with audiofrequencies on superconductors, B. Serin and C. A. Reynolds—938(L)
Formation of boundary between normal-conducting and superconducting metal, M. P. Garfunkel and B. Serin—834
Magnetic properties of hollow superconducting Pb sphere, Julius Babiskin—104
Magnetic threshold field curve, R. P. Hudson—382(L)
Meissner effect in alloys of In-Tl and Sn-Bi, E. Callen, W. F. Love, and F. C. Nix—715(A)
Studies with torsion pendulum, Arthur L. Lathrop—743(A)
Superconductive transition in pure metals, W. F. Love—715(A)
Of V, A. Wexler and W. S. Corak—85
Thermal conductivity
Of metals, P. H. Sidles and G. C. Danielson—710(A)
Thermal diffusion
Distribution of components of ternary isotopic mixture along Clusius-Dickel column, F. K. Elder, Jr., and R. E. McDonald—500(L)
Thermionic emission; Emitting surfaces
BaSrO cathode supported on insulator, George E. Moore and H. W. Allison—389(A)
Chemical reactions in BaO on W emitters, R. C. Hughes, P. P. Coppola, and H. T. Evans—388(A)
Diffusion phenomena in oxide cathode, E. S. Rittner—389(A)
Electrical conductivity and thermoelectric power of (BaSr)O and BaO, J. R. Young—388(A)
Electronic properties of BaS, W. Grattidge and H. John—389(A)
$I-V$ characteristics of "L-cathode," E. S. Rittner and R. H. Ahlert—390(A)

Thermionic emission; Emitting surfaces (continued)
Influence of field on temperature saturated emissions from semiconducting cathodes, K. Lehovec—705(A)
Interpretation of periodic deviation data for highly refactory metals, E. A. Coomes—392(A)
Luminescence of BaO, Virgil L. Stout—390(A)
Photoconductivity study of activation of BaO, H. B. DeVore—390(A)
Photoelectric emission from BaO in accelerating field, Paul E. Carroll and E. A. Coomes—389(A)
Physical processes in "*L*" cathode, D. L. Shaefer and J. E. White—390(A)
P—*N* transition of oxide-coated cathode, erratum, Y. Ishikawa, T. Sato, K. Okumura, and T. Sasaki—1065(L)
Retarding potential method of measuring electrical conductivity of oxide coated cathodes, I. L. Sparks—705(A)
Study of evaporated films of BaO using electron diffraction, Paul Russell—705(A)
Use of radioactive isotopes in study of evaporation from thermionic cathodes, W. F. Leverton and W. G. Shepherd—389(A)

Thermodynamics
Of fields, A. E. Scheidegger and C. D. McKay—721(A)
Information and thermodynamics, Jerome Rothstein—135(L)
Infrared and Raman spectra and calculated thermodynamical properties of $CF_2=CHCl$, J. Rud Nielsen, C. Y. Liang, and D. C. Smith—740(A); of CH_3-CH_2F and CH_3-CHF_2, D. C. Smith, R. A. Saunders, J. Rud Nielsen, and E. E. Ferguson—739(A)
Phase transitions in adsorbed films, Lothar Meyer and Earl Long—1035
Raman and infrared spectral data, force constants, and thermodynamic properties for CBr_2Cl_2, Abram Davis, Forrest F. Cleveland, and Arnold G. Meister—707(A)
Supercooling of H_2O, B. Luyet—746(A)

Thermoelectric effects
Adiabatic thermal changes in $BaTiO_3$ ceramic at low temperatures, Roland W. Schmitt—1; Roland W. Schmitt and R. T. Swim—743(A)
Of (BaSr)O and BaO, J. R. Young—388(A)
Electrical phenomena during freezing of dilute aqueous solutions, Marvin E. Backman—759(A)

Thermoluminescence
Color centers and thermoluminescence in alkali halides, J. Sharma—692(L)

Thermomagnetic effects
Adiabatic thermomagnetic effects, Herbert B. Callen—16

Ultrasonics (see **Acoustics**)

Vacuum tubes (see **Electronic tubes**)

Van der Waals forces
In magnetic fields, Henry Margenau and D. E. Harrison—707(A)

Wave mechanics (see **Mechanics, quantum,** etc.)

Wave motion
Experimental laboratory studies of elastic wave propagation, W. L. Roever—744(A)
Propagation of Rayleigh waves on surface of viscoelastic solid, C. W. Horton—744(A)
Transient waves through steel produced by impulsive loading, William A. Allen and Clyde L. McCrary—769(A)
Wave propagation ducts in geophysics, Lynn G. Howell—744(A)

X-rays, absorption, diffraction, scattering, reflection, refraction, and polarization
Absorption of Se in soft x-ray region, M. Parker Givens and Walter P. Siegmund—313
Gometrical optics and theory of small angle scattering, George H. Vineyard—633
New method of obtaining focused images with x-rays, G. M. Ramachandran—378(L)
Point focusing monochromator for low angle x-ray diffraction, L. Shenfil, W. E. Danielson, and J. W. M. DuMond—710(A)
Reflection of x-rays and x-ray microscope, L. M. Rieser, Jr.—764(A)
X-ray diffusion in infinite medium, L. V. Spencer and Fannie Stinson—662
X-ray study of lattice imperfections, P. H. Miller, Jr.—709(A)

X-rays, spectra and spectroscopy, wavelength measurements (see also **X-rays, emission**)
Auger enhancement of $M\alpha$ x-ray satellite lines, F. R. Hirsh, Jr.—685(L)
Curved quartz crystal x-ray spectrometer, John E. Edwards—160(A)
Energy levels in KCl, L. G. Parratt and E. L. Jossem—729(A)
K excitation potentials of elements, G. L. Rogosa—716(A)
M_3 and M_4 x-ray absorption edges of Ta, Donald D. Doughty and J. W. McGrath—1040(L)

Zeeman effect
Of positronium, Martin Deutsch and Sanborn C. Brown—1047(L)
Rotation magnetic moments of $^1\Sigma$-molecules, J. R. Eshbach and M. W. P. Strandberg—24

THE AMERICAN INSTITUTE OF PHYSICS

INCORPORATED

57 East 55 Street New York 22, N.Y.

MEMBER SOCIETIES:

American Physical Society
KARL K. DARROW, *Secretary*, Columbia University, New York 27, New York.

Optical Society of America
ARTHUR C. HARDY, *Secretary*, Massachusetts Institute of Technology, Cambridge 39, Massachusetts.

Acoustical Society of America
WALLACE WATERFALL, *Secretary*, 57 East 55th Street, New York 22, New York.

Society of Rheology
G. J. DIENES, *Secretary*, Brookhaven National Laboratory, Upton, Long Island, New York.

American Association of Physics Teachers
R. F. PATON, *Secretary*, University of Illinois, Urbana, Illinois.

AFFILIATED SOCIETIES:

American Crystallographic Association
Electron Microscopy Society of America
Physical Society of Pittsburgh
Physics Club of Chicago
Physics Club of Philadelphia
Cleveland Physics Society
Physics Club of the Lehigh Valley
Sigma Pi Sigma

ASSOCIATES:

Over seventy-five leading industrial enterprises and other institutions which contribute to the support of the Institute.

JOURNALS:

The Physical Review
S. A. GOUDSMIT, *Editor*, Brookhaven National Laboratory, Upton, Long Island, New York.

Reviews of Modern Physics
J. W. BUCHTA, *Editor*, University of Minnesota, Minneapolis, Minnesota.

Journal of the Optical Society of America
WALLACE R. BRODE, *Editor*, National Bureau of Standards, Washington 25, D. C.

The Journal of the Acoustical Society of America
FOSTER A. FIRESTONE, *Editor*, 57 East 55th Street, New York 22, New York.

American Journal of Physics
THOMAS H. OSGOOD, *Editor*, Michigan State College, East Lansing, Michigan.

The Review of Scientific Instruments
GAYLORD P. HARNWELL, *Editor*, Randal Morgan Laboratory of Physics, University of Pennsylvania, Philadelphia, Pennsylvania.

The Journal of Chemical Physics
JOSEPH E. MAYER, *Editor*, Institute for Nuclear Studies, University of Chicago, Chicago 37, Illinois.

Journal of Applied Physics
ELMER HUTCHISSON, *Editor*, Case Institute of Technology, Cleveland 6, Ohio.

Physics Today
GAYLORD P. HARNWELL, *Editorial Director*; RUSSELL B. GRAVES, *Managing Editor*, American Institute of Physics, 57 East 55 Street, New York 22, New York.

OFFICERS
GEORGE R. HARRISON, *Chairman*, Massachusetts Institute of Technology
GAYLORD P. HARNWELL, *President*, Columbia University

GOVERNING BOARD:
KARL K. DARROW
G. J. DIENES
S. A. GOUDSMIT
G. P. HARNWELL
GEORGE R. HARRISON
J. V. HUNT
RUDOLPH KINGSLAKE
HUGH S. KNOWLES
C. C. LAURITSEN
F. W. LOOMIS
WILLIAM F. MEGGERS
GEORGE B. PEGRAM
I. I. RABI
DUANE ROLLER
FREDERICK SEITZ
FRANCIS G. SLACK
JOHN C. STEPHENSON
RICHARD M. SUTTON
MARK W. ZEMANSKY

Consultant on Physiology
MERVIN LOEB

ADMINISTRATIVE STAFF
HENRY A. BARTON, *Director*
WALLACE WATERFALL, *Executive Secretary*
THEODORE VOORHEES, *Advertising Manager*
RUTH F. BRYANS, *Publication Manager*
BETTY H. GOODWIN, *Assistant Secretary*
EILEEN B. NEUBERGER, *Circulation Manager*
KATHRYN SEITZ, *Assistant Treasurer*

THE American Institute of Physics was founded in 1931 as a federation of leading societies in the field of Physics. It combines into one operating agency those functions on behalf of physics which can best be done by the societies jointly. Its purpose is the advancement and diffusion of physics and its applications to human welfare. To this end it publishes for itself or the Societies the scientific journals listed on this page; promotes unity and effectiveness of effort among all who are professional in physics; renders numerous direct services to physicists and to the public; and cooperates with governmental agencies, research councils, educational institutions, technical industries, and other bodies in such manner as to realize the opportunities and fulfill the responsibilities of physics as an important and constructive human activity.

The Physical Review

Resonance Conditions in
Radiative Correction for
Interaction of a Charged
Symmetry Effects in
Thermodynamic Displacement
Isotope Effect in the
Resonance of Antimonide
Differential Range Spectrum
Energy of a Bloch Wall on
Neutron Capture γ-Rays
Proton-Proton Scattering at
Some Experiments on Fluor
Phase Transitions in Antiferro
Letters to the Editor:
Exchange Integral
Radioactivity of
Masses of Hg^{197},
Mt and Mt X-Ray
Electromagnetic
Polarization of the
Dielectric Constant and
Cloning of the Proton
Ionization Loss of
Transmutation and
Critical Velocity of
Test for the
Proposed Rest of the
Radiations of Hg^{197}, Hg^{203},
Energy Absorption
Zeeman Effect and
Multiple Coulomb
Bernoulli's Theorem
Natural Substitution
Magic Numbers and
Attempt to Produce
Scattering of 84-Mev
Elastic Scattering of
Absorption Requirement
Application of Quantum
Recoil γ-Transition
Probing the Space-Charge
Electron Interferometer
Stopping Power of
Electromagnetic
Velocity of 310-Mev
Elastic and Plastic
Pure Nuclear Elastic
Photodissociation of
Silver-Activated
Books
Author Index to Volume 82
Analytic Subject Index to Volume 82
Volume Table of Contents